Transitions between effusive and explosive activity at Merapi volcano, Indonesia: a volcanological and petrological study of the 2006 and 2010 eruptions

A thesis submitted to the School of Environmental Sciences of the University of East Anglia in partial fulfilment of the requirements for the degree of Doctor of Philosophy

Katie Jane Preece

February 2014

Abstract

The 2010 explosive eruption (VEI 4) of Merapi volcano, Indonesia, was the volcano's largest since 1872. In contrast, volcanism over the last century has been characterised by dome-building and gravitational dome collapse, such as in 2006 (VEI 1). The driving forces behind effusive and explosive activity, as well as factors that affect transitions in eruptive style are investigated through petrological and textural analysis, using the well-documented 2006 and 2010 eruptions as case-studies. Pre- and syn-eruptive crystallisation and degassing processes are examined via whole rock geochemical analysis, mineral compositions and thermobarometry, quantitative textural analysis of feldspar microlites and analysis of volatiles and light lithophile elements in melt inclusions. These data were gathered from a detailed set of stratigraphically controlled samples, correlated to eruptive chronology and style, which were collected during several field campaigns. Both the 2006 and 2010 eruptions produced basaltic andesite, similar in terms of major and trace element compositions. A major zone of crystallisation is proposed at between ~ 14 and 29 km depth, although crystallisation occurs throughout the crust. Magmatic temperatures are estimated to be ~920–1020 °C. Maximum H_2O contents reach 3.94 wt.% in 2010 melt inclusions and up to 3.73 wt.% in those from 2006. CO_2 concentrations are < 200 ppm, although they may reach up to 695 ppm in some melt inclusions from the 2010 eruption. An exsolved brine phase was present during both eruptions which "buffered" melt Cl concentrations and enriched Li at shallow depths within the conduit or edifice. Eruptive style and transitions at Merapi are linked to magma ascent rate, crystallisation and open- and closed-degassing processes, which can be influenced by magma influx. The findings of this work are crucial for understanding the full range of eruptive behaviour that Merapi is capable of producing.

Contents

List of Tables

List of Figures

The Eruption of Mt. Merapi at Night, Java. Raden Saleh (1866)

"…The roaring was horrifying…one saw masses of rock sliding down in great quantities, without interruption…the noise grew more violent, and a moment later the densest mass of ash, like thick clouds of dust, was seen having the shape of a wooly, curling and weltering colossus, sliding downslope…"

(Anonymous, 1867)

From Voight *et al.* (2000)

Acknowledgements

I would first and foremost like to thank my supervisors Dr Jenni Barclay and Dr Ricky Herd at UEA, as well as Dr Ralf Gertisser at Keele University. I am grateful to all of you for giving me the opportunity to work on such an interesting subject, and I appreciate all of the intellectual insight, advice, constructive feedback and good humour shared with me over the course of the last few years. Jenni, I thank you for your enthusiasm, support and discussions, especially those involving coffee and cake. I am very grateful to the Barclay-Renfrew family for showing me such hospitality during the course of the Ph.D. Ricky, thank you for sharing your endless knowledge of all things volcanological and for your calm, level-headed approach to everything. Ralf, thank you for your encouragement, discussions, guidance and for giving me the opportunity to go to Merapi. I also thank you for your engaging lectures and fieldtrips during my Undergraduate days at Keele, which instilled in me a love of volcanology and petrology and made me realise that I wanted to try and be a volcanologist.

I am indebted to the many people I've been lucky enough to learn from and collaborate with in the field during 4 trips to Merapi. I am especially grateful to Dr Sylvain Charbonnier and Dr Jean-Christophe Komorowski for assistance during fieldwork and for sharing their thoughts about the 2006 and 2010 Merapi eruptions. I am thankful to Dr Aurélie Germa, Dr Susanna Jenkins and Indonesian colleagues from BPPTK for help with sample collection during fieldwork. Dr Nigel Cassidy and Dr Luigia Nuzzo are acknowledged for sampling assistance at Merapi back in 2008. Thank you to our Indonesian driver and friend Biyanto, who took us to wherever we wanted to go with a smile and a John Denver tape. Thank you to Dr Antonius Ratdomopurbo for discussions about Merapi, monitoring data and lava dome growth and collapse during the 2006 eruption and to Prof. Val Troll for thought-provoking discussions about the Merapi magmatic system. David Damby is thanked for kindly sharing with us some preliminary samples from 2010.

I am grateful to Dr Kim Berlo for assistance at the ion probe and for discussions about the melt inclusions data. Thank you Dr Jake Lowenstern for very kindly carrying

out ATR micro-FTIR analysis of selected melt inclusions, as well as for helpful discussions about the melt inclusions data.

I am grateful to Bertrand Lézé for patient technical assistance and advice when using the SEM and during XRF analysis. Dr John Brindle is also thanked for general laboratory support and advice at UEA. Thanks to Dr Chiara Petrone and Dr Iris Buisman for assistance when using the electron microprobe at the University of Cambridge, as well as to Dr Andy Tindle at the Open University. Thank you to Dr Cees-Jan de Hoog at the NERC Ion Microprobe Facility, The University of Edinburgh for assistance with the ion microprobe and for useful discussions about the data. I appreciate the help given to me by technical staff at Keele University and would like to thank Peter Greatbatch and Dave Wilde for making endless thin sections and for assistance polishing grain mounts

To my office mates in the "The Rock", you have made the past few years in office 3.16 such a friendly, fun and productive place to work: Jennie, Mel and Mel, Maria, Johanna, Tom, Kostas, Rachel, Alex, Sian, Letty and Nuhu, thank you!

I acknowledge NERC for providing funding the research, as well as VMSG, The Mineralogical Society, Cities on Volcanoes, IAVCEI and UEA who all provided extra funding for conference attendance and fieldwork.

Last but not least, a big thank you to my examiners Prof. David Pyle and Prof. Roland von Glasow for taking the time to review this work and for interesting and stimulating discussion in my viva.

Chapter 1: Introduction

This thesis is an investigation of the driving forces behind effusive and explosive activity at Merapi volcano and the factors influencing the transitions between the two styles. Using the 2006 and 2010 eruptions as case studies, the thesis integrates volcanological, textural and petrological data in order to investigate degassing and crystallisation processes during magma storage and ascent. Whole rock and mineral compositions, together with quantitative microlite textural analysis and melt inclusion data aim to elucidate pre- and syn-eruptive factors that contributed to eruptive style and variations thereof.

The cataclysmic 2010 eruption of Merapi was the volcanoes largest since 1872 (*e.g.* Surono *et al*., 2012). On 26 October 2010, after nearly two months of enhanced levels of seismicity and ground deformation, Merapi erupted explosively generating PDCs that travelled down the southern slopes, killing 35 people. In stark contrast to other recent eruptions at Merapi, no lava dome grew before the eruption and there was little warning time before the first high-energy explosion tore across the southern flanks. A lava dome then rapidly extruded and further explosions continued daily, for approximately two weeks, before activity started to decrease in the middle of November. At the peak of activity on 5 November, PDCs travelled 16 km south of summit, resulting from laterally directed explosions of the rapidly extruding dome, subsequently followed by sub-Plinian fountain collapse. During the 2010 eruptive episode (VEI 4) more than 200 people were killed, making this most recent eruption the greatest volcanic disaster at Merapi in 80 years. The 2010 eruption was dramatically different to other recent eruptions at Merapi, including the preceding 2006 eruption (VEI 1). In 2006, activity consisted of prolonged (> 3 months) dome extrusion, punctuated by repeated gravitational dome collapses generating block-and-ash-flows (BAFs). This type of activity has occurred so frequently at Merapi during the last 200 years that PDCs generated by gravitational dome collapse are often referred to as ‘Merapi-type nuées ardentes’.

1.1. Lava domes and their eruptions

Effusive, dome-forming eruptions are common at silicic and intermediate volcanoes worldwide. Lava domes are defined as being mounds of rock extruded from a volcanic vent, which forms as viscous magma cools relatively quickly after emerging onto a planetary surface (Fink and Anderson, 2000). Their diameter may vary from a few meters up to several kilometres and the height can vary between a few meters to > 1 km. Their morphology can vary according to conditions of eruption and cooling rate and the yield strength of the lava. 'Peléean' domes are steep-sided and have a relatively smooth surface, which is punctuated by protruding spines, as seen at Mt. Pelée (Martinique) in 1902 and 1932-33. Less-steep sided domes, composed of sequentially emerged lobes with smooth or blocky surfaces, have been observed at Mount St. Helens (USA), Pinatubo (Philippines), Redoubt and Katmai (USA). 'Platy' or 'endogenous' domes are those with an even lower profile, a rough and blocky carapace and often with transverse ridges. This type of dome is common at Merapi (Indonesia) and La Soufrière (St. Vincent) volcanoes. 'Axisymmetric' domes have a tendency to be constrained by local topography and have nearly flat upper surfaces that are highly corrugated, such as Little Glass Mountain (Medicine Lake, California) and Big Obsidian Flow (Newberry, Oregon) (Fink and Anderson, 2000).

The main hazard posed by lava domes, apart from the effusive activity itself, is the unpredictable nature of their growth. They may grow passively for long periods of time (months or years), with the possibility that the dome may become unstable and collapse, generating pyroclastic density currents (PDCs), or that dome growth may transition into periods of more explosive activity. Fluctuations in dome discharge and transitions between effusive and explosive behaviour (or vice versa) have repeatedly been observed at many volcanoes around the world, such as Mount St. Helens (USA), Pinatubo (Philippines), Santiaguito (Guatemala), Lascar (Chile), Galeras (Colombia), Soufrière Hills (Montserrat) and Unzen (Japan) to name just a few. Understanding the factors responsible for these variations in activity is crucial for monitoring and long-term hazard assessment.

1.2. Effusive-explosive transitions

Early work stated that the transition from explosive (*e.g.*, Plinian) to effusive activity was due to stratification of volatiles in the magma body, suggesting that changes in activity reflect the original, heterogeneous distribution of volatiles in the source magma body (*e.g.* Heiken, 1978; Eichelberger and Westrich, 1981; Fink, 1983). This model was subsequently challenged by work which showed that eruptive variations result from varying degrees of gas loss during ascent and transitions between open- and closed-system degassing (*e.g.* Taylor *et al*., 1983; Eichelberger *et al*., 1986). During open-system degassing, exsolved volatiles are separated from the melt and lost via permeable flow through the conduit walls or the conduit, which often results in a gas poor, effusive eruption. Closed-system degassing is an equilibrium process, in which exsolved volatiles remain with the melt, entrained in the magma as bubbles, rather than escaping. Closed-system degassing therefore leads to an increase in vesicularity and a greater capacity for explosive eruptions. The degree of degassing can be significantly influenced by magma ascent rate, with rapid magma ascent hindering gas loss and increasing the potential for an explosive eruption (Sparks, 1978; Stasiuk et al., 1996; Barclay *et al*., 1996). Magma ascent rate is a function of a complex interplay of factors including pressure in the magma storage region, magmatic flux, conduit geometry, and properties of the magma, such as composition, density, viscosity and crystallinity (*e.g.* Scandone and Malone, 1985; Jaupart and Allegre, 1991; Woods and Koyaguchi, 1994; Massol and Jaupart, 1999; Costa *et al*., 2007; Scandone *et al*., 2007; Rutherford, 2008). In dome eruptions, degassing during ascent increases the viscosity of the magma (*e.g.* Hess and Dingwell, 1996), and causes crystallisation which acts to further increase the viscosity (*e.g.* Lejeune and Richet, 1995), causing rheological stiffening (Sparks, 1997) and introducing complex non-linearities into the dynamics of conduit flow and dome extrusion (Villemant and Boudon, 1998; Melnik and Sparks, 1999, 2005; Barmin *et al*., 2002). Models show that the rheological changes induced in the magma by degassing and crystallisation can generate large overpressures at shallow levels in the conduit, which may build to critical levels to produce explosive activity (Sparks, 1997; Melnik and Sparks, 1999, 2005, Barmin *et al*., 2002.) Large variations in discharge rate and eruptive behaviour can occur as a consequence of small changes in volatile content, crystal size distribution and temperature (Melnik and Sparks, 2005). Therefore, degassing and crystallisation are not only influenced by magma ascent rate, but in a

complex feedback mechanism, they also have influence upon magma ascent via the rheological changes that they induce. During magma ascent, crystallisation is driven by adiabatic decompression (*e.g.* Cashman and Blundy, 2000; Martel, 2012). The solubility of volatiles, including H_2O, is pressure-related (*e.g.* Zhang, 1999), therefore depressurisation of a melt during ascent leads to a decrease in its dissolved volatile content. This results in an increase in liquidus temperature of the magma and of anhydrous minerals, particularly plagioclase (*e.g.* Tuttle and Bowen, 1958; Burnham, 1979; Moore and Carmichael, 1998) (Fig. 1.1). The resulting temperature difference between the liquidus temperature and the actual magmatic temperature (referred to as undercooling or ΔT), results in and controls microlite crystal nucleation and growth, as a function of decompression conditions during magma ascent (*e.g.* Cashman, 1992; Geschwind and Rutherford, 1995; Hammer *et al.*, 1999, 2000; Nakada and Motomura, 1999; Cichy *et al.*, 2011; Martel, 2012) (Fig. 1.1). Most natural and experimental studies have focussed on a particular eruptive behaviour of a volcano, with comparatively less attention paid to the transitions between eruptive style (Castro and Gardner, 2008; Martel, 2012).

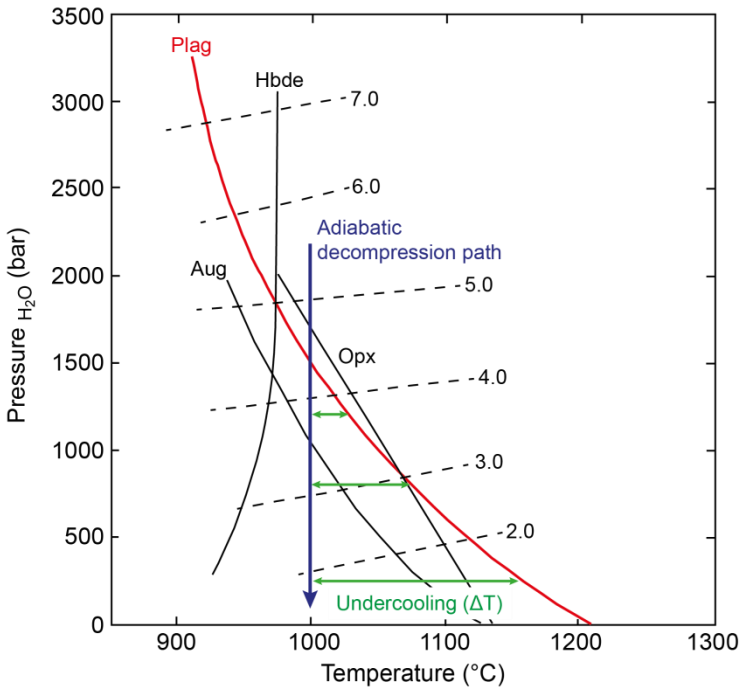

Fig. 1.1 Phase diagram for a hydrous andesitic melt (modified after Moore and Carmichael, 1998). Black dashed lines correspond to H_2O content (wt.%). Plag (plagioclase), Aug (augite), Hbde (hornblende), Opx (orthopyroxene) liquidus lines. Note the large change in plagioclase liquidus temperature with decreasing pressure and H_2O content. As a consequence, during adiabatic decompression of magma during ascent, the difference between magmatic temperature and plagioclase liquidus temperature (undercooling) increases with decreasing pressure and water content, resulting in plagioclase microlite crystallisation

1.3. Overview of Merapi volcano

Merapi volcano (110.44°E, 7.542°S) is an almost 3000 m high basaltic to basaltic-andesite volcanic complex, located 25–30 km north of the city of Yogyakarta in Central Java, Indonesia (Fig 1.2). It lies at the southern-most end of a chain of 4 stratovolcanoes, comprising (north to south) Ungaran, Telomoyo, Merbabu and Merapi (Fig. 1.2). Merapi lies in the Sunda arc, a volcanic island chain formed by the subduction of the Indo-Australian plate beneath the Eurasian plate (Hamilton, 1979) (Fig. 1.3). Merapi is one of Indonesia's most active volcanoes, with frequent eruptions posing a persistent threat to the surrounding population, buildings and infrastructure. Approximately 1.1 million people live in 300 villages above 200 m elevation on the slopes of Merapi, with an estimated 440,000 of these people inhabiting high risk areas, prone to pyroclastic flows, surges and lahars (Thouret *et al*., 2000). Yogyakarta city (~ 1.6 million inhabitants) is one of the most important cities in Indonesia in terms of economic activity and historical inheritance (Thouret *et al*., 2000; Pallister *et al*., 2013). Merapi is also situated close to the archaeological temples of Borobudor (40 km northwest of Yogyakarta) and Prambanan (17 km East of Yogyakarta), both listed as UNESCO World Heritage Sites. Eruptions during the latter part of the 20th Century and early 21st Century have occurred approximately every 2–8 years (Ratdomopurbo *et al*., 2013), making Merapi a dangerous and high risk volcano for people living on its flanks. During this time, activity has mainly consisted of lava dome growth and subsequent gravitational collapse to generate small volume PDCs. This type of activity has occurred frequently in past years, including recently in 1992, 1994, 1997-98, 2001-02 and 2006, usually lasting for a few weeks or months each time. In contrast to the mainly effusive dome-forming activity of the 20th Century, the geological record shows that during the Holocene, larger explosive (subplinian) eruptions with a VEI 3 or 4, as well as fountain collapse pyroclastic flows, were commonplace at Merapi (*e.g.* del Marmol, 1989; Berthommier, 1990; Andreastuti, 1999; Andreastuti *et al*.,2000; Camus et al., 2000; Newhall *et al*., 2000; Voight *et al*., 2000; Gertisser, 2001; Gertisser et al., 2003a; Gertisser *et al*., 2012a).

In the 1990's, Merapi was designated as 1 of 16 Decade Volcanoes by the International Association of Volcanology and Chemistry of the Earth's Interior (IAVCEI), as part of the United Nations' International Decade for Natural Disaster

Reduction. The consequent research resulted in considerable advances in our knowledge of Merapi and a collection of papers was published in the Journal of Volcanology and Geothermal Research, vol. 100; 2000. Since then, the cataclysmic 2010 eruption resulted in renewed research interest in Merapi, with another special edition of Journal of Volcanology and Geothermal Research published (vol. 261; 2013).

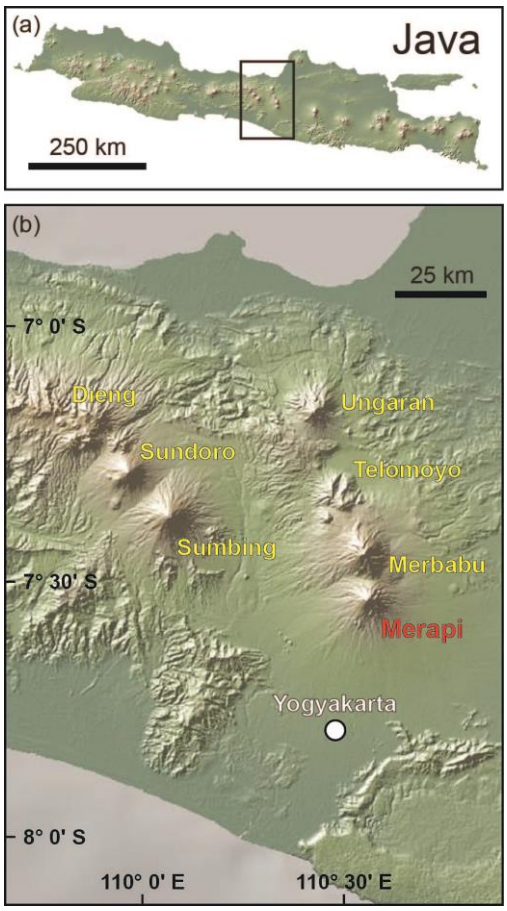

Fig 1.2 (a) Geographical location of Merapi volcano in Central Java, (b) Merapi is situated north of the city of Yogyakarta and surrounded by other geologically young stratovolcanoes (Modified after Gertisser *et al*., 2012a)

1.4. Tectonic and geological setting

Indonesian volcanism is related to several distinct subduction zones, namely the Sunda, Banda, Sangihe and Halmahera arc systems (Fig. 1.3). Merapi belongs to the Sunda arc, which extends from the Andaman Islands, north of Sumatra in the west, to Flores in the east (Fig. 1.3). Quaternary volcanism in the Sunda arc is associated with the northwards subduction of the Indo-Australian plate beneath the Eurasian plate, at a

rate of 7cm / year near Java, and 6 cm / year further west, near Sumatra (Widiyantoro and Van der Hilst, 1997).

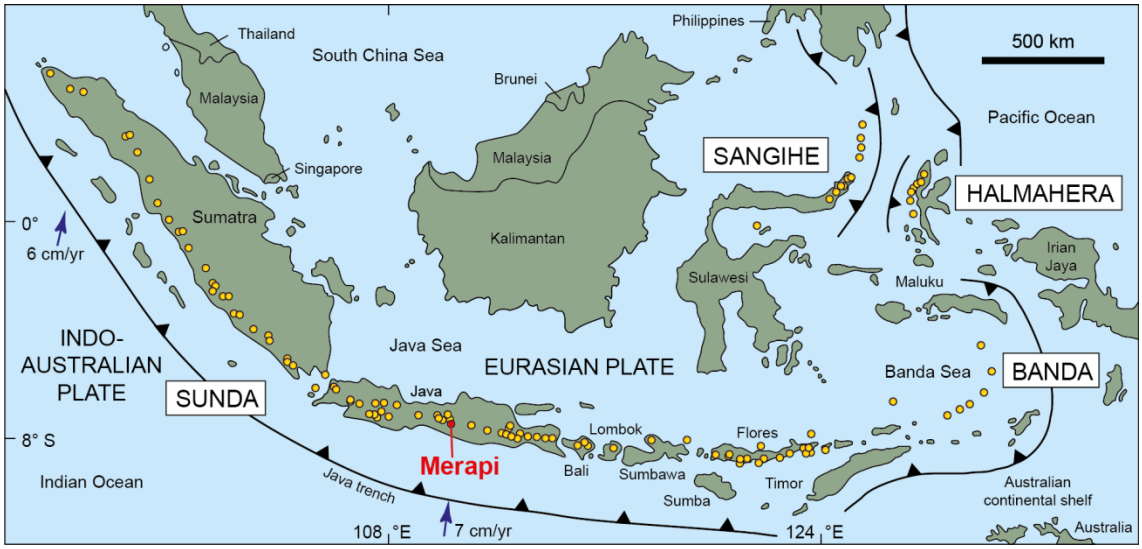

Fig.1.3 Map of the Indonesian subduction zone system showing location of Merapi and the general tectonic setting (after Hamilton, 1979). Yellow circles indicate locations of active volcanoes (after Simkin and Siebert, 1994). Arrows indicate the direction of the Indo-Australian plate motion relative to the Eurasian plate with convergence rates from Widiyantoro and Van der Hilst (1997). (Modified after (Gertisser and Keller, 2003b)

The Sunda arc is not an archetypal continental- or oceanic-type arc, but has a character that is transitional between the two. Previous work determined that the age of the subducting slab decreases across arc from west to east and that the composition and thickness of the overriding plate also change (Hamilton, 1979). The overriding plate was thought to be composed of continental crust in the west of the arc, becoming progressively more oceanic to the east, so that in the west, Sumatra overlies continental crust, islands to the east of Java are oceanic crust, and Java is underlain by quasi-continental crust, oceanic in composition and continental in thickness (Hamilton, 1979; Edwards *et al.*, 1993). Seismic surveys revealed that the crust below Sumatra is ~ 25 km thick, below Java ~ 20 km thick, beneath Bali ~18 km thick, thinning to 5–10 km beneath Flores (Curray *et al.*, 1977). The change in thickness was thought to reflect the progressive eastwards migration of a series of subduction zones in the evolution of the Indonesian islands since the late Palaeozoic (Katili, 1975). However, more recent work suggests that continental basement is more widespread than previously thought. The south-eastern part of the Eurasian plate is called Sundaland and is considered to be the continental core of SE Asia (Hamilton, 1979). It had been formed by the early Mesozoic through the amalgamation of continental blocks (Hall, 2002) and is therefore, not a

single homogeneous block of continental crust. Terranes of arc and ophiolitic material were accreted to the southern margin of Sundaland during the late Cretaceous, forming the crust (Hamilton, 1979; Hall, 2002). Cretaceous zircons found in clastic rocks on Java support that the arc was accreted during the Cretaceous (Smyth *et al*., 2005, 2007). However, older zircons dating from the Archaean and the Cambrian have been found and interpreted to originate from a continental fragment of Gondwana (possibly western Australian), which rifted during the Mesozoic and collided with SE Asia (Smyth *et al*., 2005, 2007). This Gondwanan fragment is thought to now underlie East Java, in the Southern Mountains region and extend beneath western Sulawesi to the north-west (Smyth *et al*.,2005; 2007) (Fig. 1.4). The boundary between the East Java Gondwana fragment and the Cretaceous crust to the west is thought to coincide with the Progo-Muria fault, running close to Yogyakarta and Merapi (Smyth *et al*., 2007) (Fig. 1.4). Other rifted Australian fragments are thought to lie in Sumatra, Sulawesi, Sumba and Borneo, and well as Tibet and West Burma (Hall and Sevastjanova, 2012). A detailed reconstruction of the evolution of the Indonesian region in the Late Jurassic–Cenozoic is given in Hall (2012).

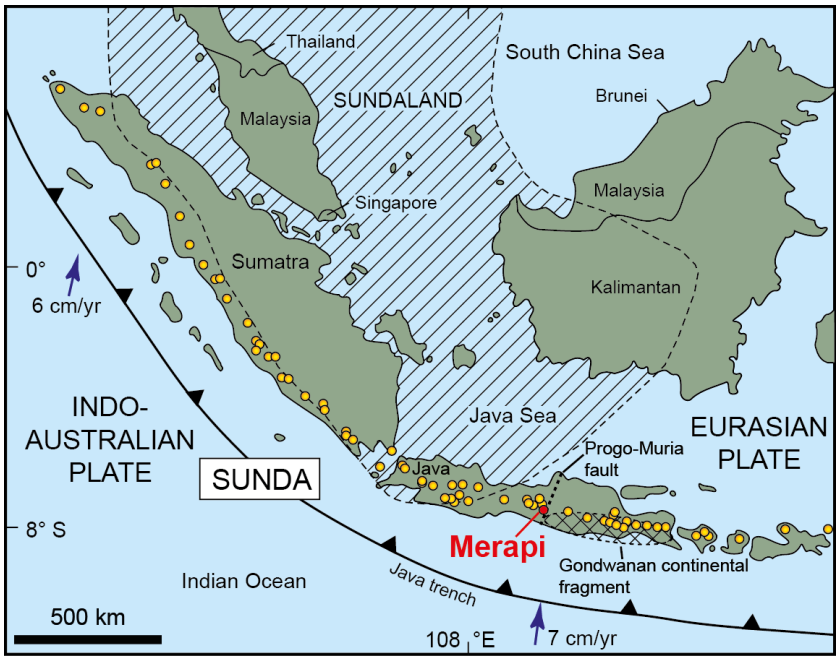

Fig1.4 Map showing the location of the Mesozoic Sundaland core, possible locality of Gondwanan fragment beneath East Java, and the Progo-Muria fault, with boundaries after Smyth *et al*. (2007). Base map modified after Gertisser and Keller (2003b)

Geochemical investigation of the arc reveals a progressive increase in Sr isotope ratios across West and Central Java, correlating with inferred changes in lithospheric thickness, and a significant change in crustal thickness between Central and East Java, perhaps representing the south-east boundary of Sundaland (Whitford *et al*., 1979; Handley, 2006; Dempsey, 2013). Along arc Hf and Nd isotope ratios suggest that the subducted sediment source is heterogeneous and reflects variations in sediment composition on the down-going plate along Java (Handley, 2006; Handley *et al*., 2011).

Seismic and tomographic studies reveal that beneath Central Java, the dipping angle of the subducting slab gradually increases from almost horizontal beneath the offshore part to the south (0–150 km), to 45° (150–250 km) to 70–80° north of Java (> 250 km) (Koulakov *et al*., 2007, 2009; Luehr *et al*., 2013). A low velocity zone extends from the upper crust to the upper mantle below Central Java, extending at a 45° slope from beneath the volcanic arc to meet the subducting slab at ~ 100 km depth. This is thought to represent a pathway for ascending fluids and partial melts released from the slab, and the geophysical evidence suggests that this part of the arc has a high magma flux possibly allowing for the development of large crustal magma reservoirs and voluminous eruptions in the future (Luehr *et al*., 2013). Another low velocity zone has also been discovered in the crust, north of Merapi, called the Merapi-Lawu anomaly, and thought reflect a high fluid and partial melt content in the crust in this area (Koulakov *et al*., 2007, 2009).

Basement rocks, of uncertain character, extend to ~ 25 km depth in Central Java and are overlain by upper crustal sediments (Curray *et al*., 1977; Hamilton, 1979). The upper crustal sediments at Merapi are composed of Cretaceous to Neogene limestones, marls, and volcaniclastic units (Van Bemmelen, 1949). The geology of Java has been divided into four east-west trending stratigraphic-tectonic zones (van Bemmelen, 1949; Smyth *et al*., 2005). From south to north these are (1) the Southern Mountain Zone consisting of remnants of an Eocene-Miocene volcanic arc, with deposits of siliciclastic, volcaniclastic, volcanic and carbonate rocks; (2) the Central Volcanic Zone which is the present day volcanic arc, active since the late Miocene; (3) the Kendeng Zone which contains thick sequences of Eocene-Miocene volcanogenic and pelagic sediment; (4) the Rembang Zone which includes shelf edge deposits such as Eocene-Pliocene shallow marine clastic sediments and carbonates. The currently active central Java volcanic arc

partially overlies the Kendeng Zone, in which sediment thickness ranges from ~ 8 to 11 km (Smyth *et al*., 2005 and references therein).

1.5. Geological evolution of Merapi

Merapi is a complex volcanic edifice consisting of a currently active stratovolcano which has grown on top of remnants of an older volcanic edifice. Van Bemmelen (1949, 1956) was the first to describe the volcanic complex and recognised the older and newer portions. He proposed that a catastrophic eruption occurred in 1006 AD which resulted in the collapse of the western side of the old edifice along the Kukusan fault, leaving a horseshoe-shaped crater or Somma rim on the north and eastern flanks, and leading to the migration of the Mataram Kingdom from Central to East Java (Fig. 1.5). However, Djumarma *et al*. (1986) cited new archaeological evidence that the Mataram Kingdom moved in 928–929 A.D. and found no archaeological evidence for such a catastrophic (Somma rim-forming) eruption either in 928–929 A.D. or in 1006 A.D. Since the work of van Bemmelen (1949, 1956), more recent studies have built upon the idea of an Old and New Merapi, although ideas are somewhat conflicting (del Marmol, 1989; Berthommier, 1990; Camus *et al*., 2000; Newhall *et al*., 2000; Gertisser, 2001; Gertisser *et al*., 2012a). Del Marmol (1989) and Newhall *et al*. (2000) defined "Old Merapi" as preceeding the debris avalanche failure and "New Merapi" as the subsequent growth of the present stratovolcano. Newhall *et al*. (2000) dated the oldest deposit of "Old Merapi" at 9,630 ± 60 ^{14}C years B.P., although admitted that construction began earlier. According to Newhall *et al*. (2000), debris avalanche failure of the "Old Merapi" edifice occurred at ~ 1,900 ^{14}C years B.P. based on their youngest pyroclastic flow deposit found on the eastern side of the volcano, assuming that the Somma rim stopped all later pyroclastic flows from travelling in an easterly direction. "New Merapi" then began to grow soon after. However, this young date has been disputed by (Gertisser 2001; Gertisser and Keller, 2003a) who report a younger (1,590 ± 40 ^{14}C years B.P.) pyroclastic flow deposit on the north-east side of Merapi, find pyroclastic deposits as old as 8,380 ± 230 ^{14}C years B.P. on the western flanks and suggest that the apparent lack of any young debris-avalanche deposits cast doubt on a collapse as young as 1,900 ^{14}C years B.P. Newhall *et al*. (2000) also defined a "Proto-Merapi" stage ("Very Old Merapi", del Marmol, 1989). Newhall *et al*. (2000)

concluded that Gunung Plawangan and Gunung Turgo ("Gunung", abbr. "G." = Indo. "mountain"), two steep-sided hills on Merapi's southern flank rising above the villages of Turgo and Kaliurang, represent erosional remnants of the earliest, "Proto-Merapi" cone and precede "Old Merapi" (Fig 1.6). Camus *et al*. (2000) divided the evolution of Merapi into four different stages: "Ancient" (40,000 years B.P. to 14,000 years B.P.), "Middle" (14, 000 years B.P. to 2200 years B.P.), "Recent" (2,200 years B.P. to 1786 A.D.) and "Modern" (1786 A.D. to Present). Gunung Plawangan and G. Turgo belong to "Ancient Merapi", with one lava flow from G. Plawangan dated at 40 ± 18 ka using a U-Th mineral-whole rock isochron (Berthommier 1990; Camus *et al*., 2000). They also dated Gunung Bibi, another distinct hill, situated on the north-east flank of Merapi. Based on a ^{40}K-^{40}Ar age of 0.67 ± 0.25 Ma, they interpreted this structure to have formed before "Ancient Merapi" and attributed it as a remnant of an older "Pre-Merapi" (Fig. 1.6). However, this was questioned by Newhall *et al*. (2000) who doubted the reliability of the age given the weathered nature of G. Bibi rocks, and suggested that it is more likely to be a vent that erupted through and built up on the "Old Merapi" flank. Camus *et al*. (2000) postulated that during the time of "Middle Merapi", a Mount St. Helens-type edifice collapse occurred between 6,700–2,200 B.P. and interpret G. Gendol and the surrounding hills to the south-west of Merapi as being part of the resulting debris-avalanche deposit (Fig 1.6). However, this interpretation was strongly questioned by Newhall *et al*. (2000) who found no evidence of a debris-avalanche deposit and suggested that it has probably been buried by younger deposits. In an attempt to reassess and clarify the geological evolution of Merapi, Gertisser *et al*. (2012a) produced further radiocarbon, ^{40}K-^{40}Ar and ^{40}Ar-^{39}Ar ages to integrate with stratigraphic field data. They dated G. Plawangan and G. Turgo at 135 ± 3 ka and 138 ± 3 ka, respectively, suggesting that they are older than previously thought and ascribe them to "Proto-Merapi", agreeing with Newhall *et al*. (2000) that they likely represent ruins of an ancient volcano. Although the rocks of G. Bibi are highly weathered, a fresh block exposed by a recent landslide was dated at 109 ± 60 ka, via the ^{40}Ar-^{39}Ar method on amphiboles. Despite the large error, G. Bibi is still older than the Somma, the base of which dates at 30 ka. The age is also younger than the age reported in Berthommier (1990) and Camus *et al*. (2000), although it is still considered part of an older "Proto-Merapi" edifice. They dated the beginning of "Old Merapi" to ~ 30 ka, which was subsequently destroyed by one, or possibly several, flank failures, the latest of which

occurred after 4.8 ± 1.5 ka, marking the end of the "Old Merapi" stage. Consequently, "New Merapi" is younger than 4.8 ± 1.5 ka (Gertisser *et al*., 2012a).

Fig. 1.5 Photograph showing the modern active cone of "New Merapi" and the remnants of "Old Merapi" taken from Kali Gendol, south of Merapi in August 2008

1.6. Eruptive history of Merapi

Historical records of Merapi and its eruptive activity date back to geological observations in the 18th Century, when F. van Boekhold may have been the first ever European to climb to the summit in 1786 (van Boekhold, 1792). More systematic investigations began in the early 20th Century, with work by Grandjean (1931a-c), Kemmerling (1932), Escher (1933a, b), Newmann van Padang (1933), Hartmann (1935) and van Bemmelen (1949) amongst others (for a comprehensive review see Voight *et al*., 2000). Early work defined three types of nuées ardentes to describe the eruptive activity of Merapi. The first type are the "Merapi-type" nuées ardentes (Escher, 1933a, b; Macdonald, 1972), resulting from gravitational dome collapse. This type was subsequently divided in two sub-types by Bardintzeff (1984), with the Merapi-type *sensu stricto* incorporating material from a fully solidified dome without any fresh glass, and the Arenal-type, which is derived from a dome with a portion of the interior still liquid. The second type is the "St. Vincent-type" (Esher 1933a; Macdonald, 1972),

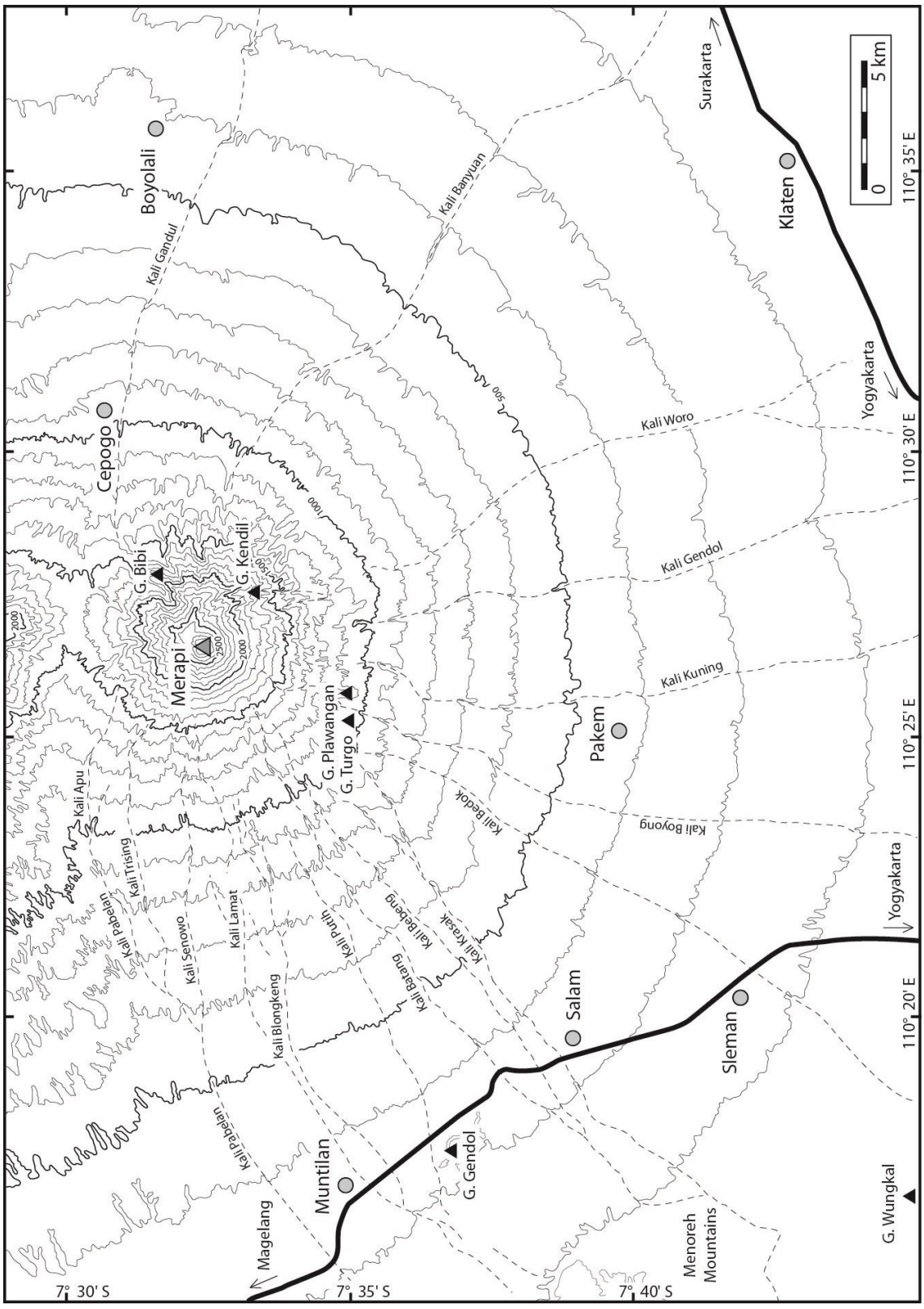

Fig.1.6 Topographic sketch map of Merapi showing major river valleys (dashed lines) and major towns (grey circles), the Merapi summit and surrounding hills of Gunung Bibi, Gunung Turgo and Gunung Plawangan. (Modified after Gertisser, 2001)

which results from the collapse of an eruption fountain. Grandjean (1931a-c) argued that a third type occurred in 1930. This "Peléean-type" was envisaged to be generated by a directed blast, although others workers disputed this (Kemmerling, 1932; Newmann van Padang, 1933) whilst Escher (1933b) accepted it to be a possibility. Hartmann (1935) classified Merapi activity into four groups (A, B, C, D) related to the gas content of the erupting magma, arranged from A-D in order of increasing explosivity.

More recent field studies (del Marmol, 1989; Berthommier, 1990; Andreastuti, 1999; Camus et al., 2000; Newhall *et al*., 2000; Andreastuti *et al*., 2000; Gertisser, 2001; Gertisser *et al*., 2012a) have revealed that although recent eruptive behaviour typically consists of VEI 1-3 eruptions generating PDCs from gravitational dome collapse, other types of activity have occurred at Merapi in the past. As well as the BAF deposits emplaced via gravitational dome collapse, other types of deposit have been identified at Merapi and classed according to dominant component lithology, including (i) pyroclastic flow deposits dominated by moderately vesicular breadcrust bombs, (ii) those dominated by moderately vesicular cauliform-textured clasts and (iii) pumice-rich PDC deposits, dominated by moderate to highly vesicular light grey pumiceous clasts (Gertisser, 2001; Gertisser *et al*., 2012a) (Fig1.7). Pyroclastic flow deposits dominated by breadcrust bombs, often more basic in composition (Gertisser, 2001) are interpreted to have formed by fountain collapse related to Vulcanian-type activity. The most prominent breadcrust bomb flow at Merapi has been tentatively linked to the VEI 4 eruption of 1872 (Newhall *et al*., 2000). Pyroclastic flow deposits rich in cauliform-textured clasts have also been attributed to similar Vulcanian-type activity. Pyroclastic fall and tephra fall deposits rich in pumiceous material are prominent within the geological record during the mid- to late-Holocene (< ~ 4000 yrs BP). These are evidence of larger subplinian-type eruptions of VEI 3-4 (Andreastuti, 1999; Andreastuti *et al*., 2000; Newhall et al., 2000; Gertisser, 2001; Gertisser et al., 2003a; Gertisser *et al*., 2012a) (Fig 1.7). It should be noted that the VEI 4 eruptions are an order of magnitude larger than any recorded historical eruption at Merapi, except those that occurred in 1872 and 2010, and produced conspicuous, cm- to dm-thick pumice lapilli fallout deposits (*e.g.* Gertisser et al., 2012a).

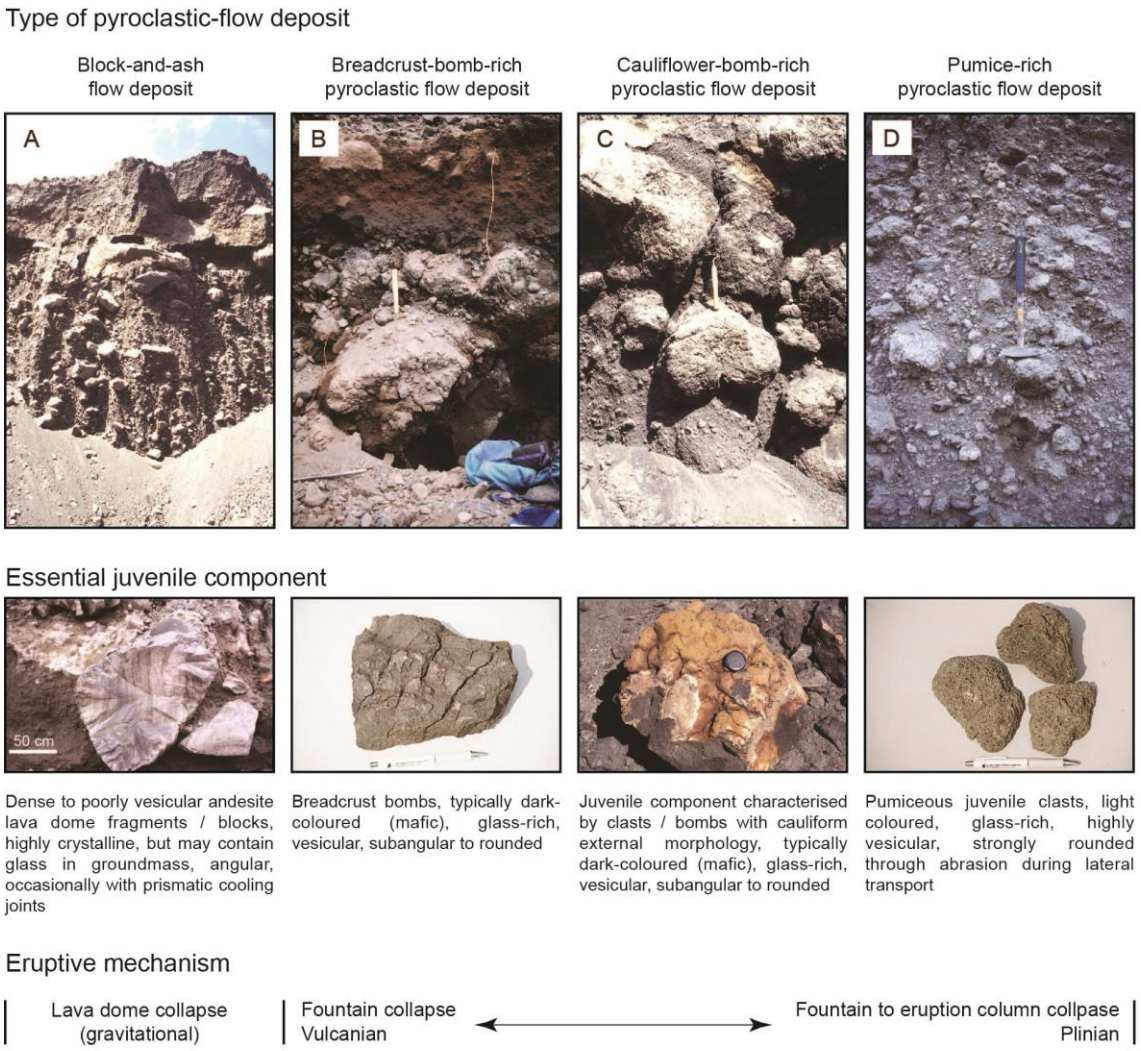

Fig 1.7 Types of small-volume pyroclastic flow deposit previously identified at Merapi based on dominant juvenile component with inferred generation mechanism. (Modified after Gertisser *et al*., 2012a)

The radiocarbon record has been used to help to constrain past eruptions of Merapi and currently consists of dates back to nearly 14,000 years (cal. years BP) (Gertisser *et al*., 2012a and references therein). The majority of these dates are within the last 2000 years, as the older record is fragmentary with older deposits comparatively rare due to burial by newer deposits. The radiocarbon record reveals that over the last 2000 years, activity at Merapi has been persistent, with 126 ages recorded (an average of one eruption every 15.9 years assuming that each radiocarbon date represents a single eruption) (Gertisser *et al*., 2012a). In comparison there have been 29 eruptions in the 19th Century (average of one eruption every 3.4 years) and 25 eruptions in the 20th Century (average of one eruption every 4 years) (Venzke *et al*., 2002; Siebert *et al*.,

2011; Gertisser *et al*., 2012). Historical accounts date back as far as the 16th Century, although the record only becomes more complete after the 18th Century (Fig1.8).

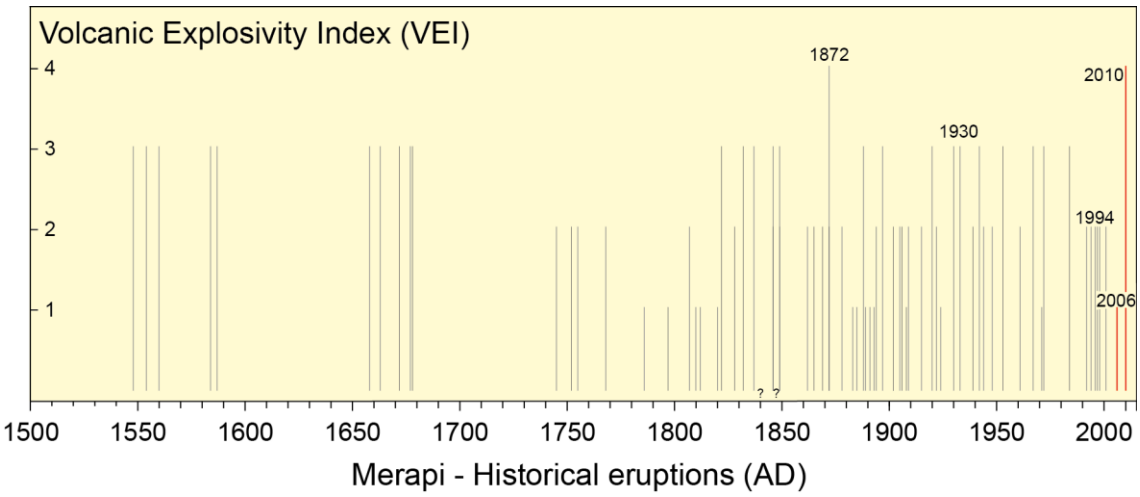

Fig. 1.8 Historical eruptions of Merapi with data from Venzke *et al*. (2002) and Siebert *et al*. (2011). (Modified after Gertisser *et al*. 2011)

It has been noted that there was a shift in the style of activity from the 19th to the 20th Centuries (Voight *et al*., 2000; Newhall *et al*., 2000). Records show that during the 1800s, explosive eruptions and some associated fountain-collapse pyroclastic flows occurred and were larger (up to VEI 4) than any produced in the 20th Century. In comparison, throughout the 20th Century and early 21st Century, eruptive activity at Merapi has been typically characterised by effusive dome-forming eruptions often resulting in PDCs associated with gravitational collapse. Below are brief descriptions of examples of notable eruptions that occurred during the 19-20th Centuries:

1822-1823: This eruption (VEI 3 or 4) began unexpectedly with violent explosions on 27 December 1822, developing into a paroxysm on 29 and 30 December (Hartmann, 1935; Voight *et al*., 2000). Pyroclastic flows travelled mainly towards the west and south-west, in the Gandul, Apu, Lamat, Blongkeng, Batang, Gendol and Woro river valleys, with lapilli and ash fall recorded in the settlements of Boyolali, Muntilan, Magelang and Yogyakarta (Fig 1.6). Explosions continued until 10 January 1823, accompanied by hot lahars. Approximately 50 people were killed by PDCs and a similar number by hot lahars. In mid-January 1823, a new lava dome began to extrude.

1872: Explosions began suddenly with no precursors on 15 April 1872, destroying a pre-existing dome. The early phase lasted from 15-17 April, with a paroxysm from 17-20 April, before the eruption (VEI 4) ended suddenly on 20 April (Voight *et al*., 2000). Fountain-collapse nuées ardentes travelled radially from the vent in the Apu, Trising, Senowo, Blongkeng, Batang, Woro and Gendol valleys (Fig 1.6). PDCs and tephra fall destroyed all villages above 1000m elevation.

1930: This was the largest and most destructive eruption of the 20th Century (VEI 3), resulting in the death of 1369 people, 2100 animals and destroying 20 km^2 land (Voight *et al*., 2000) (Fig. 1.9). Tremors were recorded in January 1930 and increased until 25 November, until just after the first appearance of a new lava dome, when lava broke out from underneath pre-existing domes (BNEIVS, no. 39-40; Voight *et al*., 2000). Effusion remained steady until 18 December, when PDCs began to travel up to ~ 12 km to the west, resulting in BAF deposits filling the Senowo, Batang and Blonkeng valleys, mantled by surge and fall deposits (Voight *et al*., 2000) (Fig. 1.6). The exact eruption mechanism of the 1930 eruption has been somewhat disputed. A large summit depression, 850 m long and open at the western side, suggests the gravitational collapse of the old dome complex as well as the juvenile lava (Voight *et al*., 2000). Potentially, vertical or directed explosions (Peléean-type) may have also occurred, as proposed at the time by Grandjean (1931a-c), although this was disputed by some contemporaneous workers (Kemmerling, 1932; Newmann van Padang, 1933). Recent workers (Voight *et al*., 2000) suggest that explosive activity during the 1930 eruption may have been possible, as rapid unloading of the dome complex could promote explosive activity in pressurised magma. The activity in 1930 highlights the possible destabilising influence of extrusion of fresh lava undermining pre-existing domes, as well as the influence of heavy rainfall that occurred at the time.

1961: After about 2 years of previous quiescence, the VEI 3 eruption began on 19 March 1961, with noises of avalanches reported, although the summit was covered by clouds. Incandescence was visible on 11 April, indicating fresh lava venting through the 1957 lava dome. Two days later, 18 dome collapse nuées ardentes, were emplaced up to 3.5 km in Kali Batang on the SW flanks. The frequency and runout distance of nuées ardentes increased over the following days and on 18 April, a large nuée travelled 6.5 km in the Batang, partially destroying Gendeng village. On 20 April, an "explosion

type" nuées ardentes destroyed the village of Gendeng (BVSI, no. 104). New lava effusion over the following week was followed by incandescent jets and explosions, producing fountain-collapse nuées ardentes in the Batang, Senowo, Woro and Gendol. Paroxysmal activity occurred on 8 May, when a dense black ash plume generated 17 nuées ardentes, up to 7 km in the Batang, followed by larger ones up to 12 km distance. Despite evacuations warnings well in advance, 6 people were killed and another 6 were severely injured. An effusive phase followed, with frequent rockfalls, until 27–28 November, when the majority of the dome was destroyed by 119 dome-collapse nuées ardentes, reaching 8 km in the Batang. The collapses may have been related to torrential rainfall.

1994: The 1994 eruption (VEI 2) began with dome growth early in the year, adding a new lobe towards the southwest. From February 1994, rockfalls produced a build-up in a southern run-out channel, allowing later rockfalls to spill out of the channel and travel towards the Kali Boyong ("Kali" abbr. "K." = Indo. "river"). On 22 November, the dome collapsed over a 7 hour period generating PDCs that travelled towards the south-southwest and towards the south in the Boyong and Bedog valleys, with run-out distances up to 6.5 km from the summit (Abdurachman *et al*., 2000; Voight *et al*., 2000) (Fig 1.9). In the Boyong valley, near the villages of Turgo and Kaliurang, there were 95 casualties and 64 deaths (Shelley and Voight, 1995; Abdurachman *et al*., 2000).

1997: The 1997 eruption (VEI 2) comprised dome collapse PDCs on 14 January 1997, which travelled up to 6 km from the summit towards the southwest (Fig. 1.9). On the 17 January, a vulcanian explosion generated a fountain-collapse PDC and a 4 km high plume (Voight *et al*., 2000).

1998: In May 1998, seismic unrest and summit deformation were detected before a new dome was visible on 11 July. Between 11–19 July, 128 BAFs were emplaced in valleys on the western flanks, including the Senowo, Lamat, Putih and Sat, with surge deposits affecting the interfluve areas (Schwarzkopf *et al*., 2005) (Fig1.9).

The two most recent eruptions in 2006 and 2010 are described in detail in Chapter 2 and are the focus of this thesis. In brief, the 2006 eruption consisted of effusive dome-growth and gravitational collapse to produce BAFs, whereas the 2010 eruption comprised explosive activity as well as rapid dome extrusion and designated as

a VEI 4 eruption (a magnitude larger than any historical eruption apart from 1872). Although, throughout the 20th Century, activity has mainly consisted of effusive dome growth and subsequent gravitational collapse to produce "Merapi-type" PDCs, the larger and more explosive activity that more commonly occurred in the 19th Century should also be considered "typical" for Merapi, as recently demonstrated by the 2010 eruption. The fact that larger subplinian (VEI 3–4) eruptions were commonplace during the mid- to late-Holocene, evidenced by tephra fall deposits in the geological record (Andreastuti *et al*., 2000; Gertisser, 2001; Gertisser et al., 2012a) should also not be overlooked. For this reason, the term "Merapi-type" will not be used in this thesis. The variety of activity evidenced at Merapi ranging from effusive, dome-forming eruptions to explosive vulcanian and subplinian types should all be considered for long-term hazard assessment.

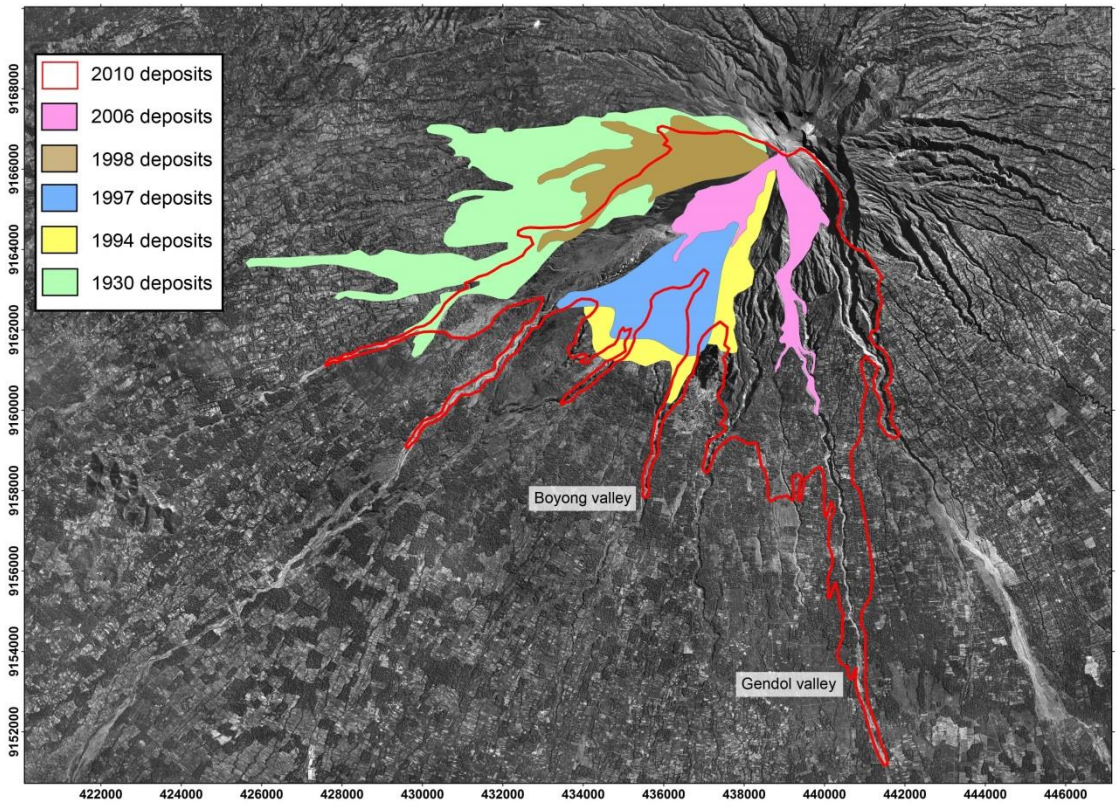

Fig. 1.9 Distribution map of recent Merapi PDC deposits (After Gertisser *et al*., 2011)

1.7. Merapi magmatic system

Merapi rocks are basaltic to basaltic andesite in composition, although the majority of recent eruptive products are basaltic andesite (~ 56–57 wt.% SiO_2) (*e.g.* del

Marmol, 1989; Berthommier, 1990; Gertisser, 2001). Trace element patterns are typical for volcanic products from a subduction-related tectonic setting, with enrichment of large ion lithophile elements (LILE), U, Th, Pb and to a lesser extent light rare earth elements (LREE) relative to high field strength elements (HFSE) such as Zr, Hf, Nb, Ta and Ti (Gertisser and Keller, 2003b). The main mineral phases are plagioclase feldspar, clinopyroxene, orthopyroxene, Fe-Ti oxides and amphibole (*e.g.* del Marmol, 1989; Gertisser, 2001). Recent rocks are high-K in composition, although they shifted from having a medium-K affinity at ~1,900 years B.P. (Gertisser and Keller, 2003a, b). This transition is thought to be related to variable contribution of subducted sediments to the mantle wedge, rather than via shallow level crustal processes (Gertisser and Keller, 2003a, b; Debaille *et al*., 2006). As well as the change to high-K basaltic andesite compositions, during the last ~ 2,000 years, cyclic transitions between basaltic (~ 52–53 wt.% SiO_2) to basaltic andesite related to eruption frequency have been noted (Andreastuti, 1999; Andreastuti et al., 2000; Gertisser, 2001; Gertisser and Keller, 2003a). During periods of lower eruptive frequency, basaltic andesite is generated by fractional crystallisation of a parental basaltic melt. Conversely, periods of high eruptive frequency coincide with shifts in whole rock compositions from basaltic andesite towards more basaltic compositions, thought to be due to influxes of primitive magma into a continuously active magma chamber, triggering eruptions (Gertisser and Keller, 2003a).

The plumbing system of Merapi is thought to consist of multiple magma storage and crystallisation regions, ranging over almost the entire thickness of the crust (*e.g.* Gertisser, 2001; Chadwick *et al*., 2013; Costa *et al*., 2013), although details are still controversial. Ratdomopurbo and Poupinet (2000) detected a shallow aseismic zone at a depth of 1.5–2.5 km below the summit, which was interpreted to be a small shallow magma reservoir into which magma is injected from greater depths and stored temporarily before eruption. Shallow storage region(s) have also been proposed based upon Bouguer gravity anomaly data (Saepuloh *et al*., 2010). However, other geophysical studies have failed to find evidence for a shallow storage region. Tiede *et al*. (2005) did find a low density body within the Merapi edifice, although could not confirm whether this can be attributed to a magmatic body. A decrease in resistivity below the summit, near the conduit, has also been noted but is thought to be caused by the presence of saline fluids rather than by melt (Müller *et al*., 2002; Müller and Hack,

2004; Commer *et al*., 2005). GPS and tilt data also failed to detect a shallow magma storage region, but did indicate a deeper magma storage region at 8.5 ± 0.4 km below the summit (Beauducel and Cornet, 1999), which is broadly consistent with the depth of a second aseismic zone observed by Ratdomopurbo and Poupinet (2000) at > 5 km below the summit. It is therefore possible that if a shallow storage region(s) exists it is either too small or diffuse to be observed by certain techniques, or is ephemeral with magma only stored there before an eruption. Indeed, Beauducel and Cornet (1999) do not rule out the existence of a shallower storage region because their data originates from a different time period to that of Ratdomopurbo and Poupinet (2000).

Petrological data have also helped to shed light on the magmatic system and processes at Merapi. Mineral equilibria in lavas and pyroclastic rocks reveal a major magma storage region at mid- to lower-crustal levels (14–19 km) (Gertisser, 2001). This is corroborated by the petrological study of magmatic inclusions, which are interpreted to reveal crystallisation occurring at between ~ 3 and 45 km depth, with the bulk of magma stored in the mid- to lower-crust (12-18 km), and small pockets of magma stored in the top few kilometres of the crust (Chadwick *et al*., 2013) (Fig. 1.10a). Other petrological and textural studies suggest magma storage at > 10 km depth, as well as residence at < 10 km depth (Innocenti *et al*., 2013a, b). Recent petrological work by Costa *et al*. (2013) defines three zones of crystallisation: (1) a deep reservoir at 30 ± 3 km depth, evidenced by some amphibole and high-Al clinopyroxene crystals. It is thought that this is the region where the basaltic andesite is generated, probably by fractionation of a more primitive magma. Here, the basaltic andesite contains ~ 4–6 wt.% H_2O at 1050°C; (2) a second zone at 13 ± 2 km recorded by amphibole, some high-Al clinopyroxene and Ca-rich plagioclase. In this region, magma still probably contains ~ 4–6 wt.% H_2O, but CO_2 and SO_2 are probably degassing. Also at this depth, crustal carbonate assimilation is thought to occur, contributing to the volatile budget of the system, potentially intensifying and sustaining eruptions (Chadwick *et al.*, 2007; Deegan *et al*., 2010; Troll *et al*., 2012) (3) a shallow (< 10 km depth) region where lower An plagioclase and low-Al clinopyroxene are crystallising, along with orthopyroxene. This region is envisaged to be largely degassed and crystal-rich (Fig. 1.10b).

A complex interplay of magmatic processes are thought to act at Merapi, including: the interaction between magma stored in various parts of the plumbing system (i.e. shallower, degassed magma and hotter, deeper, more volatile magma) (Costa *et al*., 2013), mixing and mingling with a more mafic magma, resulting in the remobilisation of the basaltic andesite (Gertisser and Keller, 2003a; Chadwick *et al*., 2013), mixing of distinct basaltic andesite batches (Chadwick *et al*., 2013), and contamination via assimilation of carbonate crustal rocks (*e.g.* Troll *et al*., 2012; 2013).

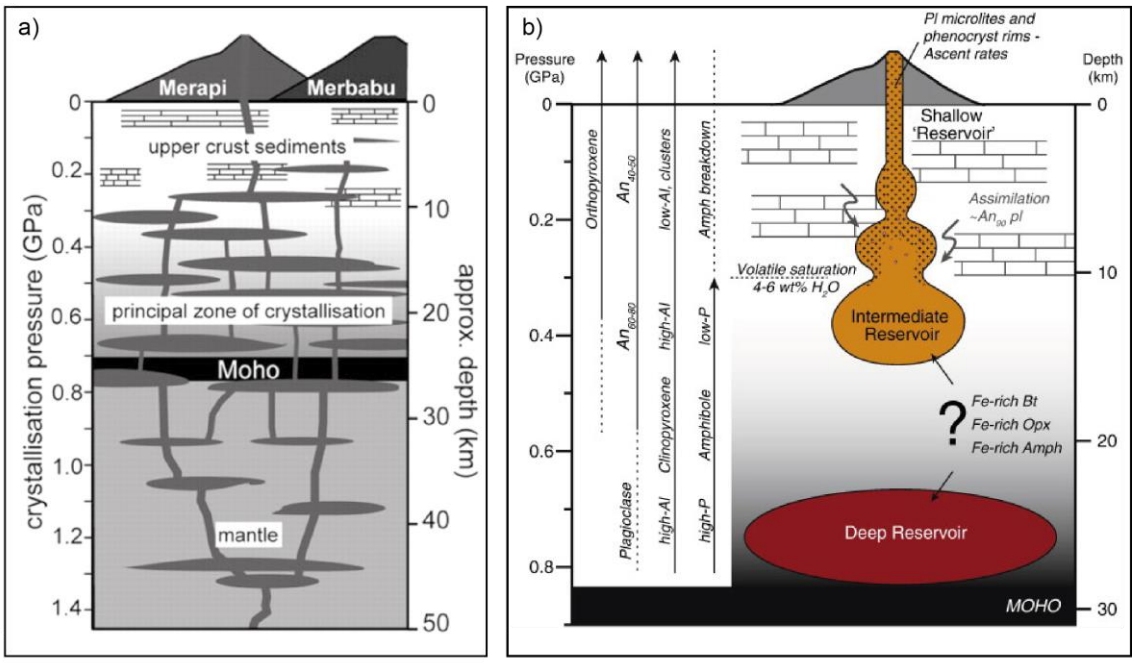

Fig. 1.10 Recently published hypotheses of the structure of the Merapi plumbing system based on petrological data: a) Chadwick (2008), modified after Deegan et al., 2010; b) Costa et al. (2013). Both models show multiple storage regions throughout the crust, with zones of deeper and shallower crystallisation. However, the depths and structure of these regions vary in the two models

1.8. Rationale and outline of the thesis

Although Merapi is a well-studied volcano, recent activity has highlighted some fundamental questions, both relevant to Merapi, as well as other similar volcanoes worldwide. For example, the processes that determine eruptive style at Merapi are still not clear and there are still some uncertainties regarding the structure of the Merapi magmatic system, especially at shallow depths. The two most recent Merapi eruptions, 2006 and 2010, provide ideal case studies to gain insight into the driving forces behind contrasting dome-forming and explosive eruptions and the transition between the two styles, representing "end-members" of recent Merapi activity. The two eruptions were

well monitored and documented, allowing a detailed set of samples to be collected and linked to eruption chronology and eruptive mechanism. Volcanological, petrological and textural analysis of the well constrained samples has been carried out, with the aim of elucidating pre- and syn-eruptive magmatic processes, such as conditions of magma storage and ascent associated with effusive and explosive eruptions. The 2006 samples provide insights into variations in crystallisation and degassing processes within an individual dome-forming eruption and are compared to the those processes occurring before and during the explosive 2010 eruption. 2010 samples give insights into the driving forces behind the effusive-explosive transition occurring within a single eruption. The thesis is presented in the following way:

- Chapter 2 provides detailed background information on the 2006 and 2010 eruptions, including eruption chronology, monitoring data and a description of the deposits and juvenile components.

- Chapter 3 presents quantitative microlite textural analysis and petrological data of the 2006 samples, with the aim of elucidating short timescale variations of shallow magma ascent and conduit processes during an effusive dome-forming eruption, as well as providing insight into magma storage at Merapi. This chapter is based on the following paper published in the recent Merapi special edition 'Merapi Eruption' of Journal of Volcanology and Geothermal Research and slightly modified for the purpose of the thesis: Preece, K., Barclay J., Gertisser, R., Herd, R.A., 2013. Textural and micro-petrological variations in the eruptive products of the 2006 dome-forming eruption of Merapi volcano, Indonesia: implications for sub-surface processes. Journal of Volcanology and Geothermal Research 261, 98–120.

- Chapter 4 investigates magma storage and ascent conditions prior to the effusive and explosive phases of 2010 eruption using quantitative textural analysis of feldspar microlites, mineral geobarometry and whole rock geochemical data, linked to field data.

- Chapter 5 examines degassing and crystallisation processes that occurred prior to both eruptions, using volatile and light lithophile element data, augmented by major element concentrations in silicate melt inclusions. Insights into

magma storage and ascent are gained from geobarometry of the melt inclusions and the host clinopyroxene phenocrysts. This chapter has been submitted as the following paper, and is currently in review: Preece, K., Gertisser, R., Barclay, J., Berlo, K., Herd, R.A. Pre- and syn-eruptive degassing and crystallisation processes of the 2006 and 2010 eruptions of Merapi volcano, Indonesia. Contributions to Mineralogy and Petrology (In Review).

- Chapter 6 is a synthesis and discussion of all the data presented in this thesis. It aims to link together the data to shed light on conditions of magma storage and ascent during effusive and explosive eruptions at Merapi, inter- and intra-eruptive variations and how they may influence eruptive style at Merapi and other volcanoes.

- Chapter 7 presents the main conclusions from this work.

Chapter 2: An Overview of the 2006 and 2010 Eruptions of Merapi Volcano

The 2006 eruption is an example of the effusive, dome-forming activity that has frequently occurred at Merapi over the last century. In contrast, the 2010 eruption began with explosions in the absence of dome growth. These initial explosions were followed by less than one week of rapid dome growth which terminated in paroxysmal explosions, before further rapid dome extrusion ensued. These two contrasting eruptions provide ideal case-studies to characterise the driving forces behind effusive and explosive eruptions at Merapi, and to determine the factors that contribute to transitions between the two styles. Linking together monitoring data, activity reports and previously published data, this chapter outlines the chronology of each eruption, the eruptive style and the deposits produced at each stage. This information provides the basis for the field sampling strategy. Collected samples are correlated with eruptive origin and chronology, laying the foundations for the petrological and textural data that are presented in this thesis to be linked with eruption dynamics.

2.2. The 2006 eruption of Merapi volcano

2.2.1. Chronology of the 2006 eruption

The 2006 eruption began after nearly five years of quiescence following the previous eruption in 2001. The chronology of the 2006 eruption presented here is largely based upon online reports from the Smithsonian Institution (BGVN 2006, 2007), information provided by the Centre of Volcanology and Geological Hazard Mitigation (CVGHM) and a comprehensive review of the 2006 dome growth and collapse provided in Ratdomopurbo *et al*. (2013). The deposits were surveyed and sampled in July–August 2008 (Chapter 3).

Early eruptive precursors began approximately a year before eruption, with increased seismic activity and deformation beginning in early 2005. Low-frequency (LF) seismic activity increased, which is typically attributed to resonance of fluid-filled

cavities due to pressure perturbations (Budi-Santoso *et al*., 2013). In addition, summit displacement and inflation of 2 cm was measured with EDM (electronic distance measurement) in January to March 2005, as well as a slight increase in SO_2 emissions. In July 2005, volcano-tectonic (VT) earthquakes, which result from brittle fracture of rocks under stress during volcanic activity (Jousset *et al*., 2013), were recorded alongside a 4 cm decrease in EDM lines and accompanied by another slight increase in SO_2. During December 2005, 2–3 VT events were recorded per day, which increased to 6–8 events per day in March 2006, and by mid-April 2006 the frequency of VT events had increased to 15 per day. The frequency of multi-phase (MP) seismic events, which can be related to magma flow in the upper conduit and dome growth (Budi-Santoso *et al*., 2013), also increased, with ~ 10–20 recorded per day in December 2005, increasing to 40 per day in March 2006, until a sharp increase to 150 per day in mid-April 2006. The total cumulative displacement of the summit area before the 2006 eruption, as recorded by EDM, was 40 cm on the northwest rim and 2.4 m on the southern rim. On the southern side, the displacement seemed to occur in two stages, with constant displacement of ~ 20 mm per day until the end of March 2006, when displacement increased to 60 mm per day, throughout April 2006. On 19 March 2006, the volcano alert level was raised from 1 "*aktif normal*" (normal) up to 2 "*Waspada*" (on guard), on a scale of 1–4, and 10,000 residents were warned about a possible evacuation. Due to the increasing unrest, the alert level was raised from 2 to 3 "*Siaga*" (standby) at 15:00 on 12 April, with an exclusion zone of 8 km enforced. Seismicity, summit deformation and SO_2 flux remained high until 26 April, when hourly seismic events decreased, and ground deformation stopped. This is interpreted as fresh magma finally breaking through to the surface, alleviating pressure and reducing summit deformation and seismic events, signalling the onset of the eruption (Ratdomopurbo *et al*, 2013). A new block was observed protruding from the summit on 28 April, although the new dome was not observed until 5 May, due to the angle of the monitoring cameras. On 5 May, the dome was estimated to already have a volume of 0.13×10^6 m^3 and was growing towards the southwest, in the direction of the head of the Boyong–Krasak valleys (Fig. 2.1). Dome extrusion continued without collapse until 11 May, when the first pyroclastic flow travelled 1.5 km SW towards K. Krasak and gas or ash plumes rose to over ~ 800 m about the summit. By this time, the dome was 55 m high above the summit, had reached an estimated volume of 1.0×10^6 m^3 and had grown to fill the gap

between the 1997 and the 2001 domes on the west side of the summit (Fig. 2.1). It is estimated that over the period 1–11 May, the dome grew at an average rate of 1 m^3 s^{-1}. At 09:40 on 13 May, the alert level was raised from 3 to the maximum level 4 "*Awas*" (beware) and by 16 May > 22,000 people had been evacuated. During this time, pyroclastic flows were occurring daily, with runout distances of 3 to 4 km on the SW flanks. On 22 May, the dome had reached an estimated volume of 2.3 x 10^6 m^3. CVGHM recommended that residents living on the north-northwestern flanks of the volcano, near the Apu, Trising, Senowo, Lamat and Sat rivers, and on the southeast, near the Woro river, were safe to return to their homes. Residents from villages within a 7 km radius of the summit and within 300m of the banks of the Krasak/Bebeng, Bedok, Boyong and Gendol rivers, remained evacuated. Between 11 and 27 May, dome growth continued, punctuated by gravitational dome collapse, with an estimated extrusion rate of 1.9 m^3 s^{-1}.

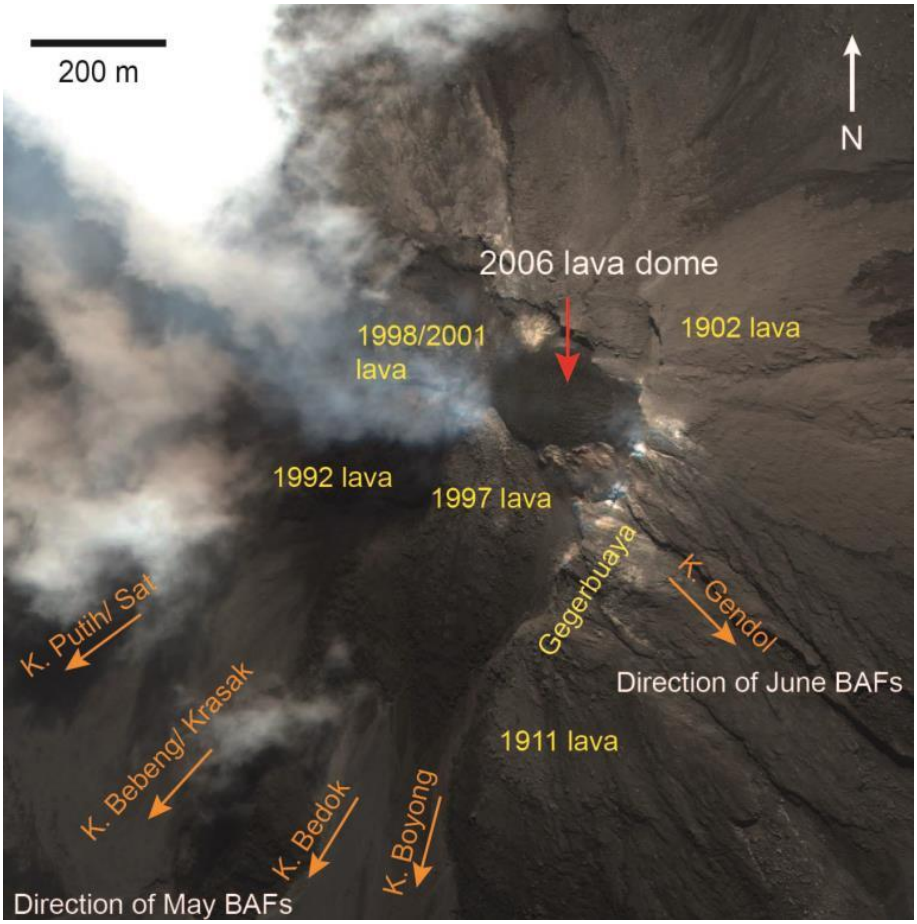

Fig. 2.1 Merapi summit viewed by the IKONOS satellite on 11 May 2006 with the 2006 lava dome clearly visible. Previous lavas domes and headwaters on the SW and S flanks are labelled based on Ratdomopurbo *et al*. (2013)

On 27 May, the dome had a volume of 2.6 x 10^6 m^3 and was 84 m high. At 05:53 on 27 May, a M_W 6.3 tectonic earthquake occurred near Bantul (7.962 °S, 110.458 °E) ~ 40 km SSE of the volcano (Walter *et al*., 2007), at a focal depth of 10 km. The earthquake resulted in 5749 deaths, 38,568 injuries, the destruction of 127,000 homes, with 600,000 people displaced from the Bantul-Yogyakarta area and an estimated monetary loss of ~ 3.1. billion US dollars. Hours after the earthquake, pyroclastic flows at Merapi became more frequent and the direction of flows also changed. On the same day, some small pyroclastic flows began to travel to the SE for the first time, towards the head of the K. Gendol (Fig. 2.2). Over the coming days, the proportion of pyroclastic flows travelling to the Gendol valley began to increase, until on 1 June, all flows were channelled in this direction. Between 27 May and 8 June, dome effusion rates also increased to 3.3 m^3 s^{-1} and by 8 June the dome was 98 m high, with an estimated volume of 4.1 x 10^6 m^3. The change in flow direction after the 27 May earthquake is probably due to the formation of instabilities in the summit region. Near the summit, the Gegerbuaya wall (Indonesian for "crocodile back") collapsed in several steps on 4 June, creating an opening on the summit towards the SE (Fig. 2.3). Prior to its collapse, the Gegerbuaya wall had formed a barrier that prevented pyroclastic flows from travelling southwards and entering the Gendol valley. Only the uppermost portion of the wall remained, supporting the 100 m high lava dome. On 9 June, a major pyroclastic flow, which reached 4 km in the Gendol valley, was generated when the remaining segment of Gegerbuaya collapsed, along with a portion of the 2006 dome. This collapse formed a small depression in the 2006 dome and a loss of ~ 18 m in height (Fig. 2.3). The largest dome collapse event occurred on 14 June. CVGHM reports suggest that a prolonged collapse event lasting ~ 3.5 hours occurred, but subsequent analysis of seismic data suggests that two sustained dome-collapse events produced pyroclastic flows, with runout distances of ~ 5 and 7 km in the Kali Gendol (Charbonnier and Gertisser, 2008; Lube *et al*., 2011) (Fig. 2.2). The first collapse began at 11:46, generating BAFs that travelled 5 km in the Kali Gendol, stopping near the village of Kaliadem. The second dome collapse event was the largest of the entire 2006 eruption, occurring in the afternoon from 14:46 to 15:50, lasting ~ 64 minutes. This flow resulted in the destruction of a region of Kaliadem village, as BAFs escaped the Gendol valley near a sabo dam producing overbank flows (Charbonnier and Gertisser, 2008; Lube *et al*., 2011; Gertisser *et al*., 2012b) (Fig. 2.2). Two search and rescue workers who were assisting with evacuation efforts were killed by overbank pyroclastic

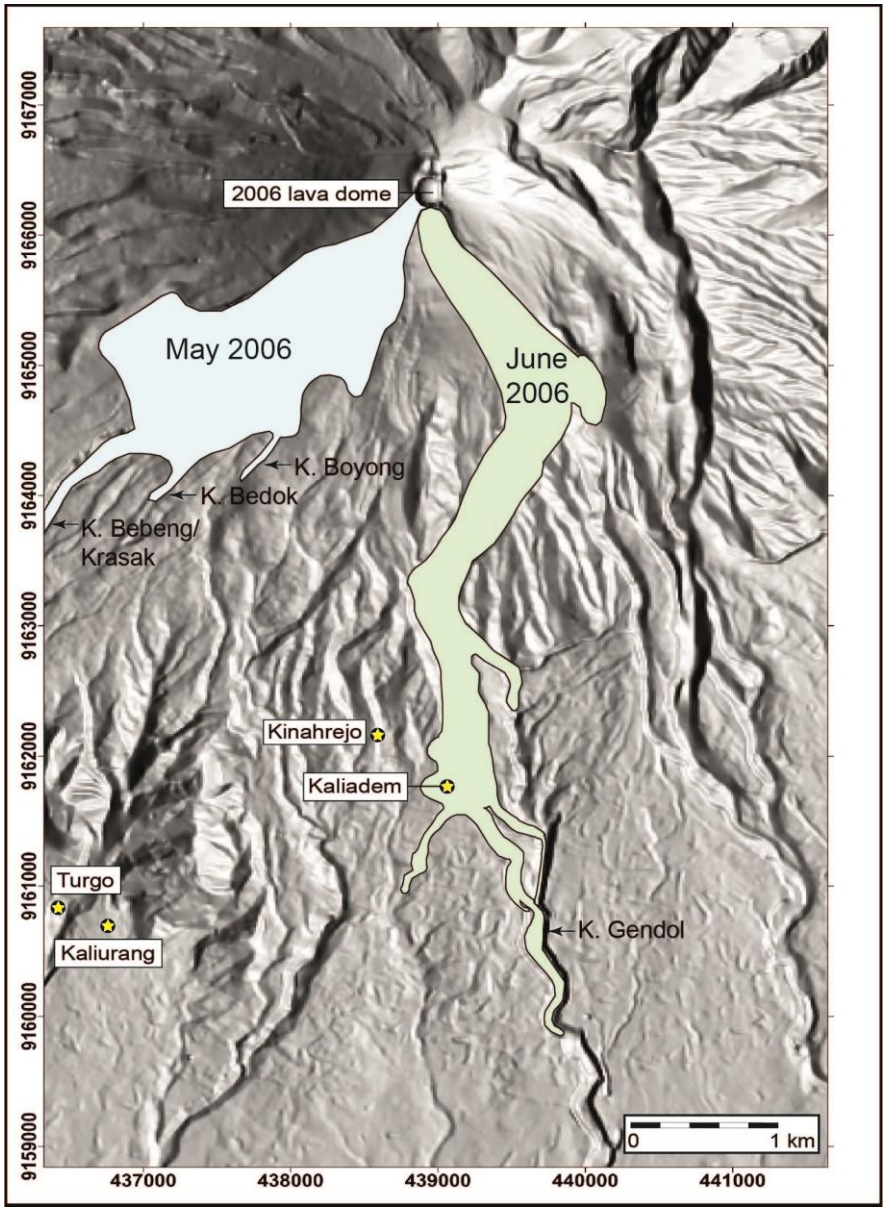

Fig. 2.2 Distribution of the May and June 2006 deposits on the south-western and southern flanks respectively (modified after Charbonnier and Gertisser, 2008), superimposed onto a digital elevation model (C. Gerstenecker, Technische Universität, Darmstadt, Germany)

flows as they sought refuge in an underground bunker in Kaliadem. Excavation teams retrieved their bodies from the bunker, which was buried under ~ 2m of deposit and concluded that both men died due to burns. On 14 June, the majority of the lava dome collapsed, leaving a depression in the summit. Activity levels remained high, and on the 15 June BAFs reached a distance of 4.5 km in the Gendol valley. Daily pyroclastic flows continued between 16–19 June, as the dome continued to grow. Between 21 and 27 June, seismic signals indicated the occurrence of daily rockfalls and pyroclastic

flows, although due to inclement weather, flows were only observed on 24 June and reached a maximum runout distance of 4 km in the K. Gendol. Gas and ash plumes reached a height of 1.5 km above the summit. By late June, dome extrusion rates had decreased to ~ 1.2 x 10^6 m^3 s^{-1} (Ratdomopurbo *et al*., 2013). After 28 June, pyroclastic flows and rockfalls began to decrease in frequency and intensity and on 10 July the alert level was lowered to level 3 in all areas except for the southern slopes. After this time, pyroclastic flows were no longer observed, although incandescent rock avalanches were reported almost daily until August, with runout distances up to ~ 2 km SE towards K. Gendol. On 17 July, the alert level was lowered to 3 in the south. Dome growth continued at low rates until October 2006 (Ratdomopurbo *et al*., 2013; Walter *et al*., 2013).

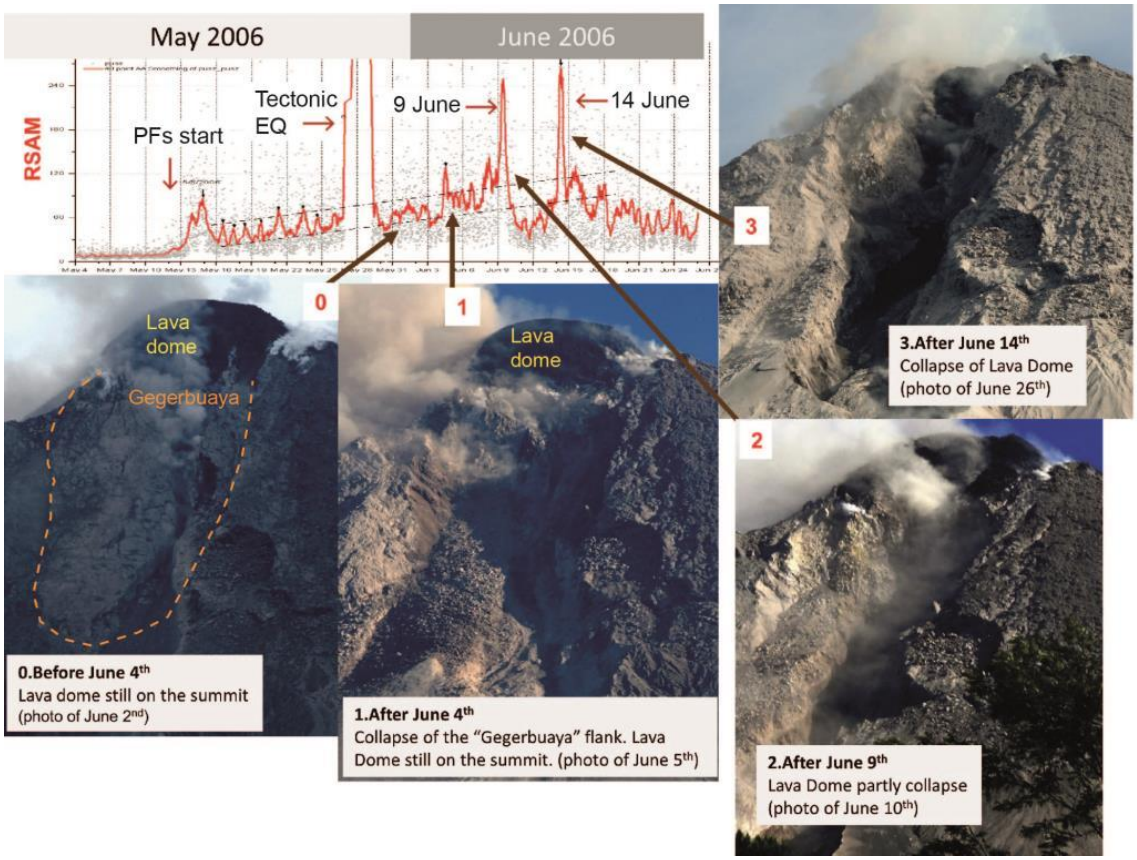

Fig 2.3 Lava dome and Gegerbuaya collapse during 2006 with RSAM trace of corresponding stages (modified after Ratdomopurbo *et al*., 2013). Time 0: photograph taken on 2 June, before Gegerbuaya collapse; Time 1: photograph taken on 5 June, the day after the majority of the Gegerbuaya wall collapse; Time 2: The remnants of Gegerbuaya wall collapsed along with a portion of the dome on 9 June, photograph taken on 10 June, showing a the opening to the SE and a scar on the lava dome; Time 3 Summit dome on 26 June, after the main collapse of 14 June. All photos taken from 4 km SE of the summit

2.2.2. Deposits of the 2006 eruption

The first BAFs of the 2006 eruption, from 11 May, were emplaced in valleys on the southwest flanks of Merapi, until the flow direction changed to the southeast and south towards K. Gendol at the end of May. BAFs were emplaced mainly into the Krasak, Bebeng, Bedok and Boyong valleys, with runout distances of < 4 km. After the tectonic earthquake on 27 May, flows were increasingly channelled towards K. Gendol and by 1 June, all flows were channelled to the Kali Gendol (Fig. 2.2).

The pristine 2006 BAFs in the Kali Gendol and surrounding areas were mapped in September 2006, before the rainy season, by Charbonnier and Gertisser (2008, 2011) and Charbonnier (2009) (Fig. 2.4). Important details regarding the 14 June BAF deposits and the mechanism of valley avulsion were added by Lube *et al.* (2011). The 2006 BAFs and BAF deposits have also been investigated via numerical modelling (Charbonnier and Gertisser, 2009), with satellite imagery (Thouret *et al.*, 2010) and using geophysical techniques (Gertisser *et al.*, 2012b). Four deposit types associated with the 2006 eruption have been identified (Charbonnier and Gertisser, 2008; Thouret *et al.*, 2010; Gertisser *et al.*, 2012b), including: 1) a valley-confined facies, consisting of basal avalanche deposits between 2 and 8 m thick, 2) an overbank facies, formed when the basal avalanche escaped the channel and spread laterally over interfluve areas, 3) a secondary valley-filling facies, formed by the re-channelling of unconfined flows into surrounding valleys, and 4) a 10–50 cm thick dilute ash-cloud surge facies often deposited along valley margins,. The volume of the June 2006 deposits in and around the Kali Gendol has been estimated at 8.7 x 10^6 m^3 (Charbonnier, 2009; Charbonnier and Gertisser, 2011). The valley-confined deposits in K. Gendol consist of 9 overlapping lobes, which reach between 2 and 7 km from the summit (Charbonnier and Gertisser, 2008) (Fig. 2.4). The farthest reaching lobe, Lobe 1, corresponds to the BAF that was emplaced in the afternoon of 14 June, with subsequent overlapping lobes (Lobes 2–9) emplaced from 15 June to early July (Fig. 2.4). They are typically < 100m wide and each is exposed for tens to hundreds of metres along the flow axis. Each lobe is a massive mixture of decimetre- to metre-sized blocks, set within a matrix of fine lapilli to medium ash.

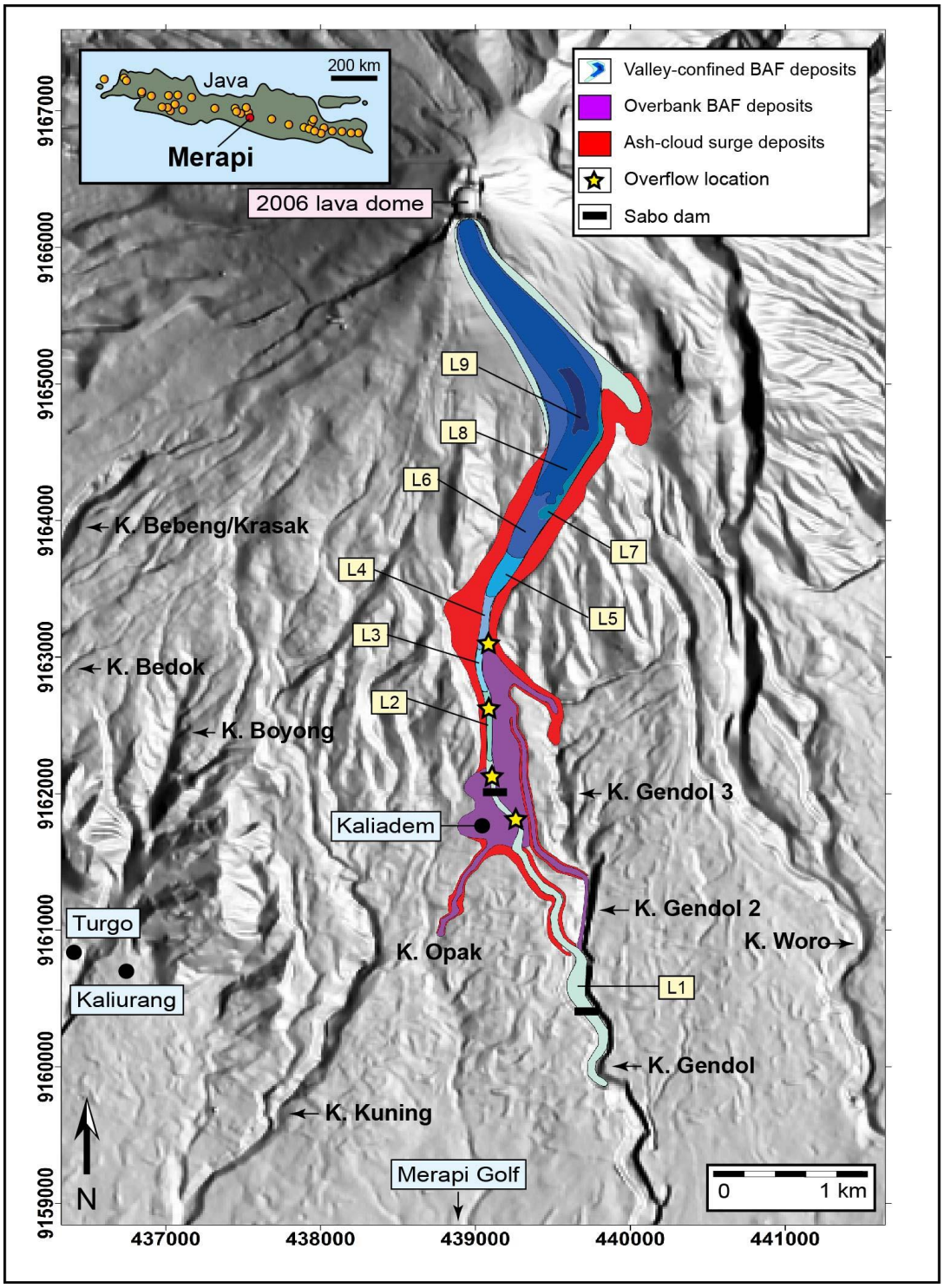

Fig. 2.4 Map of the June 2006 block and ash flow (BAF) deposits in the K. Gendol and surrounding area (modified after Charbonnier and Gertisser, 2008), superimposed onto a digital elevation model (C. Gerstenecker, Technische Universität, Darmstadt, Germany). The valley-filling BAFs generating during the peak of the eruption on 14 June and subsequent ones emplaced until early July are shown as individual overlapping lobes (L1-L9). Sabo dams, are illustrated by black bars and locations of BAF overflow are shown by yellow stars. Co-ordinates are in UTM

Clast componentry of the 2006 deposits was divided into 6 main components (Charbonnier and Gertisser, 2008) as follows:

- Type 1: light grey scoria
- Type 2: dark grey scoria
- Type 3: light grey dense clasts
- Type 4: dense prismatically jointed clasts
- Type 5: hydrothermally-altered clasts
- Type 6: oxidised clasts

Types 1–4 are juvenile 2006 lava, whereas Types 5 and 6 represent old dome fragments or lava flows that were incorporated into the 2006 deposits. Charbonnier and Gertisser (2008) reported differences in componentry between lobes. The most abundant clast type in most lobes is the light grey scoria (Type 1) with an average content of ~ 40 % by volume. Dense prismatically jointed clasts (Type 4) are only found within Lobe 1, indicating that the dome collapse which generated the largest 14 June pyroclastic flows incorporated material from the inside of the dome. Lobes 1 and 5 have a higher proportion of hydrothermally altered clasts (Type 5) and Lobe 9 is enriched with dark grey scoria (Type 2). The overbank deposits, found between 3.5 and 5 km from the summit, with a mean thickness of 3 m, have a higher content of vesicular (scoriaceous) clasts. It is thought that valley fills from previous deposits, channel bends and anthropogenic barriers, such as sabo dams, influenced the course of the pyroclastic flows and increased their capacity to overspill the valley confines, producing overbank flows (Charbonnier and Gertisser, 2008; Thouret *et al*., 2010; Lube *et al*., 2011; Gertisser *et al.*, 2012b). Basal avalanche deposits were estimated to have a minimum temperature of 400 °C, with flow velocities of 13.5–43.8 m s^{-1} based on vertical flow run-up (Charbonnier and Gertisser, 2008), or ~ 18.5 m s^{-1} based on eye-witness reports of travel time (Lube *et al*., 2011). Ash-cloud velocities were estimated to be 24.2–62.6 m s^{-1} (Charbonnier and Gertisser, 2008).

2.3. The 2010 eruption of Merapi volcano

2.3.1. Chronology of the 2010 eruption

The 2010 eruption was Merapi's largest and most explosive for more than a century (Surono *et al*., 2012). The first signs of unrest began approximately a year before eruption, with 4 VT swarms occurring on 31 October 2009, 6 December 2009, 1 February 2010 and 10 June 2010 (Surono *et al*., 2012; Budi-Santoso *et al*., 2013). In November 2009, EDM data showed that deflation following the 2006 eruption had reversed and the volcano was beginning to inflate. In early September 2010, seismicity levels increased, both in terms of the number of earthquakes and the seismic energy released. An increase in seismicity was accompanied by an increase in ground deformation, as well as the temperature, CO_2 and H_2S levels of summit fumaroles. This led to the alert level being raised from 1 to 2 on 20 September 2010. Further increases in unrest occurred in October, including further VT and MP earthquakes, associated with the movement of magma (Surono *et al*., 2012; Budi-Santoso *et al*., 2013; Jousset *et al*., 2013). Large increases of CO_2/SO_2, CO_2/HCl and CO_2/H_2O were detected in fumarolic gases in the months leading up to eruption, with a dramatic increase in CO_2 abundance from 10 mol.% in September 2010 up to 35–63 mol.% on 20 October, interpreted to be due to a progressive shift to degassing of a deeper magmatic source (Surono *et al*., 2012). On 21 October, the alert level was again increased, from 2 to 3. From 23 to 26 October, there were small steam and ash emissions (BGVN 2011). During this time, summit inflation on the southern flank also increased dramatically, to levels of > 500 mm per day, compared to < 10 mm per day in early September. The cumulative inflation measured on the southern flank was 3 m. Seismic activity also dramatically increased, with 194 "Guguran" or rockfall earthquakes, 80 VT and 588 MP earthquakes detected on 24 October, and 454 Guguran, 222 VT and 624 MP earthquakes detected on 25 October (Budi-Santoso *et al*., 2013). The rapid escalation of unrest and unprecedented levels of deformation and seismic activity between 23 and 25 October, led CVGHM to increase the alert level to 4 on 06:00 local time on 25 October (Pallister *et al*., 2013). Tens of thousands of people had to be evacuated within a 10 km radius of the summit. 35 hours later, at 17:02 local time on 26 October, Merapi erupted. The initial explosion destroyed the remnants of the 2006 dome and created a new summit crater, excavating an estimated ~ 6 $x10^6$ m^3 of non-juvenile material (Pallister *et al*., 2013). A volcanic plume rose to 12 km altitude and released a greater amount of

SO_2 emissions than during previous recent eruptions (Surono *et al*., 2012). Pyroclastic flows travelled 8 km from the summit in the Kali Gendol and Kali Kuning valleys. The event killed 35 people including the renowned spiritual guardian of Merapi, Mbah Marijan, who refused to evacuate the village of Kinahrejo, on the southern flank. In addition, 150 buildings were damaged in an area of 7.5 km^2 (Jenkins *et al*., 2013). On 25 October, 19 hours before the eruption, a M7.7 tectonic earthquake occurred ~ 1,200 km NW of Merapi, near the Mentawai Islands, off the coast of Central Sumatra. This was followed by several aftershocks (M6.1 and 6.2) just prior to the eruption, as well as one just after 26 October eruption (M 5.8). The earthquakes triggered tsunamis that hit the Mentawai islands, killing at least 428 people (BGVN 2011). However, apart from the close timing and regional proximity, the link between the earthquake and the onset of eruption remains ambiguous. Additional but smaller explosions occurred on 29 October, 31 October and 1 November. 150 LF earthquakes were recorded, attributed to the movement of magma and gas within the edifice (Surono *et al*., 2012). From 1 November (or from 29 October according to Komorowski *et al*. (2013)) to 4 November, a new lava dome rapidly built up within the crater that had been produced on 26 October (Fig. 2.5). Dome effusion rates were estimated to be 25 m^3 s^{-1} and by 4 November the volume of the dome had reached ~ 5 x 10^6 m^3 (Surono *et al*., 2012; Pallister *et al*., 2013) (Fig. 2.5). During the start of dome growth, SO_2 emissions were relatively low compared to during previous explosions, but on 3–4 November, SO_2 emissions a few orders of magnitude higher than recorded in previous eruptions were detected. Seismic activity also increased, accompanied by a series of explosions, some of which were reportedly heard in Yogyakarta, and pyroclastic flows that reached 12 km runout distance (Fig. 2.5). This prompted the evacuation zone to be extended to a radius of 15 km on 3 November. On 4 November, seismic tremors, often associated with resonance in fluid-filled cavities, fluid flow or degassing (Budi-Santoso *et al*., 2013) were felt up to 15 km away. The exclusion zone was further extended to a 20 km radius, so that a total of ~ 300,000 people were now evacuated from the surrounding area. At 23:56 on 4 November, a tectonic earthquake was recorded (Surono *et al*., 2012; Komorowski *et al*., 2013; Budi-Santoso *et al*., 2013; Jousset *et al*., 2013). Minutes later, at 00:02 on 5 November local time, the paroxysmal phase occurred, with explosions generating a 17 km high ash column, pyroclastic flows which travelled nearly 16 km on the southern flanks, and forming a new 400 m diameter crater and a canyon near the summit extending into the Kali Gendol headwaters (Fig. 2.6).

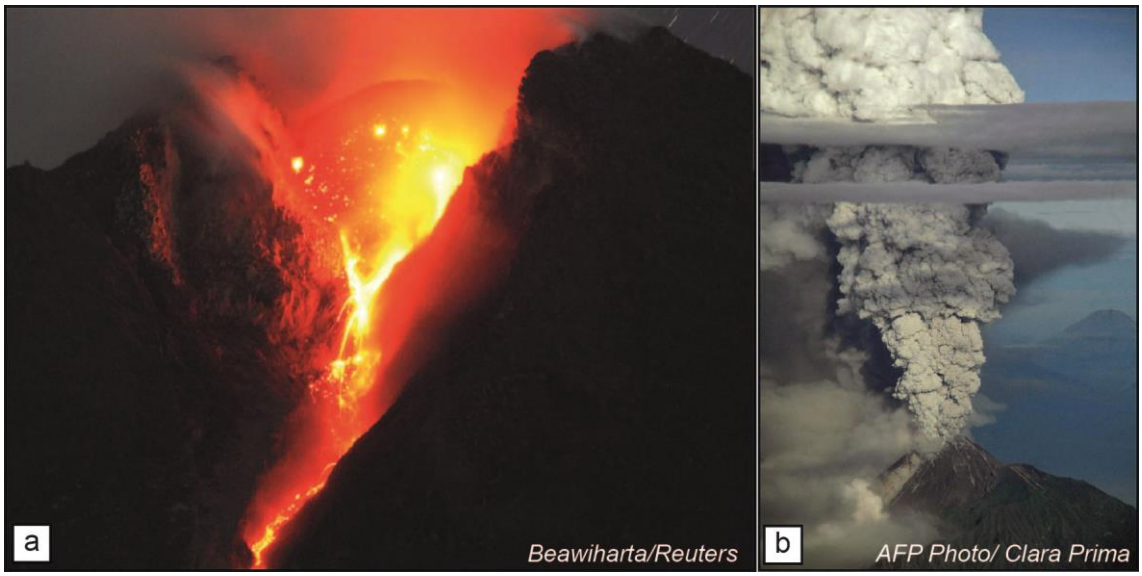

Fig. 2.5 (a) The 2010 dome, as photographed on 3 November 2010, during rapid dome growth at rates of 25 m^3 s^{-1} (Photo credit: Beawiharta/ Reuters), (b) Sustained eruption column on 4 November 2010 (Photo credit: AFP Photo/ Clara Prima)

The death toll remains somewhat ambiguous, with some reports suggesting that 367 fatalities occurred in total (Surono *et al*., 2012), whereas others suggest that the number who were killed as a direct consequence of the PDCs is likely closer to ~ 120 (Jenkins *et al*., 2013). In either case, the 2010 eruption resulted in the highest number of fatalities since the 1930 eruption, when > 1300 people died (*e.g.* Voight *et al.*, 2000). More than 1300 buildings were damaged, alongside infrastructure and many trees were felled in an area of 22 km^2 (Jenkins *et al*., 2013). The pyroclastic surges were estimated to have had a temperature of 200–300 °C, based upon examination of wood, plastics and other debris left behind in villages, as well as medical reports about the condition of victims' bodies (Jenkins *et al*., 2013). A large number of the fatalities occurred due to overbank PDCs in Bronggang village, which had not yet been evacuated (Fig. 2.7). However, it should be noted that due to the timely forecasts by CVGHM, an estimated 10,000–20,000 lives were saved (Surono *et al*., 2012). Ash fell in Yogyakarta and "sand-sized" tephra fell up to 15 km away. Residents up to 240 km away reported that "heavy grey ash" blanketed trees, cars and roads (BGVN 2011). From 5–20 November, Yogyakarta airport was closed, with 1350 flights cancelled (Picquout *et al*., 2013). RADARSAT satellite images collected on 6 November show that rapid extrusion at an average rate of 35 m^3 s^{-1} produced a new lava dome with a volume of 1.5 x 10^6 m^3 in less than 12 hours (Pallister *et al*., 2013). Dome growth was accompanied by

incandescent jetting of gas as well as pyroclastic flows which travelled up to 4 km in the Senowo valley on the western flank. Ash plumes rose to an altitude of 16.8 km. On 7 November, an explosion was heard, ash plumes rose to 6 km altitude and pyroclastic flows travelled 5 km. Dome growth ceased on 8 November, and on 9 November CVGHM noted a reduction in the intensity of activity. The exclusion zone was reduced from 20 to 15 km on 14 November, and then down to 5 km on 19 November. The alert level was decreased from 4 to 3 on 3 December. Although the primary volcanic threat had decreased, lahars were still a major hazard. During the first rainy season, lahars occurred primarily on the western flank, especially in the Kali Putih drainage (Surono *et al*., 2012). In the first rainy season, between October 2010 and May 2011, 240 lahars were recorded, with runout distances up to > 15 km, resulting in 3 fatalities, the damage of 860 houses and destruction of 14 sabo dams and 21 bridges (de Bélizal *et al*., 2013).

Fig. 2.6 Photographs taken of Merapi before and after the 2010 eruption, depicting the change in summit morphology. The eruption has resulted in the formation of a deep crater and a deep scar to the SE leading into the headwaters of the Kali Gendol, known as the Gendol Breach (From Surono *et al*., 2012)

2.3.2. Deposits of the 2010 eruption

Visual observations of the eruption were difficult due to the fact that the 2010 eruption occurred in the rainy season and inclement weather conditions often made for poor visibility during the day, as well as the fact that the paroxysmal phase occurred during the night. To overcome this, a range of satellite data was used during the monitoring efforts, including information on SO_2 emissions from the Ozone Mapping Instrument (OMI), SAR images from RADARSAT-2 and TerraSAR-X sources, high-resolution infrared data from GeoEye-1 and WorldView-2 sensors and thermal data from the ASTER sensor. Increased satellite frequency and rapid data processing were made possible by several national and international agreements, including the

International Charter for Space and Major Disasters (Pallister *et al*., 2013). In addition to satellite data recorded at the time of eruption, subsequent field studies of the deposits have proved vital in piecing together further details of the eruption (Charbonnier *et al*., 2013; Komorowski *et al*., 2013; Cronin *et al*., 2013). For example, the exact generation mechanism of the pyroclastic flows that led to the destruction and fatalities in Kinahrejo on 26 October initially remained unclear. Reports of booming noises and explosions suggested that there might have been collapse of eruption fountains, or even horizontally directed blasts. However, following field investigation it seems clear that the destruction in Kinahrejo was caused by ash-cloud surges that detached from pyroclastic flows channelled in the Gendol valley (*e.g.* Gertisser *et al*., 2011). From field study and satellite imagery, Charbonnier *et al*. (2013) recognise 23 PDC events in 2010, including 5 main channelled flows, 15 overbank flows derived from overspill and re-channelling, as well as two main surge events, with the total non-DRE volume of the 2010 deposits estimated at ~ 36.3 x 10^6 m^3. The total volume is distributed between valley-filling deposits (50.2 %), overbank deposits (39.3 %) and surges and fallout tephra (10.5 %). An estimated > 70 % of the deposits were generated on 4–5 November. Komorowski *et al*. (2013) divided the 2010 eruption chronology and associated deposits into 8 stages (Table 2.1) as follows:

- Stage 1: unrest and magmatic intrusion (31 Oct. 2009–26 Oct. 2010)
- Stage 2: initial explosions (26 Oct. 2010)
- Stage 3: recurrent rapid dome growth and destruction (29 Oct.–4 Nov. 2010)
- Stage 4: paroxysmal dome explosions and collapse (5 Nov. 2010)
- Stage 5: retrogressive summit collapse (5 Nov. 2010)
- Stage 6: subplinian fountain collapse (5 Nov. 2010)
- Stage 7: rapid dome growth with alternating effusive and explosive activity (5–8 Nov. 2010)
- Stage 8: declining ash venting and degassing (8–23 Nov. 2010)

The 5 November (Stage 4) deposits were mapped in detail by Komorowski *et al*. (2013) and integrated with the monitoring record (Fig. 2.7). Stage 4 consisted of an 11 minute sequence of five laterally-directed explosions, generating high-energy PDCs with runout distances up to 15.5 km. The event began at 00:02 on 5 November, with two initial minor explosions, followed by the largest explosion at 00:06 and two smaller subsequent explosions. Komorowski *et al*. (2013) identified 5 types of PDCs which

were generated during Stage 4, leading to a complex stratigraphy: (1) unconfined high-energy turbulent stratified PDCs, which are distributed over a 3–4 km wide area up to a distance of 8.4 km from the summit; (2) secondary, valley-confined, block-poor concentrated PDCs that formed from sedimentation of high-energy primary PDC on steep slopes in valleys; (3) valley-confined block-rich concentrated PDCs that reached up to 15.5 km distance in K. Gendol and ~ 8.5 km in K. Opak; (4) overbank PDC deposits originating from overspill of valley-confined block-rich PDCs and (5) dilute PDCs that detached from the main valley-confined block-rich PDCs and propagated laterally for 50–400 m in distal areas. The estimated height of the PDCs reached up to 330 m, with an internal velocity of ~ 100 m s^{-1} within the first 3 km from the summit. Specifically focussing on the Stage 4 unconfined lithofacies, Komorowski *et al*. (2013) identify 3 depositional units, Unit 0, Unit 1 and Unit 2. Unit 0 was only found in one locality in Kinahrejo and consists of poorly-sorted coarse ash to fine lapilli layer, 3–5 cm thick. Unit 1 and Unit 2 are interpreted to have been generated in explosions 3 and 4 respectively. Both display bi-partite layering, with a lower layer (L1) and an upper layer (L2). Unit 1 varies in thickness from ~ 150 cm in proximal areas to ~ 1 cm at 8.5 km distance from the summit. L1 is clast-supported, fines-depleted, poorly-sorted and predominantly composed of lapilli-sized clasts but also some blocks/bombs, as well as coarse ash. L2 is rich in fines, well-sorted and sometimes displays wavy cross and planar stratification. Unit 2 is similar to Unit 1, but is finer grained and thinner compared to Unit 1, with a maximum thickness of 53 cm, and is recorded at fewer sites. Komorowski *et al*. (2013) noted that the Merapi 'blast' during Stage 4 was similar to historical blasts at Pelée (Martinque), Mt. Lamington (Papua New Guinea), Bezymianny (Russia) and Mount St. Helens (USA), although Merapi devastated a smaller area, the impact was remarkable considering the comparatively smaller volume of magma involved. It is thought that the interaction with local topography at Merapi was partly responsible for the devastation caused. The expanding gas and solids expelled during the explosion were channelled into an inclined chute at the headwaters of the K. Gendol, known as the Gendol Breach (Fig. 2.6), which acted as a "cannon barrel", before most of the flow was deflected by the Gunung Kendil ridge, guiding the flow into the Gendol Funnel. This is a relatively narrow (~ 120 m across) constriction in the upper K. Gendol, which acted as a venturi structure, causing an increase in speed, dynamic pressure and kinetic energy.

The 2006 and 2010 eruptions of Merapi provide excellent case-studies to examine the driving forces behind effusive and explosive behaviour and factors that contributed to transitions in eruptive style. Both eruptions were well-monitored and documented, allowing for all samples and data to be correlated to eruptive chronology and behaviour.

Table 2.1 Summary of the chronology, eruptive phenomena and style, deposits and impact of the 2010 eruption. (Modified after Komorowski *et al*., 2013). Data in Surono *et al*. (2012); Budi-Santoso *et al*, (2013); Charbonnier *et al*. (2013); Jenkins *et al*. (2013) ; Jousset *et al*. (2013) ; Pallister *et al*. (2013)

Date/ Time	Stage	Eruptive Phenomena	Eruptive Deposits	Eruptive Style	Eruptive Impact
31 Oct. 2009 – 26 Oct. 2010	1	Non-eruptive. Escalating unrest and increase in seismicity, ground deformation, heat flux, SO_2 and CO_2 emissions	Rockfalls < 1.5 km	Unrest and intrusion	None
26 – 29 Oct.	2	Explosion from gas-rich stalled intrusion, forming a crater 200m diam., 100m deep. Unconfined dilute and valley-confined PDCs up to 5.4 km in K. Opak and 6.8 km in K. Gendol	Surge deposits with vesicular material, BAFs, ash fallout	Initial explosions	35 direct PDC deaths, 150 buildings damaged over 7.5 km^2
29 Oct. – 4 Nov.	3	Incandescence on 29 Oct. Rapid dome growth (25 m^3 s^{-1}). Explosions on 30 Oct., 31 Oct., 1 Nov., 2 Nov., 3 Nov., causing unconfined dilute PDCs 5-6 km distance in S, W-NW. Many valley-confined PDCs with runout distances up to 12 km	Surge deposits with vesicular material, BAFs, ash fallout	Rapid dome growth and recurrent destruction	At least 3 evacuated villages damaged. Lahars on 3-4 Nov. destroy bridges
5 Nov. *00:02 – 00:13*	4	11 minute sequence of 5 laterally directed dome explosions, generating dilute unconfined PDCs and valley confined PDCs up to 15.5 km in K. Gendol and 8 km in K. Opak	Surges, BAFs, ash fallout	Paroxysmal dome explosions and collapse	Damage to 22 km^2, direct PDC deaths, > 1000 buildings damaged, extensive tree blowdown
5 Nov. *00:13 – 01:57*	5	Retrogressive dome collapse, crater widened ~ 300x400m, 150-200m deep. PDCs 15.5 km in K. Gendol, with localised valley overspilling	Surges, BAFs, accretionary lapilli ash fall	Retrogressive summit collapse	Dilute and concentrated PDCs over 5 km^2. ~ 120 direct PDC deaths > 12 km distance, ~ 900 buildings damaged, tree blowdown in overspill areas
5 Nov. *02:11 – 04:21*	6	Ash venting and convective column collapse. Valley confined PDCs to 15.5 km in K. Gendol, with some local overspilling	Pumice and scoria flow. Ash fall out	Subplinian fountain collapse	Unknown direct deaths and building damage
5 – 8 Nov.	7	Sustained and declined ash venting, degassing, lava fountains, sporadic explosions. Unprecedented rapid dome growth on 6 Nov. (35 m^3 s^{-1}). Few valley-confined PDCs < 5 km in K. Gendol	BAFs, ash fallout	Rapid dome growth with alternating effusive/ explosive activity	Effects of ash fall
8 – 23 Nov.	8	Declining ash venting, degassing and lava fountains. Deflation of new dome, a few valley-confined PDCs in K. Gendol < 3 km	Ash fallout, BAFs	Declining ash venting and degassing	None

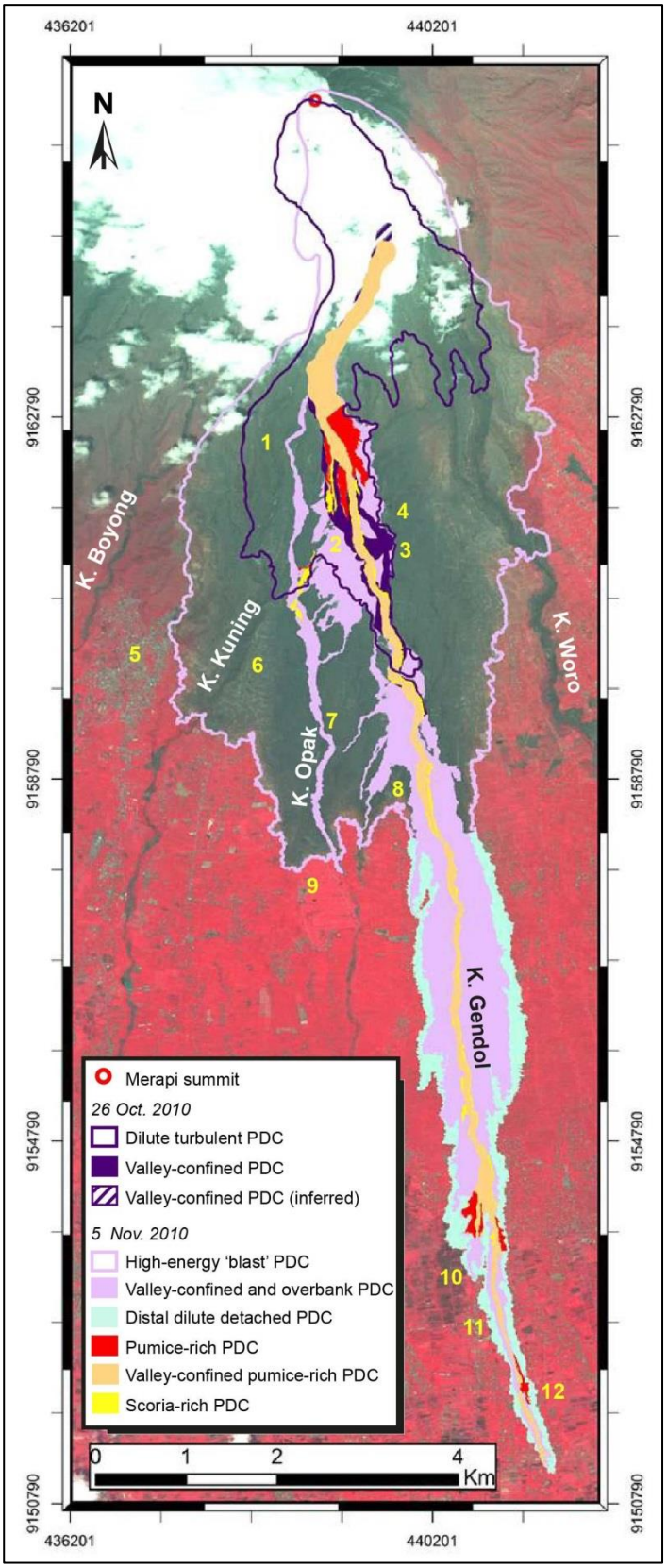

Fig 2.7 Distribution map of the 26 October and 5 November deposits (modified after Komorowski *et al*., 2013). Yellow numbers indicate selected localities damaged by or nearby deposits (1) Kinahrejo; (2) Kaliadem; (3) Kalitengah Kidul; (4) Kalitengah Lor; (5) Kaliurang; (6) Umbulharjo; (7) Petung; (8) Kopeng; (9) Merapi golf course; (10) Bakalan; (11) Bronggang; (12) Plumbung

Chapter 3: The 2006 Eruption of Merapi: Textural and Petrological Constraints on Pre- and Syn-Eruptive Magmatic Processes

3.1. Introduction

Magma ascent and conduit dynamics exert a profound control over eruptive behaviour, influencing whether an eruption will be effusive or explosive (*e.g.* Eichelberger *et al.*, 1986; Jaupart and Allègre, 1991; Woods and Koyaguchi, 1994). The style of magma ascent and syn-eruptive degassing during ascent plays a large role in determining the style of eruption of compositionally similar magmas (*e.g.* Hildreth and Drake, 1992; Platz *et al.*, 2007; Constantini *et al.*, 2011). For example, open-system degassing, where magma degasses freely during ascent, typically results in a less explosive eruption compared to a partly closed system, where gas is prevented from escaping, more often resulting in explosive activity (*e.g.* Westrich *et al.*, 1988; Stix *et al.*, 1993). Degassing also influences the physical and rheological properties of magma by affecting the permeability, viscosity and crystallinity, which in turn affect the style of eruption (*e.g.* Eichelberger *et al.*,1986; Mastin, 2005; Edmonds and Herd, 2007; Hale *et al.*, 2007). It is therefore crucial to better understand magma ascent processes and syn-eruptive degassing and their respective influence upon eruptive behaviour in order to aid in future hazard assessment of volcanic eruptions.

During magma ascent, crystallisation of groundmass microlites may occur due to adiabatic decompression and accompanying devolatilisation (*e.g.* Cashman, 1992; Geschwind and Rutherford, 1995; Hammer *et al.*, 1999, 2000). As magma ascends prior to eruption, decompression leads to volatile exsolution and degassing of H_2O. The resulting H_2O loss causes an increase in the stability of anhydrous minerals, particularly plagioclase, and an increase in the liquidus temperature of the anhydrous minerals. As a corollary of the increase in liquidus temperature, there is an increase in the relative undercooling (ΔT), defined as the difference between the temperature of the liquidus and that of the magma, causing the melt to crystallise. The style of crystallisation

depends upon the kinetics and relative importance of crystal nucleation and crystal growth, as a consequence of ΔT (Lofgren, 1980; Kirkpatrick, 1981; Swanson *et al.*, 1989). For example, a large ΔT favours nucleation of new crystals, leading to the formation of many smaller crystals, whereas smaller ΔT leads to a growth dominated regime, resulting in fewer but larger crystals. At very high undercooling however, low rates of diffusion, due to high melt viscosity at low H_2O content (Hess and Dingwell, 1996), mean that the magma does not crystallise, but is quenched to glass upon eruption. Microlite textures are therefore an indication of the relative undercooling of the magma, determined by its decompression path. In the case of dome-forming eruptions, magma may also reside for prolonged periods of time near the surface, at elevated temperatures within the dome, allowing for the possibility of further groundmass crystallisation to occur (Sparks *et al.*, 2000). The final groundmass texture is a result of the often complex ascent path of a magma, i.e. ascent rate, depth and style, which may be continuous or intermittent, with temporary stalling at one or several levels in the crust, as well as any post-extrusion, near-surface crystallisation that may take place during dome residence.

Previous investigations into groundmass crystallisation have utilized natural volcanic samples (*e.g.* Cashman, 1992; Wolf and Eichelberger, 1997; Hammer *et al.*, 1999, 2000; Nakada and Motomura, 1999; Noguchi *et al.*, 2006, 2008; Suzuki and Fujii, 2010), decompression experiments (*e.g.* Geschwind and Rutherford, 1995; Hammer and Rutherford, 2002; Couch *et al.*, 2003a; Brugger and Hammer, 2010a; Martel, 2012), as well as numerical modelling of crystallisation and magma ascent (*e.g.* Brandeis and Jaupart, 1987; Melnik and Sparks, 1999, 2005; Clarke *et al.*, 2007; Melnik *et al*., 2011).

Previous work (Hammer *et al.*, 2000) carried out on the feldspar microlite textures of recent dome-forming eruptions at Merapi has investigated processes of magma ascent and the resultant degassing-induced crystallisation over timescales of several years, using samples produced in distinct episodes of dome extrusion between 1986 and 1995. The study found a correlation between microlite number density and effusive flux, indicating that crystallisation conditions (ΔT) and resultant microlite textures were determined by magma ascent rate that was cyclic over the time period studied.

This chapter presents a detailed textural and petrological case study of the exceptionally well-documented 2006 eruptive episode, with the aim of elucidating the short timescale variations (> 3 month duration) of shallow magma ascent and conduit processes during a single dome-forming (effusive) eruption cycle at Merapi (Charbonnier and Gertisser, 2008; Ratdomopurbo *et al*., 2013). Chronologically controlled sampling and textural analysis of juvenile dome material, incorporated into several block-and-ash flow (BAF) deposits during successive dome collapse events during the course of the eruption, provide a detailed insight into sub-surface magmatic processes. When compared to the products of the more explosive 2010 eruption (*e.g.* Surono *et al*., 2012; Pallister *et al*., 2013), these data allow the relation of those textural features to differences in magma ascent processes and their control on eruptive mechanisms and behaviour.

3.2. Background

3.2.1. Recent eruptive history of Merapi

Throughout the last two centuries, activity at Merapi has been almost continuous, with eruptions occurring every few years, typically consisting of prolonged periods of dome growth followed by multiple gravitational dome collapses (VEI 1–2), to produce BAFs [see Voight *et al*. (2000) for a detailed summary]. This type of activity has become so synonymous with Merapi that small volume pyroclastic flows from gravitational dome collapse are often termed "Merapi-type" nuées ardentes. However, more explosive eruptions (up to VEI 4; Voight *et al.,* 2000) have occurred during this time, notably in 1872 and, possibly, in 2010, and were more common in pre-historical time (Andreastuti *et al*., 2000; Camus *et al*., 2000; Newhall *et al*., 2000; Gertisser and Keller, 2003a; Gertisser et al., 2012a). Variations in magma supply from depth, magma ascent rate, the degassing behaviour during ascent and the assimilation of crustal carbonates are thought to be important factors that control whether Merapi erupts effusively or explosively (Newhall *et al.,* 2000; Chadwick *et al*., 2007; Gertisser and Keller, 2003a; Deegan *et al*., 2010;Gertisser *et al*., 2011; Troll *et al*., 2012).

3.2.2. Merapi magma plumbing system

There is both petrological and geophysical evidence for the structure of the magma plumbing system at Merapi. Gertisser (2001) found evidence, based on thermobarometric calculations, of a major magma storage region at mid- lower crustal levels. There is also petrological evidence of a storage region at mid- upper crustal levels, where crustal carbonate contamination contributes to the volatile budget of the system, intensifying and sustaining eruptions (Deegan *et al*., 2010; Troll *et al*., 2012; Troll *et al*., 2013). Costa *et al*. (2013) present further petrological data to elucidate the magma storage conditions before the 2006 and 2010 eruptions, concluding that there are three main zones of crystallisation, consisting of a deep reservoir (~ 30 km depth), a second zone at ~ 11 km and a shallow, crystal-rich region at < 10 km depth. Petrological evidence, based on magmatic inclusions, also reveals crystallisation at Merapi occurs at multiple depths (~ 2–45 km depth), with the bulk of it occurring at mid-crustal levels (Chadwick *et al*., 2013). Geophysical studies also indicate the presence of multiple magma storage regions at Merapi. GPS and tilt data suggest an average source depth for magma storage at 8.5 ± 0.4 km below the summit (Beauducel and Cornet, 1999), consistent with an aseismic zone at > 5 km depth below the summit (Ratdomopurbo and Poupinet, 2000). As well as a deeper source, one or potentially two shallower storage regions have been proposed, linked to the deeper storage region(s) via an inclined conduit, based upon Bouguer gravity anomaly data (Saepuloh *et al*., 2010). In addition, a shallow aseismic zone located at 1.5–2.5 km depth below the summit has been proposed and is interpreted to be an ephemeral storage region, where magma is temporarily stored as it migrates from the deeper reservoir(s) before eruption (Ratdomopurbo and Poupinet, 2000). A low density region between 0.8–1.8 km below the summit has also been postulated from gravity data, although it is not clear if this is a zone of magma storage (Tiede *et al*., 2005). The plumbing system at Merapi is therefore complex and believed to consist of multiple regions of magma storage and crystallisation. These range over almost the entire thickness of the crust, with a main magma storage zone within the lower crust, linked via a network of other regions of crystallisation in the mid- to shallow-crust, to a shallow magma storage region within the edifice, which is probably small and ephemeral.

3.2.3. The 2006 eruption of Merapi volcano

The 2006 eruption is a well characterized example of extrusive, dome-forming activity at Merapi (Charbonnier and Gertisser, 2008, 2009, 2011; Lube *et al*., 2011; Gertisser *et al.,* 2012b). The onset of the eruption (VEI 1) is estimated from monitoring data to be 26 April 2006 (Ratdomopurbo, 2011). Lava dome extrusion probably began on 1 May, although it was not directly observed until 5 May (Ratdomopurbo *et al.,* 2013), after approximately 10 months of increased seismicity and summit deformation (Fig. 3.1). The first dome collapses occurred on 11 May 2006, and continued during May, with BAFs channelled and emplaced in river valleys, herein referred to as "Kali", abbreviated as "K.", (Indo. = river), on the south-west flank of the volcano, including Kali Bebeng, Kali Krasak, Kali Boyong and Kali Bedok, with run-out distances of less than 4 km. On 22 May, the dome volume was estimated to be ~ 2.3×10^6 m^3. A M_w 6.3 tectonic earthquake occurred ~ 40 km south of Merapi on 27 May, after which, a considerable increase in dome collapse events was noted (Walter *et al.,* 2007; Charbonnier and Gertisser, 2008; Troll *et al.,* 2012). On 4 June, the dome was estimated to have reached a height of 100 m above the former summit and a volume of ~ 4.0×10^6 m^3 (BGVN 32:02) and between 1 May and 8 June, extrusion rates were estimated to increase from 1.0 m^3 s^{-1} to 3.3 m^3 s^{-1} (Ratdomopurbo *et al.,* 2013). Throughout the beginning of June, activity increased and BAFs were emplaced daily into valleys on the southern flank of the volcano, predominantly into the Kali Gendol drainage channel, instead of into the valleys on the south-western flanks, due to progressive collapse of the "Gegerbuaya" wall (Indo. = "crocodile back") near the summit. The peak of activity on 14 June 2006 consisted of multiple phases of dome collapse (Charbonnier and Gertisser, 2008; Lube *et al*., 2011; Gertisser *et al*., 2012b) in the morning and afternoon, with flows in the morning travelling 5 km and the afternoon flows travelling 7 km in the K. Gendol (Lobe 1; Charbonnier and Gertisser, 2008). The largest flows in the afternoon over-topped the valley walls and devastated surrounding interfluvial areas and partially destroyed the village of Kaliadem, ~ 5 km from the summit (Fig 3.1), resulting in two fatalities (Gertisser *et al*., 2012b). Subsequently, during the second half of June, activity began to decrease with further smaller BAFs emplaced in the Kali Gendol, resulting in at least eight overlapping lobes (Lobes 2-9; Charbonnier and Gertisser, 2008; Fig. 3.1). Dome extrusion rates decreased to ~ 1.2 m^3 s^{-1} during late June (Pallister *et al*., 2013). Lobe 10, not recorded in Charbonnier and Gertisser (2008), was formed by a

small collapse of remnants of the 2006 dome after September 2006, possibly even during 2007 (Fig 3.1). Alert levels were reduced to normal in early October 2006, signalling the end of the eruption.

3.3. Sampling and analytical methodology

3.3.1. Sampling the 2006 deposits

There is some inherent uncertainty when sampling BAF deposits as it is not possible to know the exact extrusion date and original dome location of each clast, as well as the degree of homogeneity of clast origin within the deposit. Theoretically, two end-member scenarios of dome growth and collapse to emplace subsequent lobes during an eruption are: (i) the extrusion and growth of one dome followed by incremental collapse of portions of that dome, so that samples represent various regions of the same dome, and (ii) the extrusion and total collapse of one dome, followed by further extrusion and collapse, so that samples taken from subsequent lobes represent distinct, time-ordered, extrusive periods. The growth and collapse of the 2006 lava dome was somewhere between these two idealised end-member scenarios (Fig. 3.2), with on-going sustained extrusion at variable rates, punctuated by contemporaneous collapses of portions of the dome that could be sampled immediately after the eruption from the well characterized and pristine BAF deposits (Charbonnier and Gertisser, 2008). As such, the 2006 deposits at Merapi present an unparalleled opportunity to study a detailed collection of BAF samples from an exceptionally well documented and monitored recent dome-forming Merapi eruption. The detailed monitoring record (Ratdomopurbo *et al.*, 2013) and comprehensive field descriptions (Charbonnier and Gertisser, 2008) allow the samples to be related directly to the eruptive activity during the 2006 episode. The individual BAFs of the 2006 eruption emplaced within the Gendol valley, as well as the surrounding interfluvial overbank deposits, have previously been described, with successive overlapping flow lobes defined within the valley (Fig. 3.1; Charbonnier and Gertisser, 2008). The most common juvenile components are various types of grey scoria originating from either the exterior of the dome or vesiculated interior regions, as well as denser blocks which are often prismatically jointed and interpreted to originate in the interior of the dome (Charbonnier and Gertisser, 2008).

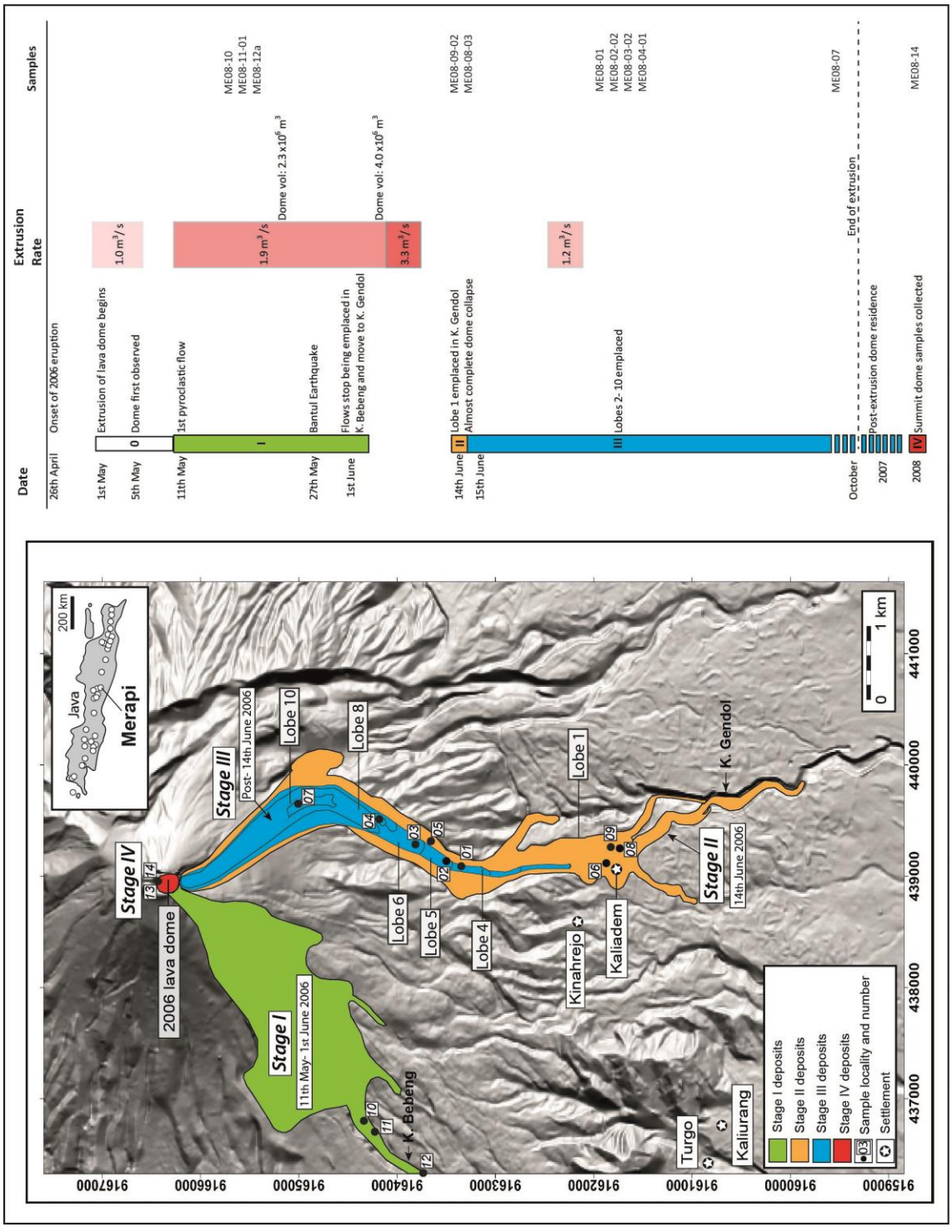

Fig. 3.1 Map of the 2006 eruption deposits (after Charbonnier and Gertisser, 2008), with deposits grouped into four stages based upon emplacement date. Stages are indicated by Roman numerals in the column at right. Sample localities are marked as black circles, with sample names abbreviated (*e.g.* sample "ME08-01" labelled as "01" on map). Inset shows a map of the island of Java, and Merapi's location, alongside other active volcanoes in Java (shown as open circles). A timeline of the 2006 eruptive events, extrusion rates (Ratdomopurbo *et al*., 2013; Pallister et al., 2013) and deposit stage emplacement times (Stages I–IV), with a summary of samples taken from those stages used in textural analysis, are also shown

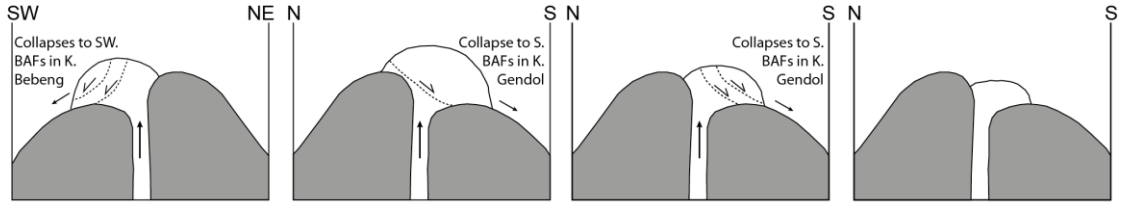

Stage I	Stage II	Stage III	Stage IV
Dome extrusion began on 1 May 2006 at a rate of 1.0 m^3 s^{-1}. The first dome collapse occurred on 11 May, with BAFs emplaced daily on SW flanks until 1 June. Continued endogenous dome growth during this period, with extrusion through the central vent at rates gradually increasing to 1.9 m^3 s^{-1}. Early collapses sampled the dome margins and later collapses more of the interior portions of the dome.	The largest collapse occurred on 14 June 2006, resulting in the destruction of most of the dome and BAFs emplaced in Kali Gendol to the S. The collapse was preceded by extrusion rates of 3.3 m^3 s^{-1}. Scoriaceous samples represent the exterior margins of the dome and dense clasts originate from the interior.	Dome extrusion, at an estimated rate of 1.2 m^3 s^{-1}, continued after 14 June, forming a new dome at the surface. Growth continued until September 2006, with continued emplacement of BAFs in Kali Gendol, to form overlapping lobes.	Extrusion ceased in September 2006. Stage IV scoria was sampled from the surface of the remnant dome at the summit during fieldwork in August 2008.

Fig. 3.2 Simplified sketch of the evolution of the 2006 lava dome relating to the origin of samples in Stages I–IV

. These will be referred to as "scoria" and "dense" components, respectively. For the purpose of this study, the 2006 deposits have been assigned to four eruption stages, based on the deposit map of Charbonnier and Gertisser (2008) and monitoring records (Ratdomopurbo *et al.,* 2013) (Fig 3.1). Stage I is defined as the period from the onset of BAF emplacement on 11 May until 1 June 2006. During this time the BAFs were channelled towards the southwest, such that our samples from Kali Bebeng (on the southwest flank) were emplaced during this time and represent material that collapsed from both the exterior and interior portions of the 2006 dome (Fig 3.2). Stage II occurred on 14 June, when the existing dome almost entirely collapsed and the largest flows travelled up to 7 km in Kali Gendol (Lobe 1 of Charbonnier and Gertisser, 2008). Stage III is the time-period between 15 June 2006 and 2007, when overlapping Lobes 2–10 were emplaced in Kali Gendol. Samples from this stage originate from the new dome that grew at slower rates post-14 June. Stage IV is the last stage and is represented by samples taken from the surface of un-collapsed remnants of the 2006 summit dome during fieldwork in August 2008 (Fig 3.2).

In addition to the 2006 samples (Appendix A), lava dome samples from the highly explosive 2010 eruption of Merapi have been analysed for comparison. The samples were collected from the widespread BAF deposits emplaced during the cataclysmic events on 5 November 2010 and consist of dark, glass-rich and dense lava fragments, interpreted to represent dome material that was extruded rapidly within a few days between the end of October 2010 and the dominantly explosive dome-collapse

events of 5 November that completely destroyed this dome (Surono *et al*., 2012; Charbonnier *et al*., 2013; Pallister *et al*., 2013, Komorowski *et al*., 2013).

3.3.2. Geochemical analysis

Whole-rock compositions of 2006 and 2010 samples were obtained from interior portions of fresh samples, which were washed in purified water in a sonic bath, dried overnight at > 100°C and powdered before fused glass discs and pressed powder pellets were prepared for major and trace element analysis by X-ray fluorescence (XRF) using a Bruker AXS S4 Pioneer instrument at the University of East Anglia. Loss on ignition (LOI) was carried out by heating ~ 1 g of sample powder in a furnace at 1050°C for 4 hours. Feldspar and groundmass glass compositions were determined using Cameca SX-100 electron microprobes at the University of Cambridge and The Open University. Mineral phases were analysed using a beam size of either 1 or 5 μm beam, a 15kV accelerating voltage and 10 nA beam current. Groundmass glass was analysed using a 5-10 μm beam size, using a 15kV accelerating voltage and 4–10 nA beam current. Na was always counted first to minimise alkali migration. Natural silicate minerals were used as primary standards to calibrate the instruments and as secondary, in-run standards to monitor precision and accuracy during mineral analyses. Rhyolitic glasses, including KE-12, a peralkaline obsidian from Kenya, were used as secondary, in-run standards to monitor glass analyses.

3.3.3. Textural analysis

All textural analyses of microlites were carried out using back-scattered electron (BSE) images of carbon-coated, polished thin sections, acquired with a JEOL JSM 5900 LV Scanning Electron Microscope (SEM) at the University of East Anglia, using an accelerating voltage of 20 kV and a working distance of 10 mm at 1500x magnification. Multiple BSE images were taken over continuous areas, sizes of which varied depending upon microlite density. The images were then digitally stitched together and feldspar microlite crystals were outlined manually using *Adobe Illustrator*. At least ~ 600 crystals were measured in each sample. The average atomic number of the

plagioclase microlites is close to that of the glass and consequently, the grey-scale values in the BSE images are similar for both so that automatic selection of the crystals was not possible. Digitised images were subsequently converted to high-resolution tiff files, from which crystal measurements could be made using *ImageJ (version 1.42q)*. Individual crystal area, mean crystal area, area % occupied by feldspar, the total area analysed and crystal dimensions (short and long axes) were measured, the latter using a best fit ellipsoid method. Microlite number density (N_A) was calculated by dividing the number of whole crystals in the analysed area by the area of groundmass. Errors were calculated by dividing each total area into two halves, vertically and horizontally, and calculating the standard deviation of the measurements to obtain the variability within the sample. The total area analysed is free of phenocrysts and vesicles and includes only groundmass.

Stereological conversion of 2D measurements to 3D data may be complicated as a consequence of random intersection through a 3D sample (Underwood, 1970; Royet, 1991). The intersection will seldom cut straight through the centre of a particle and therefore intersection sizes will be variable, even in a population containing one size of particles, an effect known as the cut-section effect. However, Higgins (1994; 2000) showed that crystal habits may be recognized from random 2D sections through known 3D shapes. For example, for a tablet shaped particle, the most common 2D intersection shape will be a rectangle with a width close to the smallest 3D dimension and the length closest to the intermediate 3D dimensions. For a particle with a prismatic habit, the most frequent intersection will be cut perpendicular to the longest axis, resulting in a square shape. Using this principle, 2D length and width data have been converted to 3D crystal habits using *CSDslice* (Morgan and Jerram, 2006) to produce a characteristic aspect ratio (short, *S*: intermediate, *I*: long axis, *L*) for each sample. This compares the 2D measurements of the random crystal intersections in the sample to a database of random sections through particles with 703 different known habits, providing a best match shape and an estimate of reliability, R^2. For a good statistical fit, at least 200-300 crystals should be measured and the R^2 value should be > 0.8 (Morgan and Jerram, 2006). As well as the cut-effect described above, there is a lower probability of intersecting a smaller crystal than a larger one, known as the intersection probability effect. A free software, *CSDCorrections (version 1.39)* (Higgins, 2000), which corrects for these stereological artefacts was utilized to produce crystal size distribution (CSD)

data and plots. An estimation of the rock fabric, crystal aspect ratio and crystal roundness must all be input before accurate CSD data can be generated. For these samples the rock fabric was massive and the crystal aspect ratio calculated with *CSDslice* was used. Crystal roundness was visually estimated to be 0.3 (on a scale from 0-1, where 0 is a euhedral block and 1 is an ellipsoid), although it has been suggested that the roundness factor does not strongly affect the calculations (Higgins and Roberge, 2007). As previously suggested (Higgins, 2000), the number of logarithmic size intervals, or bins, was set at 5 per decade so that each bin is 1.6 times the size of the next smallest bin, and any bins containing less than 5 crystals were removed from the CSD as they are not precise.

3.4. Results

3.4.1. Petrographic overview

Rocks from the 2006 eruption are porphyritic with phenocryst (~ 500–2000 μm in length), microphenocryst (~ 50–500 μm) and groundmass microlite (< 50 μm) crystal populations. Phenocrysts and microphenocrysts of plagioclase, clinopyroxene, orthopyroxene and amphibole are present, with titanomagnetite only occurring as microphenocrysts. The groundmass is composed of microlites of feldspar, clinopyroxene, orthopyroxene, titanomagnetite and glass, with no amphibole microlites present. Apatite is a common accessory phase and occurs as microlites and often as inclusions within pyroxene and plagioclase. Rare pyrrhotite has been noted as inclusions in amphibole.

Feldspar microlites in the 2006 products range in composition from $An_{60}Ab_{38}Or_2$ to $An_5Ab_{54}Or_{41}$ (Fig 3.3) and frequently have alkali-rich rims of anorthoclase and more K-rich alkali feldspar (sanidine) (Table 3.1). The abundance and mean size of the microlites vary between samples. Crystal morphology is typically euhedral and occasionally with swallow-tailed, hopper or skeletal textures (Fig 3.3).

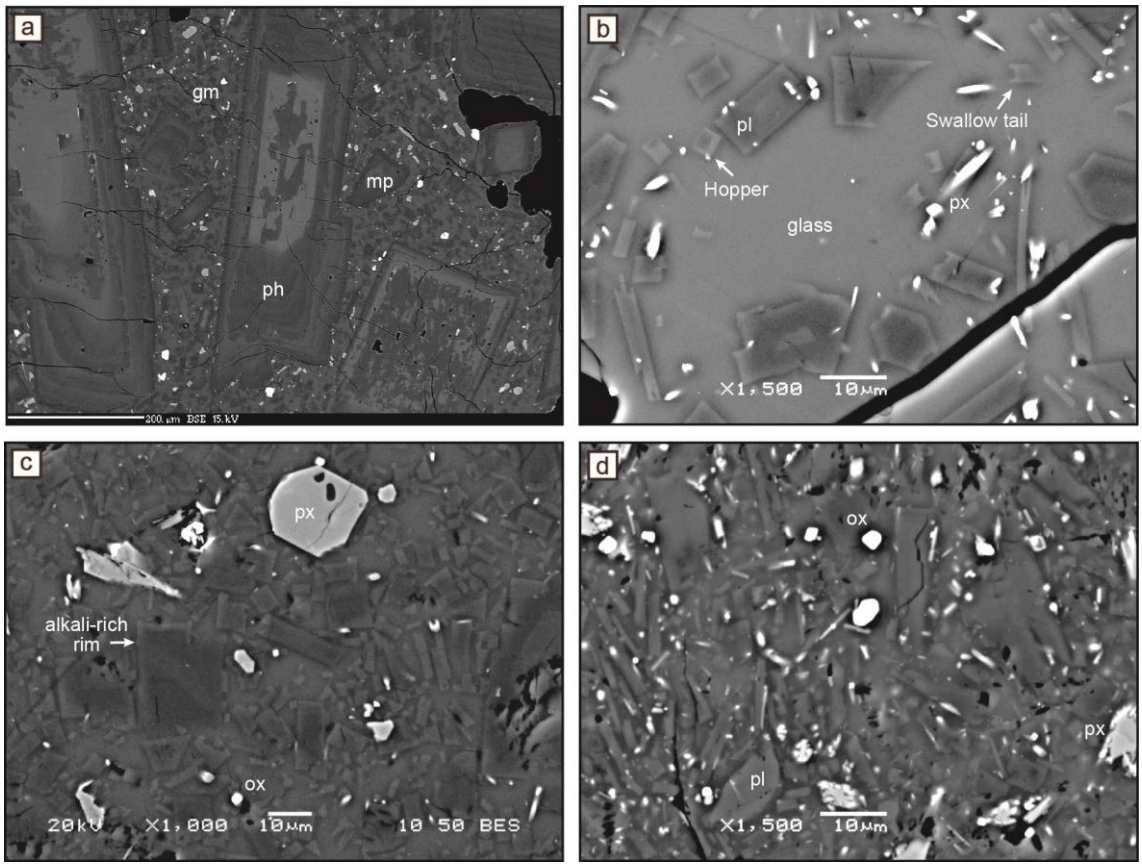

Fig. 3.3 Back-scattered electron (BSE) images of samples from the 2006 (a–c) and 2010 (d) eruption. (a) Representative sample (ME08-01) showing feldspar phenocryst (ph), microphenocryst (mp) and groundmass microlite (gm) crystal populations. (b) Groundmass feldspar microlites with hopper and swallowtail crystal shapes (sample ME08-01, Lobe 4; Stage III). (c) Groundmass feldspar microlites with paler, grey coloured alkali-rich rims (sample ME08-14, 2006 summit dome sampled in 2008; Stage IV). (d) Representative BSE image of the groundmass microlite textures of the rapidly growing lava 2010 lava dome (M11-15) prior to the 5 November paroxysm. Mineral abbreviations: pl = plagioclase; px = pyroxene; ox = Fe-Ti oxide

Amphibole is titanian magnesiohastingsite, following the classification of Leake *et al.* (1997), with the proportion of ferric iron calculated stoichiometrically on a 13eCNK basis (Fig 3.4). Amphibole is present as both phenocrysts and microphenocrysts, as well as within cumulate inclusions (Fig 3.4). Crystals are either homogenous or slightly zoned in composition, with rims containing either higher or lower concentrations of Al_2O_3 than the cores. Overall, Al_2O_3 ranges between 10.3–14.3 wt. % and Mg # between 0.57–0.68. Amphibole phenocrysts are typically surrounded by breakdown rims composed of small crystals of plagioclase, pyroxene and magnetite, although reaction rims are not present bordering all crystals. The extent of breakdown is

Table 3.1 Representative feldspar microlite compositions of samples from Stages I to IV of the 2006 eruption and representative dome samples from the 2010 eruption. Localities: KB = Kali Bebeng; L = Lobe (1, 4, 6, 8, 10); SD = 2006 summit dome (sampled in 2008); KG = Kali Gendol. Lithology types: S = 2006 scoria, D = dense dome blocks. FeO* = All iron reported as FeO. All analyses are in Appendix D.

Stage	Locality	Lithology	Sample	SiO_2	Al_2O_3	FeO*	CaO	Na_2O	K_2O	Total	Ab (mol%)	An (mol%)	Or (mol%)
I	KB	S	ME08-10	64.42	21.48	0.60	3.79	6.43	3.27	99.99	60.2	19.6	20.2
I	KB	S	ME08-10	58.31	25.88	0.58	8.25	6.03	0.95	99.99	53.7	40.7	5.6
II	L1	S	ME08-09-02	56.68	26.39	1.07	8.76	5.84	0.64	99.38	52.6	43.6	3.8
II	L1	S	ME08-09-02	59.38	25.18	0.76	7.09	6.56	1.25	100.22	58.0	34.7	7.3
II	L1	D	ME08-08-03	60.32	23.81	0.71	6.44	6.88	1.79	99.95	59.2	30.6	10.1
II	L1	D	ME08-08-03	56.32	27.25	0.51	9.68	5.74	0.61	100.11	49.9	46.6	3.5
III	L4	S	ME08-01	57.41	26.44	0.71	8.70	6.20	0.83	100.29	53.7	41.6	4.7
III	L4	S	ME08-01	60.33	24.22	0.61	6.16	7.07	1.40	99.80	62.0	29.9	8.1
III	L6	S	ME08-03-02	58.23	25.57	0.51	7.96	6.43	1.01	99.72	55.9	38.3	5.8
III	L8	S	ME08-04-01	63.13	21.45	0.76	4.06	7.20	2.64	99.25	64.4	20.1	15.5
III	L8	S	ME08-04-01	59.60	25.04	0.62	7.50	6.26	1.29	100.30	55.6	36.8	7.5
III	L10	S	ME08-07	59.73	24.63	0.52	6.46	7.14	1.21	99.68	62.1	31.0	6.9
III	L10	S	ME08-07	61.10	23.52	0.50	5.51	7.30	2.01	99.94	62.6	26.1	11.3
IV	SD	S	ME08-14	54.51	27.88	0.58	11.02	4.87	0.39	99.26	43.4	54.3	2.3
IV	SD	S	ME08-14	64.28	21.02	0.51	3.39	7.40	3.09	99.67	65.5	16.6	18.0
2006 (all)	*KB*	*S*	*Max. An (mol%) - ME08-10*	*52.42*	*29.52*	*0.59*	*12.12*	*4.19*	*0.33*	*99.17*	*37.7*	*60.3*	*1.9*
2006 (all)	*L6*	*S*	*Max. Or (mol%) - ME08-03-02*	*67.03*	*18.64*	*0.68*	*0.99*	*6.08*	*7.08*	*100.49*	*53.9*	*4.8*	*41.3*
2010	KG	D	M11-07	53.19	28.90	0.74	12.15	4.61	0.31	99.90	40.0	58.2	1.7
2010	KG	D	M11-07	51.52	30.21	0.92	13.69	3.74	0.23	100.31	32.6	66.1	1.3
2010	KG	D	M11-07	51.73	30.45	0.79	13.72	3.66	0.23	100.58	32.1	66.6	1.3
2010	KG	D	M11-27-2	49.99	30.67	0.79	14.38	3.26	0.21	99.29	28.7	70.1	1.2
2010	KG	D	DD10	51.56	30.68	0.69	13.69	3.66	0.18	100.46	32.3	66.7	1.0
2010	KG	D	DD10	51.73	30.40	0.82	13.62	3.68	0.23	100.48	32.4	66.2	1.3
2010	KG	D	DD10	57.59	27.04	0.50	9.01	6.22	0.53	100.88	53.9	43.1	3.0
2010	KG	D	DD10	51.46	30.36	0.83	13.52	3.63	0.24	100.04	32.2	66.4	1.4
2010	KG	D	DD10	51.67	30.30	0.87	13.55	3.61	0.22	100.21	32.1	66.6	1.3
2010	KG	D	DD10	51.72	29.36	0.78	12.62	3.92	0.28	98.68	35.4	63.0	1.7

variable between samples, with amphiboles in dense material taken from 14 June 2006 (sample ME08-08-03) showing minimal breakdown textures compared to all other 2006 samples (Fig 3.4).

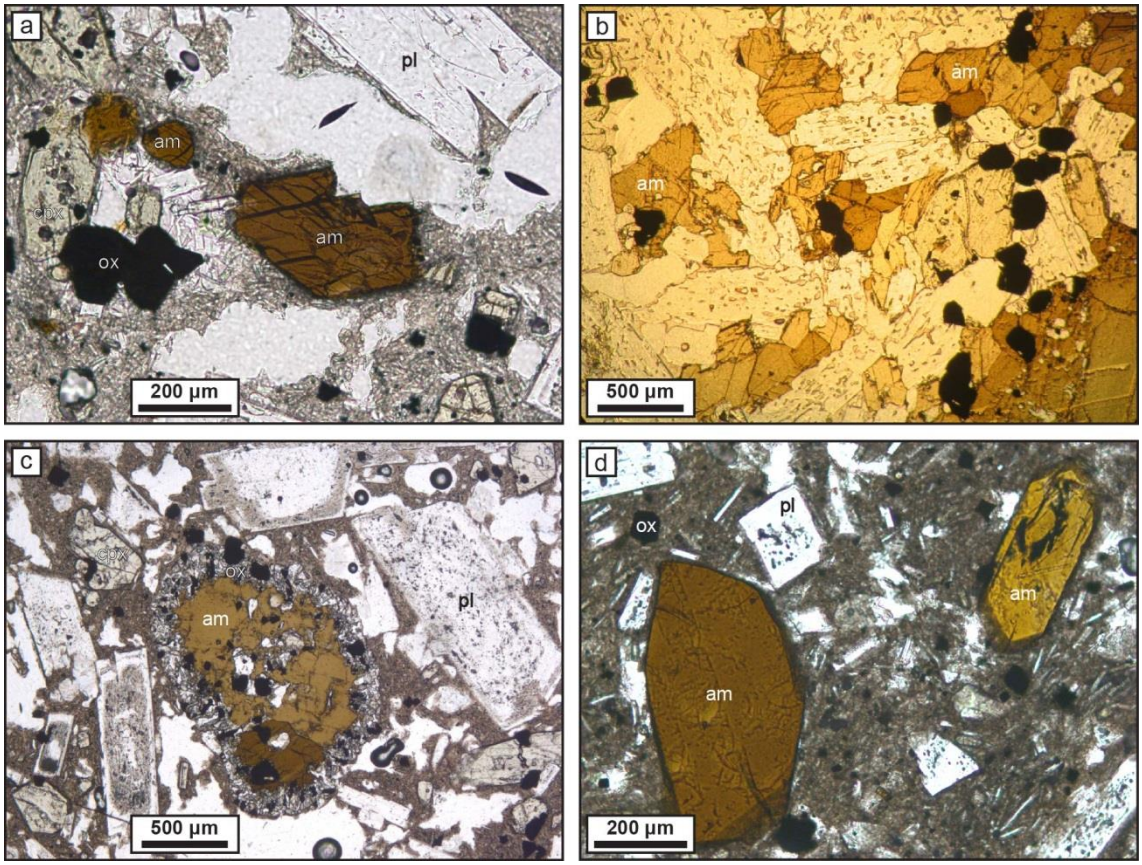

Fig. 3.4 Photomicrographs (taken in plane polarized light) of representative amphibole textures in the 2006 and 2010 eruption products of Merapi. (a) Amphibole phenocrysts with very thin breakdown rims consisting of plagioclase, clinopyroxene and Fe-Ti-oxide in a dense dome sample taken from Lobe 1 emplaced on 14 June 2006 (Stage II). (b) Fresh amphibole within an amphibole- and plagioclase-rich cumulate inclusion found within Lobe 1 from 14 June 2006 (Stage II). (c) Amphibole surrounded by a reaction or breakdown rim composed of smaller crystals of plagioclase, clinopyroxene and Fe-Ti-oxide in a scoriaceous samples taken from Lobe 8 emplaced after 14 June 2006 (Stage III). (d) Fresh amphibole phenocrysts in a dense dome sample from the rapidly growing lava dome prior to the 5 November paroxysm in 2010. Mineral abbreviations: am = amphibole; pl = plagioclase; cpx = clinopyroxene; ox = Fe-Ti oxide

Pyroxene crystals are euhedral to subhedral and in some samples the microlites may occasionally display swallow-tail or hopper textures. Phenocrysts and microphenocrysts frequently host melt inclusions and abundant inclusions of magnetite. Clinopyroxene crystals are classed as augite and less frequently extending into the range of diopside (Wo_{39-47}, En_{35-45}, Fs_{13-17}). Orthopyroxene is more commonly present as microphenocrysts and microlites and ranges between En_{60-68}, Fs_{28-36}, Wo_{1-8}, classified as enstatite and occasionally pigeonite in the scheme of Morimoto (1988) (Fig. 3.5).

Titanomagnetite crystals are anhedral or irregularly shaped, ranging in ulvöspinel content from 22–62 mol.% (Fig 3.5), and are often exsolved to variable extents, showing trellis-type exsolution, consisting of ilmenite lamellae parallel to the {111} planes of the titanomagnetite host (Buddington and Lindsley, 1964; Haggerty, 1993).

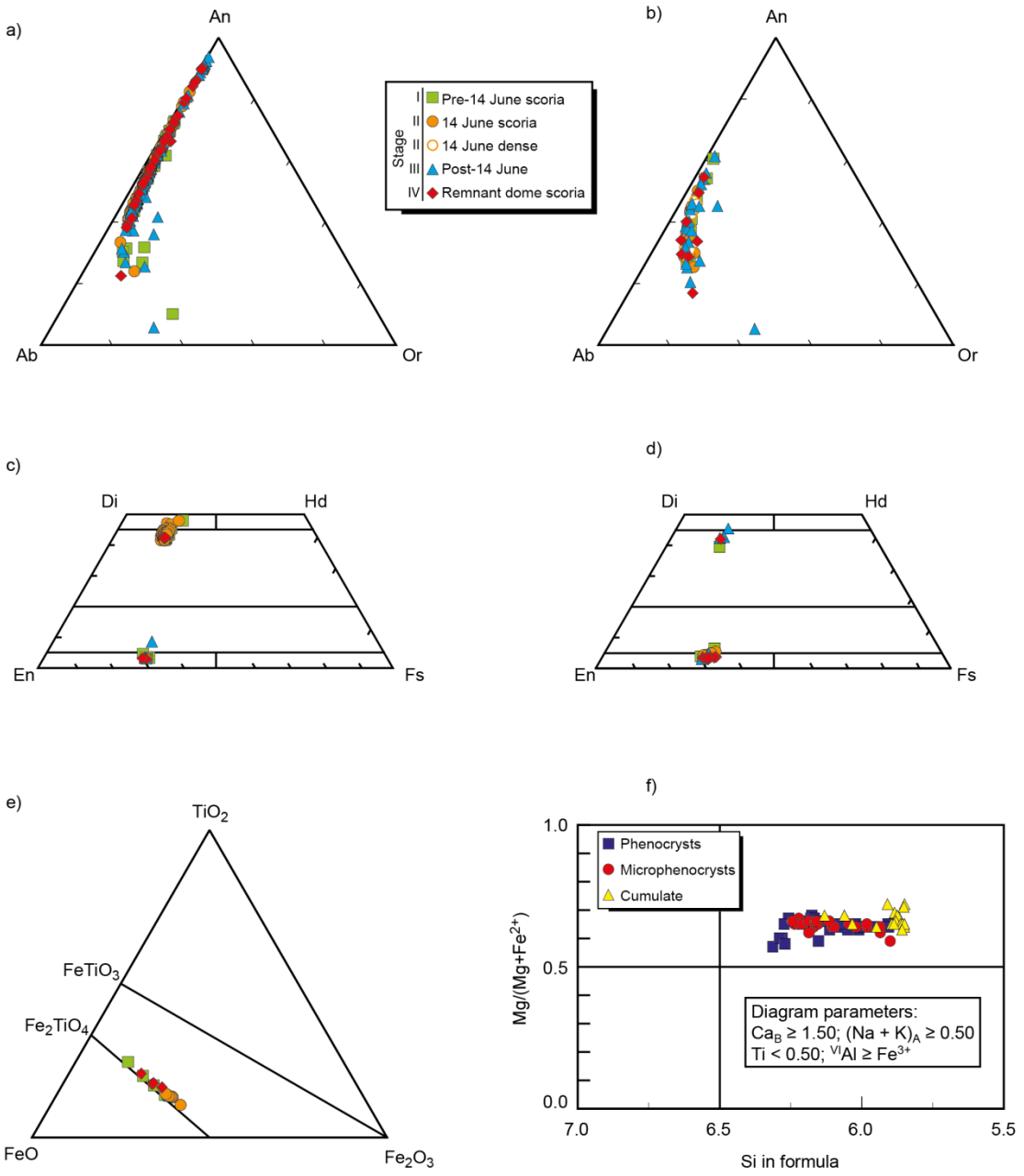

Fig. 3.5 Mineral compositions of the 2006 eruptive products a) feldspar phenocrysts and microphenocrysts, b) feldspar microlites, c) pyroxene phenocrysts and microphenocrysts, d) pyroxene microlites, e) Fe-Ti oxides microphenocryst and microlites, f) amphibole phenocrysts, microphenocrysts and those from cumulate inclusions within 2006 lava. See Appendix D for data

3.4.2. Whole rock geochemistry and groundmass glass compositions

The bulk compositions of the 2006 rocks are typical of, and similar to, products formed by other recent dome eruptions at Merapi (del Marmol, 1989; Boudon *et al.*, 1993; Camus *et al.*, 2000; Andreastuti *et al.*, 2000; Gertisser and Keller, 2003a, 2003b; Gertisser *et al.*, 2012a). They lie within a narrow compositional range (Table 3.2) and are classed as high-K basaltic andesite in the scheme of Le Maitre *et al.* (2002). SiO_2 values range from 55.2–56.1 wt. % and total alkalis range between 6.0 and 6.2 wt. % (Fig 3.6). With increasing SiO_2, Na_2O and K_2O contents also increase, whereas MgO, CaO, TiO_2 and $Fe_2O_3^*$ contents decrease. Al_2O_3 and P_2O_5 show no systematic correlation with SiO_2 concentrations (Fig 3.6). Samples taken from the remnant 2006 summit dome in 2008 are the most SiO_2 enriched (55.8–56.1 wt. %; Fig. 3.6) and plot outside the trends in MgO, TiO_2, $Fe_2O_3^*$ and Al_2O_3 against SiO_2 defined by the other samples. Dome samples from the 2010 eruption (Table 3.2) lie within a similar compositional range (54.7–55.6 wt.% SiO_2; Fig, 3.6). The bulk rock (magma) compositions at Merapi are similar for long periods of time (Fig 3.6h) and the ascent variations within the 2006 eruption and the difference between effusive eruptions (as in 2006) and the more explosive 2010 events cannot be directly related to different magma compositions. All whole rock data is listed in Appendix C.

Although bulk rock compositions are basaltic andesite, the groundmass glass is rhyodacite to rhyolite (69.9–75.3 wt. % SiO_2; Table 3.3), consistent with the high abundance of crystals in these samples. SiO_2 is positively correlated with total groundmass crystallinity. CaO, Na_2O, Al_2O_3, FeO^* and P_2O_5 all display negative trends with crystallinity. MgO and K_2O contents do not show any systematic variation with increasing crystallinity and TiO_2 displays an overall negative trend (Fig 3.7). The variation in glass composition for each sample and at each specific groundmass crystallinity suggests that glass composition is affected by local, rather than global equilibrium, with the glass compositions varying locally as a function of small-scale variations in crystallinity.

Table 3.2 Whole rock major and trace element compositions (XRF) of samples from Stages I to IV of the 2006 eruption and representative dome samples from the 2010 eruption. Localities: KB = Kali Bebeng; L = Lobe (1, 4, 5, 6, 8, 10); SD = 2006 summit dome (sampled in 2008); KG = Kali Gendol. Lithology types: S = 2006 scoria, D = Fe_2O_3.

Stage	I	I	I	I	I	II	II	II	II	II	II	II	II	III	III	III
Locality	KB	KB	KB	KB	KB	L1	L1	L1	L1	L1	L1	L1	L1	L4	L5	L5
Lithology	S	S	S	S	D	S	S	S	S	S	S	S	D	S	S	S
Sample	ME08-10	ME08-11-01	ME08-11-02	ME08-11-03	ME08-12	ME08-05-01	ME08-05-02	ME08-06	ME08-09-02	ME08-09-03	ME08-09-04	ME08-09-05	ME08-08-03	ME08-01	ME08-02-01	ME08-02-02
Major elements (wt%)																
SiO_2	55.18	54.90	54.85	55.05	55.78	55.27	55.31	55.75	55.27	55.11	54.84	55.20	55.54	55.16	55.08	55.42
TiO_2	0.72	0.74	0.72	0.72	0.71	0.72	0.71	0.71	0.71	0.71	0.73	0.71	0.70	0.71	0.70	0.72
Al_2O_3	18.98	18.96	18.89	19.03	19.24	19.08	19.04	19.36	19.03	18.94	18.90	19.04	19.10	19.06	19.05	19.05
Fe_2O_3*	7.58	7.75	7.67	7.51	7.45	7.55	7.44	7.49	7.44	7.51	7.69	7.38	7.38	7.48	7.32	7.57
MnO	0.19	0.20	0.20	0.19	0.19	0.19	0.19	0.19	0.19	0.19	0.20	0.19	0.19	0.19	0.19	0.19
MgO	2.39	2.46	2.45	2.39	2.37	2.39	2.35	2.36	2.32	2.38	2.42	2.32	2.28	2.36	2.27	2.38
CaO	8.06	8.10	8.12	8.07	7.94	8.01	7.97	8.10	7.98	8.02	8.03	7.95	7.89	8.00	7.92	8.05
Na_2O	3.88	3.90	3.86	3.88	3.89	3.91	3.92	3.95	3.90	3.86	3.85	3.95	3.97	3.90	3.92	3.92
K_2O	2.15	2.14	2.13	2.14	2.18	2.16	2.17	2.16	2.17	2.16	2.13	2.18	2.19	2.16	2.17	2.15
P_2O_5	0.31	0.32	0.30	0.30	0.30	0.30	0.30	0.31	0.31	0.31	0.31	0.31	0.30	0.31	0.30	0.30
LOI	-0.03	-0.06	-0.01	0.08	0.02	-0.10	-0.03	-0.04	0.07	0.08	0.08	0.06	-0.10	0.08	0.06	0.01
Total	99.41	99.41	99.18	99.36	100.07	99.48	99.37	100.34	99.39	99.27	99.18	99.29	99.44	99.41	98.98	99.76
Trace elements (ppm)																
Sc	10	11	12	11	10	9	11	11	11	13	11	<10	12	11	10	11
V	139	149	148	148	135	137	140	120	141	144	155	139	141	132	136	139
Cr	<10	<10	<10	<10	<10	<10	<10	<10	<10	<10	<10	<10	<10	<10	<10	<10
Ni	<10	<10	<10	<10	<10	<10	<10	<10	<10	<10	<10	<10	<10	<10	<10	<10
Rb	48	49	48	49	49	49	48	47	48	48	48	48	50	49	49	48
Sr	547	544	540	544	547	544	544	557	543	539	538	545	543	550	547	540
Ba	503	495	498	499	507	496	495	523	496	493	485	505	511	507	499	495
Pb	22	23	22	23	23	24	23	22	22	23	24	24	23	22	24	22
Th	<10	<10	<10	<10	<10	<10	<10	10	<10	<10	<10	<10	<10	<10	<10	<10
Zr	106	106	105	106	106	107	106	106	108	107	106	107	109	107	107	106
Nb	<10	<10	<10	<10	<10	<10	<10	<10	<10	<10	<10	<10	<10	<10	<10	<10
Y	24	24	23	23	23	23	24	23	24	24	23	24	24	24	24	24

Table 3.2. Continued.

Stage	III	III	III	III	III	III	IV	IV	IV	IV	2010	2010	2010	2010	2010
Locality	L6	L6	L8	L8	L8	L10	SD	SD	SD	SD	KG	KG	KG	KG	KG
Lithology	S	S	S	S	S	S	S	S	S	S	D	D	D	D	D
Sample	ME08-03-01	ME08-03-02	ME08-04-01	ME08-04-02	ME08-04-03	ME08-07	ME08-13-01	ME08-13-02	ME08-13-03	ME08-14	M11-01	M11-04	M11-12	M11-15	M11-27
Major elements (wt%)															
SiO_2	55.38	55.15	55.27	55.18	55.40	55.20	55.86	55.32	55.08	55.47	54.04	55.40	54.77	54.34	54.80
TiO_2	0.71	0.72	0.72	0.72	0.71	0.72	0.72	0.71	0.71	0.70	0.74	0.73	0.74	0.74	0.72
Al_2O_3	19.20	18.85	19.04	18.90	19.08	19.06	18.78	18.84	18.62	19.01	19.14	19.12	19.13	19.19	19.06
Fe_2O_3*	7.42	7.63	7.51	7.56	7.48	7.48	7.48	7.39	7.49	7.41	7.73	7.65	7.79	7.86	7.56
MnO	0.19	0.20	0.19	0.20	0.19	0.19	0.19	0.19	0.19	0.19	0.19	0.19	0.20	0.19	0.19
MgO	2.32	2.45	2.39	2.41	2.37	2.36	2.35	2.30	2.36	2.30	2.49	2.34	2.42	2.46	2.34
CaO	7.99	8.01	8.06	8.03	8.03	8.01	7.76	7.67	7.74	7.85	8.22	7.96	8.13	8.20	7.90
Na_2O	3.95	3.88	3.88	3.89	3.94	3.91	3.96	3.92	3.84	3.92	3.84	4.00	3.80	3.70	3.85
K_2O	2.17	2.15	2.15	2.15	2.15	2.16	2.21	2.16	2.15	2.19	2.05	2.17	2.08	2.09	2.13
P_2O_5	0.30	0.32	0.31	0.31	0.31	0.31	0.26	0.26	0.29	0.33	0.31	0.32	0.32	0.32	0.32
LOI	-0.11	0.08	-0.06	-0.07	-0.09	-0.05	0.04	0.10	0.11	0.00	-0.14	-0.06	-0.15	-0.19	-0.06
Total	99.52	99.44	99.46	99.28	99.57	99.35	99.61	98.86	98.58	99.37	98.61	99.82	99.23	98.90	98.81
Trace elements (ppm)															
Sc	10	10	10	10	11	12	10	12	10	13	12	11	13	11	10
V	136	138	140	136	137	136	140	147	148	141	159	146	153	159	145
Cr	<10	<10	<10	<10	<10	<10	<10	<10	<10	<10	<10	<10	<10	<10	<10
Ni	<10	<10	<10	<10	<10	<10	<10	<10	<10	<10	<10	<10	<10	<10	<10
Rb	49	49	49	48	49	49	50	49	50	48	45	48	46	47	48
Sr	550	545	542	544	549	548	533	529	528	543	540	540	540	547	542
Ba	515	512	501	504	503	501	511	504	489	504	480	496	476	483	487
Pb	22	20	23	23	23	22	<20	24	30	23	23	24	22	21	23
Th	<10	10	<10	<10	<10	<10	<10	<10	<10	10	<10	<10	<10	10	9
Zr	107	107	107	106	106	107	109	107	108	109	106	110	107	105	109
Nb	<10	<10	<10	<10	<10	<10	<10	<10	<10	<10	<10	<10	<10	<10	<10
Y	24	24	23	23	23	24	23	22	23	24	23	25	24	24	23

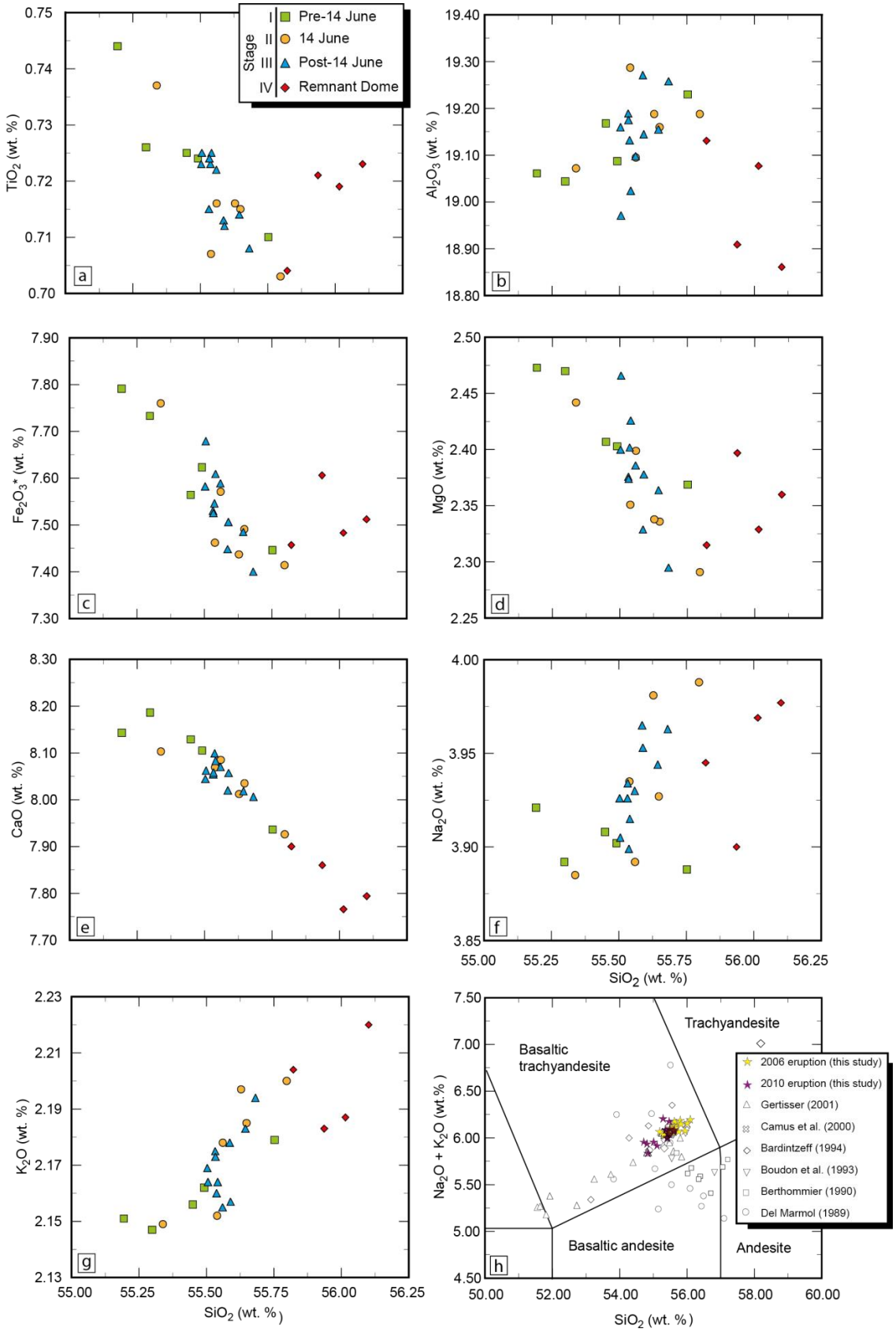

Fig. 3.6 (a–g) Bulk rock major element variation diagrams of 2006 products. (h) Total alkali vs. silica (TAS) diagram of 2006 products and the 2010 lava dome, plotted alongside previously published data of other recent dome-forming eruptions at Merapi. All analyses are normalized to 100 wt. %, free of volatiles

Table 3.3 Groundmass glass compositions of 2006 eruptive products. Localities: KB = Kali Bebeng; L = Lobe (1, 4, 6, 8, 10); SD = 2006 summit dome (sampled in 2008); Lithology types: S = 2006 scoria, D = dense dome blocks. FeO* = All iron reported as FeO*.

Stage	Locality	Lithology	Sample	SiO_2	TiO_2	Al_2O_3	FeO*	MnO	MgO	CaO	Na_2O	K_2O	P_2O_5	Total
I	KB	S	ME08-10	74.70	0.43	12.74	2.13	0.08	0.18	0.44	3.59	6.77	0.05	101.11
				73.82	0.48	12.72	2.21	0.12	0.22	0.44	3.95	6.55	0.06	100.57
				74.05	0.46	12.30	2.29	0.02	0.23	0.49	4.01	6.40	0.05	100.29
				73.91	0.49	12.40	2.48	0.08	0.23	0.27	3.78	6.40	0.08	100.12
				74.79	0.47	12.75	2.45	0.09	0.18	0.56	3.71	6.52	0.09	101.60
				75.32	0.42	12.70	2.06	0.09	0.14	0.42	3.39	6.58	0.06	101.17
				74.44	0.43	13.36	1.50	0.02	0.12	0.35	3.68	6.56	0.06	100.50
II	L1	S	ME08-09-02	72.14	0.54	13.49	2.51	0.08	0.21	0.68	3.98	6.65	0.10	100.38
				71.80	0.58	13.43	2.69	0.10	0.21	0.66	3.89	6.58	0.11	100.04
				72.22	0.53	13.65	2.50	0.15	0.20	0.65	4.03	6.49	0.11	100.54
				72.26	0.57	13.55	2.68	0.12	0.20	0.71	4.00	6.38	0.11	100.57
				72.27	0.58	13.48	2.47	0.13	0.22	0.65	3.83	6.37	0.14	100.13
				72.23	0.57	14.16	2.72	0.06	0.20	0.69	4.10	6.49	0.09	101.31
				72.46	0.62	13.42	2.37	0.18	0.24	0.66	3.97	6.41	0.13	100.46
				72.29	0.57	13.54	2.60	0.07	0.24	0.61	4.10	6.09	0.13	100.24
				71.02	0.57	13.86	2.67	0.11	0.22	0.67	4.18	6.34	0.09	99.72
II	L1	D	ME08-08-03	72.69	0.46	13.50	2.06	0.07	0.21	0.60	3.72	6.50	0.07	99.89
				73.70	0.46	13.64	2.09	0.14	0.25	0.62	3.98	6.54	0.04	101.45
				74.11	0.49	12.97	2.36	0.15	0.25	0.59	3.65	6.25	0.11	100.94
				74.29	0.44	13.24	2.12	0.08	0.17	0.60	3.77	6.49	0.11	101.31
				74.05	0.52	12.80	2.51	0.09	0.30	0.59	3.54	6.48	0.08	100.96
				73.74	0.46	13.32	2.22	0.08	0.20	0.63	3.70	6.35	0.05	100.76
III	L4	S	ME08-01	70.54	0.45	14.48	2.53	0.03	0.23	0.81	4.50	6.21	0.12	99.92
				69.87	0.55	14.55	2.76	0.14	0.30	0.82	4.44	6.28	0.13	99.84
				70.72	0.44	14.84	2.59	0.19	0.33	0.77	4.49	6.17	0.12	100.64
				70.12	0.50	14.82	2.96	0.10	0.26	0.81	4.32	6.48	0.11	100.47
				70.10	0.47	14.41	2.49	0.13	0.25	0.82	4.40	6.37	0.13	99.58
				70.16	0.51	14.36	2.40	0.09	0.22	0.76	4.40	6.32	0.11	99.32
				70.39	0.50	14.53	2.59	0.15	0.21	0.86	4.32	6.31	0.11	99.98
				70.73	0.54	14.06	2.44	0.12	0.22	0.70	4.42	6.06	0.10	99.40
				70.88	0.51	14.37	2.79	0.15	0.22	0.79	4.30	6.36	0.15	100.51
				70.31	0.49	14.95	2.41	0.08	0.22	0.81	4.23	6.62	0.09	100.21
				70.74	0.52	14.69	2.51	0.19	0.17	0.81	4.42	6.40	0.10	100.54
III	L6	S	ME08-03-02	74.62	0.46	12.53	2.75	0.13	0.25	0.53	3.19	6.36	0.02	100.84
				73.61	0.45	12.90	2.40	0.12	0.17	0.60	3.68	6.39	0.04	100.35
				74.40	0.51	12.37	2.38	0.14	0.13	0.37	3.67	6.34	0.08	100.39
				74.78	0.45	12.62	2.49	0.09	0.28	0.40	3.59	6.43	0.05	101.19
				74.22	0.44	12.64	2.39	0.10	0.25	0.57	3.54	6.41	0.08	100.63
				74.46	0.42	12.65	2.28	0.07	0.25	0.60	3.75	6.25	0.05	100.78
				74.92	0.48	12.49	2.32	0.11	0.21	0.60	3.51	6.40	0.09	101.12
				74.66	0.48	12.71	2.06	0.07	0.34	0.49	3.46	6.36	0.07	100.70
				74.33	0.49	12.30	2.42	0.17	0.23	0.59	3.63	6.20	0.05	100.40
				74.25	0.46	12.50	2.47	0.04	0.28	0.52	3.64	6.42	0.02	100.61
III	L8	S	ME08-04-01	72.57	0.58	13.60	2.57	0.04	0.20	0.58	4.25	6.34	0.09	100.83
				72.78	0.52	13.33	2.53	0.08	0.25	0.63	3.97	6.35	0.12	100.56
				71.70	0.60	13.58	2.60	0.15	0.25	0.53	4.14	6.38	0.10	100.03
				72.76	0.54	13.84	2.80	0.10	0.28	0.90	3.57	6.12	0.13	101.04
				72.79	0.48	13.41	2.67	0.21	0.24	0.62	4.04	6.46	0.13	101.05
				72.72	0.50	13.74	2.70	0.02	0.24	0.57	3.90	6.48	0.12	100.99
				71.79	0.45	14.71	2.35	0.13	0.22	0.86	4.39	5.85	0.07	100.82
				73.05	0.48	13.97	2.53	0.00	0.20	0.59	4.42	6.63	0.11	101.97
				72.37	0.50	13.42	2.56	0.13	0.23	0.64	4.09	6.56	0.10	100.61
III	L10	S	ME08-07	72.88	0.49	13.46	2.35	0.09	0.20	0.64	4.14	6.73	0.08	101.06
				72.28	0.47	13.93	2.25	0.15	0.30	0.55	4.14	6.62	0.07	100.77
				72.17	0.54	13.53	2.51	0.09	0.24	0.58	3.87	6.53	0.10	100.16
				72.24	0.46	13.40	2.36	0.16	0.25	0.54	3.98	6.35	0.07	99.82
				73.23	0.51	13.78	2.23	0.09	0.23	0.54	3.99	6.51	0.08	101.20
				73.28	0.49	13.59	2.20	0.13	0.28	0.52	4.13	6.42	0.09	101.10
				72.87	0.45	13.60	2.41	0.11	0.24	0.56	4.07	6.50	0.12	100.92
				73.36	0.49	13.61	2.40	0.20	0.29	0.59	4.04	6.50	0.10	101.58
				73.35	0.48	13.47	2.44	0.06	0.20	0.56	3.84	6.67	0.08	101.14
				72.35	0.49	13.38	2.38	0.09	0.20	0.59	4.08	6.64	0.13	100.35
IV	SD	S	ME08-14	75.30	0.45	12.09	2.19	0.11	0.10	0.42	3.52	6.24	0.10	100.51
				74.65	0.48	13.46	1.70	0.04	0.09	0.48	4.12	5.91	0.09	101.02
				73.10	0.40	13.94	1.58	0.04	0.11	0.38	4.07	7.02	0.08	100.71

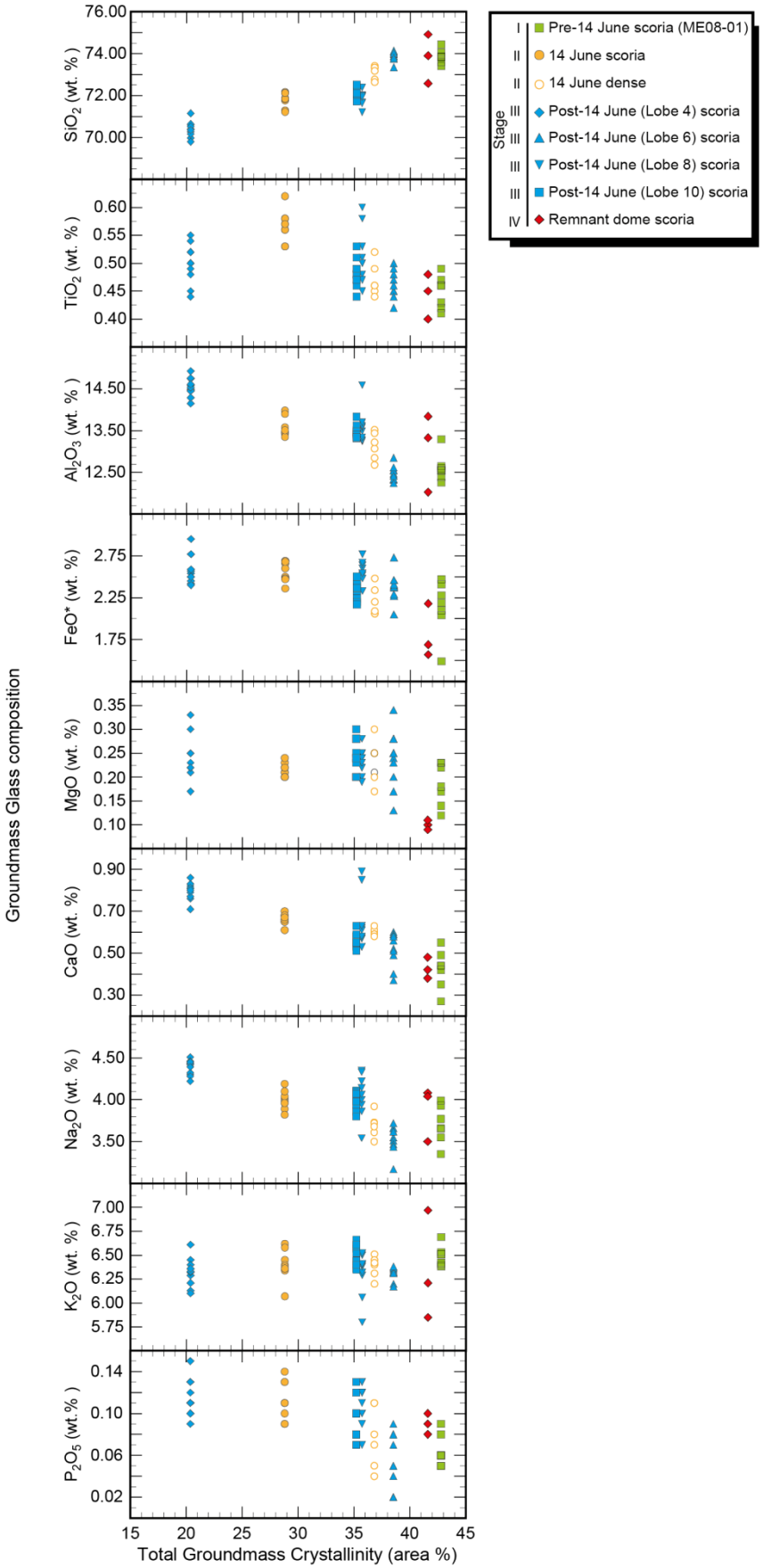

Fig. 3.7 Groundmass glass compositions plotted against the total groundmass crystallinity (area %) measured in various 2006 samples. This crystallinity measurement includes all microlite mineral phases present (i.e. feldspar, clinopyroxene, orthopyroxene, Fe-Ti oxide and accessory apatite)

3.4.3. Textural analysis of feldspar microlites

The groundmass textures of the 2006 samples are temporally variable, with differences observed between samples collected from separate stages of the eruption. Textural data are summarised in Table 3.4. Visual examination of BSE images reveals that feldspar microlites, which are the most abundant groundmass phase, vary in their size, morphology and abundance between samples (Fig 3.8). Samples generally possess either many smaller (< 10 μm) feldspar microlites or fewer larger (> 10 μm) microlites, depending upon which stage of the eruption they represent.

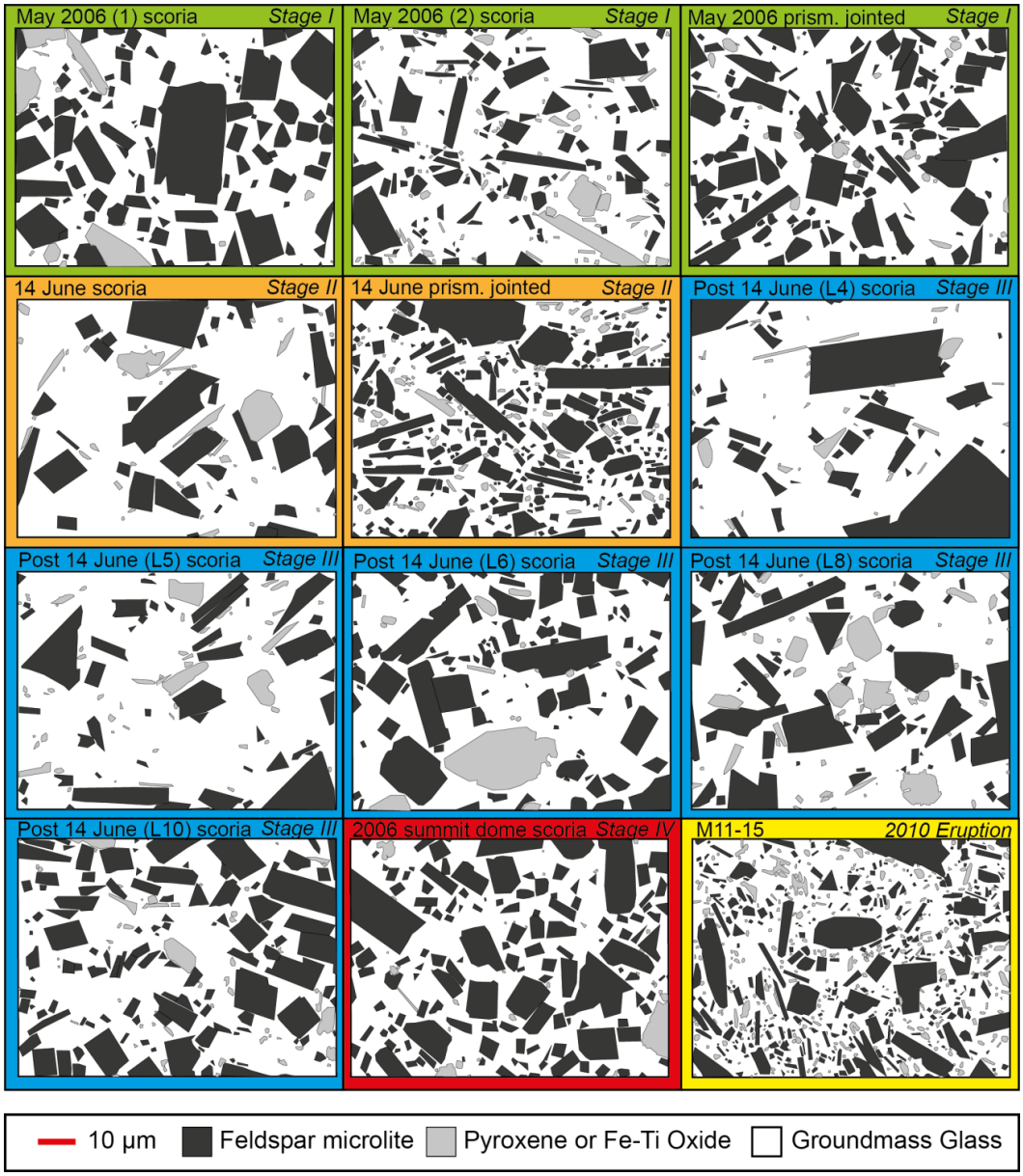

Fig. 3.8 Representative images of groundmass microlites used in the textural analysis of eleven samples from the 2006 eruption and one sample from the 2010 eruption. Images are digitised from BSE images; black areas represent feldspar microlites, grey areas represent pyroxene and Fe-Ti oxide microlites and white area indicates groundmass glass. See Appendix G for full analyses

Table 3.4 Textural variation of feldspar microlites in samples from Stages I to IV of the 2006 eruption and in a representative dome sample from the 2010 eruption. Localities: KB = Kali Bebeng; L = Lobe (1, 4, 5, 6, 8, 10); SD = 2006 summit dome (sampled in 2008); KG = Kali Gendol. Lithology types: S = 2006 scoria, D = dense dome blocks. *n** denotes number of crystals measured in each sample. Numbers in brackets indicate standard errors of measurements of N_A, area % feldspar and mean crystal area.

Stage	Locality	Lithology	Sample	2D areal measurements							3D volume measurements		
				*n**	Total area (μm^2)	N_A (mm^{-2})	Area % feldspar	φ	Mean crystal area (μm^2)	Gm. glass (area %)	Aspect Ratio / R^2	No. density by volume	Vol. from inter area
I	KB	S	ME08-10	614	26985	22753 (1158)	38.5 (2.4)	0.40	16.9 (1.1)	57.23	1.00:1.25:2.20 / 0.8350	4870000	38.51
I	KB	S	ME08-11-01	640	39257	16303 (644)	20.6 (0.6)	0.22	12.7 (0.6)	74.36	1.00:1.50:5.50 / 0.6793	2230000	20.36
I	KB	D	ME08-12	603	31755	18989 (1244)	34.2 (2.9)	0.36	18.2 (2.6)	62.55	1.00:1.40:3.40 / 0.7920	3420000	34.37
II	L1	S	ME08-09-02	602	89845	6700 (292)	26.2 (2.7)	0.27	39.1 (4.4)	71.20	1.00:1.50:5.00 / 0.7648	515000	26.19
II	L1	D	ME08-08-03	615	13039	47166 (3972)	32.5 (2.4)	0.48	6.9 (1.0)	63.19	1.00:1.15:1.60 / 0.7593	17300000	32.87
III	L4	S	ME08-01	635	88317	7190 (362)	18.9 (2.9)	0.22	24.8 (4.9)	79.63	1.00:1.50:4.50 / 0.7728	1030000	18.01
III	L5	S	ME08-02-02	648	86861	7460 (428)	21.9 (3.8)	0.23	29.3 (6.6)	74.27	1.00:1.40:4.00 / 0.8682	990000	21.87
III	L6	S	ME08-03-02	625	40636	15380 (426)	33.8 (3.6)	0.36	22.0 (2.5)	61.48	1.00:1.50:3.40 / 0.7914	3080000	33.74
III	L8	S	ME08-04-01	617	53249	11587 (893)	31.8 (2.7)	0.33	27.4 (4.3)	64.30	1.00:1.25:5.50 / 0.8457	1030000	31.83
III	L10	S	ME08-07	595	33313	17861 (1097)	32.0 (0.5)	0.33	17.9 (1.1)	64.80	1.00:1.40:2.40 / 0.8008	3650000	31.99
IV	SD	S	ME08-14	693	31647	21898 (1326)	37.6 (0.8)	0.39	17.2 (1.3)	58.41	1.00:1.20:1.70 / 0.8318	4700000	37.56
2010	KG	D	M11-15	678	10682	63471 (2798)	27.8 (1.0)	0.29	4.4 (0.3)	67.73	1.00:1.60:5.00 / 0.7245	17500000	27.86

Microlite abundance may be expressed in terms of microlite number density (N_A), which describes the number of crystals per unit area (mm^2). The N_A density of scoria samples ranges from ~ 6700–22,700 mm^{-2}, with the highest densities in samples taken from Kali Bebeng, Lobe 10 and the dome in 2008. Samples erupted after 14 June 2006 (Lobes 4, 5, 6 and 8) have lower number densities and the 14 June scoria has the smallest N_A of all the samples analysed. The dense sample taken from the 14 June deposits has the highest N_A of all the samples, measured at 47,166 mm^{-2}. The mean crystal area ranges from ~ 13–39 μm^2, with the largest crystals observed in the scoria from 14 June and the smallest crystals in scoria samples from May 2006, post-14 June samples (Lobe 10) and the summit dome sampled in 2008. The dense sample from 14 June has the smallest size crystals of all samples, with a mean area of 6.9 μm^2. Crystal shape information may also be obtained from the BSE images and calculated aspect ratios are listed in Table 3.4. The shortest axis (S) is defined as 1.00, the intermediate dimension (*I*) ranges from 1.15 to 1.50 and the long dimension (*L)* ranges from 1.60 to 5.50. *S/L* is greatest (i.e. blocky, equant crystals) in the dense sample from 14 June as well as scoriaceous samples taken from deposits emplaced in May 2006, after 14 June (Lobe 10) and the summit dome in 2008, whereas in samples from earlier post-14 June lobes and other samples from May, *S/L* values are lower and represent more elongated crystal habits. More elongated, prismatic crystal shapes correlate with larger mean microlite sizes and lower number densities, in contrast to the blocky shapes, which correlate with smaller crystal sizes and higher number densities (Fig 3.9). Feldspar microlite crystallinity (φ) is expressed as the fraction of groundmass area that is occupied by feldspar microlites, measured using the calculations of Hammer *et al*. (2000), on a vesicle-, phenocryst-, Fe-Ti oxide- and pyroxene-microlite-free area, meaning that the remaining area is composed only of groundmass glass. Crystallinity is a function of both crystal size and crystal abundance. Samples may be divided into two groups based on their feldspar microlite crystallinity. The first group has higher φ values, between 0.33-0.48 and includes samples from May 2006, post-14 June Lobes 6, 8, and 10, the summit dome in 2008 and the dense clasts in the May and 14 June BAF deposits. The second group contains scoria samples from May 2006, 14 June and post-14 June (Lobes 4 and 5) that have lower crystallinities ranging from 0.22 to 0.27. There is a positive correlation between φ and N_A (Fig 3.9b) In comparison, textural analysis of the 2010 dense dome lava yields a N_A value of

63,471 mm^{-2}, feldspar groundmass crystallinity (φ) of 0.29 and a mean crystal area of 4.4 μm^2. The estimated aspect ratio is 1.00: 1.60: 5.00 (Fig 3.9).

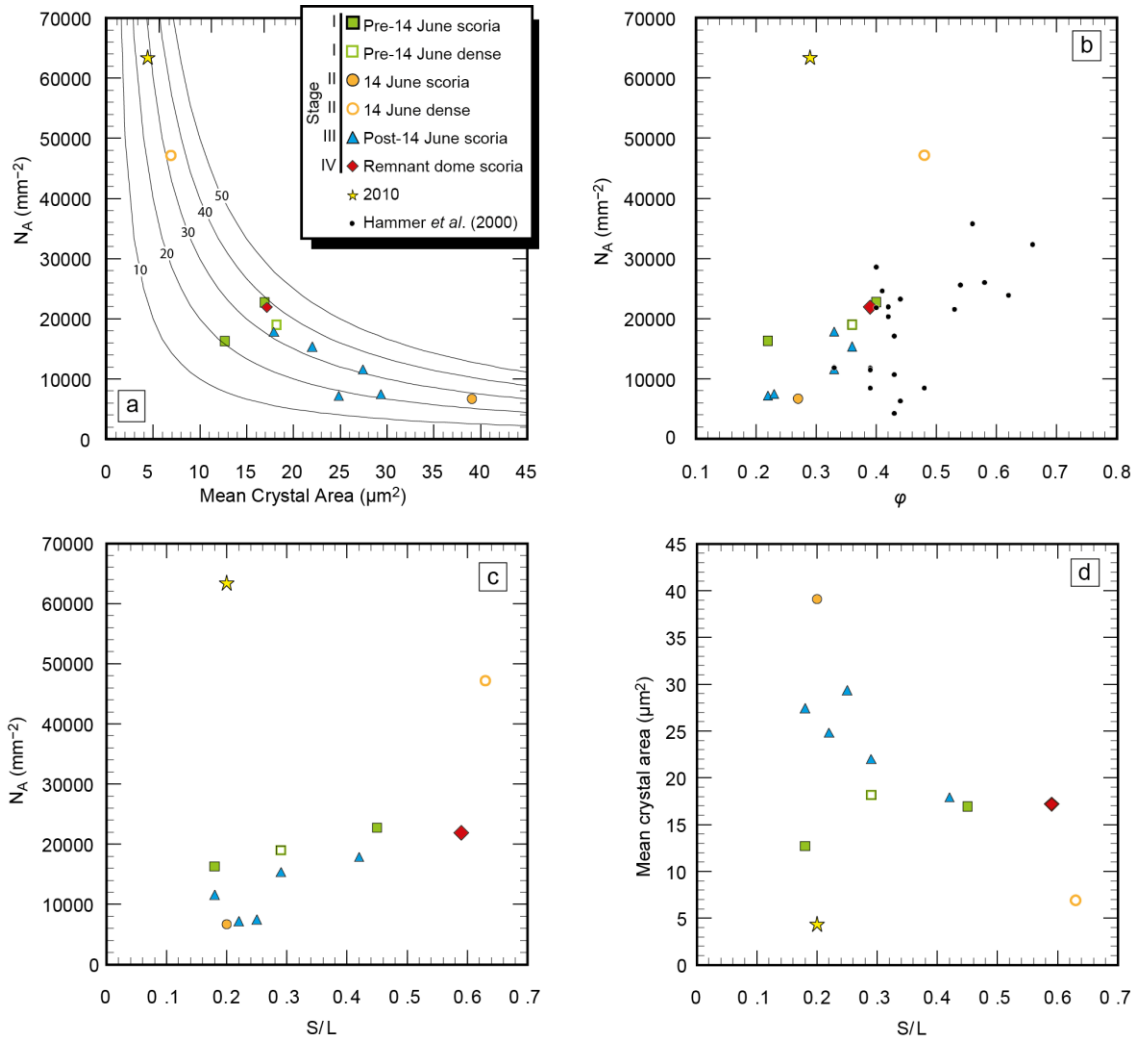

Fig. 3.9 Variation of textural parameters in 2006 eruptive products and 2010 dense dome. (a) Areal feldspar microlite number density (N_A mm^{-2}) vs. mean crystal area (μm^2), with solid lines indicating modelled microlite crystallinity at a particular N_A and crystal size, labelled with percentage values. (b) Areal feldspar microlite number density (N_A mm^{-2}) vs. groundmass feldspar microlite crystallinity (φ), including previously published data of samples from the 1986–87, 1992–93, 1994 and 1995 eruptions (Hammer *et al.*, 2000). (c) Areal feldspar microlite number density (N_A mm^{-2}) vs. S/L or short to long axis ratio. (d) Mean crystal area (μm^2) vs. S/L

3.4.4. Crystal Size Distributions (CSDs)

In order to fully investigate the crystal population, it is helpful to convert 2-dimensional intersection measurements into 3D data. The CSD of a rock may be defined as the number of crystals of a mineral per unit volume, within a series of

defined size intervals. A typical CSD plot considers the population density (a measure of the number of crystals per unit volume of the population), plotted against crystal size. The CSDs in this study all display curved trends, which may be divided into 2–3 straight line segments (Fig 3.10). Based upon their CSDs, the samples may be divided into two groups. The first group displays lower y-axis intercept values (n^o), indicative of the final nucleation density (based upon only the steepest segment of the CSD) of between 18.11 to 20.39 mm^{-4}, as well as less steep slopes, which extend to larger crystal sizes. Samples within this group include scoria from May 2006, 14 June and post-14 June, taken from Lobes 4, 5 and 8. In comparison, the second group has relatively higher y-axis intercepts (20.85–21.65 mm^{-4}), steeper slopes and it does not include the largest size intervals. This group includes scoria and dense samples from May 2006, dense 14 June material, post-14 June scoria from Lobes 6 and 10, as well as scoria taken from the summit dome in 2008 (Fig 3.10). These two groups are broadly consistent with the high and low crystallinity groups, as described in the previous section, with the nucleation-dominated group consisting of similar samples as the high φ group, and the growth-dominated group coinciding with the low φ group. The 2010 dense dome sample has a relatively higher y-axis intercept of 23.17 mm^{-4}, with the CSD array displaced to higher population density values than the 2006 samples (Fig 3.10).

A decrease in population density at the smallest crystal sizes results in a left-hand "downturn" in the CSDs for some samples. This decrease in the number of the smallest crystals has previously been noted in both natural and experimental samples and attributed to inadequate spatial resolution (Marsh, 1998; Hammer *et al*., 1999) and stereological problems when compensating for intersection probability effects at small sizes (Cashman 1988; Brugger and Hammer, 2010b; Higgins, 2010). In the analysed images, 1 μm is represented by 9 pixels, so the spatial resolution is adequate to distinguish the smaller crystal sizes and the downturn cannot be attributed to this factor. It is therefore proposed that the left-hand downturn is due to conversion errors in the CSD software for smaller size classes, resulting from a lower probability of intersecting smaller crystals, and therefore not discussed further.

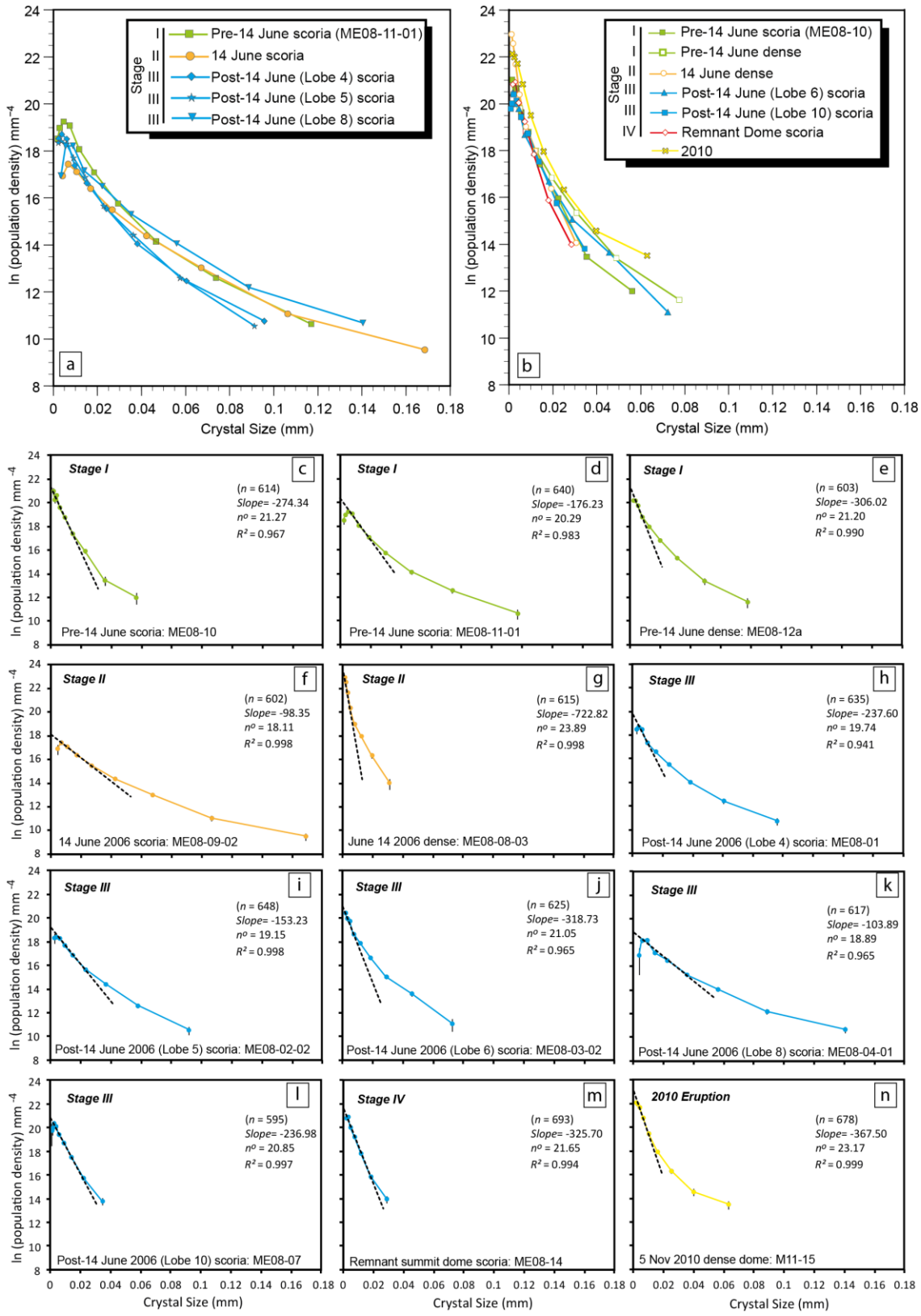

Fig. 3.10 Crystal Size Distribution (CSD) plots of feldspar microlite crystals from the 2006 and 2010 eruptions. (a) CSDs of samples within the "growth-dominated" group. (b) CSDs of samples within the "nucleation-dominated" group. (c–n) Individual CSDs for each sample (grey solid line), with a regression line fitted to the steepest initial part of the CSD curve (black dashed line), values for the slope of these regressed lines, the y-axis intercepts or nucleation densities (n^o) and R^2 values given. *n* denotes the number of crystals analysed in each sample

3.5. Discussion

3.5.1. Textural variations during the 2006 eruption

Textural measurements can be linked with the 2006 eruption sequence. Groundmass microlites can reveal important information about the style of crystallisation, which can be used to elucidate shallow conduit processes and magma ascent paths (*e.g.* Hammer *et al*., 1999, 2000; Nakada and Motomura, 1999; Cichy *et al*., 2011). In general, temporal trends in the 2006 samples display an increase in crystal number density with time, a decrease in mean microlite size, a progression towards more equant crystals from more prismatic habits and an overall increase in crystallinity (Fig. 3.11). Early erupted scoria and dense clasts from Stage I that were emplaced in Kali Bebeng, when early flows travelled towards the southwest between 11 May and 1 June 2006 (Ratdomopurbo *et al*., 2013), show variable number densities, feldspar microlite crystallinites and mean crystal areas (Fig. 3.11). Stage II samples taken from Lobe 1, emplaced during the largest pyroclastic flows on the 14 June 2006, show distinct textural characteristics compared to samples from earlier as well as later emplaced deposits. Scoriaceous clasts have the lowest N_A, the largest mean crystal size and a feldspar microlite crystallinity of 0.27 (Fig. 3.11). By contrast, dense blocks display the highest N_A and the smallest sized crystals of all samples analysed, with a crystallinity of 0.48, the highest of all analysed samples. Stage III samples erupted after the 14 June collapse, taken from Lobes 4, 5, 6, 8, and 10, and Stage IV samples taken from the remnant 2006 dome in 2008 show progressively increasing N_A, generally increasing φ and decreasing mean crystal areas (Fig. 3.11). These textural differences are due to variations of ΔT during crystallisation, which may occur during ascent and dome residence. Samples that have experienced significant amounts of crystallisation while on the dome would exhibit high degrees of crystallinity and low volumes of residual glass. This is not consistent with the analysed samples, as even the sample analysed from Stage IV, which resided at or near the dome surface for approximately 2 years, has a φ of 0.39 and 58 % of the groundmass area is residual glass. Dense samples representing the interior of the dome, which were held at elevated temperatures before being quenched have ~ 63 % residual groundmass glass and display variable microlite textures. In comparison, samples which have been interpreted to have spent prolonged periods (weeks to months) crystallising in domes at Montserrat and Mount St. Helens

have a more extensive, sometimes nearly holocrystalline groundmass, with much lower amounts of residual glass, which is often devitrified (Sparks *et al*., 2000; Pallister *et al*., 2008). Therefore, although it is possible that a small degree of crystallisation took place within the dome, we suggest that groundmass crystallisation predominantly occurred during ascent and, as such, the observed textures reflect the magmatic conditions during this time. As melts exsolve H_2O and become increasingly SiO_2-rich, the resulting viscosity increase means that crystallisation kinetics become increasingly sluggish and microlite growth is retarded (Cashman, 1988; Wolf and Eichelberger, 1997). For this reason, continued crystallisation in the dome becomes increasingly difficult. Another possibility for the lack of extensive crystallisation within the dome may be that the samples did not reside for long enough periods of time within the dome to undergo significant amounts of dome crystallisation before emplacement.

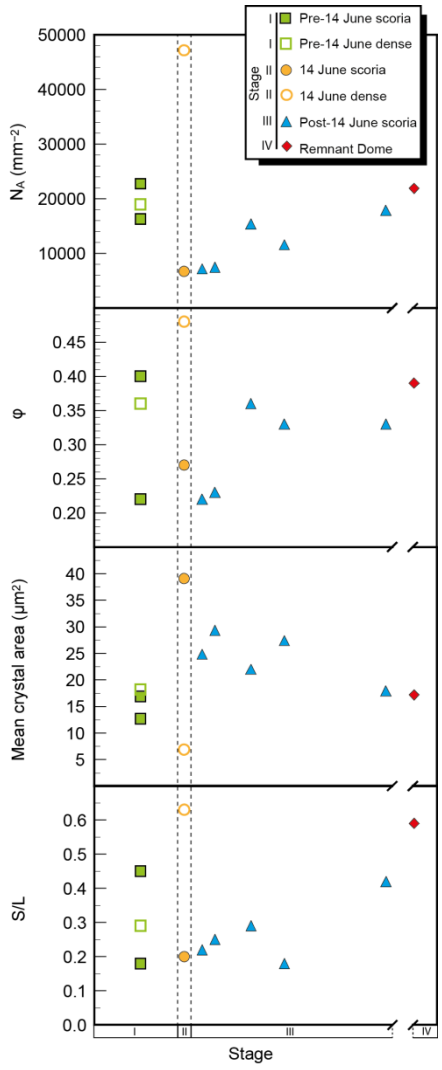

Fig. 3.11 Temporal variations in feldspar microlite textural parameters in scoria and dense samples produced throughout the 2006 eruption

As a consequence, textural variations seen within Stage I samples of the 2006 eruption are interpreted to be the result of the variations in ascent rate during this period. During Stage I, extrusion rates increased from ~ 1.0 m^3 s^{-1} at the beginning of dome formation to ~ 1.9 m^3 s^{-1} during 11-27 May (Ratdomopurbo *et al*., 2013). As the samples represent material that may have extruded any time between the onset of the eruption on 26 April and 1 June, when almost all flows stopped travelling to the south-west, the preferred interpretation of the observed range in number densities are the increasing lava extrusion (and presumably ascent) rates, which lead to higher degrees of ΔT and, consequently, higher degrees of nucleation, resulting in higher N_A. In an alternative model, the range in number density could indicate sampling of different parts of the lava dome, i.e., marginal versus core facies, as initial collapses are likely to have affected the margin of the growing dome and subsequent collapses may have tapped more interior regions of the growing dome. However, as discussed above, the microlites predominantly formed during ascent and further crystallisation within the dome is largely inhibited by anhydrous, near-surface conditions. Therefore, the textural variations within these samples reflect differing ascent conditions rather than differing circumstances of dome residence. The difference in microlite textures in Stage II is a result of the scoriaceous and dense components having been sourced from different parts of the dome, which experienced different ascent conditions. The dense dome fragments within the 2006 deposits are interpreted to originate from the interior of the dome (Charbonnier and Gertisser, 2008). Field evidence from examination of the 2006 remnant lava dome in 2008 supports this interpretation, as the outer facies of the lava dome was observed to be scoriaceous. Therefore, it is suggested that the scoriaceous material represents earlier erupted material from the outside margin of the dome, erupted when extrusion rates were lower, and the dense material represents a later stage of mainly endogenous dome growth, extruded just before the 14 June collapse, when extrusion rates had reached 3.3 m^3 s^{-1} (Ratdomopurbo *et al*., 2013), the maximum during the 2006 eruptive episode. This interpretation is supported by the presence of amphibole microphenocrysts and phenocrysts with minimal breakdown rims in the dense 14 June 2006 sample (sample ME08-08-03), indicative of fast magma ascent from depth (Fig. 3.4). Progressive textural variations in samples from Stages III and IV record progressive changes in crystallisation conditions, notably a general increase in the degree of undercooling, as recorded by increasing N_A. In a previous study of microlite textures at Merapi, Hammer *et al*. (2000) found a positive correlation of N_A

with ascent rate. However, during the post-14 June period (Stage III), extrusion rates decreased to ~ 1.2 m^3 s^{-1} (Pallister *et al*., 2013) and therefore presumably so did the ascent rate. The slower magma ascent rate during this period is also recorded by amphibole crystals with decompression breakdown rims composed of plagioclase, pyroxene and oxides (Fig. 3.4). In contrast with the Stage I samples that were emplaced by dome collapses which progressively sampled more of the interior of the dome, each lobe of the Stage III sampled both exterior and interior portions of the dome, evidenced by the presence of both scoriaceous and dense clasts in each lobe (Charbonnier and Gertisser, 2008). The progressive increase in N_A in Stage III and IV samples, caused by an increase in ΔT, may be explained by the magma stalling temporarily and equilibrating at shallower depths. Liquidus temperatures increase with decreasing pressure and loss of H_2O, resulting in higher degrees of undercooling at shallower depths during isothermal ascent of magma (Hammer et al., 1999, 2000; Cashman and Blundy, 2000; Hammer and Rutherford, 2002; Cashman and McConnell, 2005; Brugger and Hammer, 2010a). Consequently, higher undercooling during stalling at shallow levels would lead to an increased nucleation rate, producing the abundant small microlites seen in these samples. In addition to crystal number density, the groundmass crystallinity (φ) also progressively increases in the Stage III and IV samples. An increase in overall crystallinity also favours stalling at shallow depths resulting in increased time to crystallise. An increase in groundmass crystallinity would result in an increase in bulk viscosity, further promoting stalling of the magma at shallow depths, where H_2O degassing and the increase in SiO_2 content further increases the viscosity of the melt. For example, calculated viscosities, using *KWare Magma*, of a rhyodacite at 900 °C increase by two orders of magnitude when 50 vol.% crystals are added, and an increase in viscosity by two orders of magnitude takes place when H_2O contents decrease from 4 wt.% to 1 wt.%.

Overall, the Merapi microlites display prismatic and equant morphologies, becoming increasingly equant with increasing N_A and decreasing size (Fig. 3.9), with occasional hopper and swallowtail crystals, especially in samples emplaced in early post-14 June lobes (Lobes 4 and 5). Previous studies have linked plagioclase crystal morphology to the degree of undercooling (*e.g.* Lofgren, 1974, 1980; Corrigan, 1982; Couch *et al.*, 2003a), with crystals changing from tabular to hopper to swallowtail to dendritic morphologies, becoming more acicular with increasing ΔT. In the Merapi

samples this increase in aspect ratio, with crystals becoming less acicular and more equant, seen especially in later erupted samples which have a higher N_A and presumably formed at higher ΔT, is therefore counterintuitive. However, decompression experiments have shown that both decompression rate and pressure have an effect on crystal morphology, which may help to explain the textures seen within the Merapi samples. Experiments have found that as decompression rate slows, plagioclase changes from hopper, swallowtail and acicular forms to more tabular or equant shapes (Szramek *et al*., 2006; Brugger and Hammer, 2010a) and that during higher-pressure decompression (from 150 to 50 MPa) crystal growth is dominant, whereas at lower pressure decompression (from 50 to 15 MPa) crystal nucleation prevails (Martel and Schmidt, 2003). This may explain why in late-stage erupted samples, especially those taken from Lobe 10 and the summit dome in 2008, the N_A is high and the crystals are equant in shape. As noted above, textural analysis of the microlites in this study suggests that these samples were stalled at shallow levels, leading to high ΔT at relatively low P and therefore high N_A, with the relatively slow rates of shallow ascent and decompression at the late stages of eruption also favouring nucleation, with resulting crystals having equant shapes. By contrast, samples taken from flows emplaced on 14 June and soon after (Lobes 4 and 5) show few but larger crystals, which are more prismatic and sometimes skeletal or swallowtail. Comparison of these textures with those from experiments of similar compositions (Martel and Schmidt, 2003; Szramek *et al*., 2006) implies faster decompression from a deeper initial starting point, consistent with the interpretations above.

The textural data are in broad agreement with the geophysical (Ratdomopurbo and Poupinet, 2000) and petrological models (*e.g.* Costa *et al*., 2013) of the Merapi magmatic system. The late 2006 samples appear to have stalled at shallow depths, perhaps in an ephemeral shallow storage region as previously revealed via seismic studies (Ratdomopurbo and Poupinet, 2000). Faster ascended magma, such as that represented by the 14 June dense samples, rose directly from depths within the amphibole stability field, without stalling in the shallow system. These findings are consistent with other petrological studies suggesting a complex plumbing system consisting of magma storage and crystallisation regions at multiple depths within the crust (*e.g.* Gertisser, 2001; Chadwick *et al*., 2013; Costa *et al*., 2013).

3.5.2. Crystal Size Distribution analysis and microlite crystallisation

The curved CSDs reflect changes in the ratio and rates of growth and nucleation of microlites during magma ascent, as a function of changing ΔT. Different microlite sizes reflect magmatic conditions at different depths, for example, growth of existing crystals is dominant in the lower conduit, and in the shallower system, nucleation begins to dominate, leading to steeper slopes for smaller crystal sizes (Melnik *et al*., 2011). The fact that the CSDs are curved rather than kinked suggests progressive changes in ΔT during ascent, rather than distinct events of nucleation and growth. CSD analysis reveals two groups of samples. One group displays a stronger gradient with a more pronounced change in crystal size with population density, with higher y-axis intercepts (n^o), indicative of nucleation density, and overall smaller crystal sizes. The other group of samples have weaker gradients, with lower y-axis intercepts and larger crystal sizes (Fig 3.10). These groups may be described as "nucleation-dominated" and "growth-dominated", respectively. The nucleation-dominated group consists of scoria and dense samples that have crystallised at conditions of higher undercooling than the growth-dominated samples. Although the CSDs are curved, the curves may be approximated by 2–3 straight line segments. Crystallisation time estimates may be obtained from the slope of these CSD segments, if the crystal growth rate is known, using the following equation (Marsh, 1988): $Slope = -1/G\tau$, where G is growth rate and τ is crystallisation time. Growth rates of groundmass plagioclase due to water exsolution during magma ascent are generally estimated to be between 10^{-6} and 10^{-8} mm s^{-1} (Brugger and Hammer, 2010b). When minimum and maximum crystallisation times are calculated for the Merapi microlites using this range of growth rates (10^{-6}, 10^{-7} and 10^{-8} mm s^{-1}), the estimated times range over three orders of magnitude for each sample, with a shortest estimate of 23 minutes and a longest of 11.8 days, based only upon the slope of the steepest segment of the CSD, which represents the smallest crystals, preserving a record of the most recent crystallisation before eruption. Based upon a comparison with decompression experiments, Brugger and Hammer (2010b) suggest that the most accurate growth rate for decompression-induced crystallisation of plagioclase is 10^{-8} mm s^{-1}. When using this growth rate, Merapi microlites are estimated to have crystallised over a time period of between 38 to 282 hours, or 1.6 to 11.8 days, based upon the steepest slope (Table 3.5), which agrees with experiments that have determined groundmass crystallisation to occur over a period of days after a decrease in

pressure (Geschwind and Rutherford, 1995). The monitoring record reveals an increase in precursory signals beginning in 2005, which increased ~ 1 month prior to the onset of eruption. Summit deformation began to rapidly increase after 18 April 2006, until on 26 April displacement stopped and real-time seismic amplitude measurement (RSAM) signals decreased. This is interpreted to be caused by a sudden loss in pressure due to degassing of magma below the summit, understood to be the onset of the 2006 eruption (Ratdomopurbo *et al*., 2013). A second drop in RSAM signals was also noted on 1 May, related to the opening of the summit and the onset of dome extrusion. Calculated microlite crystallisation times for the largest microlites (based on the shallowest segments of the CSDs) in early erupted samples taken from Kali Bebeng, range from 16–23 days, possibly reflecting the time period seen in the monitoring record when the movement of magma to shallow levels began to cause summit deformation. The five day period between 26 April and 1 May, when magma moved from inside the edifice to the surface, is similar to calculated crystallisation times of the smallest microlites (based on the steepest slopes), for early erupted samples, which range from ~ 4–6 days. The apparent correspondence between calculated crystallisation times and estimated ascent rates based on the monitoring data suggests that microlite crystallisation occurred at shallow depths, within the edifice. It also indicates that differently sized microlites may preserve evidence of different stages of magma ascent, with the larger microlite population within a sample revealing information about early ascent and the smaller crystals within a sample revealing evidence of crystallisation conditions at the latest stages of ascent. However, given the complexity in relating the samples to eruption time in Stage I and potentially permissive crystal growth rates, this relation must be viewed with caution.

The nucleation rate (J) may be calculated using the y-axis intercept (n^o) of the CSD and the following equation (Marsh, 1988): $J = n^o G$, where the growth rate (G) is 10^{-8} mm s^{-1}. Estimated nucleation rates for the Merapi microlites are between 7.33×10^{-1} and 2.25×10^{2} nuclei mm $^{-3}$ s^{-1}, based only using the steepest section of the CSD, therefore based on the smallest and latest formed crystals, giving evidence of conditions just before extrusion (Table 3.5). However, both growth and nucleation rates vary with the degree of undercooling (*e.g.* Kirkpatrick, 1977; Dowty, 1980; Hammer and Rutherford, 2002; Couch *et al*., 2003a), and as a consequence, it is possible that

calculated crystallisation times and nucleation rates may be underestimated for samples which have experienced higher undercooling.

3.5.3. Insights from compositional variations of feldspar microlites throughout the 2006 eruption

Variations in magma ascent, as evidenced by microlite textural differences, also affect microlite compositions. For example, anorthite content increases with increasing water pressure and temperature (*e.g.* Couch *et al*., 2003b). If crystallisation occurred during continuous ascent, microlite compositions would reflect this by showing a range of anorthite contents. If the magma had stalled for a period of time during ascent, there may be a predominance of a certain anorthite content in the microlite population, representative of the water pressure and temperature of the magma at the time of stalling. Although the very smallest crystals (< ~ 3 μm diameter) were too small to analyse, the compositions of the larger microlites provide information about the magma system during ascent. Analysed microlites from Stage I range in composition between $An_{19\text{-}60}$, with most analyses between $An_{40\text{-}50}$ (Fig 3.12). Stage II microlites are more restricted compositionally, with anorthite contents between 28–49 mol%, but with a similar peak at $An_{40\text{-}50}$. Anorthite contents of Stage III microlites include lower An compositions, ranging from $An_{5\text{-}45}$, with the majority of analyses between $An_{30\text{-}40}$. Stage IV microlites show a more even spread between $An_{17\text{-}54}$, with the most abundant compositions between $An_{20\text{-}40}$ (Table 3.1). The fact that the over 50% of the Stage III microlites analysed have between 30–40 mol% anorthite is consistent with the interpretation that this magma temporarily stalled within the shallow crust before extrusion, leading to a predominance of crystals within a small compositional range. Decompression experiments at between 825–925 °C (Couch *et al*., 2003b) show that microlites of between 30–40 mol% anorthite form at water pressures between 25–50 MPa. This pressure is equivalent to shallow depths of ~ 1–2 km, consistent with the depths of the proposed shallow ephemeral magma storage region (Ratdomopurbo and Poupinet, 2000) and with the textural evidence that Stage III magma temporarily stalled, crystallising in this region (Fig 3.13).

Table 3.5 Crystal Size Distribution (CSD) analysis results and calculated crystallisation times and nucleation rates for samples from stages I to IV of the 2006 eruption and representative dome samples from the 2010 eruption: Section 1 = steepest CSD segment; section 3 = shallowest segment. Localities: KB = Kali Bebeng; L = Lobe (1, 4, 5, 6, 8, 10); SD = 2006 summit dome (sampled in 2008); KG = Kali Gendol. Lithology types: S = 2006 scoria, D = dense dome blocks.

						Crystallisation time					Nucleation rate		
						$G = 10^{-6}$	$G = 10^{-7}$	$G = 10^{-8}$			$G = 10^{-6}$	$G = 10^{-7}$	$G = 10^{-8}$
Stage	Locality	Lithology	Sample	Section	Slope	T (hours)	T (hours)	T (hours)	CT (days)	$(\ln)n^0$ (mm^{-4})	J (no/mm^3s^{-1})	J (no/mm^3s^{-1})	J (no/mm^3s^{-1})
I	KB	S	ME08-10	1	274.34	1.01	10.13	101.25	4.22	21.27	1720.71	172.07	17.21
				2	185.49	1.50	14.98	149.75	6.24	20.06	513.11	51.31	5.13
				3	70.53	3.94	39.38	393.84	16.41	15.97	8.60	0.86	0.09
I	KB	S	ME08-11a	1	176.23	1.58	15.76	157.62	6.57	20.29	649.69	64.97	6.50
				2	103.63	2.68	26.80	268.05	11.17	18.93	166.58	16.66	1.67
				3	49.45	5.62	56.17	561.73	23.41	16.38	12.94	1.29	0.13
I	KB	D	ME08-12a	1	306.02	0.91	9.08	90.77	3.78	21.20	1607.59	160.76	16.08
				2	129.84	2.14	21.39	213.94	8.91	19.58	317.19	31.72	3.17
				3	62.24	4.46	44.63	446.30	18.60	16.45	13.98	1.40	0.14
II	L1	S	ME08-09-02	1	98.35	2.82	28.24	282.44	11.77	18.11	73.29	7.33	0.73
				2	54.83	5.07	50.66	506.62	21.11	16.82	20.18	2.02	0.20
				3	24.60	11.29	112.92	1129.18	47.05	13.69	0.88	0.09	0.01
II	L1	D	ME08-08-03	1	722.82	0.38	3.84	38.43	1.60	23.88	23493.74	2349.37	234.94
				2	472.41	0.59	5.88	58.80	2.45	22.66	6922.20	692.22	69.22
				3	216.59	1.28	12.83	128.25	5.34	20.64	923.79	92.38	9.24
III	L4	S	ME08-01	1	237.60	1.17	11.69	116.91	4.87	19.74	372.59	37.26	3.73
				2	116.22	2.39	23.90	239.01	9.96	18.43	100.63	10.06	1.01
				3	56.33	4.93	49.31	493.13	20.55	16.07	9.56	0.96	0.10
III	L5	S	ME08-02-02	1	153.23	1.81	18.13	181.28	7.55	19.15	206.75	20.67	2.07
				2	74.40	3.73	37.34	373.36	15.56	17.18	29.03	2.90	0.29
III	L6	S	ME08-03-02	1	318.73	0.87	8.72	87.15	3.63	21.05	1379.52	137.95	13.80
				2	166.91	1.66	16.64	166.42	6.93	19.82	406.87	40.69	4.07
				3	91.41	3.04	30.39	303.88	12.66	17.75	50.98	5.10	0.51
III	L8	S	ME08-04-01	1	103.89	2.67	26.74	267.38	11.14	18.89	159.57	15.96	1.60
				2	63.34	4.39	43.86	438.55	18.27	17.35	34.31	3.43	0.34
				3	29.15	9.53	95.29	952.93	39.71	14.78	2.63	0.26	0.03
III	L10	S	ME08-07	1	236.98	1.17	11.72	117.22	4.88	20.85	1136.25	113.63	11.36
				2	153.54	1.81	18.09	180.92	7.54	19.11	198.64	19.86	1.99
IV	SD	S	ME08-14	1	325.70	0.85	8.53	85.29	3.55	21.65	2531.30	253.13	25.31
				2	180.00	1.54	15.43	154.32	6.43	19.12	201.24	20.12	2.01
2010	KD	D	M11-15	1	367.50	0.76	7.56	75.59	3.15	23.17	11515.96	1151.60	115.16
				2	208.22	1.33	13.34	133.41	5.56	20.74	1017.89	101.79	10.18
				3	71.42	3.89	38.89	388.94	16.21	16.37	12.83	1.28	0.13

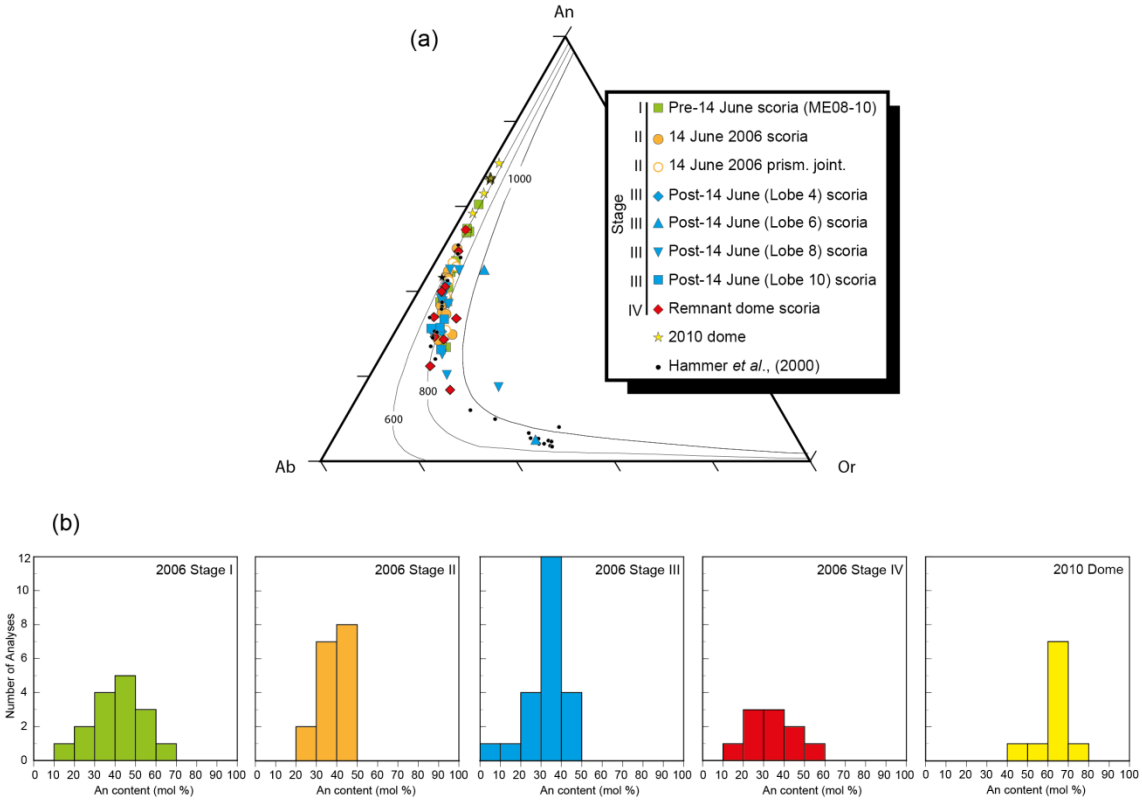

Fig. 3.12 (a) Feldspar microlite compositions in the feldspar ternary (An-Ab-Or) diagram. Microlites are from the 2006 and 2010 eruptions, plotted together with previously published data of microlite compositions from other recent dome-forming eruptions in 1986–87, 1992–93, 1994 and 1995 (Hammer *et al.*, 2000). Curves represent isothermal sections of the dry ternary solvus at 600, 800 and 1000 °C, calculated using SOLVCALC (Wen and Nekvasil, 1994). (b) Histograms of the anorthite content in microlites from Stages I–IV of the 2006 eruption, as well as from the 2010 dome

Although many are too fine to analyse, plagioclase microlites in the 2006 samples are frequently seen in BSE images to be mantled by lighter grey coloured alkali-rich rims of anorthoclase and more K-rich alkali feldspar (sanidine). The grey-scale of these lighter rims is similar to the grey-scale of the smallest microlites, implying that the small microlites are also alkali-rich in composition. The presence of alkali feldspar rims on microlites has previously been reported in recent erupted products at Merapi (Bardintzeff, 1984; Hammer *et al.*, 2000) and interpreted by Hammer *et al.* (2000) as a consequence of degassing; after degassing the position of the two feldspar + liquid curve moves towards An, relocating the remaining liquid from the plagioclase + liquid field to the alkali feldspar + liquid field. Such a process has also been invoked to explain microlite compositions of the Tenjo eruption of Kozu Island, Japan (Noguchi *et al.*, 2006) and the 1815 eruption of Tambora (Gertisser *et al.*, 2012c),

as well as microphenocryst compositions of Monte Nuovo, Italy (D'Oriano *et al.*, 2005). Microlite compositions are shown with isothermal sections of the dry ternary solvus, calculated using SOLVCALC (Wen and Nekvasil, 1994) at 0.5 kbar (Fig 3.12). The dry solvus position is not sensitive to pressure changes between 0–3 km, the region of expected degassing in the conduit, so depth only controls feldspar composition in terms of the extent of H_2O degassing (Hammer *et al*., 2000). The microlite compositions with respect to the dry solvus do not imply that microlite crystallisation occurred at different temperatures during cooling between ~ 600–1000 °C, but rather that changes in H_2O activity changed the position of the liquidus and therefore the composition of the crystallizing feldspar. Consequently, our compositional data for the 2006 microlites are consistent with the model of Hammer *et al.* (2000) for samples from previous Merapi dome eruptions; i.e., they show enrichment in alkalis due to degassing and compositional evolution of the residual melt phase, reaching a rhyolitic composition (Table 3.3).

3.5.4. Magma ascent during the 2010 eruption of Merapi

In stark contrast with the > 3 month-long, effusive (dome-building) activity that occurred in 2006, the subsequent eruption in 2010 was short duration (< 1 month), more explosive and did not begin with the extrusion of a new lava dome (Surono *et al*., 2012; Pallister *et al*., 2013). During 1–4 November rapid dome growth took place at an estimated rate of 25 m^3 s^{-1}, (Pallister *et al*., 2013) nearly 8 times that of the peak extrusion rates during the 2006 eruptive episode (peak of 3.3 m^3 s^{-1} (Ratdomopurbo *et al*, 2013) and produced a lava dome with a volume of ~5 x10 m^3 (Pallister *et al*., 2013). This dome was subsequently destroyed during the largest explosive event, on 5 November, when pyroclastic density currents travelled up to 15 km in the Kali Gendol [see Charbonnier *et al*. (2013) and Komorowski *et al*. (2013) for detailed work on the 2010 deposits].

Initial investigation of groundmass microlite textures of dense dome blocks from the rapidly growing 2010 lava dome, collapsed on 5 November 2010, show a similar φ to the 2006 samples, a relatively small mean microlite area and higher N_A (Table 3.4). These textural observations are evidence of higher relative undercooling and a

crystallisation regime dominated by nucleation relative to growth. These preliminary results are in accord with the substantially higher observed extrusion rates in 2010 (*e.g.* Pallister *et al*., 2013). High rates of magma ascent, created higher degrees of undercooling, resulting in a higher degree of crystal nucleation in comparison to other recent dome-forming eruptions at Merapi. Amphibole crystals in the 2010 lava dome that extruded after the initial explosions of 26–29 October 2010 are mostly pristine or display only minimal degrees of breakdown in comparison with most 2006 samples, in agreement with fast magma ascent rates from depth (Fig 3.4).

The microlites from the 2010 eruption cover a similar compositional range as those from 2006, but also extend to more An-rich compositions (up to ~ An_{70}), with 50 % of analysed microlites between An_{60-70} (Fig 3.12). These high-An microlites may have formed at higher temperatures and water pressures compared to the lower-An microlites in the 2006 samples. The presence of high-An microlites has been observed in natural samples from other dome-forming volcanoes including Mount Pelée, Martinique (Martel *et al.,* 2000, 2006), Unzen, Japan (Noguchi *et al*., 2008) and Soufrière Hills, Montserrat (Couch *et al.,* 2003b; Humphreys *et al.,* 2009). It is possible that the An-rich microlites in the 2010 Merapi magma were formed via influx and interaction with a hotter, deeper magma. These findings are consistent with other petrological data (Costa *et al*., 2013) as well as gas monitoring data from the 2010 eruption, which suggests the presence of a deep degassing source prior to 5 November, speculated to be a new input of mafic magma (Surono *et al.,* 2013). Future work on the comparison of groundmass textures from other 2010 samples, produced during other stages of the eruption, will give further insights into magma ascent dynamics and the driving forces behind the more explosive 2010 eruption (Chapter 4).

3.5.5. Comparison of the 2006 eruption with other recent dome-forming Merapi eruptions: a textural perspective

Previous analysis of Merapi microlites (Hammer *et al*., 2000) found similarities in N_A and φ between samples from dome eruptions in 1992–93, 1994 and 1995, indicating cyclic conditions of crystallisation during magma ascent. Hammer *et al*. (2000) also observed changes in groundmass texture over time, with samples from the

beginning of the 1995 eruption, produced when effusion rates were high, displaying higher N_A than samples erupted near the end of the 1995 eruption, produced when effusion rates decreased. This correlation between effusion rate and N_A suggests that ΔT is controlled by magma ascent rate. However, although peak effusion rates were an order of magnitude higher in 2006 (3.3 m^3 s^{-1} pre-14 June 2006, compared with 0.32 m^3 s^{-1} estimated maximum extrusion rate in 1994), values of N_A are similar to the previous eruptions, implying that conditions of nucleation were similar despite the higher extrusion rate. Values of φ are lower for a particular N_A than in previous eruptions, signifying that crystal growth was less dominant in 2006 than in the previous eruptions, due to differing ΔT (Fig 3.9b). Textural changes with time throughout the 2006 eruption are also in contrast with those seen in 1995, with no clear correlation between effusion rate and N_A. Therefore, although ascent rate contributes to the degree of ΔT and N_A, other factors influencing undercooling such as magma ascent path, source depth and near-surface degassing also play a part in controlling the final groundmass texture. Our results show that these factors were variable over short timescales throughout the 2006 eruption, elucidated by detailed sampling of the different stages of the eruption (Fig. 3.13). Textural analysis of the 2006 samples also provide an insight into the evolution of the Merapi plumbing system during the eruption, with samples showing textural evidence of rapid magma ascent from a magma storage region at depths within the amphibole stability field, as well as later erupted samples suggesting stalling of the magma at shallow depths within the edifice, probably within an ephemeral reservoir (Fig 3.13).

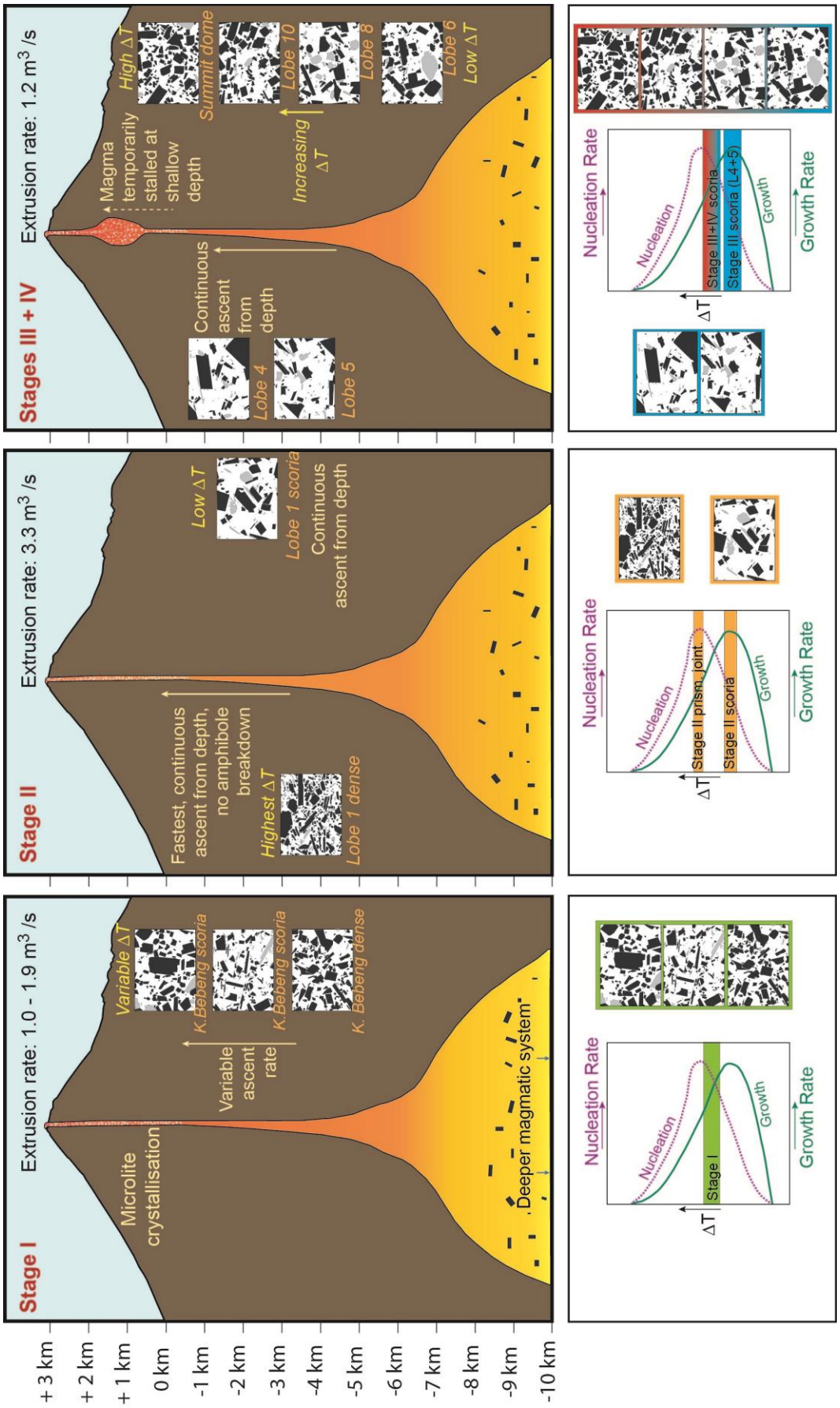

Fig. 3.13 Schematic diagram of the evolution of the shallow magmatic system and variation in ascent processes at Merapi during the various stages of the 2006 eruption

3.6. Summary

The final groundmass microlite textures in the natural samples from the prolonged 2006 eruption of Merapi are the result of a combination of variable rates of magma ascent, coupled with varying modes of dome collapse. Although complex in detail, quantitative textural analysis of sample groups from the four main stages of the eruption, alongside other petrological, geochemical and monitoring data, provide important constraints on the dominant magma ascent and dome collapse processes, and their variations over short timescales during a single, prolonged dome-forming eruption at Merapi. Stage I of the 2006 eruption consisted of variable magma ascent and extrusion rates, likely coupled with variations in the rate of crystallisation within the margin and core of the growing lava dome, and resulting in variable feldspar microlite textures. Calculated crystallisation times correlate reasonably well with the monitoring record of magma moving at shallow depths within the edifice during this stage. The textures of Stage II samples favour rapid magma ascent from depths within the amphibole stability field. Samples from Stages III and IV of the 2006 eruption suggest that magma batches stalled temporarily at shallower levels before being extruded. In contrast to the typical dome-forming eruption cycle of Merapi in 2006, the textures (as well as other petrological features, *e.g.* Costa *et al*., 2013) indicate that magmas associated with the highly explosive and unusual eruption of Merapi in 2010 ascended at faster rates than in 2006, possibly influenced by interaction with hotter, more mafic magma at depth.

Chapter 4: Volcanological, petrological and textural insights into effusive-explosive transitions during the 2010 Merapi eruption

4.1. Introduction

Transitions between effusive and explosive activity are commonly observed at many subduction zone volcanoes worldwide. Understanding the driving forces behind eruptive style and factors that influence changes in activity is crucial for hazard assessment and monitoring efforts. Previous research into the causes of eruptive style has included studies of petrological and textural studies of natural samples (*e.g.* Barclay *et al*., 1996; Hammer *et al*., 1999; Platz *et al*., 2006; Koleszar *et al*., 2012), decompression experiments (*e.g*. Geschwind and Rutherford, 1995; Szramek *et al*., 2006; Castro and Gardner, 2008; Martel, 2012) and numerical modelling (*e.g*. Jaupart and Allègre, 1991; Woods and Koyaguchi, 1994; Villemant and Boudon, 1998; Melnik and Sparks, 1999, 2005; Barmin *et al*., 2002; Clarke *et al*., 2007; Degruyter *et al*., 2012) and suggests that a variety of interrelated factors influence eruptive style. Studies have shown that eruptive activity is related to the rate, volume and composition of magma supply and influx to a magma chamber (*e.g.* Woods and Koyaguchi, 1994; Cashman and McConnell, 2005; Constantini *et al*., 2011). For example, magmatic influx has been identified as an eruption trigger in many previous studies (*e.g.* Murphy *et al*., 2000; Ridolfi *et al*., 2008; Suzuki *et al*., 2013). Magmatic influx to a chamber may in turn affect magma ascent dynamics, influencing the rate of magma ascent and whether ascent is sustained or pulsatory in its nature (Wolf and Eichelberger, 1997; Scandone *et al*., 2007). Magma ascent rate governs, and is governed by, volatile exsolution during decompression, with fast ascent often linked to closed-system degassing which results in increased potential for explosive activity, and slower ascent linked to open-system degassing and often more effusive activity (*e.g*. Jaupart and Allègre, 1991; Martel *et al*., 2000; Szramek *et al*., 2006; Villemant *et al*., 2008). At shallow depths, degassing and crystallisation influence magma rheology and may determine the style of eruption (*e.g*. Melnik and Sparks, 1999, 2005; Barmin *et al*., 2002; Degruyter *et al*., 2012). Extensive,

shallow-level, degassing-induced crystallisation may effectively seal the conduit, resulting in pressure build-up and an explosive eruption, if pressure exceeds a critical threshold related to magma strength (*e.g.* Stix *et al.*, 1993; Sparks, 1997, Melnik and Sparks, 1999, 2005; Edmonds and Herd, 2007; Burgisser *et al.*, 2011). Therefore, a complex interplay between deep and shallow processes related to magma storage, influx, ascent and the rheological changes caused by crystallisation and degassing are known to influence the final eruptive behaviour, often via complex feedback mechanisms.

This chapter focusses on the cataclysmic (VEI 4) 2010 Merapi eruption, during which several transitions between explosive and effusive eruptive phases occurred. As described in more detail in Chapter 2, the 2010 eruption was the largest at Merapi since 1872 and hence, is the first time a larger than "normal" eruption has been well-monitored at Merapi, with seismic, ground deformation and gas emission data available. This eruption therefore provides an ideal case-study in which to examine the driving forces behind transitions in eruptive styles during a single eruption. Comparison with the effusive 2006 eruption provides further insights into the factors that govern whether Merapi erupts explosively or effusively. A well-constrained sample suite representing different stages of the 2010 eruption is linked to eruption chronology, allowing the petrological and textural features to be interpreted in light of eruptive style. Processes occurring deeper in the magmatic system, in the magma reservoir(s), are revealed by whole rock geochemistry, analysis of mineral compositions and thermobarometry of phenocrysts from samples of different stages of the 2010 eruption and compared with those from the 2006 eruption. Shallow magmatic processes occurring in the edifice and conduit are investigated via quantitative textural and compositional analysis of feldspar microlites. Together, the petrological and textural analyses highlight important pre- and syn-eruptive processes occurring in the Merapi magmatic system that acted to influence eruptive behaviour, including deep magma influx and variations in ascent rate which influenced degassing and crystallisation.

4.2. Sampling the 2010 deposits

In order to collect samples for petrological and textural analysis and to relate them to eruption chronology and dynamics, fieldwork was carried out in February 2011,

July 2011 and August 2013. During this time, varying lithologies were identified, sampled and linked to eruption stages, based on the scheme of Komorowski *et al.* (2013). Field localities, stratigraphic sections and sample localities are all documented in Appendix B.

- **Stage 2 (26–29 October 2010) and Stage 3 (29 October–4 Nov 2010): Pre-5 November deposits**

As described in Chapter 2 (Section 2.3.2), Stage 1 of the 2010 eruption (Komorowski *et al*., 2013) was a period of increased volcanic unrest, consisting of increased seismicity, deformation, heat and gas flux (*e.g*. Surono *et al*., 2012). The first deposits were produced on 26 Oct 2010, related to the first explosion and mark the beginning of the eruption and the beginning of Stage 2. Stage 2 and Stage 3 eruptive products were sampled soon after eruption, in February 2011, in dilute PDC (surge) deposits, predominantly in and around Kinahrejo village, as well as on the interfluve regions near Kali Gendol, Kali Woro and Kali Opak (Fig. 1.6). In and around Kinahrejo, 4 or 5 surges occurred during these two stages, with each surge emplacing a unit consisting of two layers. Typically, the lower layer is composed of massive, grey-coloured or 'salt and pepper' coarse ash to fine lapilli, comprised of scoriaceous or dense clasts, herein referred to as "Pre-5 November scoria" and "Pre-5 November dense clasts", respectively. The upper layer is usually a brown-orange or grey coloured fine ash, which is often stratified. The coarser basal layer is interpreted to have formed via emplacement of the dilute PDC, with the upper fine ash layer emplaced due to ash settling as the surge waned and sedimentation rates decreased. Sometimes the ash is rich in plagioclase crystals. Bulk ash samples were taken, as well as lapilli-sized clasts of scoriaceous and dense lithologies (Fig 4.1). Although valley-confined Stage 2 and Stage 3 BAFs were buried by subsequent flows at the time of initial fieldwork in February 2011, some were exposed due to erosion in river valleys and were sampled during fieldwork in July 2011 and August 2013. Component analysis of these BAFs revealed that they are composed of non-juvenile, hydrothermally altered and accidental lithics, as well as light grey dense crystalline clasts, occasional white pumice and abundant grey scoria which is interpreted to correspond to the scoriaceous lapilli (Pre-5 Nov. scoria) sampled in the surge deposits. The dense lapilli (Pre-5 Nov. dense clasts) within the surge layers are interpreted to correspond to the light grey dense crystalline clasts in the

valley-confined facies, as the groundmass textures are very similar when examined with an SEM (see Stage 4 deposits below). Stage 3 was also characterised by rapid (25 m^3 s^{-1}) dome extrusion (See Chapter 2).

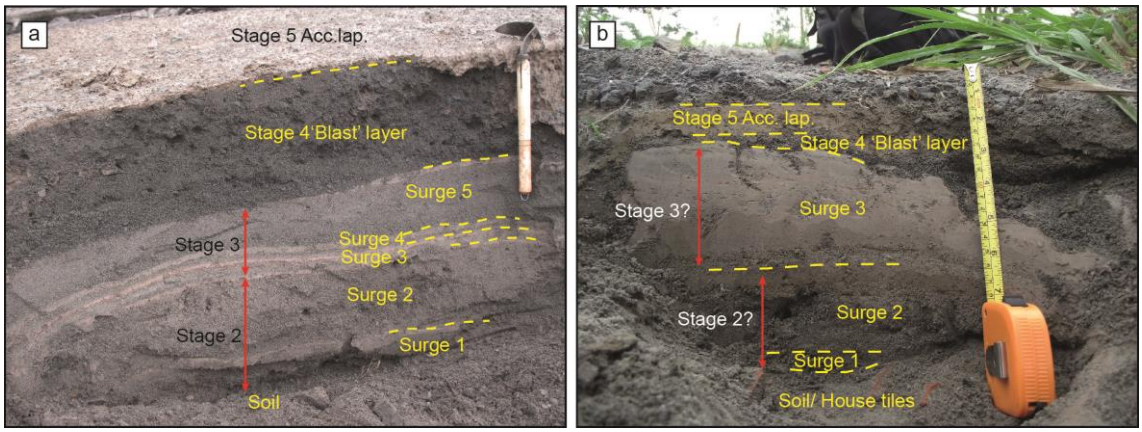

Fig. 4.1 Examples of dilute PDC (surge) deposits emplaced during Stages 2 and 3. (a) Section at Locality 06 on hills north of Kinahrejo village, composed of 5 surge units formed during Stages 2 and 3, all with a coarser lower layer and a fine ash upper layer. Above the surges is the Stage 4 'blast' unit, topped by Stage 5 accretionary lapilli-bearing ash (Photo taken in Feb. 2011). (b) Section at Locality 55 in Kinahrejo village showing 3 surge units, with the Stage 4 'blast' layer and Stage 5 accretionary lapilli-bearing ash above (Photo taken in August 2013). For more details see Appendix B

- **Stage 4 deposits: (5 November 2010)**

Stage 4 deposits are those produced on 5 November, via a series of paroxysmal dome explosions and collapses (Komorowski *et al*., 2013). Stage 4 facies include valley-confined BAFs and associated overbank deposits which were generated via the breakout of confined flows onto interfluve areas, as documented by Charbonnier *et al*. (2013), as well as high-energy, dilute PDC (surge) or 'blast' deposits, documented in detail by Komorowski *et al*. (2013) (Fig 4.2). The 'blast' deposits have bi-partite layering, with the lower layer coarser than the upper (Komorowski *et al*., 2013). The lower layer is clast-supported, fines-depleted, consisting mostly of lapilli, but also may contain blocks or bombs, sometimes up to ~ 20 cm in diameter, as well as containing coarse ash. The upper unit is composed of fine to coarse ash, which sometimes has wavy cross- and planar-stratification (Fig 4.2e). Lapilli pipes are often present, originating from the top of the lower unit (Fig 4.2h). Komorowski *et al*. (2013) identify two 'blast' units (U1 and U2) originating from the two paroxysmal explosions, both with bi-partite layering (U1-L1, U1-L2, U2-L1 and U2-L2). Unit 2 is similar to Unit 1 and is distributed over a similar area, although Unit 2 is typically finer grained, thinner

and outcrops are less abundant. While the two paroxysmal explosions generated these unconfined dilute PDC deposits, channelling of the basal, high particle-concentration portion of the PDCs resulted in emplacement of valley-confined BAFs and unconfined (overbank) flows. The valley-confined BAFs are massive, poorly-sorted and often reversely-graded. They may contain lapilli pipes formed via post-depositional gas escape of the deposit and carbonised plant material, are frequently encrusted with sublimates and may be oxidised towards the top. Stage 4 deposits are almost monolithological, in that their componentry is dominated by dark grey to black coloured, dense fragments of the dome that grew during Stage 3 and which was destroyed by the Stage 4 explosions (Fig 4.2a-c). As well as these dense dome fragments, dark grey to black scoriaceous dome fragments also occur within Stage 4 deposits. Light grey coloured, dense, crystalline material is found as abundant inclusions within the juvenile dome material (Fig 4.2a). Inclusions range in size from a few millimetres to a few centimetres and have angular shapes, indicating brittle behaviour of the light grey material, although occasionally it forms wavy bands through the dome material, indicating ductile behaviour. Large blocks (up to several metres in diameter) of the light grey dense material have also been found loose within the PDC deposits. They are prismatically jointed, indicating that they were hot at the time of eruption and therefore originate from the eruption and are not accidental lithics picked up by the flow (Fig 4.2d). As stated above, it is also probable that the pre-5 November dense lapilli found in Stage 2 and Stage 3 surge and BAF deposits is the same light grey dense material. The light grey dense material is interpreted to originate from a 'plug' of cooled, rigid magma that resided at shallow depth within the magmatic system and was partially re-heated, fragmented and incorporated into the juvenile 2010 magma (Gertisser *et al*., in prep). As well as the light grey dense inclusions, calc-silicate xenolith inclusions are also frequently observed within the 2010 dome lava. They are green and white in colour and originate from interaction of the magma with the surrounding crustal carbonate rocks underlying Merapi. They are frequently observed in Merapi eruptive products from 2010, 2006 and other recent eruptions (*e.g*. Clocchiatti *et al*., 1982; Gertisser and Keller, 2003b; Chadwick *et al*., 2007; Deegan *et al*., 2010; Troll *et al*., 2013). Also forming inclusions within the 2010 dome rocks are frequent magmatic cumulates that are composed of coarse-grained plagioclase, amphibole and clinopyroxene and interpreted to originate deep within the Merapi system.

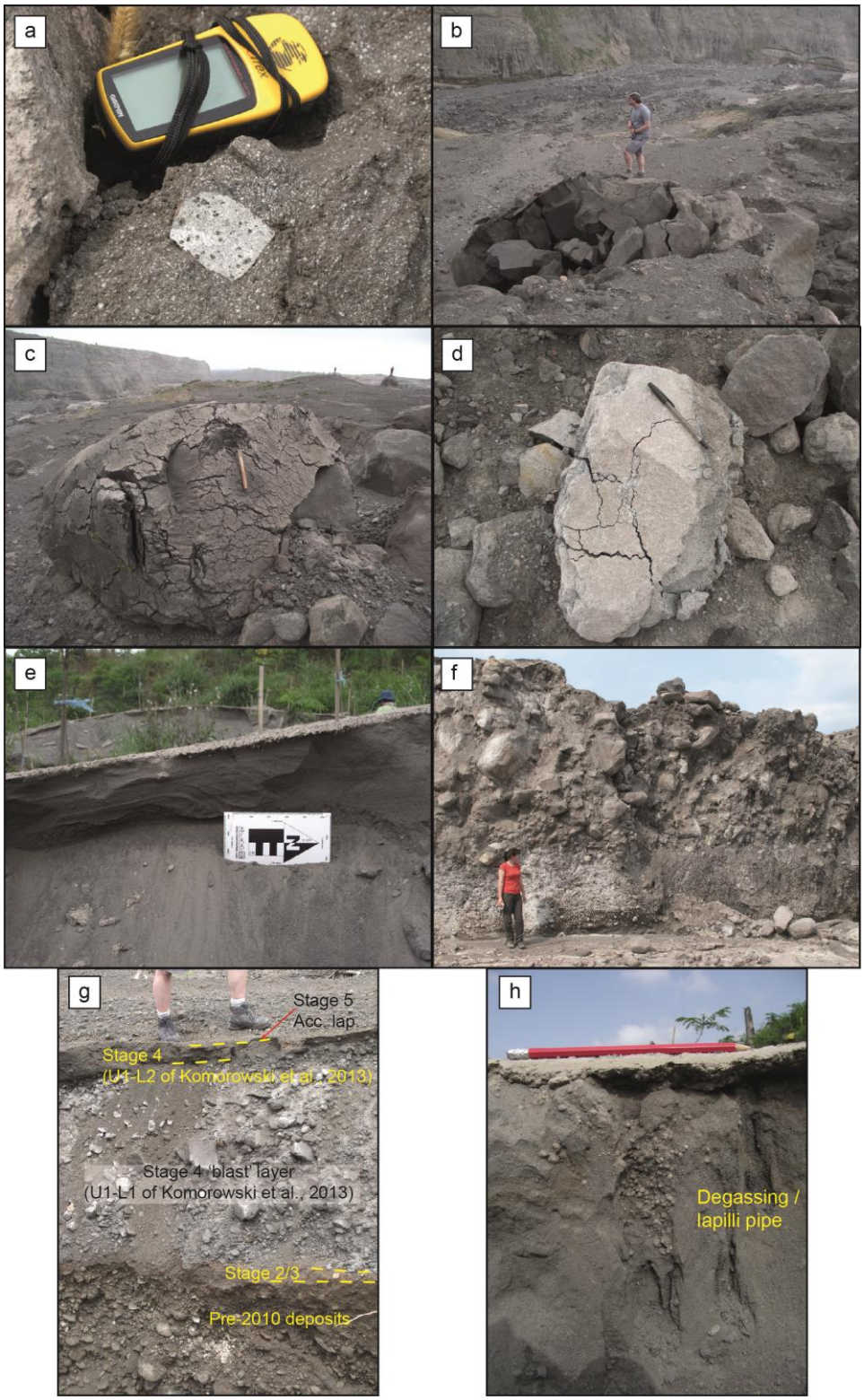

Fig 4.2 Stage 4 deposits and lithologies. (a) Dark dense dome clast, with visible plagioclase, pyroxene and occasional amphibole phenocrysts, hosting a light grey inclusion which has visible phenocrysts of pyroxene. (b) Large prismatically jointed dense dome block in K. Gendol. (c) Rare block with breadcrust texture (d) Prismatically jointed light grey dense block in K. Gendol overbank deposits near Kepuharjo. (e) Upper layer of 'blast' deposit showing cross stratification, correlated with U1-L2 of Komorowski *et al.* (2013) at Locality 19. (f) Typical reversely graded BAF deposit from Stage 4/5 at Locality 21. (g) Stage 4 'blast' unit showing bi-partite layering, with a coarse lower layer and a finer-grained upper layer at Locality 05. (h) Lapilli pipe found in the upper layer (U1-L2) of the 'blast' deposit at Locality 19 near Kinahrejo. See Appendix B for further information

Fig 4.3 Photographs showing damage to landscape and villages due to the 2010 eruption. (a) Ridges north of Kinahrejo with scoured soil and blown down trees. Tree orientation indicates flow direction from Kali Gendol towards Kinahrejo. (b) Melted plastic cassette player in Kinahrejo. (c) Remnants of house in Kinahrejo, razed to the ground by Stage 4 'blasts'. (d) Overturned and burnt car in Kinahrejo, covered by Stage 4 lapilli and blocks. (e + f) Houses destroyed in Kinahrejo. Walls remain partly standing as they were partially protected by local topography. (g) Kali Gendol channel, near Kepuharjo, filled with BAF deposits, with wide-reaching overbank deposits either side. (h) House destroyed by overbank deposits in Wukirsari, Lower K. Gendol

As described in Chapter 2, the 2010 eruption caused considerable loss of life and damage to settlements and infrastructure. This was especially apparent after the 5 November paroxsymal eruption on the southern flanks of Merapi. Figure 4.3 documents some impact of the eruption, observed during fieldwork in February and July 2011.

- **Stage 5 deposits: (5 November 2010)**

Activity during stage 5 consisted of retrogressive summit dome collapse followed by a brief (< 15 minutes) eruptive lull (Komorowski *et al*., 2013). This produced BAFs consisting of variable lithologies, including dense and scoriaceous 2010 dome clasts, light grey dense clasts as well as variable non-juvenile lithics (Fig 4.4).

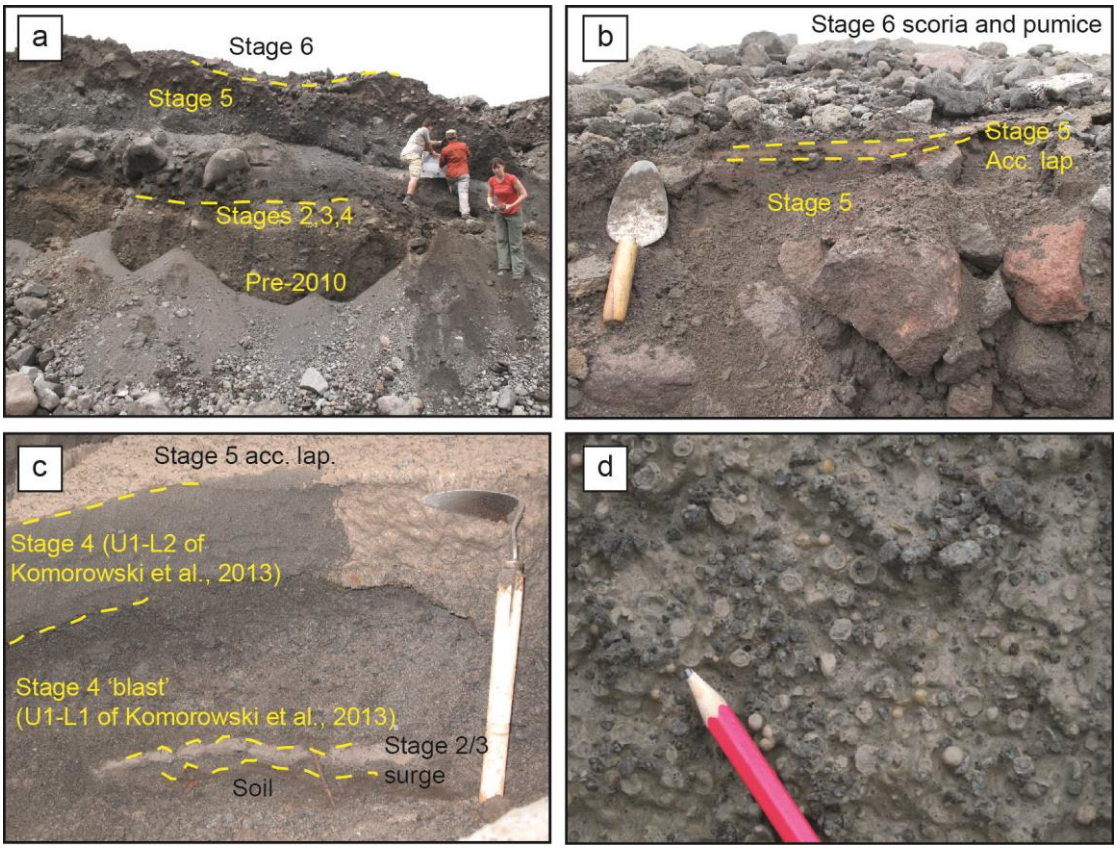

Fig. 4.4 Examples of Stage 5 deposits, (a + b) Overbank deposit at Locality 35 near Kinahrejo sabo dam, including Stage 5 red-pink coloured flow and accretionary lapilli-bearing ash layer. Below Stage 5 are deposits from Stages 2, 3 and 4 and above the accretionary lapilli-bearing ash layer are the Stage 6 scoriaceous and pumiceous flows. (c) Distinctive orange accretionary lapilli-bearing ash layer stratigraphically above the Stage 4 'blast' deposit at Locality 08 on the ridges north of Kinahrejo. Stage 4 has bi-partite layering, with the lower coarser layer composed of coarse ash and lapilli, with an upper layer of stratified ash. (d) Close up of accretionary lapilli layer at Locality 08. See Appendix B for more details

The deposits often have a distinctive reddish-pink colour . The eruptive lull at the end of Stage 5 allowed for the deposition of a layer consisting of orange-pink coloured fine ash with abundant accretionary lapilli (Fig 4.4). This accretionary lapilli layer forms a distinctive marker horizon across the southern flanks either stratigraphically above the Stage 5 BAFs in the valleys, or above Stage 4 'blast' deposits on interfluve areas. Both dense and scoriaceous dome samples were collected from Stage 5 deposits. Although the dome clasts from Stage 4 and 5 were emplaced at different times, the source dome was extruded during Stage 3 and therefore are classed as the same lithology type.

- **Stage 6 deposits: (5 November 2010)**

Stage 6 activity consisted of ash venting and recurrent fountain collapse, generating PDCs (Komorowski *et al*., 2013). Stage 6 deposits related to fountain collapse are rich in scoriaceous or pumiceous clasts. In particular, a Stage 6 PDC rich in grey scoriaceous clasts (herein referred to as "grey scoria") was sampled in the Kali Gendol and on the Kali Gendol interfluve areas (Fig 4.5). The deposit also contains juvenile dome fragments as well as various non-juvenile lithics. Scattered on the surface of the scoria-rich flow deposits in and around the Kali Gendol are abundant white pumice clasts, also interpreted to be associated with the Stage 6 fountain collapse events (Fig 4.5). White pumice was also collected from the ridges north of Kinahrejo, where they were scattered on the surface of the Stage 5 accretionary lapilli layer, scattered around the surface near to the Kinahrejo 'Forest Gate' as well as being found in reworked deposits in Kali Putih on the western flanks (See Appendix B for localities). In addition, comparatively 'dense' and geochemically distinct white pumices were discovered scattered on proximal surge deposits on a ridge north of Gunung Kendil and in Kali Putih (Fig 4.5).

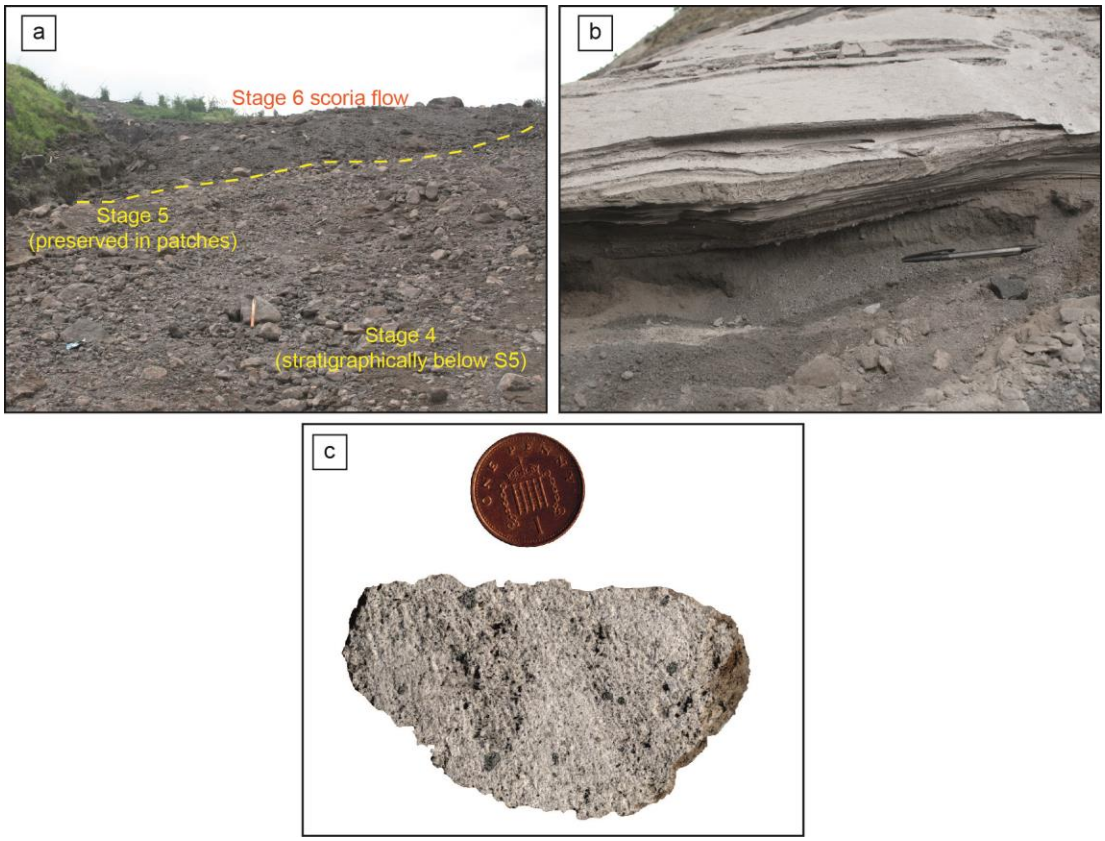

Fig. 4.5 Examples of Stage 6 deposits and samples. (a) Stage 6 scoria flow, emplaced stratigraphically above Stage 5 and 4 flows, at Locality 35, near the sabo dam at Kinahrejo. (b) Surge layers north of Gunung Kendil where comparatively 'dense' pumice lapilli were collected, Locality 36. (c) Photograph of typical white pumice clast with visible vesicles and dark-coloured clinopyroxene phenocrysts

The main 2010 lithology types that are used in this study for petrological and textural analysis and/ or referred to in the thesis are summarised in Table 4.1.

Table 4.1 Main lithology types collected from the 2010 deposits and referred to throughout this thesis

Date	Stage	Lithology sampled
26-29 Oct	2	Ash
		Pre-5 November scoria clasts
		Pre-5 November dense clasts (Light grey inclusion material?)
29 Oct- 4 Nov	3	Ash
		Pre-5 November scoria clasts
		Pre-5 November dense clasts (Light grey inclusion material?)
5 Nov	4	Dome (dense)
		Dome (scoriaceous)
		Light grey inclusion material
5 Nov	5	Dome (dense)
		Dome (scoriaceous)
		Light grey inclusion material
		Accretionary lapilli
5 Nov	6	Grey scoria
		White pumice
		'Dense' pumice

4.3. Analytical Methodology

Major elements were analysed by XRF at the University of East Anglia, as described in Chapter 3 (Section 3.3.2). Trace elements were analysed by ICP-MS at Acme Analytical Laboratories, Vancouver, Canada (http://acmelab.com). Samples were crushed to a fine powder using a tungsten carbide mill at the University of East Anglia and further preparation was carried out at Acme Labs. Rare earth elements and refractory elements were analysed from sample splits fused with lithium borate before being digested in dilute acid. Precious metals and base metals (*i.e.* Au, Ag, As, Bi, Cd, Cu, Hg, Mo, Ni, Pb, Sb, Se, Tl, Zn) were analysed from sample splits that were digested in hot (95 °C) aqua regia. All results are listed in Appendix C

Mineral compositions (Appendix D) were analysed using Cameca SX100 electron microprobes at the University of Cambridge and at The Open University. Minerals were analysed with 1, 5 or 10 μm beam diameter, a 15–20 kV accelerating voltage and 10–20 nA bean current. Volatiles were analysed with extended peak counting times. Na was always measured first to minimise migration effects. In-house natural mineral standards were used for calibration and as secondary standards during analytical runs.

Textural analysis of feldspar microlites was carried out on representative samples of dense and scoriaceous dome (Stage 4), grey scoria and white pumice (Stage 6) (Appendix G). Textural analysis was carried out using the methodology outlined in Chapter 3 (Section 3.3.3) with backscatter electron (BSE) images. However, some modifications to the method were made in order to account for the vesicularity of some of the 2010 samples. The parameters φ and N_A, as well as calculation of CSDs must be done on a vesicle-free basis in order to allow fair comparison between samples. Vesicle correction was needed for the scoriaceous dome, white pumice and one grey scoria sample, although a second grey scoria sample did not need to be corrected for vesicularity, as a large enough groundmass area was found which comprised only groundmass glass and microlites, with no vesicles. The vesicle area was measured automatically using the threshold function of *ImageJ* and the area occupied by the vesicles calculated. Vesicles in BSE images can easily be selected by the threshold function, as they are black and contrast highly with the brighter groundmass glass and mineral phases. The area occupied by vesicles can then be subtracted from the total

sample area, so that all calculations of φ and N_A are carried out on vesicle-free basis. The area % of vesicles can then be entered into the *CSDCorrections* program (Higgins, 2000), which corrects for this in the calculation of population density.

4.4. Results

4.4.1. Whole rock geochemistry

Whole rock geochemical analysis was carried out in order to determine any differences between the composition of juvenile 2010 products as well to compare to those from 2006 and other recent eruptions. Merapi 2010 rocks are classed as high-K basaltic andesite, with all products containing between 52.6 and 58.1 wt.% SiO_2 on a volatile-free basis (Fig. 4.6). However, most juvenile components identified (*i.e.* dense and scoriaceous dome clasts, white pumice and grey scoria) have ~ 54.5–55.7 wt.% SiO_2, similar to the 2006 products (Preece *et al.*, 2013) and those from other 20th century dome eruptions (Gertisser *et al.*, 2012a) (Fig. 4.6). The light grey dense inclusion material generally has less evolved compositions (52.62–54.96 wt.% SiO_2) and the ash sampled from surge and fall deposits is generally more SiO_2 rich (55.10–58.09 wt.% SiO_2). With increasing SiO_2 content, TiO_2, Fe_2O_3, MgO and CaO contents decrease, whereas Al_2O_3, Na_2O and K_2O contents increase. P_2O_5 remains at similar concentrations of ~ 0.27–0.33 wt.% (Fig. 4.6).

Trace element concentrations for all 2010 lithologies are similar to each other and are similar to 2006 rocks, with concentrations also similar to values reported for other recent Merapi high-K series rocks that are characteristic of the Merapi eruptive products younger than ~ 1900 y BP (Gertisser and Keller, 2003b; Gertisser *et al.*, 2012a).Concentrations of incompatible trace elements such as Rb, Ba, Zr and Pb increase with increasing SiO_2. V and Sr are negatively correlated with SiO_2, whereas Ce remains at ~65–85 ppm (Fig. 4.7). Trace element patterns of 2010 rocks normalised to N-MORB (Sun and McDonough, 1989) are typical of subduction-related magmas. They show an enrichment of large ion lithophile elements (LILE) such as Rb, Ba, K and Sr, and to a lesser extent enrichment of light rare earth elements (LREE) in comparison to heavy rare earth elements (HREE) and high field strength elements (HFSE) such as Nb, Ta, Zr, Hf and Ti (Fig. 4.8). HREE are depleted compared to N-MORB and negative

anomalies exist for Nb, Ta and Ti. Chondrite-normalised REE patterns of the 2010 Merapi products are also typical for a subduction-related environment, with LREE enrichment and flat HREE trends. Like all Merapi rocks, the 2010 products lack a Eu anomaly (Fig. 4.8), which is thought to be a result of the comparatively high oxygen fugacity of the Merapi magmas (Gertisser, 2001). Again, the concentrations of trace elements in 2010 rocks are similar to each other and to those produced in 2006, as well as reported values and normalised patterns of other recent high-K rocks at Merapi (Gertisser and Keller, 2003b). All whole rock geochemical data is listed in Appendix C.

4.4.2. Mineralogy, petrography and mineral compositions of the 2010 products

All eruptive products from the 2010 eruption contain feldspar, clinopyroxene, orthopyroxene, Fe-Ti oxides, amphibole and accessory apatite, similar to the 2006 eruptive products (Fig 4.9). In addition, the light grey inclusion material also contains cristobalite and biotite. All mineral analyses are listed in Appendix D.

Feldspar is always present as phenocrysts (~ 500–2000 μm), microphenocrysts (~ 50–500 μm) and microlites (~ < 50 μm). Phenocrysts and microphenocrysts analysed in all 2010 products are wide ranging in composition between $An_{25}Ab_{70}Or_5$ and $An_{91}Ab_9Or_{<1}$ (Fig 4.10). Phenocrysts may be normally zoned, reversely zones, oscillatory zoned (Fig 4.9a), have sieve-textured cores or have very high-An (up to An_{91}) unzoned cores, with lower-An rims (Fig 4.9b). Rims often contain ~ 40–50 mol.% An. Microlites are generally more evolved in composition, however they may contain up to ~ 84 mol.% An. Plagioclase microlites are often mantled by alkali element-rich rims of anorthoclase and more K-rich alkali feldspar (sanidine). 2010 microlite compositions range from $An_1Ab_{41}Or_{58}$ (alkali feldspar) to $An_{84}Ab_{16}Or_{<1}$ (plagioclase) (Fig 4.10). Microlites from all lithologies possess a similar overall range of compositions, however white pumice microlites are generally more albitic and those from the light grey inclusions are predominantly alkali-rich.

Clinopyroxene is present as phenocrysts, microphenocrysts and microlites in all 2010 Merapi products, and orthopyroxene is common as microphenocrysts and microlites. Crystals of anhedral to subhedral orthopyroxene are sometimes rimmed by clinopyroxene. Phenocrysts may be zoned or unzoned and often host silicate melt (glass)

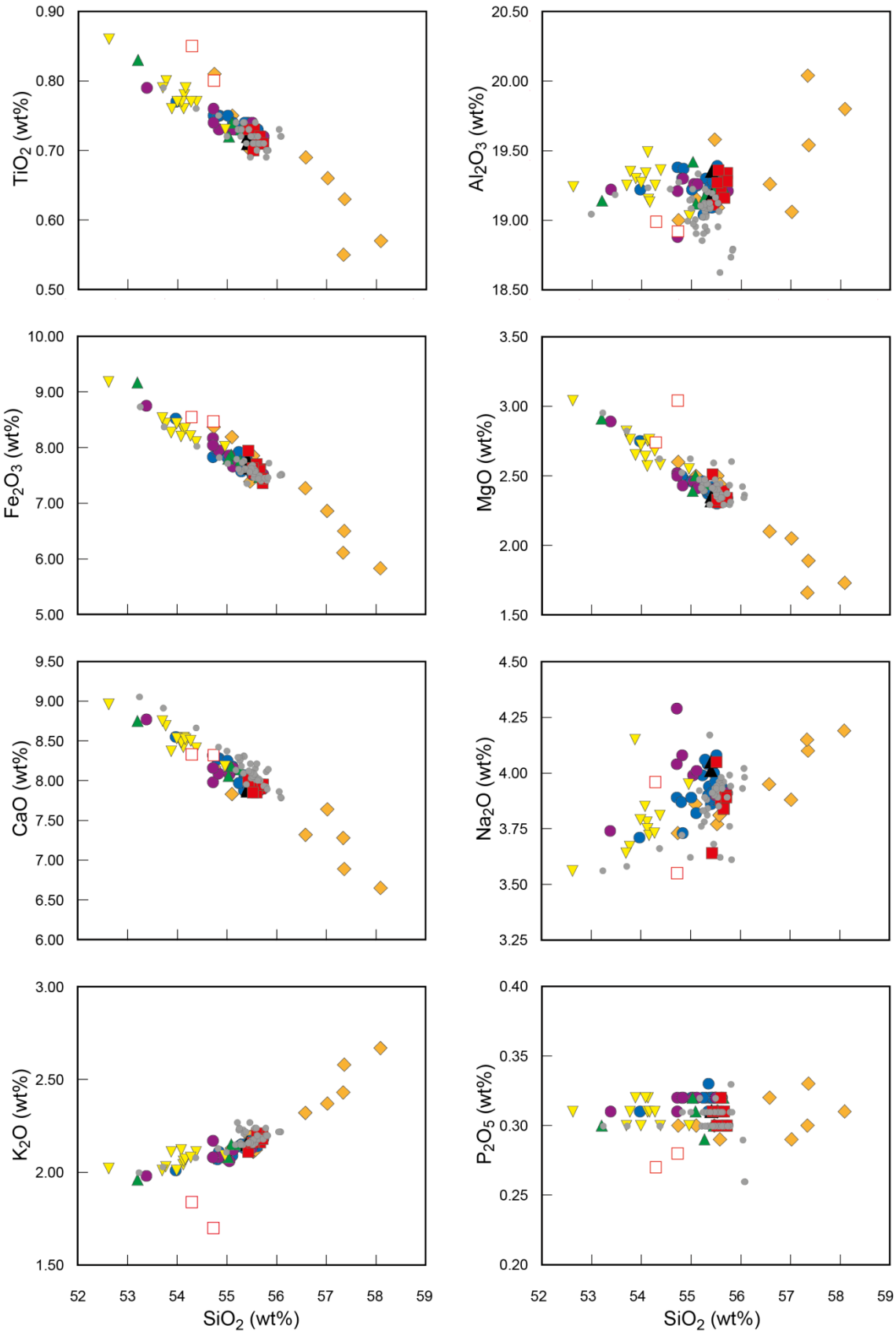

Fig4.6 Variation diagrams for major elements versus SiO_2 for various lithologies of the 2010 eruption, compared with 2006 and other 20th century products. All elements are normalised to 100 wt.% on a volatile-free basis. All iron is reported as Fe_2O_3. See Fig 4.7 for key

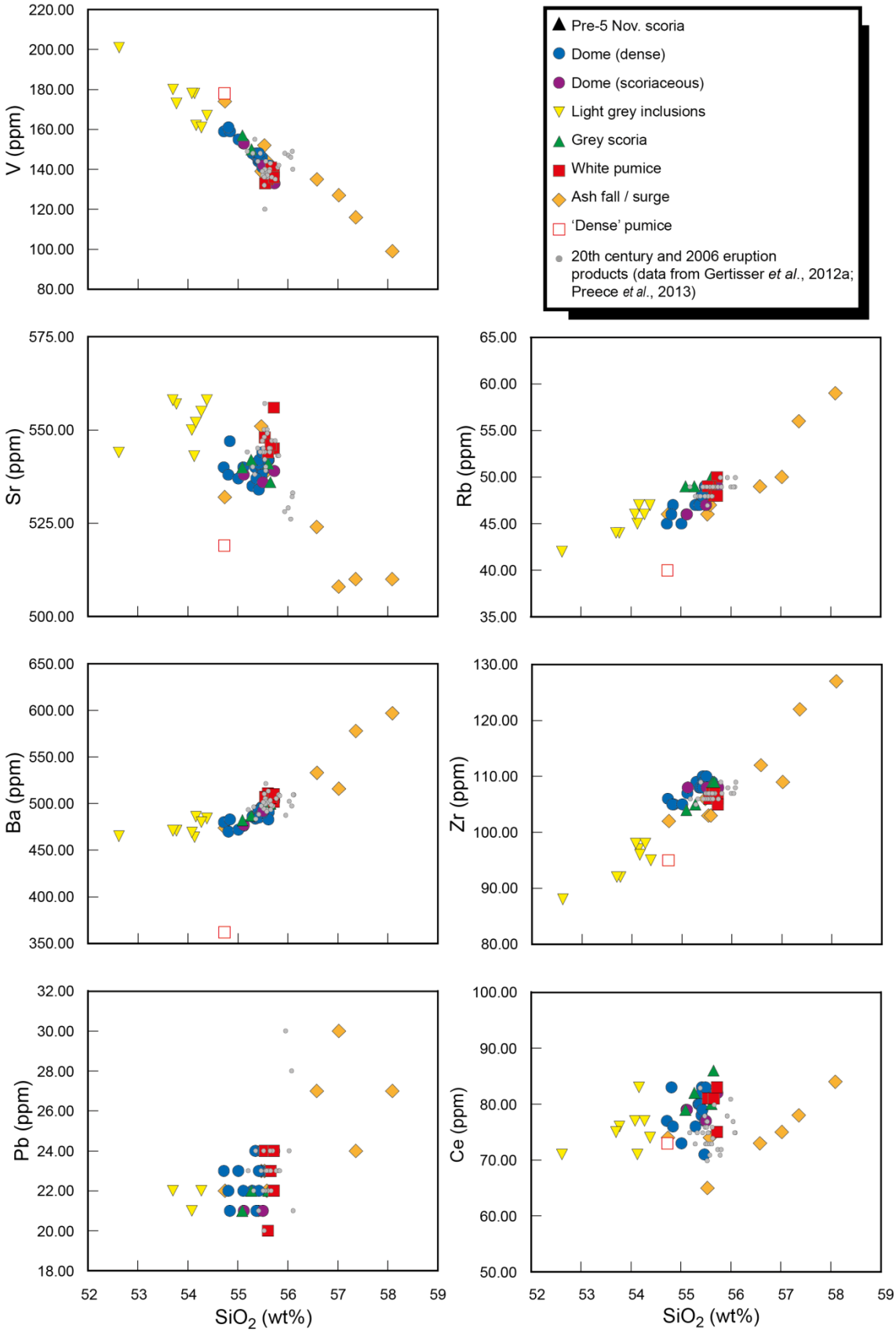

Fig. 4.7 Variation diagrams for trace elements (ppm) versus SiO_2 (wt.%) from various lithologies produced during the 2010 eruption

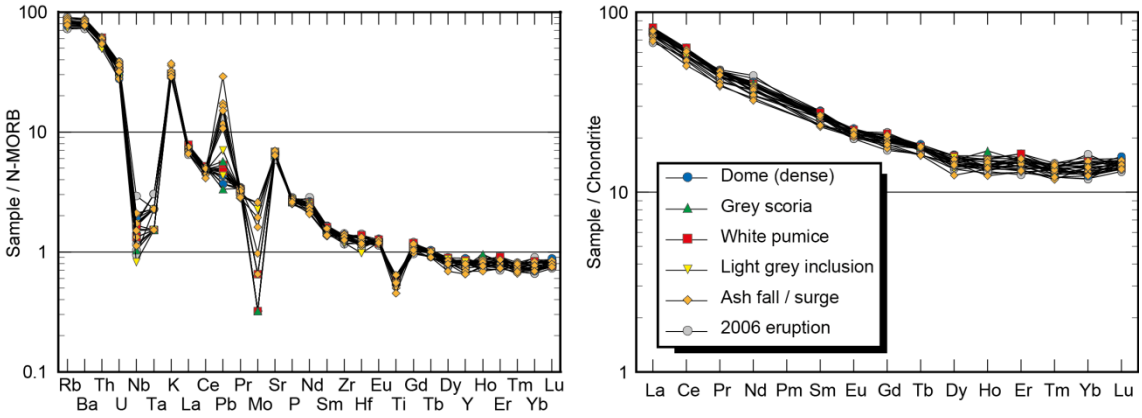

Fig. 4.8 N-MORB and chondrite-normalised trace element patters for 2010 products and 2006 rocks. All normalising values are from Sun and McDonough (1989)

inclusions, as well as inclusions of magnetite, plagioclase and apatite (Fig 4.9c). Clinopyroxene phenocrysts are classed as augite and diopside ($Wo_{39-50}En_{36-46}Fs_{10-19}$), following the scheme of Morimoto (1988) (Fig 4.10), with between 0.4 and 8.9 wt.% Al_2O_3, although the majority contain between 1.5–2.5 wt. % and have Mg# 61–85, with most between 75–85 (Mg# = 100 x Mg / (Mg + Fe^{2+}) . Occasional orthopyroxene phenocrysts were analysed and classed as enstatite ($Wo_{0.2-0.3}En_{57-70}Fs_{27-39}$) (Fig 4.10). Microlites and microphenocrysts in the 2010 products generally have more variable compositions compared to the phenocrysts. Clinopyroxene microphenocrysts and microlites are usually augite and diopside ($Wo_{40-50}En_{35-45}Fs_{13-21}$) (Fig 4.10), with 0.8–7.6 wt.% Al_2O_3 and Mg# 65–81, with most between Mg# 70–80. However, several crystals with higher Fe content were analysed and classed as hedenbergite ($Wo_{49-50}En_{8-21}Fs_{29-41}$), with 1.2–2.6 wt.% Al_2O_3 and Mg# 19–47 (Fig 4.10). These crystals were exclusively found in the dense dome lava, near a calc-silicate xenolith and were bright green when viewed in plane-polarised light. Orthopyroxene microlites ($Wo_{0.5-9}En_{45-81}Fs_{16-53}$) are classed as enstatite, pigeonite and ferrosilite (Fig 4.10). Orthopyroxene microphenocrysts and microlites contain between 0.2 and 3.6 wt% Al_2O_3 and have Mg# from 54 to 94, although the majority have Mg# ~65–75. The crystals with orthopyroxene cores and clinopyroxene rims, plot within the same Wo-En-Fs space as the other pyroxene crystals.

Amphibole is present in all samples as phenocrysts and microphenocrysts, but is absent as groundmass microlites. Amphibole is titanian magnesiohastingsite, following

the classification of Leake *et al.* (1997), with the proportion of ferric iron calculated stoichiometrically on a 13eCNK basis, which provides a maximum Fe^{3+} content (Fig 4.10). Crystals may be homogenous in composition, or zoned, often with rims of higher Al_2O_3 and MgO, and lower SiO_2, K_2O and FeO compared to the cores (Fig 4.9f). The overall range of Al_2O_3 content is 10.0–14.9 wt.% with Mg# ranging between 49 and 58, with a cluster at ~ 62–68. Of the crystals with Mg# > 68, 70 % are phenocrysts from the white pumice, with the rest being phenocrysts from the light grey inclusions. More than 55 % of the crystals with Mg# <62 are dense dome microphenocrysts. Amphiboles may be surrounded by breakdown reaction rims, composed of anhydrous minerals plagioclase, pyroxene (or olivine) and Fe-Ti oxides (Fig 4.9e). However, in contrast to 2006 products, amphiboles from 2010 frequently do not possess breakdown reaction rims.

Fe-Ti oxides occur in all samples as anhedral and irregularly shaped microphenocrysts and microlites, as well as inclusions within clinopyroxene phenocrysts. All Fe-Ti oxides are titanomagnetite and no ilmenite was found. Crystals range in ulvöspinel content from 18–59 mol.%, although most range from ~ 22 to 35 mol.% (Fig 4.10). Titanomagnetite is often exsolved to various extents showing trellis-type exsolution, consisting of ilmenite lamellae parallel to the {111} planes of the titanomagnetite host (Buddington and Lindsley, 1964; Haggerty, 1993). Rare pyrrhotite inclusions have also been observed within magnetite, amphibole and clinopyroxene hosts (Fig 4.9d).

Apatite is present as anhedral inclusions within clinopyroxene, plagioclase and amphibole phenocrysts, and rarely as groundmass microlites. Crystals contain 0.6–1.4 wt.% Cl, as well as 2.8 to 5.4 wt.% F, with the majority containing ~ 3–4 wt.% F. Although H_2O was not measured directly, Cl, F and OH occupy one site within the mineral structure, so OH can be calculated if F and Cl are known. This was done based on 24 oxygens, on the basis of H_2O filling the C-site, using an Excel spreadsheet developed and kindly provided by Andy Tindle (The Open University, UK). In the Merapi apatite crystals, the site is occupied with between 8 and 25% Cl, 36 to 71% F and between 6 and 56 % OH, with variable OH and F concentrations and relatively constant Cl.

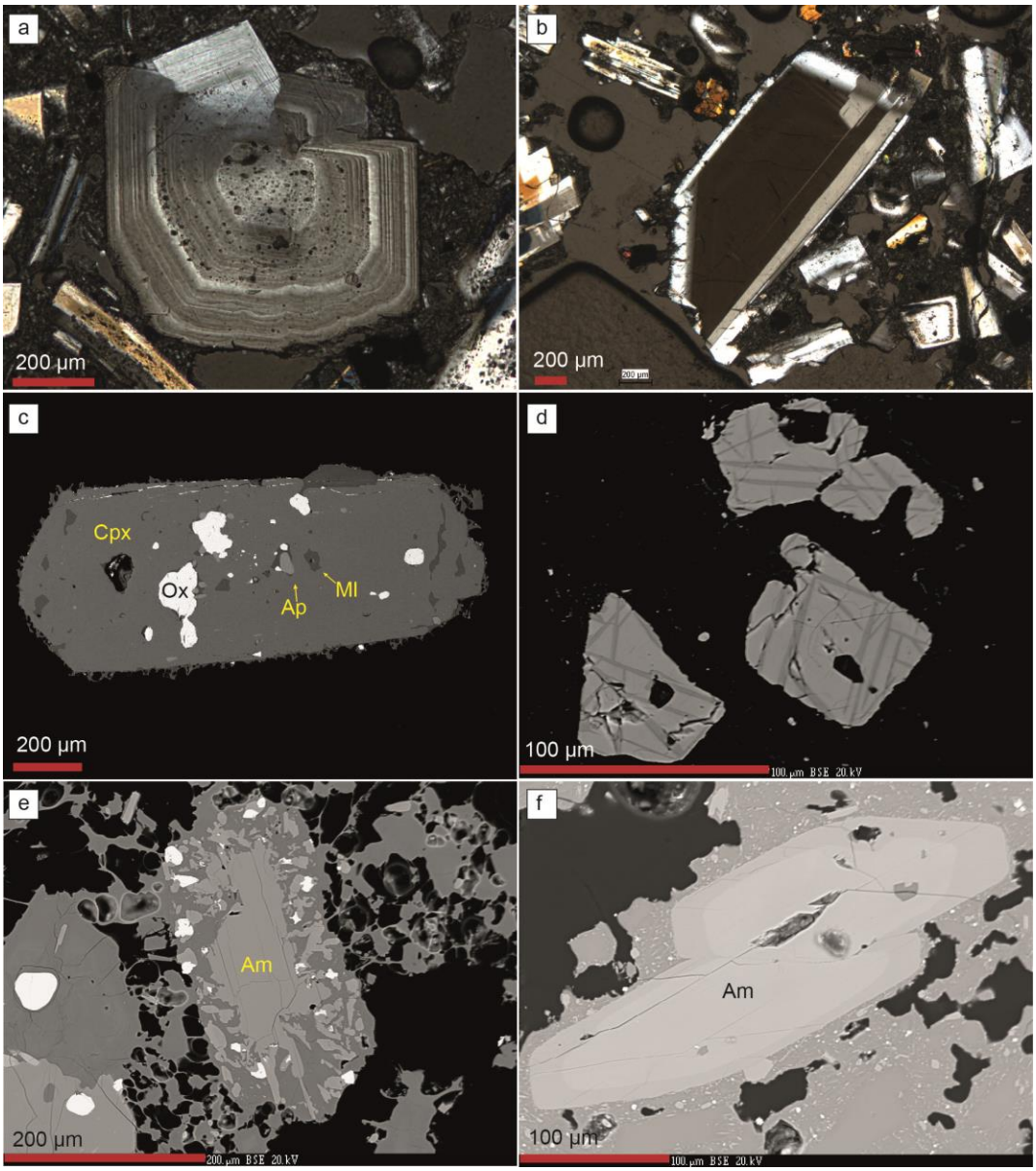

Fig 4.9: (a) Oscillatory zoned plagioclase phenocryst in dome material; (b) Plagioclase phenocryst with very high-An unzoned core, mantles by lower-An rim; (c) unzoned clinopyroxene phenocryst containing silicate melt inclusions (MI), apatite inclusions (Ap) and Fe-Ti oxide inclusions (Ox); (d) Fe-Ti exsolution lamellae; (e) amphibole phenocryst in white pumice sample, surrounded by breakdown rim; (f) pristine zoned amphibole phenocryst in dense dome sample

Within the light grey inclusion material, biotite and a crystalline SiO_2 phase, cristobalite, are also present. Biotite has not previously been observed in Merapi products before 2010. In this study it has been frequently noted in the light grey inclusion material, and Costa *et al.* (2013) also note the presence of biotite in 2010 samples. Biotite contains 0.5–3.8 wt.% F, 0.1–0.3 wt.% Cl, between 11.9 and 15.6 wt.% FeO, with Mg# 63–70. Cristobalite is observed to fill small vesicles and is pervasive within the groundmass, often with 'fish-scale' cracked morphology or a microbotryoidal texture.

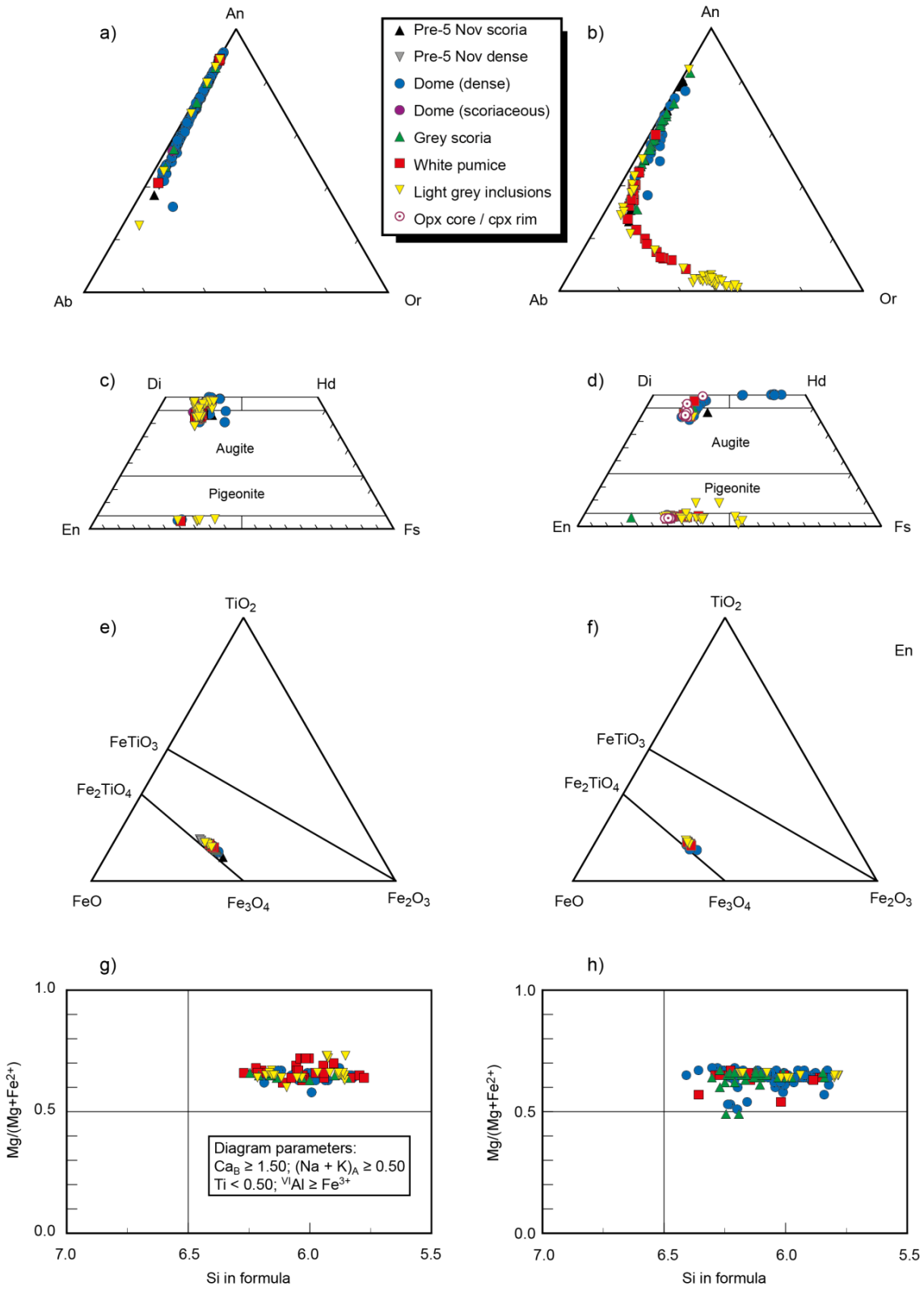

Fig. 4.10 Mineral compositions of phenocrysts, microphenocrysts and microlites from various 2010 eruptive products, (a) Feldspar phenocrysts and microphenocrysts, (b) Feldspar microlites, (c) Pyroxene phenocrysts, (d) Pyroxene microphenocrysts, microlites and crystals with opx cores / cpx rims, (e) Fe-Ti oxide microphenocrysts, (f) Fe-Ti oxide microlites, (g) amphibole phenocrysts, (h) amphibole microphenocrysts

4.4.3. Textural analysis of feldspar microlites

4.4.3.1. Textural characterisation of microlites

The groundmass textures of the 2010 eruptive products are highly variable. Textural analysis of feldspar microlites, the most abundant groundmass phase, reveals differences in crystal size, abundance and morphology between different lithologies (Fig. 4.11). Analysis was focussed on representative samples erupted on 5 November, during the climactic stages of the 2010 eruption. Analysed samples include dense and scoriaceous dome samples that were rapidly extruded from the end of October (Stage 3), before the dome was destroyed by explosions on 5 November (Stage 4). In addition to the dense and scoriaceous dome clasts produced by effusive activity, microlites were also analysed in samples of Stage 6 grey scoria and white pumice, originating from explosive activity. This analysis therefore provides a means of comparing groundmass microlite textures produced via effusive and explosive activity that occurred during 2010, as well as comparing the rapidly-emplaced dome samples of 2010, with samples of more 'typical' dome-forming activity that occurred during 2006.

Microlite abundance, expressed as areal number density (N_A), which describes the number of crystals per unit area, ranges from 5682 to 63,962 mm^{-2}. The highest number densities are in samples from the dome, especially the dense dome samples. The lowest number densities are recorded in samples of white pumice (Fig. 4.12). Mean crystal area is variable, with most samples ranging between 4–6 μm^2, with the dense dome samples at the lower end of this range and grey scoria at the higher end. The average crystal size of the white pumice microlites is an order of magnitude larger, at up to 60.46 μm^2 (Fig. 4.12). Feldspar microlite crystallinity (φ), calculated after Hammer *et al*. (2000), is the fraction of groundmass area that is occupied by feldspar microlites, on a vesicle- and phenocryst-free area, thereby taking into account the area of liquid available for late-stage crystallisation. Crystallinity is a function of both microlite abundance and size, as many small crystals may produce the same crystallinity as few large crystals. Crystallinity ranges from 0.16 to 0.37 in 2010 samples, with dense dome samples having φ of 0.28 and 0.29, the scoriaceous dome sample measured has a φ of 0.25, grey scoria samples range from 0.16 to 0.25 and the white pumice from 0.19 to 0.37 (Fig. 4.12). As well as crystal abundance and size, the morphology of the

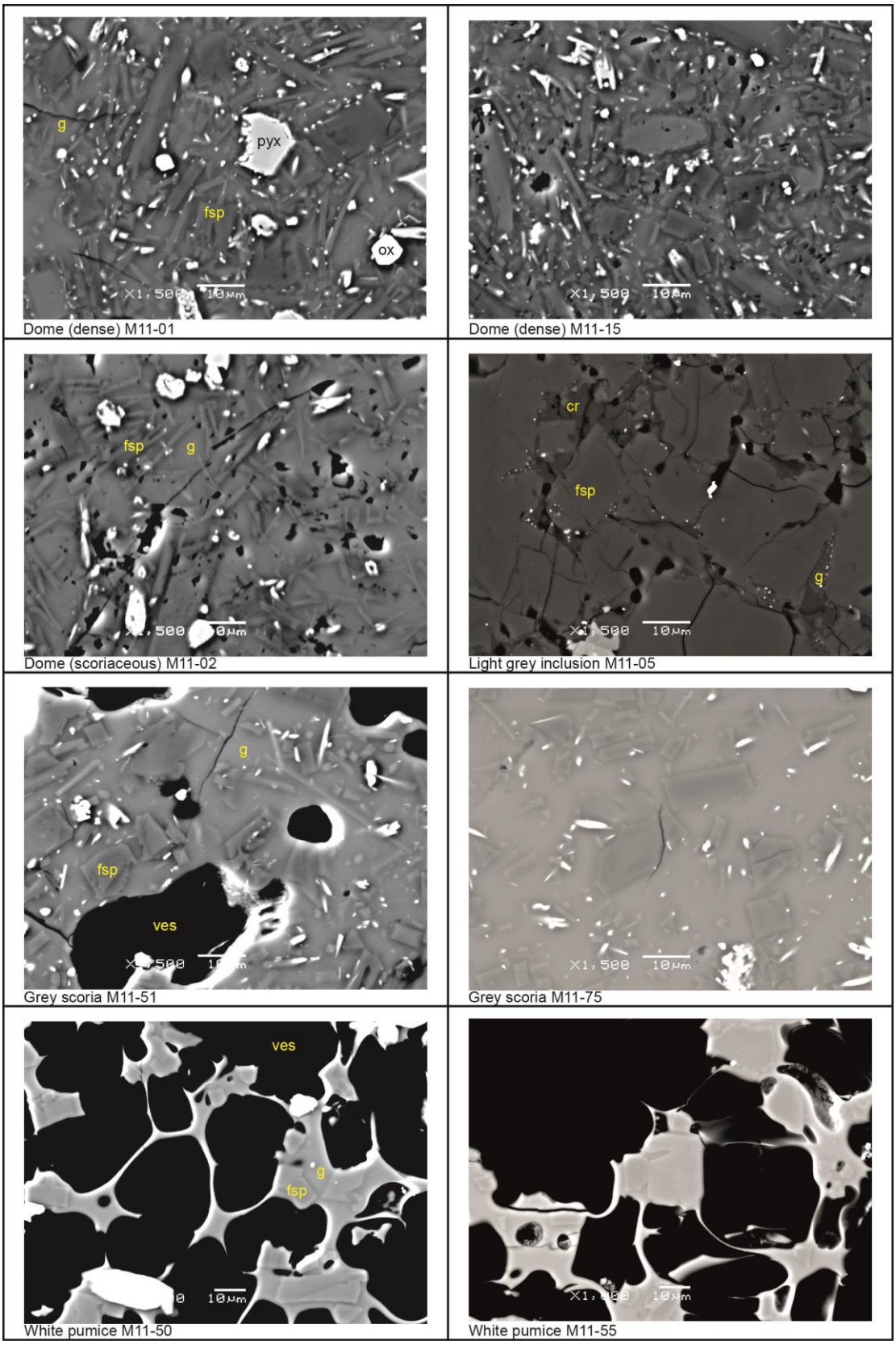

Fig.4.11 Representative BSE images of the groundmass of 2010 lithologies, showing feldspar microlites (fsp), pyroxene microlites (pyx), Fe-Ti oxide microlites (ox), groundmass glass (g) and vesicles (ves). Note presence of cristobalite (cr) and speckled appearance of groundmass glass in the light grey inclusion material. Scale bars are 10 microns. Note that all images are taken at x1500 magnification, except images of white pumice at x1000

microlites was calculated using *CSDSlice* (Morgan and Jerram, 2006). The short (S) axis is always 1.00, the intermediate (I) axis ranges from 1.10 to 3.20 and the long (L) axis ranges between 1.50 and 10.00. All microlite crystal populations were estimated with *CSDSlice* as having acicular crystal habits, apart from those in the white pumice, which are classed as having a rectangular prism habit. Short/long (S/L) axis ratios range from 0.10 to 0.67, with acicular shaped crystals having a low S/L and more blocky shaped crystals having a higher S/L. Most microlite populations had S/L < 0.20, with the dense dome crystals estimated at 0.10–0.20, the scoriaceous dome at 0.10 and the grey scoria microlites at 0.10–0.18. The white pumice microlites have higher S/L, with both sampled populations estimated at 0.67 (Fig. 4.12). Light grey inclusion material has a highly crystalline groundmass, which has not been analysed quantitatively because many microlites are touching, making discrimination of separate crystals difficult. However, qualitative observations show that the highly crystalline groundmass is composed of tabular or equant looking crystals, with low proportions of groundmass glass. The remaining glass often appears speckled, with heterogeneities of light and dark areas in backscatter images (Fig.4.11). Cristobalite is common in the groundmass.

To summarise, the 2010 products have either many small microlites (*e.g.* dense dome) or few large microlites, such as in the white pumice samples. The relatively few and large microlites of the white pumice have blocky morphologies, whereas the abundant small microlites in the dome samples are acicular in shape (Table 4.2).

Table 4.2. Textural variation of feldspar microlites in samples from the 2010 eruption. Lithology types are DD= dense dome, DS= scoriaceous dome, GS= grey scoria, WP= white pumice. *n** denotes number of feldspar crystals analysed. Numbers in brackets indicate the standard deviation for the crystal area, and the R^2 value for the crystal aspect ratio. Area % feldspar has been vesicle-corrected where necessary.

Stage	Lith.	Sample	2D areal measurements							3D volumetric measurements		
			*n**	Total Area (μm^2)	N_A (mm^{-2})	Area % fsp	φ	Mean crystal area (μm^2)	Gm. Glass (area %)	Vesicle area %	Calc. aspect ratio (R^2)	No. density by vol (mm^3)	Vol. from inter area (%)
4	DD	M11-15	678	10682	63471	27.8	0.29	4.40 (15.61)	67.73	N/A	1.00:1.60:5.00 (0.7245)	17500000	27.86
4	DD	M11-01	790	12351	63962	25.8	0.28	4.03 (16.50)	66.43	N/A	1.00:1.50:10.00 (0.6928)	8880000	25.66
4	DS	M11-02	736	15612	50150	23.88	0.25	4.76 (20.68)	70.70	6	1.00:3.20:10.00 (0.5101)	10900000	23.89
6	GS	M11-75	717	27568	26009	15.2	0.16	5.84 (16.20)	82.04	N/A	1.00:1.50:10.00 (0.7869)	2850000	14.44
6	GS	M11-51	779	18082	53338	24.48	0.25	4.59 (15.36)	72.58	18.2	1.00:1.40:5.50 (0.7512)	13600000	24.17
6	WP	M11-50	691	338454	5760	34.82	0.37	60.46 (185.32)	58.27	64.1	1.00:1.15:1.50 (0.8548)	635000	34.39
6	WP	M11-55	645	296824	5682	18.61	0.19	32.75 (123.64)	80.40	59.7	1.00:1.10:1.50 (0.8399)	998000	17.69

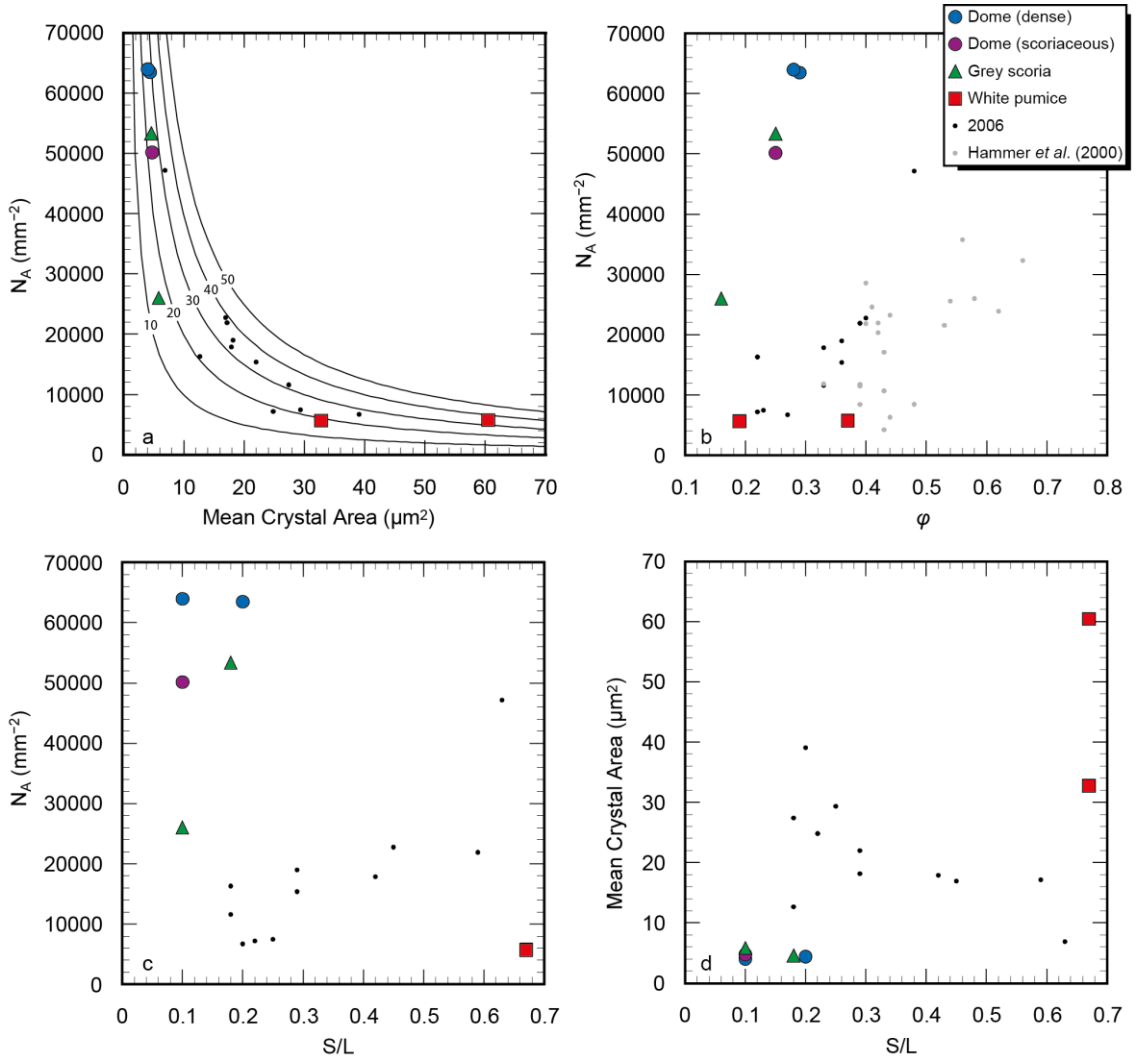

Fig. 4.12 Variation in textural parameters in 2010 products compared to those from 2006. (a) Areal feldspar microlite number density (N_A mm^{-2}) vs. mean crystal area (µm^2), with solid lines indicating modelled microlite crystallinity at a particular N_A and crystal size, labelled with percentage values. (b) Areal feldspar microlite density (N_A mm^{-2}) vs. feldspar microlite crystallinity (φ) including previously published data of samples from other recent effusive dome-forming eruptions (Hammer *et al.*, 2000). (c) Areal microlite number density (N_A mm^{-2}) vs. S/L. (d) Mean crystal area (µm^2) vs. S/L

4.4.3.2 Crystal Size Distribution (CSD) analysis

The 2-dimensional intersection measurements as outlined above, were converted into 3D data using *CSDSlice* (Morgan and Jerram, 2006) and *CSDCorrections* software (Higgins, 2000), as described in Chapter 3. Figure 4.13a shows the CSD plots of the 2010 samples, with bins containing less than 5 crystals not shown, as they are they are not precise (Higgins, 2000), whereas, for comparison, Figs4.13b-h show data from all the bins. The values reported here are based only on statistically viable bins (*i.e.* those containing > 5 crystals). The majority of the CSDs display curved trends, which may be

divided into 2 or 3 segments (Fig. 4.13). The exceptions to this are the CSD plots of white pumice samples, both of which are composed of one straight line (R^2= 0.98 and 0.99). The y-axis intercept (n^o), which is indicative of the final nucleation density, ranges from 18.78 to 23.17 mm^{-4}, with white pumice samples having the lowest intercept values, the dense dome having the highest and the scoriaceous dome and grey scoria plotting in between. This is consistent with the N_A data calculated, which also showed that the dense dome samples have the highest crystal number density and the white pumice have the lowest. As seen in the 2006 CSDs discussed in Chapter 3, the decrease in population density at the smallest sizes, resulting in a left-hand "downturn" is considered to result from conversion errors in the CSD software, resulting from a lower probability of intersecting smaller crystal sizes (Cashman, 1988; Brugger and Hammer, 201b; Higgins, 2010). Some of the calculated crystal sizes calculated with *CSDCorrection*s, do not appear to match the distribution expected from the 2D intersection data. In particular, in 2D section, the white pumice samples have a mean crystal area, larger than all of the other sample types (Table 4.2), which is not reflected in the CSD. In the CSD plot, both of the white pumice samples appear to have a lack of larger crystals, with the CSDs of all other samples extending to larger crystal sizes compared with the white pumice (Fig. 4.13). Even when the discarded bins of larger crystal sizes are taken into account, the white pumice CSDs still appear to lack the larger sized crystals (Fig. 4.13).

4.5. Discussion

4.5.1. Geochemical and petrological data

Whole rock compositions, both in terms of major and trace elements, fall within a restricted compositional range, with all juvenile 2010 products similar to one another, as well as being similar to 2006 products (Preece *et al*., 2013) and products from other recent dome forming eruptions (del Marmol, 1989; Andreastuti *et al*., 2000; Camus *et al*., 2000; Gertisser *et al*., 2012a). Since the mid-20th Century, the eruptive products of Merapi have maintained remarkably constant compositions, especially considering that a host of processes such as recharge and mixing with a more primitive magma, fractional crystallisation and crustal contamination are all invoked to play a major role in the magmatic evolution at Merapi (Camus *et al*., 2000; Gertisser and Keller, 2003a;

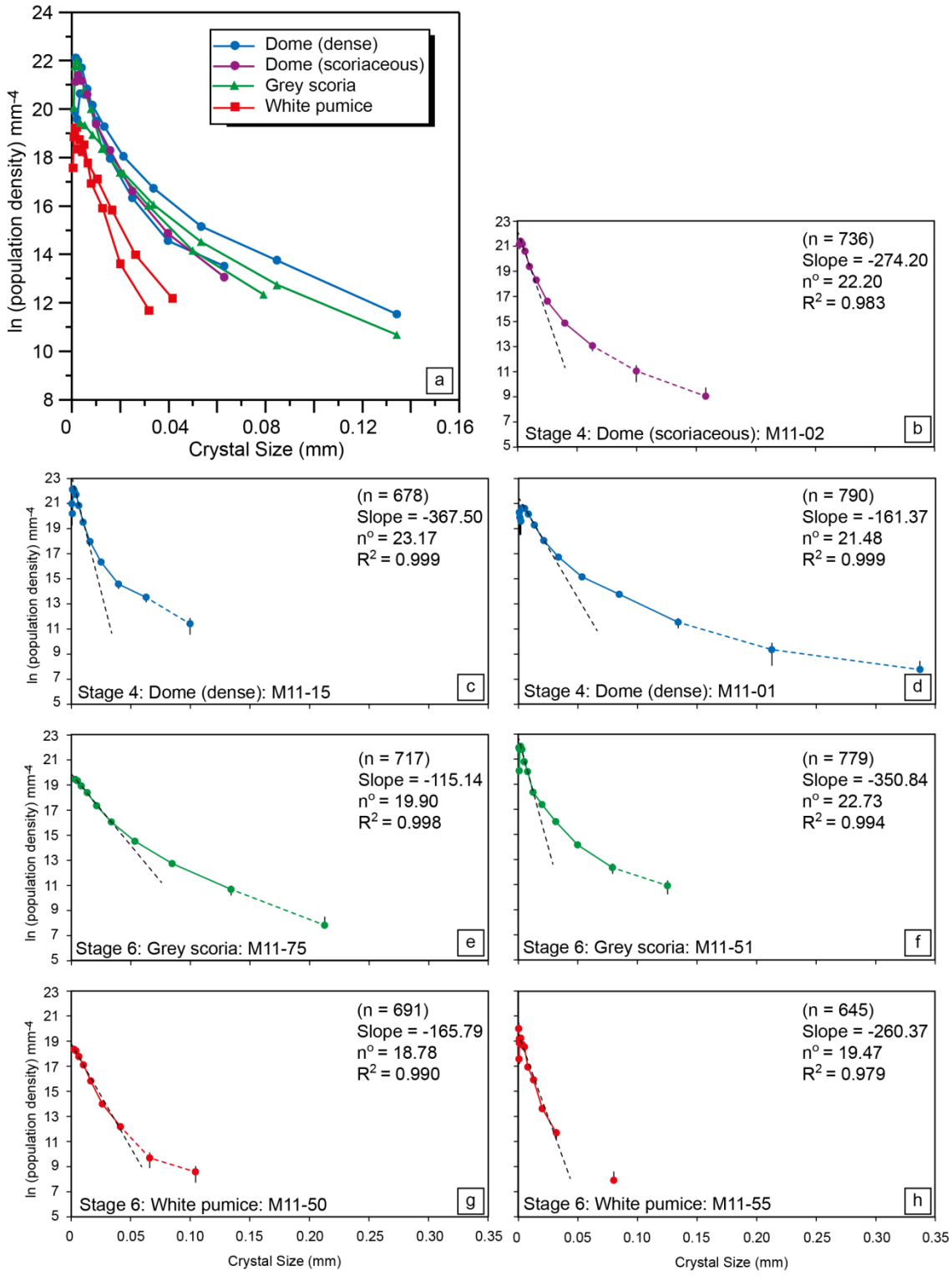

Fig. 4.13 Crystal size distribution (CSD) plots of feldspar microlites from the 2010 eruption. (a) all CSDs plotted, with bins with < 5 crystals excluded. (b–h) individual CSDs for each sample. Coloured dashed lines join excluded bins containing < 5 crystals. Black dashed lines are regression lines fitted to the steepest initial part of the CSD. Values for the slope of these regressed lines, the y-axis intercepts or nucleation densities (n^o) and R2 values given. n = number of feldspar crystals analysed

Chadwick et al., 2007; Chadwick *et al*., 2013; Costa *et al*., 2013). Gertisser and Keller (2003a) suggest that in order to maintain uniform magma compositions over decadal time periods, a continuously active magma reservoir is maintained in a quasi-steady state by balanced fractional crystallisation, recharge and eruption. The similarity in magma composition produced in 2006 and in other recent dome-forming eruptions, compared to in 2010, suggest that the magma that has produced effusive activity over the past century is also capable of producing larger magnitude explosive eruptions, as in 2010. This is in contrast to the previous VEI 4 eruption that occurred in 1872 and which has been tentatively linked to a basaltic deposit (Newhall *et al*., 2000; Gertisser, 2001), suggesting that different magma dynamics played a role in 1872 compared with 2010. Some compositional differences are observed in the 2010 products, with the ash samples apparently more evolved (more SiO_2-rich) and the light grey dense inclusion material less evolved. The Stage 2 and 3 ash compositions may be explained as an effect of crystal winnowing, as varying proportions of loose crystals may be segregated from the ash during transport. Stage 2 and 3 scoria clasts do not show more evolved compositions but, instead are similar compositions to the other juvenile clasts, supporting the idea that evolved ash compositions are due to modification during ash transport and emplacement. The light grey inclusion material is more mafic than the other juvenile 2010 products, which may be due to higher crystal content.

Mineral compositions are wide ranging but typical for Merapi products. Feldspar phenocryst compositions range between ~ An_{25}–An_{90}, although they are most frequently between ~ An_{40}–An_{90}. Costa *et al*. (2013) reported 2010 feldspar compositions within a similar range, but identified 3 groups defined by anorthite content, clustered at ~ An_{90}, An_{70} and An_{40}, interpreted to have formed at different depths within the plumbing system and affected by assimilation of crustal carbonate. The data from this study show a continuous range between ~ An_{40}–An_{90} rather than distinct clustered groups. The variety of feldspar zoning types (oscillatory, normal, reverse, sieve-textured, high-An cores) is evidence of dynamic open-system processes occurring within the Merapi magmatic system. High anorthite plagioclase phenocryst cores (up to ~ An_{90}) have previously been interpreted to be derived from crustal carbonate material at Merapi, based on a combination of anorthite content and Sr isotope analysis (Chadwick *et al*., 2007; Deegan *et al*., 2010). Phenocrysts found both in the 2006 and in the 2010 rocks with unzoned high-An cores and lower An rims, may therefore be recording crustal

contamination prior to both eruptions. If these phenocrysts are recording crustal contamination, the fact that the high-An cores are often mantled by lower An rims, suggests that the crustal contamination did not take place immediately prior to eruption. Alternatively, high-An phenocryst cores could have crystallised at higher temperatures or P_{H2O} (Couch *et al*., 2003b; Martel, 2012) or may have crystallised from a more mafic melt (Gertisser, 2001). High-An cores may be xenocrystic cores inherited from a more mafic magma, that have been incorporated into the basaltic andesite magma, where the lower-An rim was able to form. Feldspar microlite compositions are discussed in Section 4.4.2 in relation to textural analysis.

Many geothermobarometers can be used to gain an insight into the plumbing system at Merapi. However, in order to use many of these reliably it is necessary to ascertain that mineral pairs or mineral–melt pairs are indeed equilibrium pairs. For example, in order to utilise the hornblende–plagioclase thermometer (Holland and Blundy, 1994), is it necessary to know what composition plagioclase is in equilibrium with the amphibole. This is difficult to know given the wide range of feldspar compositions present in the Merapi rocks, and no inclusions of these minerals were found within each other. A similar problem was reported by Costa *et al*. (2013). Likewise, in order to employ the pyroxene–liquid thermometer (Putirka, 2008), the melt composition in equilibrium with an individual pyroxene should be determined. Melt inclusions in Merapi samples are not in equilibrium with their clinopyroxene hosts. Costa *et al*. (2013) calculated that a mafic melt would be in equilibrium with pyroxene phenocrysts, rather than the andesitic to rhyolitic melts of the melt inclusions. Therefore, thermobarometers based only upon single mineral compositions were applied.

The amphibole thermobarometer of Ridolfi and Renzulli (2012) was applied in order to establish pressure and temperature estimates for the crystallisation of amphibole phenocrysts and microphenocrysts. This thermobarometer is updated from the Ridolfi *et al*. (2010) model, and is based on thermobarometric equations obtained through multivariate least squares analysis of experimental and natural calcic amphiboles from calc-alkaline and alkaline magmas. Errors are estimated at $T \pm 23.5$ °C and $P \pm 11.5\%$ (Ridolfi and Renzulli, 2012). Results indicate that 2010 amphiboles crystallised at 328–1034 MPa (Fig. 4.14). Assuming a mean crustal density of 2800 kg/m^3 (Costa *et al*., 2013), these pressures equate to depths of crystallisation of ~ 12 to

38 km below the summit. Temperature estimates range from 888 to 1025 °C, although most are between 920 and 1020 °C. In comparison, 2006 amphiboles crystallised at a more restricted pressure range between 350 and 859 MPa (~ 13–31 km) and temperatures of 935–1022 °C (Fig. 4.14). Amphiboles in cumulate inclusions were also analysed, with results revealing that they crystallised at pressures as high as 1336 MPa (41 km). Cumulate amphibole cores crystallised at minimum pressures of 625 MPa (23 km) although rims sometimes record shallower crystallisation (minimum 440 MPa). Microphenocrysts have generally crystallised shallower than phenocrysts, with cores and rims appearing to have formed over a similar pressure range. Focussing on the 2010 amphiboles, dome, grey scoria and light grey inclusion amphiboles have crystallised over a similar pressure range (328–898, 373–897 and 354–810 MPa, respectively), whereas the white pumice incorporates amphiboles crystallised at greater pressures and depths (405–1034 MPa) (Fig. 4.14). In contrast to the results of Costa *et al*. (2013) who proposed that 2010 amphiboles crystallised at two distinct pressure ranges (~ 800 and ~350–400 MPa), the data in this study indicate a continuum of pressures between ~ 350 and 1000MPa (Fig. 4.14). This may be because more data were gathered in this study as well as the fact that this study also samples Stage 6 grey scoria and white pumice, not only Pre-5 November and dome products. The 2006 data from this study also indicate a wider range of amphibole crystallisation pressures (350 and 859 MPa) compared to those reported by Costa *et al*. (2013), albeit more restricted than those erupted in 2010. Amphiboles erupted in 2010 may sometimes display breakdown rims composed of plagioclase, clinopyroxene and magnetite, although often the amphiboles are pristine. By contrast, all amphiboles in the more slowly ascended 2006 products are reacted, except for in the 2006 Stage II dense dome clasts (see Chapter 3). Experiments on Mount St. Helens dacitic pumice show that amphiboles are only stable when the coexisting melt contains more than ~4 wt.% H_2O, and during decompression and degassing, amphiboles begin to break down within approximately 5 days, to form reaction rims of anhydrous minerals (e.g. Rutherford and Hill, 1993). This suggests that the abundant amphiboles without reaction rims in the 2010 Merapi products may have ascended from the amphibole stability to erupt at the surface within a similar timeframe.

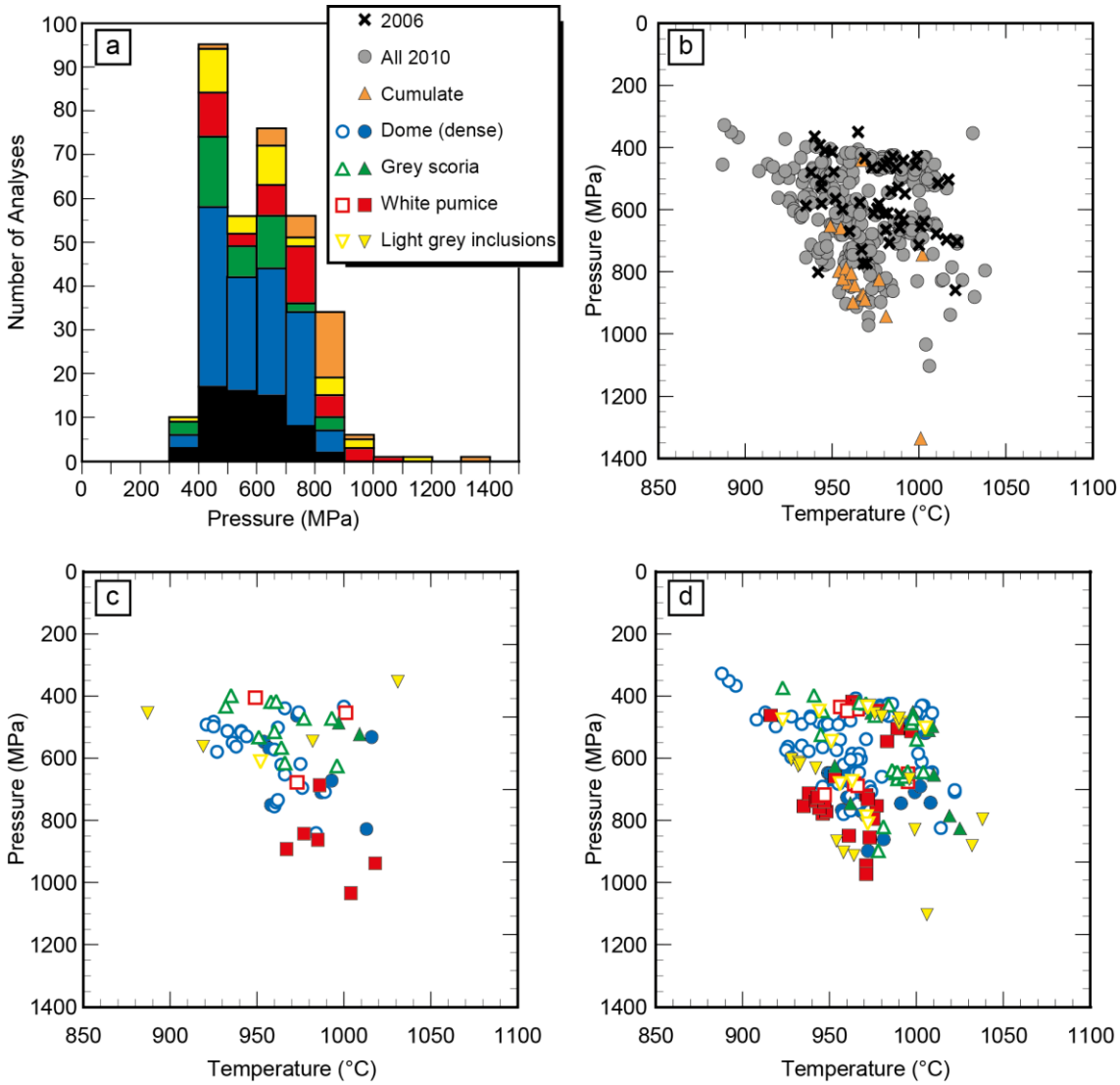

Fig. 4.14 Results of amphibole thermobarometry using the model of Ridolfi and Renzulli (2012). (a) histogram of crystallisation pressure of amphibole phenocrysts and microphenocrysts from 2010 lithologies, with amphiboles from 2006 and cumulate inclusions as a comparison, (b) temperature and pressure estimates of all measured amphiboles from 2010, 2006 and cumulates, (c) 2010 crystal rims, filled symbols are phenocrysts and open symbols are microphenocrysts, (d) 2010 crystal cores, filled symbols are phenocrysts and open symbols are microphenocrysts

Clinopyroxene barometry was carried out on clinopyroxene phenocrysts, microphenocrysts and microlites, using the structural geobarometric calculations of Nimis (1999). Barometry was carried out assuming a temperature of 1000 °C, based on previous two-pyroxene thermometry (Costa *et al*., 2013) and the mildly alkaline (MA) calibration was used, which has an error of ± 200 MPa. Pressure estimates for the 2010 clinopyroxene crystallisation range between 100–850 MPa (~3.6–30.1 km depth), with the bulk of crystallisation occurring at between ~400–700 MPa (~14–25 km) (Fig. 4.15), which is similar to the zone of major crystallisation suggested by Gertisser (2001) and Chadwick *et al*. (2013). The deepest clinopyroxenes are most often found in grey scoria

and white pumice (up to 850 MPa and 790 MPa, respectively), with nearly 50 % of the clinopyroxene that crystallised at > 650 MPa (~24 km) originating from the white pumice. Clinopyroxene barometry is discussed in more detail in Chapter 5, in relation to silicate melt inclusions. Most clinopyroxene contains ~1 to 3 wt.% Al_2O_3, although high-Al clinopyroxene (up to a maximum of 8.9 wt.% Al_2O_3) is common within the 2010 products (Fig. 4.15). In comparison, other recent dome lavas have phenocrysts containing up to 3.65 wt.% Al_2O_3 (Gertisser, 2001). The majority of high-Al clinopyroxene occurs as phenocrysts and microlites within the dome clasts, and appear to have crystallised over a range of pressures between ~350 and 850 MPa. These pressures are consistent with previous petrological modelling, which suggests that high-Al clinopyroxene at Merapi may be stable in conditions of moderate pressure–high temperature (~300 MPa and 1067 °C) as well as at high pressure–moderate temperature (~800 MPa and 985 °C) conditions (Costa *et al.*, 2013). This suggests that, in order for high-Al clinopyroxene to be stable at the lower end of the observed pressure range, magmatic temperatures must have been high. It should be noted, that if magmatic temperatures are higher than 1000 °C, then the calculated pressure estimates are maximum values. The bright green hedenbergite crystals found in dome lava, near to a calc-silicate xenolith, are interpreted to originate from the calc-silicate and are evidence of assimilation of metamorphosed crustal carbonate material.

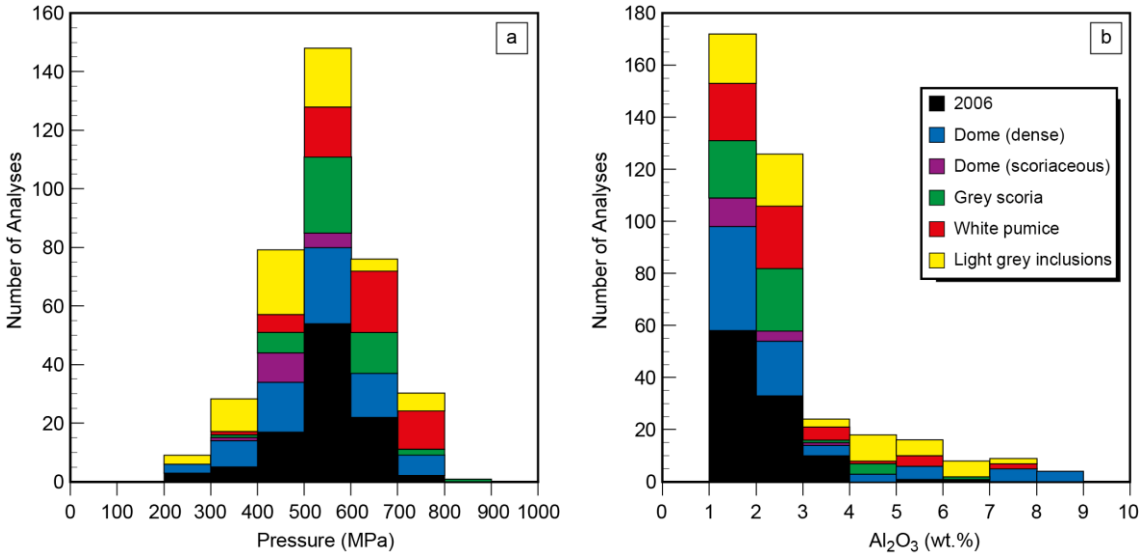

Fig. 4.15 Histograms of clinopyroxene from 2010 and 2006 (a) pressures of crystallisation, calculated using CpxBar (Nimis, 1999) with the majority of crystals from > 600 MPa from the grey scoria or white pumice, (b) Al_2O_3 content (wt.%) in pyroxene crystals, with the majority of high-Al pyroxenes originating from the dense dome

Thermobarometry of the 2010 amphibole and clinopyroxene reveals crystallisation throughout the crust at ~3–38 km depth, with cumulate amphibole recording crystallisation down to 41km. A major zone of crystallisation is situated within the mid to lower crust, at pressures of ~ 400–800 MPa (~ 14 to 29 km depth), where the bulk of amphiboles and pyroxenes crystallised prior to the 2010 and 2006 eruptions. The 2010 explosive Stage 6 grey scoria and white pumice both incorporate a large proportion of deeper crystals compared to the other lithologies, which crystallised at up to 38 km depth. High-Al clinopyroxene also suggest the presence of a hotter and deeper magma within the system. This implies an influx of deeper, hotter, magma prior to, or during the course of the 2010 eruption.

4.5.2. Crystallisation and degassing during magma ascent revealed by groundmass microlites

Analysis of the 2010 feldspar microlites reveals highly variable groundmass textures, in terms of crystal abundance, crystal morphology, mean crystal size and size distribution. The 2D intersection data and crystal size distribution (CSD) analysis reveal that the dense dome clasts and the white pumice can be considered as textural end-members of the paroxysmal 2010 products, with the dense dome groundmass composed of many, small acicular microlites and the white pumice groundmass containing relatively few, large, equant crystals. The scoriaceous dome and grey scoria samples show textural characteristics between these two end-members.

As previously discussed in Chapter 3, groundmass microlite textural differences are due to differences in undercooling (ΔT) during crystallisation, which may occur during ascent or during dome residence. The 2010 dome began to extrude sometime between 29 October (Komorowski *et al*., 2013) and 1 November (Pallister *et al*., 2013) and was destroyed by explosions early on 5 November. Therefore, the 2010 dome clasts resided for a maximum of 7 days within the dome. The Merapi 2010 dome samples (dense and scoriaceous) have a maximum φ of 0.29 with minimum of 66 % of the groundmass area being composed of glass. This is within the range of values for 2010 grey scoria and white pumice that have seen no dome residence (φ = 0.16–0.37 and groundmass glass = 58–82 area %). Comparison of the 2010 Merapi dome microlite textures with groundmass textures from samples interpreted to have crystallised on

domes at other volcanoes (*e.g.* Sparks *et al*., 2000; Pallister *et al*., 2008) show that the samples from the other studies are more extensively crystallised, sometimes nearly holocrystalline, with lower amounts of groundmass glass that is often devitrified. The dome samples from previous studies have spent weeks within the dome, allowing time for crystallisation, compared to only days for the 2010 Merapi dome. Previous studies also suggest that crystallisation kinetics become increasingly sluggish in viscous, near anhydrous, high-SiO_2 magma present within domes, making continued crystallisation increasingly difficult (Cashman, 1988; Wolf and Eichelberger, 1997). Therefore, although a small proportion of crystallisation during dome residence cannot be entirely ruled out, the microlite textures predominantly reflect conditions during magma ascent. The textures observed in the 2010 dome samples vary from those recorded in 2006 dome samples (Preece *et al*., 2013) as well as other recent Merapi domes (Hammer *et al*., 2000), further suggesting that textures reflect ascent conditions rather than dome residence.

Groundmass microlite textures are principally controlled by rates of crystal nucleation, which differ considerably depending on magmatic ascent and decompression paths (e.g. Cashman and Blundy, 2000). Crystal nucleation and growth conditions are a function of ΔT (Lofgren, 1980; Kirkpatrick, 1981). Decompression during magma ascent may induce crystallisation because declining H_2O solubility results in volatile exsolution (*e.g.* Burnham and Davies, 1971; Moore *et al*., 1998; Papale *et al*., 2006), an increase in liquidus temperatures and resultant degree of ΔT. At moderate ΔT, new crystals do not readily nucleate and crystallisation progresses primarily by growth of existing crystals. At high ΔT, nucleation dominates over crystal growth and new crystals are formed in preference of the growth of existing ones. However, at very high ΔT, as may occur during explosive eruptions, limiting rates of diffusion as a consequence of increased magma viscosity at low H_2O contents (Hess and Dingwell, 1996), mean that crystallisation is retarded and the melt quenches to glass.

Groundmass microlite textures of the 2010 dome samples are indicative of high degrees of ΔT during crystallisation. High microlite number densities, small crystal sizes and acicular morphologies, all point to nucleation-dominated crystallisation at high ΔT, forming many small crystals with high aspect ratios. Experimental evidence shows a relationship between decompression and microlite number density (Hammer

and Rutherford, 2002; Brugger and Hammer, 2010a; Martel, 2012) and dome extrusion rates have previously been correlated with microlite number density in natural samples (e.g. Nakada and Motomura, 1999; Hammer *et al*., 2000). Experiments also show crystal morphologies change from tabular and euhedral to acicular or dendritic shapes as ΔT increases (Lofgren, 1974, 1980; Corrigan, 1982) and as decompression rates increase (*e.g.* Couch *et al*., 2003; Szramek *et al*., 2006; Brugger and Hammer, 2010a). The extrusion rate of the Stage 3 2010 dome was 25 m^3 s^{-1} (Pallister *et al*., 2013). In comparison, this is nearly 8 times greater than peak extrusion rates at Merapi in 2006 (Ratdomopurbo *et al*., 2013) and 78 times greater than in 1995 (Hammer *et al*., 2000). Similarly high rates of dome effusion have been recorded during the 2006 explosive and effusive eruption of Augustine volcano (Coombs *et al*., 2010) and during the 2009 eruption of Redoubt (Diefenbach *et al*., 2012), although most dome extrusion rates worldwide are < 5 m^3 s^{-1} (Pallister *et al*., 2013). High extrusion rates and high ascent rates of the 2010 dome magma resulted in high degrees of ΔT related to degassing during fast decompression, causing nucleation-dominated crystallisation and yielding textures with many, small acicular crystals. High ascent rates are also confirmed by the lack of reaction rims on many of the amphibole phenocrysts and microphenocrysts in the dome samples. Values of N_A are higher for a given φ compared to the 2006 and other recent dome forming eruptions (Fig. 4.12b), indicating that crystallisation was dominated by high levels of nucleation in comparison to other recent eruptions. The white pumice were also formed during high rates of magma ascent in the sub-Plinian stage of the 5 November paroxysmal activity, and yet have different groundmass textures to the dome, with less numerous microlites that are relatively large in size and equant in morphology. At very high ΔT, crystallisation is retarded due to an increase in viscosity with H_2O loss. Also, sufficiently rapid ascent results in no crystallisation due to a lag time between conditions of supersaturation and crystallisation, as nucleation kinetics are more sluggish than those of gas exsolution (Hammer *et al*., 1999), attributed to the time necessary for structural reorganisation of the melt (Brugger and Hammer, 2010a). Experiments suggest that the nucleation delay may be between a few hours and 2–3 days, depending on ΔT (Couch *et al*., 2003a, b; Brugger and Hammer, 2010a; Martel, 2012). Therefore, white pumice microlites with large size, low number density and equant morphologies, were probably crystallised at lower ΔT under growth-dominated conditions, before the rapid ascent to the surface. The final rapid ascent did not result in a nucleation event and formation of many small crystals, as seen in the

dome samples, because the ascent was sufficiently rapid to hinder crystallisation. Nucleation densities are low for a given φ compared to other 2010 samples (Fig. 4.12b), indicating the crystallisation proceeded by growth of existing crystals rather than nucleation of new ones. Groundmass microlite textures in grey scoria samples are intermediate between those observed in the dome clasts and those in the white pumice, although in many respects are more closely similar to the dome samples. The crystal number densities are more variable than for other lithologies, varying from high number densities, similar to those of the dome, to densities of ~26,000 mm^{-2} intermediate between those of the dome and white pumice. Small mean crystal sizes and low aspect ratios reveal that crystals are small and acicular, as in the dome samples. High number densities of small, acicular crystals indicates crystallisation at conditions of high ΔT, although not as high as those recorded by pumice textures.

Crystal size distributions of the samples are concave-upwards curves, except the white pumice CSDs, which are straight lines. Crystal size distribution theory states that under steady state, open-system conditions, the natural log of a crystal population density has an inversely linear correlation to the size of the crystals (Marsh, 1988). For constant crystallisation under constant conditions, a population balance is produced by crystals growing into and out of a specific size rage, resulting in a straight-line CSD (Cashman and Marsh, 1988). In contrast, curved CSDs may reflect progressive changes in crystal growth and nucleation rates as a function of changing ΔT in the system. Growth of crystals is dominant in the lower conduit and nucleation begins to dominate in the upper conduit, leading to crystallisation of smaller crystals. Therefore, different microlite sizes reflect magmatic conditions at different depths (Melnik *et al*., 2011). Nucleation rates (J) were calculated using the y-axis intercept (n^o), using the equation of Marsh (1988): $J = n^o G$ where G is the growth rate. Crystal growth rates of 10^{-8} mm s^{-1}, which are thought be accurate for decompression induced crystallisation (Brugger and Hammer, 2010b) were used. Nucleation rates for the 2010 products vary over two orders of magnitude, from 1.43 to 1.15 $x10^2$ nuclei mm^{-3} s^{-1}. Using the following equation (Marsh, 1988): $Slope = -1/G\tau$, where G is growth rate and τ is crystallisation time, the crystallisation times were calculated using the slope of the CSD, with the curved CSDs split into 2 or 3 segments. Calculated crystallisation times and nucleation rates are shown in Table 4.3. Based only upon the steepest segments at smallest crystal sizes, which record the most recent crystallisation event before eruption, crystallisation

times range between 75 and 214 hours or 3 to 10 days. Larger crystals in shallower segments crystallised for between 13 and 26 days. Calculations based on the steepest segments of dome CSDs, suggest that the smallest crystals grew for between 3 and 7 days, and those in the grey scoria for between 3 to 10 days. Calculation of crystallisation times of the white pumice microlites, based upon the whole straight line CSD, are between 4 to 7 days. During 1–26 Oct, an increase in seismic activity and summit deformation mark an 'intrusive phase', believed to reflect the movement of magma to shallower regions in the system (Budi-Santoso *et al*., 2013). Before the 17 October, mainly deep (2.5–5 km below the summit) VT earthquakes were detected, after which shallow seismic activity (>1.5 km) strongly increased. This is due to the migration of magma from deeper to shallower parts of the edifice ~ 10 days before the start of the eruption (Budi-Santoso *et al*., 2013). These timescales of magma movement based on the monitoring are broadly consistent with crystallisation timescales calculated from the CSDs. Crystallisation time estimates of ~ 2–4 weeks prior to eruption for the larger sized microlites in the dome and grey scoria samples, broadly match the onset of the 'intrusive phase' at the beginning of October 2010. Seismic evidence of magma migration to shallower levels in the edifice approximately 10 days prior to eruption is consistent with the calculated crystallisation times of the smaller microlites. Crystallisation of the large white pumice microlites, which occurred ~4–7 days prior to eruption, roughly coincides with the onset of dome extrusion. However, caution must be used when interpreting the white pumice CSDs because although the 2D intersection data revealed that crystal sizes are larger than in the other 2010 lithologies, the large crystal sizes are not reflected in the CSD (Fig. 4.13). The standard deviation (1σ) of the crystal areas in the white pumice are much higher than in the other crystals (Table 4.2), suggesting that although the mean size is higher, the range in sizes is also larger. It is possible therefore that several large crystals increased the mean crystal area considerably, so that it is not representative of the whole crystal population. However, if this was the case, the large crystals would still have been measured in the CSD. Even when all bins are plotted, including those which contain < 5 crystals, the white pumice crystal sizes are still not as large compared to other 2010 samples (Fig. 4.13). One possibility for this apparent discrepancy may potentially be the shape factor and errors in the conversion of crystal intersections to crystal lengths (Higgins, 2000).

Table 4.3 Crystal Size Distribution (CSD) analysis results with calculated crystallisation times and nucleation rates from 2010 samples. Section 1= steepest CSD segment to Section 3= shallowest segment. DD= dense dome, DS= scoriaceous dome, GS = grey scoria, WP = white pumice.

				Crystallisation time					Nucleation rate		
				$G= 10^{-6}$	$G=10^{-7}$	$G=10^{-8}$			$G= 10^{-6}$	$G=10^{-7}$	$G=10^{-8}$
Lith.	Sample	Section	Slope	T (hours)	T (hours)	T (hours)	T (days)	$(ln)n^o$ (mm^{-4})	J (no/mm^3s^{-1})	J (no/mm^3s^{-1})	J (no/mm^3s^{-1})
DD	M11-15	1	367.50	0.76	7.56	75.59	3.15	23.17	11515.96	1151.60	115.16
		2	208.22	1.33	13.34	133.41	5.56	20.74	1017.89	101.79	10.18
		3	71.42	3.89	38.89	388.94	16.21	16.37	12.83	1.28	0.13
DD	M11-01	1	161.37	1.72	17.21	172.14	7.17	21.48	2129.17	212.92	21.29
		2	89.42	3.11	31.07	310.66	12.94	19.87	427.73	42.77	4.28
		3	44.82	6.20	61.97	619.71	25.82	17.55	41.82	4.18	0.42
DS	M11-02	1	274.20	1.01	10.13	101.30	4.22	22.20	4391.78	439.18	43.92
		2	184.58	1.50	15.05	150.49	6.27	21.22	1646.64	164.66	16.47
		3	92.26	3.01	30.11	301.08	12.55	18.77	141.95	14.20	1.42
GS	M11-75	1	115.14	2.41	24.13	241.25	10.05	19.90	437.24	43.72	4.37
		2	52.35	5.31	53.06	530.61	22.11	17.50	39.90	3.99	0.40
GS	M11-51	1	350.84	0.79	7.92	79.18	3.30	22.73	7438.98	743.90	74.39
		2	111.49	2.49	24.92	249.15	10.38	19.65	342.57	34.26	3.43
		3	61.99	4.48	44.81	448.13	18.67	17.25	31.11	3.11	0.31
WP	M11-50	1	165.79	1.68	16.75	167.55	6.98	18.78	142.81	14.28	1.43
WP	M11-55	1	260.37	1.07	10.67	106.69	4.45	19.47	285.29	28.53	2.85

Feldspar microlite compositions in the 2010 products are highly variable, ranging from $An_1Ab_{41}Or_{58}$ to $An_{84}Ab_{16}Or_{<1}$ (Fig. 4.16). Microlites from each lithology, generally contain similar maximum anorthite contents, although there are differences between the different crystal populations. Microlites from dome samples, range in composition between $An_{36}Ab_{53}Or_{11}$ to $An_{76}Ab_{21}Or_3$, although nearly 60 % of the measured microlites have > An_{60} (Fig. 4.16). Grey scoria microlites have a similar overall range in composition, between $An_{31}Ab_{59}Or_{10}$ and $An_{67}Ab_{31}Or_2$, although in contrast to the dome microlites, only ~ 20% of those from the grey scoria are > An_{60} (Fig. 4.16). White pumice microlites are generally more albitic, with compositions between $An_5Ab_{49}Or_{46}$ and $An_{67}Ab_{31}Or_2$. Of the white pumice microlites measured, all but one have < An_{60}, with Ab usually > Ab_{50} (Fig. 4.16). Microlites from the light grey inclusion material show the widest overall range ($An_1Ab_{41}Or_{58}$ to $An_{84}Ab_{16}Or_{<1}$), although more than 70% of these crystal are high alkali with > Or_{20} (Fig. 4.16). As previously described in Chapter 3, the microlite compositions plotted onto the An-Ab-Or ternary diagram, with isothermal sections of the dry solvus (Wen and Nekvasil, 1994) do not necessarily represent changes in crystallisation temperature between 600 and 1000 °C, but rather changes in the position of the liquidus due to degassing. High-An microlites in the dome clasts formed at higher water pressures or temperatures compared to the other microlites. Experiments show that An content increases with increasing temperature and P_{H2O} and suggest that microlites with > An_{60} crystallise at > 50 MPa at temperatures between ~900–1000 °C (Couch *et al*., 2003b; Martel, 2012). Previous work on Mount Pelée (Martel *et al*., 2006) and Soufrière Hills volcano (Humphreys *et al*., 2009) has interpreted high-An microlites to be inherited from mafic magma. It is therefore likely that the high-An microlites formed via the interaction with an influx of hotter, deeper magma, which would be consistent with other petrological work (Costa *et al*., 2013) and monitoring data from the 2010 eruption (Surono *et al*., 2012).Based on textural evidence, the relatively large, equant microlites in the white pumice are interpreted to have formed at relatively low ΔT, before rapid ascent to the surface. Large (> 60 μm^2), high-An (> An_{50}) microlites were observed in pumice samples from Soufrière Hills Volcano, Montserrat (Couch *et al*., 2003b) and interpreted to have formed at elevated P_{H2O} (>130 MPa) in the magma chamber rather than in the conduit during ascent, with the final ascent being sufficiently rapid to prevent decompression-related crystallisation. However, the Merapi white pumice microlites

generally have lower An contents compared to those from Montserrat and also compared to microlites in the 2010 dome and grey scoria. This suggests that the white pumice microlites either grew at comparatively lower temperatures, lower water pressures, or a combination of both factors. Experimental microlites with An contents < 60 mol.% crystallise at ~ < 50MPa for a magma at ~ 900−1000 °C (Couch *et al*., 2003b; Martel, 2012). This therefore suggests that if the lower An white pumice microlites are formed before very rapid ascent to the surface, then the very fast ascent and magma fragmentation before the explosive activity, only occurred within the last ~ < 2 km of ascent, rather than very fast ascent from greater depths. Similar microlites, with blocky habits and alkali compositions have been discovered in pumice pyroclasts from explosive eruptions at the Inyo volcanic chain, California (Castro and Gardner, 2008). The crystals formed at the Inyo volcanic chain are interpreted to have formed during slow decompression, which was then followed by rapid decompression and fragmentation driven by unloading, which led to explosive behaviour. Anorthoclase and high-K microlites that are predominant in the light grey inclusion material suggest that crystallisation occurred either at low P_{H2O} and/or lower temperatures. The high groundmass crystallinity, low proportions of groundmass glass and presence of cristobalite, suggests that the light grey inclusion material has spent a prolonged period of time crystallising at shallow depths within the magmatic system. The presence of cristobalite is indicative of extensive late-stage vapour-phase crystallisation as previously observed, for example, in the Mount St. Helens cryptodome in 1980 and subsequent dome rocks (Hoblitt and Harmon, 1992; Pallister *et al*., 2008). The inhomogeneous groundmass glass is similar to the glass observed from Mount St. Helens (Cashman, 1988, 1992), Santiaguito (Scott *et al*., 2012) and Soufrière Hills, Montserrat (Couch *et al*., 2003b). This texture has been interpreted as a phase separation and devitrification of the glass during shallow storage or slow extrusion (Cashman, 1992; Scott, 2012). Another groundmass phase observed in the light grey inclusions is biotite. This is rare at Merapi and has not been observed in previous eruptive products. Biotite may have a magmatic origin, but may also originate from hydrothermal alteration or derive from metasomatic skarn material (*e.g.* Ayati *et al*., 2008; Panigrahi *et al*., 2008; Afshooni *et al*., 2013; Balassone *et al*., 2013). Given that the light grey inclusion material is interpreted to have resided at shallow depths for a prolonged period of time, it is possible that the biotite has formed via hydrothermal alteration of the basaltic andesite. It is also possible that the biotite may be associated with the thermally

metamorphosed carbonate crustal material. Biotite composition, especially in terms of its FeO, MgO, MnO, TiO_2 and Al_2O_3 contents, is indicative of biotite formation. For example, the mole fraction of Mg in the octahedral site of biotite (X_{Mg}) has been used to distinguish between igneous biotite and that which formed in hydrothermal alteration zones of porphyry deposits, with the hydrothermal biotite containing higher X_{Mg} and less FeO (Selby and Nesbit, 2000; Panigrahi *et al*., 2008; Zachariáš, 2008). At Vesuvius, distinct mica compositions have been identified, depending on whether they are magmatic or associated with hydrothermal or metasomatic material (Balassone *et al*., 2013). When compared to the Vesuvius mica compositions, the Merapi biotite are most similar to the biotite of magmatic origin, as they are Al- Ti-, and Fe- rich compared to the skarn and hydrothermal types. As the light grey inclusion material has a highly crystalline groundmass, the biotite potentially formed from the presumably more evolved residual melt.

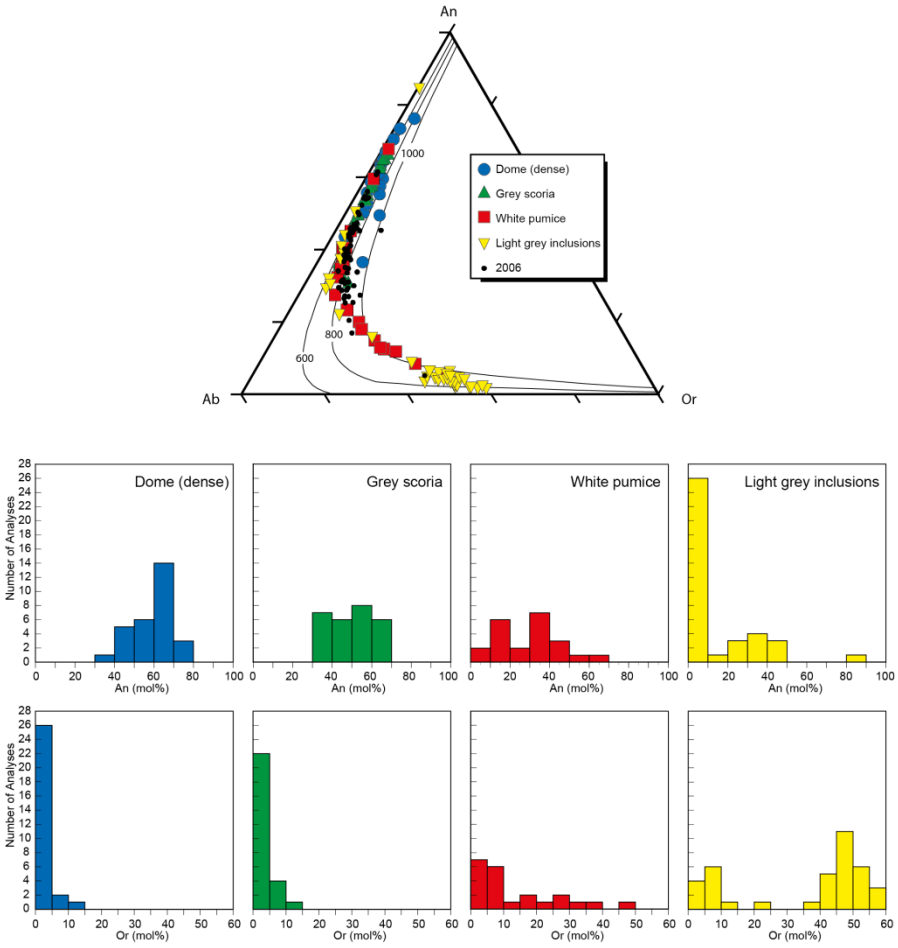

Fig. 4.16 Feldspar microlite compositions in the feldspar ternary (An-Ab-Or) diagram display differences in the compositions between the different 2010 lithologies, also reflected in the histograms. 2006 microlites are also shown for comparison. Curves on the ternary diagram represent isothermal sections of the dry ternary solvus at 600, 800 and 1000 °C, calculated using SOLVCALC (Wen and Nekvasil, 1994)

4.6. Summary

Pre-eruptive processes occurring at deep and shallow levels within the Merapi magmatic system prior to and during the 2010 eruption have been revealed through petrological and textural analysis. With detailed fieldwork, samples have been correlated with the eruption stages defined by Komorowski *et al*., (2013), allowing petrological and textural analysis to be integrated with eruption chronology and eruptive style. Samples include those erupted before, during and after the paroxysmal explosions on 5 November and consist of eruptive products of both explosive and effusive periods of activity. Samples from explosive activity during Stages 2 and 3, consist of ash, scoria and light grey dense clasts. Samples from Stage 4 and 5 deposits, emplaced during the 5 November paroxysmal explosions, consist of dense and scoriaceous material from the dome that rapidly extruded during Stage 3 and was destroyed during explosions in Stage 4 and 5. Stage 6 grey scoria and white pumice represent material that was erupted during subplinian fountaining. Whole rock major and trace element concentrations are similar in all juvenile 2010 products and are similar to rocks from the effusive 2006 eruption, as well as other recent effusive dome-forming eruptions. Thermobarometry of amphibole and clinopyroxene highlights the existence of a magma reservoir at between ~ 14 and 29 km depth, although crystallisation occurs throughout the crust. Barometry of cumulate inclusions reveals crystallisation occurring as deep as 41 km below the summit. In the 2010 samples, the range of depths of crystallisation is more variable than in 2006, often with deeper crystals in 2010. The deeper crystals, originating from ~ 25–38 km depth, are predominantly found within products of Stage 6 subplinian activity, *i.e.* the 2010 grey scoria and white pumice. Magmatic temperatures for 2006 and 2010 are estimated to be 920–1020 ± 23.5 °C. High-Al clinopyroxene and high An microlites, found in all 2010 samples, but most frequently in dense dome samples, indicate the presence of a hotter (> ~ 1000 °C), potentially more mafic, magma. Therefore, thermobarometry of the 2010 products reveals an influx of a hotter, deeper magma prior to and during the 2010 eruption. Microlite textural analysis, as well as the prevalence of amphiboles without reaction rims, demonstrates that the magma ascended at faster rates than in 2006, and rose from the depths within the amphibole stability field to the surface in less than the time it takes for amphibole breakdown rims to occur. Timescales of magmatic ascent estimated from CSD analysis, broadly match the timescales of migration of magma to shallower levels based on monitoring data. Overall petrological

and textural results suggest the explosive nature of the 2010 eruption, in comparison with the effusive 2006 eruption, was driven by an influx of hotter, deeper magma that ascended rapidly. Crystallisation and degassing processes during magma ascent further served to modify eruptive activity.

Chapter 5: Pre- and syn-eruptive degassing processes of the 2010 and 2006 eruptions

5.1. Introduction

Eruptive behaviour is governed by various factors, including magma composition, volatile content, degassing style, magmatic flux and ascent rate (*e.g.* Woods and Koyaguchi, 1994; Eichelberger, 1995; Villemant and Boudon, 1998; Melnik and Sparks, 1999; Scandone *et al*., 2007). Previous studies show that the style of degassing (open vs. closed) is pivotal in determining eruptive behaviour. During open-system degassing, exsolved volatiles are separated from the melt and are lost through various routes such as through the vent and/or the conduit walls, leading to effusive eruptive activity (Eichelberger *et al*., 1986; Melnik and Sparks, 1999; Villemant *et al*., 2008). In closed-system degassing, the exsolved volatiles remain within the system, tending to result in increased overpressure, vesicularity and capacity for explosive eruption (Wilson *et al*., 1980). Transitions between effusive dome-forming (open-system degassing) and explosive Plinian (closed-system degassing) eruptions have been related to changes in degassing regime, as well as changes in initial volatile content, changes in magma supply rate and overpressure, as well as crystallisation during ascent (*e.g.* Jaupart and Allègre, 1991; Woods and Koyaguchi, 1994; Martel *et al*., 1998; Villemant and Boudon, 1998; Melnik and Sparks, 2005; Ruprecht and Bachmann, 2010). At Merapi, previous volcanological and petrological work suggests that the eruptive style of past dome-forming and larger sub-Plinian eruptions has been governed by slow vs. fast magma ascent rate and open- vs. closed-system degassing (Gertisser, 2001; Gertisser *et al*., 2011) and that shallow-level dynamics control the eruptive behaviour (Gauthier and Condomines, 1999). In addition, crustal carbonate assimilation and the resulting CO_2 liberation has also been invoked to play a significant role in governing the explosivity of eruptions (Chadwick *et al.*, 2007; Deegan *et al*., 2010; Troll *et al*., 2012, 2013; Borisova *et al*., 2013).

Understanding the driving forces behind eruptive activity and transitions in eruptive style, which, as the 2010 eruption of Merapi demonstrated, may occur rapidly and without clear precursors during individual eruptions, is crucial for hazard assessment. Silicate melt inclusions trapped in phenocrysts potentially retain evidence about the pre-eruptive magma that may not be preserved elsewhere, providing critical information about the processes operating during magmatic evolution. For example, melt inclusions can conserve the composition and dissolved volatile concentrations of a pre-eruptive melt, and have been used to shed light on minimum pressures of crystallisation and to supply information about exsolved fluids present during crystallisation (see Lowenstern, 1995; 2003; Kent, 2008 for reviews of the subject). However the interpretation of melt inclusion volatile concentrations is challenging, both analytically and due to potential changes in the initial composition by post entrapment processes, including crystallisation and diffusive loss through the crystal lattice or cracks (*e.g.* Lowenstern, 1995).

In 2010, Merapi volcano had its largest eruption (VEI 4) since 1872 (Gertisser *et al*., 2012a; Surono *et al*., 2012). In contrast to recent prolonged and effusive dome-forming eruptions at Merapi, such as the previous eruption in 2006 (Charbonnier and Gertisser, 2008; Preece *et al*., 2013; Ratdomopurbo *et al*., 2013), the 2010 eruption began explosively before a new lava dome grew rapidly in the newly formed crater prior to explosive destruction of this dome during the peak of the eruption on 5 November 2010 and further explosive activity and extrusion of a new dome (Surono *et al*., 2012; Komorowski *et al*., 2013; Pallister *et al*., 2013). This chapter presents a comprehensive suite of melt inclusion data from samples of various stages of the cataclysmic 2010 eruption, including dense clasts from the dome that extruded before 5 November, as well as grey scoria and white pumice from the subsequent sub-Plinian stage. Data include measurements of volatiles (H_2O, CO_2, Cl, S, F), light lithophile trace elements (B, Li, Be) and major element concentrations. These data are complemented by analysis of the host clinopyroxene phenocrysts as well as groundmass glass.

The diverse and well-constrained sample set, produced by rapidly changing eruptive behaviour in 2010, is used to shed light on the driving forces behind shifts in eruptive style during a single eruptive period at Merapi. In addition, comparison of the various 2010 samples to those originating from scoriaceous dome fragments produced

during the peak of the 2006 eruption, elucidate magma storage, ascent and pre-eruptive processes during the two most recent and contrasting eruptions of Merapi that may be regarded as end-members of "Merapi-type" activity. Insights gained from this are essential to identify and understand factors controlling eruptive behaviour, with results being beneficial for hazard analysis at Merapi and possibly other dome-forming volcanoes worldwide.

5.2. Background

5.2.1. Merapi magmatic system

The plumbing system of Merapi is thought to consist of multiple magma storage and crystallisation regions, ranging over almost the entire thickness of the crust (*e.g.* Gertisser, 2001; Chadwick *et al*., 2013; Costa *et al*., 2013). Evidence for this comes from both petrological and geophysical studies. For example, geobarometry of magmatic inclusions indicates that crystallisation at Merapi occurs over a wide range of depths (~ 2–45 km), with the majority occurring at mid-crustal levels (12–18 km) (Chadwick *et al*., 2013). Mineral equilibria in lavas and pyroclastic rocks reveal a major magma storage region at mid- to lower-crustal levels (14–19 km) (Gertisser, 2001), corroborated by estimates of amphibole crystallisation at between 9 and > 20 km depth (Preece *et al*., 2011; Nadeau *et al*., 2013). Petrological data which elucidate the magma storage conditions prior to the 2006 and 2010 eruptions indicate that there were multiple zones of crystallisation at depths throughout the crust prior to both eruptions (Costa *et al*., 2013; Preece *et al*., 2013). Geophysical data also suggest the presence of multiple magma storage regions at Merapi. Tilt and GPS data indicate an average source depth for magma storage at 8.5 ± 0.4 km below the summit (Beauducel and Cornet, 1999), broadly consistent with the depth of an aseismic zone observed at > 5 km below the summit, thought to represent the presence of melt (Ratdomopurbo and Poupinet, 2000). In addition, an aseismic zone located at 1.5–2.5 km depth below the summit is interpreted to be a shallow ephemeral storage region, where magma is temporarily stored as it migrates from the deeper reservoir(s) before eruption (Ratdomopurbo and Poupinet, 2000). Shallow storage regions have also been proposed, based upon Bouguer gravity anomaly data (Saepuloh *et al*., 2010). The size of this shallow magma storage

region has been estimated at ~ 1.6–1.7 x 10^7 m^3 (Gauthier and Condomines, 1999; Le Cloarec and Gauthier, 2003).

At Merapi, CO_2 is thought to originate both from the mantle source and an input from crustal carbonate assimilation. For example, isotopic data indicate a mantle-derived origin for most volatiles at Merapi, with additional CO_2 derived from crustal contamination (Allard *et al.*, 2011). The upper crustal rocks around Merapi are comprised of a ~ 10 km thick sequence Cretaceous to Tertiary limestones, marls and volcaniclastic deposits (van Bemmelen, 1949; Hamilton, 1979; Smyth *et al*., 2005). Calc-silicate xenoliths, often dominated by wollastonite and diopside, are commonly found within Merapi lavas, providing evidence for the interaction of magma with crustal carbonate material (*e.g.* Clocchiatti *et al*., 1982; Camus *et al*., 2000; Gertisser and Keller, 2003; Chadwick *et al*., 2007; Deegan *et al.*, 2010; Troll *et al*., 2012, 2013). Magma-carbonate interaction liberates CO_2 during the conversion of crustal carbonates to the diopside and wollastonite assemblages observed in the xenoliths, which adds to the magmatic volatile budget with the potential to sustain and intensify eruptions at Merapi (Deegan *et al*., 2010; Troll *et al*., 2012, 2013). Magma-carbonate interaction at Merapi is supported by the occurrence of high $^{87}Sr/^{86}Sr$ values of high-An plagioclase phenocrysts (Chadwick *et al*., 2007), elevated $\delta^{13}C$ values in fumarolic gas (Troll *et al*., 2012) and $\delta^{18}O$ values in whole rocks and phenocrysts above typical mantle values (Gertisser and Keller, 2003; Troll *et al*., 2013; Borisova *et al*., 2013).

5.2.2. Volatile emission at Merapi

Gas emissions at Merapi are H_2O-rich (~ 84–95 mol. %), with lesser amounts of CO_2 (< 10 mol. %) and minor amounts of SO_2 and H_2S (Le Guern *et al*., 1982; Zimmer and Erzinger, 2003). Merapi is a moderate gas emitter when compared to other arc volcanoes, with an average SO_2 flux of ~ 100 Mg/day emitted from the main plume between 1987 and 1995 (Nho *et al*., 1996; Le Cloarec and Gauthier, 2003). CO_2 output during the inter-eruptive periods of 2002 and 2007 was measured at 240 Mg/day from the degassing dome, with a further 200–230 Mg/day through the soil near the dome (Toutain *et al*., 2009). Previous work has concluded that effusive volcanism at Merapi is accompanied by open-system degassing, with most of the degassing occurring within the conduit during ascent or during magma residence in a shallow magma chamber

below the summit (Le Pennec *et al*., 2001; Le Cloarec and Gauthier, 2003). Evidence of a deeper gas and magma supply to this shallower system has been reported, with inputs of deep, undegassed magma into the shallower, degassing reservoir (Gauthier and Condomines, 1999; Le Cloarec and Gauthier, 2003; Costa *et al*., 2013). For example, volcanic gases are enriched in S compared to modelled volatile phases, attributed to a deeper, reduced, mafic magma supplying S to the shallow magmatic system (Nadeau *et al*., 2010, 2013). It is estimated that the magma degassing rate is 40 times greater than the lava extrusion rate of the past 100 years (Allard *et al*., 2011). This suggests that the magma storage region is large enough to accommodate substantial amounts of unerupted, degassing magma, with continuous gas percolation through the magma system (Allard *et al.*, 2011).

5.2.3. The 2010 and 2006 eruptions of Merapi

Previous work (Komorowski *et al*., 2013) has recognised eight stages of the paroxysmal 2010 eruption, which will be referred to throughout this chapter. The onset of the eruption was heralded by unrest beginning in October 2009 (Stage 1), with increased seismic activity, ground deformation and an increase in CO_2, SO_2 and H_2S fumarolic emissions, which intensified from September 2010 onwards (Fig. 5.1). The eruption began on 26 October 2010, with initial explosions generating pyroclastic density currents (PDCs) which swept down the southern flanks (Stage 2). The 26 October explosive events destroyed the remnants of the 2006 dome, excavating an estimated $6x10^6$ m^3 non-juvenile material. Between 29 October–4 November (Stage 3), satellite images revealed that a new dome had extruded at an average rate of 25 m^3 s^{-1} (> 7.5 times greater than peak dome extrusion rates in 2006) reaching a volume of ~5 x 10^6 m^3 on 4 November (Surono *et al*., 2012; Pallister *et al*., 2013). Dome growth during this period was punctuated by gravitational collapse and explosions. On 5 November, this new dome was destroyed in a cataclysmic eruption sequence of laterally directed dome explosions, generating PDCs which travelled up to 16 km from the summit (Stage 4) (Fig. 5.1). The deposits of these explosions are dominated by juvenile dark-coloured, dense, basaltic andesite clasts from the newly-formed dome, herein referred to as dense dome material. Later on 5 November, retrogressive summit collapse occurred (Stage 5) followed by a subsequent change in activity to produce a convective column, which

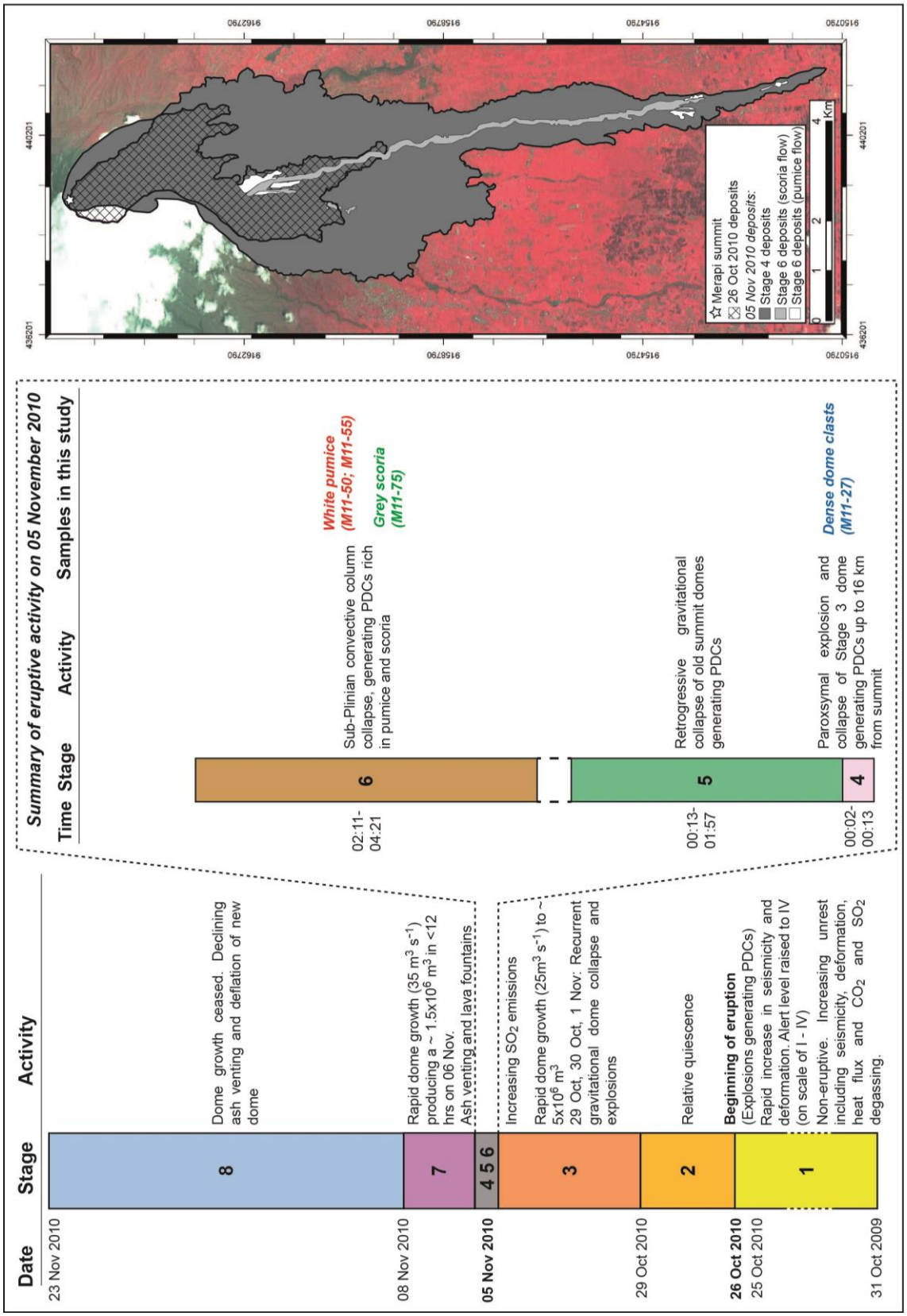

Fig. 5.1 Eruptive timeline of the 2010 eruption, with Stages based on Komorowski *et al*. (2013) and expanded section describing the paroxysmal eruptive activity of 5 November 2010 and samples used in this paper. Deposit map showing the extent of deposits emplaced on 26 October 2010, as well as during Stage 4 and Stage 6 (modified after Komorowski *et al*. 2013)

collapsed repeatedly to generate PDCs with conspicuous scoria and pumice clasts (Stage 6) (Fig. 5.1). On 6 November dome extrusion resumed at an increased rate of 35 m^3 s^{-1}, producing a new dome of ~1.5 x 10^6 m^3 in less than 12 hours (Stage 7). Declining ash venting and degassing continued until the 23 November (Stage 8). The 2010 PDCs covered an area of ~22.3 km^2, with an estimated non-DRE volume of ~ 36.3 x 10^6 m^3 (Charbonnier *et al*., 2013). Activity waned throughout November and the alert level was decreased on 3 December 2010 (Surono *et al*., 2012).

In contrast to the explosive VEI 4 eruption in 2010, previous episodes of volcanic activity at Merapi over the last century (VEI 1–3) were characterised by prolonged dome extrusion and subsequent gravitational collapse to produce block-and-ash flows or 'Merapi-type nuées ardentes' (*e.g.* Andreastuti *et al*., 2000; Newhall *et al*., 2000; Voight *et al*., 2000; Gertisser *et al*., 2012a; Surono *et al.,* 2012). The previous eruption which occurred in 2006, is a well-characterised example of a typical extrusive, dome-forming eruption at Merapi (Charbonnier and Gertisser, 2008; Gertisser *et al.*, 2012b; Preece *et al.*, 2013; Ratdomopurbo *et al*., 2013). However, it should be noted that although the 2006 eruption displayed typical Merapi dome-forming activity, peak dome extrusion rates reached 3.3 m^3 s^{-1} (Ratdomopurbo *et al*., 2013), which is high compared to other recent Merapi eruptions and the long-term average of since 1890, calculated as 0.1 x 10^6 m^3/month (Siswowidjoyo *et al*., 1995) or ~ 0.04 m^3 s^{-1}. For example, it is an order of magnitude higher than peak dome extrusion rates in 1994 (0.32 m^3 s^{-1}) (Ratdomopurbo, 1995; Hammer *et al*., 2000). The onset of the eruption (VEI 1) on 26 April 2006 occurred after ~ 10 months of increased seismicity and summit deformation (Ratdomopurbo *et al*., 2013). Throughout the eruption block-and-ash flows (BAFs) generated by gravitational dome-collapse were emplaced, at times daily, into valleys on the south-western and southern slopes of the volcano. The peak of activity on 14 June 2006 consisted of multiple phases of dome collapse (Charbonnier and Gertisser, 2008; Lube *et al*., 2011; Gertisser *et al*., 2012b) with BAFs travelling up to 7 km in the Kali Gendol valley on the southern flanks (Charbonnier and Gertisser, 2008). Alert levels were reduced to normal in early October 2006, signalling the end of the eruption.

5.3. Methodology

5.3.1. Samples and sample preparation

Various samples from the cataclysmic stages of the 2010 eruption were analysed, in particular, samples of dense dome material emplaced on 5 November (Stage 4 of Komorowski *et al*., 2013), as well as grey scoria and white pumice clasts from PDC deposits emplaced by subsequent convective fountain collapse (Stage 6 of Komorowski *et al*., 2013). Clinopyroxene-hosted silicate melt inclusions were analysed in all samples, and groundmass glass was analysed in all but the dense dome samples, as the groundmass was too crystalline to allow for accurate glass analysis. For comparison, both melt inclusions and groundmass glass were analysed from scoriaceous dome fragments from the block-and-ash flows emplaced at the peak of the 2006 eruption on 14 June 2006 (Lobe 1 of Charbonnier and Gertisser, 2008; Preece *et al*., 2013).

Grain mounts were prepared by briefly crushing rock samples in an agate mill before sieving to different size fractions. Several hundred clinopyroxene crystals were picked by hand under a binocular microscope from > 1 mm and > 500 μm sieve fractions and mounted into low volatility Struers EpoFix epoxy resin. Each grain mount was polished by hand with aluminium polishing solution down to 0.3 μm, until melt inclusions were exposed. Inclusions were only studied after polishing, with the proviso that some petrographic information may have been lost during polishing. However, this method has the advantage that many melt inclusions can be analysed quickly, giving an extensive overview of the melt inclusion population (Humphreys *et al*., 2008).

5.3.2. Analytical Methods

Melt inclusions in gold coated samples were analysed by Secondary Ion Mass Spectrometry (SIMS) for isotopes of volatiles ($^{1}H^{+}$ and $^{12}C^{+}$) and of light lithophile elements ($^{7}Li^{+}$, $^{9}Be^{+}$, $^{11}B^{+}$) using the Cameca ims-4f ion microprobe at the NERC Ion Microprobe Facility at the University of Edinburgh (UK). A sub-set of these inclusions were subsequently analysed for $^{12}C^{+}$ at high resolution in order to minimise the interference of $^{24}Mg^{2+}$ on $^{12}C^{+}$. All CO_2 data in this chapter are based on the high resolution $^{12}C^{+}$ results. Analyses were performed using a primary $^{16}O^{-}$ beam and positive secondary ion beam with an accelerating voltage of 4.5 kV. Energy filtering with a 75 ±

20 V offset, or a 50 V offset for high resolution $^{12}C^+$ measurements, was used with the purpose of minimising the transmission of unwanted molecular species. Results are based on the last 7 cycles, with the first 8 disregarded, or, for high resolution $^{12}C^+$ measurements, based on the last 8 with the first 5 disregarded, in order to abate effects of potential surface contamination and allow time for beam stabilisation. In addition to this, surface contamination was further eliminated by performing a 50 μm diameter, 10 nA raster of the sample surface for 3 minutes prior to analysis. CO_2 backgrounds were measured to be < 5 ppm using CO_2-free standards. For all analyses, ^{30}Si was used as an internal standard and corrected with SiO_2 contents as measured by electron microprobe analysis. H_2O and CO_2 were measured using $^1H^+$ and $^{12}C^+$ respectively, calibrated using dacitic to rhyolitic glass standards with known H_2O (up to 4.32 wt.%) and CO_2 (up to 10380 ppm) concentrations and using working curves as described in Blundy and Cashman (2008). Results are listed in Appendix F.

Selected melt inclusions in the same polished epoxy grain mounts were also analysed for H_2O and CO_2 using attenuated total reflectance micro-Fourier Transform Infrared spectroscopy (ATR micro-FTIR) at the USGS, Menlo Park, California. A Ge accessory crystal was used to measure evanescent wave absorption at 3450 cm^{-1} (representing total H_2O) and at 2350 cm^{-1} (representing molecular CO_2) using the methods of Lowenstern and Pitcher (2013).

Samples were viewed with SEM and analysed by electron probe only after the SIMS analysis in order to avoid possible contamination of C with the carbon coating. Major elements as well as Cl, F and S in the melt inclusions and groundmass glass were measured using Cameca SX100 electron microprobes at The Open University and the University of Cambridge. Glass was analysed using a defocussed beam diameter of 5–10 μm, an accelerating voltage of 15–20 kV and a 4–20 nA beam current for major elements and a 10–20 nA beam current for volatiles. Volatiles were analysed with extended peak counting times. Na was always measured first to minimise migration effects and in-house natural mineral standards were used for calibration. Results are listed in Appendix E. Major elements were measured in the clinopyroxene host crystals, near to the site of each melt inclusion, as well as in other clinopyroxene phenocrysts in 2010 and 2006 samples. Although there is little zonation in the pyroxene phenocrysts, attempts were always made to analyse the clinopyroxene in the same zones in which

melt inclusions were situated. Pyroxenes were analysed using a 1−5 μm beam diameter, a 15−20 kV accelerating voltage and a 15−20 nA beam current.

Back-scattered electron (BSE) images of all melt inclusions were acquired with a JEOL JSM 5900 LV SEM at the University of East Anglia, using an accelerating voltage of 20 kV and a working distance of 9 mm. All host crystals were imaged using an accelerating voltage of 20 kV and a working distance of 31−37 mm. Back-scattered electron images were then analysed in order to disregard analyses that were on cracks or occasional inclusions which contained any daughter crystals.

All melt inclusion major element data were corrected for the compositional effects of post-entrapment crystallisation (PEC) of clinopyroxene at the melt inclusion-host interface. The corrections were performed by first calculating the composition of the host clinopyroxene that should be in equilibrium with the melt inclusion using an appropriate clinopyroxene-melt equilibrium model (Nielsen and Drake, 1979). The equilibrium clinopyroxene was then added in 0.1 wt.% increments to the measured melt inclusion composition until the equilibrium clinopyroxene composition becomes identical to that of the host, using the reverse fractional crystallisation modelling function of the *Petrolog3* software (Danyushevsky and Plechov, 2011). The calculated degree of PEC is less than 10% but typically < 5%.

5.4. Results

5.4.1. Major element geochemistry

Major element compositional variations in whole rocks, melt inclusions and groundmass glass from 2010 and 2006 samples are shown in Fig. 5.2. Whole rock compositions of both the 2010 and 2006 eruptive products are high-K basaltic andesite and lie within a similar restricted compositional range (Preece *et al.*, 2013). SiO_2 concentrations are between 54.1 and 55.7 wt.% for 2010 juvenile samples and between 55.2 and 56.1 wt.% for the 2006 products. A comparison of different 2010 lithologies reveals that the compositional range of the dense dome material erupted on 5 November extends to slightly less evolved compositions (54.1−55.6 wt.% SiO_2) than the white pumice (55.5−55.7 wt.% SiO_2) and the grey scoria (55.1−55.7 wt.% SiO_2), although the

differences are marginal. There is a compositional gap of > 5 wt.% SiO_2 between the most evolved whole rock sample and the least evolved melt inclusion (Fig 5.2). The melt inclusions are mainly dacitic to rhyolitic in composition, with 63.1–72.4 wt.% SiO_2, with only two classed as andesitic (61.7 and 62.3 wt.% SiO_2) when corrected for PEC and normalised to 100% on a volatile-free basis (Table 1). Both 2010 and 2006 melt inclusions cover a similar compositional range. Melt inclusions from each 2010 lithology generally span the entire observed compositional range, although the most evolved melt inclusions (> 70 wt.% SiO_2) come exclusively from white pumice and grey scoria. Groundmass glass compositions represent the most evolved compositions (66.8–76.4 wt.% SiO_2). Overall trends of Al_2O_3, CaO, FeO^* (total iron recalculated as FeO) and MgO correlate negatively with SiO_2, and K_2O correlates positively with SiO_2 (Fig 5.2). Both TiO_2 and NaO_2 trends are inflexed, with TiO_2 concentrations decreasing until ~ 67 wt.% SiO_2 before groundmass TiO_2 concentrations increase with increasing SiO_2, and Na_2O correlating positively until ~ 67 wt.% SiO_2, where Na_2O concentrations begin to decrease.

Table 5.1 Representative analyses of melt inclusion compositions from 2010 and 2006 eruptions. Stages 4 and 6 of the 2010 eruption refer to chronology of Komorowski *et al.* (2013). Lithology types are as follows: dense dome (DD), grey scoria (GS), white pumice (WP), scoriaceous dome clasts (DS). MI denotes melt inclusion number. PEC denotes degree of post-entrapment crystallisation corrected for (%). All major elements (in wt. %) determined by electron microprobe, FeO*= total iron, all values shown are uncorrected for PEC. Volatiles (S, F, Cl) in ppm also measured by electron microprobe. H_2O (in wt. %), CO_2, Li, B, Be (in ppm) measured by ion microprobe

Eruption	Stage	Type	Sample	MI	SiO_2	TiO_2	Al_2O_3	FeO*	MnO	MgO	CaO	Na_2O	K_2O	P_2O_5	S	F	Cl	Total	PEC	Li	B	Be	H_2O	CO_2
2010	4	DD	M11-27-5	x34-18	68.78	0.34	16.81	0.83	0.07	0.20	1.92	4.87	5.12	0.16	210	760	3150	99.52	0.1	28	45	1	0.78	
2010	4	DD	M11-27-5	x34-19	67.52	0.44	15.97	2.67	0.13	0.29	1.22	5.13	6.31	0.13	105	450	2690	100.15	6.0	43	44	2	0.40	
2010	4	DD	M11-27-5	x9-93	67.03	0.50	16.73	2.40	0.06	0.09	0.57	6.52	5.82	0.13	110	1210	2880	100.26	17.0	68	41	1	1.13	5
2010	4	DD	M11-27-5	x9-94	66.38	0.77	15.70	2.35	0.11	1.86	4.65	4.30	4.26	0.16	130	650	2970	100.91		20	50	1	1.69	12
2010	4	DD	M11-27-5	x50-99	57.95	0.52	15.66	3.30	0.16	0.54	1.72	4.04	5.89	0.27	35	770	2720	90.39	5.6	41	35	2	0.16	
2010	4	DD	M11-27-5	x2-103	63.98	0.35	14.91	2.87	0.14	0.77	1.81	5.42	6.27	0.12	40	670	2770	96.99	0.3	54	44	1	0.77	
2010	4	DD	M11-27-5	x4-108	63.58	0.42	14.91	3.05	0.12	0.51	1.81	4.08	6.33	0.18	10	510	2610	95.32	4.7	39	48	2	0.22	
2010	6	GS	M11-75	x5-44	67.30	0.38	16.04	1.90	0.09	0.25	1.30	4.79	5.22	0.12	180	750	2860	97.78	6.4	25	47	2	3.39	
2010	6	GS	M11-75	x5-45	67.85	0.40	16.82	1.79	0.09	0.16	1.52	4.98	4.93	0.14	445	140	2770	99.07	9.7	25	48	2	2.79	86
2010	6	GS	M11-75	x5-46	69.15	0.50	16.60	1.76	0.08	0.23	1.38	5.40	4.90	0.12	90	1480	2620	100.52	5.5	32	41	1	3.94	
2010	6	GS	M11-75	x11-49	67.87	0.48	16.25	2.41	0.07	0.24	1.22	6.04	5.29	0.11	60		2910	100.29	6.9	30	47	2	1.08	109
2010	6	GS	M11-75	x4-50	64.73	0.42	15.89	1.93	0.06	0.54	1.61	4.70	5.13	0.17	315		3180	95.55	3.4	27	48	1	3.83	146
2010	6	GS	M11-75	x13-51	67.42	0.43	16.34	2.62	0.12	0.18	1.05	6.22	5.18	0.16	45	970	2710	100.10	7.5	34	45	2	1.27	18
2010	6	GS	M11-75	x30-53	66.06	0.50	16.48	2.25	0.09	0.36	1.55	4.62	5.46	0.14	205	1160	3470	98.01	6.1	27	49	1	3.66	65
2010	6	GS	M11-75	x41-56	62.66	0.54	16.45	2.75	0.11	0.40	1.90	4.32	4.63	0.25	180	560	2760	94.37	7.7	26	42	1	3.08	
2010	6	WP	M11-75	x25-5	70.55	0.29	14.14	2.12	0.07	0.28	0.76	4.26	5.84	0.03	45	420	2440	98.64	4.4	29	71	2	1.83	
2010	6	WP	M11-55	x25-6	68.80	0.29	14.41	2.43	0.12	0.58	1.31	4.42	6.00	0.07		1060	3810	98.92	3.1	31	70	2	1.62	
2010	6	WP	M11-55	x52-7	66.81	0.44	15.34	2.29	0.12	0.37	1.03	4.85	5.82	0.08	80	1110	3850	97.65	4.2	34	58	2	2.04	
2010	6	WP	M11-55	x36-8	70.55	0.36	14.21	2.22	0.10	0.30	0.88	4.54	5.65	0.05	50	930	2820	99.24	3.9	31	67	2	2.37	
2010	6	WP	M11-50	x20-58	62.20	0.32	17.74	2.72	0.12	0.54	3.20	4.30	4.77	0.17	390	930	3960	96.66	10.2	29	69	1	3.91	695
2010	6	WP	M11-50	x11-59	65.50	0.38	16.83	2.80	0.11	0.53	1.59	5.26	5.57	0.15	90	2390	2670	99.22	7.4	34	42	1	2.11	97
2010	6	WP	M11-50	x25-62	69.47	0.33	13.72	2.00	0.08	0.25	0.75	3.91	6.09	0.08	110	830	5130	97.29	4.8	32	84	3	1.19	
2010	6	WP	M11-50	x9-64	65.73	0.45	15.86	2.57	0.12	0.57	1.41	4.36	5.32	0.12	160	810	3220	96.94	3.7	29	40	1	3.79	534
2010	6	WP	M11-50	x4-74	67.62	0.37	16.00	2.60	0.12	0.43	1.35	4.80	5.63	0.12	140	710	2860	99.42	4.7	30	47	2	1.92	146
2010	6	WP	M11-50	x21-75	65.75	0.24	13.85	2.45	0.12	0.24	0.96	4.45	5.46	0.08	30	120	2670	93.87	5.3	26	51	2	2.23	
2010	6	WP	M11-50	x27-77	66.92	0.36	15.81	2.56	0.13	0.60	1.93	4.65	4.69	0.15	135	370	2770	98.16	1.5	23	47	2	3.28	
2010	6	WP	M11-50	x29-78	67.90	0.36	15.34	2.56	0.11	0.51	1.34	4.92	5.44	0.10	95	570	3020	98.95	2.5	30	50	2	2.46	
2010	6	WP	M11-50	x29-79	67.71	0.39	16.09	2.45	0.07	0.41	1.29	5.06	5.61	0.13	85	260	2900	99.55	3.4	33	48	2	2.31	51
2010	6	WP	M11-50	x54-80	64.27	0.28	15.24	2.67	0.11	0.97	2.16	5.00	5.26	0.14	20	1740	2470	96.52	2.2	26	45	2	1.91	31
2010	6	WP	M11-50	x71-81	68.07	0.36	15.47	2.84	0.12	0.90	2.20	4.75	5.43	0.14	90	420	2660	100.58		31	47	2	1.97	15
2010	6	WP	M11-50	x80-83	67.32	0.37	16.22	2.59	0.09	0.44	1.44	5.00	5.56	0.11	275	870	2550	99.51	3.0	31	47	1	1.88	193
2006		DS	M08-09	x79-25	68.19	0.39	16.24	1.90	0.08	0.30	1.55	4.98	4.64	0.14	245	2050	3050	98.98	5.2	28	44	1	3.33	158
2006		DS	M08-09	x85-26	66.46	0.40	16.01	2.54	0.13	0.15	1.33	6.89	5.40	0.11	95	1180	2960	99.83	2.9	47	46	2	1.13	3
2006		DS	M08-09	x79-27	64.11	0.78	16.23	2.83	0.06	0.74	1.79	6.70	6.00	0.10	285	330	2910	99.73	0.1	63	47	1	1.93	
2006		DS	M08-09	x70-28	67.79	0.42	14.95	2.96	0.12	0.67	1.52	4.66	5.86	0.13	95	1400	2930	99.54	3.1	33	51	2	0.65	1
2006		DS	M08-09	x48-86	65.69	0.41	16.35	2.52	0.11	0.34	1.15	5.07	5.97	0.17	75	1520	2780	98.23	5.3	34	42	1	0.83	
2006		DS	M08-09	x48-87	68.12	0.51	16.20	2.69	0.15	0.33	1.18	4.73	6.17	0.14	10	1140	3720	100.70	5.1	20	48	2	0.42	7
2006		DS	M08-09	x6-88	67.87	0.33	16.28	2.60	0.11	0.35	0.94	5.02	6.33	0.16	85	800	2640	100.34	4.6	35	47	2	0.82	9
2006		DS	M08-09	x10-89	62.44	0.36	16.08	1.84	0.12	0.41	1.71	4.74	4.00	0.16	345	2030	2330	92.36	2.2	30	44	1	2.65	134

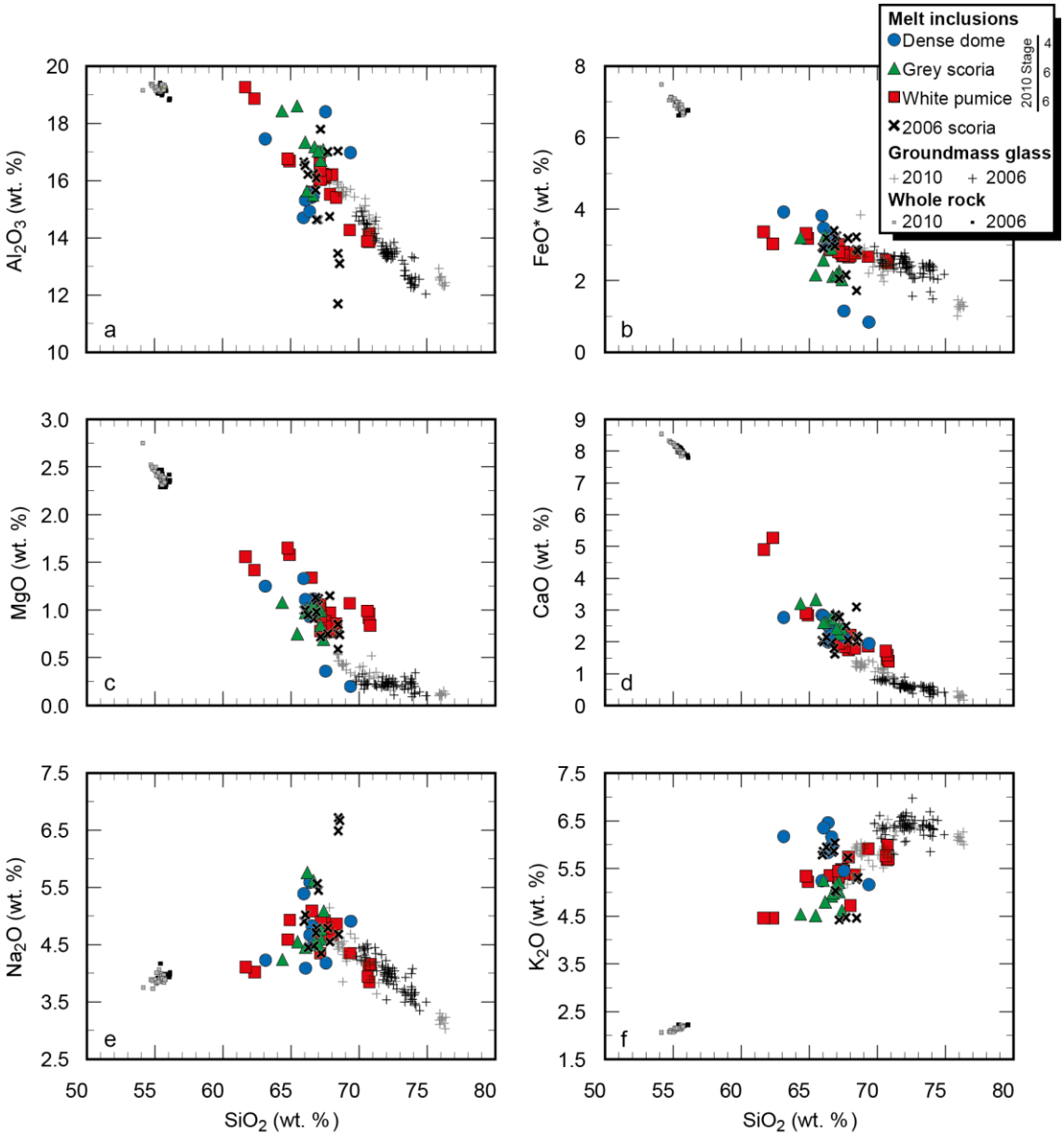

Fig. 5.2 (a-f) Major element variation diagrams showing the composition of melt inclusions from 2010 dense dome material, white pumice and grey scoria, and 2006 scoriaceous dome clasts, as well as groundmass glass and whole rock compositions from 2006 and 2010 samples. All melt inclusion compositions are corrected for PEC. All melt inclusion, groundmass glass and whole rock measurements are normalised to 100 % on a volatile-free basis. FeO* = all iron reported as FeO

5.4.2. Volatile concentrations

5.4.2.1. Interpreting the SIMS and ATR micro-FTIR data

A selected group of melt inclusions were analysed for H_2O and CO_2 using both the SIMS and ATR micro-FTIR techniques. These inclusions were primarily targeted for ATR micro-FTIR analysis because results from the preceding SIMS analysis suggested that these inclusions were enriched in CO_2 (up to ~ 3000 ppm) at medium (~ 2 wt.%) H_2O contents, relative to the degassing trend displayed by other analysed

inclusions (Fig. 5.3). This apparent CO_2 enrichment that produces compositional trends dissimilar to that modelled using equilibrium degassing has been observed previously in melt inclusions from other volcanoes and attributed to various processes. Post-entrapment modification, especially diffusion of H_2O or H^+ out of the melt inclusion has been shown to cause apparently elevated CO_2 at relatively low H_2O contents (Berlo *et al*., 2012; Reubi *et al*., 2013). Alternatively, fluxing with a CO_2-rich gas has been proposed at other volcanoes to explain enrichment of CO_2 compared to expected equilibrium degassing values, this includes, such as Jorullo (Johnson *et al*., 2008), Colima (Vigouroux *et al*., 2008), Etna (Collins *et al*., 2009) and Mount St. Helens (Blundy *et al*., 2010). An increase in the CO_2 concentration decreases the partial pressure of H_2O and the H_2O/CO_2 in the melt, shifting melt inclusion compositions isobarically towards higher CO_2 and lower H_2O concentrations. For Merapi, Nadeau *et al*. (2013) invoke a similar process in older Merapi samples, with the production and liberation of a CO_2-rich gas via crustal carbonate assimilation.

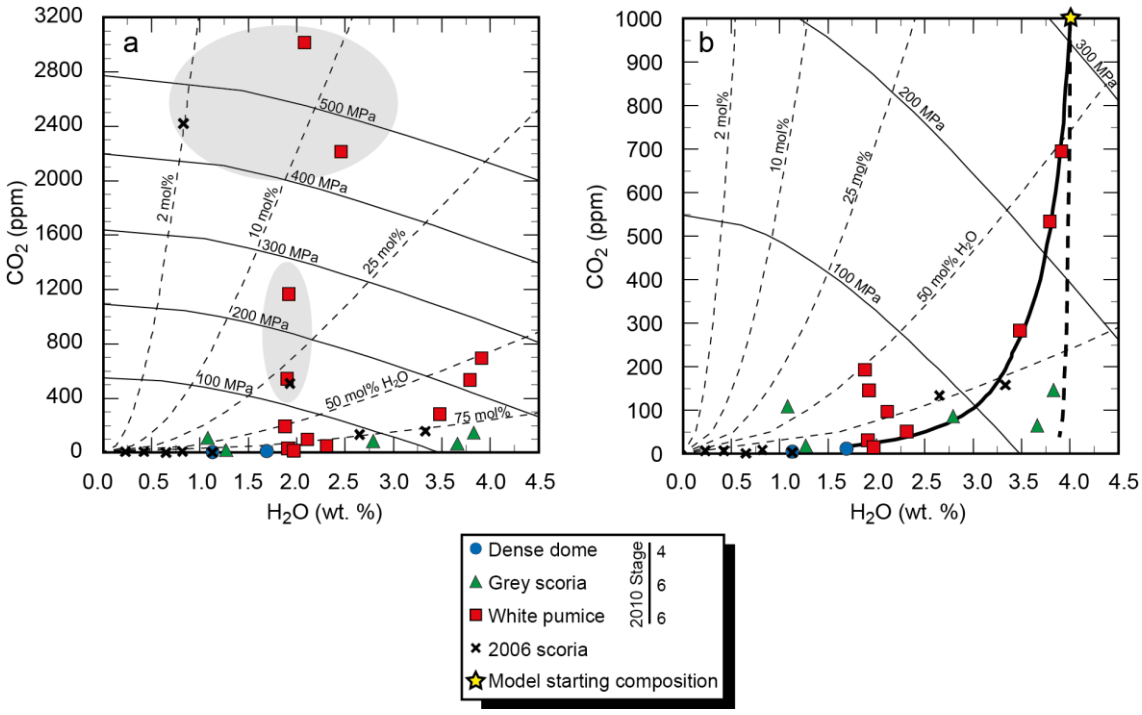

Fig. 5.3 Melt inclusion H_2O and CO_2 concentrations. (a) H_2O vs. CO_2 measured with high-resolution SIMS. All measured melt inclusions are shown including, in the shaded areas, the "high-CO_2" inclusions, some of which were subsequently re-analysed with ATR micro-FTIR. b) Enlarged view of measured melt inclusions excluding the "high-CO_2" set. Isobars (fine solid lines) and vapour isopleths (fine dashed lines) calculated with VolatileCalc (Newman and Lowenstern 2002). Closed-system decompression degassing pathway (bold solid line) with 1% exsolved vapour (bold solid line) starting at 1000 ppm CO_2 and 4.0 wt. % H_2O at 1000°C, and open-system degassing pathway starting at the same conditions (bold dashed line) calculated with VolatileCalc

ATR micro-FTIR results in this study reveal that although measured H_2O concentrations are similar to the ones acquired by SIMS, the concentration of CO_2 in the inclusions was below the detection limit (200 ppm). This discrepancy between the two data-sets is potentially caused by heterogeneities in the distribution of CO_2 in natural silicate melt inclusions. The sampling volume of the two techniques is different, with the SIMS sampling a smaller region of the inclusion than the FTIR. In this respect, the FTIR would not detect any heterogeneities, giving only an average CO_2 concentration of the inclusion, whereas the SIMS analysis is restricted to a smaller area within each inclusion, therefore allowing sampling of potential heterogeneity. This is supported by the analysis of one apparently high-CO_2 inclusion that was large enough to analyse in two distinct areas, with one measurement of 1167 ppm CO_2 and another of 146 ppm CO_2. Unfortunately, other melt inclusions were too small for multiple analyses. In light of this, the apparently elevated CO_2 values have been reported here but are not used in the reconstruction of degassing pathways and are discussed further below. The remaining CO_2 measurements are retained as they reproduce modelled trends for equilibrium degassing.

5.4.2.2. H_2O and CO_2

The highest H_2O concentrations are found in melt inclusions from the 2010 grey scoria (up to 3.94 wt.%) and white pumice (up to 3.91 wt.%) (Table 5.1). Melt inclusions from 2010 dense dome clasts are generally more degassed, although the highest measured H_2O in the dome samples is 3.62 wt.%. In comparison, melt inclusions from the scoriaceous 2006 dome fragments contain up to 3.73 wt.% H_2O (Table 5.1).

CO_2 concentrations in melt inclusions are generally less than 200 ppm, although at high H_2O concentrations, melt inclusions in the white pumice have increased CO_2 concentrations up to 695 ppm. The maximum CO_2 measured in the 2010 grey scoria and dense dome is 146 ppm and 12 ppm respectively, and in melt inclusions from the 2006 dome scoria, the maximum is 158 ppm CO_2 (Table 5.1).

5.4.2.3. F, S, Cl

Samples from 2010 show differences in fluorine concentration, depending upon lithology (Fig 5.4). Groundmass glass in white pumice samples contains 632–2199 ppm F, with the peak at between 1000–1250 ppm, whereas the groundmass glass in the grey scoria encompasses a larger range of F (180–2637 ppm), with a peak at relatively higher concentrations of 2000–2500 ppm (Fig 5.4). Fluorine concentrations in 2010 melt inclusions also vary with lithology. Those trapped in clinopyroxene phenocrysts from dense dome clasts and those from grey scoria have a similar range of F, containing up to 1400 ppm and 1480 ppm, respectively. White pumice derived inclusions contain concentrations of F up to 2390 ppm (Fig 5.4). Melt inclusions from 2006 contain up to 2050 ppm F, with the groundmass glass containing up to 2349 ppm. Fluorine concentrations in the 2010 and 2006 melt inclusions and groundmass glass are similar, although they extend to both higher and lower concentrations compared to the 1994 Merapi dome-forming eruption (Gertisser, 2001).

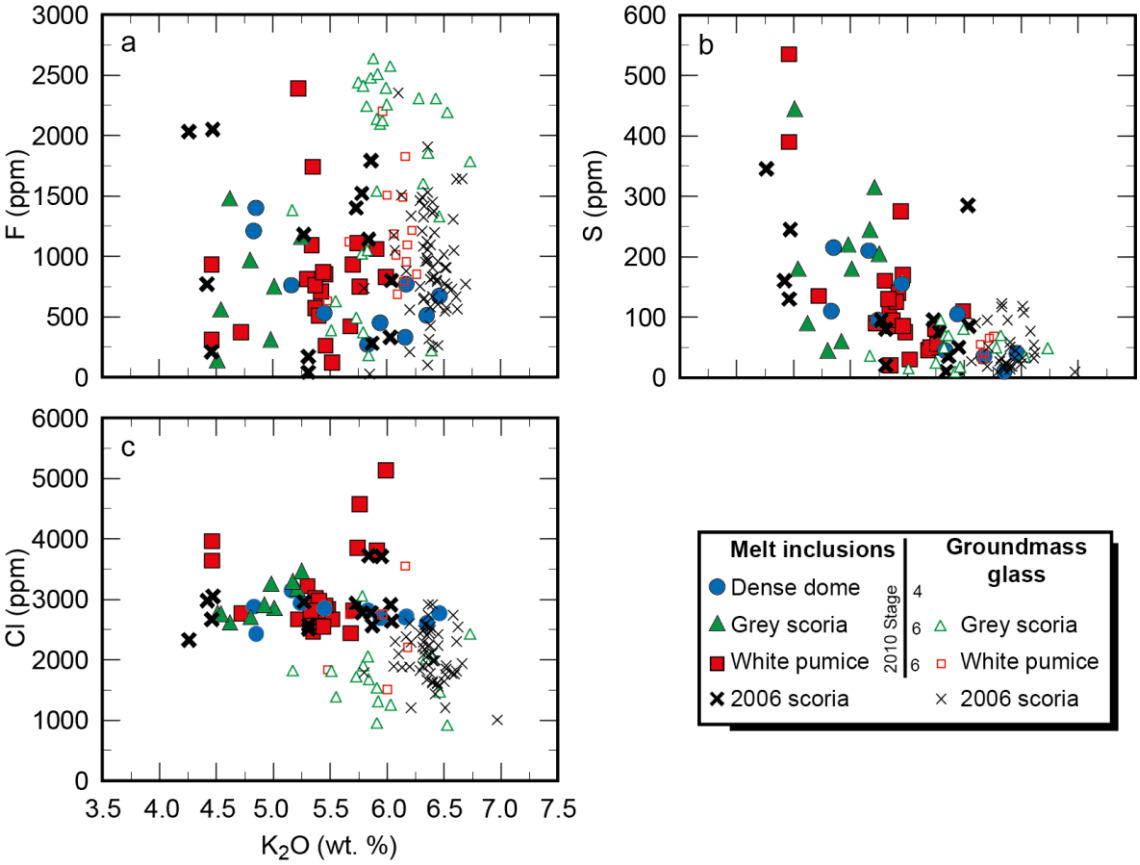

Fig. 5.4 Volatile contents in melt inclusions and groundmass glass plotted against differentiation indicator K_2O wt. %. (a) F vs. K_2O, (b) S vs. K_2O, (detection limit ~ 100 ppm) (c) Cl vs. K_2O

Sulphur is present in low concentrations in all groundmass glass, with < 100 ppm (detection limit) in 2010 glass and up to 122 ppm in 2006 glass. Melt inclusions are generally more enriched in S than groundmass, ranging up to 535 ppm S in 2010 products and up to 345 ppm in inclusions from 2006(Fig 5.4). Sulphur concentrations of the 2010 and 2006 melt inclusions and groundmass glass are similar to reported concentrations from the 1994 eruption (Gertisser, 2001).

Chlorine is more enriched in the melt inclusions than in groundmass glass in both 2010 and 2006 samples (Fig 5.4). In melt inclusions, the Cl concentration ranges from 2060–5130 ppm in 2010 eruptive products, with concentrations most frequently between 2500–3000 ppm in all sample types. The highest Cl concentrations are found in melt inclusions hosted in clinopyroxene from white pumice samples. Chlorine concentrations in melt inclusions from the 2006 samples show a comparatively narrow range from 2330–3720 ppm. The groundmass glass concentrations of Cl range from ~ 900 ppm up to 3550 ppm in samples from the 2010 eruption and are between ~1000 and 2920 ppm in those from 2006. The Cl concentrations in the 2010 and 2006 melt inclusions and groundmass glass are similar to those reported for the 1994 dome-forming eruption (Gertisser, 2001), although they extend to both higher and lower values.

5.4.3. Light lithophile elements (B, Be and Li)

Concentrations of light lithophile elements, especially those of boron and lithium, indicate differences within the melt inclusion population. Beryllium concentrations are uniform, with all measured melt inclusions containing 1–2 ppm. Lithium concentrations are more variable and range from 20–68 ppm. When plotted against H_2O and Cl (Fig 5.5), divergent L-shaped trends show enrichment of Li (> ~ 35 ppm) in melt inclusions from the 2010 dense dome material and 2006 scoria, with low H_2O concentrations and ~ 2700 ppm Cl. There is no obvious correlation between Li and SiO_2 or K_2O (Fig 5.5). The overall range in B concentration is 35–109 ppm, with enrichment (> ~ 55 ppm) occurring in melt inclusions from white pumice that contain intermediate H_2O concentrations (~ 1–2.5 wt.%) and some have enriched Cl contents (up to ~ 5000 ppm) (Fig 5.5). Boron-enriched inclusions show a positive correlation

with SiO_2 and K_2O. When plotted against each other, B and Li show a divergent L-shaped trend (Fig 5.5).

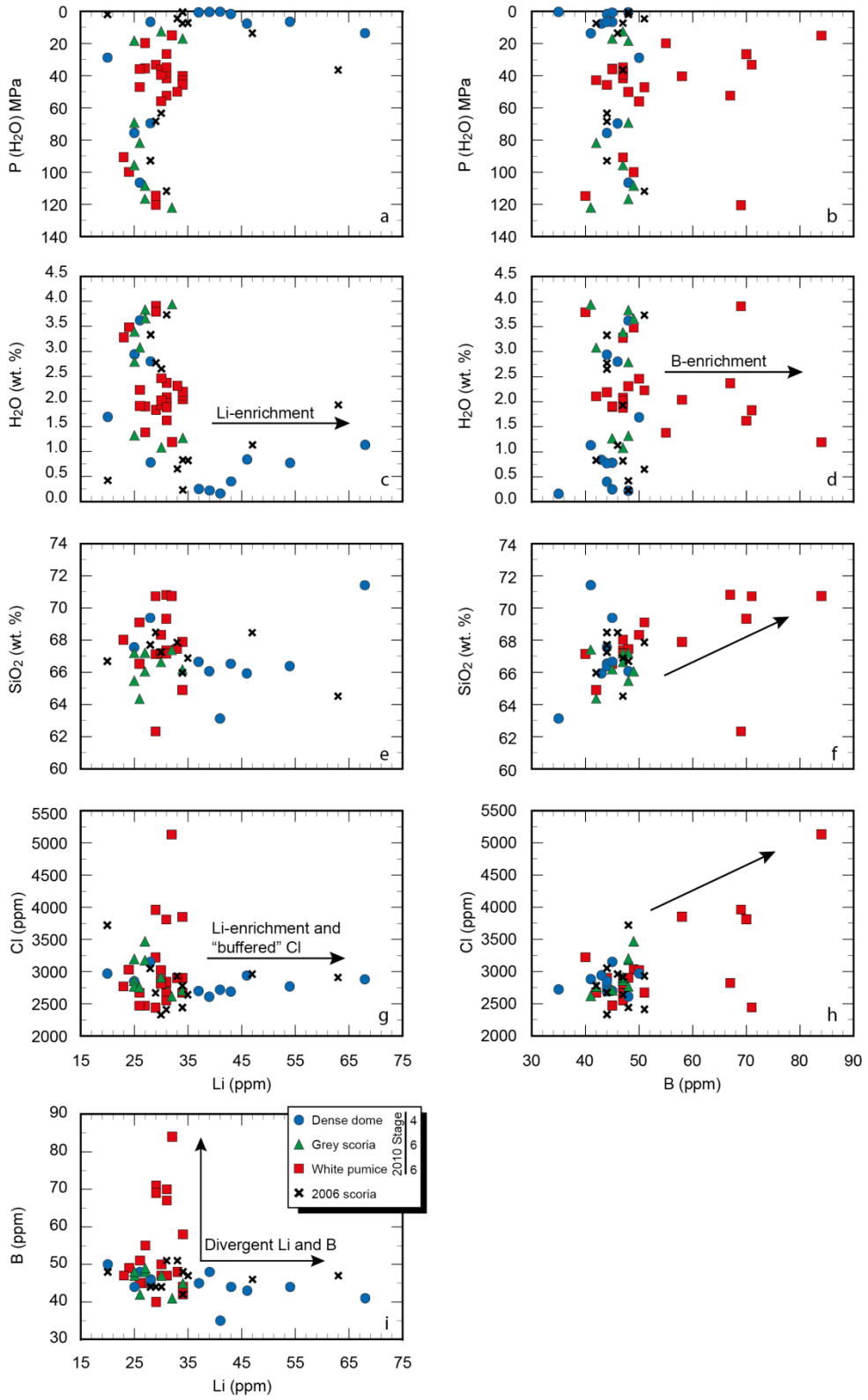

Fig. 5.5 Light lithophile elements Li and B concentrations in melt inclusions, showing that Li is enriched in melt inclusions from the 2010 dense dome clasts and the 2006 scoriaceous dome clasts, and B is enriched in white pumice melt inclusions. (a + b) Li and B vs. P H_2O, (c + d) Li and B vs. H_2O, (e + f) Li and B vs. SiO_2, (g + h) Li and B vs. Cl, (i) Li vs. B

5.4.4. Clinopyroxene compositions

The major element composition of clinopyroxene host crystals was measured alongside other clinopyroxene phenocrysts within the same eruptive products. This established whether there are systematic compositional variations between different eruptive products and whether the host crystals are representative of the larger clinopyroxene phenocryst population. Of the different 2010 lithologies, clinopyroxene from the dome samples have the widest compositional range ($Wo_{40-50}En_{33-45}Fs_{12-24}$) with the presence of crystals containing higher proportions of Wo and Fs and lower En, compared to the grey scoria ($Wo_{42-47}En_{38-44}Fs_{12-15}$) and the white pumice ($Wo_{41-48}En_{36-45}Fs_{13-16}$) (Fig 5.6). Analysed clinopyroxene phenocrysts from the 2006 dome scoria are similar in composition ($Wo_{41-48}En_{36-45}Fs_{13-17}$) as those from the 2010 eruption (Table 5.2). The magnesium number (Mg# = 100 x Mg / (Mg + Fe^{2+})) of the 2006 pyroxenes (Mg# = 76–83) also sits within the range of the 2010 phenocrysts (Mg# = 61–86). The 2010 dome samples have the largest range in Mg# (61–86), although most crystals analysed from the dome lie between Mg# 71–84 (Table 5.2). In comparison, grey scoria and white pumice samples contain clinopyroxene phenocrysts with Mg# 77–83 and Mg# 75–84, respectively. Although the majority of clinopyroxene phenocrysts from all 2010 and 2006 samples contain ~ 1–3 wt.% Al_2O_3, the 2010 dome crystals display the largest variation, with values ranging between 0.4 and 8.9 wt.%. Other lithologies from the 2010 eruption also contain relatively high-Al_2O_3 phenocrysts, with the clinopyroxene from the white pumice containing 1.4–7.0 wt.% Al_2O_3 and those from the grey scoria 1.4–4.8 wt.% Al_2O_3. This is similar to previous analyses of 2010 and 2006 Merapi clinopyroxene phenocrysts, for which concentrations of 2–8 wt.% Al_2O_3 and 1.5–6.5 wt.% are reported (Costa *et al.*, 2013). In comparison, the 2006 clinopyroxene generally encompass a more restricted range, with crystals generally containing 1.4–3.8 wt.% Al_2O_3, with only one analysis recorded at elevated Al_2O_3 contents (6.7 wt.%) (Fig 5.6). The clinopyroxene phenocrysts hosting the melt inclusions that were used for SIMS analysis generally sample the compositional range found within the entire 2010 and 2006 population of clinopyroxene phenocrysts analysed, although they do not sample the highest Al_2O_3 contents, with analysed host crystals containing a maximum of 5.6 wt.% Al_2O_3 (Table 5.2).

Table 5.2: Representative clinopyroxene compositions from 2010 and 2006 eruptive products. Stages from Komorowski *et al*. (2013). Sample types are abbreviated as follows: DD= dense dome clast, GS= grey scoria, WP= white pumice, DS=scoriaceous dome clasts. FeO* denotes total iron. Mg# = 100 x Mg / (Mg + Fe^{2+}). Clinopyroxene end-member compositions were calculated in mol.% from the ferric structural formula as follows: wollastonite (Wo) = 100 x Ca / (Ca + Mg + Fe*), enstatite (En) = 100 x Mg / (Ca + Mg + Fe*) and ferrosilite (Fs) = 100 x Fe* / (Ca + Mg + Fe*) where Fe* denotes total iron (Fe^{2+} and Fe^{3+}).

Eruption	2010	2010	2010	2010	2010	2010	2010	2010	2010	2010	2010	2010	2006	2006	2006	2006
Stage	4	4	4	4	6	6	6	6	6	6	6	6	14 Jun	14 Jun	14 Jun	14 Jun
Type	DD	DD	DD	DD	GS	GS	GS	GS	WP	WP	WP	WP	DS	DS	DS	DS
Sample	M11-25-5	M11-27-5	M11-27-5	M11-27-5	M11-75	M11-75	M11-75	M11-75	M11-55	M11-55	M11-50	M11-50	M08-09	M08-09	M08-09	M08-09
Cpx no.	x21-h1	x12-h1	x30-h1	x34-h2	x13-h1	x11-h2	x30-h1	x41-h1	x17-h1	x44-h1	x20-h1	x71-h2	x70-h2	x13-h1	x28-h1	x48-h2
SiO_2	52.44	52.33	50.59	52.41	52.66	51.80	51.80	52.44	50.68	52.02	48.04	51.71	52.15	51.32	52.65	52.10
Al_2O_3	1.80	1.74	3.68	1.67	1.79	2.18	2.60	1.86	4.17	2.05	5.56	3.23	1.89	3.11	1.61	2.38
TiO_2	0.33	0.36	0.67	0.17	0.35	0.38	0.52	0.35	0.71	0.43	0.88	0.57	0.38	0.55	0.37	0.50
Cr_2O_3	0.00	0.05	0.00	0.03	0.05	0.01	0.02	0.00	0.01	0.04	0.00	0.01	0.00	0.02	0.00	0.02
FeO*	7.66	9.18	8.56	10.93	8.77	8.43	8.52	8.60	8.50	8.94	8.71	8.83	9.23	8.84	8.78	8.67
MnO	0.46	0.73	0.40	0.58	0.61	0.48	0.47	0.56	0.30	0.67	0.26	0.54	0.72	0.58	0.72	0.54
MgO	15.33	15.19	14.07	13.61	14.93	14.89	15.00	15.09	13.93	14.91	13.01	14.05	15.09	14.16	14.87	14.49
CaO	21.20	20.16	21.78	20.92	20.55	21.38	20.83	20.62	21.88	20.57	22.16	21.14	20.18	20.97	20.49	20.80
Na_2O	0.37	0.41	0.38	0.33	0.37	0.40	0.37	0.32	0.35	0.35	0.33	0.37	0.34	0.35	0.34	0.35
Total	99.59	100.15	100.12	100.65	100.07	99.95	100.13	99.83	100.52	99.97	98.95	100.44	99.99	99.89	99.83	99.85
Ferric Form																
Si	1.944	1.938	1.874	1.950	1.952	1.918	1.915	1.946	1.870	1.931	1.804	1.913	1.935	1.909	1.958	1.937
Al	0.079	0.076	0.161	0.073	0.078	0.095	0.113	0.081	0.181	0.090	0.246	0.141	0.083	0.136	0.071	0.104
Ti	0.009	0.010	0.019	0.005	0.010	0.011	0.014	0.010	0.020	0.012	0.025	0.016	0.011	0.015	0.010	0.014
Cr	0.000	0.001	0.000	0.001	0.001	0.000	0.001	0.000	0.000	0.001	0.000	0.000	0.000	0.000	0.000	0.001
Fe3	0.041	0.056	0.080	0.040	0.023	0.075	0.053	0.030	0.064	0.048	0.121	0.027	0.049	0.040	0.017	0.018
Mg	0.847	0.839	0.777	0.755	0.825	0.822	0.827	0.835	0.767	0.825	0.728	0.775	0.835	0.785	0.824	0.803
Fe2	0.196	0.228	0.185	0.300	0.249	0.186	0.210	0.237	0.199	0.229	0.153	0.246	0.237	0.235	0.256	0.252
Mn	0.014	0.023	0.012	0.018	0.019	0.015	0.015	0.018	0.009	0.021	0.008	0.017	0.023	0.018	0.023	0.017
Ca	0.842	0.800	0.864	0.834	0.816	0.848	0.825	0.820	0.865	0.818	0.891	0.838	0.803	0.836	0.816	0.829
Na	0.027	0.029	0.027	0.024	0.026	0.029	0.026	0.023	0.025	0.025	0.024	0.027	0.024	0.025	0.025	0.025
Sum	4.000	4.000	4.000	4.000	4.000	4.000	4.000	4.000	4.000	4.000	4.000	4.000	4.000	4.000	4.000	4.000
Mg#	81.19	78.60	80.78	71.56	76.85	81.54	79.75	77.88	79.41	78.27	82.67	75.90	77.89	76.98	76.30	76.15
Wo	43.71	41.60	45.34	43.23	42.65	43.91	43.07	42.66	45.68	42.59	47.08	44.44	41.71	44.09	42.65	43.57
En	43.97	43.62	40.76	39.14	43.13	42.57	43.17	43.44	40.47	42.96	38.47	41.08	43.40	41.41	43.07	42.25
Fs	12.33	14.78	13.91	17.62	14.22	13.52	13.75	13.89	13.85	14.45	14.45	14.48	14.88	14.50	14.27	14.18

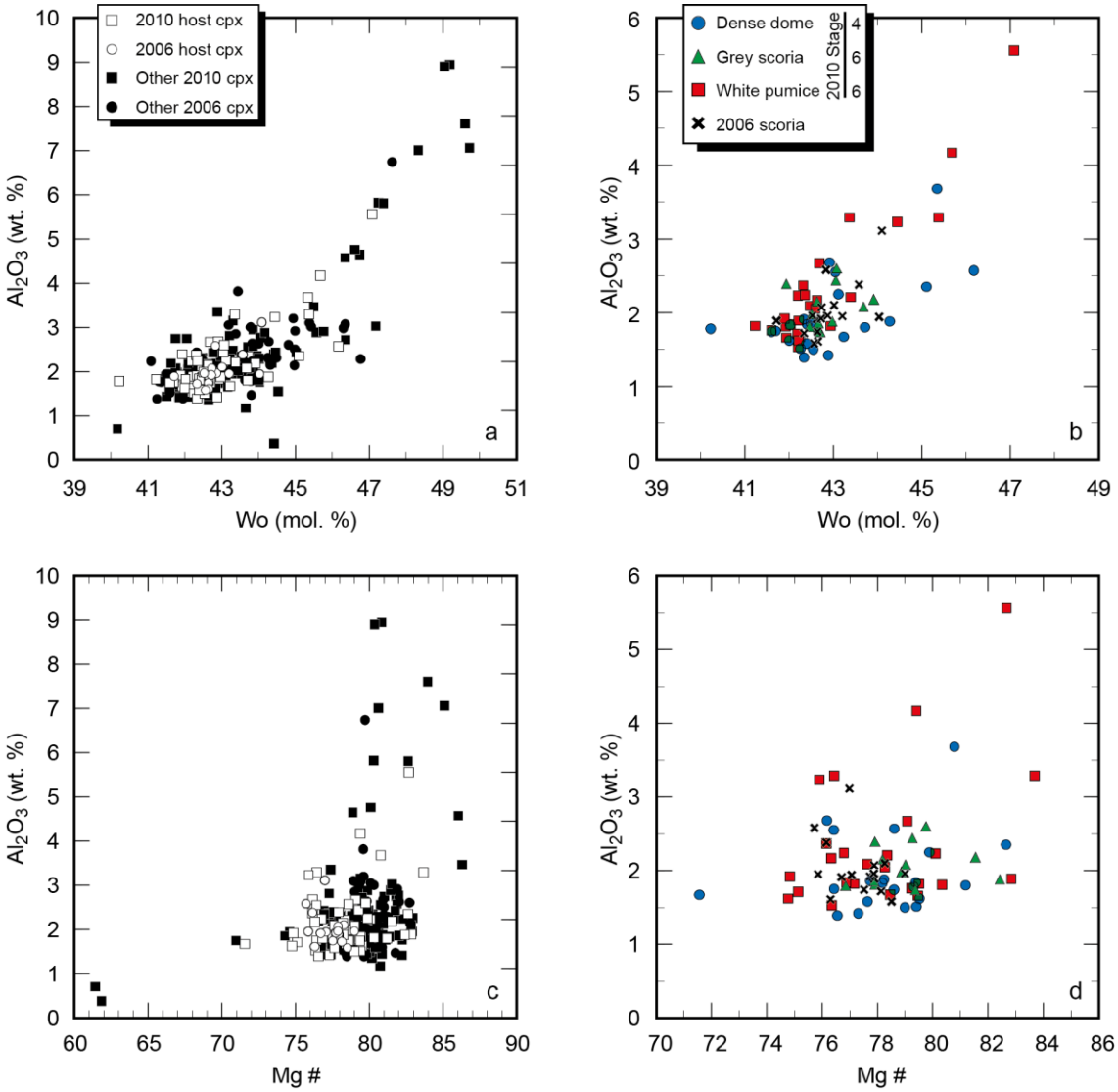

Fig. 5.6 Clinopyroxene phenocryst compositions. (a) Al_2O_3 (wt. %) vs. Wo (mol. %) (wollastonite end-member) of all measured clinopyroxene phenocrysts in 2010 and 2006 products, including the host phenocrysts (white symbols) that host melt inclusions used in this paper, as well as other phenocrysts from the same eruptive products (black symbols). (b) Al_2O_3 (wt. %) vs. Wo (mol. %) in the host phenocrysts, divided into eruptive stages. (c) Al_2O_3 (wt. %) vs. Mg # of all measured clinopyroxene phenocrysts in 2010 and 2006 products, including the host phenocrysts (white symbols) that host melt inclusions used in this paper, as well as other phenocrysts from the same eruptive products (black symbols). (d) Al_2O_3 (wt. %) vs. Mg # in the host phenocrysts, divided into eruptive stages

5.5. Discussion

5.5.1. Melt inclusion entrapment and clinopyroxene crystallisation

The wide variation of H_2O concentrations in melt inclusions over the entire compositional range suggests that some inclusions have ruptured on timescales that

were long enough to allow the escape of H_2O but not to allow chemical re-equilibration with the groundmass melt (Blundy and Cashman, 2005) (Fig. 5.7). This is consistent with the fact that the melt inclusions with the lowest H_2O concentration are from the densest (dome) samples, which have experienced a protracted cooling history at low pressure in the dome. When focussing only on the scoria and pumice samples the general trend is for lower SiO_2 and K_2O melt inclusions to have higher H_2O concentration than the higher SiO_2 and K_2O melt inclusions, which is consistent with vapour-saturated crystallisation in response to decompression (Fig. 5.7). Individual melt inclusion entrapment pressures, or the last pressures of re-equilibration assuming vapour saturation, were calculated using the Papale H_2O-CO_2 model (Papale *et al*., 2006), and using *VolatileCalc1.1* (Newman and Lowenstern, 2002), with both sets of calculations carried out at a temperature of 1000°C based upon previous thermometry of recent Merapi rocks (Gertisser, 2001; Costa *et al*., 2013). Pressure estimates calculated with each model are similar. Minimum equilibration pressures assuming volatile saturation, range from < 5 to 250 MPa using VolatileCalc. This is a similar pressure range to that previously reported for Merapi melt inclusions, which found the majority were trapped below 266 MPa (Nadeau *et al*., 2013). However, as stated above, the lowest values probably reflect the fact that some melt inclusions have ruptured during ascent. To get a better estimate of the lowest entrapment pressures, the most evolved inclusion that sits on the decompression crystallisation trend (Fig. 5.7), equilibrated at ~ 15 MPa. This reveals minimum melt inclusion equilibration at depths of ~ 0.6–9.1 km, assuming an average crustal density of 2800 kg/m^3 (Costa *et al*., 2013).

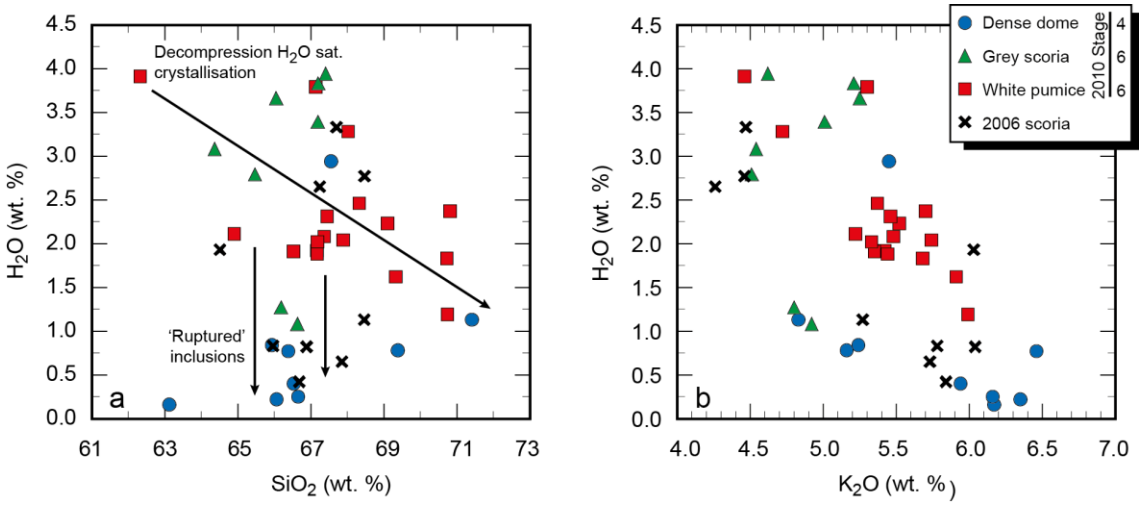

Fig. 5.7 H_2O plotted vs indicators of magmatic differentiation (a) SiO_2, (b) K_2O. Melt inclusions last equilibrated during decompression H_2O-saturated crystallisation, and evidence that some melt inclusions ruptured during ascent

The crystallisation pressure of melt inclusion-hosting clinopyroxene phenocrysts was calculated using *CpxBar*, an Excel spreadsheet based upon the clinopyroxene structural geobarometric calculations of Nimis (1999). Calculations for the Merapi clinopyroxene utilised the mildly alkaline (MA) series calibration (standard error: 200 MPa), with a temperature input of 1000°C, based upon previous two pyroxene thermometry (Gertisser, 2001; Costa *et al*., 2013). The pressure outputs for the 2010 phenocrysts are distributed between 280–790 MPa or 10.2–28.8 km (*n = 57*), with the 2006 phenocrysts lying within a similar, albeit more restricted range of 490–670 MPa, equivalent to 17.8–24.4 km (*n= 15*) (Fig 5.8). Estimates for the differing 2010 lithologies indicate that nearly 80% of the crystals originating from the white pumice crystallised at pressures above 650 MPa (23.7 km). 2010 dense dome samples include phenocrysts that have crystallised at minimum pressures of 280 MPa, compared to 360 and 390 MPa for the white pumice and grey scoria, respectively, although this difference is within the standard error of the method applied. If pressure estimates are calculated with a higher temperature of 1050°C, as previously proposed for high-Al pyroxenes (Costa *et al*., 2013), then pressure estimates decrease to 80 and 540 MPa (2.9–19.7 km) for 2010 crystals and to 230–420 MPa (8.4–15.3 km) for those erupted in 2006 .

In summary, even when the large standard errors of the clinopyroxene barometer are taken into account, pressure estimates for clinopyroxene crystallisation are greater than those of the last recorded melt inclusion equilibration pressures. Clinopyroxene phenocrysts crystallised at between ~ 10–29 km, with calculated minimum melt inclusion equilibration occurring between 0.6–9.1 km. The clinopyroxene barometry results are in agreement with previous clinopyroxene barometry carried on recent eruptive products from Merapi (Gertisser, 2001; Chadwick *et al*., 2013). Clinopyroxene crystallisation depths are in accord with other geophysical and petrological evidence concerning the magmatic plumbing system at Merapi (*e.g.* Beauducel and Cornet, 1999; Costa *et al*., 2013). The calculated melt inclusion equilibration pressures also complement those previously reported for Merapi (Nadeau *et al*., 2013). The discrepancy between the crystallisation pressure of the host clinopyroxene phenocrysts and the minimum equilibration pressure of the melt inclusions can be explained in several ways. One possible explanation is that the melt was not vapour-saturated at the

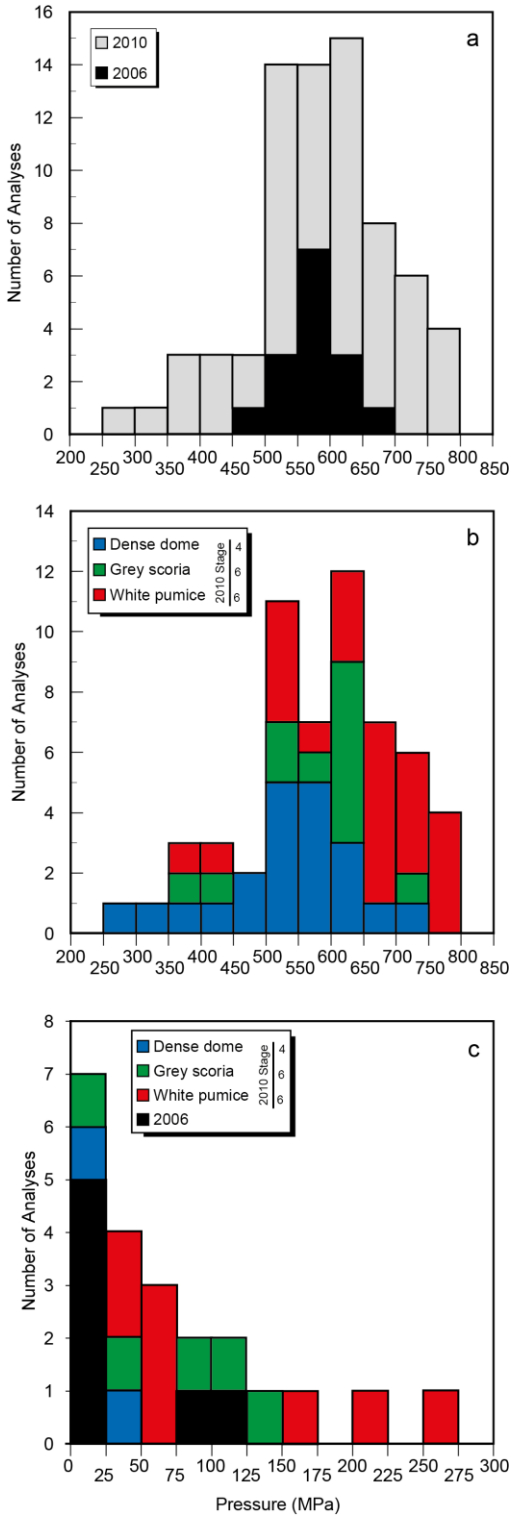

Fig. 5.8 (a + b) Histograms to show pressure (MPa) of clinopyroxene host crystallisation, calculated with CpxBar (Nimis, 1999) using the MA (mildly alkaline) calibration at 1000°C (standard error = 200 MPa). (a) Clinopyroxene host from 2006 crystallised over a more restricted pressure range than the ones from 2010. (b) 2010 clinopyroxenes, divided into eruptive stages, with the deepest crystals originated in the white pumice. (c) Histogram of last re-equilibration pressures (MPa) of melt inclusions from different 2010 stages and from 2006, calculated using VolatileCalc (Newman and Lowenstern, 2002) at 1000°C, based on melt inclusion H_2O and CO_2 concentrations

time of entrapment, therefore recording seemingly lower pressures than those of actual entrapment. This scenario is not considered likely as it is not consistent with the trends of vapour-saturated crystallisation (Fig. 5.7), nor with the presence of exsolved brine (see below), and is contradictory to previous evidence of volatile-saturated melt inclusions at Merapi (Nadeau *et al*., 2013). Another interpretation is that the inclusions are not primary but secondary, *i.e.* not trapped within hosts during initial crystallisation, but instead during subsequent partial dissolution, as previously observed for Merapi melt inclusions in amphibole and pyroxene hosts (Nadeau *et al*., 2013). However, there is no petrographic evidence for dissolution of the clinopyroxene host crystals that were analysed for this study. Therefore, the most likely explanation for the pressure difference is due to melt inclusions re-equilibrating with the magma after initial entrapment. This is consistent with the H_2O-saturated crystallisation trends, as shown in Fig. 5.7. The melt inclusions re-equilibrated over a range of pressures < 250 MPa (~ < 9km), indicating either that there was enough time for re-equilibration during ascent or that magma was stored at this pressure range for a period of time before eruption. The fact that the maximum melt inclusion re-equilibration depth of ~ 9 km matches that of previous melt inclusion studies (Nadeau *et al*., 2013), hints at the possibility that the melt has stalled at this depth. This depth is broadly consistent with geophysical (Beauducel and Cornet, 1999; Ratdomopurbo and Poupinet, 2000) and petrological (Costa *et al*., 2013) evidence for a magma storage region beneath Merapi.

5.5.2. Degassing history (CO_2 and H_2O)

Using *VolatileCalc* (at 1000°C), trends for open- and closed-system degassing were calculated and compared to the Merapi inclusions. In the open-system model, exsolved volatiles are removed from the system, whereas for closed-system runs, the exsolved vapour remains within the system, acting as a buffer on the remaining melt, including those volatiles that remain in solution in the depressurising magma. Closed-system models fit the data better than open-system ones, with the overall best fit having an initial starting point of 4.0 wt.% H_2O, 1000 ppm CO_2 and 1% exsolved vapour (Fig 5.3). This closed-system trend is mainly defined by white pumice inclusions, indicating that closed-system degassing occurred prior to the sub-Plinian explosive phase of the 2010 eruption, with the exsolved volatiles staying within the system, leading to

increasing overpressure and explosive activity. Inclusions from other stages of eruption have re-equilibrated after the majority of the CO_2 was degassed.

The heterogeneous CO_2 distribution detected in some melt inclusions may either have occurred post-entrapment, perhaps related to the rate of CO_2 diffusion, or may represent real heterogeneities in the magma. Notably, the apparent CO_2 enrichment was predominantly detected in melt inclusions from the 2010 white pumice and never in those from 2010 dome clasts, indicating that the CO_2 heterogeneity could be linked to magmatic heterogeneity locked in by eruption. In which case, the high CO_2 values would represent maximum values. In light of the FTIR data, the high-CO_2 inclusions cannot be interpreted as due to CO_2 fluxing, either from a deeper magmatic source or from carbonate assimilation, as proposed by other authors (*e.g.* Troll *et al*., 2012; Borisova *et al*., 2013; Nadeau *et al*., 2013). That is not to say that these processes do not occur at Merapi, but evidence is not preserved in these inclusions, possibly because any crustal contamination may occur late stage, at shallow depths, not allowing for the CO_2 to dissolve into or re-equilibrate with the melt. However, we do see evidence for deeper magma recharge, especially in the white pumice inclusions.

5.5.3 Evidence of pre- and syn-eruptive degassing processes from F, S and Cl

Fluorine concentrations in melt inclusions and groundmass glass are similar and within the typical range for subduction related magmas (Fig 5.4) (Aiuppa *et al*., 2009 and references therein). The results are consistent with the fact that F is highly soluble in silicate melts (*e.g.* Carroll and Webster, 1994), and generally partitions in favour of the melt relative to the vapour phase, therefore it is often not significantly extracted from the melt by degassing (*e.g.* Balcone-Boissard *et al*., 2010).

Melt inclusions from the 2010 eruption contain a range of S from below the detection limit (~ 100 ppm) up to 535 ppm. Total SO_2 emissions for the entire 2010 eruption were calculated at 0.44 Tg, based on satellite observations (Surono *et al*., 2012). Assuming the maximum S concentration in the melt inclusions (535 ppm) represents the pre-eruptive volatile content of the melt, and the S concentration in the groundmass glass (< 100 ppm) indicates post-eruptive volatile contents, then it is possible to calculate the mass and volume of magma needed to produce the 0.44 Tg of SO_2 that

were emitted during the eruption (Self *et al*., 2004). The approximate phenocryst content is 40 vol.%, and taking into account the fraction of felsic to mafic minerals in the rocks, the proportion of phenocrysts is ~ 45 wt.% (*i.e.* the melt or groundmass occupies 55 wt.%). Results indicate that the mass of degassing magma in the 2010 eruption was 9.2 x 10^{11} kg, and, taking into account the melt density of 2550 kg m^{-3} calculated from the composition of a typical dome clast using the software *Pele* (Boudreau, 1999), the corresponding melt volume is 0.36 km^3. In comparison, it has been estimated that between 0.03–0.06 km^3 of magma (DRE) was erupted during the 2010 eruption (Surono *et al*., 2012), an order of magnitude less than the calculated total volume of degassing melt in the system, indicating that a large proportion of melt did not erupt and remained in the system.

The chlorine content of the groundmass glass is generally lower than the concentration in the melt inclusion population, indicating Cl exsolution at low pressures during syn-eruptive degassing (Fig 5.9). The chlorine concentrations in the melt inclusions are similar to other arc magmas (Aiuppa *et al*., 2009 and references therein; Webster *et al*., 1999), ranging between 2060 and 5130 ppm, although nearly 90 % of the data in this study range between 2400 and 3400 ppm (Fig. 5.9), with the higher concentrations only observed in white pumice melt inclusions. The simplest explanation for relatively limited range of Cl in the melt inclusions, regardless of variations in H_2O, could be that the magma underwent decompression degassing with preferential loss of H_2O and no apparent loss of Cl (Webster *et al*., 2010; Mann *et al*., 2013). However, an alternative explanation is that the silicate melt was in equilibrium with a magmatic hydrosaline chloride liquid ± vapour (*e.g.* Shinohara, 1994; Lowenstern, 1994; Webster, 1997, 2004). Chlorine concentrations in the silicate melt are "buffered" and so remain constant as Cl reaches its solubility limit in equilibrium with the liquid phase(s). Similar indirect geochemical evidence for the presence of a hydrosaline chloride liquid from melt inclusion data has been reported at Mount Hood (Koleszar *et al*., 2012), the Bandelier Tuff, Valles Caldera (Stix and Layne, 1996) and at Vesuvius (Signorelli *et al*., 1999; Fulignati and Marianelli, 2007). The chlorine concentrations in the Merapi melt inclusions are similar to saturation values for felsic melts determined experimentally (*e.g.* Métrich and Rutherford, 1992; Webster, 1997) as well as the values recorded in natural felsic melt inclusions interpreted to have been in equilibrium with a Cl-rich

liquid (Stix and Layne, 1996; Koleszar *et al*., 2012). This evidence for the presence of a saline liquid or "brine" phase is also corroborated by the Li data (see section below).

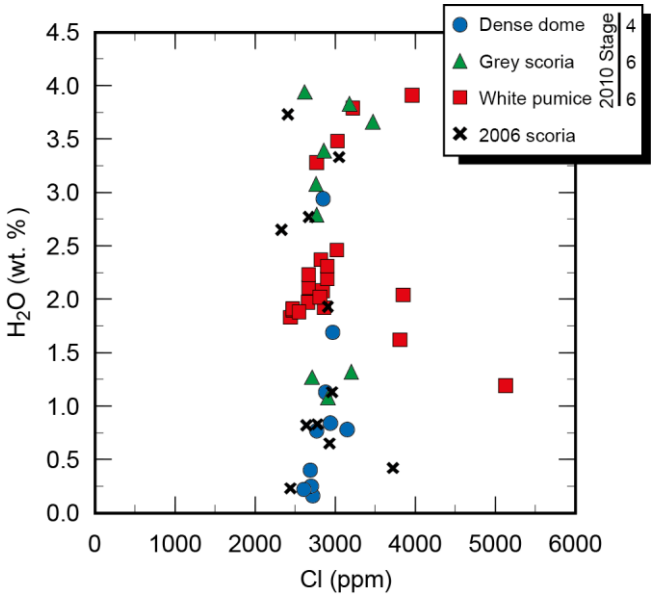

Fig. 5.9 Concentration of Cl vs. H_2O in melt inclusions. Melt inclusions from the 2010 samples as well as from the 2006 scoriaceous dome show constant Cl concentrations with variable H_2O contents, evidence that the Cl concentration in the melt was "buffered" by a hydrochloride phase. The only inclusions that deviate to higher Cl concentrations are several from the white pumice

5.5.4 Lithium and boron enrichment

Lithium is enriched in melt inclusions from the 2010 dense dome material and the 2006 scoria, which contain relatively low concentrations of H_2O. It displays an L-shaped, divergent trend when plotted against H_2O and Cl and displays no correlation with SiO_2 or K_2O (Fig 5.5). Enrichment of B occurs in melt inclusions from white pumice samples, which have mid-range H_2O content, with variable Cl, including elevated contents. These contrasting features indicate that Li and B enrichment are produced by different processes, corroborated by the decoupled relationship of Li vs. B (Fig 5.5) as well as the fact that enrichment occurs in distinct and separate lithological types.

Boron is a component of many phases within marine sediments and present in carbonates if mixed with fine detrital clays (Leeman and Sisson, 1996; Palmer and Swihart, 1996). It is therefore possible that the B enrichment in the white pumice inclusions is due to an increased degree of crustal assimilation before the explosive phase of the 2010 eruption. If this was the case, given that crystallisation and melt

inclusion equilibration is happening throughout the crust, the B enrichment should coincide with the depth range of crustal carbonate rocks (~ 0-10 km). However, B enrichment is limited to inclusions with a more restricted H_2O concentration and P_{H2O}. The majority of white pumice melt inclusions are enriched in B at P_{H2O} = ~ 15–52 MPa or ~ 0.6–1.9 km depth. Only one B-enriched inclusion last equilibrated at higher pressures and also contains significant CO_2, so pressure calculated with H_2O + CO_2 = 251 MPa or 9.1 km depth. Previous work has shown that under certain conditions, boron partitions preferentially into vapour over both melt and brine (Heinrich *et al*., 1999; Schatz *et al*., 2004). However, other work has demonstrated that B, along with Cl, may also preferentially stay in the melt during explosive volcanic eruptions (Wright *et al*., 2012). The positive correlation of B against SiO_2 in white pumice melt inclusions indicates that during the explosive stage of the 2010 eruption, B acted as an incompatible element, becoming enriched in the melt. The positive correlation of B with Cl is only seen in white pumice melt inclusions, with Cl concentrations in these inclusions increasing up to > 5000 ppm from the "buffered" concentrations seen in other the other melt inclusions. This implies that during the fast ascent of the explosive stage, B and Cl stayed in the melt with insufficient time for them to degas and insufficient time for the exsolution of a brine phase from the melt.

Lithium-enriched inclusions, only detected in 2010 dense dome samples and 2006 scoriaceous dome samples, have last equilibrated at near-surface depths, with the maximum Li enrichment in 2010 inclusions at P_{H2O} = 14.5 MPa (0.5 km depth) and P_{H2O} = 36.5 MPa (1.3 km) for maximum Li in 2006. This implies that Li enrichment is a pressure-mediated process. Lithium enrichment in early-erupted dome samples, detected in melt inclusions equilibrated at specific H_2O concentrations, has also been noted at Mount St Helens (Berlo *et al*., 2004; Blundy *et al*., 2008) and at Shiveluch (Humphreys *et al*., 2008). This has been attributed to pre-eruptive, vapour-mediated transfer of Li, derived from deeper within the magma transport system. Alternatively, Li-rich inclusions may be produced via re-equilibration with a Li-rich brine phase (Kent *et al*., 2007). An alkali-rich aqueous vapour can be produced via the degassing of an H_2O-saturated magma body. Buoyant upward migration of this vapour results in its exsolution to produce two phases; a dense alkali-rich brine and a lower density H_2O-rich vapour (Kent *et al*., 2007). The lower density H_2O-rich vapour is subsequently lost via degassing and the alkali-rich brine re-equilibrates with the melt, resulting in Li-

enriched melt inclusions. In the Merapi melt inclusions, the Li-enriched inclusions all contain similar Cl concentrations (Fig 5.5), further indicating that Li-enrichment occurred during "buffering" of the melt Cl concentrations, related to equilibration of the melt with the brine phase. The inflexed trend in SiO_2 vs. Na_2O, with decreasing Na_2O in the groundmass glass (Fig 5.2) may also be attributed to Na partitioning into the exsolving fluid phase during volatile-saturated crystallisation (Blundy *et al*., 2008).

5.5.5. Comparison of the 2010 and 2006 eruptions

In many respects, the contrasting behaviour of the 2006 and 2010 eruptions is not reflected in the eruptive products. Whole rock, melt inclusion and groundmass compositions are all similar in terms of major elements. Volatile (H_2O, CO_2, F, Cl and S) concentrations are predominantly similar. Silicate melt from early erupted products (*i.e.* dome clasts) of both 2010 and 2006 was saturated in Cl, preserving evidence of the presence of a hydrosaline fluid or "brine" phase within the magmatic system prior to each eruption. Further evidence for this comes from the fact that these same melt inclusions are enriched in Li, indicating similar shallow-level processes operating prior to the dome-building stage of each eruption.

However, there are some differences between the 2010 and 2006 products, particularly in melt inclusions originating from the white pumice, which is unique to the 2010 eruption and erupted explosively during the sub-Plinian stage. Moreover, the white pumice shows numerous distinctive features when compared to other 2010 samples. The white pumice reveals evidence of an increase in deep magma supply, highlighted by an abundance of clinopyroxene phenocrysts crystallised at > 23 km depth. This may either be due to an influx of deeper magma to shallower parts of the system, or may have been caused by the removal of the dome during Stage 4 of the eruption, increasing drawdown depth and incorporating an increased proportion of magma from greater depths. The white pumice melt inclusions are the only ones to show B enrichment and variable Cl concentrations, owing to the fast ascent rate. The deep influx of magma would have caused increased overpressure and faster magma ascent. Closed-system degassing and fast magma ascent rates, as a result of the deep influx of magma, was a primary driving force behind the explosive nature of the 2010 eruption. Melt inclusions from both eruptions re-equilibrated after entrapment, during

volatile-saturated crystallisation. The continuous range of re-equilibration depths between 9.1–0.6 km suggests that the melt region, at these depths at least, is strongly interconnected and not formed of discrete chambers.

5.6. Summary

Despite the contrasting eruptive behaviour, the 2010 and 2006 eruptive products are similar in terms of bulk rock and melt inclusion major element concentrations. In addition, the volatile contents of both melt inclusions and groundmass glass are also similar. Dome clasts from both eruptions reveal evidence of an exsolved brine phase prior to eruption, with melt inclusions from these clasts enriched in Li and with "buffered" Cl concentrations. In contrast, melt inclusions from the 2010 white pumice formed during subsequent explosive activity, equilibrated during closed-system degassing, are enriched in B and Li, and have variable Cl concentrations due to fast ascent. Clinopyroxene host phenocrysts from the white pumice crystallised at greater depths (up to 28.8 km) compared to those erupted during other stages of the 2010 eruption or those from 2006. The transition from effusive dome-forming to explosive (sub-Plinian) behaviour during the 2010 eruption was triggered by an influx of magma from depth which increased the overpressure and "overwhelmed" the system. This was further increased by a closed-system degassing regime, with exsolved volatiles staying in the system. Careful melt inclusion analysis, utilising various complementary techniques including SIMS and ATR micro-FTIR revealed no evidence in these melt inclusions for CO_2 fluxing via crustal carbonate assimilation or via degassing of a deeper magma body. This work highlights the influence of magmatic flux, magmatic degassing and ascent rate in controlling the eruptive style at Merapi volcano, and indeed other similar arc volcanoes worldwide. Variations in these factors will serve to modulate future activity, controlling whether eruptions will be effusive and dome-forming or more explosive.

Chapter 6: Synthesis and discussion

This thesis has sought to elucidate the driving forces behind effusive and explosive activity at Merapi, via petrological and textural analysis of the 2006 and 2010 eruptive products. The 2006 effusive eruption (VEI 1) was characteristic of eruptions that have occurred at Merapi over the past century, and consisted of dome-growth, punctuated by gravitational dome collapse. The 2010 eruption (VEI 4) was the largest eruption at Merapi since 1872 (e.g. Surono *et al*., 2012) and, in contrast to recent eruptions, began with explosions rather than effusion of a lava dome and displayed remarkably high extrusion rates when dome growth did later occur (Surono *et al*., 2012; Ratdomopurbo *et al*., 2013; Pallister *et al*., 2013). Activity in 2010 consisted of several explosive stages generating a series a laterally directed dome explosions (blasts), sustained eruption columns and maximum PDC runout distances of ~ 16 km, more than twice of those generated in 2006 (7 km) (Charbonnier and Gertisser 2008; Charbonnier, 2009; Charbonnier *et al*., 2013; Komorowski *et al*., 2013). The fact that the 2010 eruption was the first VEI 4 eruption since 1872, meant that this was the first time that a larger than "normal" eruption at Merapi was well-monitored, with seismic, ground deformation and gas emission data all available to enhance the interpretation of petrological data. This chapter aims to synthesise and link together the results presented in Chapters 3, 4 and 5 in order to explicate factors that were responsible for effusive and explosive eruptive style and the transition between them. In addition, findings are reviewed compared to previous activity at Merapi, as well as in a global context, compared to other similar subduction related volcanoes.

6.1. Eruptive processes in 2006 and 2010

Whole rock compositions, both in terms of major and trace element data presented in Chapters 3 and 4 are similar for the 2006 and 2010 erupted lavas and remained nearly constant throughout the duration of each eruption. This indicates that bulk magmatic composition cannot be a major factor in the change in behaviour between the 2006 and 2010 basaltic andesite eruptions. Petrological data presented in

this thesis, including geobarometry, melt inclusion volatile content and the presence of higher-Al clinopyroxene and higher-An feldspar microlites, all suggest that there was an influx of deeper (> ~ 25 km), hotter and more volatile-rich magma prior to the 2010 eruption compared to 2006. This is in agreement with other petrological and monitoring data (Surono *et al*., 2012; Jousset *et al*., 2013; Costa *et al*., 2013). Increasing fumarole gas temperatures and ratios of CO_2/SO_2, CO_2/HCl and CO_2/H_2O in months prior to the 2010 eruption, were interpreted to be due to the degassing of a deep magmatic source (Surono *et al*., 2012). SO_2 emissions during explosive phases of the 2010 eruption were up to ~ 3 orders of magnitude higher than emissions detected during eruptions between 1992 and 2007 (Surono *et al*., 2012). Costa *et al*. (2013) proposed that the 2010 eruption was preceded by an influx of deeper, hotter, more volatile-rich magma that was up to 10 times more voluminous than that in 2006. Despite the difference in recharge, whole rock compositions of erupted magma remain similar. Mafic recharge has been proposed at Merapi, based on long-term geochemical variations (Gertisser and Keller, 2003a), the presence of occasional mafic enclaves (*e.g*. Chadwick *et al*., 2013) and rare sulphide melt saturated mafic melt inclusions (*e.g*. Nadeau *et al*., 2010, 2013). The fact that whole rock compositions remain similar for long periods of time at Merapi, may potentially be due to recharge filtering processes. If a mafic magma is injected into a silicic magma, then a density filter may prevent the mafic magma erupting through the silicic material and in turn a viscosity filter may prevent the silicic magma erupting. Conditions that enable the mafic and silicic magmas to mix will form an andesite. This enables the magma to overcome the rheological barriers and erupt, explaining why only limited compositions are erupted over long periods of time (Kent *et al*., 2010; Eichelberger *et al*., 2010). All melt inclusions in this study were mainly dacitic to rhyolitic (63.1–72.4 wt.% SiO_2), with only two andesitic inclusions measured with a minimum SiO_2 of 61.7 wt.% (Chapter 5). Measured melt inclusions do not record more primitive compositions that may be associated with a deep mafic recharge. However, as discussed in Chapter 5, these melt inclusion compositions are related to decompression H_2O-saturated crystallisation, and as such, provide a record of conditions during ascent and/or relatively shallow (< 9 km) storage rather than recording an episode of deeper (~ > 25 km) magmatic flux.

The initial explosion at the onset of the 2010 eruption on 26 October was not preceded by dome extrusion, as was the case for the 5 November paroxysmic

explosions. On 26 October, it is probable that overpressure built up due to high magmatic flux and ascent rates causing an accumulation of gas, fed by the large influx of hotter, deeper magma. The fact that rapid magmatic ascent resulted in explosions rather than dome extrusion, as in later stages of the 2010 eruption, suggests that the system was effectively 'closed' prior to the 2010 eruption (Fig. 6.1). Gas accumulation due to magmatic influx and rapid ascent was not balanced by release through permeable conduit walls and fractures to the surface. Field work revealed that as well as the juvenile scoriaceous material erupted during initial explosive stages of the eruption, light grey dense material was found as lapilli, prismatically jointed blocks and as inclusions within the dense dome material (Chapter 4). The light grey dense material has an extensively crystallised groundmass, with low volumes of residual melt and contains abundant cristobalite. Based on groundmass textures, feldspar microlite compositions and the presence of cristobalite, this material is interpreted to be a 'plug' of cooled rigid magma that resided within the shallow system before being partially reheated and remobilised during eruption (Chapter 4). Cristobalite has been frequently found in lava domes, including at Unzen, Japan (Nakada and Motomura, 1999), Santiaguito, Guatemala (Scott, 2012), Soufrière Hills volcano, Montserrat (Sparks *et al*., 2000; Williamson *et al*., 2010), and Chaitén, Chile (Horwell *et al*., 2010), as well as in the 1980 cryptodome at Mount St. Helens, USA (*e.g.* Hoblitt and Harmon, 1992). As cristobalite is often precipitated within vesicles via vapour-transport after dome emplacement, the extent of cristobalite mineralisation may reduce porosity and permeability (Horwell *et al*., 2013). It is therefore possible that cristobalite crystallisation within the light grey dense inclusion material contributed to sealing gas escape pathways prior to the 2010 eruption, augmenting gas overpressure. The remnant 2006 dome may also have been a factor in sealing gas escape pathways at the onset of eruption in 2010 (Fig. 6.1). Seismic features support the fact that explosions during this initial stage of the eruption were driven by gas pressure in the conduit (Jousset *et al*., 2013). Volcano tectonic (VT), multi-phase (MP) and very long period (VLP) earthquakes, as well as unprecedented rates of summit deformation, were all detected prior to the eruption, attributed to fluid movement and pressure build-up in the conduit (Surono *et al*., 2012; Jousset *et al*., 2013, Budi-Santoso *et al*., 2013). VT earthquakes clustered at depths of 2.5–5.0 km and later at < 0.5 km depth below the summit have been attributed to magma intruding and breaching the edifice ~ 10 days prior to eruption (Budi-Santoso *et al*., 2013; Jousset *et al*., 2013). MP and VLP earthquakes detected

below the remnant 2006 dome indicate a build-up of pressure within the conduit prior to the explosive phase (Jousset *et al*., 2013). Some workers also suggested that the initial explosive activity was related to magmatic interaction with the hydrothermal system and that initial explosions were phreatomagmatic (Komorowski *et al*., 2013; Charbonnier *et al*., 2013), although an interpretation of a purely magmatic opening phase is preferred here.

Long term, time-averaged extrusion rates at Merapi between 1890 and 1992 are calculated at 1.2 x 10^6 m^3 y^{-1} (Siswowidjoyo *et al*., 1995), equivalent to 0.04 m^3 s^{-1}. This is based on eruptive episodes during that period with extrusion rates ranging from 0.01 to 0.7 m^3 s^{-1}. Similar extrusion rates were observed for individual dome-forming eruptions at Merapi between 1984 and 1996, which ranged between 0.05 and 0.32 m^3 s^{-1} (Hammer *et al*., 2000). In comparison to extrusion rates recorded for Merapi dome-forming eruptions over the last century, peak extrusion rates during the 2006 eruption were a magnitude higher, reaching a peak of 3.3 m^3 s^{-1} (Ratdomopurbo *et al*., 2013) and averaging 2.4 m^3 s^{-1} (Pallister *et al*., 2013). This led to concern during the monitoring effort of the 2006 eruption that a larger eruption would ensue, such as the ones that occurred during the 19th Century (*e.g.* 1822), which had estimated effusion rates of up to 3.5 m^3 s^{-1} (Newhall and Melson, 1983; Pallister *et al*., 2013). As summarised by Pallister *et al*. (2013), high extrusion rates may destabilise a lava dome because "(1) it creates high shear rates in the dome carapace, (2) it results in more low viscosity material in the core of the dome, (3) it causes loading of supporting rocks beneath the dome and over-steepens the dome front, (4) it favours incomplete degassing of the rising column of magma, leading to a build-up of internal gas pressure possibly to the point of transitioning to a more explosive eruption." During the 2006 eruption, scientists at the Merapi Observatory and Technology Centre in Yogyakarta (Balai Penyelidikan dan Pengembangan Teknologi Kegunungapian, or BPPTK), together with scientists from the Volcano Disaster Assistance Program (VDAP), produced an event tree (Newhall and Hoblitt, 2002) to estimate probabilities of hazardous events, using the lava extrusion rate as the principal discriminant to forecast the 2006 activity (Pallister *et al*., 2013). Using this method, it was estimated that in late-June 2006, there was a 5% probability of a large 1872-type explosive eruption. During the pre-paroxysmal dome growth stage (Stage 3) of the 2010 eruption, extrusion rates were remarkably rapid (25 m^3 s^{-1}), with a high probability of a large eruption (Surono *et al*., 2012; Pallister *et al*.,

2013). Once the juvenile magma had disrupted the 'plug' and overpressure exceeded the plug strength then rapid extrusion of the dome became possible. Rapid magma ascent and extrusion of a dense dome, evidenced by microlite textures and the presence of amphiboles without breakdown rims (Chapter 3 and 4), as well as by monitoring data (Surono *et al*., 2012; Pallister *et al*., 2013), is interpreted to be a contributing factor to the paroxysmal behaviour in 2010. Rapid magma ascent and degassing resulted in high degrees of ΔT, causing a rapid nucleation event and nucleation-dominated crystallisation of many microlites at shallow levels within the conduit. It is interpreted that open-system degassing and crystallisation of the dense dome effectively sealed the conduit, which, when combined with high magma flux rates in the conduit, led to an increase in pressurisation before the 5 November paroxysmal explosions (Fig. 6.1). Sealing of the conduit is signified by the decrease in SO_2 emissions during rapid dome growth at the beginning of November, compared to explosive stages of the eruption (Surono *et al*., 2012). Degassing and crystallisation cause rheological stiffening of the magma and an increase in viscosity (*e.g.* Sparks, 1997; Melnik and Sparks, 1999, 2005). This may result in an increase in gas overpressure if pressure increase due to crystallisation cannot be balanced via gas flow and escape to the exterior (Sparks, 1997). Rapid nucleation and crystallisation concentrates the remaining gas into smaller amounts of residual glass, so that more gas bubbles form as a result of supersaturation, promoting higher levels of bubble connectivity (Sparks, 1997; Clarke *et al*., 2007). High bubble connectivity promotes permeable gas loss, resulting in vesicle collapse and formation of a dense dome, which acts as a plug, forming conditions favourable to Vulcanian-type explosion (Clarke *et al*., 2007). Effective sealing of the conduit by the dome consequently 'closed' the system, so that magma ascending below the dome proceeded to degas via closed-system degassing, with little or no gas escape from the system (Fig. 6.1). The light grey 'plug' material may also have contributed to this, as it is found as inclusions with in the dense dome lava and as prismatically jointed clasts within the Stage 4 'blast' deposit. Evidence of closed-system degassing is seen in the magma that erupted on 5 November, subsequent to the initial Stage 4 directed dome explosions (blasts). Melt inclusions (Chapter 5) from grey scoria and white pumice clasts also preserve evidence of closed-system conditions during ascent, with higher H_2O concentrations compared to the dome melt inclusions. Volatile concentrations in melt inclusions from white pumice clasts fit with modelled concentrations predicted for a closed-system in equilibrium with 1% exsolved volatiles. It is thought that closed-

system degassing sustained explosive behaviour, generating a subplininan convective column, which collapsed to produce the scoria- and pumice-rich PDCs during Stage 6 of the 2010 eruption (Fig. 6.1). The following day, on 6 November, effusive activity returned, with even higher dome extrusion rates than previously (35 m^3 s^{-1}), accompanied by Strombolian (i.e. open-vent) jetting of gas and tephra in the morning of 6 November (Surono *et al*., 2012; Pallister *et al*., 2013). This stage represents the transition from explosive Vulcanian/subplinian activity back to effusive activity and a return to open-system behaviour. Presumably, the rapid dome extrusion that occurred on 6 November could potentially have caused further explosions by sealing the conduit as occurred during the paroxysmal stage. However, observed Strombolian-style gas and tephra fountaining suggests that the preceding explosive activity 're-opened' the system, creating a pathway for gas release after it was sealed by the dense dome. Dome growth had ceased by 8 November and was followed by dome subsidence and small gas emissions (Surono *et al*., 2012; Pallister *et al*., 2013). This indicates that waning magmatic flux inhibited further explosive behaviour. Unfortunately, no samples were collected from the 6 November dome during this study, so textural and petrological analysis of this stage could not be carried out. Although an ascent to the summit was made during fieldwork in July 2011, the 6 November dome grew inside the deep (~ 200-300 m) crater excavated by the 5 November explosions, bounded by near-vertical, and in some places unstable, crater walls. This meant that sampling the dome at that time was not attempted due to safety reasons.

Notably, the peak of both the 2006 and 2010 eruptions were preceded by regional tectonic earthquakes. On 27 May 2006, a M6.3 earthquake occurred 40 km SSE of Merapi, followed by an increase in extrusion rates and a change in pyroclastic flow direction. On 4 November 2010, a M4.2 earthquake occurred ~ 200 km south of Merapi, at 23:56 local time, just prior the climactic phase of 5 November. Several authors have suggested a probable connection between regional seismic activity and the intensification of eruptive activity at Merapi (*e.g.* Walter *et al*., 2007; Troll *et al*., 2012; Surono *et al*., 2012; Jousset *et al*., 2013). It is possible that passing seismic waves may affect the gas phase, by promoting degassing and expansion of bubbles, thereby increasing the pressure of the system (*e.g.* Brodsky *et al*., 1998; Walter *et al*., 2007; Davis *et al*., 2007; Jousset *et al*., 2013). It is therefore possible that with the magmatic system already at a critical pressurised stage, a small external force can trigger eruption

(Walter *et al*., 2007; Jousset *et al*., 2013). Jousset *et al*. (2013) stress that the main factor causing over-pressurisation at Merapi in 2010 was magma ascent, although relatively small perturbations due to passing seismic waves may have been enough to produce rapid degassing, fragmentation and eruption of an already unstable system. Alternatively, it has been proposed that the 2006 earthquake may have caused instabilities in the Merapi dome resulting in avalanching, which reduced conduit overburden and increased the pressure gradient from chamber to surface, or unloaded the magma reservoir, causing sudden vesiculation and increased activity (de' Michieli Vitturi *et al*., 2010).

Previous workers (*e.g.* Chadwick *et al*., 2007; Deegan *et al*., 2010; Troll *et al*., 2012, 2013; Borisova *et al*., 2013) have proposed that CO_2 liberation via crustal carbonate assimilation has the potential to sustain and intensify eruptions at Merapi. In addition, CO_2 liberation may be amplified by seismic events via fracturing of the limestone basement, releasing pockets of CO_2 and enhancing xenolith entrainment (Troll *et al*., 2012). Increased carbon isotope ratios ($\delta^{13}C$) measured in fumarolic gases during the 2006 eruption after the 27 May earthquake, have been attributed to addition of crustal CO_2 (Troll *et al*., 2012). Monitoring data of the 2010 eruption indicates large CO_2 emissions prior to the 2010 eruption, although this has previously been attributed to the degassing of a deep, volatile-rich magma (Surono *et al*., 2012). Evidence of crustal assimilation has been noted in this study, with calc-silicate xenoliths found within both 2006 and 2010 lavas, as well as the presence of hedenbergite crystals within the lava, in the same thin section as a calc-silicate inclusion, interpreted to have originated from the calc-silicate (Chapter 4). However, in contrast to previous studies (Nadeau *et al*., 2013), melt inclusions in this study (Chapter 5) have revealed no evidence of CO_2 fluxing. This does not mean to say that it does not occur, but that it was not detected in this set of melt inclusions. Borisova *et al*. (2013) calculated that the pre-eruptive 2010 basaltic andesite magma assimilated from 15 to 40 wt.% calc-silicate crustal material in 2010. However, this much assimilation would lead to changes in bulk rock composition. Mixing calculations involving the most evolved 2006 magma with only 1–5 wt. % carbonate ($CaCO_3$) results in CaO contents well above those observed in real erupted Merapi lavas (Costa *et al*., 2013). Although beyond the scope of this study, determining the degree of carbonate assimilation and whether the scale of crustal CO_2 liberation was larger prior to the explosive 2010 eruption compared to the effusive 2006

eruption could have important implications for future hazard analysis at Merapi, as well as other volcanoes where calc-silicate xenoliths have been recognised, such as Popocatépetl, Mexico (Schaaf *et al*., 2005), Vesuvius, Italy (Del Moro *et al*., 2001) and Alban Hills, Italy (Freda *et al*., 1997).

In summary, in 2010, a large influx of hotter, possibly mafic magma from depth, triggered faster magma ascent rates compared to those observed in 2006. When coupled with degassing in a closed system, this pressurised the system and led to explosions on 26 October. Initial explosions temporarily 'opened' the system, allowing ascending magma to degas more freely, and extrude as a lava dome, representing the transition back to effusive activity. Open-system degassing led to a rapid nucleation and crystallisation event and extrusion of dense, degassed lava. This effectively resealed the system, and closed-system degassing of the ascending magma again began to prevail, leading to a build-up of gas overpressure, until the cataclysmic explosions on 5 November. Explosions then 're-opened' the system, facilitating the transition back to effusive activity and allowing for rapid extrusion and emplacement of a dome the following day. By this stage, the eruption was waning and so further explosive activity probably did not occur due to decreasing magma flux. The influence of regional seismicity as well as crustal carbonate assimilation should also not be ignored.

In 2006, magma ascent rates were slower, promoting lower extrusion rates and providing time for sufficient gas escape to prevent over-pressurisation. This was further enhanced by magma temporarily stalling or slowing within the edifice before extrusion. Transitions between explosive and effusive activity in 2010 were driven primarily by the dynamics of magma ascent in the conduit, with degassing and crystallisation acting via feedback mechanisms, resulting in cycles of effusive and explosive activity. For example, explosive activity on 26 October and 5 November acted to 'open' the system and allow for efficient degassing, causing the transition to effusive activity. Effusive activity at the beginning of November, promoted the transition to back to explosive activity, with rapid dome growth effectively sealing the system. In other words, explosive activity enabled subsequent effusive activity, and effusive activity provoked explosive activity.

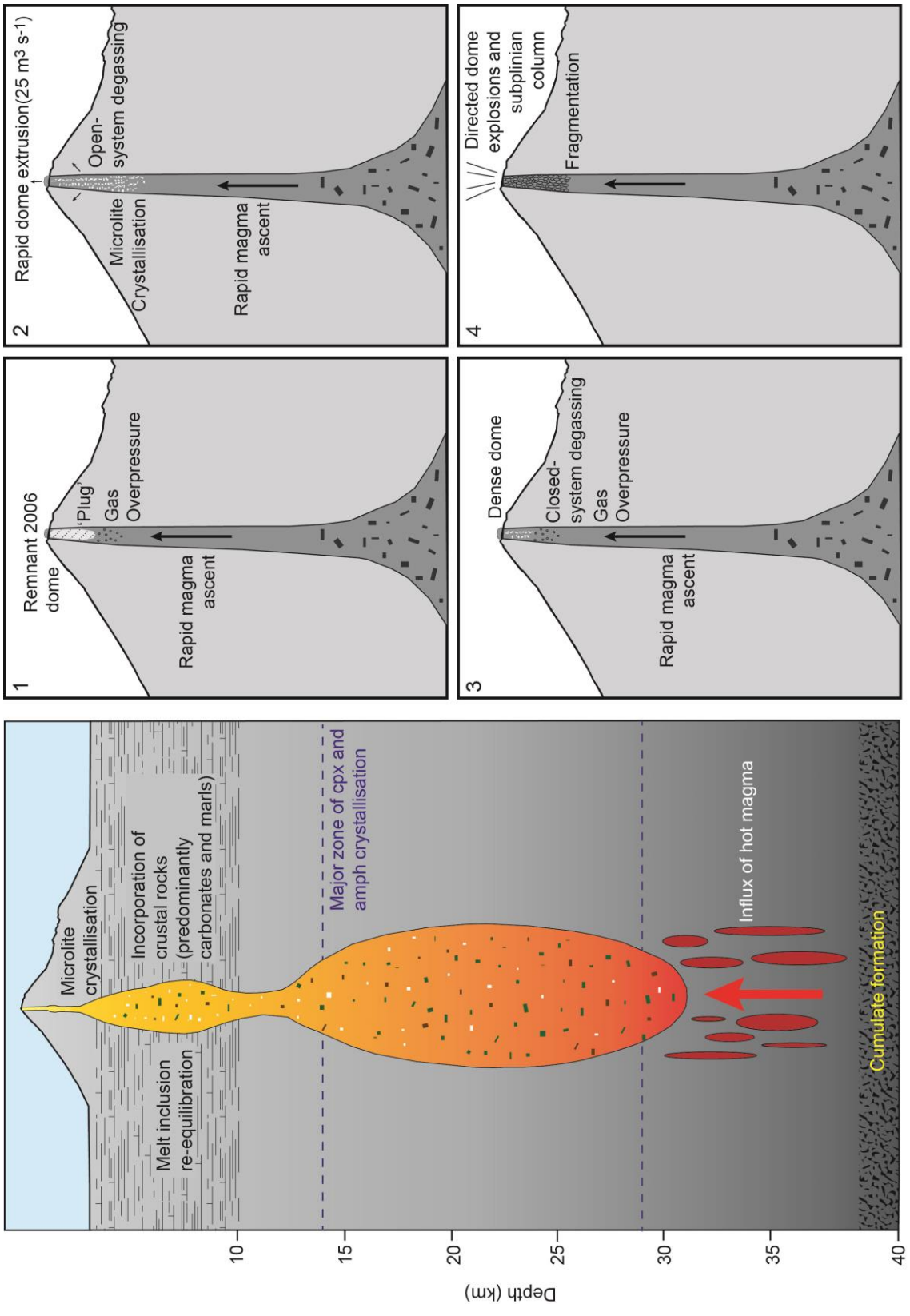

Fig 6.1 Schematic diagram of the Merapi magmatic system and effusive-explosive transitions during the 2010 eruption. (1) Pre-26 Oct. conduit with plug causing gas overpressure, before explosions opened the system, allowing for rapid dome extrusion at the beginning of Nov (2). The dense dome then sealing the system, again causing over pressure (3) before the cataclysmic explosions on 5 Nov (4)

6.2. The 2006 and 2010 eruptions in the context of past and future activity at Merapi

Over the last century, activity at Merapi has been dominated by effusive (VEI 1–2) dome-forming eruptions, but the fact that whole rock compositions were similar in both 2006 and 2010, means that Merapi magma is inherently capable of producing explosive (VEI 4 or potentially higher) eruptions. The 1872 eruption, which was the last VEI 4 eruption before 2010 (see Section 1.6 for further details), has been tentatively linked to a prominent basaltic breadcrust bomb-rich PDC deposit distributed up to a minimum of 11 km from the summit in valleys and interfluve areas on the southern flanks of Merapi (Newhall *et al*., 2000; Gertisser *et al*., 2011; Gertisser *et al*., 2012a, b). If indeed the 1872 eruption was basaltic, then magmatic parameters such as volatile content, viscosity and temperature, would have been different than in 2010, indicating that magmatic and eruption dynamics would also have been different during this explosive eruption. The geological record at Merapi also preserves evidence of frequent subplinian eruptions, up to VEI 4, during the Holocene, which produced medium-K and high-K basaltic and basaltic andesite pumiceous fallout deposits not observed during 2010 (Andreastuti *et al*., 2000; Gertisser, 2001) (section 1.6). Although no deposits preserved in the geological record at Merapi currently indicate eruptions larger than VEI 4, no deposit has yet been definitively linked to the Old Merapi collapse that created the Somma structure (< 4.8 ka) (Gertisser *et al*., 2012a) (Section 1.5). If a deposit is discovered that can be positively linked to the Somma collapse, the juvenile magma involved in this eruption could provide valuable information about the magma dynamics involved in this large-scale eruption. The potential for explosive eruptions should not be underestimated based on the lack of frequency over the last century. Further petrological and textural analysis of the breadcrust bomb-rich deposits and Holocene tephra would provide further insight into range of eruptive activity that Merapi has been capable of producing and the driving forces behind these different types of activity.

Rapid transitions in behaviour are exemplified by recent activity. The 2006 and 2010 eruptions demonstrate the capacity for dome-forming periods at Merapi to transition to explosive behaviour and the 2010 eruption demonstrates that future eruptions may begin explosively, with little warning time and without initial dome growth. Petrological evidence suggests that pre-cursors to a large eruption in the future

may include a pulse of gas-rich magma and a build-up of gas overpressure or rapid dome extrusion. Warning signs that these processes are occurring may be monitored remotely via seismic networks, satellite monitoring, gas flux and ground deformation measurements. Though most pyroclastic flows over the last century have been directed towards the west and southwest, the change in direction in 2006 and 2010 due to changes in summit morphology, mean that in forthcoming eruptions the southern flanks are likely to continue to be affected, as long as the summit morphology remains unchanged.

6.3. Global outlook

The findings of this study are pertinent to other subduction-related volcanoes, where the dynamics of magma influx, magma ascent, degassing and crystallisation may also play an important role in determining eruptive style. Worldwide, it has been estimated that 95% of dome eruptions are associated with an explosive component (Newhall and Melson, 1983). Transitions between effusive dome-forming and explosive activity have been noted at many subduction zone volcanoes, including Unzen, Japan (Noguchi *et al*., 2008); Mount St. Helens, USA (*e.g.* Fink *et al.*, 1990; Cashman and McConnell, 2005); Redoubt, USA (Wolf and Eichelberger, 1997; Coombs *et al*., 2013); Soufrière Hills, Montserrat (*e.g.* Young *et al*., 1998); Galeras, Colombia (Stix *et al*., 1993); Mt. Pelée, Martinique (Villemant and Boudon, 1998; Martel *et al*., 2000) and Mt. Taranaki, New Zealand (Platz *et al*., 2006), to name just a few. As at Merapi, evidence for recharge with hotter magma has previously been linked to remobilisation of magma, triggering and intensifying the onset of eruption and affecting ascent rate at volcanoes such as Soufrière Hills, Montserrat (Murphy *et al*., 2000); El Reventador, (Ridolfi *et al*., 2008); Villarica, Chile (Constantini *et al*., 2011) and Shinmoe-dake, Japan (Suzuki *et al*., 2013). In contrast, at Quizapu, Chile (Ruprecht and Bachmann, 2010) and Mount Hood, USA (Koleszar *et al*., 2012), recharge with hotter magma has been linked to a decrease in explosivity, via the reduction of bulk viscosity, which facilitates degassing and inhibits fragmentation. Variations in ascent rate have been linked to effusive and explosive transitions, with fast ascent promoting explosive activity and slower ascent encouraging more efficient degassing and effusive activity. This association between ascent rate and degassing style has been linked with transitions in eruptive style at

Soufrière Hills, Montserrat (Villemant *et al*., 2008); Arenal, Costa Rica (Szramek *et al.*, 2006); Mount Pelée, Martinique (Martel *et al*., 2000) and Mt. Taranaki, New Zealand (Platz *et al*., 2006). Alternatively, at the Inyo volcanic chain, USA, explosive behaviour has been linked with slow ascent followed by sudden decompression and fragmentation in the shallow conduit (Castro and Gardner, 2008). As suggested in this work during the paroxysmal stage of the 2010 Merapi eruption, closed-system degassing and crystallisation leading to gas-overpressure has also been invoked as a dominant mechanism in explosive eruptions at Galeras, Colombia (Stix *et al*., 1993); Mt. Pelée, Martinique (Villemant and Boudon, 1998; Martel, 2012) and Soufrière Hills, Montserrat (*e.g.* Voight and Elsworth, 2000; Clarke *et al*., 2007, Edmonds and Herd, 2007; Burgisser *et al*., 2011). The processes that govern effusive/explosive transitions are therefore similar at Merapi compared to other subduction volcanoes However, individual volcanic systems also need to be studied in isolation because a complex interplay of factors acts in each system to determine eruptive style. For example, as mentioned above, recharge with hotter magma may intensify eruptions at some volcanoes, and may promote effusive behaviour at others and explosive activity has been linked to fast as well as slow ascent. Therefore, although understanding of eruption dynamics has improved in recent years, via experimental and numerical modelling and verified by the petrological and textural study of natural samples, further work at Merapi and other volcanic systems is still needed.

Chapter 7: Conclusions and outlook

This thesis has investigated the driving forces behind effusive dome-forming activity, compared to more explosive activity at Merapi volcano. It has examined factors that contribute to transitions in eruptive style using the 2006 and 2010 eruptions as case studies. In particular, pre- and syn-eruptive crystallisation and degassing processes have been elucidated *via* a combination of field study, petrological and textural analysis, including quantitative microlite textural analysis, geobarometry and analysis of silicate melt inclusions. This chapter provides a summary of the main findings and conclusions that can be drawn from the work presented in this thesis. It also raises open questions about Merapi, the magmatic system and magma dynamics and provides an outlook on the scope of future work.

7.1. Conclusions

- The 2006 and 2010 eruptions both produced basaltic andesite (54.5–56.1 wt.% SiO_2) similar in terms of whole rock major and trace element compositions. Whole rock compositions remained fairly constant throughout each eruption, signifying that changing whole rock composition was not a major contributing factor to the difference in eruptive styles. This indicates that the Merapi magma which has produced dome-forming eruptions over the last century is also inherently capable of producing explosive eruptions, as was the case in 2010. The factors that contributed to the larger magnitude 2010 eruption took a maximum of four years, although perhaps as little as a few days, to modify the eruptive behaviour.

- Crystallisation at Merapi, based on petrological data from the 2006 and 2010 eruptions, occurs at depths throughout the entire crust. Amphibole and clinopyroxene barometry reveals crystallisation occurring at ~ 4–38 km below the summit. Cumulate amphibole records depths of crystallisation up to 41 km. A major zone of crystallisation is proposed at between ~ 14 and 29 km depth,

where the majority of pyroxene and amphibole phenocrysts crystallised. Melt inclusions last equilibrated at ~ 0.6–9.1 km depth, indicating a shallower magma storage region or strongly interconnected storage regions.

- Magmatic temperatures are estimated to be 920–1020 ± 23.5 °C based on amphibole thermometry from both the 2006 and 2010 eruptions. Maximum melt H_2O contents reach 3.94 wt.% in 2010 lavas and up to 3.73 wt.% in those produced in 2006. CO_2 contents in melt inclusions are generally less than 200 ppm, although are higher in melt inclusions from 2010 white pumice, up to a maximum of 695 ppm.

- Melt inclusions from both eruptions re-equilibrated with an exsolved brine phase, which acted to "buffer" melt Cl concentrations and enrich Li at shallow depths within the conduit or edifice.

- The 2010 eruption was driven by the influx of a large volume of hotter magma from depth (> ~ 25 km). This led to high magma ascent rates which had implications for degassing and crystallisation, further influencing eruptive style. Initial explosions on 26 October 2010 were triggered by rapid ascent and degassing. Gas exsolution was not balanced by gas escape, potentially due to a dense, crystalline, cristobalite-rich 'plug' sealing the conduit, which led to gas over-pressure and explosive behaviour. These initial explosions 'opened' the system allowing for subsequent rapid dome growth, open-system degassing and microlite nucleation and crystallisation. Open-system degassing and microlite crystallisation influenced the rheology of the magma and formed a dense dome which effectively re-sealed the system. This caused the transition back to closed-system degassing and a build-up of gas over-pressure, which led to the paroxysmal explosion sequence on 5 November. Once again, explosions 'opened' the system and activity transitioned back to rapid dome extrusion.

- In comparison, the effusive 2006 activity was driven by relatively lower magma ascent and extrusion rates, providing sufficient time for magma degassing to be balanced by gas escape. Open-system degassing was further enhanced by the magma ascent slowing or temporarily stalling within the edifice.

7.2. Outlook and future work

In recent years, a large progression in understanding driving forces behind a particular eruptive style and factors that can contribute to transitions in style have been made through the study of natural samples, through experiments and *via* numerical modelling. At Merapi, its designation as a "Decade Volcano" in the 1990's has prompted an upsurge in research and consequently understanding. Scientific focus has been further re-invigorated at Merapi in more recent years, following the cataclysmic 2010 eruption. This thesis has contributed to the understanding of the Merapi magmatic system; elucidating factors that influence its eruptive behaviour, specifically focussing on petrological and textural study of degassing and crystallisation processes. However, this work, as well as other recent published work, has raised questions about the Merapi system which remain. These may be key for further understanding the full range of eruptive behaviour that Merapi is capable of producing, in order to aid long-term hazard assessment at Merapi and, possibly, other similar subduction-related volcanoes.

- This study has revealed variations in magma ascent rates and magmatic undercooling in 2006 and 2010 *via* textural analysis of microlites. Decompression experiments specific to Merapi would be useful in order to further quantify ascent processes. Empirical quantification of ascent rates and styles could be gained by comparison of natural microlites with those grown during experiments carried out under different decompression conditions. For example, sets of useful experiments could include different decompression rates, decompression from different initial starting pressures, as well as continuous vs. step-wise decompression experiments to simulate magma ascent paths that may be continuous or stalled. Experiments at specific temperatures could also be useful to quantify the degree of undercooling responsible for different microlite textures. Crystal growth rates during these experiments could also be monitored, which would be used to provide a more robust estimate of crystal growth times within the natural system.

- Ascent rates and styles may also be quantified with phase stability experiments of Merapi amphiboles, tailored to the melt composition, temperature, P_{H2O} and fO_2 thought to exist at Merapi. The geobarometry in this thesis relies on the calibration used in a generic model; and it would be useful to understand the

specific stability range. More detailed study of amphibole reaction rims and their relation to experimentally produced textures could also be useful to quantify the conditions that led to de-stabilisation for samples with reaction rims.

- Establishing timescales of subsurface processes, such as magmatic influx, crystal growth and gas transfer prior to eruptions at Merapi would provide insights valuable to future monitoring efforts. For example, U-series isotope analysis of minerals would help to elucidate sub-surface processes that prevail over short and long-timescales at Merapi. U-series analysis on the 2006 and 2010 eruptions, including analysis of short-lived nuclides ^{210}Pb, ^{210}Po and ^{226}Ra in 2010 products, is currently underway as part of a NERC Urgency grant (PI: R. Gertisser; Co-I's J. Barclay, R. Herd) entitled "Understanding the driving forces behind recent changes in eruptive behaviour of Merapi volcano, Java, Indonesia". This could also be enhanced by detailed study of mineral zonation and chemical diffusion in plagioclase and pyroxene phenocrysts in order to shed further light on magmatic timescales.

- Further petrological and fumarolic gas data would help to establish the degree of crustal carbonate assimilation at Merapi, and whether or not magma – carbonate interaction is elevated during periods of heightened activity, compared to periods of "typical" activity. Work to elucidate the timescales that act between initial carbonate assimilation and CO_2 liberation may be valuable for future monitoring efforts, if the possible excess CO_2 could be detected and quantified in gas emissions prior to an eruption.

- Petrological data in this thesis have revealed a large influx of magma prior to the 2010 eruption, corroborated by monitoring data. However, what was the cause of the larger influx of magma in 2010 compared to in 2006 and will it occur again in the future? Petrological and geophysical studies have not yet revealed the reason for the large influx of magma. Petrological studies of isotopes and trace elements, as well as monitoring of gas compositions, may shed light on the deep processes occurring at Merapi. In the 2010 crisis, monitoring of ground deformation, gas emissions and seismic studies were crucial in recognising the presence of a large magmatic influx, and may help to detect a similar large influx in the future monitoring efforts. However, the interpretation of

geophysical data is often non-unique and model dependant. Petrological work provides an independent constraint on the depths of magmatic storage and influx, as well as processes such as degassing and crystallisation that may act to modulate eruptive behaviour during magma ascent. Petrological data gathered from carefully selected samples that are correlated to eruption chronology enhance the temporal record of pre-eruptive processes. Therefore, further work to integrate petrological results with detectable surface manifestations observed using geophysical monitoring would aid in interpretation of geophysical signals prior to and during future eruptive crises.

References

Abdurachman, E.K., Bourdier, J.-L., Voight, B., 2000. Nuées ardentes of 22 November 1994 at Merapi volcano, Java, Indonesia. Journal of Volcanology and Geothermal Research 100, 345-361.

Afshooni, S.Z., Mirnejad, H., Esmaeily, D., Asadi Haroni, H., 2013. Mineral chemistry of hydrothermal biotite from the Kahang porphyry copper deposit (NE Isfahan), Central Province of Iran. Ore Geology Reviews 54, 214-232.

Aiuppa, A., Baker, D.R., Webster, J.D., 2009. Halogens in volcanic systems. Chemical Geology 263, 1-18.

Allard, P., Métrich, N., Sabroux, J.-C., 2011. Volatile and magma supply to standard eruptive activity at Merapi volcano, Indonesia. Geophysical Research Abstracts 13, EGU2011-13522.

Andreastuti, S. D., Alloway, B. V., Smith, I. E. M. 2000. A detailed tephrostratigraphic framework at Merapi volcano, Central Java, Indonesia: implications for eruption predictions and hazards assessment. Journal of Volcanology and Geothermal Research 100, 51-67.

Ayati, F., Yavuz, F., Noghreyan, M., Haroni, H.A., Yavuz, R., 2008. Chemical characteristics and composition of hydrothermal biotite from the Dalli porphyry copper prospect, Arak, central province of Iran. Mineralogy and Petrology 94, 107-122.

Balassone, G., Scordari, F., Lacalamita, M., Schingaro, E., Mormone, A., Piochi, M., Petti, C., Mondillo, N., 2013. Trioctahedral micas in xenolithic ejecta from recent volcanism of the Somma-Vesuvius (Italy): Crystal chemistry and genetic inferences. Lithos 160-161, 84-97.

Balcone-Boissard, H., Villemant, B., Boudon, G., 2010. Behaviour of halogens during the degassing of felsic magmas. Geochemistry Geophysics Geosystems 11, Q09005.

Barclay, J., Carroll, M.R., Houghton, B.F., Wilson, C.J.N., 1996. Pre-eruptive volatile content and degassing history of an evolving peralkaline volcano. Journal of Volcanology and Geothermal Research 74, 75-87.

Bardinzeff, J.M., 1984. Merapi volcano (Java, Indonesia) and Merapi-type nuée ardente. Bulletin of Volcanology 47, 433-446.

Barmin, A., Melnik, O., Sparks, R.S.J., 2002. Periodic behaviour in lava dome eruptions. Earth and Planetary Science Letters 199, 173-184.

Beauducel, F., Cornet, F. H., 1999. Collection and three- dimensional modeling of GPS and tilt data at Merapi volcano, Java. Journal of Geophysical Research 104, 725-736.

Berthommier, P.-C., 1990. Etude volcanologique du Merapi (Centre-Java): téphrostratigraphie et chronologie - produits éruptifs. Ph.D. Thesis, Université Blaise Pascal, Clermont- Ferrand, France.

Berlo, K., Blundy, J., Turner, S., Cashman, K., Hawkesworth, C., Black, S., 2004. Geochemical precursors to volcanic activity at Mount St. Helens, USA. Science 306, 1167-1169.

Berlo, K., Stix, J., Roggensack, K., Ghaleb, B., 2012. A tale of two magmas, Fuego, Guatemala. Bulletin of Volcanology 74, 377-390.

BGVN, 2006. Bulletin of the Global Volcanism Network. Smithsonian Institution, Washington DC, 31:05-31:06.

BGVN, 2007. Bulletin of the Global Volcanism Network. Smithsonian Institution, Washington DC, 32:02.

BGVN, 2011. Bulletin of the Global Volcanism Network. Smithsonian Institution, Washington DC, 36:01.

Blundy, J., Cashman, K., 2005. Rapid decompression-driven crystallisation recorded by melt inclusions from Mount St. Helens volcano. Geology 33, 793-796.

Blundy, J., Cashman, K., 2008. Petrologic reconstruction of magmatic system variables and processes. Reviews in Mineralogy and Petrology 69, 179-239.

Blundy, J., Cashman, K.V., Berlo, K., 2008. Evolving magma storage conditions beneath Mount St. Helens inferred from chemical variations in melt inclusions from the 1980-1986 and current (2004-2006) eruptions. In: Sherrod, D.R., Scott, W.E., Stauffer, P.H (Eds) A volcano rekindled: The renewed eruption of Mount St. Helens, 2004-2006. U.S. Geological Survey Professional Paper 1750.

Blundy, J., Cashman, K.V., Rust, A., Witham, F., 2010. A case for CO_2-rich arc magmas. Earth and Planetary Science Letters 290, 289-301.

BNEIVS, Bulletin of the Netherlands East Indian Volcanological Survey 1927-1935, no.1-72.

Borisova, A.Y., Martel, C., Gouy, S., Pratomo, I., Sumarti, S., Toutain, J.-P., Bindeman, I.N., de Parseval, P., Metaxian, J.-P., Surono., 2013. Highly explosive 2010 Merapi eruption: Evidence for shallow-level crustal assimilation and hybrid fluid. Journal of Volcanology and Geothermal Research 261, 193-208.

Boudon, G., Camus, G., Gourgaud, A., Lajoie, J., 1993. The 1984 nuée-ardente deposits of Merapi volcano, Central Java, Indonesia: stratigraphy, textural characteristics, and transport mechanisms. Bulletin of Volcanology 55, 327-342.

Boudreau, A.E., 1999. PELE- a version of the MELTS software program for the PC platform. Computers and Geosciences 25, 201-203.

Brandeis, G., Jaupart, C., 1987. The kinetics of nucleation and crystal growth and scaling laws for magmatic crystallization. Contributions to Mineralogy Petrology 96, 24-34.

Brodsky, E.E., Sturtevant, B., Kanamori, H., 1998. Earthquakes, volcanoes, and rectified diffusion. Journal of Geophysical Research 103, 23,827-23,838

Brugger, C.R., Hammer, J.E., 2010a. Crystallization kinetics in continuous decompression experiments: implications for interpreting natural magma ascent processes. Journal of Petrology 51, 1941-1965.

Brugger, C.R., Hammer, J.E., 2010b. Crystal size distribution analysis of plagioclase in experimentally decompressed hydrous rhyodacite magma. Earth and Planetary Science Letters 300, 246-254.

Buddington, A. F., Lindsley, D.H., 1964. Iron-titanium oxide minerals and synthetic equivalents. Journal of Petrology 5, 310-357.

Budi-Santoso, A., Lesage, P., Dwiyono, S., Sumarti, S., Subandriyo, Surono, Jousset, P., Metaxian, J.-P., 2013. Analysis of the seismic activity associated with the 2010 eruption of Merapi Volcano, Java. Journal of Volcanology and Geothermal Research 261, 153-170.

Burgisser, A., Arbaret, L., Druitt, T.H., Giachetti, T., 2011. Pre-explosive conduit conditions of the 1997 Vulcanian explosions at Soufrière Hills Volcano, Montserrat: II. Overpressure and depth distributions. Journal of Volcanology and Geothermal Research 199, 193-205.

Burnham, C.W., 1979. The importance of volatile constituents. In: Yoder, H.S. The evolution of the igneous rocks: fiftieth anniversary perspectives. Princeton University Press, 439-482.

Burnham, C.W., Davies, N.F., 1971. The role of H_2O in silicate melts: 1. P-V-T relations in the system $NaAlSi_3O_8$-H_2O to 10 kilobars and 1000°C. American Journal of Science 270, 54-79.

BVSI, Bulletin of the Volcanological Survey of Indonesia, 1961. no.104.

Camus, G., Gourgaud, A., Mossand- Berthommier, C.-P., Vincent, P.-M., 2000. Merapi (Central Java, Indonesia): an outline of the structural and magmatological evolution, with special emphasis to the major pyroclastic events. Journal of Volcanology and Geothermal Research 100, 139-163.

Carroll, M.R., Webster, J.D., 1994. Solubilities of sulfur, noble gases, nitrogen, chlorine and fluorine in magmas. In: Carroll, M.R., Holloway, J.R. (Eds.) Volatiles in Magmas, Reviews in Mineralogy and Geochemistry 30, 231-279.

Cashman, K.V., 1988. Crystallization of Mount St. Helens 1980- 1986 dacite: A quantitative textural approach. Bulletin of Volcanology 50, 194-209.

Cashman, K.V., 1992. Groundmass crystallization of Mount St. Helens dacite, 1980-1986: a tool for interpreting shallow magmatic processes. Contributions to Mineralogy and Petrology 109, 431-449.

Cashman, K. V., Blundy, J.D., 2000. Degassing and crystallization of ascending andesite and dacite. Philosophical Transactions of the Royal Society London A 358, 1487-1513.

Cashman, K.V., McConnell, S.M., 2005. Multiple levels of magma storage during the 1980 summer eruptions of Mount St. Helens, WA. Bulletin of Volcanology 68, 57-75.

Castro, J.M., Gardner, J.E, 2008. Did magma ascent rate control the explosive-effusive transition at the Inyo volcanic chain, California? Geology 36, 279-282.

Chadwick, J.P., 2008. Magma crust interaction in volcanic systems: case studies from Merapi volcano, Indonesia, Taupo Volcanic Zone, New Zealand, and Slieve Gullion, Ireland. Ph.D. Thesis, Trinity College Dublin.

Chadwick, J.P., Troll, V.R., Ginibre, C., Morgan, D., Gertisser, R., Waight, T.E., Davidson, J.P., 2007. Carbonate Assimilation at Merapi Volcano, Java, Indonesia: Insights from Crystal Isotope Stratigraphy. Journal of Petrology 48, 1793-1812.

Chadwick, J.P., Troll, V.R., Waight, T.E., van der Zwan, F.M., Schwarzkopf, L.M., 2013. Petrology and geochemistry of igneous inclusions in recent Merapi deposits: a window into the sub-volcanic plumbing system. Contributions to Mineralogy and Petrology, 165, 259-282.

Charbonnier, S.J., Gertisser, R., 2008. Field observations and surface characteristics of pristine block-and-ash flow deposits from the 2006 eruption of Merapi volcano, Java, Indonesia. Journal of Volcanology and Geothermal Research 177, 971-982.

Charbonnier, S.J., Gertisser, R., 2009. Numerical simulations of block-and-ash flows using the Titan2D flow model: examples from the 2006 eruption of Merapi Volcano, Java, Indonesia. Bulletin of Volcanology 71, 953-959.

Charbonnier, S.J., Gertisser, R., 2011. Deposit architecture and dynamics of the 2006 block-and-ash flows of Merapi Volcano, Java, Indonesia. Sedimentology 58, 1573-1612.

Charbonnier, S.J., Germa, A.M., Connor, C.B., Gertisser, R., Preece, K., Komorowski, J.-C., Lavigne, F., Dixon, T.H., Connor, L.J., 2013. Evaluation of the impact of the 2010 pyroclastic density currents at Merapi volcano from high-resolution satellite imagery analysis, field investigations and numerical simulations. Journal of Volcanology and Geothermal Research 261, 295-315.

Cichy, S.B., Botcharnikov, R.E., Holtz, F., Behrens, H., 2011. Vesiculation and microlite crystallization induced by decompression: a case study of the 1991-1995 Mt Unzen Eruption (Japan). Journal of Petrology 52, 1469-1492.

Clarke, A.B., Stephens, S., Teasdale, R., Sparks, R.S.J., Diller, K., 2007. Petrologic constraints on the decompression history of magma prior to Vulcanian explosions at the Soufrière Hills Volcano, Monterrat. Journal of Volcanology and Geothermal Research 161, 261-274.

Clocchiatti, R., Joron, J.L., Kerinec, F., Treuil, M., 1982. Quelques données préliminaires sur la lave du dôme actuel du volcan Mérapi (Java, Indonésie) et sur ses enclaves. C.R. Acad. Sc., Paris,295, 817–822.

Collins, S.J., Pyle, D.M., Maclennan, J., 2009. Melt inclusions track pre-eruption storage and dehydration of magmas at Etna. Geology 37, 571-574.

Commer, M., Helwig, S.L., Hördt, A., Tezkan, B., 2005. Interpretation of long-offset transient electromagnetic data from Mount Merapi, Indonesia, using a three-dimensional optimization approach. Journal of Geophysical Research 110, B03207.

Constantini, L., Pioli, L., Bonadonna, C., Clavero, J., Longchamp, C., 2011. A Late Holocene explosive mafic eruption of Villarrica volcano, Southern Andes: The Chaimilla deposit. Journal of Volcanology and Geothermal Research 200, 143-158.

Coombs, M.L., Bull, K.F., Vallance, J.F., Schneider, D.J., Rhoms, E.E., Wessels, R.L., McGimsey, R.G., 2010. Timing, distribution and volume of proximal products of the 2006 eruption of Augustine Volcano. In: Power, J.A., Coombs, M.L., Freymueller, J.T. (Eds.) The 2006 eruption of Augustine Volcano, Alaska. USGS Professional Paper 1769, 145-186.

Corrigan, G. M., 1982. The crystal morphology of plagioclase feldspar produced during isothermal supercooling and constant rate cooling experiments. Mineralogical Magazine 46, 433-439.

Couch, S., Sparks, R.S.J., Carroll, M.R., 2003a. The kinetics of degassing-induced crystallization at Soufrière Hills volcano, Montserrat. Journal of Petrology 44, 1477-1502.

Couch, S., Harford, C.L., Sparks, R.S.J., Carroll, M.R., 2003b. Experimental constraints on the conditions of formation of highly calcic plagioclase microlites at the Soufrière Hills volcano, Montserrat. Journal of Petrology 44, 1455-1475.

Costa, A., Melnik, O., Sparks, R.S.J., Voight, B., 2007. Control of magma flow in dykes on cyclic lava dome extrusion. Geophysical Research Letters 34, L02303.

Costa, F., Andreastuti, S., de Maisonneuve, C.B., Pallister, J.S., 2013. Petrological insights into the storage conditions, and magmatic processes that yielded the centennial 2010 Merapi explosive eruption. Journal of Volcanology and Geothermal Research 261, 209-235.

Cronin, S.J., Lube, G., Dayudi, D.S., Sumarti, S., Subrandiyo, S, Surono., 2013. Insights into the October–November 210 Gunung Merapi eruption (Central Java, Indonesia) from the stratigraphy, volume and characteristics of its pyroclastic deposits. Journal of Volcanology and Geothermal Research 261, 244-259.

Curray, J.R., Shor, G.G., Raitt, R.W., Henry, M., 1977. Seismic refraction and reflection studies of crustal structure of the eastern Sunda and western Banda arcs. Journal of Geophysical Research 82, 2479-2489.

D'Oriano, C., Poggianti, E., Bertagnini, A., Cioni, R., Landi, P., Polacci, M., Rosi, M., 2005. hanges in eruptive style during the A.D. 1538 Monte Nuovo eruption (Phlegrean Fields, Italy): the role of syn-eruptive crystallization. Bulletin of Volcanology 67, 601-621.

Danyushevsky., L.V., Plechov., P., 2011 Petrolog3: Integrated software for modeling crystallization processes. Geochemistry, Geophysics, Geosystems 12, Q07021.

Davis, M., Koenders, M.A., Petford, N., 2007. Vibro-agitation of chambered magma. Journal of Volcanology and Geothermal Research 167, 24-36.

De Bélizal, E., Lavigne, F., Hadmoko, D.S., Degeai, J.-P., Dipayana, G.A., Mataqin, B.W., Marfai, M.A., Coquet, M., Le Mauff, B., Robin, A.-K., Vidal, C., Cholik, N., Aisyah, N., 2013. Rain-triggered lahars following the 2010 eruption of Merapi volcano, Indonesia: A major risk. Journal of Volcanology and Geothermal Research 261, 330-347.

De' Michieli Vitturi, M., Clarke, A.B., Neri, A., Voight, B., 2010. Transient effects of magma ascent dynamics along a geometrically variable dome-feeding conduit. Earth and Planetary Science Letters 295, 541-553.

Debaille, V., Doucelance, R., Weis, D., Schiano, P., 2006. Multi-stage mixing in subduction zones: application to Merapi volcano (Java island, Sunda arc). Geochimica et Cosmochimica Acta 70, 723-741.

Deegan, F.M., Troll, V.R., Freda, C., Misiti, V., Chadwick, J.P., McLeod, C.L., Davidson, J.P., 2010. Magma-carbonate interaction processes and associated CO_2 release at Merapi volcano, Indonesia: insights from experimental petrology. Journal of Petrology 51, 1027-1051.

Degruyter, W., Bachmann, O., Burgisser, A., Manga, M., 2012. The effects of outgassing on the transition between effusive and explosive silicic eruptions. Earth and Planetary Science Letters 349-350, 161-170.

Del Marmol, M.-A., 1989. The petrology and geochemistry of Merapi volcano, Central Java, Indonesia. Ph.D. Thesis. The Johns Hopkins University, Baltimore, USA.

Del Moro, A., Fulignati, P., Marianelli, P., Sbrana, A., 2001. Magma contamination by direct wall rock interaction: constraints from xenoliths from the walls of a carbonate- hosted magma chamber (Vesuvius 1944 eruption). Journal of Volcanology and Geothermal Research 11, 15-24.

Dempsey, S.R., 2013. Geochemistry of volcanic rocks from the Sunda arc. Ph.D. thesis. Durham University, UK.

Diefenbach, A.K., Bull, K.F., Wessels, R.L., McGimsey, R.G., 2012. Photogrammetric monitoring of lava dome growth during the 2009 eruption of Redoubt Volcano, Journal of Volcanology and Geothermal Research 259, 308-316.

Djumarma, A., Bronto, S., Bahar, I., Suparban, F., Sukhyar, R., Newhall, C., Holcomb, R.T., Banks, N.G., Torley, R., Lockwood, J.P., Tilling, R.I., Rubin, M., del Marmol, M.A., 1986. Did Merapi volcano (Central Java) erupt catastrophically in 1006 A.D.? Abstract, IAVCEI International Volcanological Congress 1986, Rotarua, p. 236.

Dowty, E., 1980. Crystal growth and nucleation theory. In: Hargreaves, R.B. (Ed.) Physics of Magmatic Processes. Princeton Univ. Press, Princeton, United States, pp. 419-485.

Edmonds, M., Herd, R.A., 2007. A volcanic degassing event at the explosive-effusive transition. Geophysical Research Letters 34, L21310.

Edwards, C.M.H., Morris, J.D., Thirlwall, M.F., 1993. Separating mantle from slab signatures in arc lavas using B/Be and radiogenic isotope systematics. Nature 362, 530-533.

Eichelberger, J.C., 1995. Silicic volcanism: ascent of viscous magmas from crustal reservoirs. Annual Review of Erath and Planetary Sciences 23, 41-63.

Eichelberger, J.C., Westrich, H.R., 1981. Magmatic volatiles in explosive rhyolitic eruptions. Geophysical Research Letters 8, 757-760.

Eichelberger, J.C., Carrigan, C.R., Westrich, H.R., Price, R.H., 1986. Non-explosive silicic volcanism. Nature 323, 598-602.

Escher, B.G., 1931a. On a classification of central eruptions according to gas pressure of the magma and viscosity of the lava. Leidsche Geol.Med. 6, 45-49.

Escher, B.G., 1931b. On the character of the Merapi eruption in Central Java. Leidsche Geol.Med. 6, 51-58.

Fink, J.H., 1983. Structure and emplacement of a rhyolitc obsidian flow: Little Glass Mountain, Medicine Lake Highland, northern California. Geological Society of America Bulletin 94, 362-380.

Fink, J.H., Anderson, S.W., 2000. Lava domes and coulees. In: Sigurdsson, H., Houghton, B., McNutt, S.R., Rymer, H., Stix, J. (Eds.) Encycolpedia of Volcanoes. Academic Press. pp 307-319.

Freda, C., Gaeta, M., Palladino, D.M., Trigila, R., 1997. The Villa Senni Eruption (Alban Hills, central Italy): the role of H_2O and CO_2 on the magma chamber evolution and on eruptive scenario. Journal of Volcanology and Geothermal Research 78, 103-120.

Fulignati, P., Marianelli, P., 2007. Tracing volatile exsolution within the 472 AD "Pollena" magma chamber of Vesuvius (Italy) from melt inclusion investigation. Journal of Volcanology and Geothermal Research 161, 289-302.

Gauthier, P.-J., Condomines, M., 1999. ^{210}Pb-^{226}Ra radioactive disequilibria in recent lavas and radon degassing: inferences on magma chamber dynamics at Stromboli and Merapi volcanoes. Earth and Planetary Science Letters 172, 111-126.

Gertisser, R., 2001. Gunung Merapi (Java, Indonesien): Eruptionsgeschichte und Magmatische Evolution eines Hochrisiko-Vulkans. Ph.D. Thesis, Universität Freiburg, Germany.

Gertisser, R., Keller, J., 2003a. Temporal variations in magma composition at Merapi Volcano (Central Java, Indonesia): magmatic cycles during the past 2000 years of explosive activity. Journal of Volcanology and Geothermal Research 123, 1-23.

Gertisser, R., Keller, J., 2003b. Trace element and Sr, Nd, Pb and O isotope variations in medium-K and high-K volcanic rocks from Merapi volcano, Central Java,

Indonesia: evidence for the involvement of subducted sediments in Sunda arc magma genesis. Journal of Petrology 44, 457-489.

Gertisser, R., Charbonnier, S.J., Troll, V.R., Keller, J., Preece, K., Chadwick, J.P., Barclay, J., Herd, R.A., 2011. Merapi (Java, Indonesia): anatomy of a killer volcano. Geology Today 27, 57-62.

Gertisser, R., Charbonnier, S.J., Keller, J., Quidelleur, X., 2012a. The geological evolution of Merapi volcano, Central Java, Indonesia. Bulletin of Volcanology 74, 1213- 1233.

Gertisser, R., Cassidy, N.J., Charbonnier, S.J., Nuzzo, L., Preece, K., 2012b. Overbank block-and-ash flow deposits and the impact of valley-derived, unconfined flows on populated areas at Merapi volcano, Java, Indonesia. Natural Hazards 60, 623-648.

Gertisser, R., Self, S., Thomas, L.E., Handley, H.K., Van Calsteren, P., Wolff, J.A., 2012c. Processes and timescales of magma genesis and differentiation leading to the great Tambora eruption in 1815. Journal of Petrology 53, 271-297.

Geschwind, C.-H., Rutherford, M.J., 1995. Crystallization of microlites during magma ascent: the fluid mechanics of 1980- 1986 eruptions at Mount St Helens. Bulletin of Volcanology 57, 356-370.

Grandjean, J.B., 1931a. Korte Mededeeling over de uitbarsting van den Merapi op 18 December 1930. Mijningingenieur 12 (12), 4-6.

Grandjean, J.B., 1931b. De uitbartsting van den Merapi in 1930. Mijningingenieur12 (4), 47.

Grandjean, J.B., 1931c. Bijdrage tot de kennis der Gloedwolken van den Merapi van Midden-Java. Mijningingenieur 12 (12) 20-25.

Haggerty, S.E., 1993. Oxide textures – a mini-atlas. In: Lindsley, D.H. (Ed.) Oxide minerals: petrologic and magnetic significance. Reviews in Mineralogy 25, 303-321.

Hale, A. J., Wadge, G., Mühlhaus, H.B., 2007. The influence of viscous and latent heating on crystal-rich magma flow in a conduit. Geophysical Journal International 171, 1406-1429.

Hall, R., 2002. Cenozoic geological and plate tectonic evolution of SE Asia and the SW Pacific: computer-based reconstructions, model and animations. Journal of Asian Earth Science 20, 353-434

Hall, R., 2012. Late Jurassic–Cenozoic reconstructions of the Indonesian region and the Indian Ocean. Tectonophysics 570-571, 1-41.

Hall, R., Sevastjanova, I., 2012. Australian crust in Indonesia. Australian Journal of Earth Sciences 59, 827-844.

Hamilton, W., 1979. Tectonics of the Indonesian region. U.S. Geological Survey Professional Paper 1078, 1-345.

Hammer, J. E., Rutherford, M. J., 2002. An experimental study of the kinetics of decompression-induced crystallization in silicic melt. Journal of Geophysical Research 107, 1-24.

Hammer, J.E., Cashman, K.V., Hoblitt, R.P., Newman, S., 1999. Degassing and microlite crystallization during pre-climactic events of the 19991 eruption of Mt. Pinatubo, Philippines. Bulletin of Volcanology 60, 355-380.

Hammer, J.E., Cashman, K.V., Voight, B., 2000. Magmatic processes revealed by textural and compositional trends in Merapi dome lavas. Journal of Volcanology and Geothermal Research 100, 165-192.

Handley, H.K., 2006. Geochemical and Sr-Nd-Hf-O isotopic constraints on volcanic petrogenesis at the Sunda arc Indonesia. Ph.D. Thesis. Durham University.

Handley, H.K., Turner, S., Macpherson, C.G., Gertisser, R., Davidson, J.P., 2011. Hf-Nd isotope and trace element constraints on subduction inputs at island arcs: limitations of Hf anomalies as sediment input indicators. Earth and Planetary Science Letters 304, 212-223.

Hartmann, M.A., 1935. Die Ausbrüche des G. Merapi (Mittel-Java) bis zum Jahre 1883. Neues Jahrb. Für Mineral. 75, 127-162.

Heiken, G., 1978. Plinian-type eruptions in the Medicine Lake Highland, California, and the nature of the underlying magma. Journal of Volcanology and Geothermal Research 4, 375-402.

Heinrich, C.A., Günther, D., Audétat, A., Ulrich, T., Frischknecht, R., 1999. Metal fractionation between magmatic brine and vapor, determined by microanalysis of fluid inclusions. Geology 27, 755-758.

Hess, K.-U., Dingwell, D.B., 1996. Viscosities of hydrous leucogranite melts; a non-Arrhenian model. American Mineralogist 81, 1297-1300.

Higgins, M. D., 1994. Numerical modelling of crystal shapes in thin sections: Estimation of crystal habit and true size. American Mineralogist 79, 113-119.

Higgins, M. D., 2000. Measurement of Crystal Size Distributions. American Mineralogist 85, 1105-1116.

Higgins. M. D., 2010. Textural coarsening in igneous rocks. International Geology Review 53, 354-376.

Higgins, M.D., Roberge, J., 2003. Crystal Size Distribution of plagioclase and amphibole from Soufrière Hills Volcano, Montserrat: evidence for dynamic crystallization - textural coarsening cycles. Journal of Petrology 44, 1401-1411.

Higgins, M. D., Roberge, J., 2007. Three magmatic components in the 1973 eruption of Eldfell volcano, Iceland: Evidence from plagioclase crystal size distribution (CSD) and geochemistry. Journal of Volcanology and Geothermal Research 161, 247-260.

Hildreth, W., Drake, R.E., 1992. Volcán Quizapu, Chilean Andes. Bulletin of Volcanology 54, 93-125.

Hoblitt, R.P., Harmon, R.S., 1993. Bimodal density distribution of cryptodome dacite from the 1980 eruption of Mount St. Helens, Washington. Bulletin of Volcanology 55, 421-437.

Holland, T., Blundy, J., 1994. Non-ideal interactions in calcic amphiboles and their bearing on amphibole-plagioclase thermometry. Contributions to Mineralogy and Petrology 116, 433-447.

Horwell, C.J., Le Blond, J.S., Michnowicz S.A.K., Cressey, G., 2010. Cristobalite in a rhyolitic lava dome: evolution of ash hazard. Bulletin of Volcanology 72, 249-253.

Horwell, C.J., Williamson, B.J., Llewellin, E.W., Damby, D.E., Le Blond, J.S., 2013. The nature and formation of cristobalite at the Soufrière Hills volcano, Montserrat:

implications for the petrology and stability of silicic lava domes. Bulletin of Volcanology 75, 1-19.

Humphreys, M.C.S., Blundy, J.D., Sparks, R.S.J., 2008. Shallow-level decompression crystallisation and deep magma supply at Shiveluch Volcano. Contributions to Mineralogy and Petrology 155, 45-61.

Humphreys, M.C.S., Christopher, T., Hards, V., 2009. Microlite transfer by disaggregation of mafic inclusion following magma mixing at Soufrière Hills volcano, Montserrat. Contributions to Mineralogy and Petrology 157, 609-624.

Innocenti, S., del Marmol., M.-A., Voight, B., Andreastuti, S., Furman, T., 2013. Textural and mineral chemistry constraints on evolution of Merapi volcano, Indonesia. Journal of Volcanology and Geothermal Research 261, 20-37.

Innocenti, S., Andreastuti, S., Furman, T., del Marmol, M.-A., Voight, B., 2013. The pre-eruption conditions for explosive eruptions at Merapi volcano as revealed by crystal texture and mineralogy. Journal of Volcanology and Geothermal Research 261, 69-86.

Jaupart, C., Allègre, C.J., 1991. Gas content, eruption rate and instabilities of eruption regime in silicic volcanoes. Earth and Planetary Science Letters 102, 413-429.

Jenkins, S., Komorowski, J.-C., Baxter, P.J., Spence, R., Picquout, A., Lavigne, F., Surono., 2013. The Merapi 2010 eruption: An interdisciplinary impact assessment methodology for studying pyroclastic density current dynamics. Journal of Volcanology and Geothermal Research 261,316-329.

Johnson, E.R., Wallace, P.J., Cashman, K.V., Delgado Granados, H., Kent, A.J.R., 2008. Magmatic volatile contents and degassing-induced crystallization at Volcán Jorullo, Mexico: Implications for melt evolution and the plumbing systems of monogenetic volcanoes. Earth and Planetary Science Letters 269, 478-487.

Katili, J.A., 1975. Volcanism and plate tectonics in the Indonesian island arcs. Tectonophysics 26, 165-188.

Kemmerling, G.L.L., 1932. De controverse uitgeschoten gloedwolken (nuées ardentes d'explosion dirigée) of lawinen-gloedwolken (nuées ardentes d'avalanche). De Ingenieur 47, 129-137.

Kent, A.J.R., 2008. Melt inclusions in basaltic and related volcanic rocks. In: Putirka, K.D., Tepley III, F.J. (Eds.) Minerals, inclusions and volcanic processes. Reviews in Mineralogy and Petrology 69, 273-332.

Kent, A.J.R., Blundy, J., Cashman, K.V., Cooper, K.M., Donnelly, C., Pallister, J.S., Reagan, M., Rowe, M.C., Thornber, C.R., 2007. Vapor transfer prior to the October 2004 eruption of Mount St. Helens, Washington. Geology 35, 231-234.

Kirkpatrick, R.J., 1977. Nucleation and growth of plagioclase, Makaopuhi and Alae lava lakes, Kilauea Volcano, Hawaii. Geological Society of America Bulletin 88, 78-84.

Kirkpatrick, R.J., 1981. Kinetics of crystallization of igneous rocks. Reviews in Mineralogy 8, 321-398.

Koleszar, A.M., Kent, A.J.R., Wallace, P.J., Scott, W.E., 2012. Controls on long-term explosivity at andesitic arc volcanoes: Insights from Mount Hood, Oregon. Journal of Volcanology and Geothermal Research 219-220, 1-14.

Komorowski, J.C., Jenkins, S., Baxter, P.J., Picquout, A., Lavigne, F., Charbonnier, S., Gertisser, R., Preece, K., Cholik, N., Budi-Santoso, A., Surono., 2013. Paroxysmal dome explosion during the Merapi 2010 eruption: processes and facies relationships of associated high-energy pyroclastic density currents. Journal of Volcanology and Geothermal Research 261, 260-294.

Koulakov, I., Bohm, M., Asch, G., Lühm B.-G., Manzanares, A,. Brotopuspito, K.S., Fauzi, P., Purbawinata, M.A., Puspito, N.T., Ratdomopurbo, A., Kopp, H., Rabbel, W., Shevkunova, E., 2007. P and S velocity structure of the crust and the upper mantle beneath central Java from local tomography inversion. Journal of Geophysical Research 112, B08310.

Koulakov, I., Jakovlev, A., Luehr, B.G., 2009. Anisotropic structure beneath central Java from local earthquake tomography. Geochemistry Geophysics Geosystems 10, Q02011.

Le Cloarec, M.-F., Gauthier, P.-J., 2003. Merapi Volcano, Central Java, Indonesia: A case study of radionuclide behavior in volcanic gases and its implications for magma dynamics at andesitic volcanoes. Journal of Geophysical Research 108 (B5), 2243.

Le Guern, F., Gerlach, T.M., Nohl, A., 1982. Field gas chromatograph analyses of gases from a glowing dome at Merapi volcano, Java, Indonesia, 1977, 1978, 1979. Journal of Volcanology and Geothermal Research 14, 223-245.

Le Maitre, R.W., Streckeisen, A., Zanettin, B., La Bas, M. J., Bonin, B., Bateman, P., Bellieni, G., Dudek, A., Efremova, J., Keller, J., Lameyre, J., Sabine, P.A., Schmidt, R., Sørensen, H., Woolley, A.R., 2002. Igneous Rocks. A classification and glossary of terms. Recommendations of the International Union of Geological Sciences subcommission on the systematics of igneous rocks. Cambridge University Press, Cambridge, 252 pp.

Le Pennec, J.-L., Hermitte, D., Dana, I., Pezard, P., Coulon, C., Cochemé, J.-J., Mulyadi, E., Ollagnier, F., Revest, C., 2001. Electrical conductivity and pore-space topology of Merapi lavas: implications for the degassing of porphyritic andesite magmas. Geophysical Research Letters 28, 4283-4286.

Leake, B.E., Woolley, A.R., Arps, C.E.S., Birch, W.D., Gilbert, M.C., Grice, J.D., Hawthorne, F.C., Kato, A., Kinsch, H.J., Krivovichev, V.G., Linthout, K., Laird, J., Mandarino, J.A., Maresch, W.V., Nickel, E.H., Rock., N.M.S., Schumacher, J.C., Smith, D.C., Stephenson, N.C.N., Ungaretti, L., Whittaker, E.J.W., Youzhi, G., 1997. Nomenclature of amphiboles: report on the subcommittee on amphiboles of the International Mineralogical Association, Commission on New Minerals and Mineral Names. The Canadian Mineralogist, 35, 219- 246.

Leeman, W.P., Sisson, V.B., 1996. Geochemistry of boron and its implications for crustal and mantle processes. In: (Eds.) Grew., E.S., Anovitz, L.M. Boron: Mineralogy, Petrology and Geochemistry, Reviews in Mineralogy 33, 645-708.

Lejeune, A.-M., Richet, P., 1995. Rheology of crystal bearing silicate melts: an experimental study at high viscosities. Journal of Geophysical Research 100, B3, 4215-4229.

Lofgren, G., 1974. An experimental study of plagioclase crystal morphology: isothermal crystallization. American Journal of Science 274, 243-273.

Lofgren, G., 1980. Experimental studies on the dynamic crystallization of silicate melts. In: Hargreaves, R.B. (Ed.) Physics of Magmatic Processes. Princeton Univ. Press, Princeton, United States, pp. 487-551.

Lowenstern, J.B., 1994. Chlorine, fluid immiscibility and degassing in peralkaline magmas from Pantelleria, Italy. American Mineralogist 79, 353-369.

Lowenstern, J.B., 1995. Applications of silicate-melt inclusions to the study of magmatic volatiles. In: Thompson, J.F.H. (Ed.) Magmas, fluids and ore deposits. Mineralogical Association of Canada Short Course 23, 71-99.

Lowenstern, J.B., 2003. Melt inclusions come of age: volatiles, volcanoes, and Sorby's legacy. In: De Vivo, B., Bodnar, R.J. (Eds.) Melt inclusions in volcanic systems: methods, applications and problems. Developments in Volcanology 5. Elsevier Press, Amsterdam, 1-22.

Lowenstern, J.B., Pitcher, B.W., 2013. Analysis of H_2O in silicate glass using attenuated total reflectance (ATR) micro-FTIR spectroscopy. American Mineralogist 98, 1660-1668.

Lube, G, Cronin, S.J., Thouret, J.-C., Surono., 2011. Kinematic characteristics of pyroclastic density currents at Merapi and controls on their avulsion from natural and engineered channels. Geological Society of America Bulletin 123, 1127-1140.

Luehr, B.-G., Koulakov, I., Rabbel, W., Zschau, J., Ratdomopurbo, A., Brotopuspito, K.S., Fauzi, P., Sahara, D.P., 2013. Fluid ascent and magma storage beneath Gunung Merapi revealed by multi-scale seismic imaging. Journal of Volcanology and Geothermal Research 261, 7-19.

Macdonald, G.A., 1972. Volcanoes. Prentice-Hall, New York, 510 pp.

Mann, C.P., Wallace, P.J., Stix, J., 2013. Phenocryst-hosted melt inclusions record stalling of magma during ascent in the conduit and upper magma reservoir prior to vulcanian explosions, Soufrière Hills volcano, Montserrat, West Indies. Bulletin of Volcanology 75, 1-16.

Marsh, B. D., 1988. Crystal size distribution (CSD) in rocks and the kinetics and dynamics of crystallization I. Theory. Contributions to Mineralogy and Petrology 99, 277-291.

Marsh, B. D., 1998. On the interpretation of Crystal Size Distributions in magmatic systems. Journal of Petrology 39, 553-599.

Martel, C., 2012. Eruption dynamics inferred from microlite crystallization experiments: application to Plinian and dome-forming eruptions of Mt. Pelée (Martinique, Lesser Antilles). Journal of Petrology 53, 699-725.

Martel, C., Schmidt, B.C., 2003. Decompression experiments as insights into ascent rates of silicic magmas. Contributions to Mineralogy and Petrology, 44, 397-415.

Martel, C., Pichavant, M., Bourdier, J.-L., Traineau, H., Holtz, F., Scaillet, B., 1998. Magma storage conditions and control of eruption regime in silicic volcanoes: experimental evidence from Mt. Pelée. Earth and Planetary Science Letters 156, 89-99.

Martel, C., Boudier, J.-L., Pichavant, M., Traineau, H., 2000. Textures, water content and degassing of silicic andesites from recent plinian and dome-forming eruptions at Mount Pelée volcano (Martinique, Lesser Antilles arc). Journal of Volcanology and Geothermal Research 96, 191-206.

Martel, C., Radadi Ali, A., Poussineau, S., Gourgaud, A., Pichavant, M., 2006. Basalt-inherited microlites in silicic magmas: evidence from Mount Pelée (Martinique, French West Indies). Geology 34, 905-908.

Massol, H., Jaupart, C., 1999. The generation of gas overpressure in volcanic eruptions. Earth and Planetary Science Letters 166, 57-70.

Mastin, L.G., 2005. The controlling effect of viscous dissipation on magma flow in silicic conduits. Journal of Volcanology and Geothermal Research 143, 17-28.

Melnik, O., Sparks, R.S.J., 1999. Nonlinear dynamics of lava dome extrusion. Nature 402, 37-41.

Melnik, O., Sparks, R.S.J., 2005. Controls on conduit magma flow dynamics during lava dome building eruptions. Journal of Geophysical Research 110, B02209.

Melnik, O.E., Blundy, J.D., Rust, A.C., Muir, D.D., 2011. Subvolcanic plumbing systems imaged through crystal size distributions. Geology 39, 403-406.

Métrich, N., Rutherford, M.J., 1992. Experimental study of chlorine behaviour in hydrous silicic melts. Geochimica et Cosmochimica Acta 56, 607- 616.

Moore, G., Carmichael, I.S.E., 1998. The hydrous phase equilibria (to 3 kbar) of an andesite and basaltic andesite from western Mexico: constraints on water content

and conditions of phenocryst growth. Contributions to Mineralogy and Petrology 130, 304-319.

Moore, G., Vennemann, T., Carmichael, I.S.E., 1998. An empirical model for the solubility of H_2O in magma to 3 kilobars. American Mineralogist 83, 36-42.

Morgan, D. J., Jerram, D. A., 2006. On estimating crystal shape for crystal size distribution analysis. Journal of Volcanology and Geothermal Research 154, 1-7.

Morimoto, N., 1988. Nomenclature of Pyroxenes. Mineralogy and Petrology, 39, 55-76.

Müller, A., Hack, V., 2004. 3-D modeling of the deep electrical conductivity of Merapi volcano (Central Java): integrating magnetotellurics, induction vectors and the effects of steep topography. Journal of Volcanology and Geothermal Research 138, 205-222.

Müller, M., Hördt, A., Neubauer, F.M., 2002. Internal structure of Mount Merapi, Indonesia, derived from long-offset transient electromagnetic data. Journal of Geophysical Research 107, B9, 2187.

Murphy, M.D., Sparks, R.S.J., Barclay, J., Carroll, M.R., Brewer, T.S., 2000. Remobilization of andesite magma by intrusion of mafic magma at the Soufriere Hills volcano, Montserrat, West Indies. Journal of Petrology 41, 21-42.

Nadeau, O., Williams-Jones, A.E., Stix, J., 2010. Sulphide magma as a source of metals in arc-related magmatic hydrothermal ore fluids. Nature Geoscience 3, 501-505.

Nadeau, O., Williams-Jones, A.E., Stix, J., 2013. Magmatic-hydrothermal evolution and devolatilization beneath Merapi volcano, Indonesia. Journal of Volcanology and Geothermal Research 261, 50-68.

Nakada, S., Motomura, Y., 1999. Petrology of the 1991-1995 eruption at Unzen: effusion pulsation and groundmass crystallization. Journal of Volcanology and Geothermal Research 89, 173-196.

Neumann van Padang, M., 1933. De uitbarsting van den Merapi (Midden Java) in den Jahren 1930-1931. Vulkanol. En. Seismol. Med. 12, 1-16.

Newhall, C.G., Melson, W.G., 1983. Explosive activity associated with the growth of volcanic domes. Journal of Volcanology and Geothermal Research 17, 111-131.

Newhall, C.G., Hoblitt, R.P., 2002. Constructing event trees for volcanic crises. Bulletin of Volcanology 64, 3-20.

Newhall, C.G., Bronto, S., Alloway, B., Banks, N.G., Bahar, I., del Marmol, M.A., Hadisantono, R.D., Holcomb, R.T., McGeehin, J., Miksic, J.N., Rubin, M., Sayudi, S.D., Sukhyar, R., Andreastuti, S., Tilling, R.I., Torley, R., Trimble, D., Wirakusumah, A.D., 2000. 10,000 Years of explosive eruptions of Merapi Volcano, Central Java: archaeological and modern implications. Journal of Volcanology and Geothermal Research 100, 9-50.

Newman, S., Lowenstern, J.B., 2002. VOLATILECALC: a silicate melt-H_2O-CO_2 solution model written in Visual Basic for excel. Computers and Geosciences 28, 597-604.

Nho, E.-Y., Le Cloarec, M.-F., Ardouin, B., Tjetjep, W. S., 1996. Source strength assessment of volcanic trace elements emitted from the Indonesian arc. Journal of Volcanology and Geothermal Research 74, 121-129.

Nielsen., R.L., Drake, M.J., 1979. Pyroxene-melt equilibria. Geochimica Cosmochimica Acta 43, 1259-1272.

Nimis, P., 1999. Clinopyroxene geobarometry of magmatic rocks. Part 2. Structural geobarometers for basic to acid, tholeiitic and mildly alkaline magmatic systems. Contributions to Mineralogy and Petrology 135, 62-74.

Noguchi, S., Toramaru, A., Shimano, T., 2006. Crystallization of microlites and degassing during magma ascent: constraints on fluid mechanical behaviour of magma during the Tenjo eruption on Kozu Island, Japan. Bulletin of Volcanology 68, 432-449.

Noguchi, S., Toramaru, A., Nakada, S., 2008. Relation between microlite textures and discharge rate the during 1991- 1995 eruptions at Unzen, Japan. Journal of Volcanology and Geothermal Research 175, 141-155.

Pallister, J.S., Thornber, C.R., Cashman, K.V., Clynne, M.A., Lowers, H.A., Mandeville, C.W., Brownfield, I.K., Meeker, G.P., 2008. Petrology of the 2004-2006 Mount St. Helens lava dome - implications for magmatic plumbing and eruption triggering. U.S. Geological Survey Professional Paper 1750, 647-702.

Pallister, J.S., Schneider, D.J., Griswold, J.P., Keeler, R.H., Burton, W.C., Noyles, C., Newhall, C.G., Ratdomopurbo, A., 2013. Merapi 2010 eruption - chronology and extrusion rates monitored with satellite radar and used in eruption forecasting. Journal of Volcanology and Geothermal Research 261, 144-152.

Palmer., M.R., Swihart., G.H., 1996. Boron isotope geochemistry: an overview. In: (Eds.) Grew, E.S., Anovitz., L.M. Boron: Mineralogy, Petrology and Geochemistry. Reviews in Mineralogy 33, 709-744.

Panigrahi, M.K., Naik, R.K., Pandit, D., Misra, K.C., 2008. Reconstructing physico-chemical parameters of hydrothermal mineralization of copper at the Malanjkhand deposit, India, from mineral chemistry of biotite, chlorite and epidote. Geochemical Journal 42, 443-460.

Papale, P., Moretti, R., Barbato, D., 2006. The compositional dependence of the saturation surface of $H_2O + CO_2$ fluids in silicate melts. Chemical Geology 229, 78-95.

Picquout, A., Lavigne, F., Mei, E.T.W., Grancher, D., Noer, C., Vidal, C.M., Hadmoko, D.S., 2013. Air traffic disturbance due to the 2010 Merapi volcano eruption. Journal of Volcanology and Geothermal Research 261, 366-375.

Platz, T., Cronin, S., Cashman, K.V., Stewart, R.B., Smith, I.E.M., 2007. Transition from effusive to explosive phases in andesite eruptions - a case-study from the AD1655 eruption of Mt. Taranaki, New Zealand. Journal of Volcanology and Geothermal Research 161, 15-34.

Preece, K., Barclay, J., Gertisser, R., Herd, R., 2011. Petrological evidence of magma storage, ascent and extrusion at Merapi volcano, Java, Indonesia. Geophysical Research Abstracts 13, EGU2011-10518.

Preece, K., Barclay, J., Gertisser, R., Herd, R.A., 2013. Textural and micro-petrological variations in the eruptive products of the 2006 dome-forming eruption of Merapi volcano, Indonesia: implications for sub-surface processes. Journal of Volcanology and Geothermal Research 261, 98-120.

Putirka, K.D., 2008. Thermometers and barometers for volcanic systems. Reviews in Mineralogy and Geochemistry 69, 61-120.

Ratdomopurbo, A., 1995. Etude sismologique du volcan Merapi et Formation du dome de 1994. PhD Thesis, Université Joseph Fourier, Grenoble, 208 pp.

Ratdomopurbo, A., 2011. The 2006 eruption of Mt. Merapi: seismic, deformation and dome observation. Geophysical Research Abstracts 13, EGU2011-13699.

Ratdomopurbo, A., Poupinet, G., 2000. An overview of the seismicity of Merapi volcano (Java, Indonesia), 1983-1994. Journal of Volcanology and Geothermal Research 100, 193-214.

Ratdomopurbo, A., Beauducel, F., Subandriyo, J., Agung Nandaka, I.G.M., Newhall, C.G., Suharna, Sayudi, D.S., Suparwaka, H., Sunarta, S., 2013. Overview of the 2006 eruption of Mt. Merapi. Journal of Volcanology and Geothermal Research 261, 97-97.

Reubi, O., Blundy, J., Varley, N.R., 2013. Volatiles contents, degassing and crystallisation of intermediate magmas at Volcan de Colima, inferred from melt inclusions. Contributions to Mineralogy and Petrology 165, 1087-1106.

Ridolfi, F., Renzulli, A., 2012. Calcic amphiboles in calc-alkaline and alkaline magmas: thermobarometric and chemometric empirical equations valid up to 1,130°C and 2.2 GPa. Contributions to Mineralogy and Petrology 163, 877-895.

Ridolfi, F., Puerini, M., Renzulli, A., Menna, M., Toulkeridis, T., 2008. The magmatic feeding system of El Reventador volcano (Sub-Andean zone, Ecuador) constrained by texture, mineralogy and thermobarometry of the 2002 erupted products. Journal of Volcanology and Geothermal Research 176, 94-106.

Ridolfi, F., Renzulli, A., Puerini, M., 2010. Stability and chemical equilibrium of amphibole in calc-alkaline magmas: an overview, new thermobarometric formulations and application to subduction-related volcanoes. Contributions to Mineralogy and Petrology 160, 45-66.

Royet, J.-P., 1991. Stereology: a method for analyzing images. Progress in Neurobiology 37, 433-474.

Ruprecht, P., Bachmann, O., 2010. Pre-eruptive reheating during magma mixing at Quizapu volcano and the implications for the explosiveness of silicic are volcanoes. Geology 38, 919-922.

Rutherford, M.J., 2008. Magma ascent rates. In: Putirka, K.D., Tepley, F.J (Eds) Mineral, inclusions and volcanic processes. Reviews in Mineralogy and Geochemistry 69, 241-271.

Rutherford, M.J., Hill, P.M., 1993. Magma ascent rates from amphibole breakdown: an experimental study applied to the 1980-1986 Mount St. Helens eruptions. Journal of Geophysical Research 98, 19,667-19,685.

Saepuloh, A., Koike, K., Omura, M., Iguchi, M., Setiawan, A., 2010. SAR- and gravity change-based characterization of the distribution pattern of pyroclastic flow deposits as Mt. Merapi during the past 10 years. Bulletin of Volcanology 72, 221-232.

Scandone, R.S., Malone, S., 1985. Magma supply, magma discharge and readjustment of the feeding system of Mount St. Helens during 1980. Journal of Geophysical Research 23, 239-262.

Scandone, R., Cashman, K.V., Malone, S.D., 2007. Magma supply, magma ascent and style of volcanic eruptions. Earth and Planetary Science Letters 253, 513-529.

Schaaf, P., Stimac, J., Siebe, C., Macias, J.L., 2005. Geochemical evidence for mantle origin and crustal processes in volcanic rocks from Popocatépetl and surrounding monogenetic volcanoes, Central Mexico. Journal of Petrology 46, 1243-1282.

Schatz, O.J., Dolejš, D., Stix, J., Williams-Jones, A.E., Layne, G.D., 2004. Partitioning of boron among melt, brine and vapor in the system haplogranite-H_2O-NaCl at 800°C and 100 MPa. Chemical Geology 210, 135-147.

Schwarzkopf, L.M., Schminke, H.-U., Cronin, S.J., 2005. A conceptual model for block-and-ash flow basal avalanche transport and deposition, based on deposit architecture of 1998 and 1994 Merapi flows. Journal of Volcanology and Geothermal Research 139, 117-134.

Scott, J.A.J., 2012. Origin and evolution of the Santiaguito lava dome complex, Guatemala. PhD Thesis, University of Oxford, UK.

Scott, J.A.J., Mather, T.A., Pyle, D.M., Rose, W.I., Chigna, G., 2012. The magmatic plumbing system beneath Santiaguito Volcano, Guatemala. Journal of Volcanology and Geothermal Research 237-238, 54-68.

Selby, D., Nesbitt, B.E., 2000. Chemical composition of biotite from the Casino porphyry Cu-Au-Mo mineralization, Yukon, Canada; evaluation of magmatic and hydrothermal fluid chemistry. Chemical Geology 171, 77-93.

Self, S., Gertisser, R., Thordarson, T., Rampino , M.R., Wolff, J.A., 2004. Magma volume, volatile emissions, and stratospheric aerosols from the 1815 eruption of Tambora. Geophysical Research Letters 31, L20608.

Shea, T., Larsen, J.F., Gurioli, L., Hammer, J.E., Houghton, B.F., Cioni, R., 2009. Leucite crystals: surviving witnesses of magmatic processes preceding the 79 AD eruption at Vesuvius, Italy. Earth and Planetary Science Letters 281, 88-98.

Shelley, I., Voight, B., 1995. Medical effects of nuée ardent eruptions: The November 1994 eruption at Merapi Volcano. Indonesia. Proc. Merapi Decade Volcano International Workshop, UNESCO/ Volcanological Survey of Indonesia, Yogyakarta, p. 9.

Shinohara, H., 1994. Exsolution of immiscible vapor and liquid phases from a crystallizing silicate melt: Implications for chlorine and metal transport. Geochimica et Cosmochimica Acta 58, 5215- 5221.

Siebert, L., Simkin, T., Kimberly, P., 2011. Volcanoes of the world. University of California Press.

Signorelli, S.,Vaggelli, G., Romano, C., 1999. Pre-eruptive volatile (H_2O, F, Cl and S) contents of phonolitic magmas feeding the 3550-year old Avellino eruption from Vesuvius, southern Italy. . Journal of Volcanology and Geothermal Research 93, 237-256.

Simkin, T.L., Siebert, L., 1994. Volcanoes of the World. Geoscience Press, Tuscon, Arizona.

Siswowidjoyo, S., Suryo, I., Yokoyama, I., 1995. Magma eruption rates of Merapi volcano, Central Java, Indonesia during one century (1890-1992). Bulletin of Volcanology 57, 111-116.

Smithsonian Institution, 2007. Merapi. Bulletin of the Global Volcanism Network 32 (2).

Smyth, H.R., Hall, R., Hamilton, J., Kinny, P., 2005. East Java: Cenozoic basins, volcanoes and ancient basement. Proceeding, Indonesian Petroleum Association, Thirteenth Annual Convention & Exhibition.

Smyth, H.R., Hamilton, P.J., Hall, R., Kinny, P.D., 2007. The deep crust beneath island arcs: inherited zircons reveal a Gondwana continental fragment beneath East Java, Indonesia. Earth and Planetary Science Letters 258, 269-282.

Sparks, R.S.J., 1978. The dynamics of bubble formation and growth in magmas: a review and analysis. Journal of Volcanology and Geothermal Research 3, 1-37.

Sparks, R.S.J., 1997. Causes and consequences of pressurisation in lava dome eruptions. Earth and Planetary Science Letters 150, 177-189.

Sparks, R.S.J., Murphy, M.D., Lejeune, A.M., Watts, R.B., Barclay, J., Young, S.R., 2000. Control on the emplacement of the andesite lava dome of the Soufriere Hills Volcano, Montserrat by degassing-induced crystallization. Terra Nova 12, 14-20.

Stasiuk. M.V., Barclay, J., Carroll, M.R., Jaupart, C., Ratté, J.C., Sparks, R.S.J., Tait, S.R., 1996. Degassing during magma ascent in the Mule Creek vent (USA). Bulletin of Volcanology 58, 117-130.

Stix, J., Layne, G.D., 1996. Gas saturation and evolution of volatile and light lithophile elements in the Bandelier magma chamber between two caldera-forming eruptions, Journal of Geophysical Research 101, 25181- 25196.

Stix, J., Zapata, J.A., Calvache, M., Cortés, G.P., Fischer, T.P., Gómez, D., Narvaez, L., Ordoñez, M., Ortega, A., Torres, R., Williams, S.N., 1993. A model of degassing at Galeras Volcano, Colombia, 1988-1993. Geology 21, 963-967.

Sun, S.S., McDonough, W.F., 1989. Chemical and isotopic systematics of oceanic basalts: implications for mantle composition and processes. In: Saunders, A.D., Norry (Eds.) Magmatism in the Ocean Basins. Geological Society, London, Special Publications 42, 313-345.

Surono, Jousset, P., Pallister, J., Boichu, M., Buongiorno, M.F., Budisantoso, A., Costa, F., Andreastuti, S., Prata, F., Schneider, D., Clarisse, L., Humaida, H., Sumarti, S., Bignami, C., Griswold, J., Carn, S., Oppenheimer, C., Lavigne, F., 2012. The 2010 explosive eruption of Java's Merapi volcano – A '100-year' event. Journal of Volcanology and Geothermal Research 241-242, 121-135.

Suzuki, Y., Fujii, T., 2010. Effect of syneruptive decompression path on shifting intensity in basaltic sub-Plinian eruption: Implication of microlites in Yufune-2 scoria from Fuji volcano, Japan. Journal of Volcanology and Geothermal Research 198, 159-176.

Suzuki, Y., Yasuda, A., Hokanishi, N., Kaneko, S., Fujii, T., 2013. Syneruptive deep magma transfer and shallow magma remobilization during the 2011 eruption of Shinmoe-dake, Japan– Constraints from melt inclusions and phase equilibria experiments. Journal of Volcanology and Geothermal Research 257, 184-204.

Swanson, S.E., Naney, M.T., Westrich, H.R., Eichelberger, J.C., 1989. Crystallization history of Obsidian Dome, Inyo Domes, California. Bulletin of Volcanology 51, 161-176.

Szramek, L., Gardner, J.E., Larsen, J., 2006. Degassing and microlite crystallisation of basaltic andesite magma erupting at Arenal Volcano, Costa Rica. Journal of Volcanology and Geothermal Research 157, 182-201.

Taylor, B.E., Eichelberger, J.C., Westrich, H.R., 1983. Hydrogen isotopic evidence of rhyolitic degassing during shallow intrusion and eruption. Nature 306, 541-545.

Thouret, J.-C., Lavigne, F., Kelfoun, K., Bronto, S., 2000. Toward a revised hazard assessment at Merapi volcano, Central Java. Journal of Volcanology and Geothermal Research 100, 479-502.

Tiede, C., Camacho, A.G., Gerstenecker, C., Fernández, J., Suyanto, I., 2005. Modeling the density at Merapi volcano area, Indonesia, via the inverse gravimetric problem. Geochemistry Geophysics Geosystems 6, Q09011.

Tindle, A.G., Webb, P.C., 1990. Estimation of lithium contents in trioctahedral micas using microprobe data: application to micas from granitic rocks. European Journal of Mineralogy 2, 595-610.

Toutain, J.-P., Sortino, F., Baubron, J.-C., Richon, P., Surono., Sumarti, S., Nonell, A., 2009. Structure and CO2 budget of Merapi volcano during inter-eruptive periods. Bulletin of Volcanology 71, 815-826.

Troll, V.R., Hilton, D.R., Jolis, E.M., Chadwick, J.P., Blythe, L.S., Deegan, F.M., Schwarzkopf, L.M., Zimmer, M., 2012. Crustal CO_2 liberation during the 2006

eruption and earthquake events at Merapi volcano, Indonesia. Geophysical Research Letters 39, L11302.

Troll, V.R., Deegan, F.M., Jolis, E.M., Harris, C., Chadwick, J.P., Gertisser, R., Schwarzkopf, L.M., Borisova, A.Y., Bindeman, I.N., Sumarti, S., Preece, K., 2013. Magmatic differentiation processes at Merapi volcano: inclusion petrology and oxygen isotopes. Journal of Volcanology and Geothermal Research 261, 38-49.

Tuttle, O., Bowen, N., 1958. Origin of granite in light of experimental studies. Geological Society of America, Memoirs 74, 153 p.

Underwood, E. E., 1970. Quantitative Stereology. Addison-Wesley, Reading, Massachusetts, 274 pp.

van Bemmelen, R., W., 1949. The Geology of Indonesia, vol. 1A, General Geology, Government Printing Office, The Hague, Netherlands.

Van Bemmelen, R.W., 1956. The influence of geologic events on human history (an example from Central Java). Verh. Kon. Ned. Geol. Mijnb. Genoot Geol 16, 20-36.

Van Boekhold, F. (1792) Relaas van een togt naar den Brandenden berg op Java, 17/18 juli 1786. Verh Bataviaasch Genoot Kunsten Wet 6, 8-12 (2nd edn in 1827).

Venzke, E., Wunderman, R.W., McClelland, L., Simkin, T., Luhr, J.F., Siebert, L., Mayberry, G., Sennert, S. (eds) 2002. Global volcanism, 1968 to the present. Smithsonian Institution, Global Volcanism Program Digital Information Series, GVP-4 (http://www.volcano.si.edu/reports/).

Vigouroux, N., Wallace, P.J., Kent, A.J.R., 2008. Volatiles in high-K magmas from the western Trans-Mexican Volcanic Belt: Evidence for fluid fluxing and extreme enrichment of the mantle wedge by subduction processes. Journal of Petrology 49, 1589-1618.

Villemant, B., Boudon, G., 1998. Transition from dome-forming to plinian eruptive styles controlled by H_2O and Cl degassing. Nature 392, 65-69.

Villemant, B., Mouatt, J., Michel, A., 2008. Andesitic magma degassing investigated through H_2O vapour-melt partitioning of halogens at Soufrière Hills volcano, Montserrat, (Lesser Antilles). Earth and Planetary Science Letters 269, 212-229.

Voight, B., Elsworth, D., 2000. Instability and collapse of hazardous gas-pressurized lava domes. Geophysical Research Letters 27, 1-4.

Voight, B., Constantine, E.K., Siswowidjoyo, S., Torley, R., 2000. Historical eruptions of Merapi volcano, Central Java, Indonesia, 1768-1998. Journal of Volcanology and Geothermal Research 100, 69-138.

Walter, T.R., Wang, R., Zimmer, M., Grosser, H., Lühr, B., Ratdomopurbo, A., 2007. Volcanic activity influences by tectonic earthquakes: Static and dynamic stress triggering at Mt. Merapi. Geophysical Research Letters 34, L05304.

Webster, J.D., 1997. Chloride solubility in felsic melts and the role of chloride in magmatic degassing. Journal of Petrology 38, 1793- 1807.

Webster, J.D., 2004. The exsolution of magmatic hydrosaline chloride liquids. Chemical Geology 210, 33-48.

Webster, J.D., Kinzler, R.J., Mathez, E.A., 1999. Chloride and water solubility in basalt and andesite melts and implications for magmatic degassing. Geochimica and Cosmochimica Acta 63, 729- 738.

Webster, J.D., Mandeville, C.W., Goldoff, B., Coombs, M.L., Tappen, C., 2010. Augustine volcano- The influence of volatile components in magmas erupted A.D. 2006 to 2,100 years before present. In: Power, J.A., Coombs, M.L., Freymueller, J.T. (Eds.) The 2006 eruption of Augustine volcano, Alaska. U.S. Geological Survey Professional Paper 1769.

Wen, S., Nekvasil, H., 1994. SOLVCALC: an interactive graphics program package for calculating the ternary feldspar solvus and for two-feldspar geothermometry. Computers and Geosciences 20, 1025-1040.

Westrich, H.R., Stockman, H.W., Eichelberger, J.C., 1988. Degassing of Rhyolitic Magma During Ascent and Emplacement. Journal of Geophysical Research 93, 6503-6511.

Whitford, D.J., Nicholls, I.A., Taylor, S.R., 1979. Spatial variations in the geochemistry of Quaternary lavas across the Sunda arc in Java and Bali. Contributions to Mineralogy and Petrology 70, 341-356.

Widiyantoro, S., Van der Hilst, R., (1997) Mantle structure beneath Indonesia inferred from high-resolution tomographic imaging. Geophysical Journal International 130, 167-182.

Williamson, B.J., Di Muro, A., Horwell, C.J., Spieler, O., Llewellin, E.W., 2010. Injection of vesicular magma into an andesitic dome at the effusive-explosive transition. Earth and Planetary Science Letters 295, 83-90.

Wilson, L., Sparks, R.S.J., Walker, G.P.L., 1980. Explosive volcanic eruptions - IV. The control of magma properties and conduit geometry on eruption column behaviour. Geophysical Journal, Royal Astronomical Society 63, 117-148.

Wolf, K.J., Eichelberger, J.C., 1997. Syneruptive mixing, degassing, and crystallization at Redoubt Volcano, eruption of December, 1989 to May1990. Journal of Volcanology and Geothermal Research 75, 19-37.

Woods, A.W., Koyaguchi, T., 1994. Transitions between explosive and effusive eruptions of silicic magmas. Nature 370, 641-644.

Wright, H.M., Bacon, C.R., Vazquez, J.A., Sisson, T.W., 2012. Sixty thousand years of magmatic volatile history before the caldera-forming eruption of Mount Mazama, Crater Lake, Oregon. Contributions to Mineralogy and Petrology 164, 1027-1106.

Young, S.R., Sparks, R.S.J., Aspinall, W.P., Lynch, L.L., Miller, A.D., Robertson, R.E.A., Shepherd, J.B., 1998. Overview of the eruption of Soufrière Hills volcano, Montserrat, 18 July 1995 to December1997. Geophysical Research Letters 25, 3389-3392.

Zachariáš, J., 2008. Compositional trends in magmatic and hydrothermal silicates of the Petráčkova hora intrusive complex, Bohemian Massif – link between the magmatic processes and intrusion-related gold mineralization. Journal of Geosciences 53, 105-117.

Zhang, Y.X., 1999. H_2O in rhyolitic glasses and melts: Measurements, speciation and diffusion. Reviews of Geophysics 37, 493-516.

Zimmer, M., Erzinger, J., 2003. Continuous H_2O, CO_2, ^{222}Rn and temperature measurements on Merapi Volcano, Indonesia. Journal of Volcanology and Geothermal Research 125, 25- 38.

Appendices

Appendix A: 2006 and 2010 sample lists

Appendix B: 2010 field localities and logs

Appendix C: Whole rock and geochemical data (XRF and ICP-MS)

Appendix D: Mineral composition (Electron microprobe data)

Appendix E: Groundmass glass and melt inclusion compositions (Electron microprobe data)

Appendix F: Melt inclusions volatiles and light lithophile elements (SIMS data)

Appendix G: Textural analysis results

Appendices

Appendix A: 2006 and 2010 sample lists

Appendix B: 2010 field localities and logs

Appendix C: Whole rock and geochemical data (XRF and ICP-MS)

Appendix D: Mineral composition (Electron microprobe data)

Appendix E: Groundmass glass and melt inclusion compositions (Electron microprobe data)

Appendix F: Melt inclusions volatiles and light lithophile elements (SIMS data)

Appendix G: Textural analysis results

Table A1 Sample list of the 2006 Merapi eruption

Sample No.	Sample Type	Abbreviation Sample Type	Eruption Stage[1]	Locality Description	UTM-Zone	Easting	Northing
ME08-01	Lobe 4 - scoria	L4-S	III	Kali Gendol	49M	439087	9163378
ME08-02-01	Lobe 5 - scoria	L5-S	III	Kali Gendol	49M	439153	9163551
ME08-02-02	Lobe 5 - scoria	L5-S	III	Kali Gendol	49M	439153	9163551
ME08-03-01	Lobe 6 - scoria	L6-S	III	Kali Gendol	49M	439306	9163826
ME08-03-02	Lobe 6 - scoria	L6-S	III	Kali Gendol	49M	439306	9163826
ME08-04-01	Lobe 8 - scoria	L8-S	III	Kali Gendol	49M	439545	9164189
ME08-04-02	Lobe 8 - scoria	L8-S	III	Kali Gendol	49M	439545	9164189
ME08-04-03	Lobe 8 - scoria	L8-S	III	Kali Gendol	49M	439545	9164189
ME08-05-01	Lobe 1 - scoria	L1-S	II	Kali Gendol	49M	439269	9163664
ME08-05-02	Lobe 1 - scoria	L1-S	II	Kali Gendol	49M	439269	9163664
ME08-06	Lobe 1 - scoria	L1-S	II	Kali Gendol	49M	439101	9161851
ME08-07	Lobe 10 - scoria	L10-S	III	Kali Gendol	49M	436828	9164438
ME08-08-01	Lobe 1 - dense dome block	L1-D	II	Kali Gendol	49M	439294	9161754
ME08-08-02	Lobe 1 - dense dome block	L1-D	II	Kali Gendol	49M	439294	9161754
ME08-08-03	Lobe 1 - dense dome block	L1-D	II	Kali Gendol	49M	439294	9161754
ME08-09-01	Lobe 1 - scoria	L1-S	II	Kali Gendol	49M	439265	9161823
ME08-09-02	Lobe 1 - scoria	L1-S	II	Kali Gendol	49M	439265	9161823
ME08-09-03	Lobe 1 - scoria	L1-S	II	Kali Gendol	49M	439265	9161823
ME08-09-04	Lobe 1 - scoria	L1-S	II	Kali Gendol	49M	439265	9161823
ME08-09-05	Lobe 1 - scoria	L1-S	II	Kali Gendol	49M	439265	9161823
ME08-10	Kali Bebeng - scoria	KB-S	I	Kali Bebeng	49M	436744	9164357
ME08-11-01	Kali Bebeng - scoria	KB-S	I	Kali Bebeng	49M	436655	9164250
ME08-11-02	Kali Bebeng - scoria	KB-S	I	Kali Bebeng	49M	436655	9164250
ME08-11-03	Kali Bebeng - scoria	KB-S	I	Kali Bebeng	49M	436655	9164250
ME08-12	Kali Bebeng - dense dome block	KB-D	I	Kali Bebeng	49M	436228	9163637
ME08-13-01	2006 summit dome - scoria (sampled in 2008)	SD-S	IV	Merapi summit	49M	438895	9166477
ME08-13-02	2006 summit dome - scoria (sampled in 2008)	SD-S	IV	Merapi summit	49M	438895	9166477
ME08-13-03	2006 summit dome - scoria (sampled in 2008)	SD-S	IV	Merapi summit	49M	438895	9166477
ME08-14	2006 summit dome - scoria (sampled in 2008)	SD-S	IV	Merapi summit	49M	438895	9166477

[1] After Preece et al. (2013)

Table A2 Sample list of the 2010 Merapi eruption

Sample No.	Sample Type	Abbreviation Sample Type	Eruption Stage[1]	Locality No.[2]	Locality Description[2]	Unit (Log)[2]	Waypoint[2]	UTM-Zone	Easting	Northing
M11-01	Dome (dense)	DD	4/5	1	Kepuharjo Interfluve	-	221	49M	440105	9157054
M11-01Cumulate	Plutonic inclusion (magmatic cumulate)	Pl-Inc	4/5	1	Kepuharjo Interfluve	-	221	49M	440105	9157054
M11-X1	Calc-silicate xenolith	CS	4/5	1	Kepuharjo Interfluve	-	221	49M	440105	9157054
M11-02	Dome (scoriaceous)	DS	4/5	2	Kali Gendol S of Kaliadem	-	223	49M	439350	9161472
M11-04	Dome (dense)	DD	4/5	2	Kali Gendol S of Kaliadem	-	225	49M	439548	9161136
M11-05	Light-grey inclusion	LG-Inc	4/5	2	Kali Gendol S of Kaliadem	-	226	49M	439516	9160923
M11-06	Dome (scoriaceous)	DS	4/5	2	Kali Gendol S of Kaliadem	-	226	49M	439516	9160923
M11-07	Dome (dense) w/ light-grey inclusion	DD w/ LG-Inc	4/5	2	Kali Gendol S of Kaliadem	-	227	49M	439437	9160814
M11-10b	Dome (dense)	DD	4	3	Kali Opak - W Interfluve	U2	229	49M	438814	9160285
M11-12	Dome (dense)	DD	4	5	Ridges N of Kinahrejo	U4	233	49M	438498	9162807
M11-14	Ash fall / surge	A	3	7	Ridges N of Kinahrejo	U5	235 (Section 2)	49M	438771	9163127
M11-15	Dome (dense)	DD	4	8	Ridges N of Kinahrejo	U2	236	49M	438836	9162339
M11-17	Ash fall / surge (with accretionary lapilli)	A	5	8	Ridges N of Kinahrejo	U4	236	49M	438836	9162339
M11-18	White pumice	WP	6	9	Ridges N of Kinahrejo	-	237	49M	438599	9163418
M11-19a	Dome (dense)	DD	4	10	Ridges N of Kinahrejo	U5	238	49M	438648	9163336
M11-20	Dome (dense)	DD	4	11	S of Gunung Kendil	U5	240	49M	439581	9162599
M11-21	Ash fall / surge	A	3	11	S of Gunung Kendil	U4	240	49M	439581	9162599
M11-24	Dome (dense)	DD	4	12	W edge of Kali Woro	U4	242	49M	440269	9163011
M11-26a	Dome (dense)	DD	4/5	13	Kali Gendol - E Interfluve	-	244	49M	440487	9157739
M11-27-1	Dome (dense)	DD	4/5	13	Kali Gendol - E Interfluve	-	244	49M	440487	9157739
M11-27-2	Dome (dense) w/ light-grey inclusion	DD w/ LG-Inc	4/5	13	Kali Gendol - E Interfluve	-	244	49M	440487	9157739
M11-27-3	Dome (dense) w/ light-grey inclusion	DD w/ LG-Inc	4/5	13	Kali Gendol - E Interfluve	-	244	49M	440487	9157739
M11-27-4	Dome (dense) w/ light-grey inclusion	DD w/ LG-Inc	4/5	13	Kali Gendol - E Interfluve	-	244	49M	440487	9157739
M11-27-5	Dome (dense)	DD	4/5	13	Kali Gendol - E Interfluve	-	244	49M	440487	9157739
M11-27-6	Dome (dense) w/ light-grey inclusion	DD w/ LG-Inc	4/5	13	Kali Gendol - E Interfluve	-	244	49M	440487	9157739
M11-28a	Pre-5th November scoria	P5N-Sc	2	14	Ridges N of Kinahrejo	U2	246	49M	438770	9163168
M11-28b	Pre-5th November light grey dense clast	P5N-LGD	2	14	Ridges N of Kinahrejo	U2	246	49M	438770	9163168
M11-33	White pumice	WP	6	17	Kaliadem Interfluve	-	278	49M	439121	9162001
M11-34	Dome (dense) with calc-silicate xenolith	DD w/ CS	6	17	Kaliadem Interfluve	-	279	49M	439201	9161731
M11-38	Dome (dense)	DD	4/5	45	Between Kali Gendol 1 & 2	-	344	49M	439573	9161305
M11-46	Dome (dense)	DD	4	22	E Kali Gendol Interfluve Opposite Kopeng	U2	289	49M	440296	9159013
M11-48	Dome (dense) w/ light-grey inclusion	DD w/ LG-Inc	4	23	E Kali Gendol Interfluve Opposite Kopeng	U1	290	49M	440404	9158889
M11-50	White pumice	WP	6	24	Kali Gendol near Kopeng	-	291	49M	440033	9158748
M11-51	Grey scoria	GS	6	24	Kali Gendol near Kopeng	-	291	49M	440033	9158748
M11-53-B1	Dome (dense)	DD	3	26	Kali Gendol - S of Kopeng	U1	294	49M	440383	9157883

[1] After Komorowski et al. (2013); [2] see Appendix B

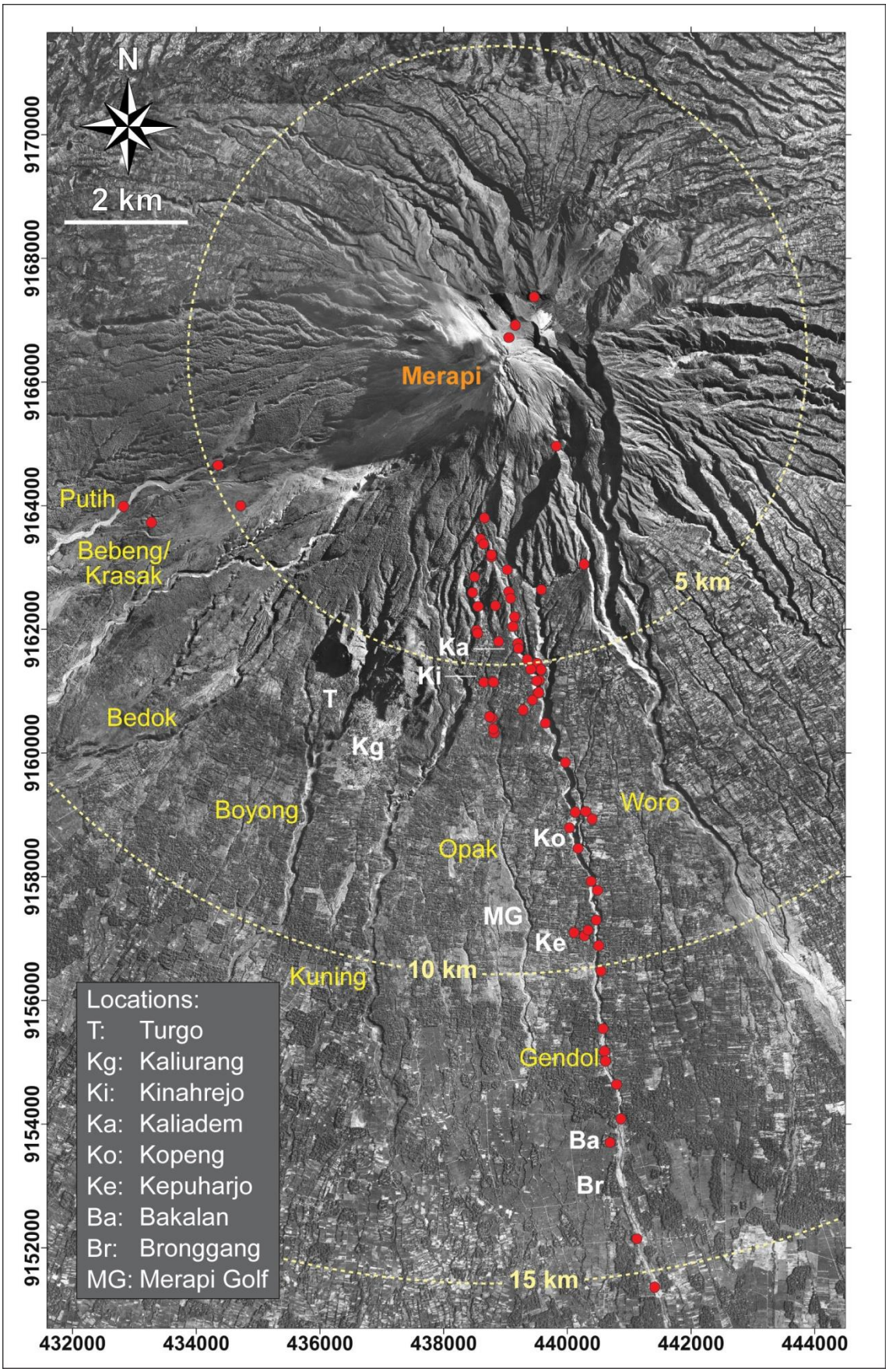

Fig. B1 Field sites and sample locations of the 2010 Merapi eruption.

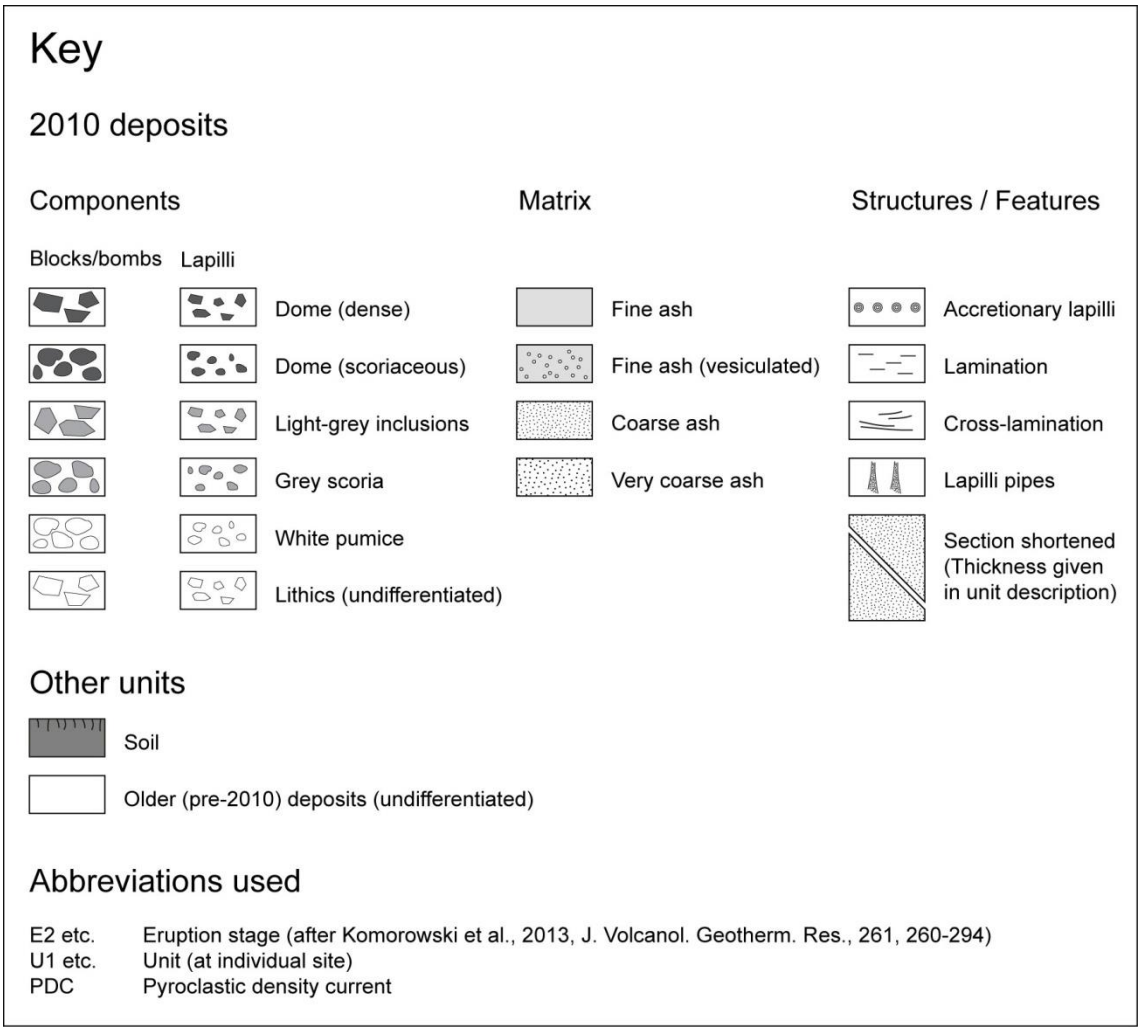

Fig. B2 Key for the field sites and stratigraphic logs of the 2010 Merapi eruption displayed below (locality numbers 1 to 56).

Locality No.:	01	Coordinates (49M):	440105 / 9157054
Locality Description:	Kepuharjo Interfluve	Samples:	M11-01, M11-01Cumulate, M11-X1
Waypoint (WP):	221		

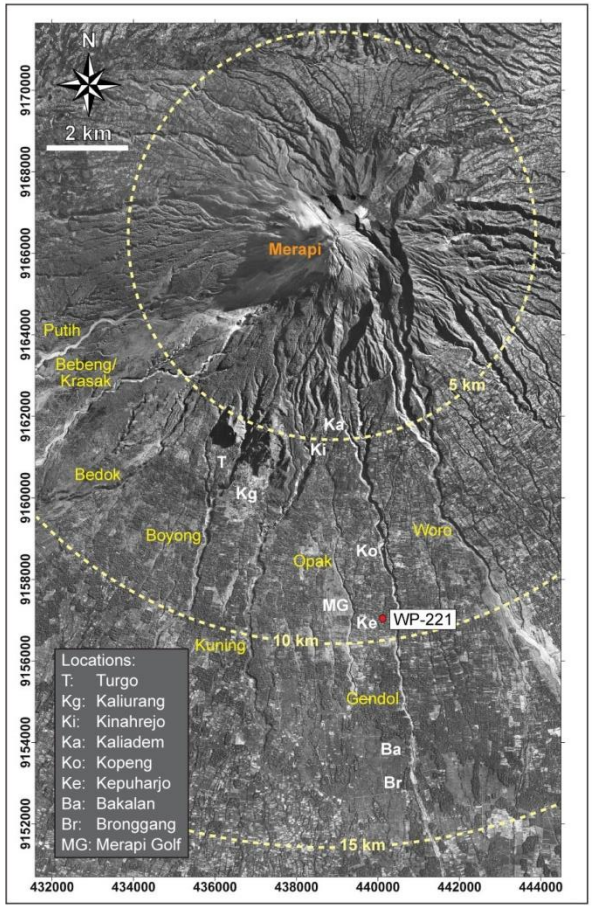

Tree damage (flow direction left to right); view across Kali Gendol towards E interfluve

Locality No.:	02	Coordinates (49M):	439350 / 9161472 (223), 439548 / 9161136 (225), 439516 / 9160923 (226), 439437 / 9160814 (227)
Locality Description:	Kali Gendol S of Kaliadem		
Waypoint (WP):	223, 225, 226 & 227	Samples:	M11-02 (223), M11-04 (225), M11-05 (226), M11-06 (226), M11-07 (227)

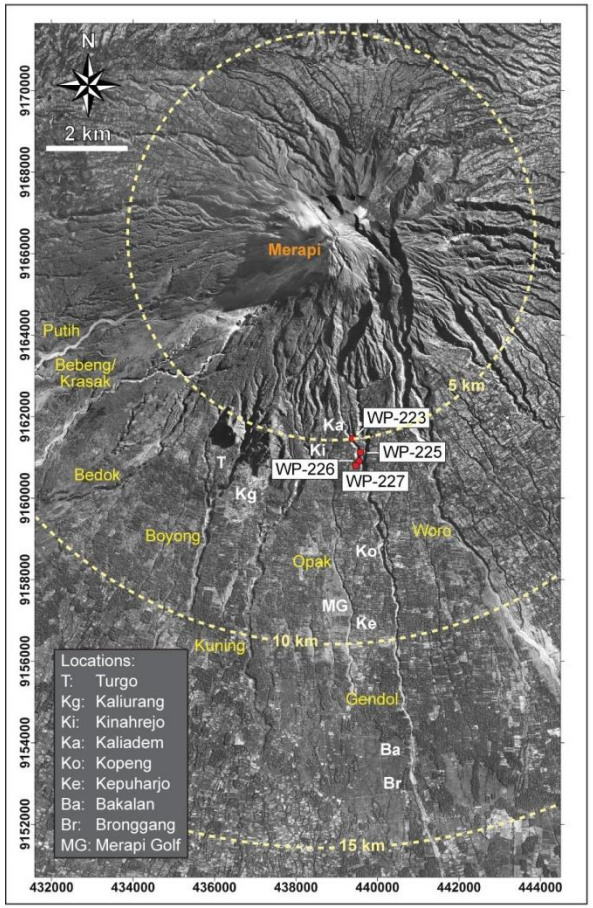

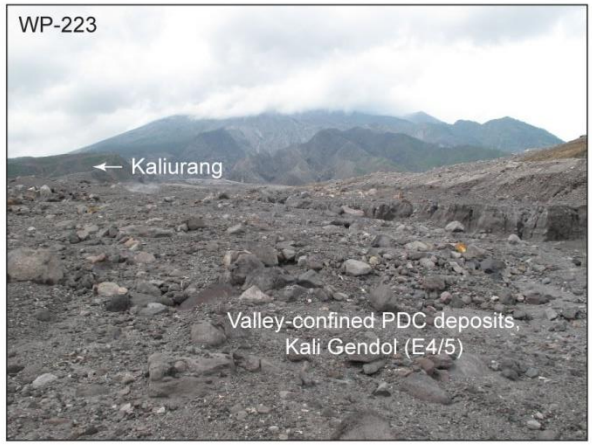

Locality No.:	03	Coordinates (49M):	438814 / 9160285
Locality Description:	Kali Opak - W Interfluve	Samples:	M11-10b
Waypoint (WP):	229		

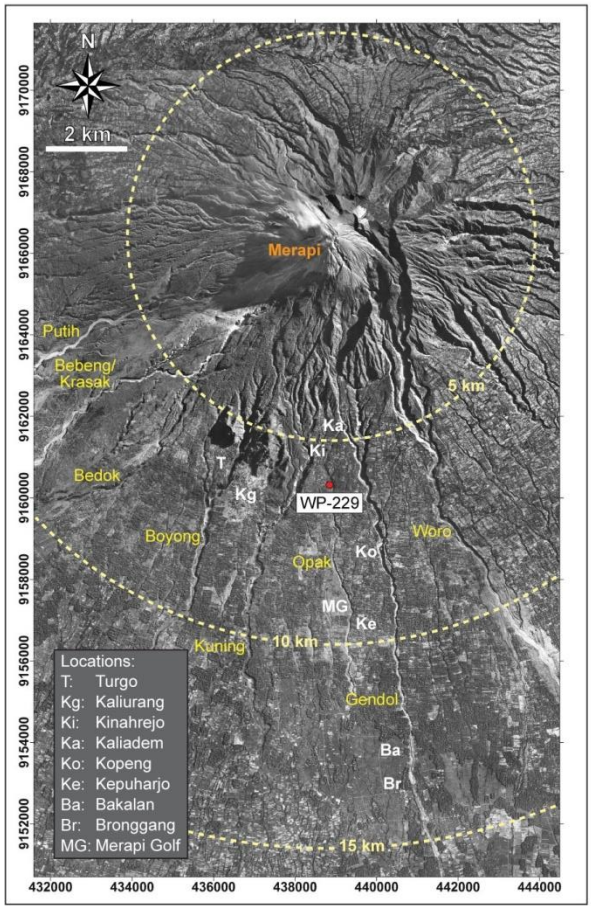

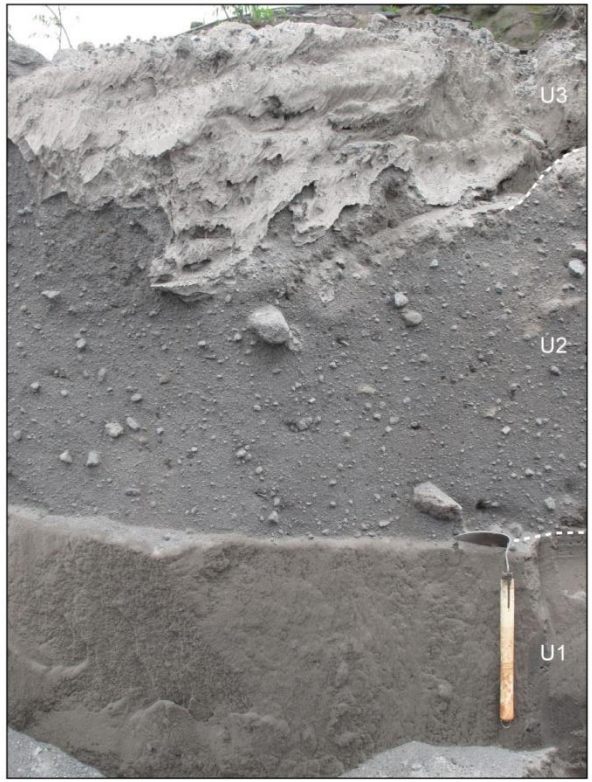

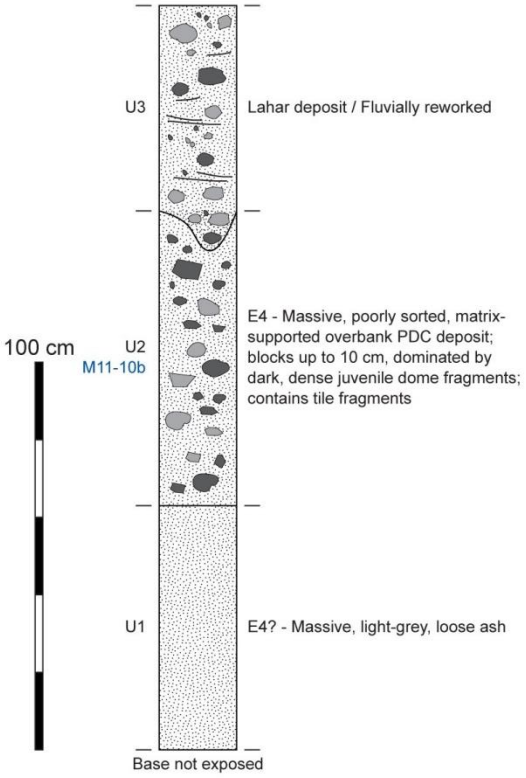

Locality No.:	04	Coordinates (49M):	438469 / 9162555
Locality Description:	Ridges N of Kinahrejo	Samples:	None
Waypoint (WP):	232		

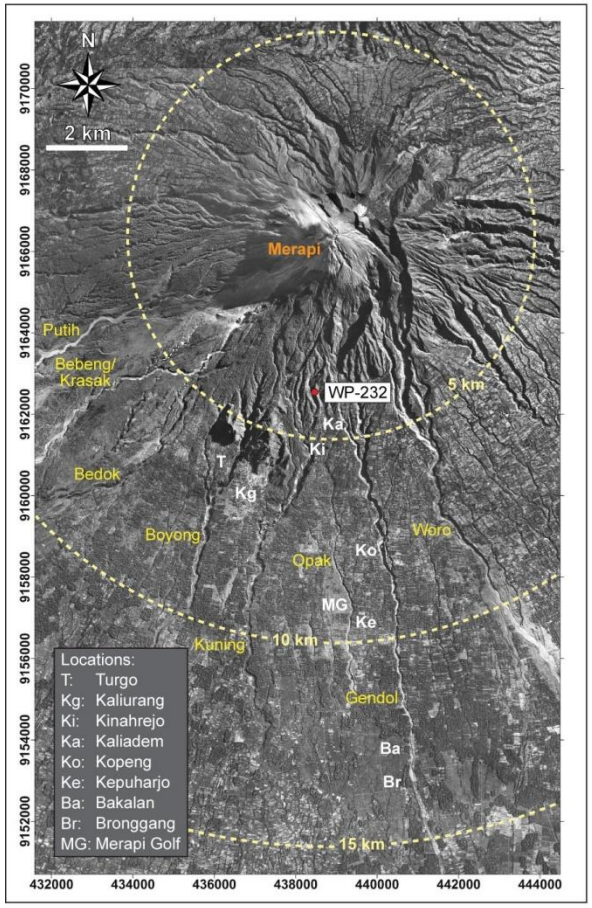

10 cm

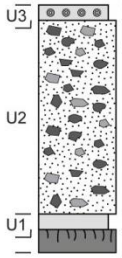

E5 - Fine ash with accretionary lapilli (AL-U4 of Komorowski et al., 2013)

E4 - Massive, poorly sorted, fines depleted, generally clast-supported PDC deposit ("blast layer"); blocks up to 15 cm; mainly dark, juvenile dome fragments (U1-L1 of Komorowski et al., 2013)

E3 - Fine grey/brown ash; ash cloud deposit from dilute PDC (surge)

Locality No.:	05	Coordinates (49M):	438498 / 9162807
Locality Description:	Ridges N of Kinahrejo	Samples:	M11-12
Waypoint (WP):	233		

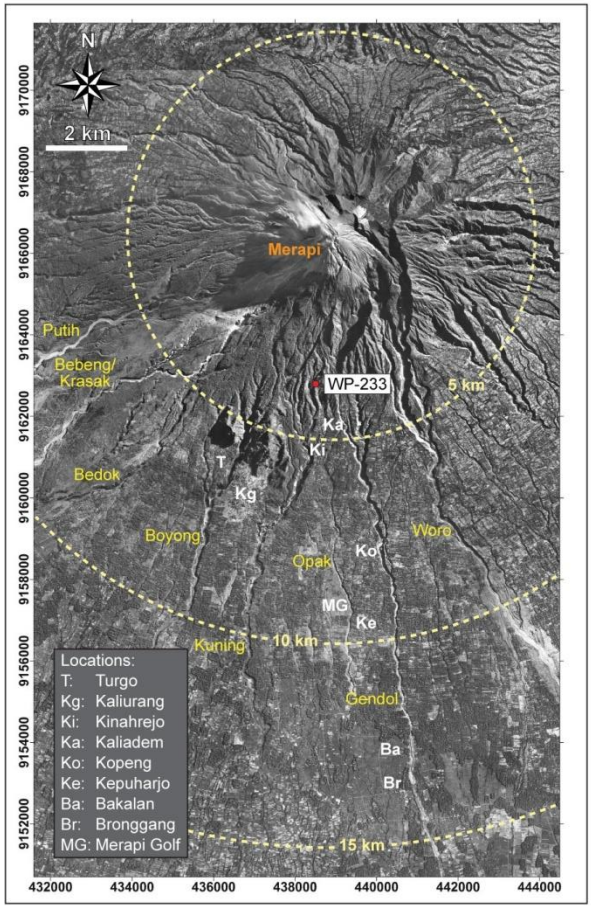

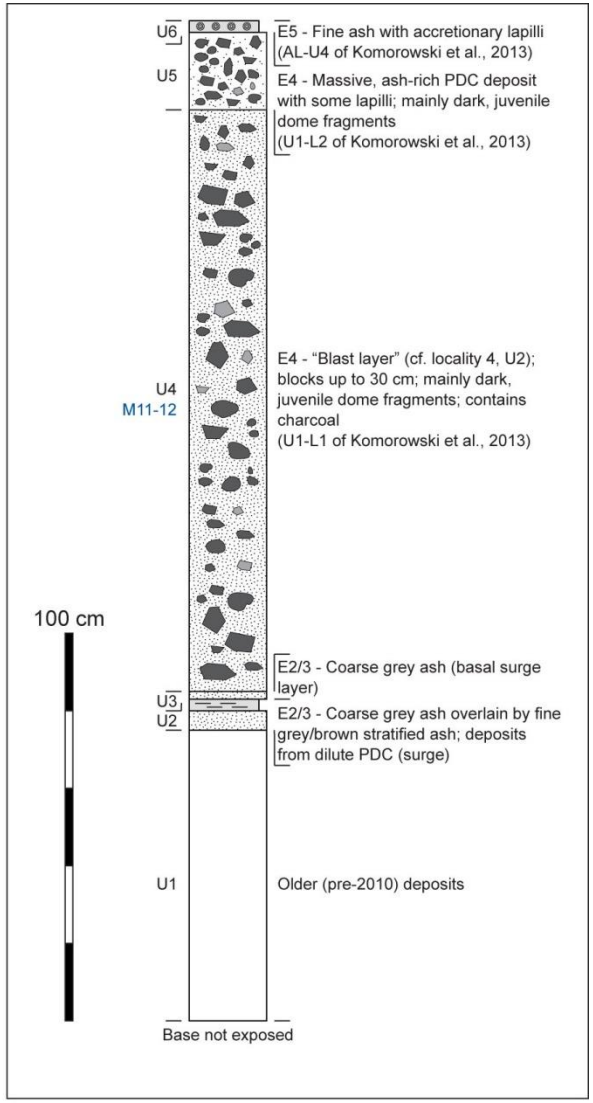

Locality No.:	06	Coordinates (49M):	438771 / 9163127
Locality Description:	Ridges N of Kinahrejo	Samples:	None
Waypoint (WP):	235 (Section 1)		

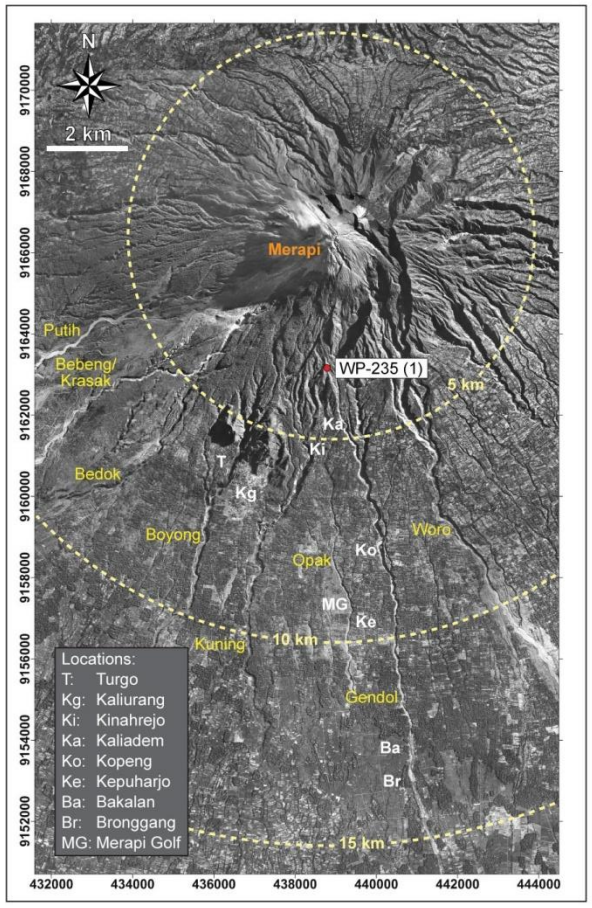

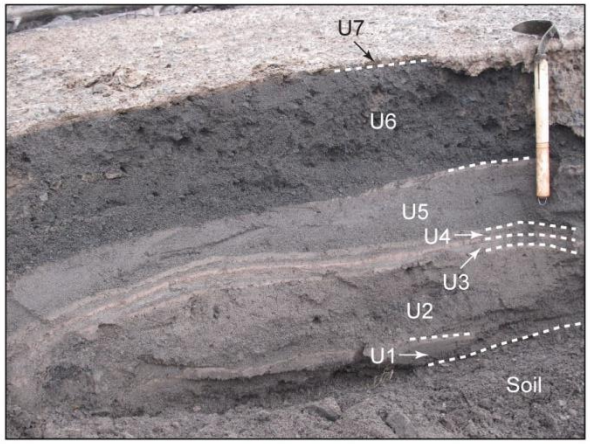

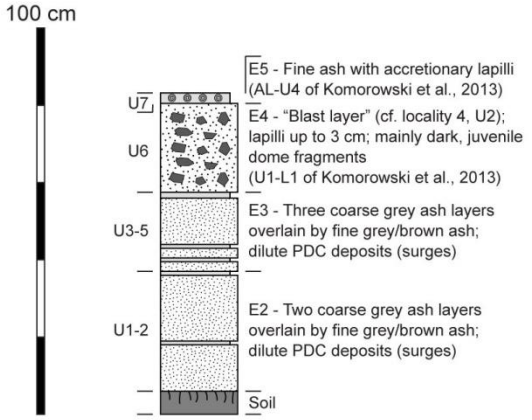

Locality No.:	07	Coordinates (49M):	438771 / 9163127
Locality Description:	Ridges N of Kinahrejo	Samples:	M11-14
Waypoint (WP):	235 (Section 2)		

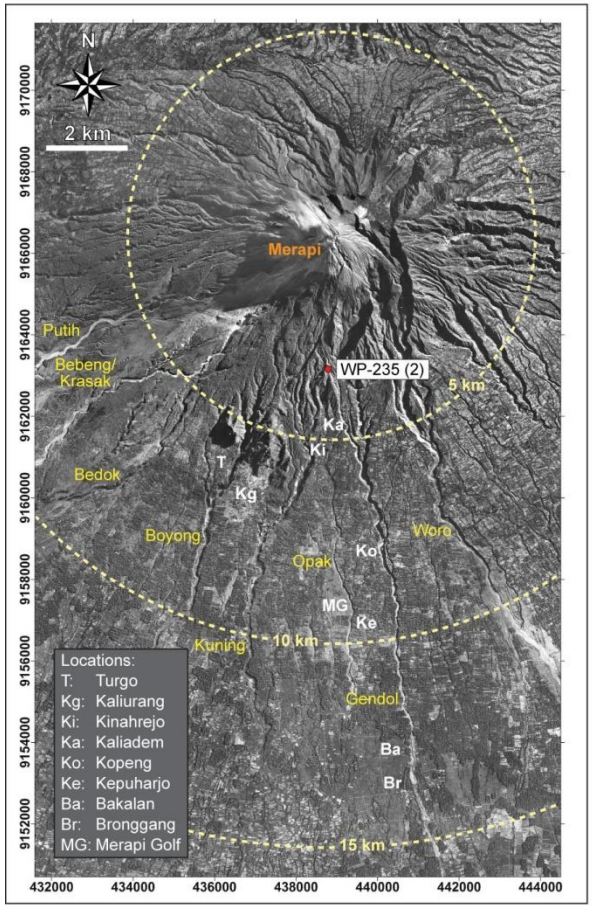

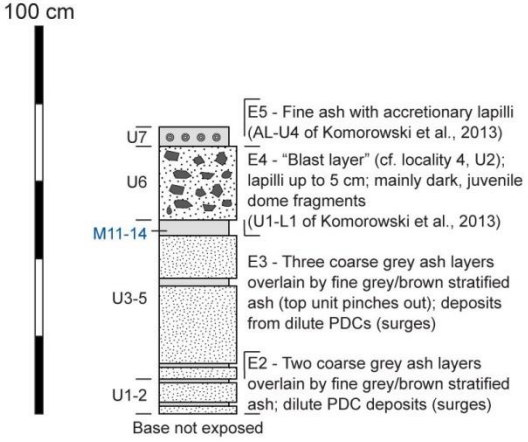

Locality No.:	08	Coordinates (49M):	438836 / 9162339
Locality Description:	Ridges N of Kinahrejo	Samples:	M11-15, M11-17
Waypoint (WP):	236		

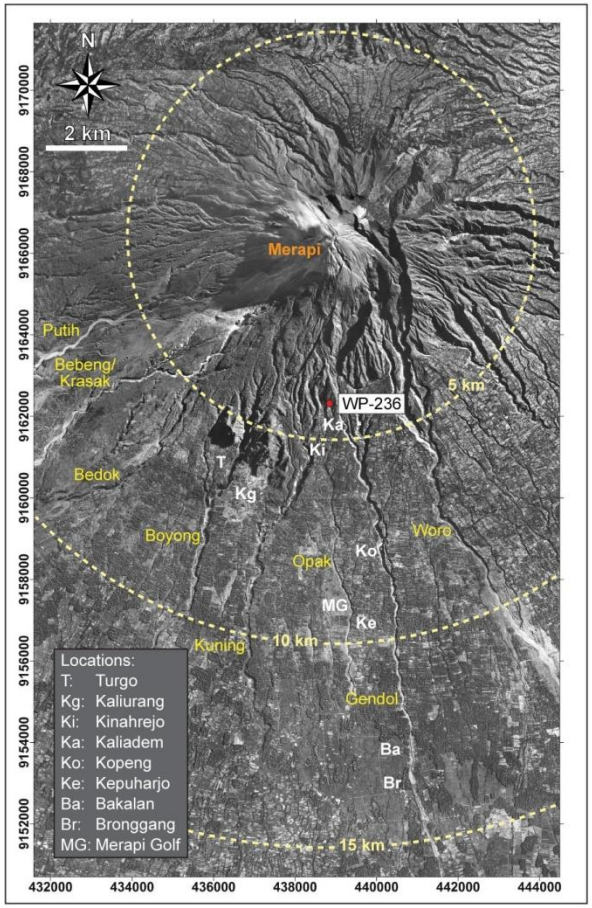

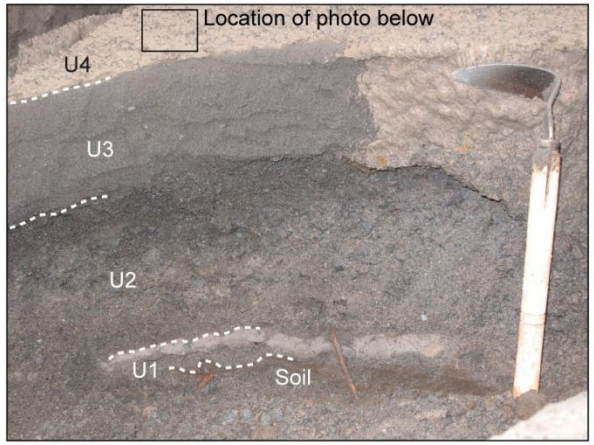

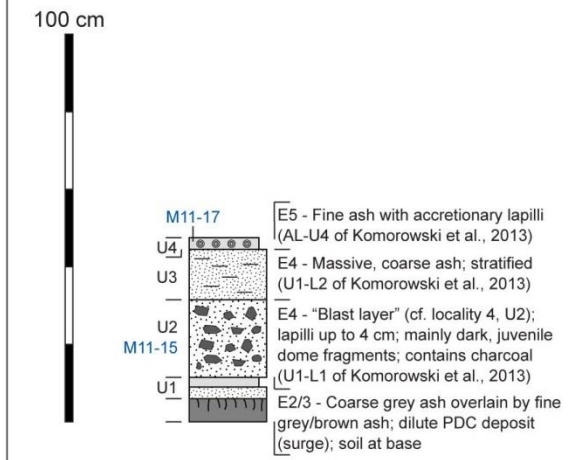

Locality No.:	09	Coordinates (49M):	438599 / 9163418
Locality Description:	Ridges N of Kinahrejo	Samples:	M11-18
Waypoint (WP):	237		

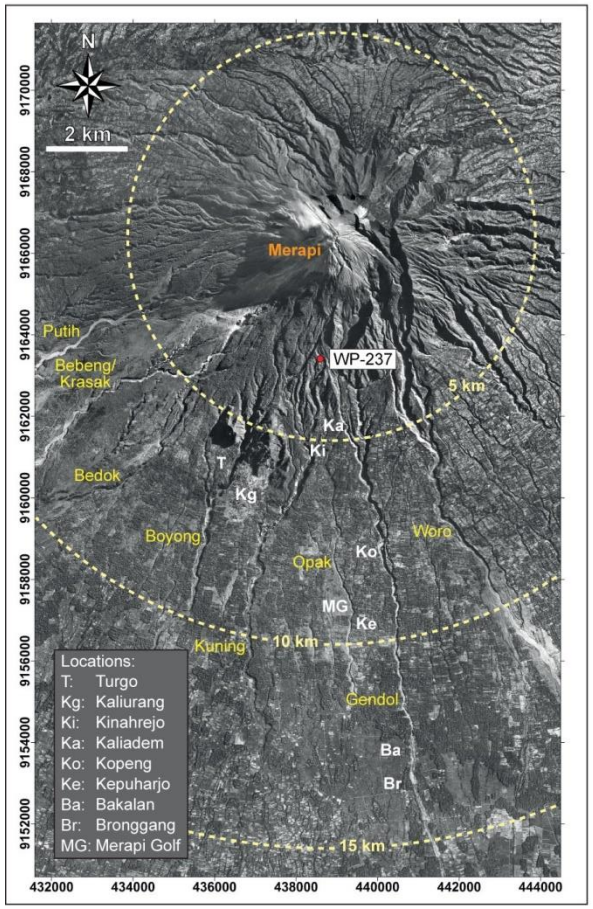

Scattered white pumice lapilli (E6) on top of E5 accretionary lapilli bearing ash (Al-U4 of Komorowski et al., 2013) (M11-18)

Locality No.:	10	Coordinates (49M):	438648 / 9163336
Locality Description:	Ridges N of Kinahrejo	Samples:	M11-19a
Waypoint (WP):	238		

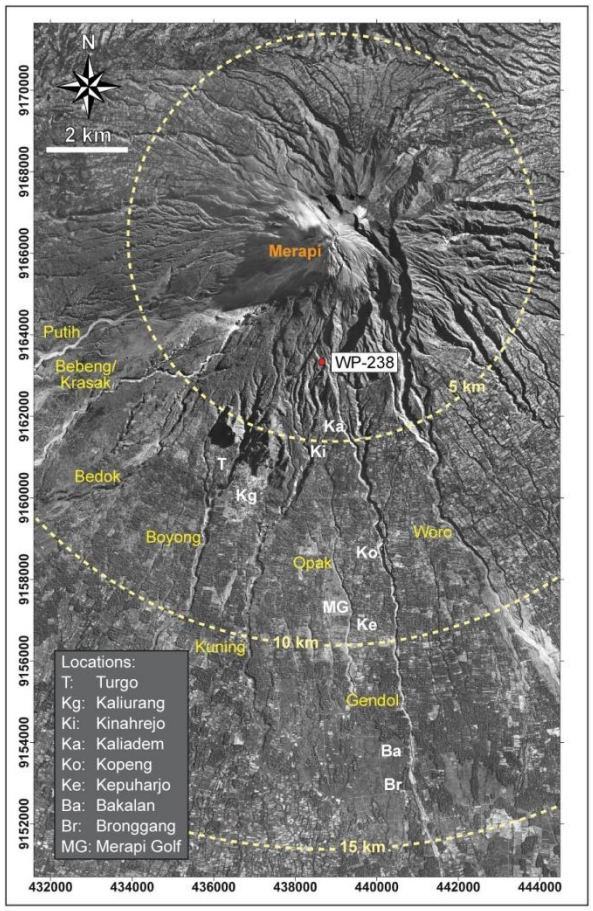

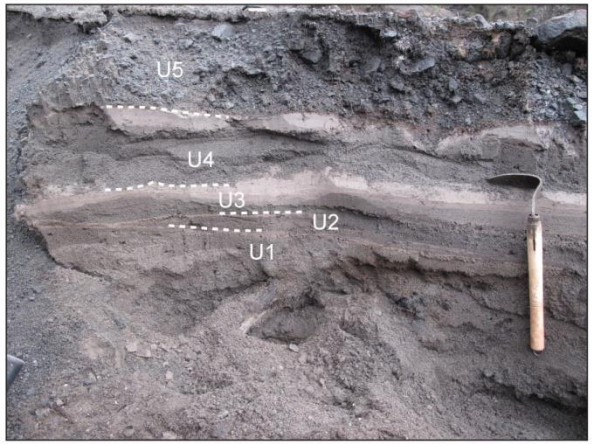

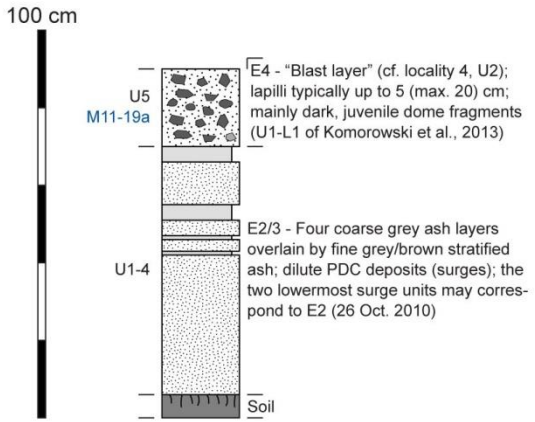

Locality No.:	11	Coordinates (49M):	439581 / 9162599
Locality Description:	S of Gunung Kendil	Samples:	M11-20, M11-21
Waypoint (WP):	240		

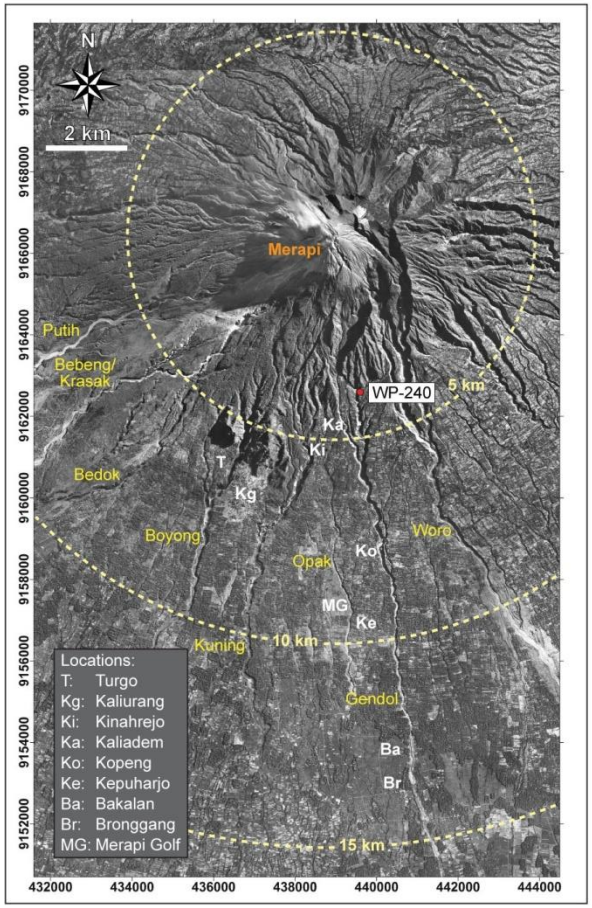

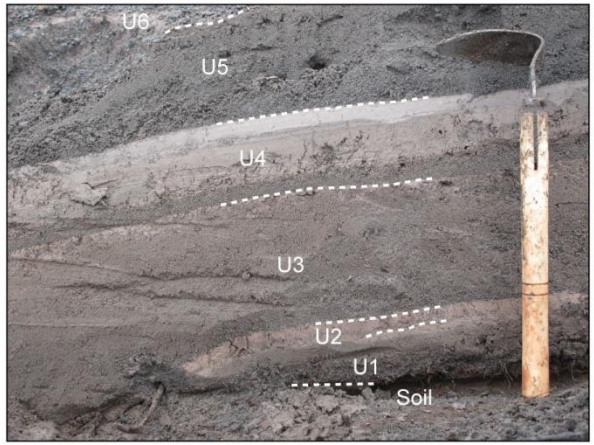

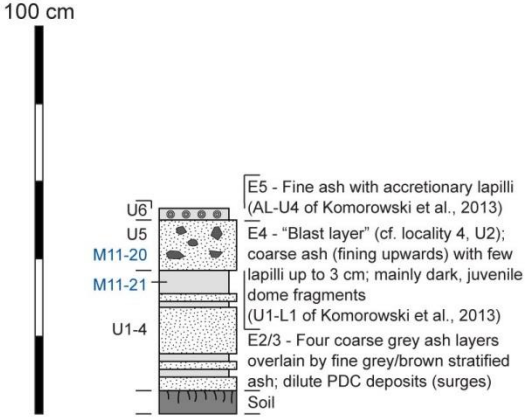

Locality No.:	12	Coordinates (49M):	440269 / 9163011
Locality Description:	W edge of Kali Woro	Samples:	M11-24
Waypoint (WP):	242		

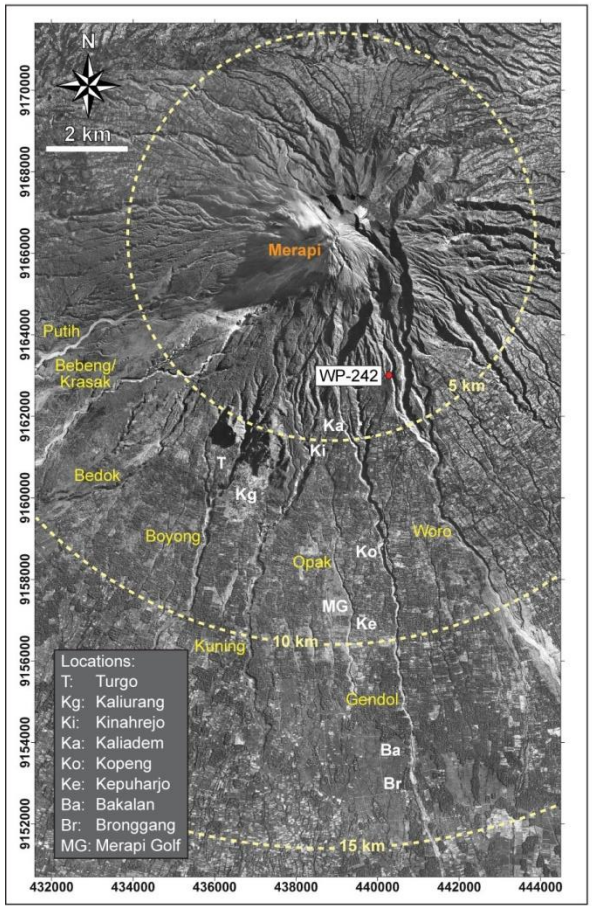

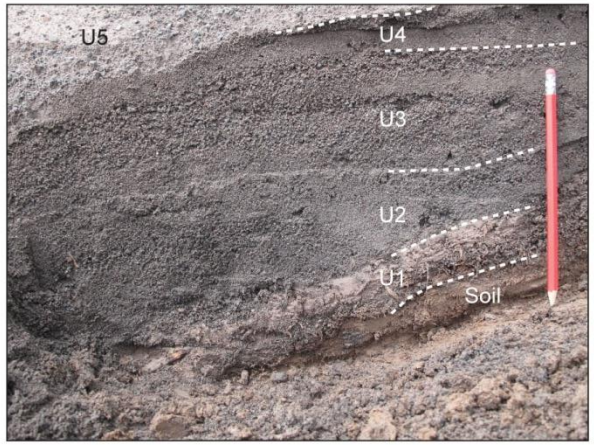

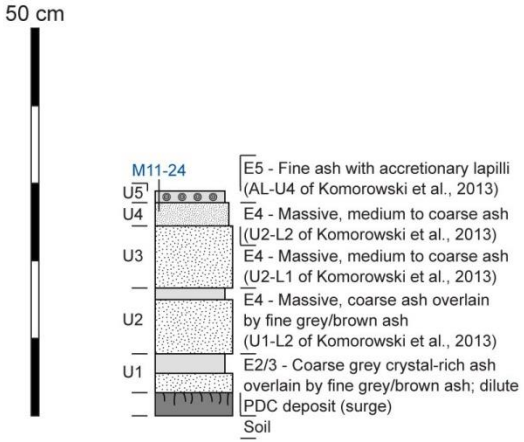

Locality No.:	13	Coordinates (49M):	440487 / 9157739
Locality Description:	Kali Gendol - E Interfluve	Samples:	M11-26a,
Waypoint (WP):	244		M11-27-1/2/3/4/5/6

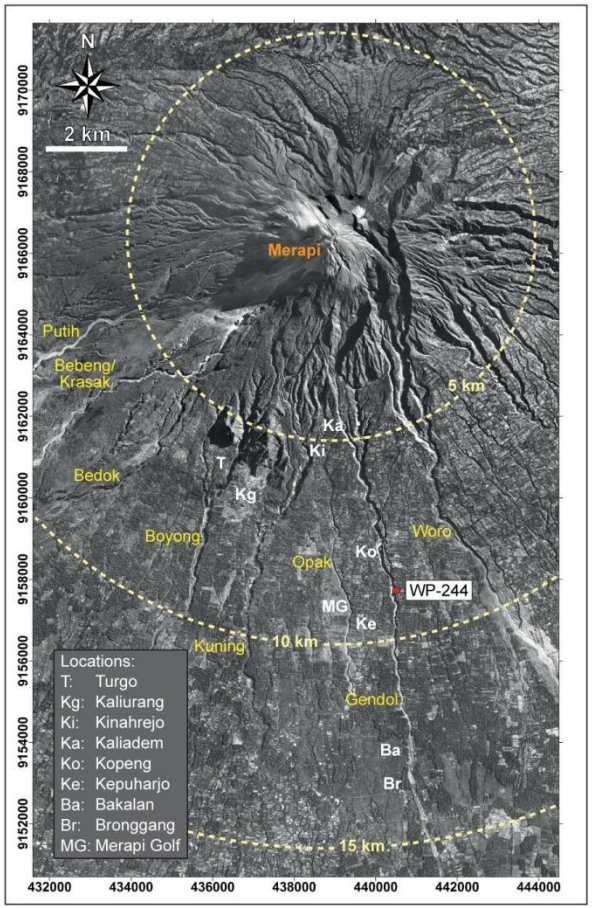

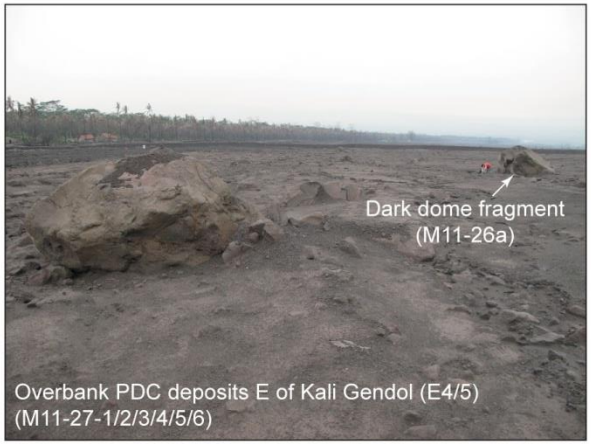

Overbank PDC deposits E of Kali Gendol (E4/5)
(M11-27-1/2/3/4/5/6)

Locality No.:	14	Coordinates (49M):	438770 / 9163168
Locality Description:	Ridges N of Kinahrejo	Samples:	M11-28a, M11-28b
Waypoint (WP):	246		

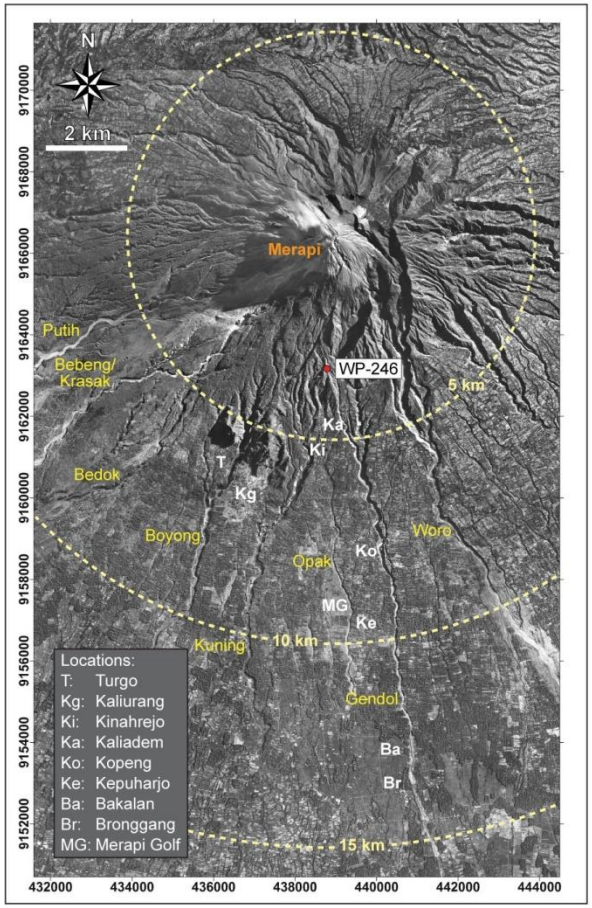

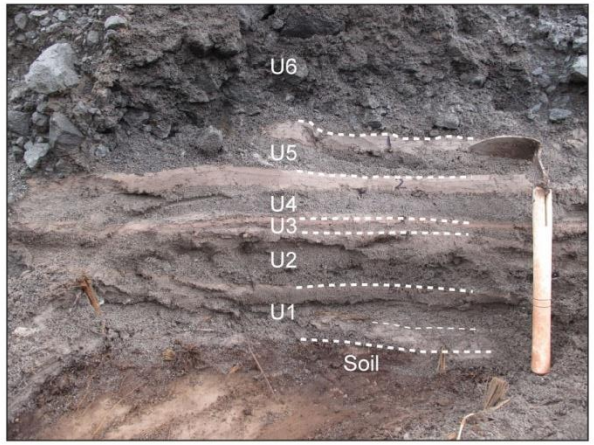

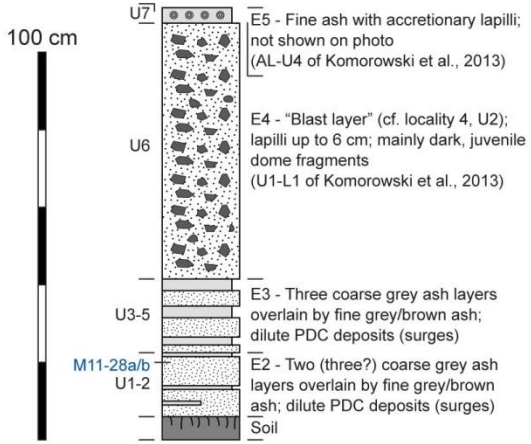

Locality No.:	15	Coordinates (49M):	438536 / 9161945
Locality Description:	Kinahrejo	Samples:	None
Waypoint (WP):	247		

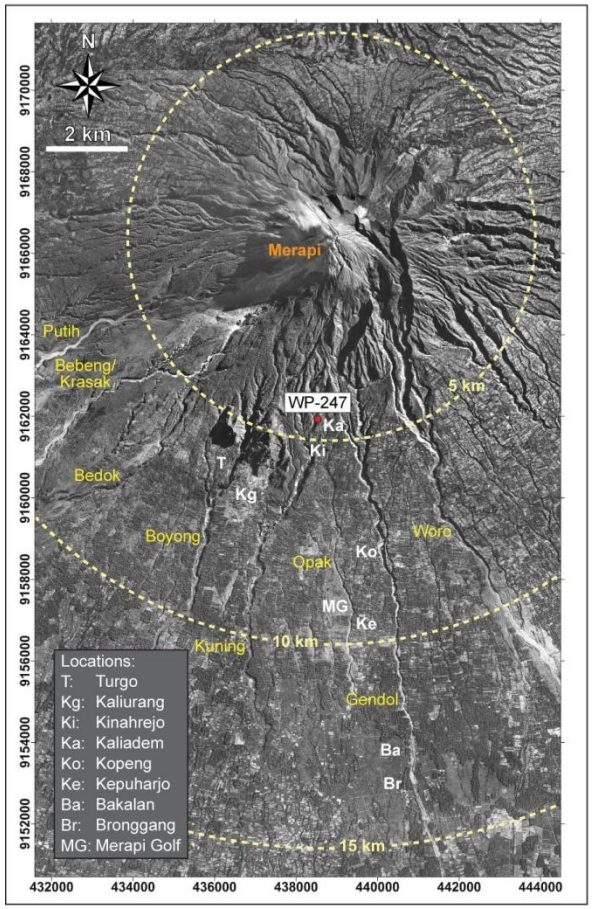

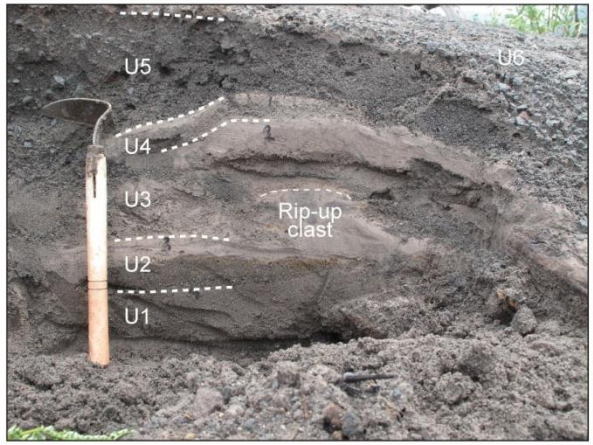

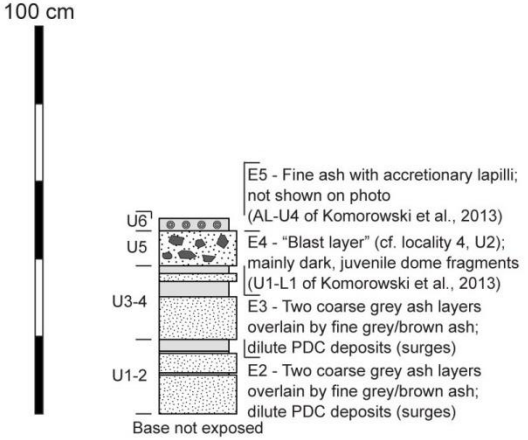

Locality No.:	16	Coordinates (49M):	438889 / 9161759
Locality Description:	Kaliadem Interfluve	Samples:	M11-80
Waypoint (WP):	275		

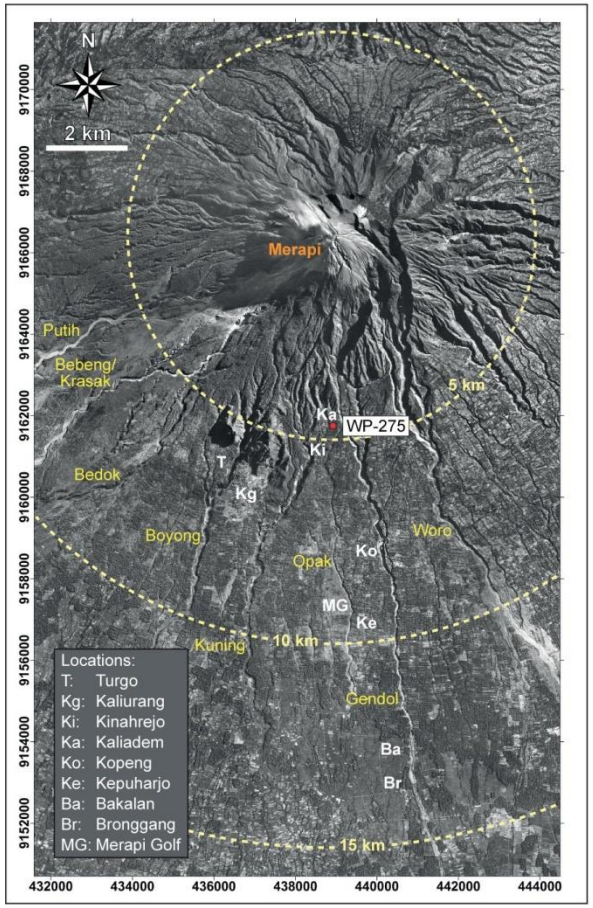

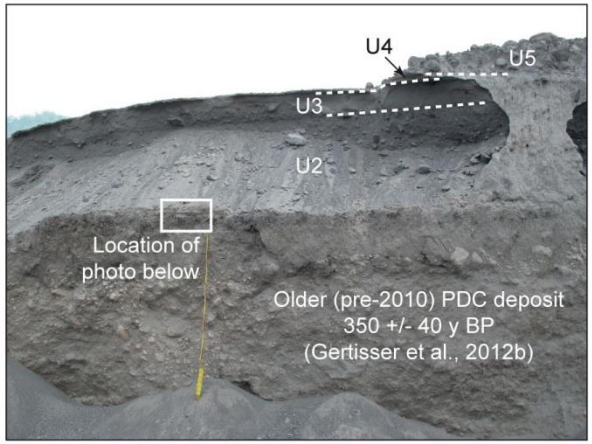

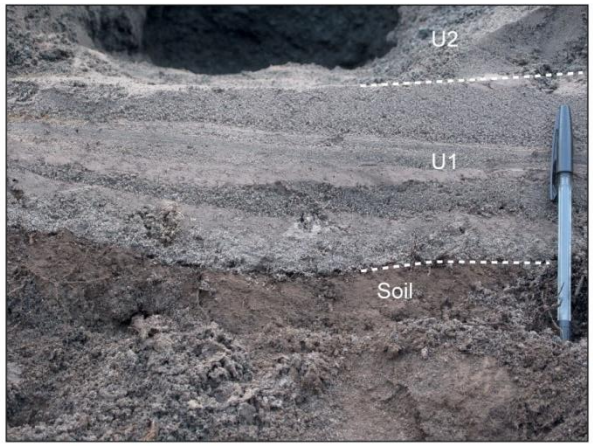

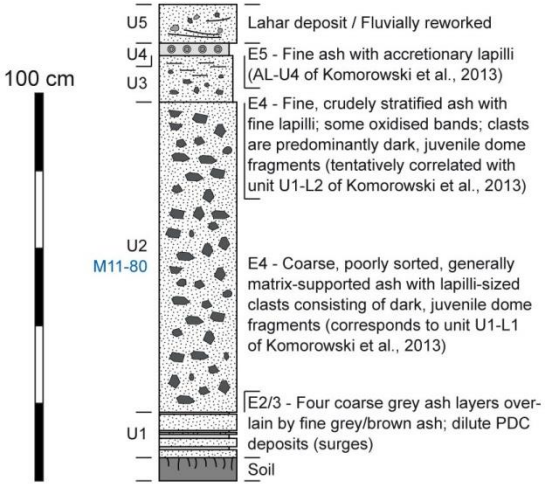

Locality No.:	17	Coordinates (49M):	439121 / 9162001 (278),
Locality Description:	Kaliadem Interfluve		439201 / 9161731 (279)
Waypoint (WP):	278 & 279	Samples:	M11-33 (278), M11-34 (279)

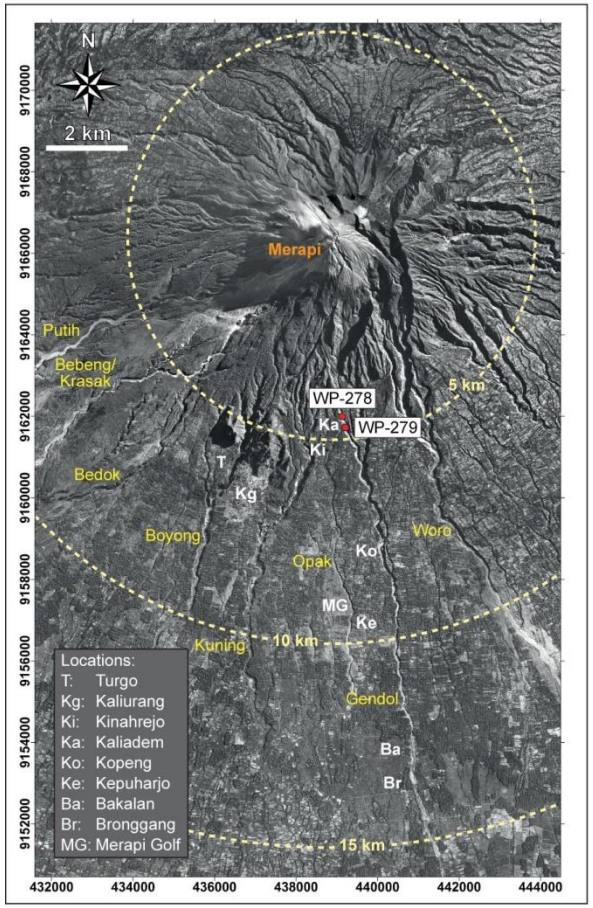


E6 scattered white pumice clasts on E6 scoria-flow surface (M11-33; M11-34)

Locality No.:	18	Coordinates (49M):	439511 / 9161406
Locality Description:	Between Kali Gendol 1 & 2	Samples:	None
Waypoint (WP):	280		

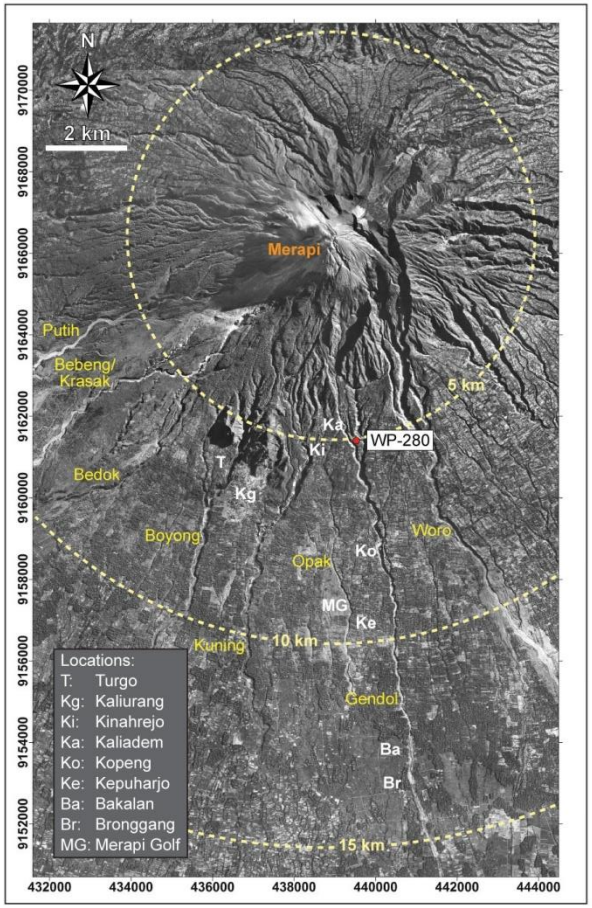

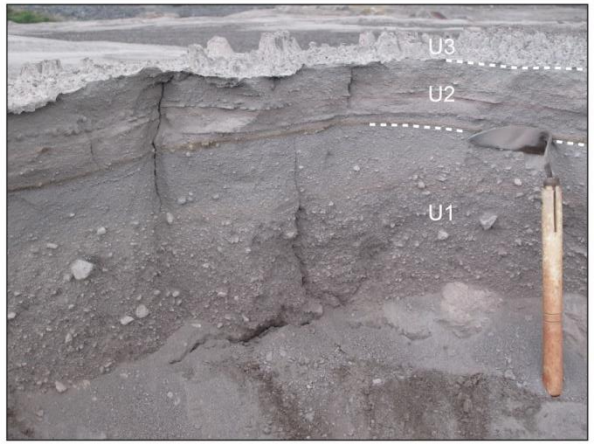

100 cm

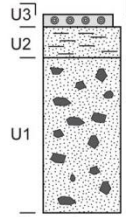

E5 - Fine ash with accretionary lapilli (AL-U4 of Komorowski et al., 2013)

E4 - Coarse, stratified ash with some oxidised bands (tentatively correlated with U1-L2 of Komorowski et al., 2013)

E4 - Coarse, reddish, matrix-supported ash with some lapilli-sized clasts consisting of dark, juvenile dome fragments (tentatively correlated with unit U1-L1 of Komorowski et al., 2013)

Base not exposed

Locality No.:	19	Coordinates (49M):	438652 / 9161101
Locality Description:	Kinahrejo - Near Mosque	Samples:	None
Waypoint (WP):	281		

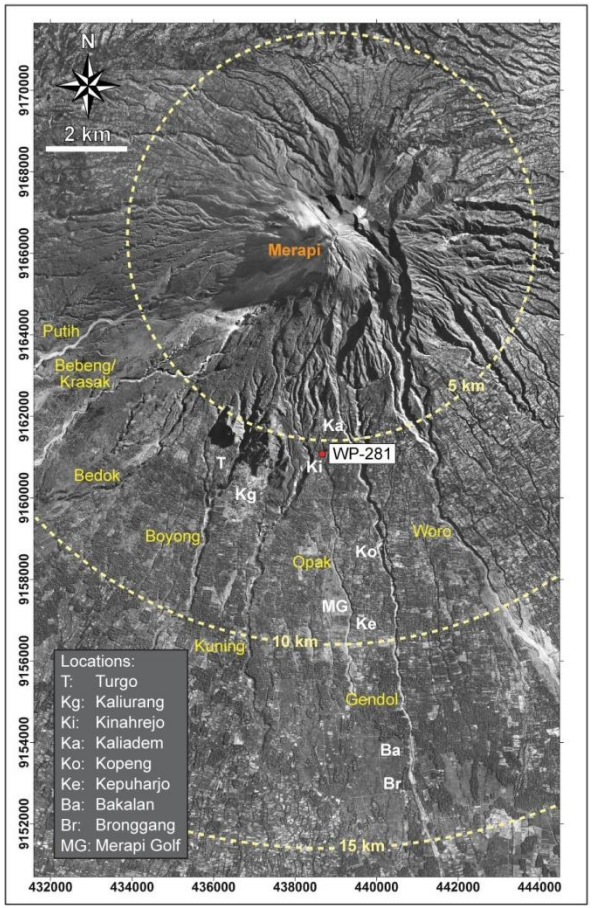

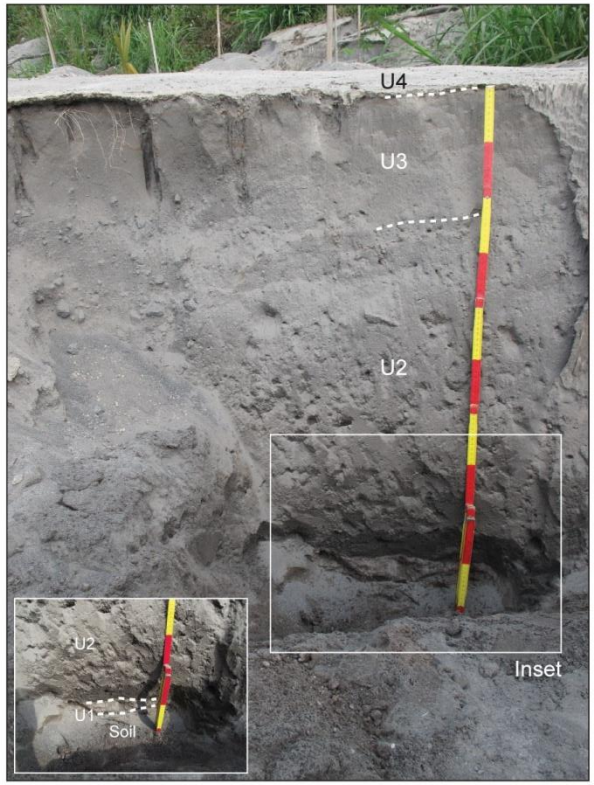

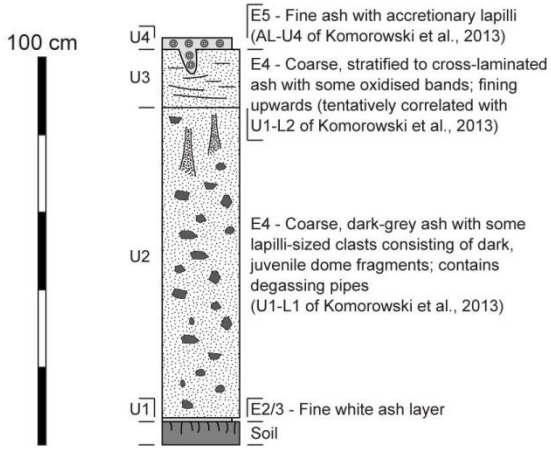

Locality No.:	20	Coordinates (49M):	439647 / 9160440
Locality Description:	Kali Gendol S of Kaliadem	Samples:	M11-87
Waypoint (WP):	285		

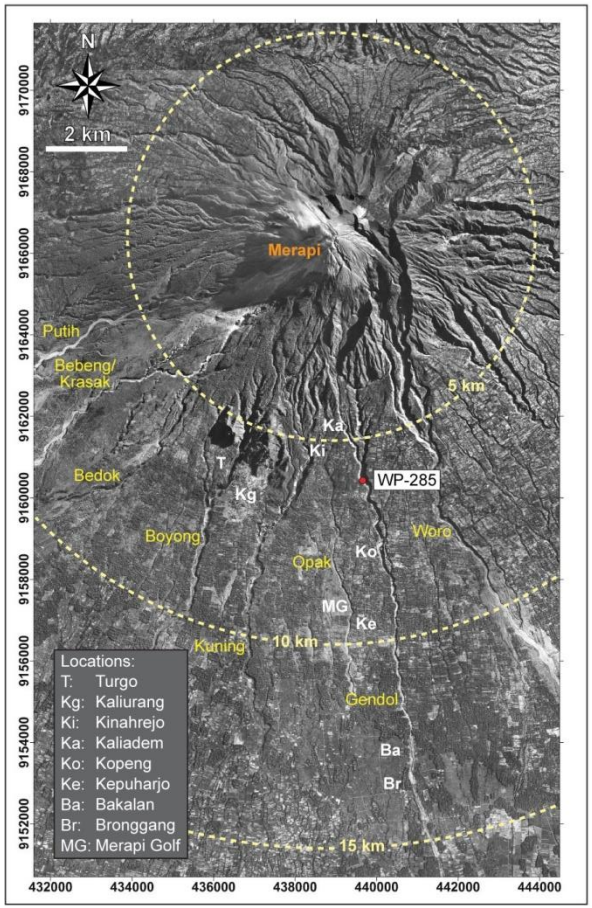

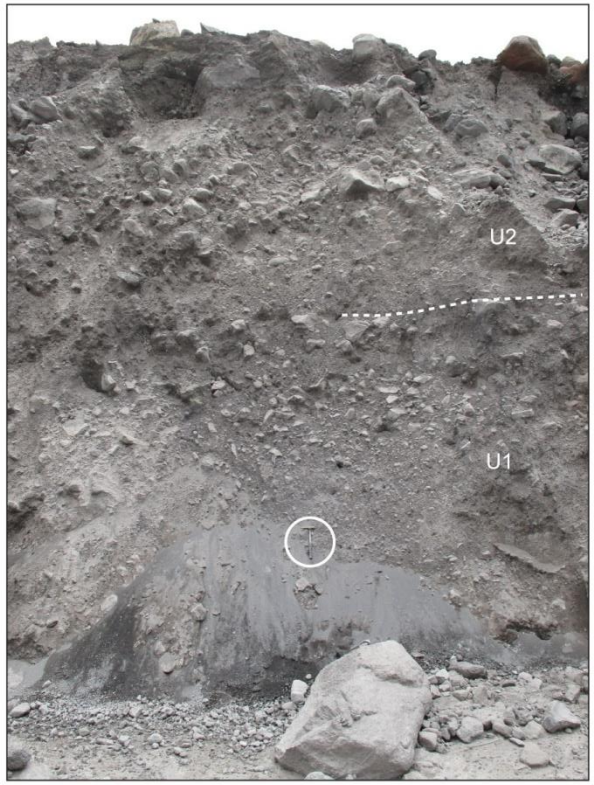

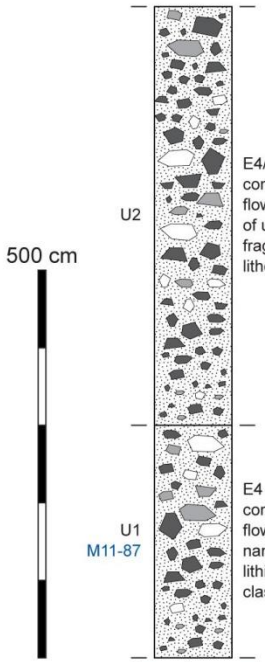

E4/5 - Massive, poorly sorted valley confined PDC deposit (block-and-ash flow deposit); coarse clast train in middle of unit; predominantly dark, juvenile dome fragments; some lithics of various lithologies; ~ 540 cm thick

E4 - Massive, poorly sorted valley confined PDC deposit (block-and-ash flow deposit); reversely graded; predominantly dark, juvenile dome fragments; lithic-poor (mainly hydrothermally altered clasts); ~ 300 cm thick

Locality No.:	21	Coordinates (49M):	440127 / 9159000
Locality Description:	Kali Gendol near Kopeng	Samples:	None
Waypoint (WP):	288		

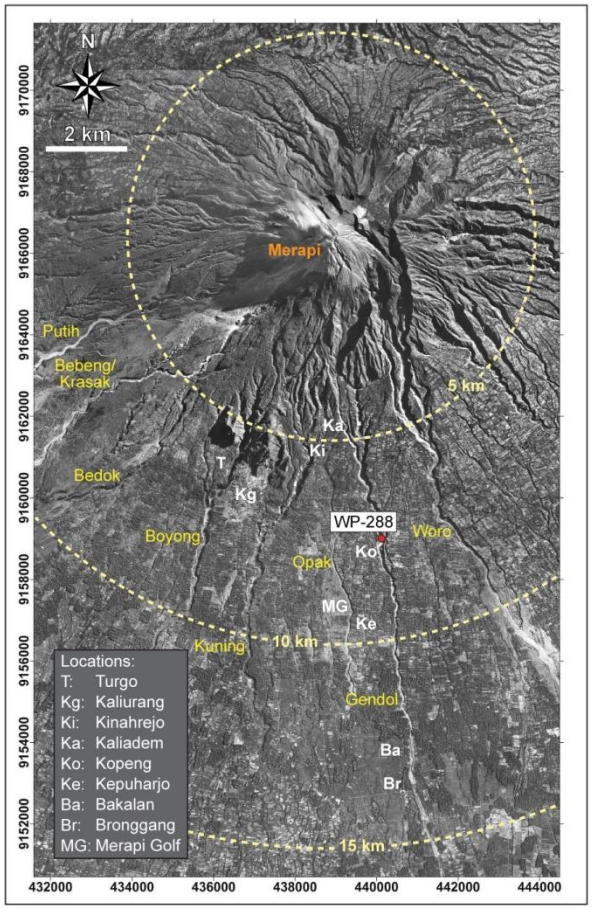

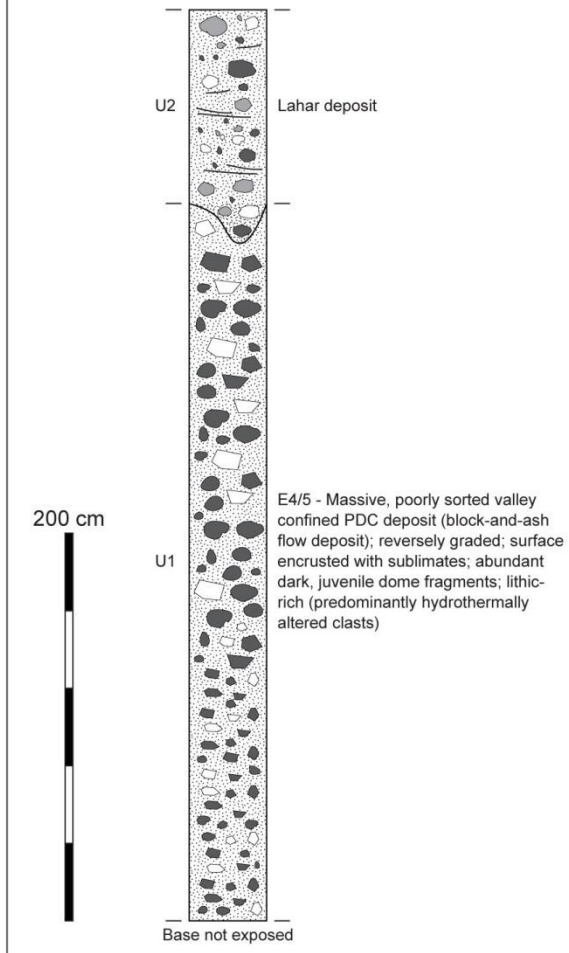

Locality No.:	22	Waypoint (WP):	289
Locality Description:	E Kali Gendol Interfluve Opposite Kopeng	Coordinates (49M): Samples:	440296 / 9159013 M11-46

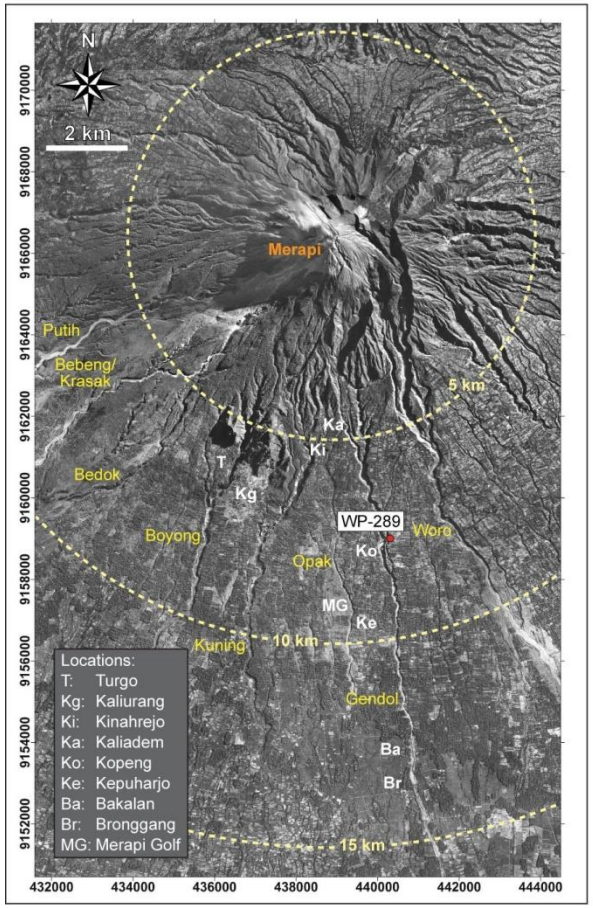

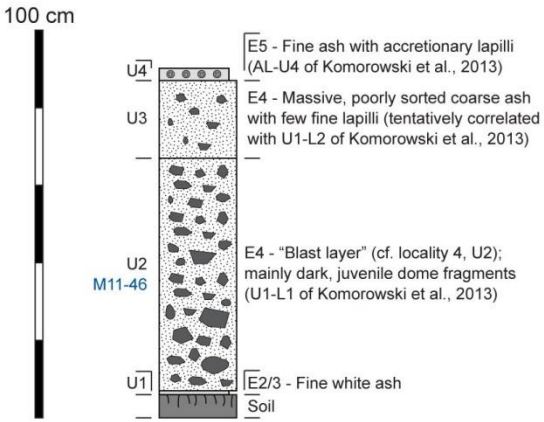

Locality No.:	23	Waypoint (WP):	290 (Sections 1 and 2)
Locality Description:	E Kali Gendol Interfluve Opposite Kopeng	Coordinates (49M):	440404 / 9158889
		Samples:	M11-48

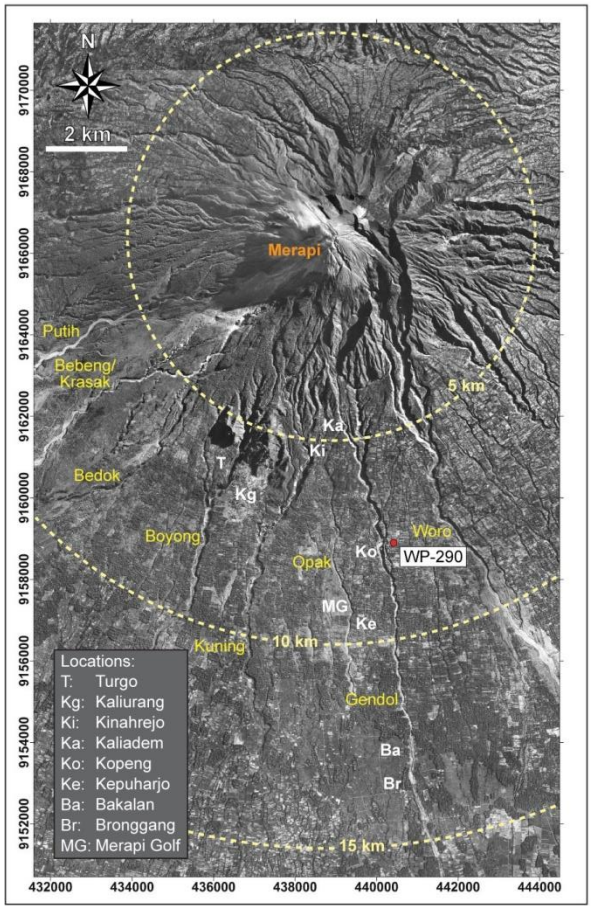

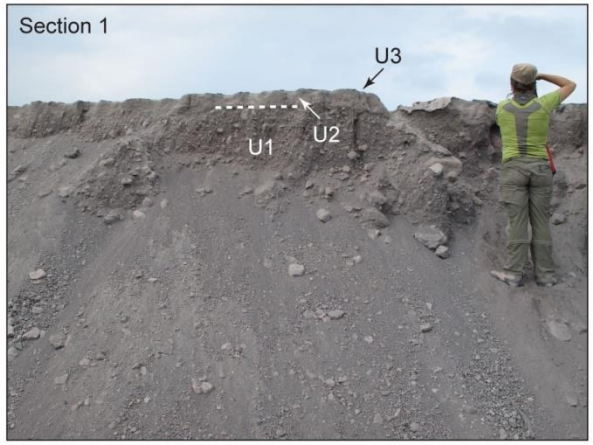

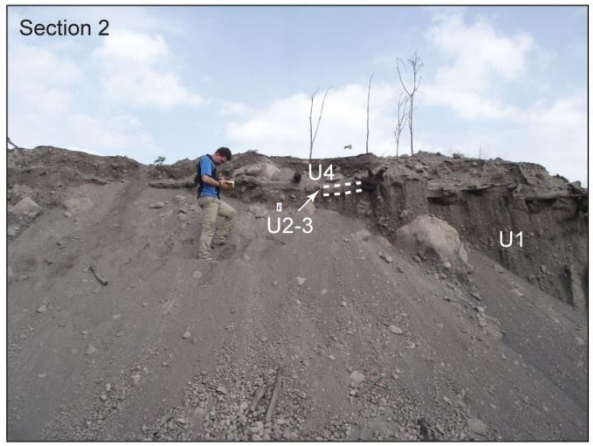

Composite section

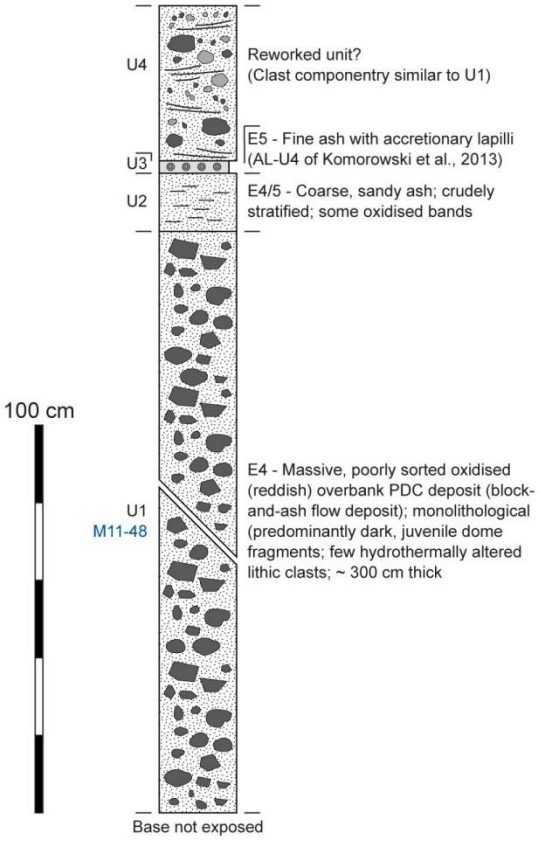

Locality No.:	24	Coordinates (49M):	440033 / 9158748
Locality Description:	Kali Gendol near Kopeng	Samples:	M11-50, M11-51
Waypoint (WP):	291		

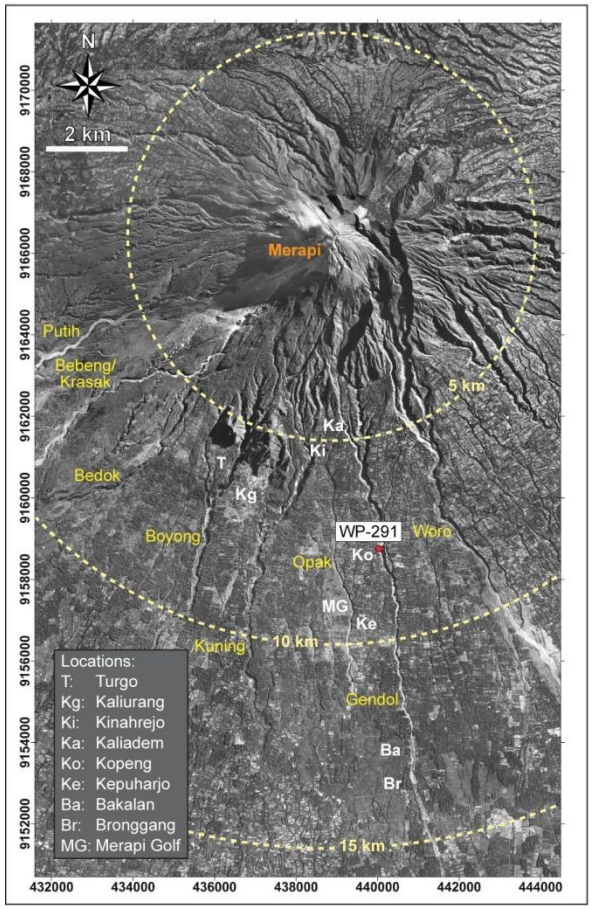

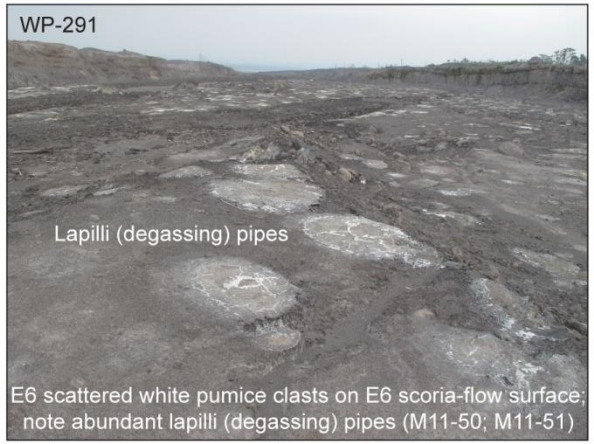

E6 scattered white pumice clasts on E6 scoria-flow surface; note abundant lapilli (degassing) pipes (M11-50; M11-51)

Locality No.:	25	Coordinates (49M):	440173 / 9158419
Locality Description:	Kali Gendol near Kopeng	Samples:	M11-93
Waypoint (WP):	292		

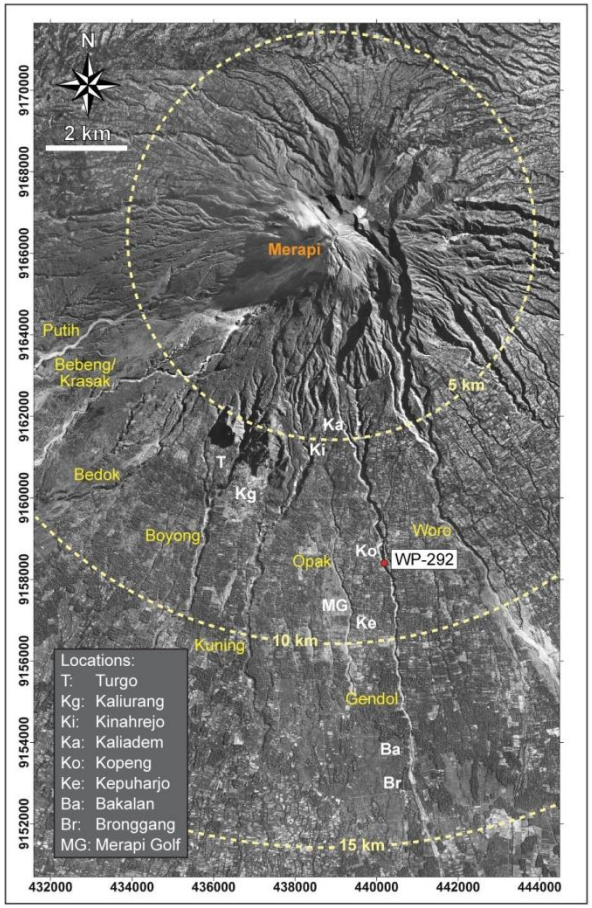

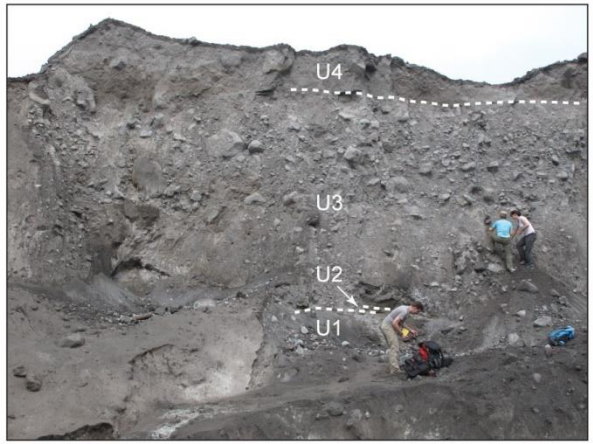

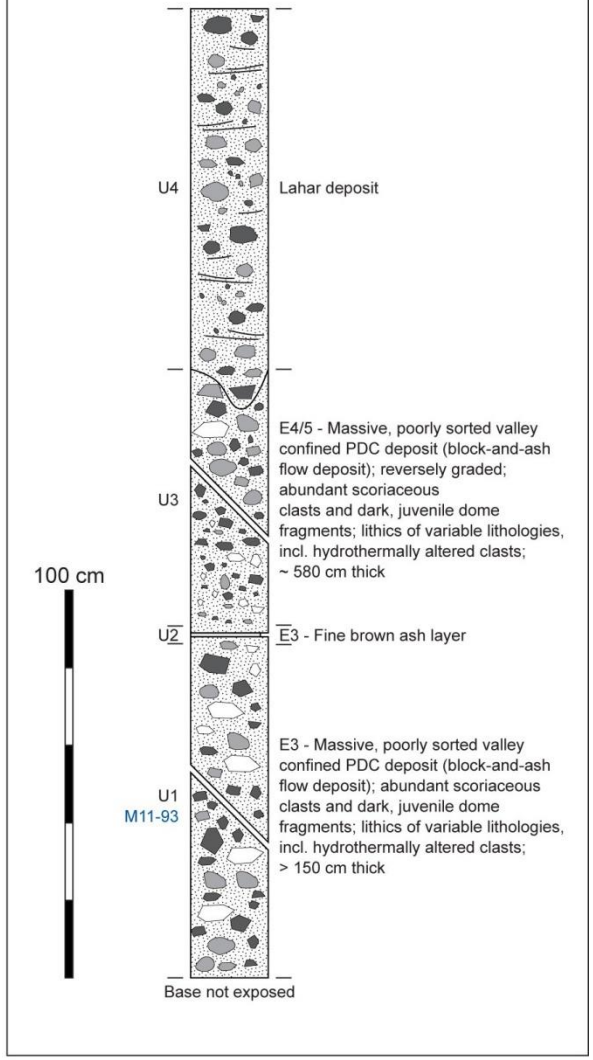

Locality No.:	26	Coordinates (49M):	440383 / 9157883
Locality Description:	Kali Gendol - S of Kopeng	Samples:	M11-53-B1, M11-53-B3, M11-53-B4
Waypoint (WP):	294		

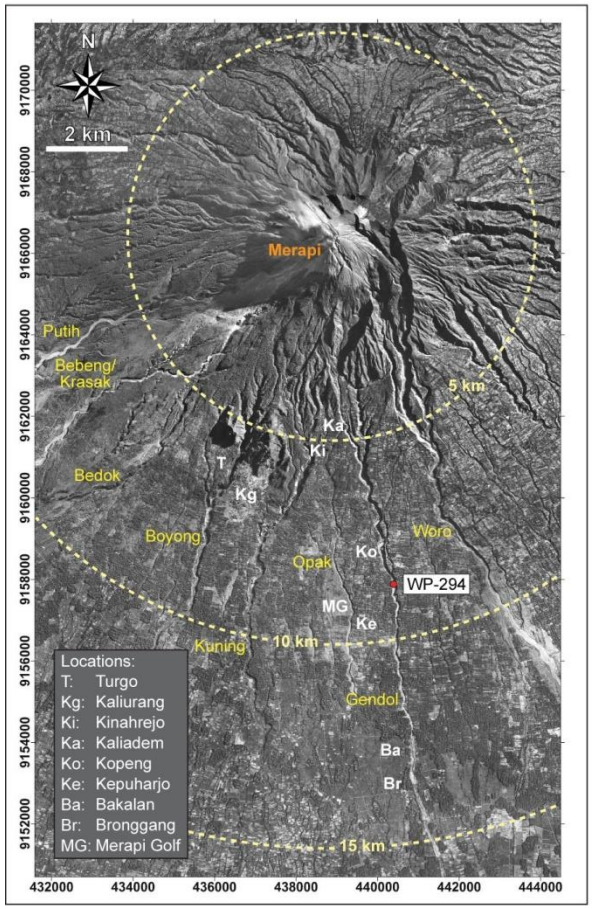

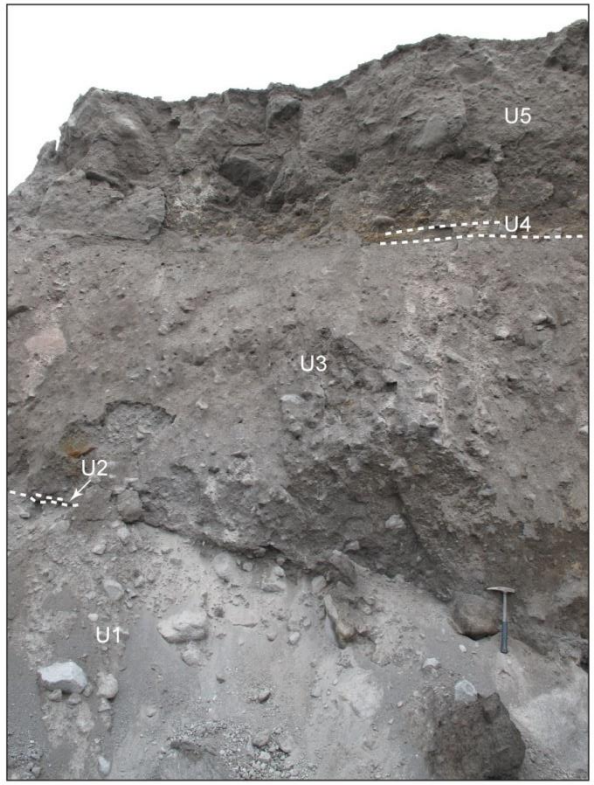

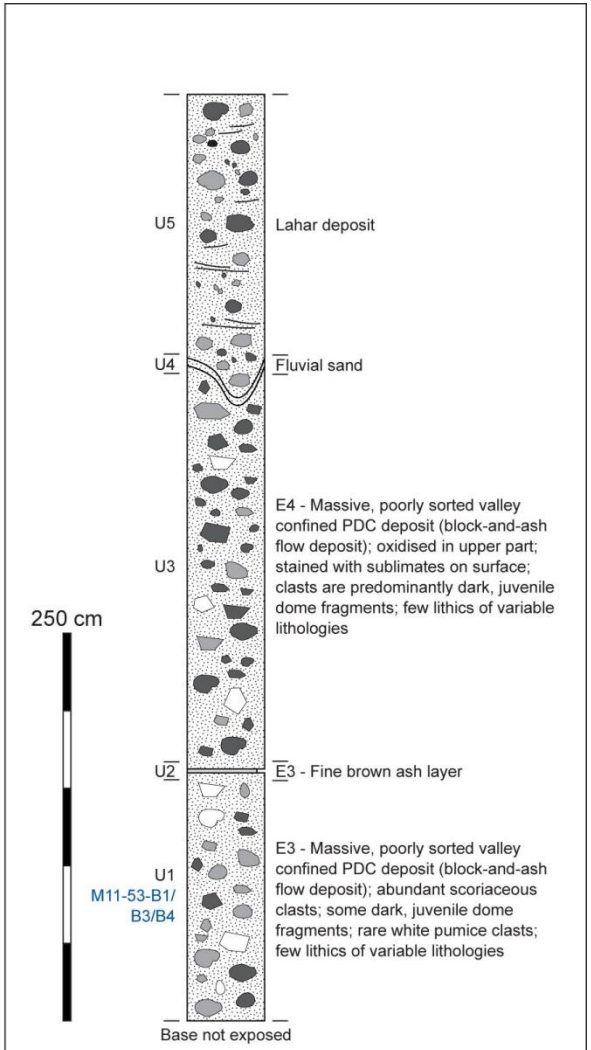

Locality No.:	27	Coordinates (49M):	440506 / 9156842
Locality Description:	Kali Gendol near Kepuharjo	Samples:	M11-54-3
Waypoint (WP):	300		

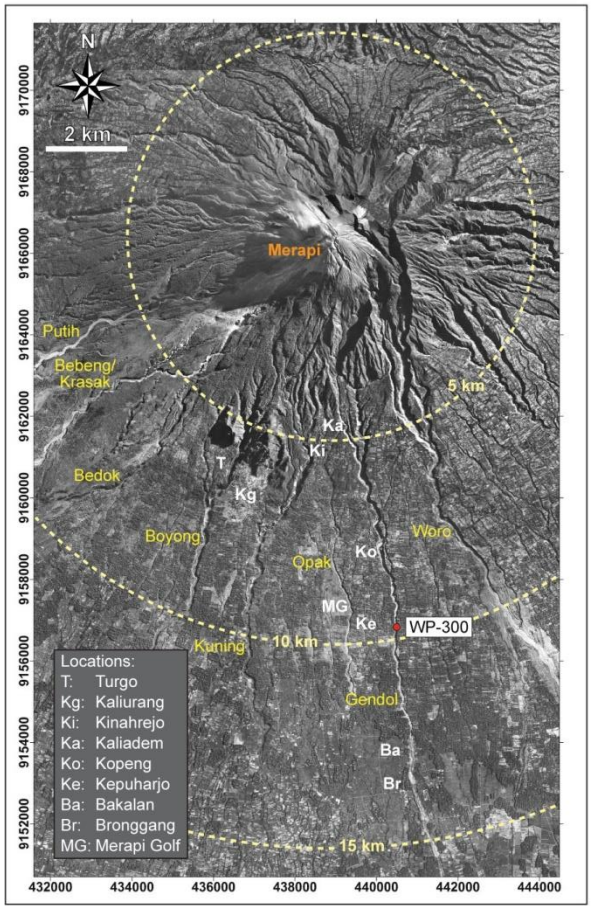

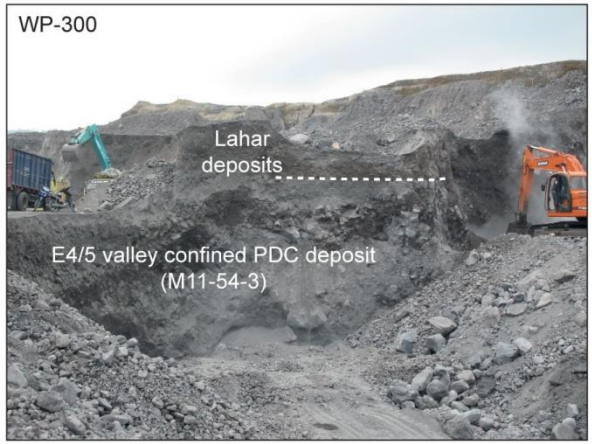

Locality No.:	28	Coordinates (49M):	440541 / 9156432 (301),
Locality Description:	Kali Gendol Interfluves		440690 / 9153657 (308)
Waypoint (WP):	301 & 308	Samples:	M11-55 (301), M11-61 (308)

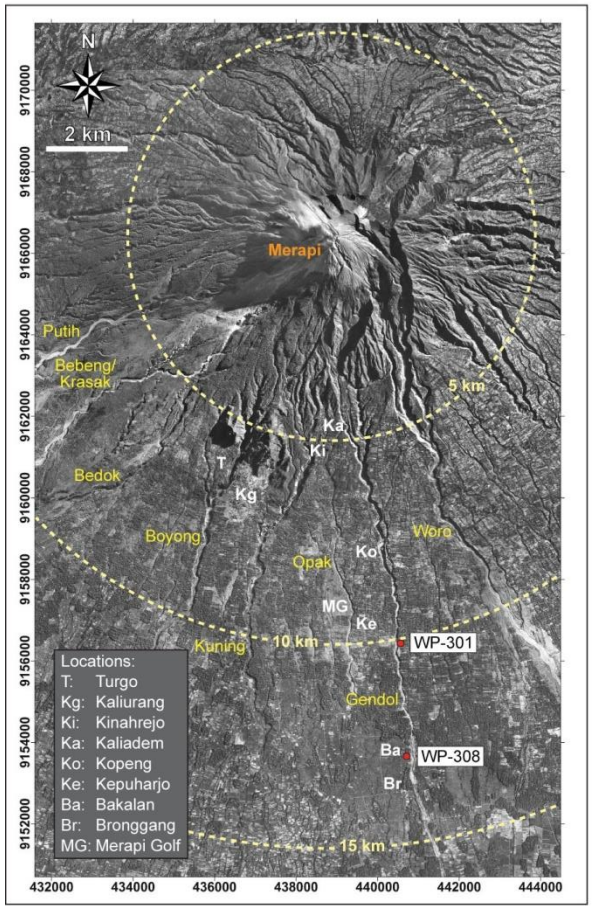

Locality No.:	29	Coordinates (49M):	440577 / 9155501
Locality Description:	Kali Gendol S of Kepuharjo	Samples:	None
Waypoint (WP):	303		

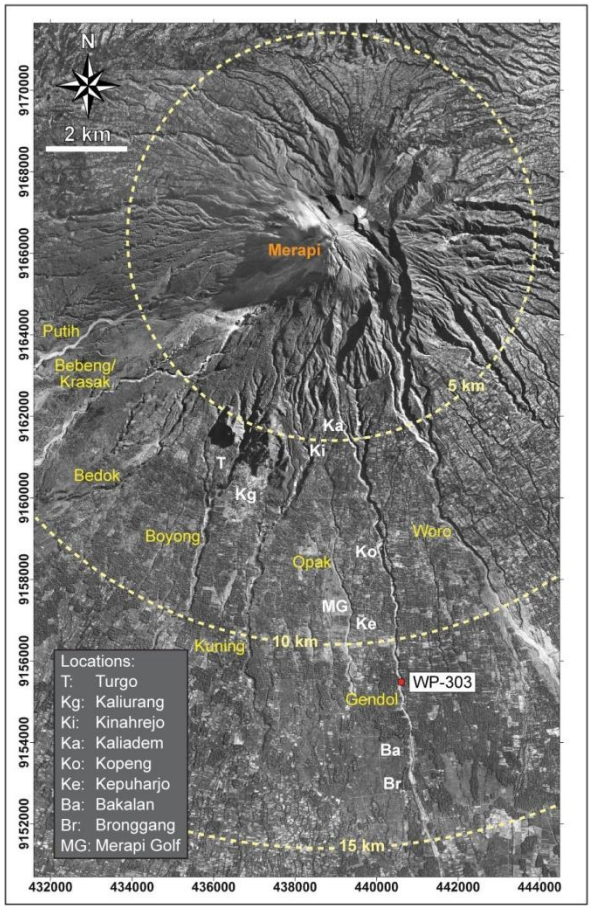

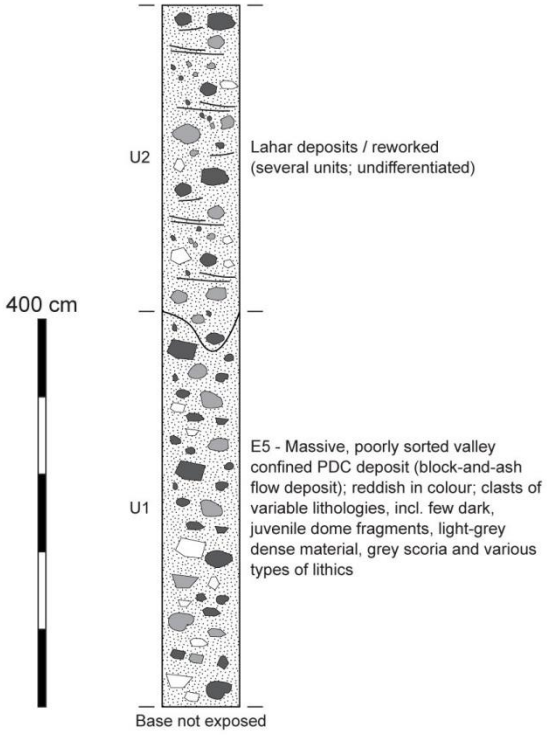

Locality No.:	30	Coordinates (49M):	440601 / 9155134
Locality Description:	Kali Gendol S of Kepuharjo	Samples:	None
Waypoint (WP):	304		

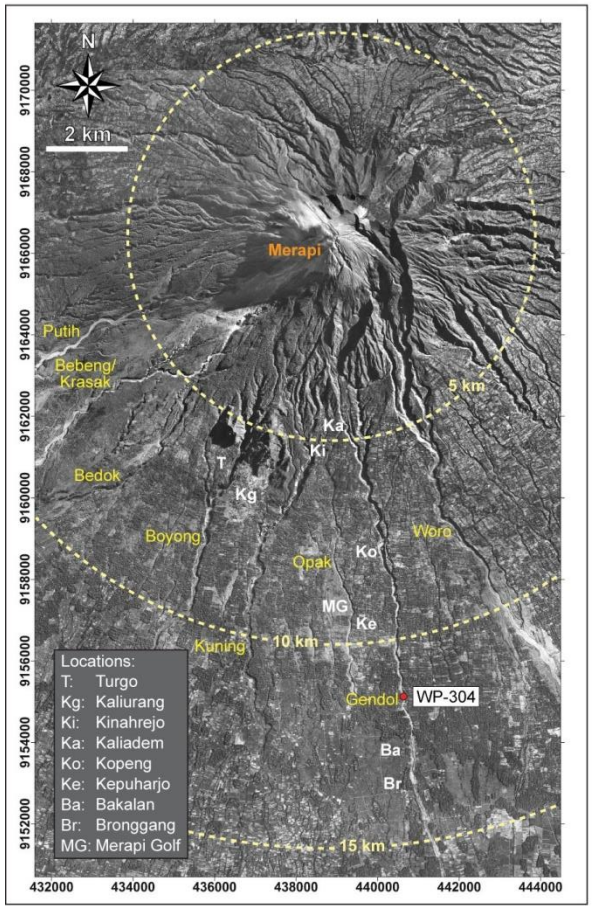

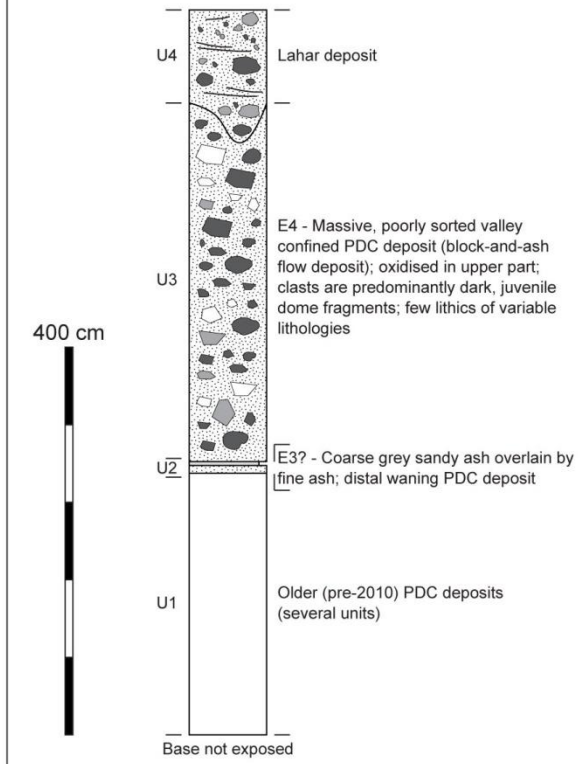

Locality No.:	31	Coordinates (49M):	440864 / 9154042
Locality Description:	Kali Gendol near Bakalan	Samples:	None
Waypoint (WP):	307		

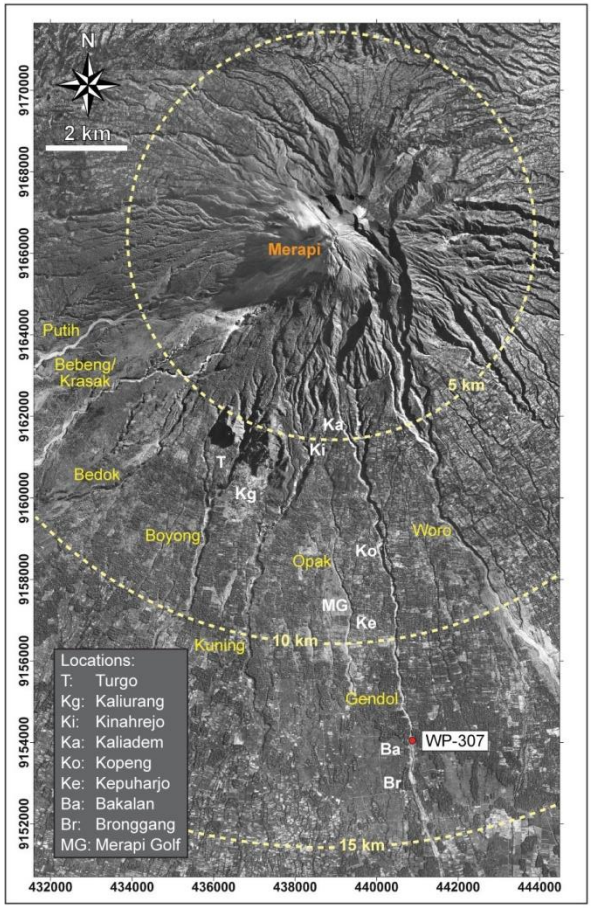

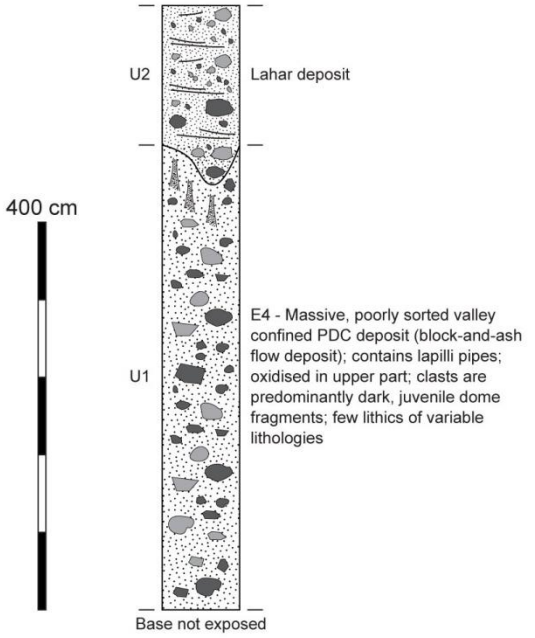

Locality No.:	32	Coordinates (49M):	441124 / 9152105
Locality Description:	Kali Gendol S of Bronggang	Samples:	None
Waypoint (WP):	311		

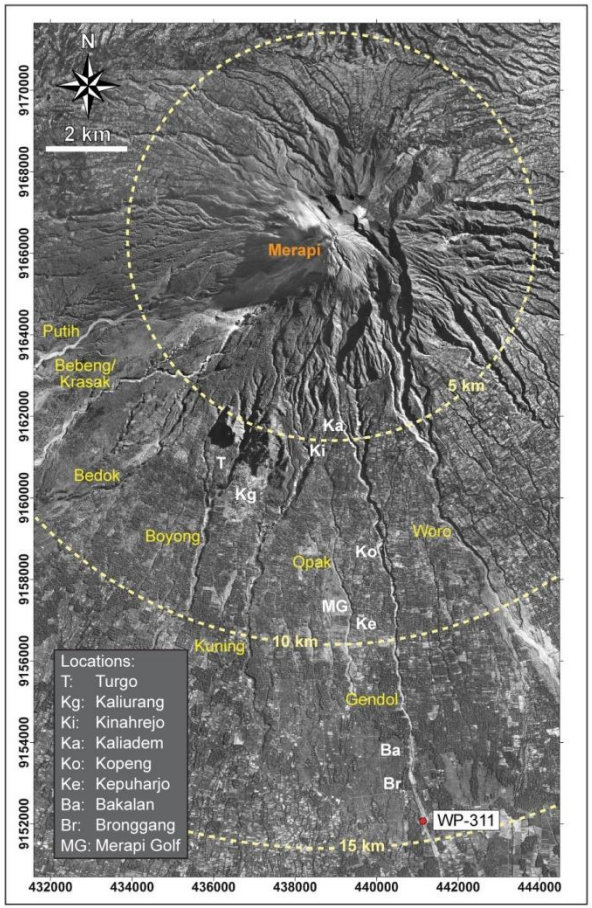

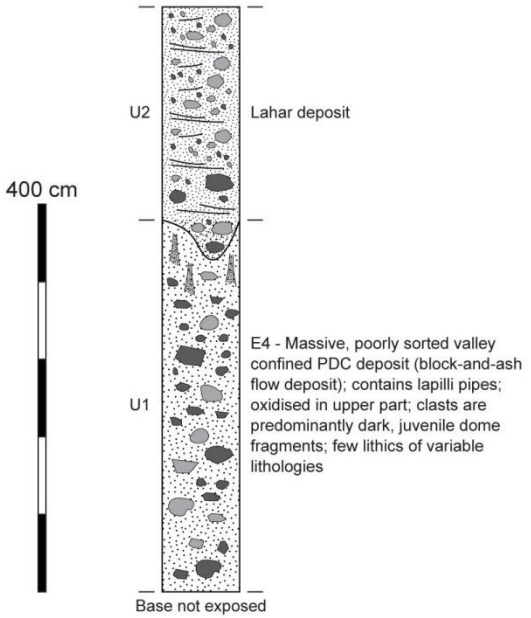

Locality No.:	33	Coordinates (49M):	441409 / 9151320
Locality Description:	Lower Kali Gendol (Max. Runout)	Samples:	M11-65
Waypoint (WP):	314		

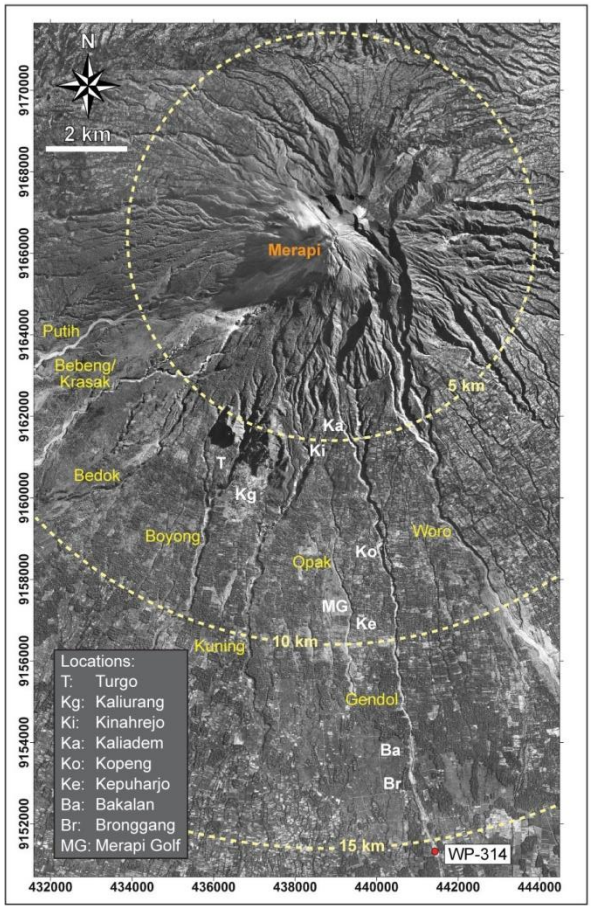

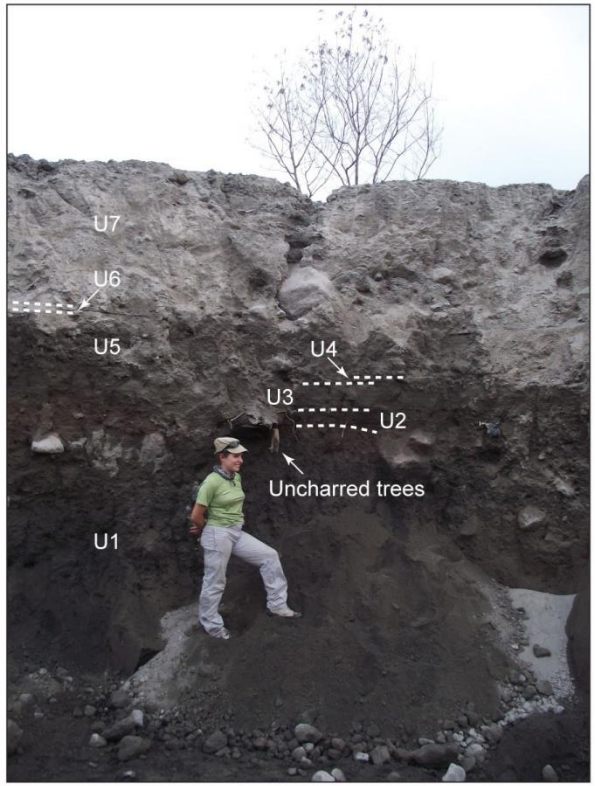

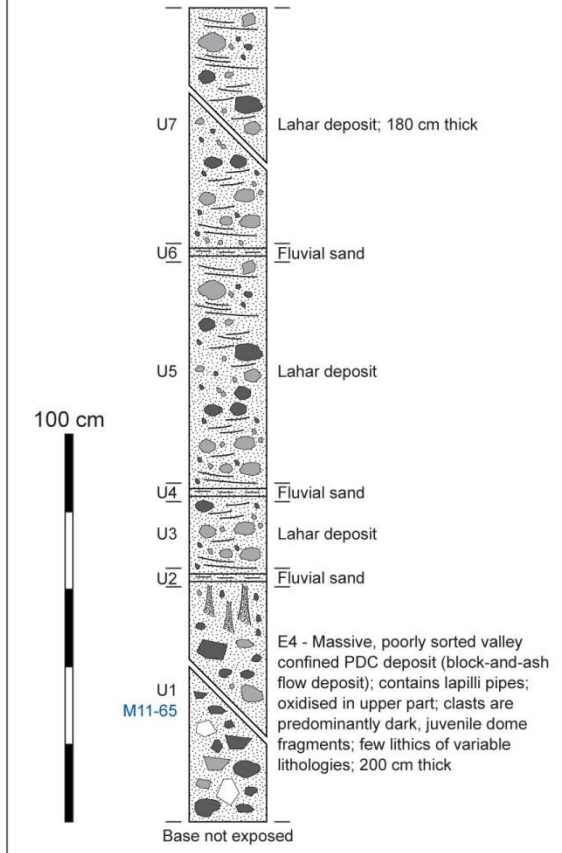

Locality No.:	34	Coordinates (49M):	434355 / 9164610 (317),
Locality Description:	Kali Putih Area		434721 / 9163959 (318)
Waypoint (WP):	317 & 318	Samples:	M11-67a/b (317); M11-68b (318)

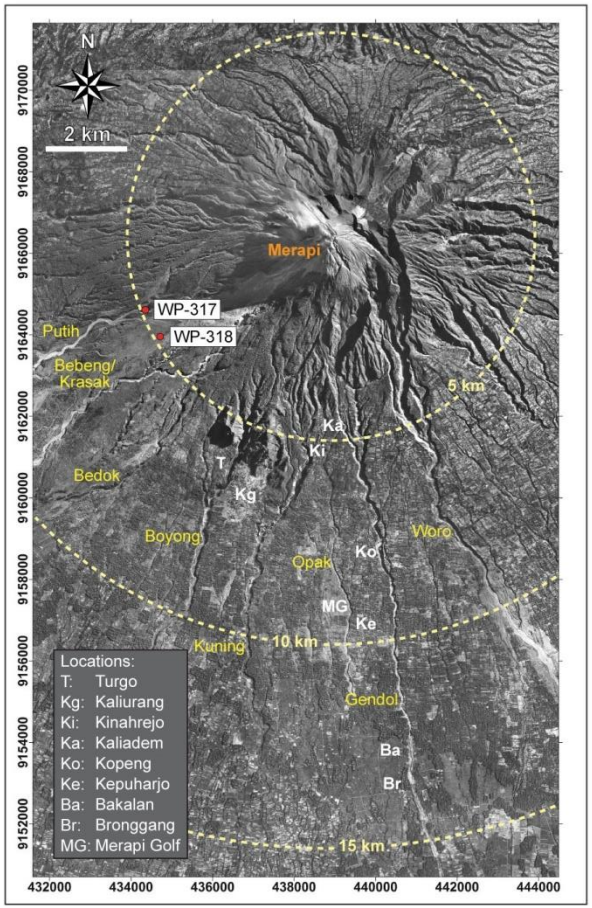

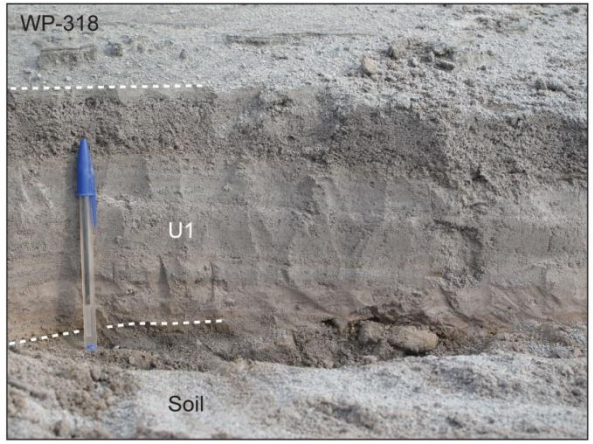

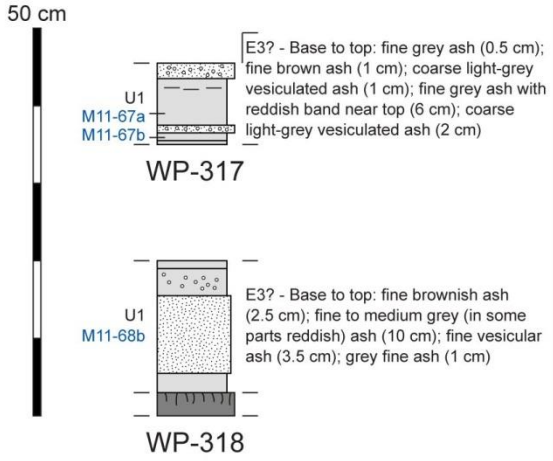

Locality No.:	35	Coordinates (49M):	438791 / 9161111 (321), 438809 / 9161103 (322)
Locality Description:	Kinahrejo - Sabo Dam		
Waypoint (WP):	321 & 322	Samples:	M11-75 (322)

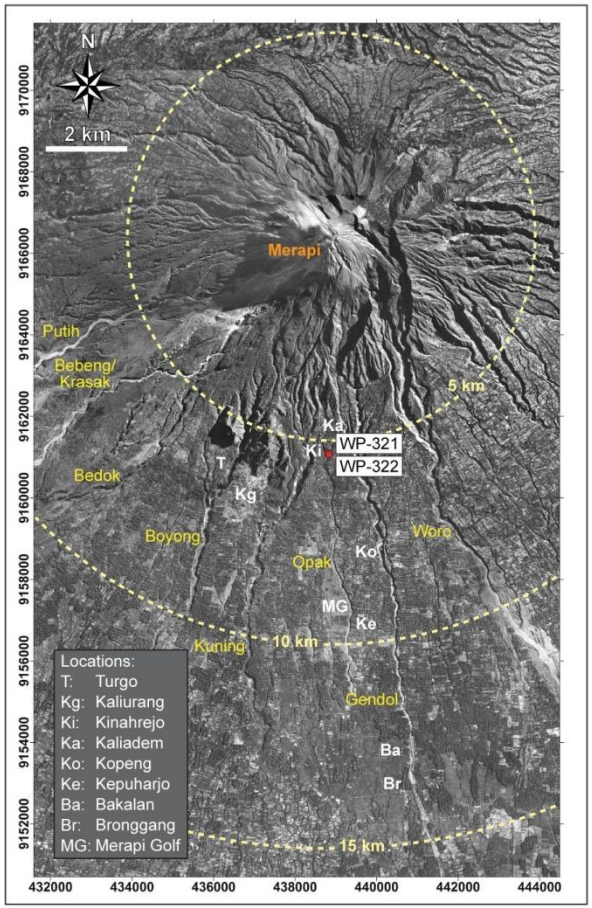

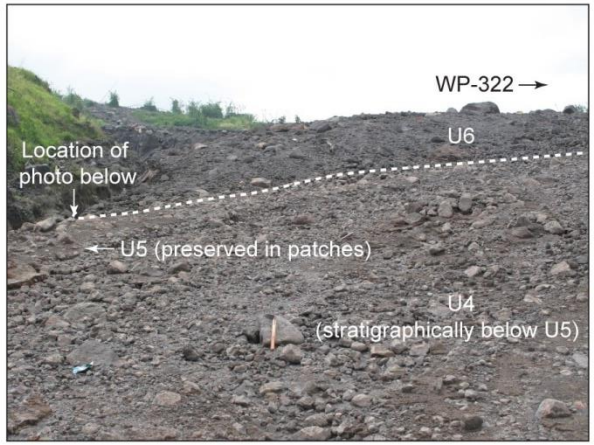

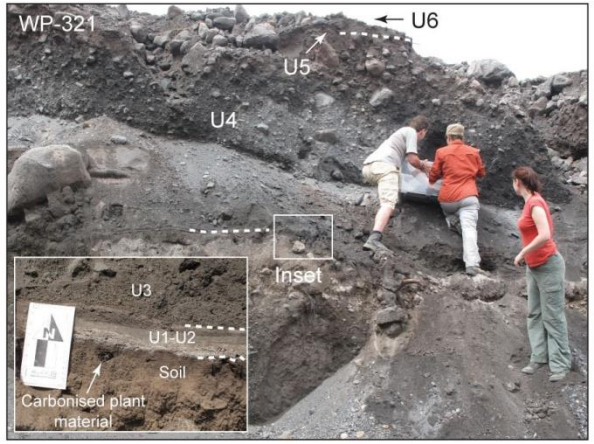

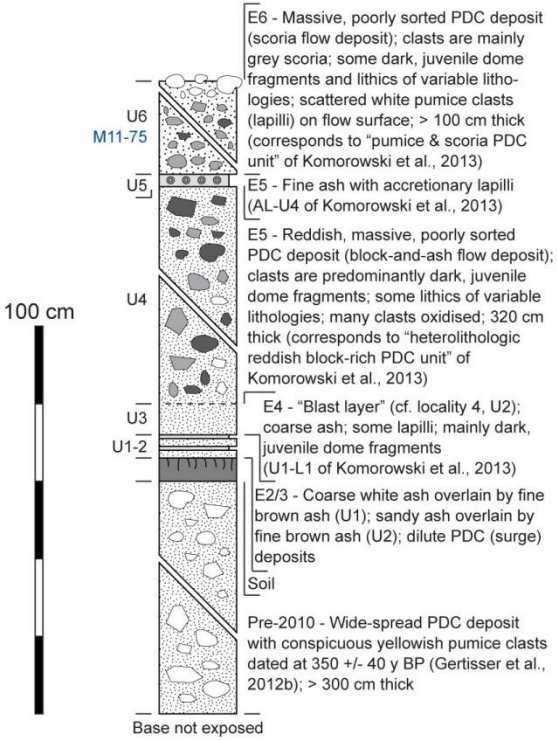

Locality No.:	36	Coordinates (49M):	439822 / 9164922
Locality Description:	Ridge N of Gunung Kendil	Samples:	M11-85
Waypoint (WP):	326		

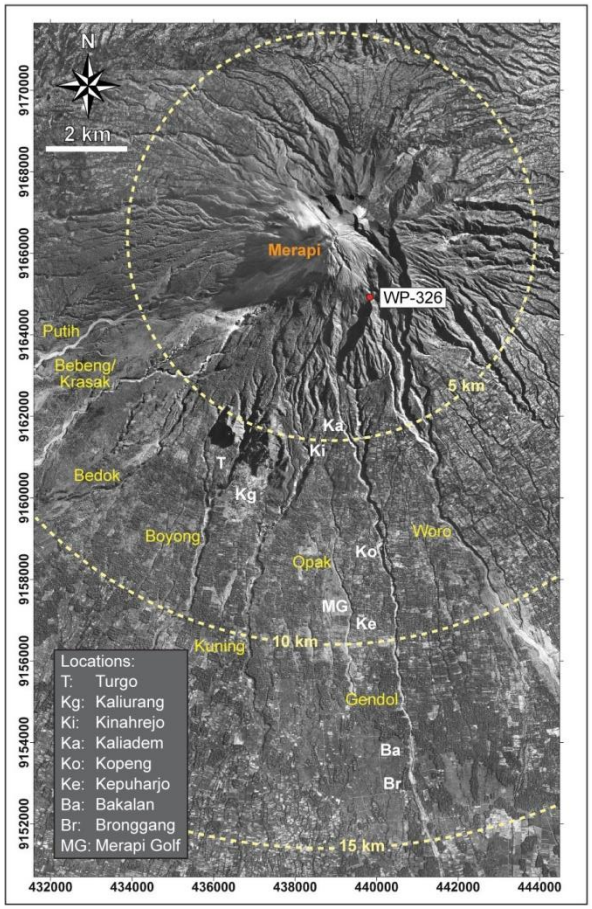

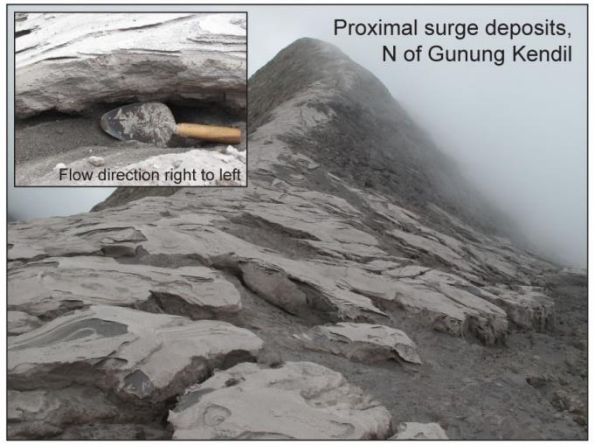

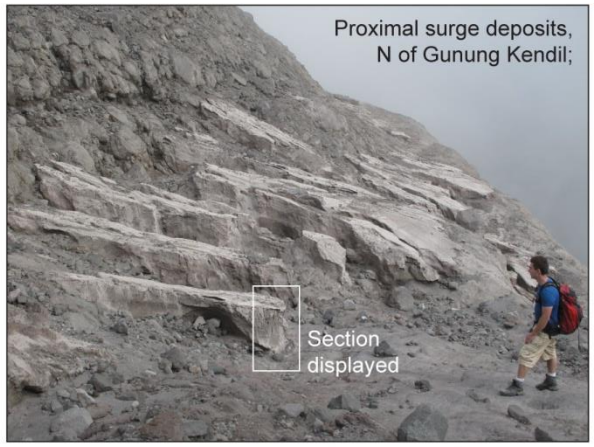

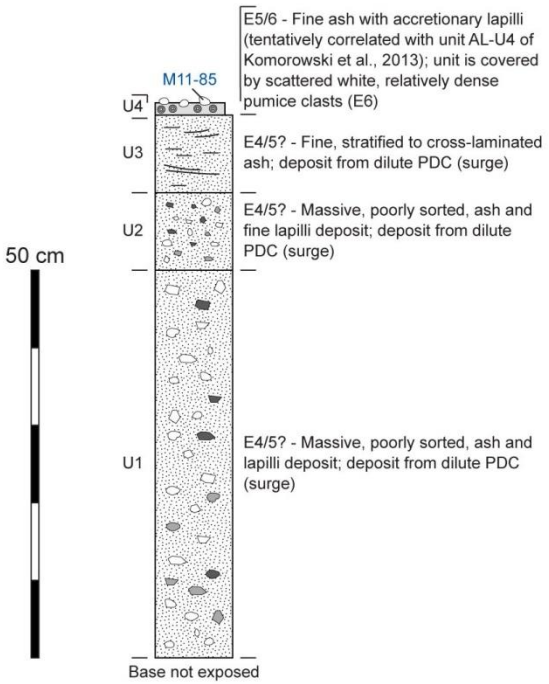

Locality No.:	37	Coordinates (49M):	438781 / 9160527
Locality Description:	Kali Opak	Samples:	M11-95, M11-96
Waypoint (WP):	330		

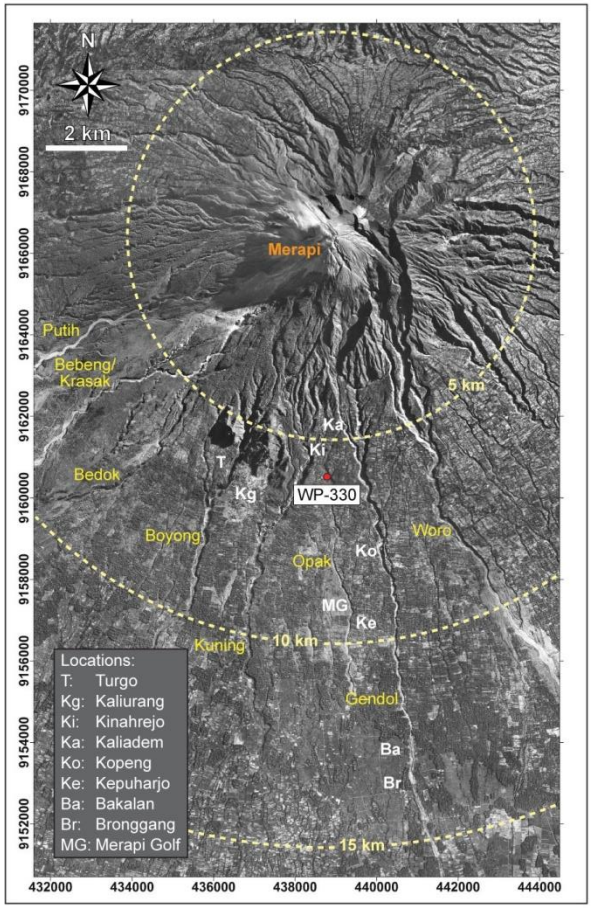

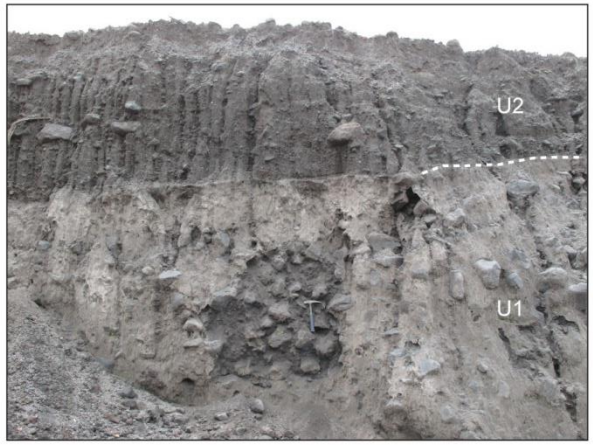

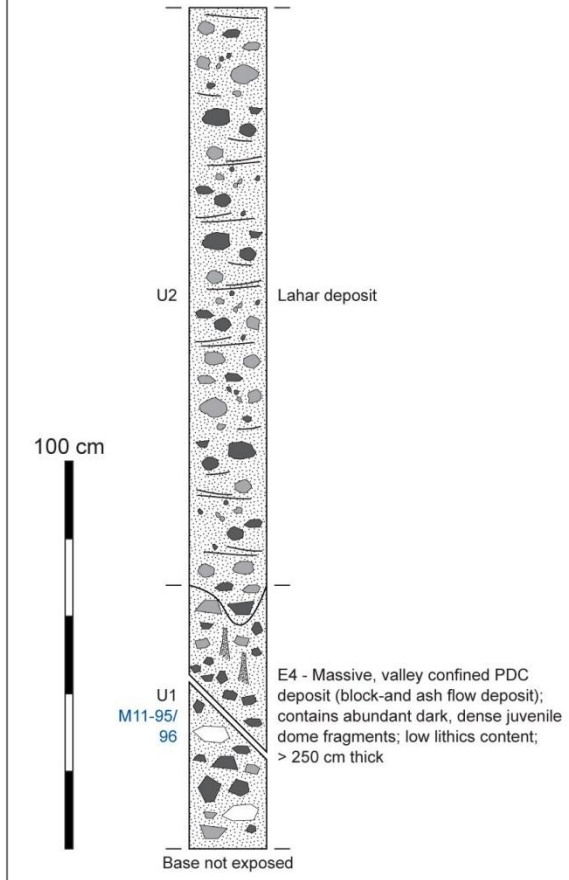

Locality No.:	38	Coordinates (49M):	438740 / 9160546 (331), 438802 / 9160349 (332)
Locality Description:	Kali Opak		
Waypoint (WP):	331 & 332	Samples:	M11-100 (332)

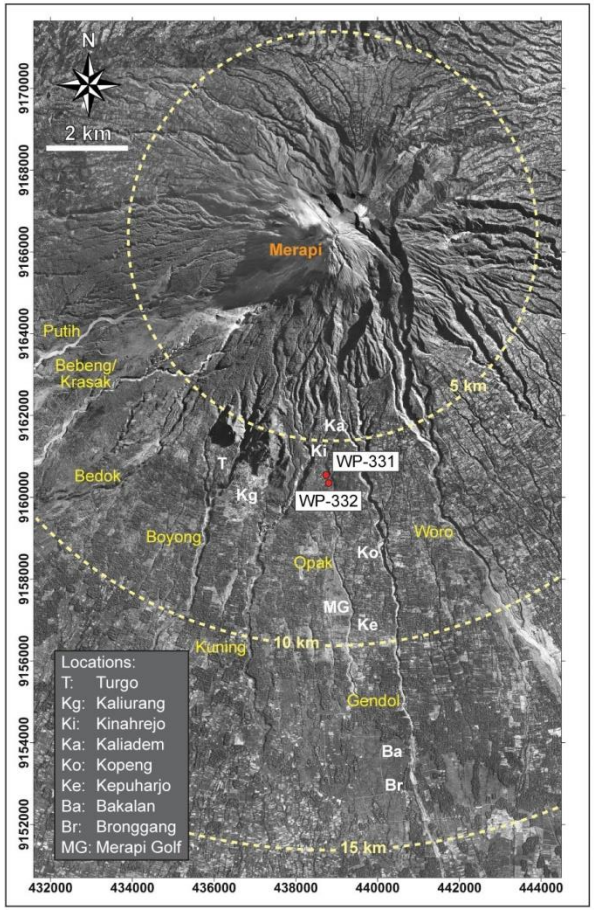

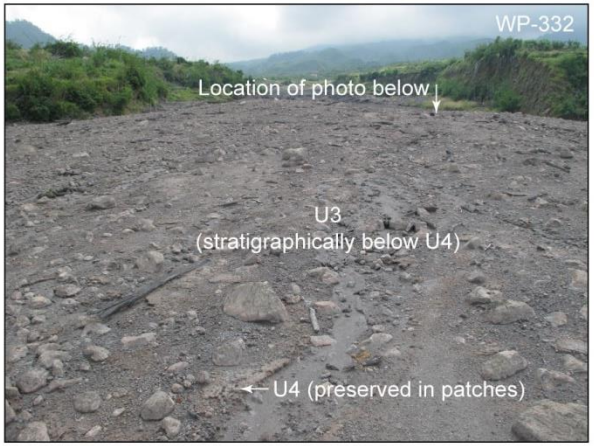

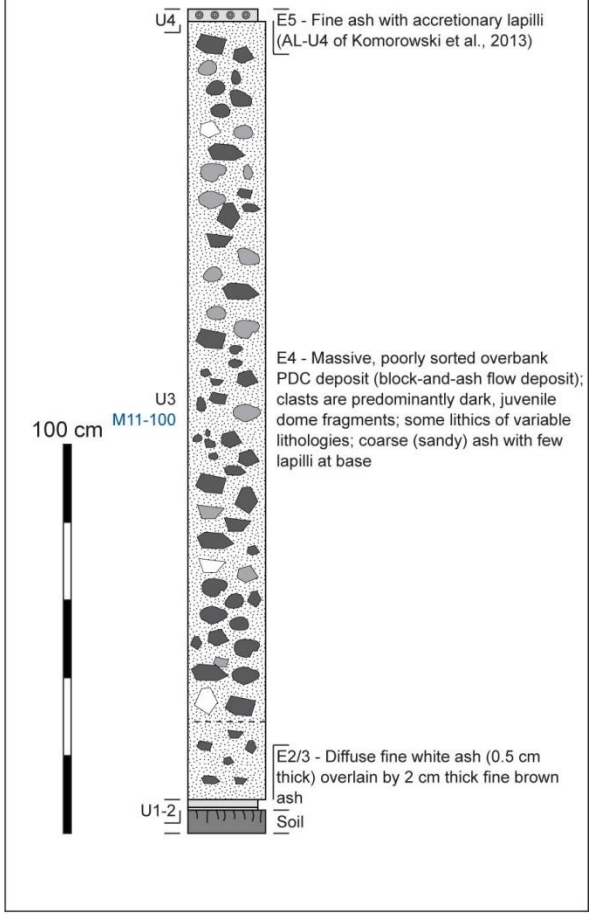

Locality No.:	39	Coordinates (49M):	440276 / 9157004 (333), 440332 / 9157098 (338)
Locality Description:	Kepuharjo Interfluve	Samples:	M11-103 (333); M11-104 (333); M11-130 (338); M11-131 (338)
Waypoint (WP):	333 & 338		

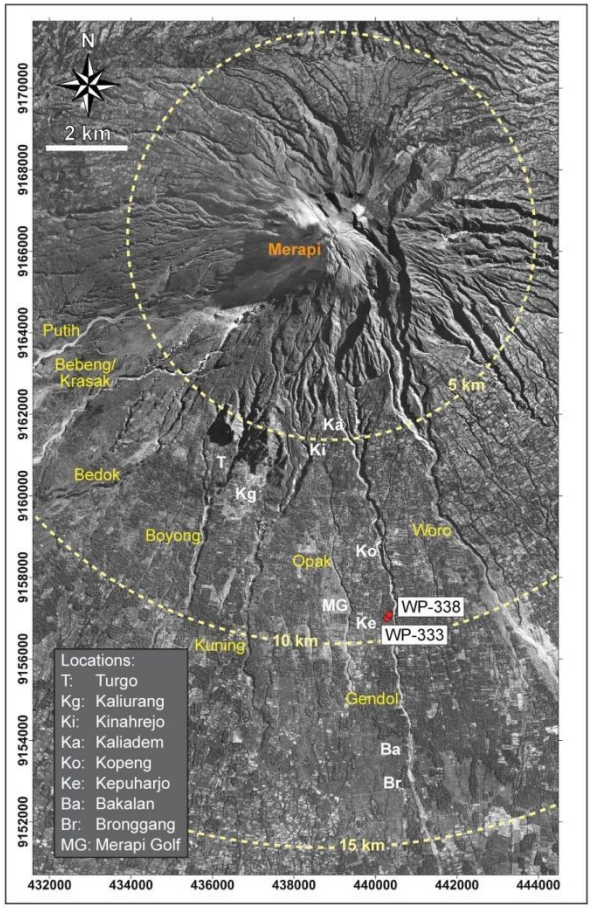

Locality No.:	40	Coordinates (49M):	439027 / 9162921
Locality Description:	Kali Gendol N of Kaliadem	Samples:	M11-127
Waypoint (WP):	335		

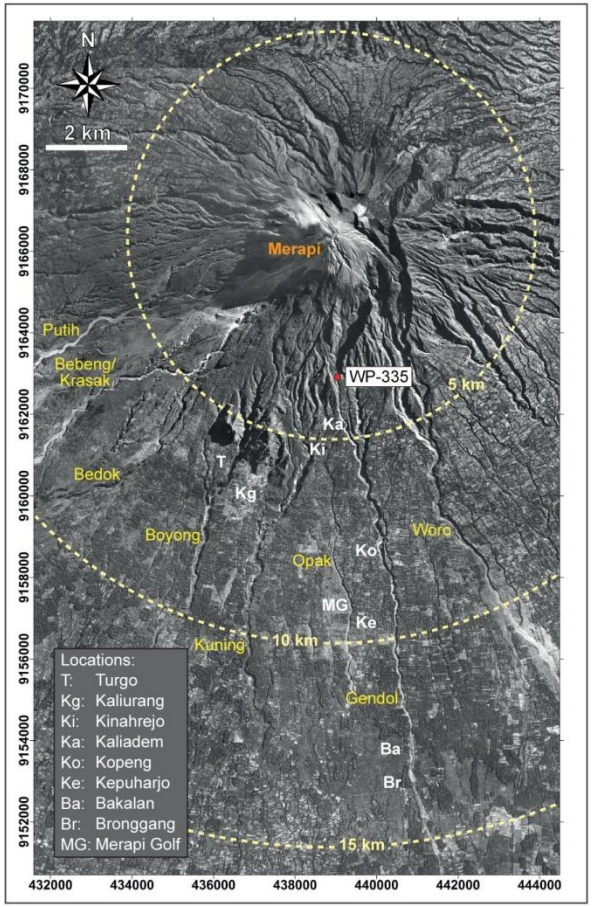

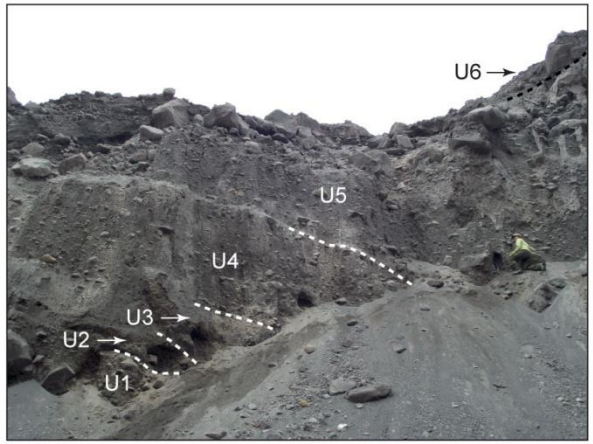

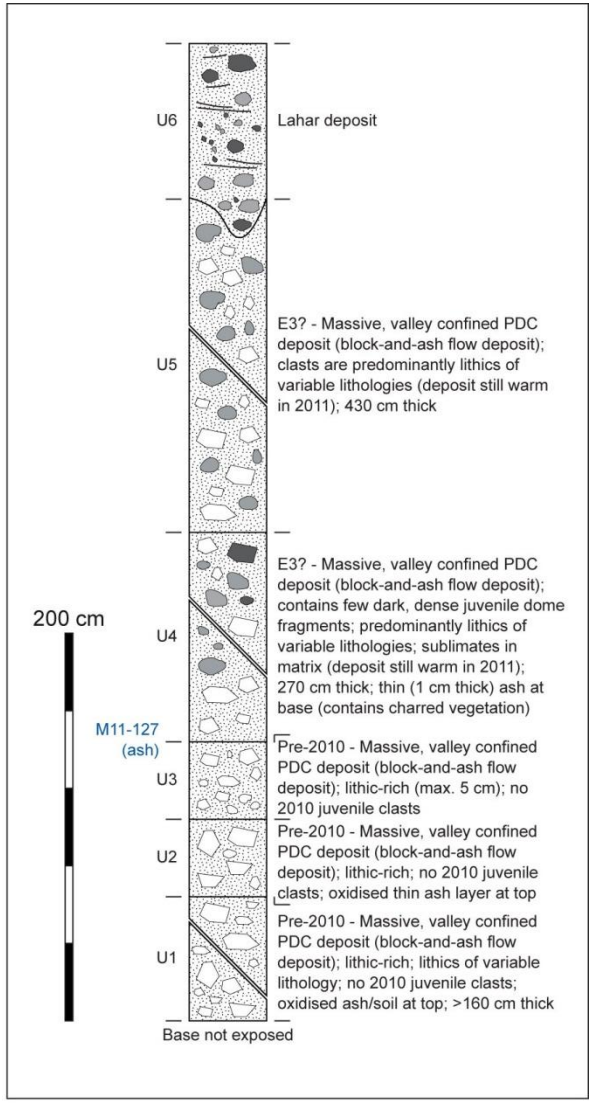

Locality No.:	41	Coordinates (49M):	440469 / 9157259
Locality Description:	Kali Gendol at Kepuharjo	Samples:	None
Waypoint (WP):	337		

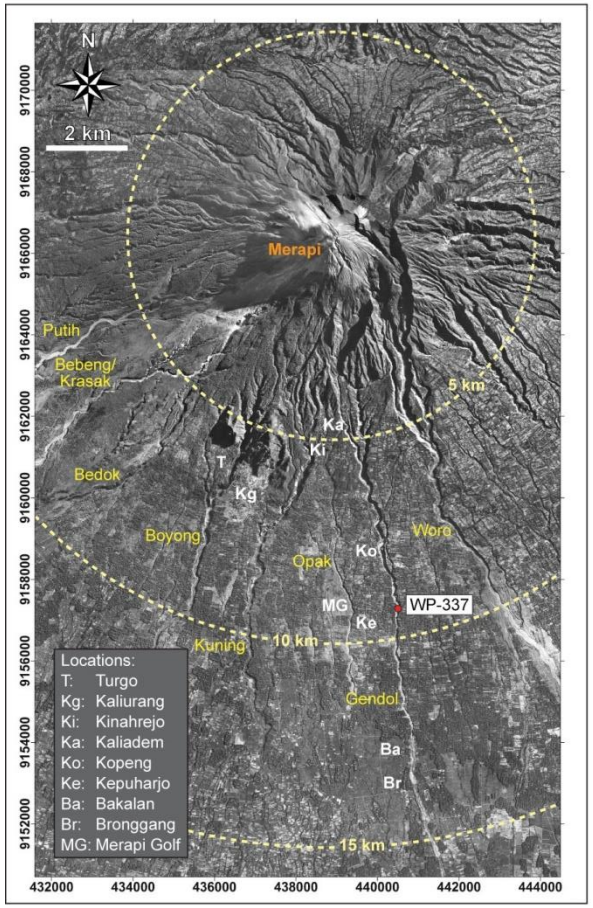

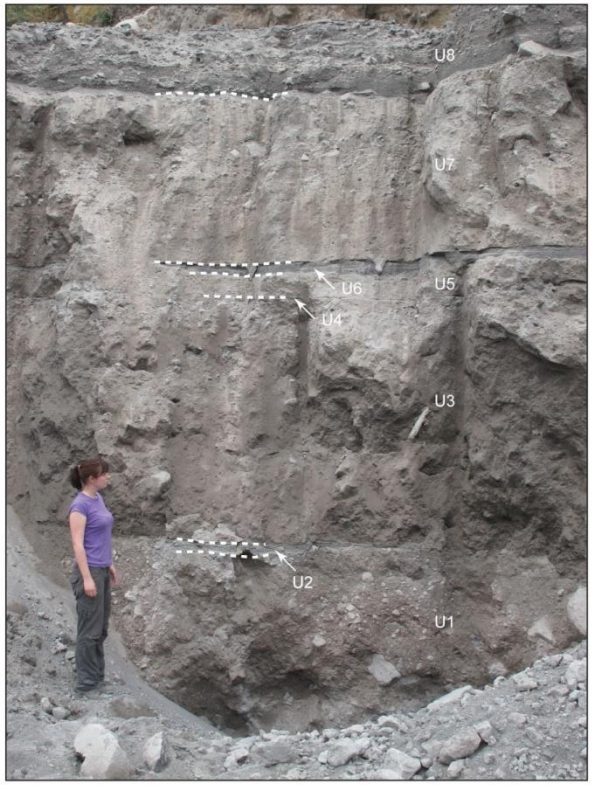

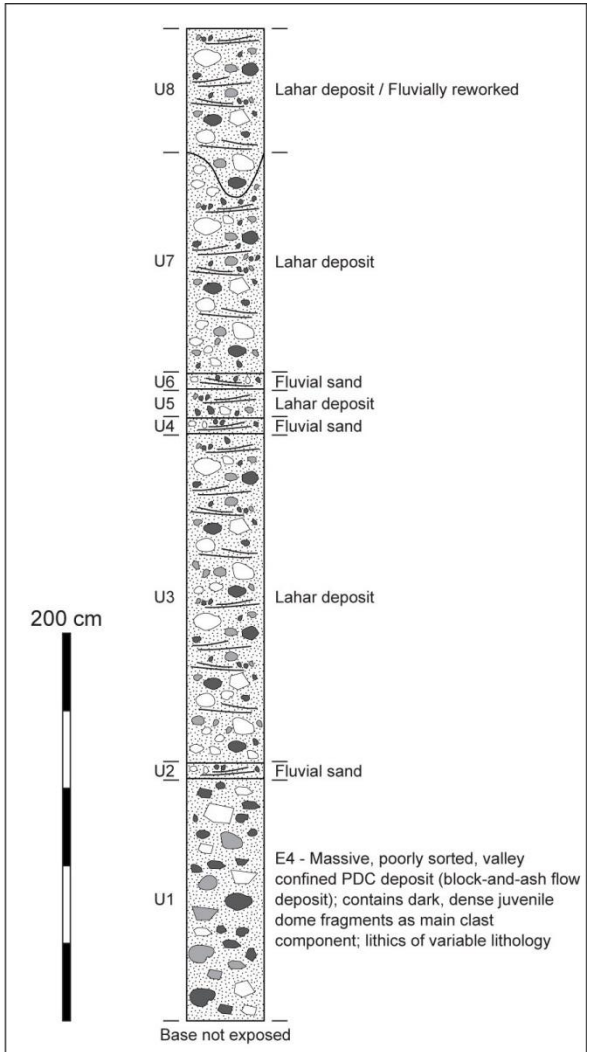

Locality No.:	42	Coordinates (49M):	440617 / 9154975
Locality Description:	Wukirsari Interfluve	Samples:	M11-133
Waypoint (WP):	339		

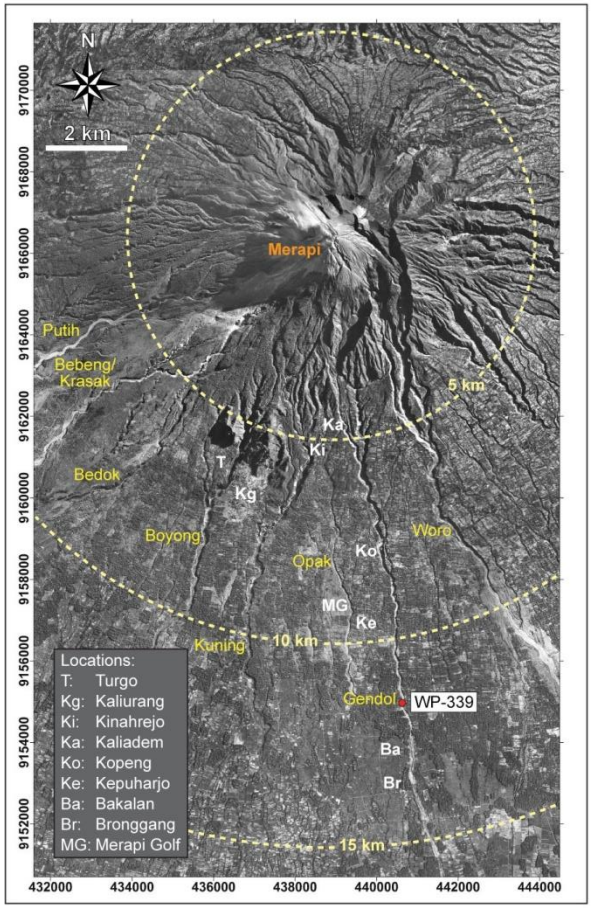

No Photo Available

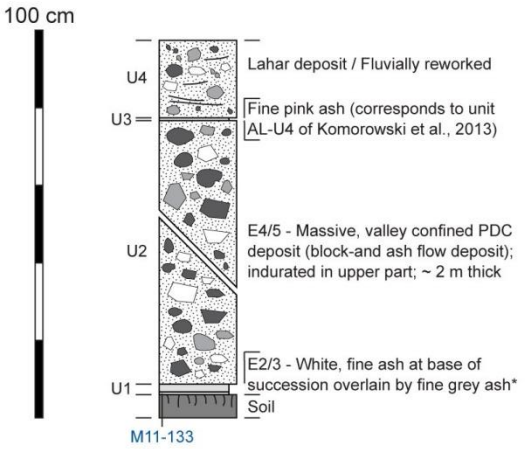

Locality No.:	43	Coordinates (49M):	440796 / 9154599
Locality Description:	Kali Gendol N of Bakalan	Samples:	M11-135
Waypoint (WP):	340		

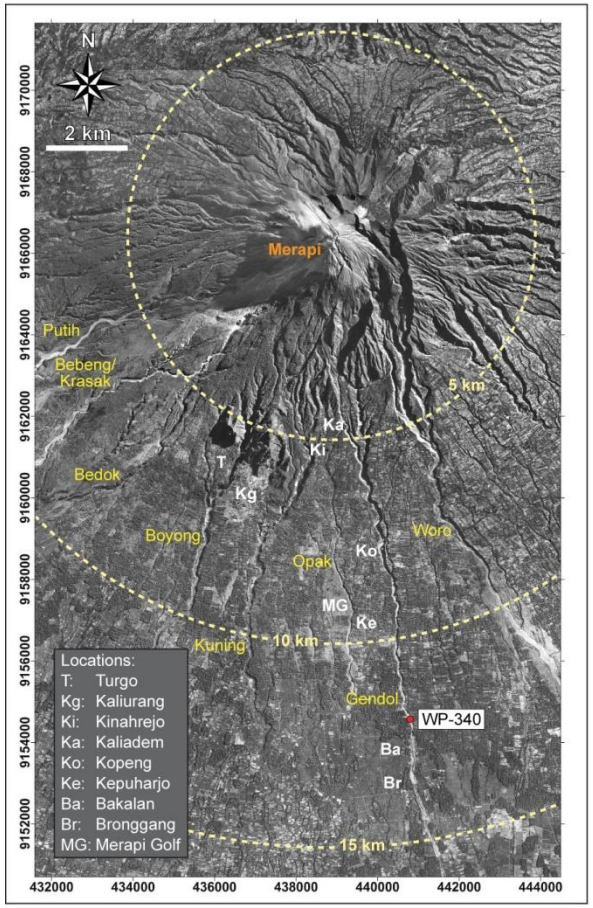

Locality No.:	44	Coordinates (49M):	439155 / 9166876 (341), 439461 / 9167331 (342), 439055 / 9166676 (343)
Locality Description:	Merapi Summit - Pasarbubar	Samples*:	M11-136a/b/c (341); M11-137 (342); M11-138a/b (343)
Waypoint (WP):	341, 342 & 343		

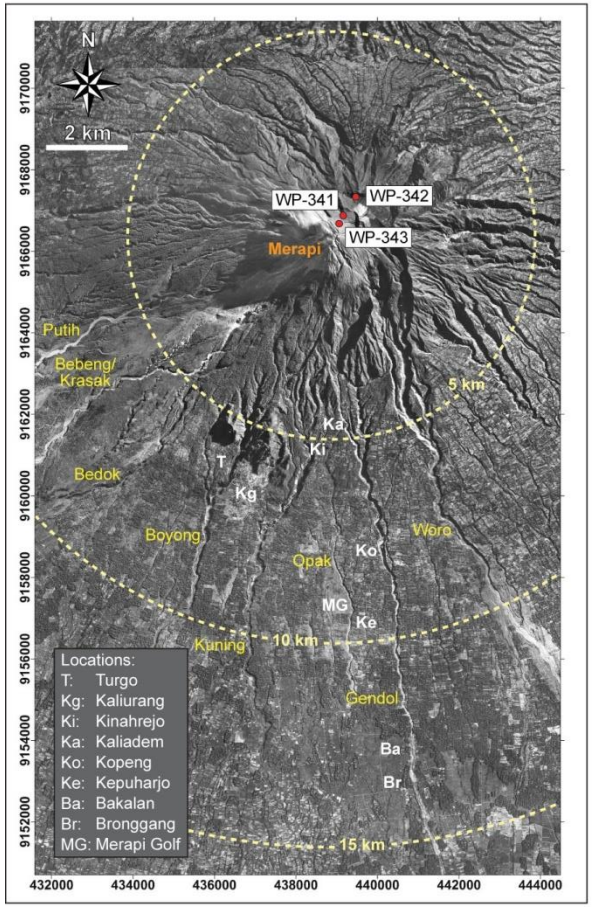

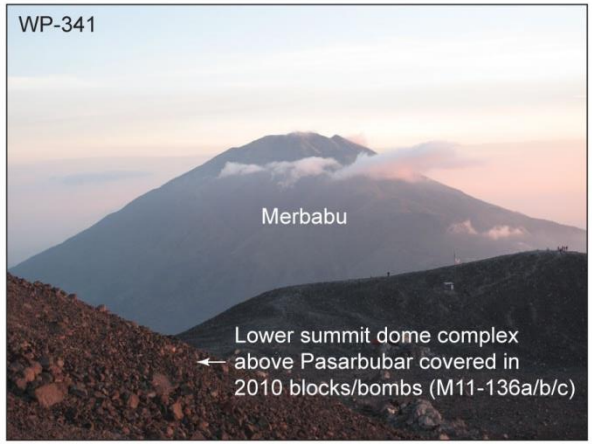

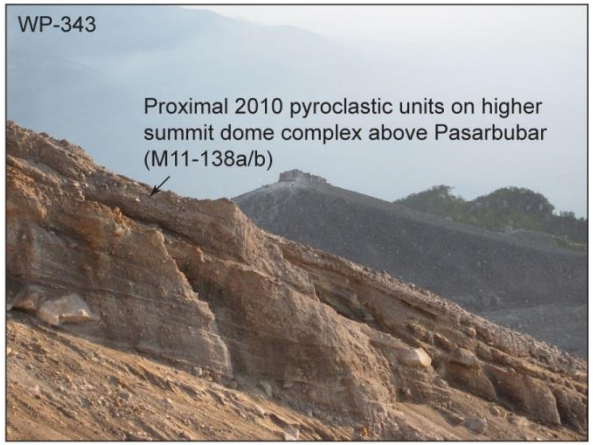

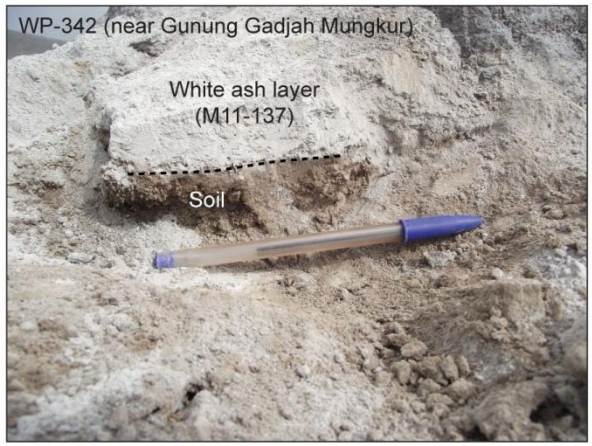

*All samples tentatively assigned to E6.

Locality No.:	45	Coordinates (49M):	439573 / 9161305
Locality Description:	Between Kali Gendol 1 & 2	Samples:	M11-38
Waypoint (WP):	344		

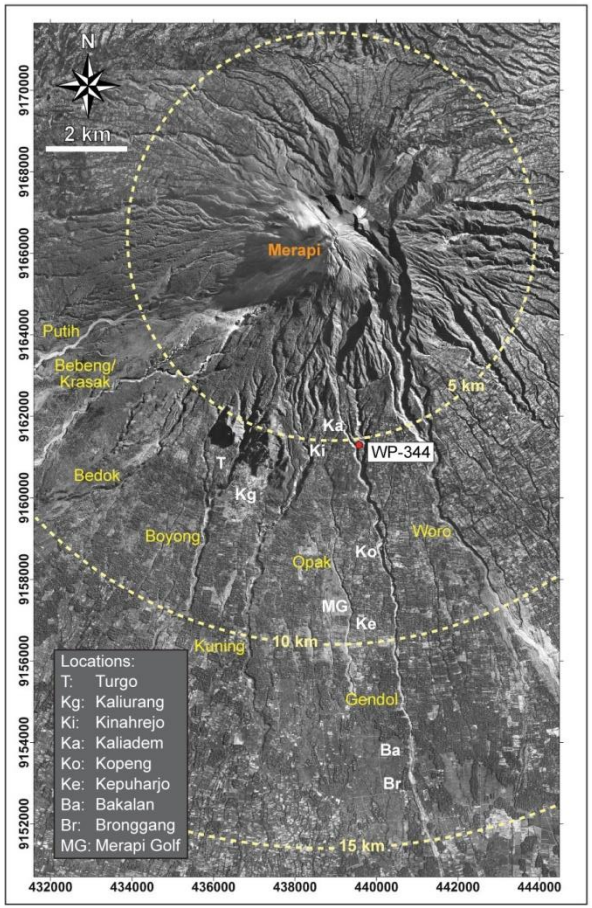

Locality No.:	46	Coordinates (49M):	439408 / 9161312
Locality Description:	Kali Gendol S of Kaliadem	Samples:	M13-26, -27, -28, -29, -33,
Waypoint (WP):	010		M13-34, -35, -37

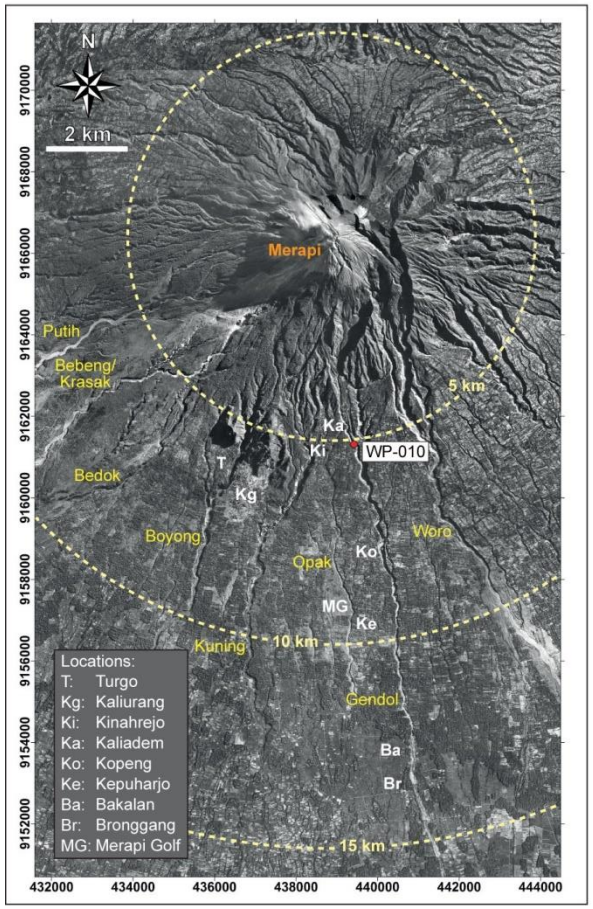

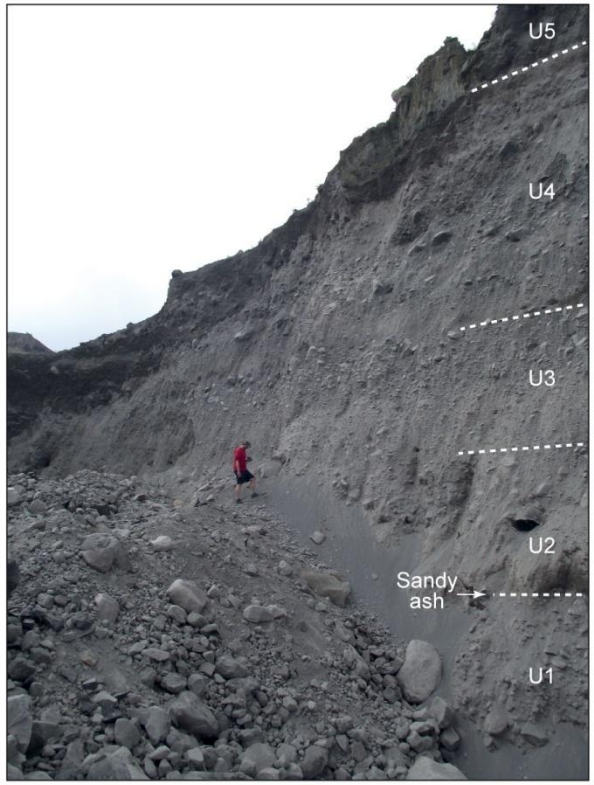

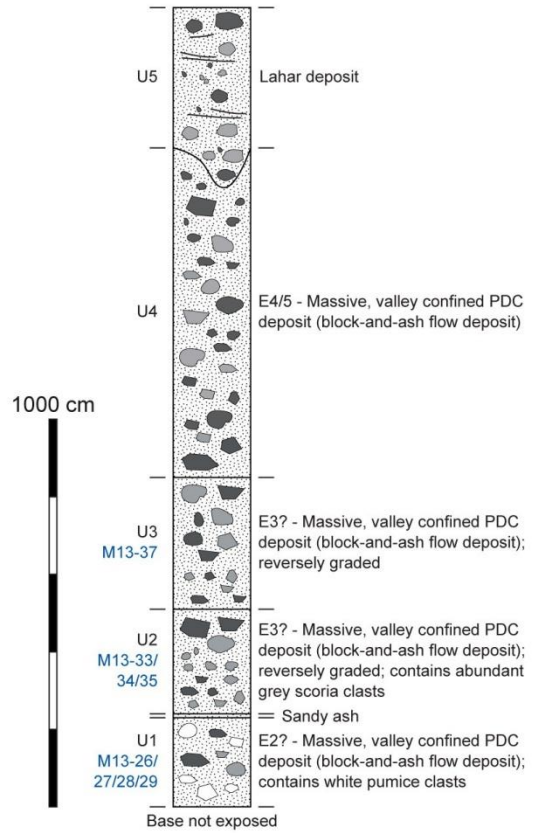

Locality No.:	47	Coordinates (49M):	439054 / 9162562
Locality Description:	Kali Gendol N of Kaliadem	Samples:	M13-07
Waypoint (WP):	016		

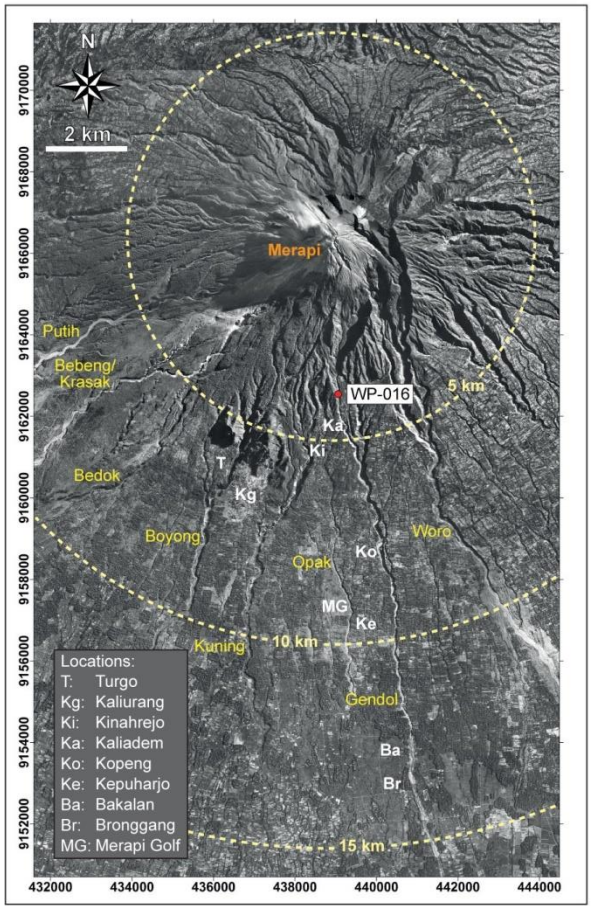

Locality No.:	48	Coordinates (49M):	439083 / 9162460
Locality Description:	Kali Gendol N of Kaliadem	Samples:	None
Waypoint (WP):	017		

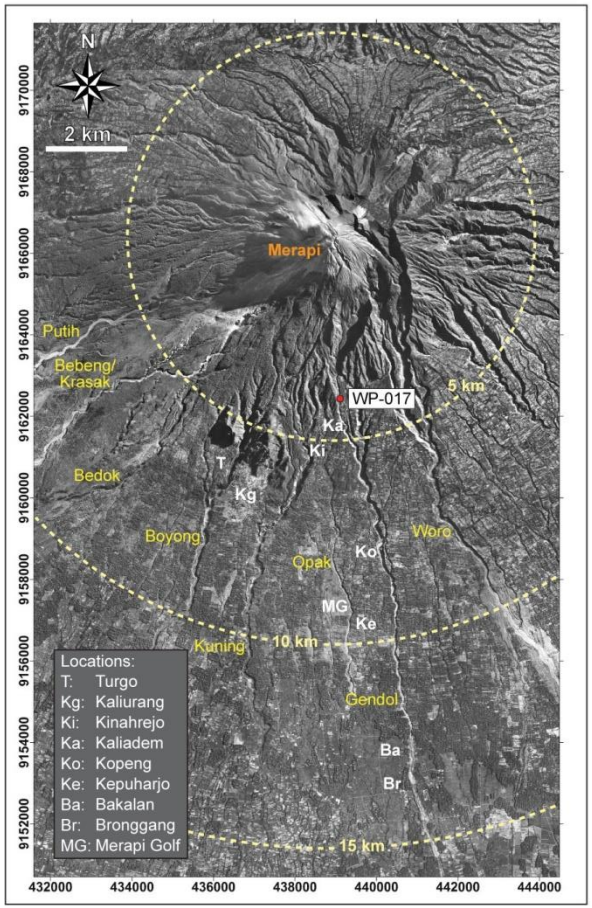

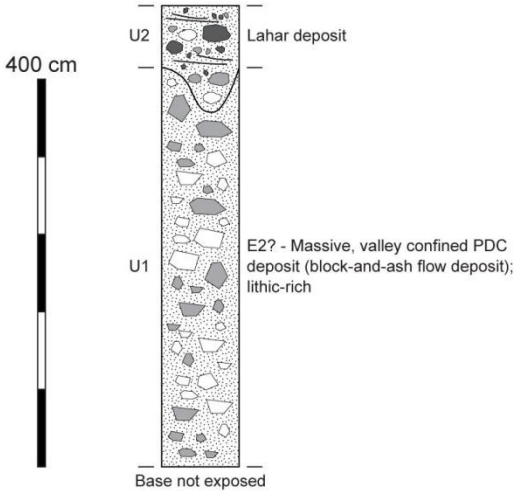

Locality No.:	49	Coordinates (49M):	433277 / 9163686
Locality Description:	Kali Putih Area	Samples:	M13-11
Waypoint (WP):	018		

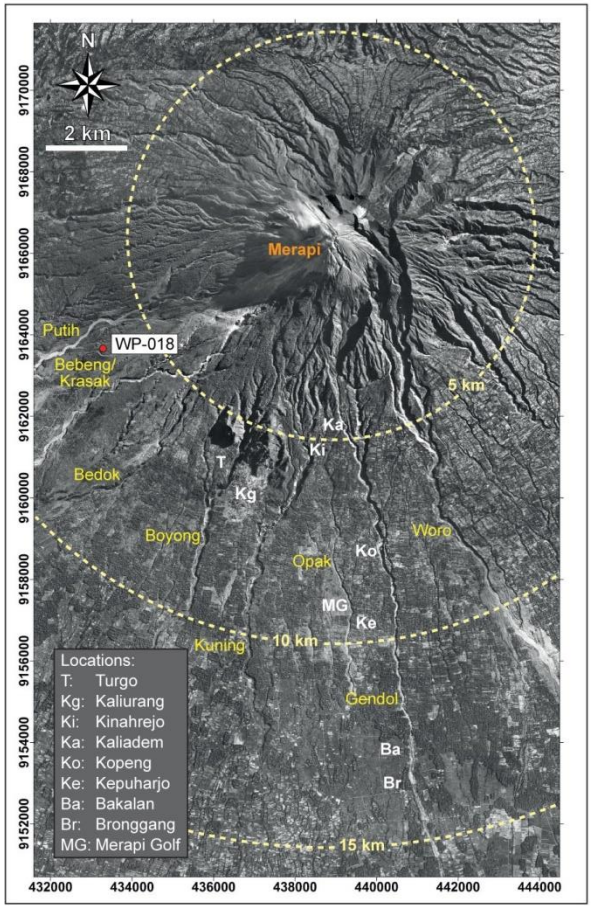

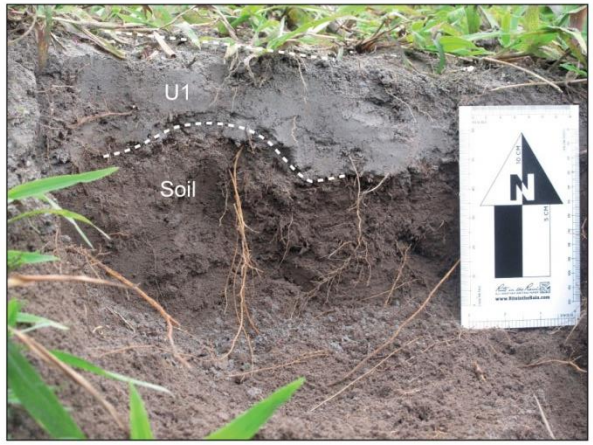

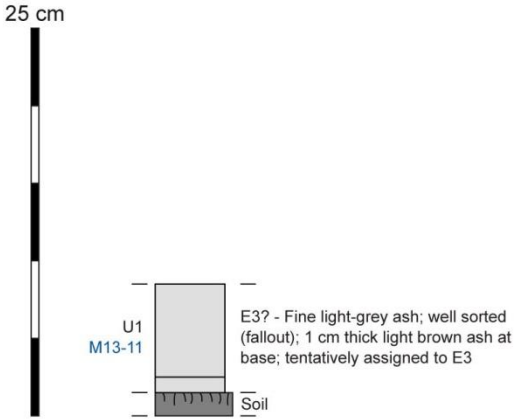

Locality No.:	50	Coordinates (49M):	432825 / 9163946
Locality Description:	Kali Putih	Samples:	M13-12
Waypoint (WP):	019		

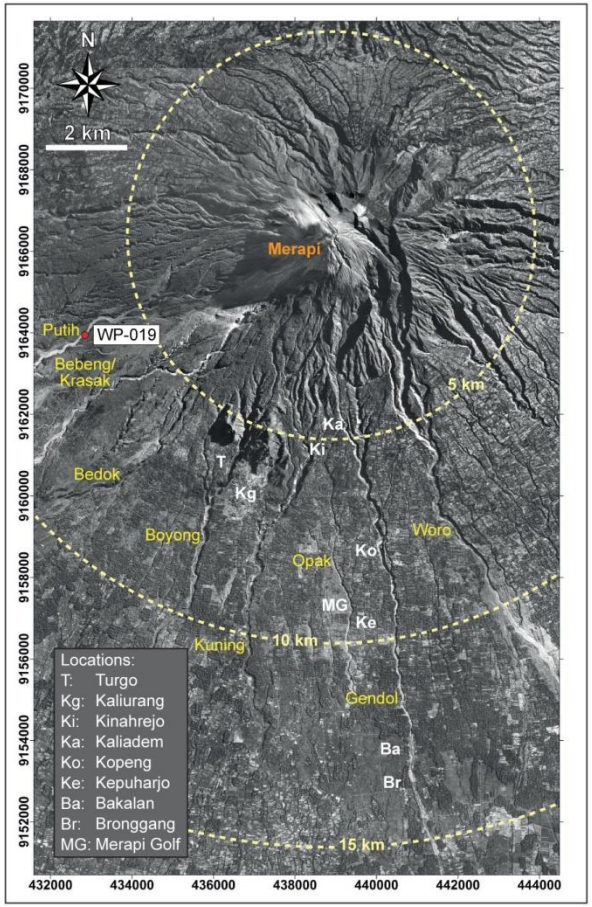

Locality No.:	51	Coordinates (49M):	439148 / 9162160
Locality Description:	Kali Gendol at Kaliadem	Samples:	M13-19; M13-20; M13-21;
Waypoint (WP):	024		M13-22; M13-23

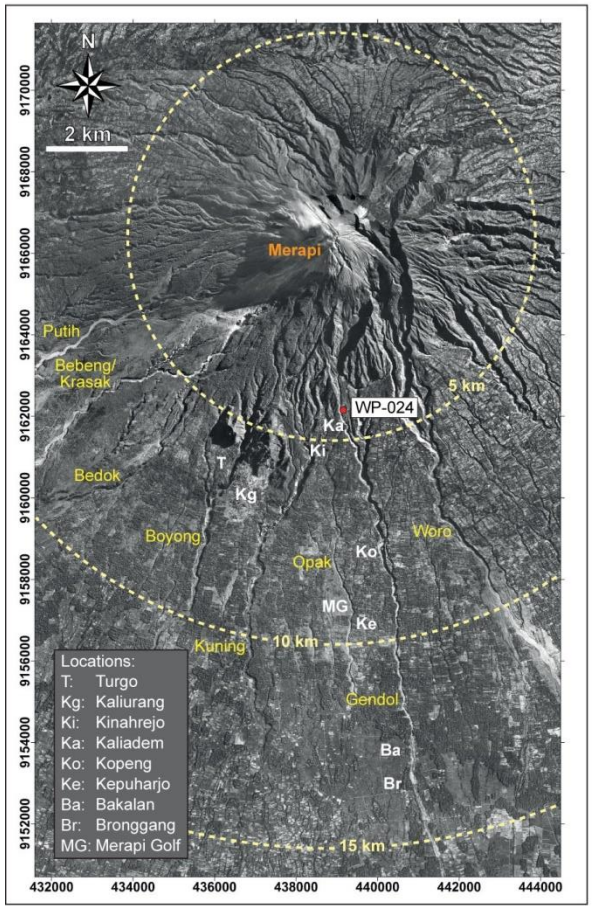

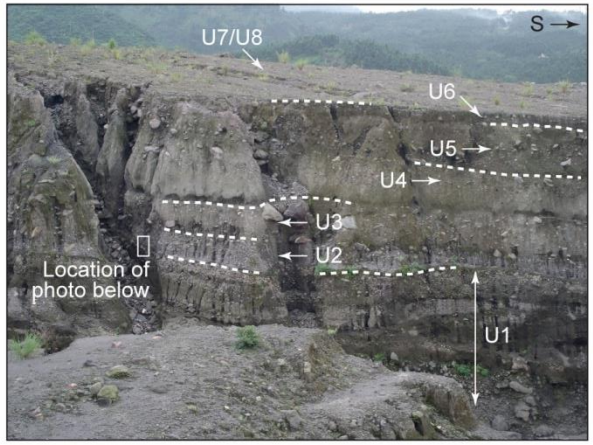

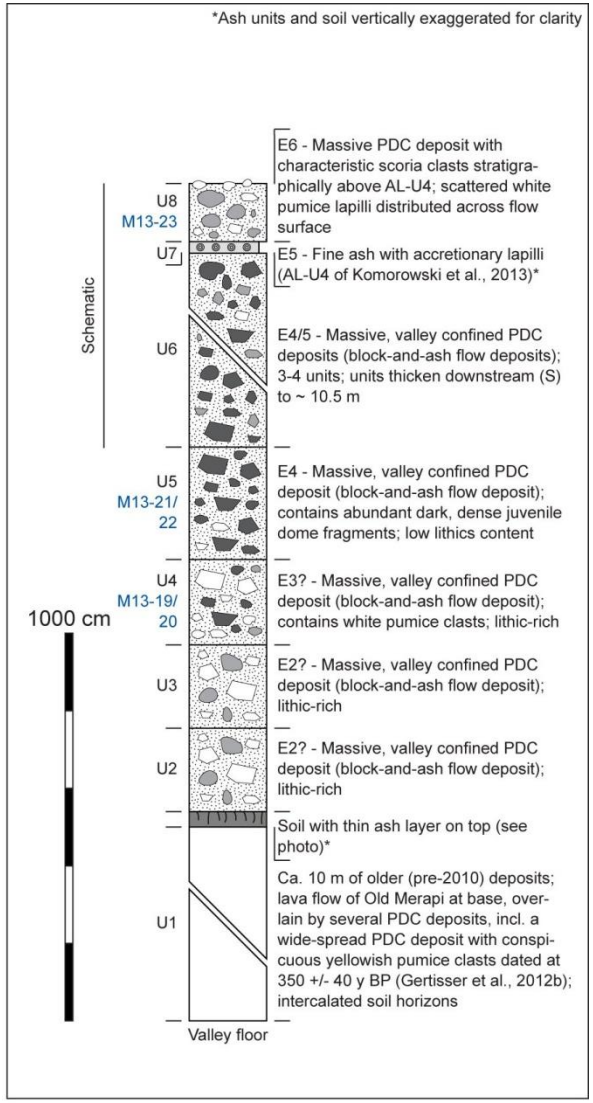

Locality No.:	52	Coordinates (49M):	439210 / 9161648
Locality Description:	Kaliadem	Samples:	M13-40, M13-41, M13-42
Waypoint (WP):	026		

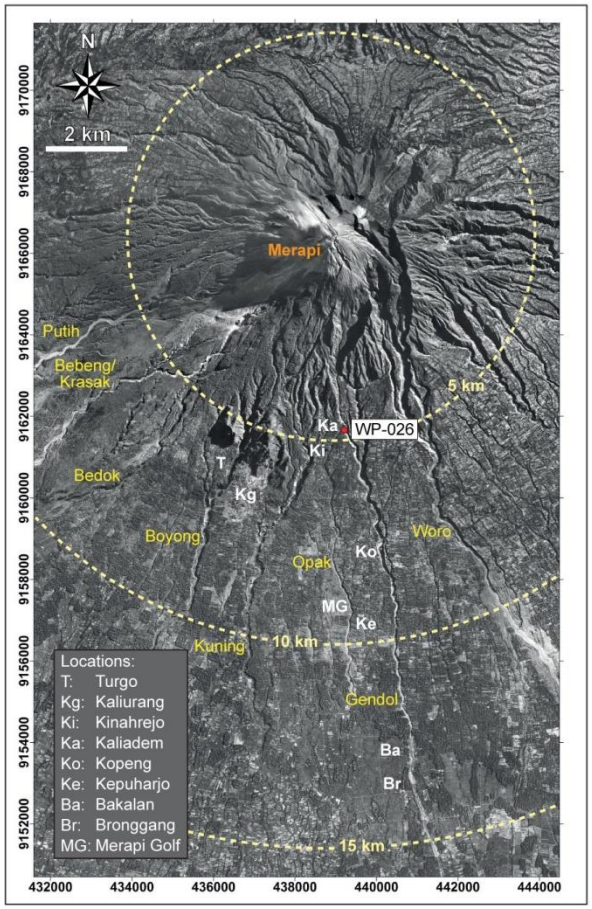

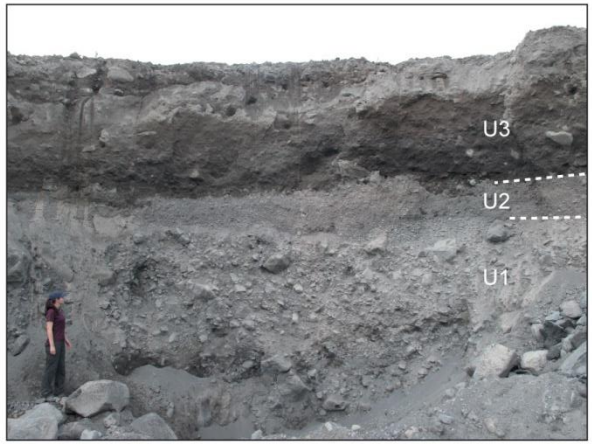

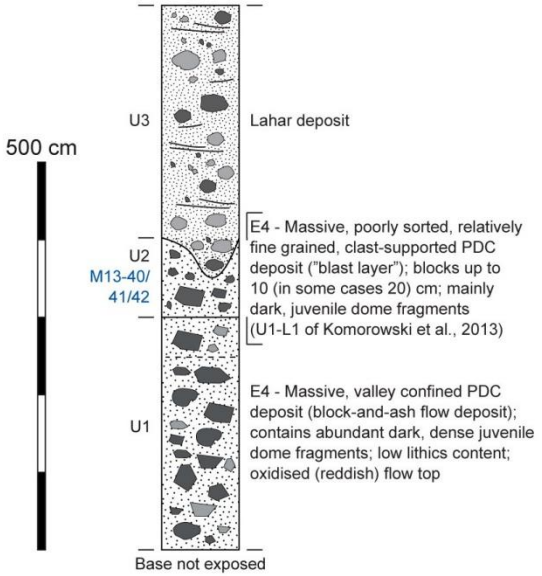

Locality No.:	53	Coordinates (49M):	438656 / 9163758
Locality Description:	Kinahrejo - Forest Gate	Samples:	M13-43
Waypoint (WP):	027		

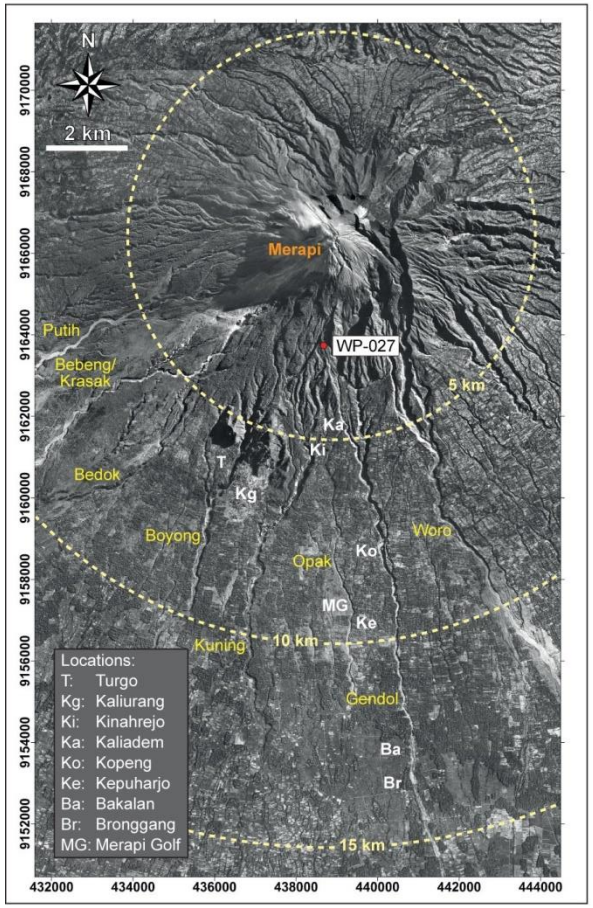


E6 scattered white pumice clasts on E4/5 surface (M13-43)

Locality No.:	54	Coordinates (49M):	438556 / 9162330
Locality Description:	Ridges N of Kinahrejo	Samples:	M13-44, M13-45,
Waypoint (WP):	029		M13-46, M13-47

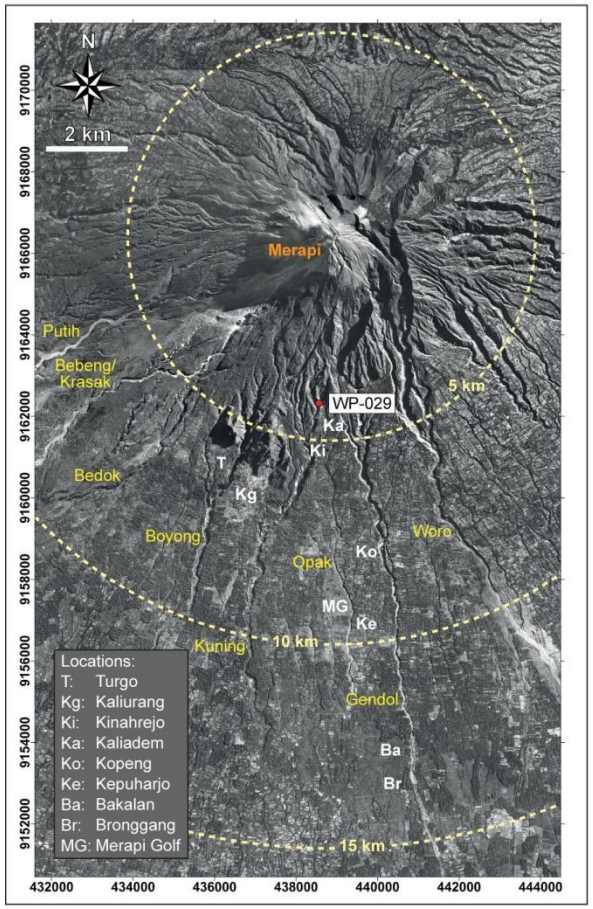

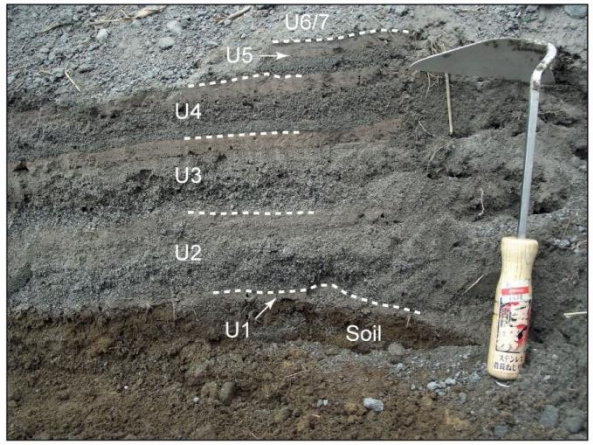

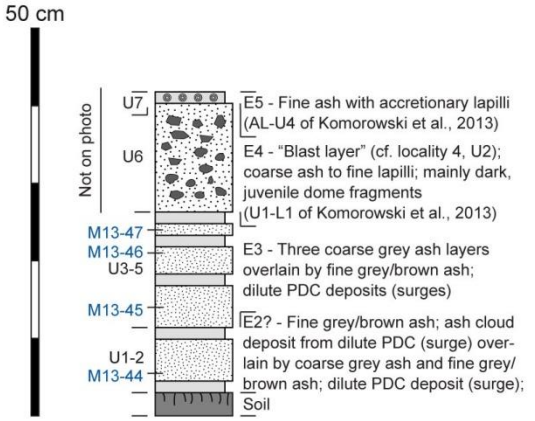

Locality No.:	55	Coordinates (49M):	438549 / 9161894
Locality Description:	Kinahrejo	Samples:	M13-48
Waypoint (WP):	030		

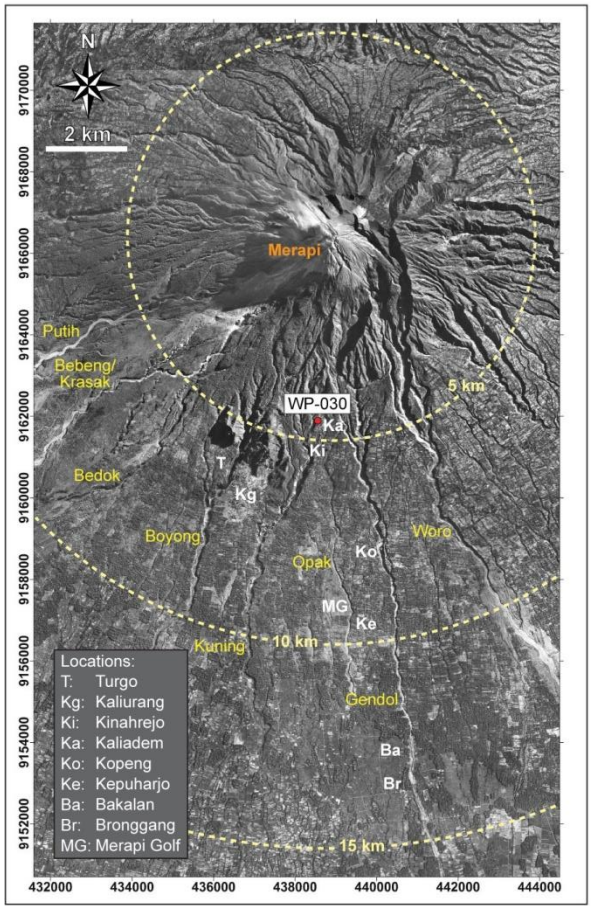

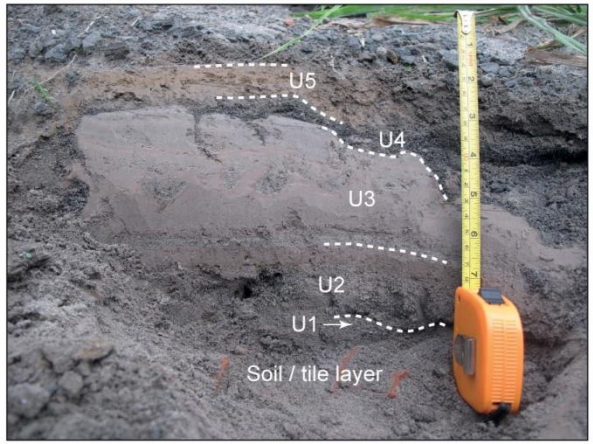

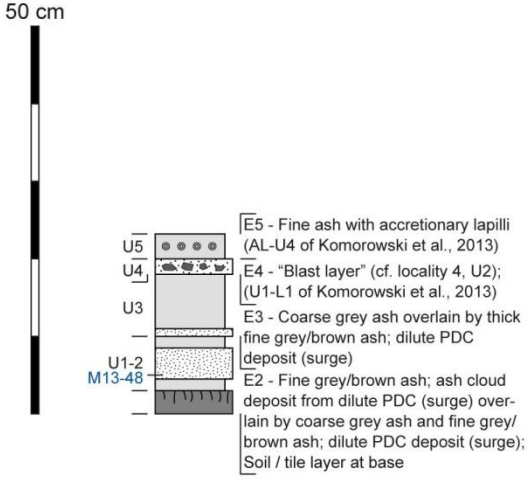

Locality No.:	56	Coordinates (49M):	439497 / 9161170 (S01), 439536 / 9160981 (S02), 439960 / 9159852 (S03), N/A (D01)
Locality Description:	Kali Gendol S of Kaliadem		
Waypoint (WP):	S01, S02, S03 & D01	Samples:	M13-60 (S01), M13-64 (S02), M13-65 (S02), M13-67 (S03), DD10 (D01)

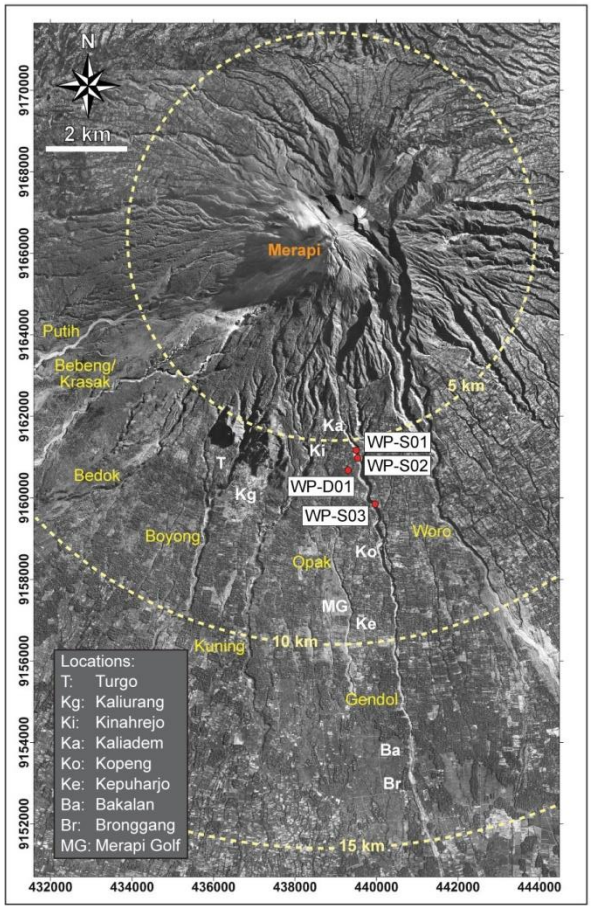

Eruption Stage:

M13-60 (E2)

M13-64 (E3)

M13-65 (E3)

M13-67 (E3)

DD10 (E4/5)

Table C1 Whole-rock major element and trace element analyses of the 2006 Merapi eruption (XRF)

Sample	ME08-01	ME08-02-01	ME08-02-02	ME08-03-01	ME08-03-02	ME08-04-01	ME08-04-02	ME08-04-03	ME08-05-01	ME08-05-02	ME08-06	ME08-07	ME08-08-03	ME08-09-01	ME08-09-02	ME08-09-03
Sample Type[1]	L4-S	L5-S	L5-S	L6-S	L6-S	L8-S	L8-S	L8-S	L1-S	L1-S	L1-S	L10-S	L1-D	L1-D	L1-S	L1-S
Eruption Stage[2]	III	III	III	III	III	III	III	III	II	II	II	II	II	IV	II	II
Major elements (wt%)																
SiO_2	55.16	55.08	55.42	55.38	55.15	55.27	55.18	55.40	55.27	55.31	55.75	55.20	55.54	55.22	55.27	55.11
TiO_2	0.71	0.70	0.72	0.71	0.72	0.72	0.72	0.71	0.72	0.71	0.71	0.72	0.70	0.71	0.71	0.71
Al_2O_3	19.06	19.05	19.05	19.20	18.85	19.04	18.90	19.08	19.08	19.04	19.36	19.06	19.10	19.34	19.03	18.94
Fe_2O_3	7.48	7.32	7.57	7.42	7.63	7.51	7.56	7.48	7.55	7.44	7.49	7.48	7.38	7.33	7.44	7.51
MnO	0.19	0.19	0.19	0.19	0.20	0.19	0.20	0.19	0.19	0.19	0.19	0.19	0.19	0.19	0.19	0.19
MgO	2.36	2.27	2.38	2.32	2.45	2.39	2.41	2.37	2.39	2.35	2.36	2.36	2.28	2.28	2.32	2.38
CaO	8.00	7.92	8.05	7.99	8.01	8.06	8.03	8.03	8.01	7.97	8.10	8.01	7.89	7.93	7.98	8.02
Na_2O	3.90	3.92	3.92	3.95	3.88	3.88	3.89	3.94	3.91	3.92	3.95	3.91	3.97	4.16	3.90	3.86
K_2O	2.16	2.17	2.15	2.17	2.15	2.15	2.15	2.15	2.16	2.17	2.16	2.16	2.19	2.21	2.17	2.16
P_2O_5	0.31	0.30	0.30	0.30	0.32	0.31	0.31	0.31	0.30	0.30	0.31	0.31	0.30	0.31	0.31	0.31
LOI	0.08	0.06	0.01	-0.11	0.08	-0.06	-0.07	-0.09	-0.10	-0.03	-0.04	-0.05	-0.10	0.22	0.07	0.08
Total	99.41	98.98	99.76	99.52	99.44	99.46	99.28	99.57	99.48	99.37	100.34	99.35	99.44	99.90	99.39	99.27
Trace elements (ppm)																
Sc	11	10	11	10	10	10	10	11	9	11	11	12	12	14	10	13
V	132	136	139	136	138	140	136	137	137	140	120	136	141	144	143	144
Cr	<10	<10	<10	<10	<10	<10	<10	<10	<10	<10	<10	<10	<10	<10	<10	<10
Ni	<10	<10	<10	<10	<10	<10	<10	<10	<10	<10	<10	<10	<10	<10	<10	<10
Cu	<10	16	25	15	24	16	51	33	<10	11	35	20	<10	11	11	<10
Zn	77	76	74	73	74	77	74	75	74	76	74	76	78	80	77	80
As	13	12	10	12	12	10	10	<10	12	11	<10	<10	<10	<10	10	12
Rb	49	49	48	49	49	49	48	49	49	48	47	49	50	48	49	48
Sr	550	547	540	550	545	542	544	549	544	544	557	548	543	545	545	539
Y	24	24	24	24	24	23	23	23	23	24	23	24	24	24	24	24
Zr	107	107	106	107	107	107	106	106	107	106	106	107	109	109	107	107
Nb	<10	<10	<10	<10	<10	<10	<10	<10	<10	<10	<10	<10	<10	<10	<10	<10
Mo	<10	<10	<10	<10	<10	<10	<10	<10	<10	<10	<10	<10	<10	<10	<10	<10
Ba	507	499	495	515	512	501	504	503	496	495	523	501	511	490	500	493
La	<20	21	<20	<20	<20	<20	<20	<20	<20	20	<20	21	<20	<20	<20	<20
Ce	77	80	75	71	73	73	77	73	76	76	70	76	71	83	74	75
Pb	22	24	22	22	20	23	23	23	24	23	22	22	23	21	22	23
Th	<10	<10	<10	<10	10	<10	<10	<10	<10	<10	10	<10	<10	<10	<10	<10
U	<10	<10	<10	<10	<10	<10	<10	<10	<10	<10	<10	<10	<10	<10	<10	<10

[1] See Appendix A; [2] after Preece et al. (2013)

Table C1 Whole-rock major element and trace element analyses of the 2006 Merapi eruption (XRF) (continued)

Sample	ME08-09-04	ME08-09-05	ME08-10	ME08-11-01	ME08-11-02	ME08-11-03	ME08-12	ME08-13-01	ME08-13-02	ME08-13-03	ME08-14
Sample Type	L1-S	L1-S	KB-S	KB-S	KB-S	KB-S	KB-D	SD-S	SD-S	SD-S	SD-S
Eruption Stage	II	II	I	I	I	I	I	IV	IV	IV	IV
Major elements (wt%)											
SiO_2	54.84	55.20	55.18	54.90	54.85	55.05	55.78	55.86	55.69	55.62	55.47
TiO_2	0.73	0.71	0.72	0.74	0.72	0.72	0.71	0.72	0.71	0.72	0.70
Al_2O_3	18.90	19.04	18.98	18.96	18.89	19.03	19.24	18.78	18.72	18.65	19.01
Fe_2O_3	7.69	7.38	7.58	7.75	7.67	7.51	7.45	7.48	7.47	7.44	7.41
MnO	0.20	0.19	0.19	0.20	0.20	0.19	0.19	0.19	0.19	0.19	0.19
MgO	2.42	2.32	2.39	2.46	2.45	2.39	2.37	2.35	2.32	2.40	2.30
CaO	8.03	7.95	8.06	8.10	8.12	8.07	7.94	7.76	7.74	7.81	7.85
Na_2O	3.85	3.95	3.88	3.90	3.86	3.88	3.89	3.96	3.99	3.90	3.92
K_2O	2.13	2.18	2.15	2.14	2.13	2.14	2.18	2.21	2.20	2.20	2.19
P_2O_5	0.31	0.31	0.31	0.32	0.30	0.30	0.30	0.26	0.26	0.29	0.33
LOI	0.08	0.06	-0.03	-0.06	-0.01	0.08	0.02	0.04	0.09	0.04	0.00
Total	99.18	99.29	99.41	99.41	99.18	99.36	100.07	99.61	99.38	99.26	99.37
Trace elements (ppm)											
Sc	11	<10	10	11	12	11	10	10	10	10	11
V	155	139	139	149	148	148	135	140	149	146	142
Cr	<10	<10	<10	<10	<10	<10	<10	<10	<10	<10	<10
Ni	<10	<10	<10	<10	<10	<10	<10	<10	<10	<10	<10
Cu	<10	<10	21	34	24	37	16	<10	12	<10	34
Zn	81	77	75	78	78	78	73	76	80	78	75
As	11	<10	<10	<10	11	<10	<10	10	12	10	<10
Rb	48	48	48	49	48	49	49	50	49	49	49
Sr	538	545	547	544	540	544	547	533	532	526	543
Y	23	24	24	24	23	23	23	23	22	23	23
Zr	106	107	106	106	105	106	106	109	108	107	107
Nb	<10	<10	<10	<10	<10	<10	<10	<10	<10	<10	<10
Mo	<10	<10	<10	<10	<10	<10	<10	<10	<10	<10	<10
Ba	485	505	503	495	498	499	507	511	511	499	510
La	<20	<20	20	21	<20	<20	<20	<20	20	23	<20
Ce	75	73	78	75	73	75	72	75	75	77	72
Pb	24	24	22	23	22	23	23	<20	21	28	23
Th	<10	<10	<10	<10	<10	<10	<10	<10	<10	<10	<10
U	<10	<10	<10	<10	<10	<10	<10	<10	<10	<10	<10

Table C2 Whole-rock trace element analyses of the 2006 Merapi eruption (ICP-MS)

Sample	ME08-01	ME08-02-02	ME08-03-02	ME08-04	ME08-07	ME08-08-03	ME08-09-01	ME08-10
Sample Type[1]	L4-S	L5-S	L6-S	L8-S	L10-S	L1-D	L1-D	KB-S
Eruption Stage[2]	III	III	III	III	III	II	II	I
Trace elements (ppm)								
Ba	481	503	508	457	499	495	488	507
Be	<1	<1	<1	<1	<1	<1	1	<1
Co	22.0	18.8	19.5	18.7	20.0	22.3	23.5	19.1
Cs	3.6	3.8	4.1	3.6	3.5	4.3	3.8	3.5
Ga	17.4	17.7	17.6	15.1	17.0	17.5	17.8	17.7
Hf	2.9	2.5	2.7	2.5	2.8	2.4	2.5	2.4
Nb	4.1	2.2	2.4	3.8	4.1	2.7	4.0	4.1
Rb	43.1	46.0	47.5	40.4	44.4	46.2	44.9	44.9
Sn	7	7	7	4	5	<1	3	4
Sr	554.2	604.1	606.4	531.0	583.0	580.9	588.9	584.4
Ta	0.3	0.3	0.2	0.3	0.4	0.2	0.4	0.4
Th	7.1	6.7	7.2	6.2	7.0	6.6	7.1	7.1
U	1.5	1.5	1.6	1.4	1.5	1.6	1.6	1.5
V	146	154	158	137	153	152	151	155
W	362.5	203.3	170.1	188.1	181.9	186.8	182.4	125.1
Zr	91.7	100.5	102.1	86.1	92.7	99.1	92.5	95.7
Y	23.1	21.6	22.8	22.4	23.3	21.6	23.1	24.7
La	17.7	19.2	19.2	16.1	17.9	18.2	17.8	18.6
Ce	34.7	37.7	38.8	34.4	36.9	37.2	37.1	37.0
Pr	4.15	4.37	4.48	3.95	4.38	4.21	4.40	4.46
Nd	16.1	17.3	20.0	17.1	18.2	18.1	17.0	18.6
Sm	3.96	4.05	4.34	3.73	4.06	3.98	4.17	4.21
Eu	1.19	1.23	1.26	1.15	1.20	1.15	1.27	1.30
Gd	3.75	4.13	4.42	3.52	3.90	3.92	4.01	4.07
Tb	0.65	0.66	0.67	0.61	0.68	0.66	0.68	0.67
Dy	3.71	3.73	3.84	3.42	3.75	3.5	3.63	3.50
Ho	0.74	0.87	0.87	0.72	0.78	0.8	0.80	0.81
Er	2.46	2.55	2.71	2.14	2.33	2.26	2.49	2.49
Tm	0.32	0.35	0.37	0.31	0.35	0.35	0.33	0.35
Yb	2.15	2.59	2.67	2.02	2.32	2.54	2.13	2.21
Lu	0.36	0.39	0.36	0.33	0.36	0.35	0.35	0.36
Mo	<0.1	0.1	<0.1	0.1	<0.1	0.2	<0.1	0.1
Cu	50.4	51.4	46.6	40.6	46.4	20	32.1	38.3
Pb	1.4	1.1	1.2	1.5	1.4	1.4	1.5	1.5
Zn	44	40	35	45	46	51	50	43
Ni	1.4	1.5	1.1	1.4	1.6	1.6	1.5	1.3
As	<0.5	<0.5	<0.5	0.5	0.5	<0.5	<0.5	0.9
Cd	<0.1	<0.1	<0.1	<0.1	<0.1	<0.1	<0.1	<0.1
Sb	<0.1	<0.1	<0.1	<0.1	<0.1	<0.1	<0.1	<0.1
Bi	<0.1	<0.1	<0.1	<0.1	<0.1	<0.1	<0.1	<0.1
Ag	<0.1	<0.1	<0.1	<0.1	<0.1	<0.1	<0.1	<0.1
Au	2.5	3.1	<0.5	0.9	1.9	1.1	0.9	1.3
Hg	0.01	<0.01	<0.01	<0.01	<0.01	<0.01	0.03	<0.01
Tl	<0.1	<0.1	<0.1	<0.1	<0.1	<0.1	<0.1	<0.1
Se	<0.5	<0.5	<0.5	<0.5	<0.5	<0.5	<0.5	<0.5

[1] See Appendix A; [2] after Preece et al. (2013)

Table C2 Whole-rock trace element analyses of the 2006 Merapi eruption (ICP-MS) (continued)

Sample	ME08-12	ME08-14						
Sample Type	KB-D	SD-S						
Eruption Stage	I	IV						
Trace elements (ppm)								
Ba	535	504						
Be	3	<1						
Co	19.9	24.3						
Cs	4.2	3.8						
Ga	19.4	18.1						
Hf	2.2	2.7						
Nb	6.8	4.0						
Rb	50.9	45.1						
Sn	2	7						
Sr	584.1	583.4						
Ta	0.3	0.4						
Th	7.0	7.3						
U	1.8	1.5						
V	166	152						
W	111.4	171.6						
Zr	105.1	95.7						
Y	22.4	23.5						
La	18.0	18.0						
Ce	36.3	36.7						
Pr	4.56	4.29						
Nd	20.8	18.5						
Sm	3.93	3.88						
Eu	1.27	1.25						
Gd	4.22	3.87						
Tb	0.63	0.65						
Dy	4.11	3.65						
Ho	0.74	0.76						
Er	2.07	2.34						
Tm	0.35	0.31						
Yb	2.76	2.01						
Lu	0.34	0.37						
Mo	0.2	0.1						
Cu	22	46.6						
Pb	1.3	3.9						
Zn	48	44						
Ni	1.5	1.5						
As	<0.5	1.4						
Cd	<0.1	<0.1						
Sb	<0.1	<0.1						
Bi	<0.1	<0.1						
Ag	<0.1	<0.1						
Au	<0.5	0.9						
Hg	<0.01	0.03						
Tl	<0.1	<0.1						
Se	<0.5	0.5						

Table C3 Whole-rock major element and trace element analyses of the 2010 Merapi eruption (XRF)

Sample	M11-01	M11-04	M11-05	M11-06	M11-10b	M11-12	M11-14	M11-15	M11-18	M11-19a	M11-20	M11-21	M11-24	M11-26a	M11-27-5	M11-33
Sample Type[1]	DD	DD	LG-Inc	SD	DD	DD	A	DD	WP	DD	DD	A	DD	DD	DD	WP
Eruption Stage[2]	4/5	4/5	4/5	4/5	4	4	3	4	6	4	4	3	4	4/5	4/5	6
Locality No.[3]	1	2	2	2	3	5	7	8	9	10	11	11	12	13	13	17
Major elements (wt%)																
SiO_2	54.04	55.40	53.76	54.28	55.45	54.77	56.33	54.34	55.16	55.07	54.73	57.13	55.00	55.19	54.80	54.69
TiO_2	0.74	0.73	0.77	0.72	0.73	0.74	0.62	0.74	0.70	0.72	0.72	0.56	0.73	0.73	0.72	0.71
Al_2O_3	19.14	19.12	19.23	18.97	19.36	19.13	19.19	19.19	19.14	19.13	18.93	19.47	19.11	19.15	19.06	18.90
Fe_2O_3	7.73	7.65	8.15	7.54	7.59	7.79	6.38	7.86	7.29	7.52	7.56	5.73	7.61	7.64	7.56	7.57
MnO	0.19	0.19	0.19	0.19	0.20	0.20	0.17	0.19	0.19	0.20	0.19	0.16	0.20	0.20	0.19	0.19
MgO	2.49	2.34	2.62	2.37	2.41	2.42	1.86	2.46	2.31	2.34	2.37	1.70	2.37	2.38	2.34	2.28
CaO	8.22	7.96	8.43	8.04	8.00	8.13	6.77	8.20	7.86	7.91	7.86	6.54	7.95	7.99	7.90	7.72
Na_2O	3.84	4.00	3.83	3.95	4.07	3.80	4.03	3.70	3.86	3.87	3.83	4.12	3.91	3.86	3.85	3.82
K_2O	2.05	2.17	2.11	2.09	2.16	2.08	2.53	2.09	2.18	2.14	2.13	2.63	2.14	2.13	2.13	2.17
P_2O_5	0.31	0.32	0.32	0.32	0.32	0.32	0.32	0.32	0.30	0.32	0.32	0.30	0.32	0.32	0.32	0.31
LOI	-0.14	-0.06	-0.34	0.03	0.00	-0.15	0.43	-0.19	0.03	-0.09	-0.10	0.72	-0.11	-0.07	-0.06	0.53
Total	98.61	99.82	99.07	98.50	100.29	99.23	98.63	98.90	99.02	99.13	98.54	99.06	99.23	99.52	98.81	98.89
Trace elements (ppm)																
Sc	12	11	13	11	14	13	10	11	12	10	11	<10	11	11	10	10
V	159	146	178	153	148	153	116	159	139	143	146	99	148	145	145	135
Cr	<10	<10	<10	<10	<10	<10	<10	<10	<10	<10	<10	<10	<10	<10	<10	<10
Ni	<10	<10	<10	<10	<10	<10	<10	<10	<10	<10	<10	<10	<10	<10	<10	<10
Cu	<10	<10	<10	<10	<10	11	26	<10	<10	12	<10	23	14	15	15	40
Zn	84	85	84	85	81	83	74	82	75	82	82	70	83	81	81	74
As	<10	<10	10	10	<10	<10	12	<10	<10	<10	<10	10	<10	<10	<10	<10
Rb	45	48	46	46	47	46	56	47	50	47	49	59	47	48	48	49
Sr	540	540	550	538	535	540	510	547	545	539	538	510	537	541	542	544
Y	23	25	23	24	24	24	23	24	23	23	24	24	25	25	23	23
Zr	106	110	98	108	109	107	122	105	106	108	109	127	108	110	109	107
Nb	<10	<10	<10	<10	<10	<10	<10	<10	<10	<10	<10	<10	<10	<10	<10	<10
Mo	<10	<10	<10	<10	<10	<10	<10	<10	<10	<10	<10	<10	<10	<10	<10	<10
Ba	480	496	469	477	486	476	578	483	502	489	496	597	486	492	487	511
La	<20	<20	<20	<20	<20	<20	24	<20	<20	<20	<20	28	22	<20	<20	21
Ce	77	71	77	79	76	79	78	76	75	81	77	84	80	83	79	81
Pb	23	24	21	21	22	22	24	21	22	21	23	27	21	22	23	20
Th	<10	<10	<10	<10	<10	<10	<10	10	10	<10	<10	11	<10	<10	9	<10
U	<10	<10	<10	<10	<10	<10	<10	<10	<10	<10	<10	<10	<10	<10	<10	<10

[1] See Appendix A; [2] after Komorowski et al. (2013); [3] see Appendix B; [4] n.a. = not analysed

Table C3 Whole-rock major element and trace element analyses of the 2010 Merapi eruption (XRF) (continued)

Sample	M11-46	M11-50	M11-51	M11-53-B1	M11-53-B3	M11-55	M11-61	M11-65	M11-67a	M11-67b	M11-68b	M11-75	M11-80	M11-85	M11-87	M11-93
Sample Type	DD	WP	D	DD	SD	WP	WP	DD	A	A	A	GS	DD	WP-D	DD	SD
Eruption Stage	4	6	6	3	3	6	6	4	3	3	3	6	4	6	4	3
Locality No.	22	24	24	26	26	28	28	33	34	34	34	35	16	36	20	25
Major elements (wt%)																
SiO_2	54.22	54.98	54.94	54.78	55.01	54.93	55.03	54.70	54.60	55.40	54.99	55.04	54.87	53.81	54.36	55.06
TiO_2	0.74	0.72	0.71	0.73	0.73	0.71	0.70	0.72	0.72	0.68	0.71	0.71	0.71	0.79	0.74	0.71
Al_2O_3	19.09	19.16	19.00	18.87	18.96	18.91	19.04	18.94	18.77	18.86	19.08	19.02	18.98	18.60	18.99	18.98
Fe_2O_3	7.83	7.46	7.46	7.68	7.57	7.49	7.35	7.56	7.72	7.12	7.52	7.39	7.41	8.33	7.73	7.43
MnO	0.19	0.19	0.19	0.20	0.20	0.19	0.19	0.20	0.19	0.17	0.19	0.19	0.19	0.18	0.20	0.19
MgO	2.47	2.29	2.34	2.39	2.39	2.36	2.31	2.37	2.46	2.06	2.41	2.32	2.31	2.99	2.43	2.31
CaO	8.18	7.87	7.79	7.96	7.95	7.85	7.85	7.93	7.79	7.17	7.87	7.82	7.86	8.18	8.15	7.81
Na_2O	3.83	3.87	3.88	3.82	3.87	3.79	3.84	3.86	3.71	3.87	3.77	3.93	3.89	3.49	3.84	3.86
K_2O	2.05	2.14	2.17	2.11	2.11	2.15	2.15	2.10	2.07	2.27	2.10	2.16	2.12	1.67	2.05	2.15
P_2O_5	0.32	0.31	0.31	0.32	0.32	0.31	0.30	0.32	0.30	0.31	0.29	0.32	0.32	0.28	0.32	0.30
LOI	0.20	0.22	0.00	0.01	0.06	0.30	0.25	0.07	0.32	0.91	0.23	0.20	0.02	0.78	0.11	0.05
Total	99.12	99.21	98.79	98.87	99.17	98.99	99.01	98.77	98.65	98.82	99.16	99.10	98.68	99.10	98.92	98.85
Trace elements (ppm)																
Sc	11	10	12	12	12	10	10	12	11	10	11	<10	11	16	12	10
V	161	133	138	144	142	141	136	148	152	135	144	139	142	178	155	133
Cr	<10	<10	<10	<10	<10	<10	<10	<10	<10	<10	<10	<10	<10	<10	<10	<10
Ni	<10	<10	<10	<10	<10	<10	<10	<10	<10	<10	<10	<10	<10	<10	<10	<10
Cu	14	<10	12	<10	11	<10	<10	<10	<10	14	15	<10	<10	<10	10	10
Zn	82	75	77	81	80	76	76	84	81	78	77	81	79	70	84	75
As	<10	10	<10	10	<10	<10	11	<10	11	10	10	11	<10	<10	<10	<10
Rb	46	49	50	48	47	48	48	48	46	49	47	48	48	40	45	49
Sr	538	548	541	538	536	546	556	534	539	524	539	536	542	519	537	539
Y	24	24	24	23	24	23	23	24	20	20	20	24	24	20	24	23
Zr	105	106	109	108	108	107	105	108	103	112	103	109	108	95	105	108
Nb	<10	<10	<10	<10	<10	<10	<10	<10	<10	<10	<10	<10	<10	<10	<10	<10
Mo	<10	<10	<10	<10	<10	<10	<10	<10	<10	<10	<10	<10	<10	<10	<10	<10
Ba	470	507	502	493	492	506	510	485	496	533	497	500	491	362	472	503
La	21	<20	<20	<20	<20	20	<20	<20	<20	<20	<20	21	<20	20	21	<20
Ce	83	81	80	78	77	81	83	82	65	73	74	86	82	73	73	82
Pb	22	24	22	21	21	23	24	23	23	27	22	23	23	<20	23	24
Th	<10	<10	<10	<10	<10	<10	<10	<10	10	10	10	10	<10	<10	<10	<10
U	<10	<10	<10	<10	<10	<10	<10	<10	<10	<10	<10	<10	<10	<10	<10	<10

Table C3 Whole-rock major element and trace element analyses of the 2010 Merapi eruption (XRF) (continued)

Sample	M11-95	M11-96	M11-100	M11-103	M11-104	M11-127	M11-130	M11-133	M11-135	M11-136a	M11-136b	M11-136c	M11-137	M11-138a	M11-138b	M13-07
Sample Type	DD	LG-Inc	DD	LG-Inc	LG-Inc	A	LG-Inc	A	LG-Inc	DD	GS	LG-Inc	A	GS	LG-Inc	A
Eruption Stage	4	4	4	4/5	4/5	3	4/5	2/3	4/5	6	6	6	6	6	6	Post-2010
Locality No.	37	37	38	39	39	40	39	42	43	44	44	44	44	44	44	47
Major elements (wt%)																
SiO_2	55.02	53.34	54.92	53.77	53.69	54.35	53.38	54.49	51.98	54.96	54.46	53.94	54.23	54.47	53.49	56.41
TiO_2	0.72	0.79	0.71	0.78	0.76	0.63	0.79	0.69	0.85	0.73	0.73	0.76	0.80	0.72	0.77	0.54
Al_2O_3	19.03	19.20	19.03	18.99	19.04	18.17	19.14	19.23	19.01	19.04	18.90	19.20	18.82	18.89	18.92	19.72
Fe_2O_3	7.44	8.36	7.48	8.28	8.12	6.54	8.48	7.26	9.07	7.65	7.78	8.03	8.29	7.66	8.22	6.01
MnO	0.19	0.19	0.19	0.20	0.20	0.16	0.20	0.18	0.20	0.20	0.19	0.19	0.20	0.19	0.19	0.14
MgO	2.31	2.74	2.35	2.74	2.65	1.95	2.80	2.28	3.00	2.39	2.47	2.56	2.58	2.40	2.72	1.63
CaO	7.90	8.62	7.94	8.46	8.41	7.28	8.70	7.83	8.85	8.01	8.09	8.34	8.09	8.02	8.44	7.16
Na_2O	3.89	3.64	3.92	3.69	3.69	3.70	3.62	3.83	3.52	3.87	3.80	3.78	3.69	3.79	3.71	4.08
K_2O	2.12	2.01	2.12	2.06	2.06	2.26	2.00	2.15	2.00	2.11	2.13	2.09	2.06	2.12	2.04	2.39
P_2O_5	0.32	0.31	0.32	0.31	0.31	0.28	0.30	0.29	0.31	0.33	0.31	0.30	0.30	0.29	0.32	0.30
LOI	-0.03	-0.35	-0.02	-0.33	-0.35	3.29	-0.26	0.74	-0.21	-0.11	0.04	-0.32	0.11	0.58	0.21	1.55
Total	98.91	98.85	98.96	98.95	98.58	98.61	99.15	98.97	98.58	99.18	98.90	98.87	99.17	99.13	99.03	99.93
Trace elements (ppm)																
Sc	11	13	<10	12	12	10	13	11	15	11	12	12	12	10	11	n.a.[4]
V	140	173	141	162	161	127	180	139	201	147	157	167	174	150	178	n.a.
Cr	<10	<10	<10	<10	<10	<10	<10	<10	<10	<10	<10	<10	<10	<10	<10	n.a.
Ni	<10	<10	<10	<10	<10	<10	<10	<10	<10	<10	<10	<10	<10	<10	<10	n.a.
Cu	<10	<10	<10	<10	21	11	<10	<10	12	<10	<10	<10	<10	<10	<10	n.a.
Zn	80	77	81	79	76	69	77	78	78	84	80	75	84	76	82	n.a.
As	11	<10	11	<10	<10	14	<10	10	<10	11	11	<10	11	<10	<10	n.a.
Rb	48	44	49	47	46	50	44	48	42	47	49	47	46	49	45	n.a.
Sr	542	557	544	552	555	508	558	551	544	540	540	558	532	542	543	n.a.
Y	24	22	25	24	23	20	23	23	23	25	23	23	21	23	24	n.a.
Zr	109	92	110	96	98	109	92	106	88	108	104	95	102	105	97	n.a.
Nb	<10	<10	<10	<10	<10	<10	<10	<10	<10	<10	<10	<10	<10	<10	<10	n.a.
Mo	<10	<10	<10	<10	<10	<10	<10	<10	<10	<10	<10	<10	<10	<10	<10	n.a.
Ba	483	471	490	486	480	516	471	496	465	484	482	484	474	487	464	n.a.
La	<20	<20	21	20	<20	24	<20	<20	<20	<20	<20	<20	<20	23	<20	n.a.
Ce	82	76	83	83	77	75	75	81	71	80	79	74	74	82	71	n.a.
Pb	24	<20	24	<20	22	30	22	23	<20	24	21	<20	22	22	<20	n.a.
Th	10	<10	10	<10	<10	10	<10	<10	<10	<10	<10	<10	<10	<10	<10	n.a.
U	<10	<10	<10	<10	<10	<10	<10	<10	<10	<10	<10	<10	<10	<10	<10	n.a.

Table C3 Whole-rock major element and trace element analyses of the 2010 Merapi eruption (XRF) (continued)

Sample	M13-11	M13-12	M13-19	M13-20	M13-21	M13-22	M13-23	M13-26	M13-27	M13-28	M13-29	M13-33	M13-34	M13-35	M13-37	M13-40
Sample Type	A	WP-D	WP	SD	DD	SD	GS	WP	LG-Inc	GS	GS	LG-Inc	DD	P5N-Sc	P5N-Sc	DD
Eruption Stage	3	6	3	3	4	4	6	2	2	2	2	3	3	3	3	4
Locality No.	49	50	51	51	51	51	51	46	46	46	46	46	46	46	46	52
Major elements (wt%)																
SiO_2	54.60	53.80	55.19	54.85	55.58	55.25	54.84	55.06	53.99	53.02	55.43	54.07	54.01	55.35	55.43	55.34
TiO_2	0.74	0.84	0.70	0.76	0.70	0.73	0.72	0.73	0.76	0.83	0.72	0.76	0.77	0.72	0.71	0.73
Al_2O_3	18.98	18.82	19.14	18.92	19.41	19.33	19.35	18.98	19.44	19.08	19.22	19.37	19.23	19.16	19.36	19.08
Fe_2O_3	8.12	8.47	7.54	8.19	7.52	7.89	7.77	7.89	8.31	9.14	7.76	8.30	8.53	7.78	7.63	7.94
MnO	0.18	0.18	0.18	0.19	0.18	0.19	0.19	0.19	0.18	0.19	0.19	0.19	0.19	0.19	0.19	0.19
MgO	2.48	2.72	2.30	2.53	2.30	2.47	2.38	2.49	2.56	2.90	2.37	2.66	2.75	2.35	2.32	2.46
CaO	7.76	8.25	7.83	8.00	7.89	8.11	8.03	7.96	8.40	8.72	7.88	8.40	8.56	7.88	7.87	7.99
Na_2O	3.82	3.92	3.81	4.30	4.08	4.00	3.99	3.62	3.77	3.54	3.94	4.16	3.71	4.01	4.05	4.00
K_2O	2.11	1.82	2.14	2.17	2.14	2.07	2.07	2.10	2.04	1.95	2.16	2.12	2.01	2.15	2.16	2.14
P_2O_5	0.30	0.27	0.30	0.32	0.30	0.32	0.32	0.31	0.31	0.30	0.30	0.32	0.31	0.31	0.31	0.32
LOI	0.73	0.53	0.72	0.25	0.06	0.24	0.01	0.83	-0.24	0.19	0.33	-0.09	-0.20	0.19	0.21	0.22
Total	99.82	99.62	99.85	100.48	100.16	100.60	99.67	100.16	99.52	99.86	100.30	100.26	99.87	100.09	100.24	100.41
Trace elements (ppm)																
Sc	n.a.	n.a.	n.a.	n.a.	n.a.	n.a.	n.a.	n.a.	n.a.	n.a.	n.a.	n.a.	n.a.	n.a.	n.a.	n.a.
V	n.a.	n.a.	n.a.	n.a.	n.a.	n.a.	n.a.	n.a.	n.a.	n.a.	n.a.	n.a.	n.a.	n.a.	n.a.	n.a.
Cr	n.a.	n.a.	n.a.	n.a.	n.a.	n.a.	n.a.	n.a.	n.a.	n.a.	n.a.	n.a.	n.a.	n.a.	n.a.	n.a.
Ni	n.a.	n.a.	n.a.	n.a.	n.a.	n.a.	n.a.	n.a.	n.a.	n.a.	n.a.	n.a.	n.a.	n.a.	n.a.	n.a.
Cu	n.a.	n.a.	n.a.	n.a.	n.a.	n.a.	n.a.	n.a.	n.a.	n.a.	n.a.	n.a.	n.a.	n.a.	n.a.	n.a.
Zn	n.a.	n.a.	n.a.	n.a.	n.a.	n.a.	n.a.	n.a.	n.a.	n.a.	n.a.	n.a.	n.a.	n.a.	n.a.	n.a.
As	n.a.	n.a.	n.a.	n.a.	n.a.	n.a.	n.a.	n.a.	n.a.	n.a.	n.a.	n.a.	n.a.	n.a.	n.a.	n.a.
Rb	n.a.	n.a.	n.a.	n.a.	n.a.	n.a.	n.a.	n.a.	n.a.	n.a.	n.a.	n.a.	n.a.	n.a.	n.a.	n.a.
Sr	n.a.	n.a.	n.a.	n.a.	n.a.	n.a.	n.a.	n.a.	n.a.	n.a.	n.a.	n.a.	n.a.	n.a.	n.a.	n.a.
Y	n.a.	n.a.	n.a.	n.a.	n.a.	n.a.	n.a.	n.a.	n.a.	n.a.	n.a.	n.a.	n.a.	n.a.	n.a.	n.a.
Zr	n.a.	n.a.	n.a.	n.a.	n.a.	n.a.	n.a.	n.a.	n.a.	n.a.	n.a.	n.a.	n.a.	n.a.	n.a.	n.a.
Nb	n.a.	n.a.	n.a.	n.a.	n.a.	n.a.	n.a.	n.a.	n.a.	n.a.	n.a.	n.a.	n.a.	n.a.	n.a.	n.a.
Mo	n.a.	n.a.	n.a.	n.a.	n.a.	n.a.	n.a.	n.a.	n.a.	n.a.	n.a.	n.a.	n.a.	n.a.	n.a.	n.a.
Ba	n.a.	n.a.	n.a.	n.a.	n.a.	n.a.	n.a.	n.a.	n.a.	n.a.	n.a.	n.a.	n.a.	n.a.	n.a.	n.a.
La	n.a.	n.a.	n.a.	n.a.	n.a.	n.a.	n.a.	n.a.	n.a.	n.a.	n.a.	n.a.	n.a.	n.a.	n.a.	n.a.
Ce	n.a.	n.a.	n.a.	n.a.	n.a.	n.a.	n.a.	n.a.	n.a.	n.a.	n.a.	n.a.	n.a.	n.a.	n.a.	n.a.
Pb	n.a.	n.a.	n.a.	n.a.	n.a.	n.a.	n.a.	n.a.	n.a.	n.a.	n.a.	n.a.	n.a.	n.a.	n.a.	n.a.
Th	n.a.	n.a.	n.a.	n.a.	n.a.	n.a.	n.a.	n.a.	n.a.	n.a.	n.a.	n.a.	n.a.	n.a.	n.a.	n.a.
U	n.a.	n.a.	n.a.	n.a.	n.a.	n.a.	n.a.	n.a.	n.a.	n.a.	n.a.	n.a.	n.a.	n.a.	n.a.	n.a.

Table C3 Whole-rock major element and trace element analyses of the 2010 Merapi eruption (XRF) (continued)

Sample	M13-41	M13-42	M13-43	M13-60	M13-64	M13-65	M13-67									
Sample Type	SD	LG-Inc	WP	LG-Inc	SD	DD	SD									
Eruption Stage	4	4	6	2	3	3	3									
Locality No.	52	52	53	56	56	56	56									
Major elements (wt%)																
SiO_2	54.67	54.23	55.45	55.00	53.45	55.54	54.69									
TiO_2	0.74	0.77	0.70	0.73	0.79	0.73	0.73									
Al_2O_3	19.19	19.35	19.24	19.04	19.24	19.25	19.25									
Fe_2O_3	8.03	8.47	7.62	8.03	8.76	7.86	7.93									
MnO	0.19	0.19	0.19	0.19	0.19	0.19	0.19									
MgO	2.50	2.73	2.33	2.55	2.89	2.38	2.42									
CaO	8.15	8.57	7.84	8.19	8.78	7.91	8.07									
Na_2O	4.04	3.81	4.04	3.95	3.74	4.05	4.07									
K_2O	2.08	2.02	2.16	2.09	1.98	2.15	2.07									
P_2O_5	0.31	0.30	0.30	0.30	0.31	0.31	0.32									
LOI	0.40	-0.27	0.27	0.11	0.03	0.08	0.14									
Total	100.30	100.17	100.14	100.18	100.16	100.45	99.88									
Trace elements (ppm)																
Sc	n.a.	n.a.	n.a.	n.a.	n.a.	n.a.	n.a.									
V	n.a.	n.a.	n.a.	n.a.	n.a.	n.a.	n.a.									
Cr	n.a.	n.a.	n.a.	n.a.	n.a.	n.a.	n.a.									
Ni	n.a.	n.a.	n.a.	n.a.	n.a.	n.a.	n.a.									
Cu	n.a.	n.a.	n.a.	n.a.	n.a.	n.a.	n.a.									
Zn	n.a.	n.a.	n.a.	n.a.	n.a.	n.a.	n.a.									
As	n.a.	n.a.	n.a.	n.a.	n.a.	n.a.	n.a.									
Rb	n.a.	n.a.	n.a.	n.a.	n.a.	n.a.	n.a.									
Sr	n.a.	n.a.	n.a.	n.a.	n.a.	n.a.	n.a.									
Y	n.a.	n.a.	n.a.	n.a.	n.a.	n.a.	n.a.									
Zr	n.a.	n.a.	n.a.	n.a.	n.a.	n.a.	n.a.									
Nb	n.a.	n.a.	n.a.	n.a.	n.a.	n.a.	n.a.									
Mo	n.a.	n.a.	n.a.	n.a.	n.a.	n.a.	n.a.									
Ba	n.a.	n.a.	n.a.	n.a.	n.a.	n.a.	n.a.									
La	n.a.	n.a.	n.a.	n.a.	n.a.	n.a.	n.a.									
Ce	n.a.	n.a.	n.a.	n.a.	n.a.	n.a.	n.a.									
Pb	n.a.	n.a.	n.a.	n.a.	n.a.	n.a.	n.a.									
Th	n.a.	n.a.	n.a.	n.a.	n.a.	n.a.	n.a.									
U	n.a.	n.a.	n.a.	n.a.	n.a.	n.a.	n.a.									

Table C4 Whole-rock trace element analyses of the 2010 Merapi eruption (ICP-MS)

Sample	M11-X1	M11-X1[4]	M11-05	M11-12	M11-14	M11-18	M11-21	M11-27-5
Sample Type[1]	CS	CS	LG-Inc	DD	A	WP	A	DD
Eruption Stage[2]	4/5	4/5	4/5	4	3	6	3	4/5
Locality No.[3]	1	1	2	5	7	9	11	13
Trace elements (ppm)								
Ba	18	19	474	486	557	510	543	491
Be	<1	1	<1	<1	<1	<1	2	<1
Co	8.0	8.8	14.1	13.1	12.0	12.8	12.0	12.1
Cs	0.9	1.2	3.4	3.5	4.0	3.9	4.3	3.9
Ga	4.3	3.5	16.7	17.5	17.8	17.5	17.0	17.2
Hf	3.6	3.4	2.4	2.5	2.3	2.8	2.7	2.4
Nb	6.2	4.4	4.0	3.9	4.8	3.9	4.0	3.8
Rb	10.0	10.6	42.2	42.9	50.2	46.7	50.5	44.6
Sn	4	5	<1	<1	2	1	5	<1
Sr	79.3	79.2	572.4	584.7	592.2	588.4	571.1	595.2
Ta	0.3	0.2	0.3	0.3	0.3	0.2	0.3	0.3
Th	3.5	3.2	6.9	6.5	7.4	7.3	7.4	7.1
U	1.1	1.0	1.6	1.5	1.7	1.7	1.6	1.3
V	27	30	175	161	140	151	125	147
W	1.0	0.6	<0.5	<0.5	0.9	0.6	0.8	<0.5
Zr	126.7	129.4	85.6	92.8	102.4	96.7	104.7	95.3
Y	9.9	9.6	23.1	24.0	21.0	23.9	20.3	24.7
La	10.8	11.9	17.5	18.7	18.9	18.4	18.7	18.0
Ce	20.5	20.3	35.5	34.8	37.8	36.4	38.0	37.2
Pr	2.78	2.68	4.18	4.41	4.53	4.37	4.46	4.41
Nd	11.9	11.6	18.1	19.2	18.1	18.7	17.7	18.1
Sm	2.10	2.13	4.03	4.15	4.00	3.99	3.59	4.27
Eu	0.54	0.48	1.22	1.31	1.22	1.29	1.19	1.26
Gd	2.19	2.03	4.05	4.18	4.09	3.97	3.89	4.13
Tb	0.30	0.31	0.65	0.68	0.67	0.66	0.66	0.69
Dy	1.60	2.00	3.42	3.82	3.83	3.72	3.55	4.04
Ho	0.28	0.32	0.78	0.80	0.86	0.80	0.77	0.79
Er	0.83	1.00	2.34	2.61	2.37	2.41	2.53	2.21
Tm	0.15	0.13	0.34	0.34	0.37	0.33	0.33	0.35
Yb	0.90	0.96	2.17	2.37	2.53	2.20	2.22	2.09
Lu	0.14	0.14	0.34	0.38	0.38	0.35	0.38	0.38
Mo	<0.1	n.a.[5]	0.7	0.1	0.5	0.2	0.3	0.1
Cu	17.9	n.a.	31.1	16.7	20.0	16.9	18.5	16.6
Pb	0.6	n.a.	2.1	1.3	3.5	1.6	5.2	1.4
Zn	2	n.a.	50	41	38	51	34	43
Ni	3.8	n.a.	2.2	1.3	1.2	1.5	1.4	1.4
As	0.8	n.a.	1.7	0.7	0.9	<0.5	0.7	<0.5
Cd	<0.1	n.a.	<0.1	<0.1	<0.1	<0.1	<0.1	<0.1
Sb	<0.1	n.a.	<0.1	<0.1	<0.1	<0.1	<0.1	<0.1
Bi	<0.1	n.a.	<0.1	<0.1	0.2	<0.1	0.1	<0.1
Ag	<0.1	n.a.	<0.1	<0.1	<0.1	<0.1	<0.1	<0.1
Au	<0.5	n.a.	2.8	1.3	4.7	1.4	2.2	7.7
Hg	<0.01	n.a.	<0.01	<0.01	0.02	<0.01	<0.01	<0.01
Tl	<0.1	n.a.	<0.1	<0.1	<0.1	<0.1	<0.1	<0.1
Se	<0.5	n.a.	<0.5	<0.5	<0.5	<0.5	<0.5	<0.5

[1] See Appendix A; [2] after Komorowski et al. (2013); [3] see Appendix B; [4] duplicate analysis; [5] n.a. = not analysed

Table C4 Whole-rock trace element analyses of the 2010 Merapi eruption (ICP-MS) (continued)

Sample	M11-55	M11-67B	M11-68B	M11-75	M11-80	M11-93	M11-130	M11-133
Sample Type	WP	A	A	GS	DD	DS	LG-Inc	A
Eruption Stage	6	3	3	6	4	3	4/5	2/3
Locality No.	28	34	34	35	16	25	39	42
Trace elements (ppm)								
Ba	518	539	519	499	526	516	469	519
Be	1	2	2	2	2	1	<1	1
Co	14.8	11.8	12.6	13.3	13.2	12.6	16.3	13.2
Cs	3.8	3.6	3.2	3.6	3.9	3.5	3.4	4.0
Ga	17.7	18.0	17.9	18.0	17.9	17.6	17.1	17.8
Hf	2.8	2.6	2.7	2.5	2.7	2.4	2.0	2.4
Nb	3.1	4.9	3.1	2.4	4.4	3.6	1.9	2.6
Rb	47.7	48.5	45.6	46.4	46.5	46.9	41.1	46.7
Sn	1	<1	<1	<1	<1	<1	<1	<1
Sr	612.7	580.0	605.5	578.2	615.9	605.5	606.8	623.7
Ta	0.2	0.3	0.2	0.2	0.3	0.2	0.2	0.2
Th	6.6	7.2	6.7	6.6	7.2	7.0	5.9	6.7
U	1.6	1.8	1.3	1.6	1.5	1.5	1.3	1.7
V	158	140	153	150	153	154	191	149
W	0.8	0.7	<0.5	0.6	<0.5	<0.5	<0.5	<0.5
Zr	101.0	103.6	97.8	99.9	100.9	100.9	87.9	99.1
Y	22.5	18.2	19.4	21.3	22.1	21.4	21.9	22.0
La	19.5	17.5	16.8	18.9	19.3	19.0	17.8	18.7
Ce	38.8	33.4	32.9	37.8	38.5	37.7	34.9	37.1
Pr	4.36	3.89	3.69	4.42	4.50	4.47	4.14	4.25
Nd	18.4	17.3	15.6	17.1	19.0	18.8	18.1	16.2
Sm	4.24	3.54	3.61	4.05	4.31	4.12	3.96	4.09
Eu	1.20	1.18	1.25	1.29	1.26	1.28	1.22	1.28
Gd	4.34	3.68	3.60	4.01	4.30	4.06	3.98	4.26
Tb	0.67	0.60	0.60	0.67	0.69	0.68	0.66	0.67
Dy	4.04	3.16	3.69	3.81	4.07	3.82	3.97	3.87
Ho	0.86	0.76	0.70	0.96	0.90	0.80	0.85	0.83
Er	2.71	2.21	2.15	2.47	2.60	2.45	2.29	2.54
Tm	0.35	0.30	0.34	0.36	0.36	0.33	0.32	0.36
Yb	2.52	2.34	2.11	2.46	2.37	2.44	2.32	2.34
Lu	0.36	0.36	0.34	0.38	0.40	0.37	0.34	0.36
Mo	0.1	0.8	0.6	0.1	0.1	0.1	0.7	0.2
Cu	16.4	17.8	18.6	12.6	13.6	23.9	16.3	24.0
Pb	1.4	8.7	4.9	1.7	1.1	1.0	1.3	3.2
Zn	52	43	47	40	38	40	48	38
Ni	1.5	1.6	1.6	1.3	1.0	1.3	2.2	1.4
As	<0.5	3.4	1.9	<0.5	<0.5	<0.5	<0.5	<0.5
Cd	<0.1	<0.1	<0.1	<0.1	<0.1	<0.1	<0.1	<0.1
Sb	<0.1	<0.1	<0.1	<0.1	<0.1	<0.1	<0.1	<0.1
Bi	<0.1	1.0	0.6	<0.1	<0.1	<0.1	<0.1	<0.1
Ag	<0.1	<0.1	<0.1	<0.1	<0.1	<0.1	<0.1	<0.1
Au	4.1	95.8	14.1	2.3	0.5	0.7	1.0	1.2
Hg	0.02	<0.01	<0.01	<0.01	0.02	<0.01	0.01	<0.01
Tl	<0.1	0.2	0.2	<0.1	<0.1	<0.1	<0.1	<0.1
Se	<0.5	0.6	0.9	<0.5	<0.5	<0.5	<0.5	<0.5

Table C4 Whole-rock trace element analyses of the 2010 Merapi eruption (ICP-MS) (continued)

Sample	M11-137							
Sample Type	A							
Eruption Stage	6							
Locality No.	44							
Trace elements (ppm)								
Ba	484							
Be	3							
Co	14.8							
Cs	2.8							
Ga	16.8							
Hf	2.4							
Nb	3.5							
Rb	43.4							
Sn	<1							
Sr	572.6							
Ta	0.2							
Th	6.5							
U	1.5							
V	171							
W	<0.5							
Zr	92.7							
Y	18.2							
La	16.4							
Ce	30.9							
Pr	3.75							
Nd	15.1							
Sm	3.60							
Eu	1.21							
Gd	3.78							
Tb	0.60							
Dy	3.60							
Ho	0.77							
Er	2.18							
Tm	0.31							
Yb	2.10							
Lu	0.34							
Mo	0.8							
Cu	15.6							
Pb	4.5							
Zn	52							
Ni	1.8							
As	1.0							
Cd	<0.1							
Sb	<0.1							
Bi	0.4							
Ag	<0.1							
Au	9.1							
Hg	0.01							
Tl	0.2							
Se	<0.5							

Table D1 Feldspar analyses of the 2006 Merapi eruption[1]

Sample	ME08-01	ME08-01	ME08-01	ME08-01	ME08-01	ME08-01	ME08-01	ME08-01	ME08-01	ME08-01	ME08-01	ME08-01	ME08-01	ME08-01
Sample Type[2]	L4-S	L4-S	L4-S	L4-S	L4-S	L4-S	L4-S	L4-S	L4-S	L4-S	L4-S	L4-S	L4-S	L4-S
Point	2 / 1 .	2 / 2 .	2 / 3 .	2 / 4 .	2 / 5 .	2 / 6 .	2 / 7 .	2 / 8 .	2 / 9 .	2 / 10 .	2 / 11 .	2 / 12 .	2 / 13 .	2 / 14 .
Comment[3]	ph-c	ph	ph	ph	ph	ph	ph	ph	ph	ph	ph	ph	ph	ph
SiO_2	52.30	51.83	52.41	52.35	52.41	55.11	56.03	54.82	55.34	56.51	56.10	56.26	55.44	56.19
TiO_2	0.02	0.02	0.02	0.03	0.01	0.02	0.03	0.03	0.04	0.03	0.04	0.03	0.02	0.03
Al_2O_3	29.58	29.68	29.80	29.56	29.67	27.73	27.29	28.37	27.83	26.87	27.50	27.10	27.08	27.12
FeO	0.44	0.45	0.49	0.50	0.47	0.53	0.46	0.54	0.51	0.47	0.45	0.46	0.48	0.51
MgO	0.03	0.04	0.05	0.03	0.05	0.06	0.02	0.04	0.04	0.07	0.05	0.03	0.04	0.05
CaO	12.59	12.92	12.62	12.56	12.37	10.41	9.51	10.86	10.23	9.29	9.83	9.60	10.35	9.52
SrO	0.18	0.08	0.15	0.18	0.15	0.11	0.13	0.09	0.06	0.15	0.13	0.10	0.11	0.11
BaO	0.05	0.05	0.03	0.02	0.26	0.13	0.01		0.01	0.07	0.03	0.11	0.13	0.01
Na_2O	4.08	3.98	4.18	4.14	4.35	5.30	5.68	5.11	5.34	5.92	5.76	5.81	5.62	5.73
K_2O	0.29	0.26	0.30	0.28	0.27	0.48	0.53	0.41	0.42	0.62	0.54	0.53	0.49	0.53
Sum	99.56	99.35	100.05	99.66	100.01	99.89	99.73	100.33	99.83	100.00	100.42	100.04	99.82	99.78
Si	2.390	2.376	2.384	2.390	2.388	2.498	2.534	2.474	2.503	2.550	2.523	2.539	2.517	2.539
Al	1.593	1.603	1.597	1.590	1.593	1.481	1.455	1.509	1.483	1.429	1.458	1.441	1.449	1.444
Ti	0.001	0.001	0.001	0.001	0.000	0.001	0.001	0.001	0.001	0.001	0.001	0.001	0.001	0.001
Fe	0.017	0.017	0.019	0.019	0.018	0.020	0.017	0.020	0.019	0.018	0.017	0.017	0.018	0.019
Mg	0.002	0.003	0.003	0.002	0.003	0.004	0.002	0.003	0.003	0.005	0.003	0.002	0.003	0.003
Sr	0.005	0.002	0.004	0.005	0.004	0.003	0.003	0.002	0.002	0.004	0.003	0.003	0.003	0.003
Ba	0.001	0.001	0.001	0.000	0.005	0.002	0.000	0.000	0.000	0.001	0.001	0.002	0.002	0.000
Ca	0.617	0.634	0.615	0.614	0.604	0.505	0.461	0.525	0.496	0.449	0.474	0.464	0.503	0.461
Na	0.361	0.354	0.369	0.366	0.384	0.466	0.498	0.448	0.469	0.518	0.502	0.509	0.495	0.502
K	0.017	0.015	0.017	0.016	0.016	0.028	0.030	0.023	0.024	0.036	0.031	0.030	0.028	0.030
Sum	5.002	5.006	5.010	5.005	5.015	5.008	5.002	5.006	5.000	5.011	5.013	5.009	5.019	5.003
Ab (mol%)	36.3	35.3	36.8	36.7	38.3	46.6	50.3	44.9	47.4	51.7	49.9	50.7	48.2	50.5
An (mol%)	62.0	63.2	61.4	61.6	60.2	50.6	46.6	52.7	50.2	44.8	47.1	46.3	49.1	46.4
Or (mol%)	1.7	1.5	1.7	1.7	1.6	2.8	3.1	2.3	2.4	3.6	3.1	3.0	2.8	3.1

[1] Major element oxides in wt.%; number of cations based on 8 oxygens; [2] see Appendix A; [3] ph = phenocryst, mph = microphenocryst, m = microlite, c = core, r = rim

Table D1 Feldspar analyses of the 2006 Merapi eruption (continued)

Sample	ME08-01	ME08-01	ME08-01	ME08-01	ME08-01	ME08-01	ME08-01	ME08-01	ME08-01	ME08-01	ME08-01	ME08-03-02	ME08-03-02	ME08-03-02
Sample Type	L4-S	L4-S	L4-S	L4-S	L4-S	L4-S	L4-S	L4-S	L4-S	L4-S	L4-S	L6-S	L6-S	L6-S
Point	2 / 15 .	2 / 16 .	2 / 17 .	2 / 18 .	2 / 19 .	2 / 21 .	2 / 22 .	13 / 1 .	14 / 1 .	15 / 1 .	16 / 1 .	3 / 1 .	3 / 2 .	3 / 3 .
Comment	ph	ph	ph	ph	ph	ph	ph-r	m	m	m	m	ph-c	ph	ph
SiO_2	56.35	56.72	56.19	56.47	55.36	57.42	63.29	57.41	60.33	57.21	60.86	56.83	56.34	53.25
TiO_2	0.02	0.02	0.02	0.03	0.03	0.04	0.12	0.03	0.03	0.02	0.03	0.03	0.03	0.04
Al_2O_3	27.32	26.87	26.98	26.63	27.23	25.59	21.99	26.44	24.22	25.15	24.09	26.72	26.93	29.29
FeO	0.53	0.51	0.47	0.48	0.49	0.36	0.88	0.71	0.61	1.11	0.63	0.44	0.54	0.52
MgO	0.06	0.03	0.04	0.06	0.05	0.05	0.18	0.05	0.01	0.87	0.03	0.05	0.07	0.07
CaO	9.55	9.02	9.56	9.10	10.02	7.95	4.92	8.70	6.16	7.84	6.26	8.99	9.44	11.64
SrO	0.20	0.11	0.11	0.16	0.17	0.05	0.07	0.12	0.07	0.11	0.06	0.07	0.13	0.11
BaO	0.10	0.14	0.02	0.08	0.07	0.16	0.23	0.09	0.20	0.17	0.33	0.01		0.06
Na_2O	5.73	6.10	5.66	5.87	5.45	6.33	7.00	6.20	7.07	6.09	6.88	5.97	5.91	4.46
K_2O	0.54	0.60	0.55	0.57	0.47	0.76	1.93	0.83	1.40	0.84	1.63	0.62	0.56	0.34
Sum	100.42	100.12	99.68	99.47	99.36	98.77	100.67	100.59	100.11	99.49	100.82	99.73	99.93	99.85
Si	2.535	2.556	2.544	2.560	2.519	2.614	2.812	2.577	2.703	2.599	2.712	2.565	2.545	2.421
Al	1.448	1.427	1.440	1.423	1.460	1.373	1.151	1.399	1.279	1.347	1.265	1.421	1.434	1.569
Ti	0.001	0.001	0.001	0.001	0.001	0.001	0.004	0.001	0.001	0.001	0.001	0.001	0.001	0.001
Fe	0.020	0.019	0.018	0.018	0.019	0.014	0.033	0.027	0.023	0.042	0.024	0.017	0.020	0.020
Mg	0.004	0.002	0.003	0.004	0.003	0.004	0.012	0.003	0.001	0.059	0.002	0.003	0.005	0.005
Sr	0.005	0.003	0.003	0.004	0.005	0.001	0.002	0.003	0.002	0.003	0.002	0.002	0.003	0.003
Ba	0.002	0.003	0.000	0.001	0.001	0.003	0.004	0.002	0.004	0.003	0.006	0.000	0.000	0.001
Ca	0.460	0.436	0.464	0.442	0.488	0.388	0.234	0.418	0.296	0.381	0.299	0.435	0.457	0.567
Na	0.500	0.533	0.497	0.516	0.481	0.559	0.603	0.539	0.614	0.536	0.595	0.523	0.518	0.393
K	0.031	0.034	0.032	0.033	0.027	0.044	0.110	0.047	0.080	0.049	0.093	0.036	0.032	0.020
Sum	5.006	5.013	5.000	5.003	5.004	5.000	4.964	5.016	5.003	5.020	4.998	5.003	5.012	5.000
Ab (mol%)	50.4	53.1	50.1	52.1	48.3	56.4	63.7	53.7	62.0	55.5	60.3	52.6	51.4	40.1
An (mol%)	46.4	43.5	46.7	44.6	49.0	39.1	24.7	41.6	29.9	39.5	30.3	43.8	45.4	57.8
Or (mol%)	3.1	3.4	3.2	3.3	2.8	4.4	11.6	4.7	8.1	5.0	9.4	3.6	3.2	2.0

Table D1 Feldspar analyses of the 2006 Merapi eruption (continued)

Sample	ME08-03-02	ME08-03-02	ME08-03-02	ME08-03-02	ME08-03-02	ME08-03-02	ME08-03-02	ME08-03-02	ME08-03-02	ME08-03-02	ME08-03-02	ME08-03-02	ME08-03-02	ME08-03-02
Sample Type	L6-S	L6-S	L6-S	L6-S	L6-S	L6-S	L6-S	L6-S	L6-S	L6-S	L6-S	L6-S	L6-S	L6-S
Point	3 / 4 .	3 / 5 .	3 / 6 .	3 / 7 .	3 / 8 .	3 / 9 .	3 / 10 .	3 / 11 .	3 / 12 .	3 / 13 .	3 / 14 .	3 / 15 .	3 / 16 .	3 / 17 .
Comment	ph	ph	ph	ph	ph	ph	ph	ph	ph	ph	ph	ph	ph	ph
SiO_2	45.52	45.52	45.63	47.43	52.45	54.52	55.23	55.30	55.98	55.45	56.02	56.63	56.81	56.02
TiO_2	0.01	0.02	0.02	0.01	0.02	0.03	0.03	0.03	0.03	0.02	0.03	0.03	0.03	0.03
Al_2O_3	34.27	34.40	34.10	32.99	29.55	28.41	27.75	27.43	27.57	27.61	27.28	26.82	26.84	27.13
FeO	0.46	0.44	0.54	0.44	0.48	0.44	0.42	0.55	0.46	0.51	0.39	0.49	0.44	0.43
MgO	0.01	0.01	0.02	0.04	0.05	0.04	0.04	0.04	0.05	0.04	0.05	0.05	0.04	0.03
CaO	17.80	17.75	17.46	16.06	12.47	10.78	10.43	10.04	9.69	10.08	9.66	9.13	8.94	9.60
SrO	0.14	0.16	0.16	0.15	0.17	0.15	0.12	0.14	0.08	0.18	0.10	0.14	0.12	0.15
BaO		0.01			0.10	0.05	0.03	0.09	0.03	0.03	0.04	0.09	0.05	0.03
Na_2O	1.26	1.13	1.33	2.10	4.32	5.05	5.25	5.44	5.66	5.32	5.63	6.02	6.01	5.78
K_2O	0.05	0.05	0.07	0.07	0.26	0.39	0.40	0.49	0.55	0.51	0.53	0.55	0.57	0.62
Sum	99.55	99.49	99.35	99.28	99.88	99.85	99.75	99.56	100.10	99.75	99.74	99.96	99.85	99.83
Si	2.112	2.111	2.120	2.194	2.391	2.471	2.502	2.512	2.523	2.512	2.533	2.555	2.562	2.534
Al	1.874	1.880	1.867	1.798	1.587	1.518	1.482	1.468	1.464	1.474	1.454	1.426	1.426	1.446
Ti	0.000	0.001	0.001	0.000	0.001	0.001	0.001	0.001	0.001	0.001	0.001	0.001	0.001	0.001
Fe	0.018	0.017	0.021	0.017	0.018	0.017	0.016	0.021	0.017	0.019	0.015	0.019	0.016	0.016
Mg	0.001	0.001	0.002	0.003	0.003	0.002	0.003	0.003	0.004	0.003	0.004	0.003	0.003	0.002
Sr	0.004	0.004	0.004	0.004	0.005	0.004	0.003	0.004	0.002	0.005	0.003	0.004	0.003	0.004
Ba	0.000	0.000	0.000	0.000	0.002	0.001	0.001	0.002	0.001	0.001	0.001	0.002	0.001	0.001
Ca	0.885	0.882	0.869	0.796	0.609	0.523	0.506	0.489	0.468	0.489	0.468	0.441	0.432	0.465
Na	0.113	0.102	0.120	0.189	0.382	0.443	0.461	0.479	0.495	0.467	0.493	0.526	0.525	0.507
K	0.003	0.003	0.004	0.004	0.015	0.023	0.023	0.028	0.032	0.030	0.031	0.032	0.033	0.036
Sum	5.009	5.001	5.008	5.004	5.013	5.002	4.998	5.007	5.007	4.999	5.001	5.010	5.003	5.013
Ab (mol%)	11.3	10.3	12.1	19.1	38.0	44.8	46.5	48.1	49.7	47.4	49.7	52.7	53.0	50.3
An (mol%)	88.4	89.4	87.5	80.5	60.5	52.9	51.1	49.1	47.1	49.6	47.2	44.1	43.6	46.2
Or (mol%)	0.3	0.3	0.4	0.4	1.5	2.3	2.3	2.8	3.2	3.0	3.1	3.2	3.3	3.5

Table D1 Feldspar analyses of the 2006 Merapi eruption (continued)

Sample	ME08-03-02	ME08-03-02	ME08-03-02	ME08-03-02	ME08-03-02	ME08-03-02	ME08-03-02	ME08-03-02	ME08-03-02	ME08-03-02	ME08-03-02	ME08-03-02	ME08-03-02	ME08-03-02
Sample Type	L6-S	L6-S	L6-S	L6-S	L6-S	L6-S	L6-S	L6-S	L6-S	L6-S	L6-S	L6-S	L6-S	L6-S
Point	3 / 18 .	3 / 19 .	3 / 20 .	3 / 21 .	3 / 22 .	3 / 23 .	3 / 24 .	3 / 25 .	3 / 26 .	3 / 27 .	3 / 28 .	3 / 29 .	3 / 30 .	3 / 31 .
Comment	ph	ph	ph	ph	ph	ph	ph	ph	ph	ph	ph	ph	ph	ph
SiO_2	60.53	55.39	55.76	55.88	57.23	57.14	57.69	56.46	56.01	56.06	56.11	55.74	53.63	52.63
TiO_2	0.33	0.02	0.02	0.02	0.03	0.03	0.02	0.03	0.01	0.02	0.02	0.02	0.03	0.01
Al_2O_3	22.62	27.46	27.55	27.31	26.48	26.38	26.26	27.16	27.11	27.34	27.22	27.28	28.94	29.37
FeO	1.42	0.39	0.54	0.50	0.42	0.47	0.51	0.47	0.44	0.45	0.44	0.50	0.52	0.58
MgO	0.25	0.06	0.04	0.03	0.02	0.06	0.03	0.05	0.04	0.06	0.05	0.02	0.04	0.05
CaO	6.62	9.86	9.78	9.85	8.70	8.65	8.52	9.48	9.78	9.68	9.60	9.83	11.56	12.06
SrO	0.09	0.09	0.13	0.16	0.12	0.15	0.11	0.17	0.11	0.15	0.12	0.11	0.14	0.16
BaO			0.13	0.10		0.12	0.06	0.12	0.01	0.09	0.03	0.10	0.06	
Na_2O	5.20	5.52	5.50	5.59	6.05	6.07	6.12	5.72	5.64	5.57	5.69	5.72	4.74	4.35
K_2O	2.12	0.54	0.49	0.51	0.67	0.66	0.66	0.59	0.52	0.52	0.53	0.49	0.37	0.33
Sum	99.21	99.33	99.96	99.97	99.78	99.71	99.99	100.25	99.77	99.94	99.84	99.82	100.04	99.53
Si	2.741	2.517	2.520	2.526	2.581	2.581	2.595	2.542	2.535	2.531	2.536	2.524	2.434	2.403
Al	1.207	1.471	1.467	1.455	1.407	1.404	1.392	1.441	1.446	1.455	1.449	1.456	1.548	1.581
Ti	0.011	0.001	0.001	0.001	0.001	0.001	0.001	0.001	0.000	0.001	0.001	0.001	0.001	0.000
Fe	0.054	0.015	0.020	0.019	0.016	0.018	0.019	0.018	0.017	0.017	0.017	0.019	0.020	0.022
Mg	0.017	0.004	0.003	0.002	0.002	0.004	0.002	0.003	0.003	0.004	0.004	0.002	0.003	0.003
Sr	0.002	0.002	0.003	0.004	0.003	0.004	0.003	0.004	0.003	0.004	0.003	0.003	0.004	0.004
Ba	0.000	0.000	0.002	0.002	0.000	0.002	0.001	0.002	0.000	0.002	0.001	0.002	0.001	0.000
Ca	0.321	0.480	0.474	0.477	0.420	0.419	0.410	0.457	0.474	0.468	0.465	0.477	0.562	0.590
Na	0.456	0.486	0.482	0.490	0.529	0.532	0.534	0.500	0.495	0.488	0.499	0.502	0.417	0.385
K	0.123	0.032	0.028	0.029	0.039	0.038	0.038	0.034	0.030	0.030	0.030	0.028	0.021	0.019
Sum	4.933	5.006	5.001	5.005	4.998	5.001	4.994	5.003	5.004	5.000	5.003	5.013	5.010	5.008
Ab (mol%)	50.7	48.7	49.0	49.2	53.6	53.8	54.3	50.4	49.5	49.5	50.2	49.9	41.7	38.7
An (mol%)	35.7	48.1	48.1	47.9	42.5	42.4	41.8	46.1	47.5	47.5	46.8	47.3	56.2	59.3
Or (mol%)	13.6	3.2	2.9	3.0	3.9	3.8	3.9	3.4	3.0	3.1	3.1	2.8	2.1	1.9

Table D1 Feldspar analyses of the 2006 Merapi eruption (continued)

Sample	ME08-03-02	ME08-03-02	ME08-03-02	ME08-03-02	ME08-03-02	ME08-03-02	ME08-03-02	ME08-03-02	ME08-03-02	ME08-03-02	ME08-03-02	ME08-03-02	ME08-03-02	ME08-03-02
Sample Type	L6-S	L6-S	L6-S	L6-S	L6-S	L6-S	L6-S	L6-S	L6-S	L6-S	L6-S	L6-S	L6-S	L6-S
Point	3 / 32 .	3 / 33 .	3 / 34 .	3 / 35 .	3 / 36 .	3 / 37 .	3 / 38 .	3 / 39 .	3 / 40 .	3 / 42 .	3 / 43 .	13 / 1 .	14 / 1 .	16 / 1 .
Comment	ph	ph	ph	ph	ph	ph	ph	ph	ph	ph	ph-r	m	m	m
SiO_2	53.67	53.65	53.04	53.71	54.26	54.96	55.37	56.14	55.69	56.65	64.92	58.58	58.23	67.03
TiO_2	0.02	0.03	0.04	0.03	0.02	0.04	0.02	0.03	0.02	0.02	0.16	0.02	0.03	0.06
Al_2O_3	28.45	28.61	29.10	28.66	28.13	27.69	27.14	26.92	27.61	25.87	19.76	25.96	25.57	18.64
FeO	0.46	0.52	0.49	0.50	0.59	0.43	0.52	0.53	0.60	0.55	0.98	0.57	0.51	0.68
MgO	0.03	0.04	0.06	0.04	0.05	0.04	0.06	0.06	0.04	0.02	0.08	0.02	-0.01	0.01
CaO	11.13	11.22	11.55	11.16	10.47	10.06	9.60	8.91	9.63	8.29	3.44	7.94	7.96	0.99
SrO	0.13	0.20	0.13	0.08	0.11	0.12	0.17	0.13	0.12	0.10	0.02	0.10		
BaO	0.02	0.13	0.04	0.06	0.13	0.09	0.03	0.06		0.09	0.16	0.10	0.04	0.25
Na_2O	4.90	4.84	4.58	4.85	5.26	5.43	5.77	5.97	5.69	6.31	6.10	6.39	6.43	6.08
K_2O	0.36	0.42	0.37	0.39	0.44	0.53	0.55	0.65	0.54	0.83	3.92	0.99	1.01	7.08
Sum	99.22	99.68	99.41	99.51	99.53	99.38	99.29	99.42	99.96	98.72	99.58	100.67	99.82	100.81
Si	2.452	2.445	2.421	2.447	2.473	2.501	2.522	2.548	2.517	2.587	2.916	2.618	2.624	2.992
Al	1.532	1.536	1.566	1.539	1.511	1.485	1.457	1.440	1.471	1.392	1.046	1.367	1.358	0.981
Ti	0.001	0.001	0.001	0.001	0.001	0.001	0.001	0.001	0.001	0.001	0.005	0.001	0.001	0.002
Fe	0.018	0.020	0.019	0.019	0.022	0.016	0.020	0.020	0.023	0.021	0.037	0.021	0.019	0.025
Mg	0.002	0.003	0.004	0.003	0.003	0.002	0.004	0.004	0.003	0.001	0.005	0.001	0.000	0.001
Sr	0.003	0.005	0.003	0.002	0.003	0.003	0.005	0.003	0.003	0.003	0.001	0.003		
Ba	0.000	0.002	0.001	0.001	0.002	0.002	0.001	0.001	0.000	0.002	0.003	0.002	0.001	0.004
Ca	0.545	0.548	0.565	0.545	0.511	0.490	0.469	0.433	0.466	0.406	0.166	0.380	0.384	0.047
Na	0.434	0.427	0.406	0.428	0.465	0.479	0.510	0.525	0.499	0.559	0.531	0.553	0.562	0.526
K	0.021	0.024	0.022	0.023	0.026	0.031	0.032	0.038	0.031	0.048	0.225	0.056	0.058	0.403
Sum	5.009	5.012	5.008	5.008	5.016	5.010	5.019	5.013	5.012	5.020	4.934	5.003	5.006	4.980
Ab (mol%)	43.4	42.8	40.9	43.0	46.4	47.9	50.5	52.7	50.1	55.2	57.6	55.9	55.9	53.9
An (mol%)	54.5	54.8	56.9	54.7	51.0	49.0	46.4	43.5	46.8	40.1	18.0	38.4	38.3	4.8
Or (mol%)	2.1	2.4	2.2	2.3	2.6	3.1	3.2	3.8	3.1	4.7	24.4	5.7	5.8	41.3

Table D1 Feldspar analyses of the 2006 Merapi eruption (continued)

Sample	ME08-03-02	ME08-04-01	ME08-04-01	ME08-04-01	ME08-04-01	ME08-04-01	ME08-04-01	ME08-04-01	ME08-04-01	ME08-04-01	ME08-04-01	ME08-04-01	ME08-04-01	ME08-04-01
Sample Type	L6-S	L8-S	L8-S	L8-S	L8-S	L8-S	L8-S	L8-S	L8-S	L8-S	L8-S	L8-S	L8-S	L8-S
Point	17 / 1 .	2 / 1 .	5 / 1 .	6 / 1 .	6 / 2 .	6 / 3 .	6 / 4 .	6 / 5 .	6 / 6 .	6 / 7 .	6 / 8 .	6 / 9 .	6 / 10 .	6 / 11 .
Comment	m	m	m	ph-r	ph	ph	ph	ph	ph	ph	ph	ph	ph	ph
SiO_2	56.47	58.61	58.10	56.85	56.31	50.91	45.96	45.48	45.32	45.28	45.56	45.28	45.00	44.87
TiO_2	0.03	0.13	0.02	0.03	0.02	0.02	0.01	0.01	0.01	0.01	0.01	0.01	0.00	0.01
Al_2O_3	26.39	24.89	25.43	25.09	26.78	30.33	33.95	34.37	34.63	34.18	34.39	34.59	34.44	34.72
FeO	0.60	0.85	0.55	0.97	0.47	0.51	0.58	0.54	0.55	0.58	0.56	0.56	0.54	0.52
MgO	0.04	0.04	0.04	0.51	0.04	0.04	0.03	0.02	0.03	0.03	0.03	0.04	0.03	0.03
CaO	9.11	7.60	7.76	8.69	9.28	13.89	17.73	17.80	17.91	17.88	17.93	18.14	18.25	18.48
SrO	0.00	0.03	0.09	0.11	0.12	0.13	0.10	0.11	0.10	0.08	0.11	0.10	0.10	0.11
BaO	0.07													
Na_2O	4.97	6.36	6.36	6.02	5.75	3.40	1.34	1.10	1.08	1.12	1.09	1.07	0.95	0.88
K_2O	1.83	1.26	0.90	0.81	0.55	0.23	0.05	0.04	0.04	0.02	0.03	0.03	0.03	0.03
Sum	99.52	99.81	99.27	99.12	99.31	99.47	99.74	99.48	99.68	99.21	99.71	99.81	99.37	99.63
Si	2.567	2.644	2.629	2.593	2.554	2.336	2.127	2.110	2.099	2.108	2.109	2.096	2.094	2.083
Al	1.414	1.323	1.356	1.349	1.431	1.640	1.852	1.879	1.890	1.875	1.877	1.887	1.889	1.899
Ti	0.001	0.004	0.001	0.001	0.001	0.001	0.000	0.000	0.000	0.000	0.000	0.000	0.000	0.000
Fe	0.023	0.032	0.021	0.037	0.018	0.020	0.022	0.021	0.021	0.023	0.022	0.022	0.021	0.020
Mg	0.003	0.003	0.003	0.035	0.003	0.003	0.002	0.001	0.002	0.002	0.002	0.002	0.002	0.002
Sr	0.000	0.001	0.002	0.003	0.003	0.004	0.003	0.003	0.003	0.002	0.003	0.003	0.003	0.003
Ba	0.001	0.000	0.000	0.000	0.000	0.000	0.000	0.000	0.000	0.000	0.000	0.000	0.000	0.000
Ca	0.444	0.367	0.376	0.425	0.451	0.683	0.879	0.885	0.889	0.892	0.889	0.900	0.910	0.919
Na	0.438	0.556	0.558	0.532	0.505	0.302	0.120	0.099	0.097	0.101	0.098	0.096	0.086	0.079
K	0.106	0.072	0.052	0.047	0.032	0.013	0.003	0.003	0.002	0.001	0.002	0.002	0.002	0.002
Sum	4.997	5.004	4.998	5.021	4.998	5.001	5.008	5.001	5.004	5.005	5.002	5.008	5.006	5.007
Ab (mol%)	44.3	55.9	56.6	53.0	51.1	30.3	12.0	10.1	9.8	10.2	9.9	9.6	8.6	7.9
An (mol%)	44.9	36.9	38.1	42.3	45.7	68.4	87.7	89.7	90.0	89.7	89.9	90.2	91.2	92.0
Or (mol%)	10.8	7.3	5.3	4.7	3.2	1.3	0.3	0.3	0.2	0.1	0.2	0.2	0.2	0.2

Table D1 Feldspar analyses of the 2006 Merapi eruption (continued)

Sample	ME08-04-01	ME08-04-01	ME08-04-01	ME08-04-01	ME08-04-01	ME08-04-01	ME08-04-01	ME08-04-01	ME08-04-01	ME08-04-01	ME08-04-01	ME08-04-01	ME08-04-01	ME08-04-01
Sample Type	L8-S	L8-S	L8-S	L8-S	L8-S	L8-S	L8-S	L8-S	L8-S	L8-S	L8-S	L8-S	L8-S	L8-S
Point	6 / 12 .	6 / 13 .	6 / 14 .	6 / 15 .	6 / 16 .	6 / 17 .	6 / 18 .	6 / 19 .	6 / 20 .	7 / 2 .	7 / 3 .	7 / 4 .	7 / 5 .	7 / 7 .
Comment	ph	ph	ph	ph	ph	ph	ph	ph	ph	ph	ph	ph	ph	ph
SiO_2	44.58	44.17	45.19	45.20	45.24	44.99	44.89	45.10	44.84	57.06	55.02	55.50	53.05	51.81
TiO_2	0.01	0.01	0.01	0.01	0.01	0.01	0.01	0.01	0.01	0.03	0.03	0.02	0.02	0.02
Al_2O_3	34.56	34.57	33.99	34.32	33.65	34.16	34.05	34.20	34.04	26.35	27.77	27.16	29.06	29.48
FeO	0.52	0.53	0.54	0.55	0.55	0.53	0.55	0.53	0.57	0.49	0.48	0.48	0.48	0.53
MgO	0.02	0.03	0.03	0.03	0.03	0.03	0.03	0.03	0.03	0.04	0.04	0.04	0.04	0.03
CaO	18.55	18.61	18.13	18.14	17.90	18.42	18.00	18.32	18.05	8.91	10.27	9.90	11.92	12.93
SrO	0.08	0.08	0.12	0.09	0.11	0.09	0.08	0.08	0.09	0.14	0.12	0.13	0.13	0.10
BaO														
Na_2O	0.86	0.70	1.04	1.05	1.09	1.00	1.02	1.00	1.01	5.92	5.22	5.58	4.38	3.90
K_2O	0.02	0.03	0.04	0.03	0.04	0.03	0.03	0.03	0.02	0.57	0.46	0.47	0.31	0.24
Sum	99.20	98.73	99.10	99.43	98.62	99.28	98.67	99.32	98.64	99.52	99.42	99.28	99.42	99.06
Si	2.079	2.071	2.108	2.101	2.119	2.097	2.102	2.100	2.101	2.580	2.500	2.524	2.422	2.381
Al	1.900	1.910	1.869	1.880	1.858	1.876	1.879	1.877	1.880	1.404	1.487	1.456	1.563	1.596
Ti	0.000	0.000	0.000	0.000	0.000	0.000	0.000	0.000	0.000	0.001	0.001	0.001	0.001	0.001
Fe	0.020	0.021	0.021	0.022	0.022	0.021	0.022	0.021	0.022	0.018	0.018	0.018	0.018	0.020
Mg	0.002	0.002	0.002	0.002	0.002	0.002	0.002	0.002	0.002	0.003	0.003	0.003	0.002	0.002
Sr	0.002	0.002	0.003	0.002	0.003	0.003	0.002	0.002	0.002	0.004	0.003	0.003	0.003	0.003
Ba	0.000	0.000	0.000	0.000	0.000	0.000	0.000	0.000	0.000	0.000	0.000	0.000	0.000	0.000
Ca	0.927	0.935	0.906	0.903	0.898	0.920	0.903	0.914	0.906	0.432	0.500	0.482	0.583	0.637
Na	0.078	0.064	0.094	0.094	0.099	0.090	0.093	0.090	0.092	0.519	0.460	0.492	0.388	0.348
K	0.001	0.002	0.002	0.002	0.002	0.002	0.002	0.002	0.001	0.033	0.027	0.027	0.018	0.014
Sum	5.010	5.007	5.006	5.007	5.003	5.011	5.005	5.007	5.006	4.993	4.999	5.007	4.999	5.001
Ab (mol%)	7.7	6.4	9.4	9.4	9.9	8.9	9.3	8.9	9.2	52.8	46.6	49.1	39.2	34.8
An (mol%)	92.2	93.4	90.4	90.4	89.8	90.9	90.5	90.9	90.7	43.9	50.7	48.2	59.0	63.8
Or (mol%)	0.1	0.2	0.2	0.2	0.2	0.2	0.2	0.2	0.1	3.3	2.7	2.7	1.8	1.4

Table D1 Feldspar analyses of the 2006 Merapi eruption (continued)

Sample	ME08-04-01	ME08-04-01	ME08-04-01	ME08-04-01	ME08-04-01	ME08-04-01	ME08-04-01	ME08-04-01	ME08-04-01	ME08-04-01	ME08-04-01	ME08-04-01	ME08-04-01	ME08-04-01
Sample Type	L8-S	L8-S	L8-S	L8-S	L8-S	L8-S	L8-S	L8-S	L8-S	L8-S	L8-S	L8-S	L8-S	L8-S
Point	7 / 8 .	7 / 9 .	7 / 10 .	7 / 11 .	7 / 12 .	7 / 13 .	8 / 1 .	8 / 2 .	8 / 3 .	8 / 4 .	8 / 6 .	8 / 7 .	8 / 8 .	8 / 9 .
Comment	ph	ph	ph	ph	ph	ph-c	ph-r	ph	ph	ph	ph	ph	ph	ph
SiO_2	49.37	54.16	48.80	58.06	61.10	50.83	56.49	55.23	57.14	56.25	52.17	55.36	54.21	55.65
TiO_2	0.02	0.03	0.02	0.47	0.08	0.02	0.03	0.02	0.03	0.02	0.02	0.02	0.03	0.02
Al_2O_3	31.23	28.29	31.54	25.07	22.75	29.63	26.78	27.84	26.53	26.76	29.49	27.60	28.01	27.85
FeO	0.56	0.57	0.57	1.88	0.79	0.49	0.49	0.48	0.45	0.46	0.51	0.48	0.45	0.50
MgO	0.03	0.04	0.03	0.28	0.05	0.03	0.05	0.05	0.04	0.04	0.04	0.04	0.04	0.05
CaO	14.50	11.04	15.28	8.21	5.22	13.60	9.33	10.40	8.85	9.45	12.48	10.16	10.79	10.34
SrO	0.12	0.10	0.11	0.07	0.08	0.12	0.08	0.10	0.13	0.13	0.12	0.11	0.13	0.09
BaO														
Na_2O	2.93	4.82	2.64	5.14	6.72	3.35	5.68	5.17	6.02	5.63	4.14	5.23	5.02	5.24
K_2O	0.18	0.46	0.15	1.99	2.85	0.33	0.54	0.40	0.59	0.52	0.29	0.49	0.46	0.47
Sum	98.95	99.51	99.15	101.21	99.64	98.42	99.47	99.69	99.78	99.25	99.26	99.52	99.14	100.24
Si	2.282	2.465	2.257	2.606	2.758	2.356	2.557	2.501	2.576	2.553	2.390	2.511	2.475	2.507
Al	1.702	1.517	1.719	1.326	1.210	1.618	1.429	1.486	1.410	1.431	1.592	1.475	1.507	1.479
Ti	0.001	0.001	0.001	0.016	0.003	0.001	0.001	0.001	0.001	0.001	0.001	0.001	0.001	0.001
Fe	0.022	0.022	0.022	0.070	0.030	0.019	0.019	0.018	0.017	0.017	0.019	0.018	0.017	0.019
Mg	0.002	0.003	0.002	0.019	0.003	0.002	0.003	0.003	0.003	0.002	0.003	0.003	0.003	0.003
Sr	0.003	0.003	0.003	0.002	0.002	0.003	0.002	0.003	0.003	0.003	0.003	0.003	0.003	0.002
Ba	0.000	0.000	0.000	0.000	0.000	0.000	0.000	0.000	0.000	0.000	0.000	0.000	0.000	0.000
Ca	0.718	0.538	0.757	0.395	0.252	0.675	0.452	0.504	0.427	0.459	0.613	0.494	0.528	0.499
Na	0.263	0.426	0.237	0.447	0.588	0.301	0.499	0.454	0.526	0.496	0.368	0.460	0.444	0.458
K	0.010	0.026	0.009	0.114	0.164	0.019	0.031	0.023	0.034	0.030	0.017	0.028	0.027	0.027
Sum	5.003	5.001	5.006	4.995	5.010	4.995	4.993	4.994	4.998	4.993	5.006	4.994	5.006	4.995
Ab (mol%)	26.5	43.0	23.6	46.8	58.5	30.3	50.8	46.3	53.3	50.3	36.9	46.8	44.5	46.5
An (mol%)	72.4	54.3	75.5	41.3	25.1	67.8	46.1	51.4	43.3	46.6	61.4	50.3	52.9	50.7
Or (mol%)	1.1	2.7	0.9	11.9	16.3	1.9	3.1	2.4	3.5	3.1	1.7	2.9	2.7	2.8

Table D1 Feldspar analyses of the 2006 Merapi eruption (continued)

Sample	ME08-04-01	ME08-04-01	ME08-04-01	ME08-04-01	ME08-04-01	ME08-04-01	ME08-04-01	ME08-04-01	ME08-04-01	ME08-04-01	ME08-04-01	ME08-04-01	ME08-04-01	ME08-04-01
Sample Type	L8-S	L8-S	L8-S	L8-S	L8-S	L8-S	L8-S	L8-S	L8-S	L8-S	L8-S	L8-S	L8-S	L8-S
Point	8 / 10 .	8 / 11 .	8 / 12 .	8 / 13 .	8 / 14 .	8 / 15 .	8 / 16 .	8 / 17 .	8 / 18 .	8 / 19 .	8 / 20 .	1 / 1 .	1 / 2 .	1 / 3 .
Comment	ph	ph	ph	ph	ph	ph	ph	ph	ph	ph	ph-c	ph-c	ph	ph
SiO_2	54.71	66.20	53.96	55.21	55.28	53.82	53.80	51.63	47.55	48.33	55.10	50.83	51.87	52.76
TiO_2	0.02	0.06	0.02	0.03	0.02	0.03	0.02	0.02	0.02	0.01	0.03	0.03	0.02	0.03
Al_2O_3	27.46	19.39	28.27	27.92	27.35	28.25	28.26	29.80	32.47	32.23	27.94	30.64	30.04	29.37
FeO	0.46	0.81	0.52	0.59	0.46	0.51	0.49	0.51	0.51	0.51	0.44	0.47	0.47	0.50
MgO	0.05	0.02	0.05	0.07	0.05	0.05	0.04	0.04	0.03	0.04	0.04	0.02	0.05	0.04
CaO	10.19	1.10	11.28	10.51	9.94	11.25	11.08	13.15	16.31	15.88	10.47	13.97	12.97	12.19
SrO	0.11	0.01	0.12	0.11	0.12	0.13	0.12	0.13	0.11	0.14	0.09	0.16	0.11	0.24
BaO												0.11	0.05	0.02
Na_2O	5.22	7.56	4.66	5.14	5.43	4.80	4.76	3.85	2.05	2.35	5.23	3.45	3.96	4.40
K_2O	0.47	5.02	0.38	0.50	0.49	0.39	0.38	0.24	0.10	0.12	0.46	0.24	0.27	0.33
Sum	98.70	100.18	99.28	100.10	99.14	99.22	98.97	99.37	99.18	99.62	99.82	99.94	99.86	99.94
Si	2.504	2.955	2.462	2.495	2.517	2.458	2.461	2.367	2.204	2.227	2.495	2.325	2.367	2.403
Al	1.481	1.020	1.520	1.487	1.468	1.521	1.524	1.610	1.774	1.751	1.491	1.652	1.616	1.577
Ti	0.001	0.002	0.001	0.001	0.001	0.001	0.001	0.001	0.001	0.000	0.001	0.001	0.001	0.001
Fe	0.018	0.030	0.020	0.022	0.018	0.020	0.019	0.020	0.020	0.020	0.017	0.018	0.018	0.019
Mg	0.003	0.001	0.003	0.004	0.003	0.003	0.003	0.003	0.002	0.002	0.003	0.001	0.004	0.003
Sr	0.003	0.000	0.003	0.003	0.003	0.004	0.003	0.003	0.003	0.004	0.002	0.004	0.003	0.006
Ba	0.000	0.000	0.000	0.000	0.000	0.000	0.000	0.000	0.000	0.000	0.000	0.002	0.001	0.000
Ca	0.500	0.053	0.551	0.509	0.485	0.550	0.543	0.646	0.810	0.784	0.508	0.685	0.634	0.595
Na	0.463	0.654	0.412	0.451	0.480	0.425	0.423	0.342	0.184	0.210	0.459	0.306	0.350	0.388
K	0.028	0.286	0.022	0.029	0.029	0.023	0.022	0.014	0.006	0.007	0.027	0.014	0.016	0.019
Sum	5.000	5.002	4.994	5.001	5.002	5.004	4.998	5.005	5.004	5.005	5.002	5.008	5.008	5.012
Ab (mol%)	46.8	65.9	41.8	45.6	48.3	42.6	42.8	34.1	18.4	20.9	46.2	30.5	35.0	38.7
An (mol%)	50.4	5.3	56.0	51.5	48.8	55.2	55.0	64.5	80.9	78.3	51.1	68.1	63.4	59.3
Or (mol%)	2.8	28.8	2.2	2.9	2.9	2.3	2.2	1.4	0.6	0.7	2.7	1.4	1.6	1.9

Table D1 Feldspar analyses of the 2006 Merapi eruption (continued)

Sample	ME08-04-01	ME08-04-01	ME08-04-01	ME08-04-01	ME08-04-01	ME08-04-01	ME08-04-01	ME08-04-01	ME08-04-01	ME08-04-01	ME08-04-01	ME08-04-01	ME08-04-01	ME08-04-01
Sample Type	L8-S	L8-S	L8-S	L8-S	L8-S	L8-S	L8-S	L8-S	L8-S	L8-S	L8-S	L8-S	L8-S	L8-S
Point	1 / 4 .	1 / 5 .	1 / 6 .	1 / 7 .	1 / 8 .	1 / 9 .	1 / 10 .	1 / 11 .	1 / 12 .	1 / 13 .	1 / 14 .	1 / 15 .	1 / 16 .	1 / 17 .
Comment	ph	ph	ph	ph	ph	ph	ph	ph	ph	ph	ph	ph	ph	ph
SiO_2	54.19	55.95	56.69	56.45	57.00	57.15	56.04	55.02	56.63	56.13	57.05	57.10	56.87	55.96
TiO_2	0.02	0.03	0.03	0.04	0.03	0.03	0.02	0.03	0.02	0.03	0.03	0.02	0.02	0.01
Al_2O_3	28.70	27.74	26.90	27.52	27.09	26.82	27.32	28.02	27.04	27.36	26.43	26.75	26.91	27.63
FeO	0.52	0.44	0.39	0.43	0.47	0.51	0.47	0.45	0.45	0.47	0.46	0.38	0.41	0.42
MgO	0.04	0.03	0.04	0.04	0.04	0.07	0.03	0.03	0.03	0.06	0.03	0.03	0.05	0.06
CaO	11.20	10.16	9.31	9.75	9.35	9.17	9.61	10.51	9.39	9.73	8.94	9.17	9.25	10.04
SrO	0.14	0.14	0.20	0.18	0.12	0.04	0.14	0.09	0.13	0.09	0.08	0.16	0.16	0.12
BaO	0.00	0.10		0.05			0.10	0.01	0.02	0.02		0.17	0.01	0.12
Na_2O	4.99	5.42	6.00	5.62	6.06	6.02	5.65	5.29	5.73	5.69	6.00	5.91	5.88	5.45
K_2O	0.43	0.49	0.58	0.51	0.55	0.56	0.50	0.47	0.62	0.52	0.63	0.62	0.55	0.46
Sum	100.23	100.50	100.21	100.66	100.72	100.44	99.87	99.92	100.05	100.09	99.63	100.33	100.13	100.29
Si	2.452	2.515	2.553	2.532	2.552	2.564	2.532	2.490	2.551	2.530	2.577	2.567	2.558	2.519
Al	1.530	1.469	1.428	1.454	1.430	1.418	1.455	1.494	1.435	1.453	1.407	1.417	1.427	1.466
Ti	0.001	0.001	0.001	0.002	0.001	0.001	0.001	0.001	0.001	0.001	0.001	0.001	0.001	0.000
Fe	0.020	0.017	0.015	0.016	0.018	0.019	0.018	0.017	0.017	0.018	0.017	0.014	0.016	0.016
Mg	0.002	0.002	0.003	0.003	0.002	0.005	0.002	0.002	0.002	0.004	0.002	0.002	0.003	0.004
Sr	0.004	0.004	0.005	0.005	0.003	0.001	0.004	0.002	0.004	0.002	0.002	0.004	0.004	0.003
Ba	0.000	0.002	0.000	0.001	0.000	0.000	0.002	0.000	0.000	0.000	0.000	0.003	0.000	0.002
Ca	0.543	0.489	0.449	0.469	0.448	0.441	0.465	0.510	0.453	0.470	0.433	0.442	0.446	0.484
Na	0.437	0.472	0.524	0.488	0.526	0.523	0.495	0.465	0.500	0.497	0.525	0.515	0.513	0.476
K	0.025	0.028	0.033	0.029	0.032	0.032	0.029	0.027	0.036	0.030	0.036	0.035	0.032	0.026
Sum	5.013	5.000	5.011	4.999	5.011	5.004	5.002	5.008	4.999	5.006	4.999	5.000	5.000	4.998
Ab (mol%)	43.5	47.7	52.0	49.5	52.3	52.5	50.0	46.4	50.6	49.9	52.8	51.9	51.8	48.2
An (mol%)	54.0	49.4	44.7	47.5	44.6	44.3	47.1	50.9	45.8	47.1	43.5	44.5	45.0	49.1
Or (mol%)	2.5	2.9	3.3	3.0	3.1	3.2	2.9	2.7	3.6	3.0	3.6	3.6	3.2	2.7

Table D1 Feldspar analyses of the 2006 Merapi eruption (continued)

Sample	ME08-04-01	ME08-04-01	ME08-04-01	ME08-04-01	ME08-04-01	ME08-04-01	ME08-04-01	ME08-04-01	ME08-04-01	ME08-04-01	ME08-04-01	ME08-04-01	ME08-04-01	ME08-04-01
Sample Type	L8-S	L8-S	L8-S	L8-S	L8-S	L8-S	L8-S	L8-S	L8-S	L8-S	L8-S	L8-S	L8-S	L8-S
Point	1 / 18 .	1 / 19 .	1 / 20 .	1 / 21 .	1 / 22 .	1 / 23 .	1 / 24 .	1 / 25 .	1 / 26 .	1 / 27 .	1 / 28 .	1 / 29 .	1 / 30 .	1 / 31 .
Comment	ph	ph	ph	ph	ph	ph	ph	ph	ph	ph	ph	ph	ph	ph
SiO_2	53.90	54.43	56.61	57.37	56.84	56.50	57.28	56.21	56.38	55.93	55.31	56.43	56.52	56.51
TiO_2	0.03	0.02	0.03	0.03	0.03	0.03	0.02	0.03	0.04	0.03	0.02	0.02	0.04	0.03
Al_2O_3	28.96	28.11	27.08	26.70	26.99	26.91	26.48	27.14	27.02	27.47	27.50	26.89	27.44	27.16
FeO	0.49	0.51	0.37	0.40	0.42	0.48	0.47	0.55	0.52	0.55	0.43	0.45	0.49	0.45
MgO	0.04	0.04	0.03	0.04	0.04	0.02	0.05	0.03	0.04	0.03	0.04	0.03	0.04	0.05
CaO	11.63	10.76	9.50	9.07	9.29	9.43	8.95	9.62	9.41	10.03	10.23	9.38	9.74	9.52
SrO	0.04	0.07	0.12	0.12	0.16	0.19	0.12	0.15	0.11	0.09	0.17	0.12	0.15	0.13
BaO	0.06	0.01	0.20	0.06	0.11	0.05	0.16		0.02	0.09	0.19	0.05		0.17
Na_2O	4.67	5.10	5.84	6.15	5.86	5.84	6.13	5.57	5.85	5.54	5.33	5.79	5.82	5.78
K_2O	0.37	0.44	0.52	0.66	0.56	0.56	0.67	0.57	0.59	0.52	0.47	0.59	0.52	0.57
Sum	100.19	99.50	100.29	100.60	100.33	100.05	100.35	99.89	99.99	100.29	99.77	99.76	100.81	100.36
Si	2.439	2.476	2.547	2.570	2.555	2.549	2.575	2.539	2.544	2.520	2.510	2.551	2.532	2.542
Al	1.545	1.507	1.436	1.410	1.430	1.431	1.403	1.445	1.437	1.459	1.471	1.433	1.449	1.440
Ti	0.001	0.001	0.001	0.001	0.001	0.001	0.001	0.001	0.001	0.001	0.001	0.001	0.001	0.001
Fe	0.019	0.020	0.014	0.015	0.016	0.018	0.018	0.021	0.020	0.021	0.016	0.017	0.019	0.017
Mg	0.003	0.003	0.002	0.003	0.003	0.001	0.003	0.002	0.003	0.002	0.002	0.002	0.003	0.003
Sr	0.001	0.002	0.003	0.003	0.004	0.005	0.003	0.004	0.003	0.002	0.004	0.003	0.004	0.003
Ba	0.001	0.000	0.004	0.001	0.002	0.001	0.003	0.000	0.000	0.002	0.003	0.001	0.000	0.003
Ca	0.564	0.525	0.458	0.435	0.448	0.456	0.431	0.466	0.455	0.484	0.497	0.454	0.467	0.459
Na	0.409	0.450	0.510	0.534	0.510	0.511	0.535	0.488	0.512	0.484	0.469	0.508	0.506	0.504
K	0.021	0.026	0.030	0.038	0.032	0.032	0.038	0.033	0.034	0.030	0.027	0.034	0.030	0.033
Sum	5.003	5.008	5.003	5.010	5.000	5.006	5.009	4.997	5.009	5.006	5.002	5.003	5.010	5.005
Ab (mol%)	41.2	45.0	51.1	53.0	51.6	51.1	53.2	49.4	51.2	48.5	47.2	51.0	50.4	50.6
An (mol%)	56.7	52.5	45.9	43.2	45.2	45.6	42.9	47.2	45.5	48.5	50.1	45.6	46.6	46.1
Or (mol%)	2.1	2.6	3.0	3.7	3.2	3.3	3.8	3.3	3.4	3.0	2.7	3.4	3.0	3.3

Table D1 Feldspar analyses of the 2006 Merapi eruption (continued)

Sample	ME08-04-01	ME08-04-01	ME08-04-01	ME08-04-01	ME08-04-01	ME08-04-01	ME08-04-01	ME08-04-01	ME08-04-01	ME08-04-01	ME08-04-01	ME08-04-01	ME08-04-01	ME08-04-01
Sample Type	L8-S	L8-S	L8-S	L8-S	L8-S	L8-S	L8-S	L8-S	L8-S	L8-S	L8-S	L8-S	L8-S	L8-S
Point	1 / 32 .	1 / 33 .	1 / 34 .	1 / 35 .	1 / 36 .	1 / 37 .	1 / 38 .	1 / 39 .	1 / 40 .	1 / 41 .	1 / 42 .	1 / 43 .	14 / 1 .	15 / 1 .
Comment	ph	ph	ph	ph	ph	ph	ph	ph	ph	ph	ph	ph-r	mph	mph
SiO_2	56.33	55.19	55.96	56.42	53.03	51.59	51.98	52.97	53.64	56.37	58.59	61.52	54.56	69.58
TiO_2	0.03	0.03	0.01	0.12	0.03	0.04	0.03	0.03	0.03	0.03	0.02	0.02	0.02	0.22
Al_2O_3	27.24	27.65	27.63	26.01	29.23	30.55	30.09	29.39	28.64	27.07	25.62	23.66	28.15	17.47
FeO	0.41	0.51	0.54	1.07	0.53	0.68	0.54	0.56	0.56	0.55	0.60	0.57	0.51	1.17
MgO	0.06	0.05	0.05	0.21	0.06	0.06	0.04	0.07	0.05	0.07	0.03	0.04	0.05	0.08
CaO	9.64	10.15	9.79	9.67	12.11	13.33	12.89	12.30	11.21	9.32	7.71	5.48	10.79	1.71
SrO	0.13	0.21	0.06	0.11	0.10	0.11	0.14	0.15	0.18	0.11	0.09		0.14	0.01
BaO		0.10			0.13			0.03	0.03	0.09	0.15	0.16		
Na_2O	5.61	5.40	5.67	5.23	4.41	3.76	4.10	4.38	4.87	5.74	6.67	7.24	4.88	5.11
K_2O	0.55	0.52	0.54	0.90	0.37	0.21	0.20	0.31	0.37	0.57	0.89	1.78	0.40	3.78
Sum	99.99	99.84	100.26	99.82	100.02	100.35	100.01	100.24	99.57	99.95	100.38	100.53	99.53	99.16
Si	2.539	2.503	2.520	2.561	2.412	2.345	2.367	2.405	2.444	2.545	2.626	2.741	2.479	3.081
Al	1.447	1.478	1.466	1.391	1.567	1.637	1.615	1.572	1.538	1.441	1.353	1.243	1.508	0.912
Ti	0.001	0.001	0.000	0.004	0.001	0.001	0.001	0.001	0.001	0.001	0.001	0.001	0.001	0.007
Fe	0.015	0.019	0.020	0.040	0.020	0.026	0.021	0.021	0.021	0.021	0.022	0.021	0.019	0.043
Mg	0.004	0.004	0.003	0.014	0.004	0.004	0.003	0.005	0.003	0.004	0.002	0.003	0.004	0.006
Sr	0.003	0.005	0.002	0.003	0.003	0.003	0.004	0.004	0.005	0.003	0.002		0.004	0.000
Ba	0.000	0.002	0.000	0.000	0.002	0.000	0.000	0.001	0.001	0.002	0.003	0.003	0.000	0.000
Ca	0.466	0.493	0.472	0.470	0.590	0.649	0.629	0.598	0.547	0.451	0.370	0.262	0.525	0.081
Na	0.490	0.474	0.495	0.460	0.389	0.331	0.362	0.386	0.430	0.502	0.580	0.626	0.430	0.439
K	0.031	0.030	0.031	0.052	0.022	0.012	0.011	0.018	0.021	0.033	0.051	0.101	0.023	0.214
Sum	4.997	5.009	5.010	4.996	5.009	5.007	5.012	5.010	5.012	5.001	5.012	5.000	4.993	4.782
Ab (mol%)	49.6	47.6	49.6	46.8	38.9	33.3	36.1	38.5	43.0	51.0	57.9	63.3	44.0	59.8
An (mol%)	47.2	49.4	47.3	47.8	59.0	65.4	62.7	59.7	54.8	45.7	37.0	26.5	53.7	11.1
Or (mol%)	3.2	3.0	3.1	5.3	2.2	1.2	1.1	1.8	2.2	3.3	5.1	10.2	2.4	29.1

Table D1 Feldspar analyses of the 2006 Merapi eruption (continued)

Sample	ME08-04-01	ME08-04-01	ME08-04-01	ME08-04-01	ME08-04-01	ME08-04-01	ME08-04-01	ME08-04-01	ME08-07	ME08-07	ME08-07	ME08-07	ME08-07	ME08-07
Sample Type	L8-S	L8-S	L8-S	L8-S	L8-S	L8-S	L8-S	L8-S	L10-S	L10-S	L10-S	L10-S	L10-S	L10-S
Point	16 / 1 .	1 / 1 .	2 / 1 .	3 / 1 .	4 / 1 .	1 / 1 .	5 / 1 .	12 / 1 .	4 / 1 .	4 / 2 .	4 / 3 .	4 / 4 .	4 / 5 .	4 / 6 .
Comment	mph	m	m	m	m	m-c	m-r	m-c	ph-c	ph	ph	ph	ph	ph
SiO_2	55.98	64.64	65.77	59.32	61.28	66.97	64.51	60.38	53.43	52.90	52.23	52.65	53.48	54.79
TiO_2	0.03	0.14	0.18	0.04	0.01	0.20	0.10	0.09	0.01	0.02	0.01	0.02	0.01	0.01
Al_2O_3	26.86	19.52	18.36	24.37	23.40	18.53	20.04	24.31	29.02	28.39	29.27	28.87	28.18	27.61
FeO	0.51	1.08	1.22	0.49	0.49	1.15	0.81	1.03	0.47	0.42	0.46	0.46	0.38	0.49
MgO	0.05	0.20	0.15	0.03	0.01	0.18	0.05	0.38	0.03	0.04	0.03	0.04	0.06	0.07
CaO	9.34	3.04	2.29	6.38	5.16	2.46	3.25	7.03	11.32	10.99	11.55	11.35	10.63	9.79
SrO	0.12	0.05		0.11	0.05				0.14	0.12	0.14	0.14	0.12	0.09
BaO		0.25	0.24	0.18	0.21				0.05		0.03		0.05	
Na_2O	5.53	6.42	5.84	6.98	7.20	5.71	5.77	5.95	4.75	4.97	4.59	4.73	5.07	5.63
K_2O	0.52	3.75	4.82	1.44	2.12	4.62	4.37	1.69	0.38	0.38	0.35	0.37	0.43	0.49
Sum	98.96	99.18	98.89	99.36	99.93	99.88	98.93	100.88	99.70	98.22	98.68	98.63	98.45	99.03
Si	2.548	2.918	2.976	2.683	2.749	2.987	2.912	2.689	2.433	2.442	2.404	2.423	2.461	2.501
Al	1.441	1.039	0.979	1.299	1.237	0.974	1.066	1.276	1.557	1.545	1.588	1.566	1.528	1.486
Ti	0.001	0.005	0.006	0.001	0.000	0.007	0.004	0.003	0.000	0.001	0.000	0.001	0.000	0.000
Fe	0.020	0.041	0.046	0.019	0.018	0.043	0.030	0.038	0.018	0.016	0.018	0.018	0.015	0.019
Mg	0.003	0.013	0.010	0.002	0.001	0.012	0.003	0.025	0.002	0.003	0.002	0.003	0.004	0.005
Sr	0.003	0.001		0.003	0.001	0.000	0.000	0.000	0.004	0.003	0.004	0.004	0.003	0.002
Ba	0.000	0.004	0.004	0.003	0.004	0.000	0.000	0.000	0.001	0.000	0.001	0.000	0.001	0.000
Ca	0.455	0.147	0.111	0.309	0.248	0.117	0.157	0.335	0.552	0.543	0.570	0.560	0.524	0.479
Na	0.488	0.562	0.512	0.612	0.626	0.494	0.505	0.513	0.419	0.444	0.410	0.422	0.452	0.498
K	0.030	0.216	0.278	0.083	0.121	0.263	0.252	0.096	0.022	0.022	0.021	0.022	0.025	0.028
Sum	4.989	4.947	4.924	5.014	5.006	4.897	4.929	4.975	5.009	5.019	5.017	5.015	5.014	5.019
Ab (mol%)	50.1	60.8	56.8	60.9	62.9	56.5	55.2	54.3	42.2	44.0	41.0	42.1	45.2	49.5
An (mol%)	46.8	15.9	12.3	30.8	24.9	13.4	17.2	35.5	55.6	53.8	56.9	55.8	52.3	47.6
Or (mol%)	3.1	23.3	30.9	8.3	12.2	30.1	27.6	10.1	2.2	2.2	2.1	2.1	2.5	2.8

Table D1 Feldspar analyses of the 2006 Merapi eruption (continued)

Sample	ME08-07	ME08-07	ME08-07	ME08-07	ME08-07	ME08-07	ME08-07	ME08-07	ME08-07	ME08-07	ME08-07	ME08-07	ME08-07	ME08-07
Sample Type	L10-S	L10-S	L10-S	L10-S	L10-S	L10-S	L10-S	L10-S	L10-S	L10-S	L10-S	L10-S	L10-S	L10-S
Point	4 / 8 .	4 / 9 .	4 / 10 .	4 / 11 .	4 / 12 .	4 / 13 .	4 / 14 .	4 / 15 .	4 / 16 .	4 / 17 .	4 / 19 .	4 / 20 .	4 / 21 .	4 / 22 .
Comment	ph	ph	ph	ph	ph	ph	ph	ph	ph	ph	ph	ph	ph	ph
SiO_2	55.16	54.70	54.90	54.14	55.32	54.85	55.92	55.59	55.43	55.10	54.01	55.11	54.21	55.84
TiO_2	0.03	0.02	0.03	0.02	0.01	0.02	0.02	0.04	0.03	0.02	0.02	0.02	0.02	0.03
Al_2O_3	27.35	27.59	27.86	28.03	27.59	27.61	27.24	27.43	27.57	27.34	28.55	28.03	28.31	27.17
FeO	0.48	0.41	0.48	0.51	0.46	0.43	0.44	0.44	0.48	0.47	0.46	0.46	0.51	0.37
MgO	0.04	0.04	0.05	0.03	0.04	0.04	0.04	0.03	0.03	0.03	0.04	0.04	0.06	0.03
CaO	9.68	9.89	10.09	10.59	9.78	10.01	9.60	9.67	9.95	9.78	11.04	10.15	10.93	9.57
SrO	0.17	0.12	0.14	0.13	0.15	0.16	0.12	0.13	0.17	0.15	0.17	0.08	0.14	0.07
BaO	0.03	0.11	0.08	0.21		0.02	0.03	0.14		0.03		0.05	0.04	
Na_2O	5.71	5.65	5.46	5.18	5.68	5.40	5.85	5.75	5.56	5.66	4.86	5.59	5.17	5.74
K_2O	0.54	0.48	0.44	0.40	0.51	0.55	0.52	0.49	0.47	0.51	0.38	0.53	0.43	0.56
Sum	99.19	99.02	99.53	99.28	99.56	99.10	99.79	99.72	99.71	99.12	99.56	100.07	99.82	99.44
Si	2.514	2.499	2.495	2.473	2.511	2.502	2.530	2.519	2.512	2.513	2.458	2.491	2.463	2.534
Al	1.469	1.486	1.492	1.509	1.476	1.484	1.453	1.465	1.473	1.470	1.531	1.493	1.516	1.453
Ti	0.001	0.001	0.001	0.001	0.000	0.001	0.001	0.001	0.001	0.001	0.001	0.001	0.001	0.001
Fe	0.018	0.016	0.018	0.019	0.017	0.017	0.017	0.017	0.018	0.018	0.017	0.017	0.019	0.014
Mg	0.003	0.003	0.003	0.002	0.003	0.003	0.003	0.002	0.002	0.002	0.003	0.003	0.004	0.002
Sr	0.004	0.003	0.004	0.004	0.004	0.004	0.003	0.003	0.004	0.004	0.004	0.002	0.004	0.002
Ba	0.001	0.002	0.001	0.004	0.000	0.000	0.001	0.002	0.000	0.001	0.000	0.001	0.001	0.000
Ca	0.473	0.484	0.491	0.518	0.476	0.489	0.465	0.470	0.483	0.478	0.538	0.492	0.532	0.465
Na	0.505	0.500	0.481	0.459	0.500	0.477	0.513	0.505	0.489	0.500	0.429	0.490	0.455	0.505
K	0.031	0.028	0.026	0.024	0.030	0.032	0.030	0.029	0.027	0.030	0.022	0.031	0.025	0.032
Sum	5.019	5.022	5.012	5.013	5.015	5.010	5.015	5.014	5.008	5.016	5.002	5.021	5.019	5.007
Ab (mol%)	50.1	49.4	48.2	45.9	49.7	47.8	50.9	50.3	48.9	49.6	43.4	48.4	45.0	50.4
An (mol%)	46.9	47.8	49.2	51.8	47.3	49.0	46.1	46.8	48.4	47.4	54.4	48.6	52.6	46.4
Or (mol%)	3.1	2.8	2.6	2.4	3.0	3.2	3.0	2.8	2.7	2.9	2.2	3.0	2.4	3.2

Table D1 Feldspar analyses of the 2006 Merapi eruption (continued)

Sample	ME08-07	ME08-07	ME08-07	ME08-07	ME08-07	ME08-07	ME08-07	ME08-07	ME08-08-03	ME08-08-03	ME08-08-03	ME08-08-03	ME08-08-03	ME08-08-03
Sample Type	L10-S	L10-S	L10-S	L10-S	L10-S	L10-S	L10-S	L10-S	L1-D	L1-D	L1-D	L1-D	L1-D	L6-S
Point	4 / 23 .	4 / 24 .	4 / 27 .	18 / 1 .	19 / 1 .	20 / 1 .	21 / 1 .	22 / 1 .	8 / 1 .	9 / 1 .	10 / 1 .	11 / 1 .	12 / 1 .	6 / 1 .
Comment	ph	ph	ph-r	m	m	m	m	m	m	m	m	m	m	m
SiO_2	54.77	52.86	61.68	56.90	59.73	61.10	59.75	59.63	60.32	56.32	57.22	60.50	57.95	57.05
TiO_2	0.03	0.02	0.12	0.03	0.04	0.02	0.06	0.04	0.05	0.03	0.02	0.03	0.03	0.02
Al_2O_3	27.98	29.01	22.13	26.26	24.63	23.52	24.40	24.50	23.81	27.25	26.64	24.11	25.41	26.55
FeO	0.46	0.62	0.87	0.68	0.52	0.50	0.57	0.65	0.71	0.51	0.58	0.47	0.56	0.57
MgO	0.04	0.04	0.06	0.04	0.02	0.03	0.05	0.02	0.03	0.04	0.06	0.05	0.03	0.04
CaO	10.29	11.75	5.31	8.73	6.46	5.51	6.80	6.56	6.44	9.68	9.36	6.50	7.88	8.69
SrO	0.18	0.13	0.00	0.13	0.10	0.10	0.12	0.04	0.07	0.15	0.12	0.10	0.10	0.10
BaO	0.01		0.11	0.06	0.12	0.23	0.07		0.16	0.09		0.18	0.12	
Na_2O	5.25	4.63	6.46	6.29	7.14	7.30	6.61	6.98	6.88	5.74	5.64	6.99	6.22	6.01
K_2O	0.45	0.36	2.18	0.80	1.21	2.01	1.46	1.53	1.79	0.61	0.80	1.48	1.03	0.84
Sum	99.49	99.45	98.94	99.93	99.96	100.34	99.91	100.02	100.28	100.46	100.45	100.48	99.37	99.87
Si	2.490	2.417	2.790	2.572	2.681	2.736	2.686	2.680	2.707	2.534	2.569	2.705	2.625	2.574
Al	1.499	1.563	1.180	1.399	1.303	1.241	1.292	1.298	1.259	1.445	1.410	1.270	1.356	1.412
Ti	0.001	0.001	0.004	0.001	0.001	0.001	0.002	0.001	0.002	0.001	0.001	0.001	0.001	0.001
Fe	0.017	0.024	0.033	0.026	0.020	0.019	0.021	0.025	0.027	0.019	0.022	0.018	0.021	0.022
Mg	0.003	0.003	0.004	0.003	0.001	0.002	0.003	0.001	0.002	0.003	0.004	0.003	0.002	0.002
Sr	0.005	0.003	0.000	0.004	0.003	0.003	0.003	0.001	0.002	0.004	0.003	0.003	0.003	0.003
Ba	0.000	0.000	0.002	0.001	0.002	0.004	0.001	0.000	0.003	0.002	0.000	0.003	0.002	0.000
Ca	0.501	0.576	0.258	0.423	0.310	0.264	0.327	0.316	0.310	0.467	0.450	0.311	0.382	0.420
Na	0.463	0.411	0.566	0.551	0.621	0.634	0.576	0.608	0.599	0.501	0.491	0.606	0.546	0.526
K	0.026	0.021	0.126	0.046	0.069	0.115	0.084	0.087	0.102	0.035	0.046	0.084	0.060	0.049
Sum	5.004	5.017	4.962	5.026	5.012	5.017	4.996	5.017	5.012	5.010	4.995	5.004	4.999	5.007
Ab (mol%)	46.8	40.8	59.6	54.0	62.1	62.6	58.3	60.1	59.2	49.9	49.7	60.5	55.3	52.9
An (mol%)	50.6	57.1	27.1	41.4	31.0	26.1	33.2	31.2	30.6	46.6	45.6	31.1	38.7	42.2
Or (mol%)	2.6	2.1	13.3	4.5	6.9	11.3	8.5	8.6	10.1	3.5	4.7	8.4	6.0	4.9

Table D1 Feldspar analyses of the 2006 Merapi eruption (continued)

Sample	ME08-09-02	ME08-09-02	ME08-09-02	ME08-09-02	ME08-09-02	ME08-09-02	ME08-09-02	ME08-09-02	ME08-09-02	ME08-09-02	ME08-09-02	ME08-09-02	ME08-09-02	ME08-09-02
Sample Type	L1-S	L1-S	L1-S	L1-S	L1-S	L1-S	L1-S	L1-S	L1-S	L1-S	L1-S	L1-S	L1-S	L1-S
Point	6 / 2 .	6 / 3 .	6 / 4 .	6 / 5 .	6 / 6 .	6 / 8 .	6 / 9 .	6 / 10 .	6 / 11 .	6 / 13 .	6 / 15 .	6 / 16 .	6 / 17 .	6 / 18 .
Comment	ph	ph	ph	ph	ph	ph	ph	ph	ph	ph	ph	ph	ph	ph
SiO_2	52.20	51.77	57.37	54.84	49.95	50.13	52.75	54.84	50.95	50.53	52.18	52.53	53.89	50.25
TiO_2	0.03	0.01	0.03	0.03	0.02	0.02	0.02	0.03	0.02	0.02	0.03	0.03	0.02	0.02
Al_2O_3	29.33	29.52	26.33	27.93	30.59	30.73	28.47	27.50	29.83	30.43	29.49	29.35	28.39	30.86
FeO	0.57	0.62	0.48	0.47	0.56	0.53	0.54	0.47	0.48	0.55	0.57	0.47	0.50	0.55
MgO	0.06	0.06	0.04	0.04	0.03	0.04	0.04	0.04	0.03	0.03	0.04	0.04	0.04	0.03
CaO	12.40	12.81	8.94	10.65	14.21	13.97	12.15	10.33	13.13	13.78	12.83	12.27	11.25	14.23
SrO	0.14	0.13	0.10	0.13	0.13	0.12	0.13	0.11	0.10	0.11	0.10	0.13	0.10	0.13
BaO														
Na_2O	4.06	3.87	6.04	5.01	3.06	3.29	4.14	5.10	3.56	3.39	4.02	4.11	4.76	3.16
K_2O	0.24	0.36	0.63	0.43	0.21	0.23	0.34	0.45	0.24	0.21	0.31	0.30	0.34	0.19
Sum	99.05	99.16	99.98	99.53	98.77	99.07	98.61	98.87	98.36	99.04	99.58	99.24	99.29	99.46
Si	2.396	2.378	2.583	2.490	2.311	2.312	2.429	2.505	2.358	2.328	2.386	2.404	2.458	2.309
Al	1.586	1.598	1.397	1.495	1.668	1.670	1.545	1.480	1.627	1.652	1.589	1.583	1.526	1.671
Ti	0.001	0.001	0.001	0.001	0.001	0.001	0.001	0.001	0.001	0.001	0.001	0.001	0.001	0.001
Fe	0.022	0.024	0.018	0.018	0.022	0.020	0.021	0.018	0.018	0.021	0.022	0.018	0.019	0.021
Mg	0.004	0.004	0.003	0.003	0.002	0.003	0.003	0.003	0.002	0.002	0.003	0.003	0.003	0.002
Sr	0.004	0.004	0.003	0.003	0.003	0.003	0.004	0.003	0.003	0.003	0.003	0.003	0.003	0.004
Ba	0.000	0.000	0.000	0.000	0.000	0.000	0.000	0.000	0.000	0.000	0.000	0.000	0.000	0.000
Ca	0.610	0.631	0.431	0.518	0.704	0.690	0.600	0.505	0.651	0.680	0.628	0.601	0.550	0.701
Na	0.361	0.344	0.527	0.441	0.274	0.295	0.370	0.452	0.319	0.303	0.356	0.365	0.421	0.281
K	0.014	0.021	0.036	0.025	0.012	0.014	0.020	0.026	0.014	0.012	0.018	0.018	0.020	0.011
Sum	4.998	5.005	4.999	4.994	4.998	5.007	4.992	4.993	4.994	5.003	5.006	4.995	4.999	5.001
Ab (mol%)	36.7	34.6	53.0	44.8	27.7	29.5	37.4	45.9	32.4	30.4	35.5	37.1	42.5	28.3
An (mol%)	61.9	63.3	43.4	52.7	71.1	69.1	60.6	51.4	66.1	68.3	62.7	61.1	55.5	70.6
Or (mol%)	1.4	2.1	3.6	2.5	1.3	1.4	2.0	2.6	1.5	1.3	1.8	1.8	2.0	1.1

Table D1 Feldspar analyses of the 2006 Merapi eruption (continued)

Sample	ME08-09-02	ME08-09-02	ME08-09-02	ME08-09-02	ME08-09-02	ME08-09-02	ME08-09-02	ME08-09-02	ME08-09-02	ME08-09-02	ME08-09-02	ME08-09-02	ME08-09-02	ME08-09-02
Sample Type	L1-S	L1-S	L1-S	L1-S	L1-S	L1-S	L1-S	L1-S	L1-S	L1-S	L1-S	L1-S	L1-S	L1-S
Point	7 / 2 .	7 / 3 .	7 / 4 .	7 / 5 .	7 / 6 .	7 / 7 .	7 / 8 .	7 / 10 .	7 / 11 .	7 / 12 .	7 / 13 .	7 / 15 .	8 / 1 .	8 / 2 .
Comment	ph	ph	ph	ph	ph	ph	ph	ph	ph	ph	ph	ph-c	ph-r	ph
SiO_2	51.41	48.25	47.93	47.10	54.99	55.52	55.98	56.88	56.78	56.68	56.44	56.94	58.11	52.83
TiO_2	0.02	0.02	0.01	0.01	0.01	0.03	0.02	0.02	0.02	0.02	0.02	0.03	0.10	0.02
Al_2O_3	29.45	31.56	32.16	32.68	27.12	26.57	26.41	26.98	26.15	26.28	26.51	26.63	24.43	29.38
FeO	0.49	0.57	0.59	0.59	0.55	0.47	0.48	0.48	0.48	0.50	0.47	0.47	0.78	0.54
MgO	0.04	0.04	0.03	0.03	0.03	0.04	0.04	0.04	0.04	0.03	0.04	0.04	0.08	0.04
CaO	13.03	15.52	15.78	16.28	10.18	9.25	9.33	9.18	9.00	8.97	9.20	9.33	6.74	12.20
SrO	0.14	0.09	0.11	0.09	0.10	0.09	0.09	0.12	0.09	0.10	0.10	0.10	0.08	0.12
BaO														
Na_2O	3.87	2.43	2.28	1.91	5.28	5.66	5.63	5.89	5.98	5.84	5.79	5.86	6.92	4.23
K_2O	0.23	0.13	0.10	0.09	0.51	0.55	0.55	0.57	0.56	0.61	0.55	0.55	0.94	0.30
Sum	98.68	98.61	99.01	98.80	98.78	98.19	98.55	100.18	99.12	99.03	99.11	99.96	98.17	99.69
Si	2.373	2.245	2.223	2.191	2.516	2.548	2.559	2.557	2.579	2.576	2.564	2.566	2.658	2.407
Al	1.602	1.730	1.758	1.792	1.462	1.437	1.423	1.430	1.400	1.407	1.419	1.414	1.317	1.578
Ti	0.001	0.001	0.000	0.000	0.000	0.001	0.001	0.001	0.001	0.001	0.001	0.001	0.003	0.001
Fe	0.019	0.022	0.023	0.023	0.021	0.018	0.018	0.018	0.018	0.019	0.018	0.018	0.030	0.021
Mg	0.003	0.003	0.002	0.002	0.002	0.003	0.003	0.003	0.003	0.002	0.003	0.003	0.005	0.003
Sr	0.004	0.002	0.003	0.003	0.003	0.002	0.002	0.003	0.002	0.003	0.003	0.003	0.002	0.003
Ba	0.000	0.000	0.000	0.000	0.000	0.000	0.000	0.000	0.000	0.000	0.000	0.000	0.000	0.000
Ca	0.645	0.774	0.784	0.812	0.499	0.455	0.457	0.442	0.438	0.437	0.448	0.451	0.330	0.596
Na	0.346	0.219	0.205	0.172	0.468	0.503	0.499	0.514	0.527	0.514	0.510	0.512	0.613	0.374
K	0.013	0.008	0.006	0.005	0.030	0.032	0.032	0.033	0.032	0.036	0.032	0.032	0.055	0.017
Sum	5.005	5.003	5.004	5.001	5.002	5.000	4.995	5.000	5.000	4.994	4.997	4.998	5.014	4.999
Ab (mol%)	34.5	21.9	20.6	17.4	47.0	50.8	50.5	52.0	52.8	52.1	51.5	51.5	61.4	37.9
An (mol%)	64.2	77.4	78.8	82.1	50.0	45.9	46.2	44.7	43.9	44.3	45.3	45.3	33.1	60.4
Or (mol%)	1.3	0.8	0.6	0.5	3.0	3.2	3.3	3.3	3.3	3.6	3.2	3.2	5.5	1.8

Table D1 Feldspar analyses of the 2006 Merapi eruption (continued)

Sample	ME08-09-02	ME08-09-02	ME08-09-02	ME08-09-02	ME08-09-02	ME08-09-02	ME08-09-02	ME08-09-02	ME08-09-02	ME08-09-02	ME08-09-02	ME08-09-02	ME08-09-02	ME08-09-02
Sample Type	L1-S	L1-S	L1-S	L1-S	L1-S	L1-S	L1-S	L1-S	L1-S	L1-S	L1-S	L1-S	L1-S	L1-S
Point	8 / 3 .	8 / 4 .	8 / 5 .	8 / 6 .	8 / 7 .	8 / 8 .	8 / 9 .	8 / 10 .	8 / 11 .	8 / 12 .	8 / 13 .	8 / 14 .	8 / 15 .	1 / 1 .
Comment	ph	ph	ph	ph	ph	ph	ph	ph	ph	ph	ph	ph	ph	ph
SiO_2	56.08	56.37	55.61	54.49	54.36	54.40	54.53	54.81	53.79	55.03	53.21	54.75	53.96	50.92
TiO_2	0.03	0.02	0.02	0.02	0.02	0.03	0.02	0.02	0.02	0.02	0.02	0.03	0.02	0.02
Al_2O_3	26.55	26.94	27.46	27.90	28.21	28.14	27.86	28.02	28.38	27.46	28.63	28.06	28.34	30.63
FeO	0.50	0.50	0.47	0.47	0.49	0.46	0.47	0.48	0.48	0.50	0.47	0.48	0.47	0.44
MgO	0.04	0.05	0.04	0.04	0.05	0.04	0.05	0.04	0.04	0.05	0.04	0.05	0.05	0.05
CaO	9.26	9.16	10.14	10.72	10.84	10.74	10.80	10.56	11.25	10.18	11.78	10.68	11.14	13.45
SrO	0.13	0.13	0.10	0.13	0.11	0.11	0.13	0.12	0.12	0.13	0.12	0.11	0.12	0.12
BaO														0.07
Na_2O	5.71	5.78	5.27	4.98	4.91	5.01	4.93	5.17	4.82	5.36	4.50	4.99	4.83	3.52
K_2O	0.56	0.56	0.47	0.43	0.41	0.42	0.43	0.41	0.41	0.47	0.34	0.40	0.39	0.22
Sum	98.87	99.52	99.59	99.17	99.39	99.36	99.22	99.64	99.33	99.23	99.10	99.55	99.33	99.45
Si	2.556	2.551	2.519	2.485	2.474	2.476	2.486	2.487	2.455	2.507	2.436	2.486	2.460	2.334
Al	1.426	1.437	1.466	1.499	1.513	1.510	1.497	1.498	1.527	1.475	1.544	1.501	1.523	1.655
Ti	0.001	0.001	0.001	0.001	0.001	0.001	0.001	0.001	0.001	0.001	0.001	0.001	0.001	0.001
Fe	0.019	0.019	0.018	0.018	0.019	0.018	0.018	0.018	0.018	0.019	0.018	0.018	0.018	0.017
Mg	0.003	0.003	0.003	0.003	0.003	0.003	0.003	0.003	0.003	0.003	0.003	0.003	0.003	0.003
Sr	0.003	0.003	0.003	0.003	0.003	0.003	0.003	0.003	0.003	0.003	0.003	0.003	0.003	0.003
Ba	0.000	0.000	0.000	0.000	0.000	0.000	0.000	0.000	0.000	0.000	0.000	0.000	0.000	0.001
Ca	0.452	0.444	0.492	0.524	0.528	0.524	0.527	0.514	0.550	0.497	0.577	0.519	0.544	0.661
Na	0.505	0.507	0.463	0.440	0.433	0.442	0.435	0.455	0.426	0.473	0.399	0.439	0.427	0.313
K	0.033	0.032	0.027	0.025	0.024	0.024	0.025	0.023	0.024	0.027	0.020	0.023	0.023	0.013
Sum	4.998	4.999	4.992	4.998	4.997	5.001	4.995	5.002	5.006	5.005	5.001	4.994	5.003	5.001
Ab (mol%)	51.0	51.5	47.1	44.5	44.0	44.7	44.1	45.8	42.6	47.4	40.1	44.7	43.0	31.7
An (mol%)	45.7	45.2	50.1	52.9	53.6	52.9	53.4	51.8	55.0	49.8	58.0	52.9	54.7	67.0
Or (mol%)	3.3	3.3	2.8	2.5	2.4	2.5	2.5	2.4	2.4	2.7	2.0	2.4	2.3	1.3

Table D1 Feldspar analyses of the 2006 Merapi eruption (continued)

Sample	ME08-09-02	ME08-09-02	ME08-09-02	ME08-09-02	ME08-09-02	ME08-09-02	ME08-09-02	ME08-09-02	ME08-09-02	ME08-09-02	ME08-09-02	ME08-09-02	ME08-09-02	ME08-09-02
Sample Type	L1-S	L1-S	L1-S	L1-S	L1-S	L1-S	L1-S	L1-S	L1-S	L1-S	L1-S	L1-S	L1-S	L1-S
Point	1 / 2 .	1 / 3 .	1 / 4 .	1 / 5 .	1 / 6 .	1 / 7 .	1 / 8 .	1 / 9 .	1 / 10 .	1 / 11 .	1 / 12 .	1 / 13 .	1 / 16 .	1 / 17 .
Comment	ph	ph	ph	ph	ph	ph	ph	ph	ph	ph	ph	ph	ph	ph
SiO_2	50.90	51.16	51.59	52.49	53.22	53.47	54.52	55.84	56.75	56.71	55.73	56.60	55.72	54.38
TiO_2	0.03	0.02	0.02	0.03	0.04	0.02	0.02	0.03	0.02	0.03	0.03	0.03	0.02	0.02
Al_2O_3	30.58	30.71	30.22	29.45	29.34	28.86	28.20	27.38	26.93	26.47	27.68	26.79	27.23	26.21
FeO	0.46	0.46	0.41	0.47	0.30	0.42	0.43	0.53	0.42	0.38	0.47	0.39	0.51	0.39
MgO	0.04	0.05	0.04	0.03	0.03	0.03	0.05	0.05	0.05	0.06	0.03	0.04	0.04	0.05
CaO	13.36	13.36	13.10	12.23	11.67	11.30	10.64	9.73	9.06	8.85	9.82	9.04	9.54	10.53
SrO	0.08	0.17	0.14	0.13	0.09	0.13	0.05	0.17	0.16	0.10	0.13	0.13	0.15	0.17
BaO	0.05			0.01	0.02		0.06	0.07			0.24	0.12	0.04	0.11
Na_2O	3.65	3.65	3.79	4.35	4.57	4.87	5.19	5.73	6.03	6.12	5.58	6.01	5.58	5.69
K_2O	0.24	0.25	0.29	0.32	0.34	0.39	0.43	0.50	0.57	0.56	0.50	0.56	0.55	0.53
Sum	99.37	99.85	99.60	99.50	99.67	99.49	99.60	100.03	99.99	99.30	100.21	99.71	99.40	98.14
Si	2.335	2.336	2.358	2.398	2.421	2.437	2.476	2.523	2.557	2.571	2.515	2.558	2.530	2.517
Al	1.653	1.653	1.628	1.586	1.573	1.550	1.510	1.458	1.430	1.414	1.472	1.427	1.457	1.430
Ti	0.001	0.001	0.001	0.001	0.001	0.001	0.001	0.001	0.001	0.001	0.001	0.001	0.001	0.001
Fe	0.018	0.017	0.016	0.018	0.011	0.016	0.016	0.020	0.016	0.014	0.018	0.015	0.019	0.015
Mg	0.003	0.003	0.003	0.002	0.002	0.002	0.004	0.003	0.003	0.004	0.002	0.003	0.003	0.003
Sr	0.002	0.004	0.004	0.004	0.002	0.004	0.001	0.004	0.004	0.003	0.004	0.003	0.004	0.004
Ba	0.001	0.000	0.000	0.000	0.000	0.000	0.001	0.001	0.000	0.000	0.004	0.002	0.001	0.002
Ca	0.657	0.654	0.641	0.599	0.569	0.552	0.518	0.471	0.438	0.430	0.475	0.438	0.464	0.522
Na	0.325	0.324	0.336	0.385	0.403	0.430	0.457	0.502	0.527	0.538	0.488	0.526	0.491	0.511
K	0.014	0.015	0.017	0.018	0.020	0.023	0.025	0.029	0.033	0.033	0.029	0.033	0.032	0.031
Sum	5.007	5.006	5.004	5.010	5.003	5.014	5.009	5.012	5.007	5.007	5.007	5.006	5.002	5.038
Ab (mol%)	32.6	32.6	33.8	38.4	40.6	42.8	45.7	50.1	52.8	53.8	49.2	52.8	49.7	48.0
An (mol%)	66.0	65.9	64.5	59.7	57.4	54.9	51.8	47.0	43.9	43.0	47.9	43.9	47.0	49.1
Or (mol%)	1.4	1.5	1.7	1.8	2.0	2.3	2.5	2.9	3.3	3.3	2.9	3.3	3.2	2.9

Table D1 Feldspar analyses of the 2006 Merapi eruption (continued)

Sample	ME08-09-02	ME08-09-02	ME08-09-02	ME08-09-02	ME08-09-02	ME08-09-02	ME08-09-02	ME08-09-02	ME08-09-02	ME08-09-02	ME08-09-02	ME08-09-02	ME08-09-02	ME08-09-02
Sample Type	L1-S	L1-S	L1-S	L1-S	L1-S	L1-S	L1-S	L1-S	L1-S	L1-S	L1-S	L1-S	L1-S	L1-S
Point	1 / 18 .	1 / 19 .	1 / 20 .	1 / 21 .	1 / 22 .	1 / 23 .	1 / 24 .	1 / 25 .	1 / 26 .	1 / 27 .	1 / 28 .	1 / 29 .	1 / 30 .	1 / 31 .
Comment	ph	ph	ph	ph	ph	ph	ph	ph	ph	ph	ph	ph	ph	ph
SiO_2	54.47	55.80	52.44	52.25	53.87	53.62	53.69	52.83	52.47	52.11	52.62	53.32	54.43	54.35
TiO_2	0.03	0.04	0.03	0.04	0.01	0.03	0.03	0.01	0.02	0.01	0.03	0.02	0.02	0.02
Al_2O_3	28.16	27.21	29.76	29.97	28.99	29.15	28.99	29.30	30.08	29.95	29.33	28.79	28.52	28.20
FeO	0.54	0.50	0.49	0.54	0.56	0.47	0.55	0.54	0.44	0.54	0.51	0.50	0.47	0.49
MgO	0.14	0.02	0.03	0.04	0.03	0.04	0.05	0.02	0.03	0.05	0.05	0.01	0.04	0.05
CaO	10.58	9.63	12.25	12.66	11.52	11.60	11.42	12.02	12.91	12.77	12.15	11.57	10.91	10.78
SrO	0.14	0.17	0.16	0.11	0.06	0.10	0.10	0.14	0.12	0.08	0.19	0.18	0.10	0.14
BaO	0.14		0.02	0.03	0.08		0.01	0.07		0.04	0.03	0.09	0.01	0.09
Na_2O	5.17	5.69	4.30	4.09	4.69	4.64	4.69	4.37	4.12	4.14	4.36	4.69	5.06	5.09
K_2O	0.48	0.53	0.33	0.30	0.38	0.35	0.31	0.32	0.34	0.28	0.32	0.34	0.39	0.43
Sum	99.89	99.59	99.87	100.02	100.19	100.06	99.87	99.63	100.55	100.00	99.59	99.54	99.96	99.71
Si	2.473	2.530	2.389	2.377	2.439	2.431	2.437	2.410	2.376	2.374	2.403	2.433	2.465	2.471
Al	1.507	1.454	1.598	1.607	1.547	1.557	1.551	1.575	1.606	1.608	1.579	1.549	1.522	1.511
Ti	0.001	0.001	0.001	0.001	0.000	0.001	0.001	0.000	0.001	0.000	0.001	0.001	0.001	0.001
Fe	0.021	0.019	0.019	0.020	0.021	0.018	0.021	0.021	0.017	0.020	0.020	0.019	0.018	0.018
Mg	0.009	0.001	0.002	0.003	0.002	0.003	0.003	0.002	0.002	0.003	0.003	0.001	0.003	0.003
Sr	0.004	0.004	0.004	0.003	0.002	0.003	0.003	0.004	0.003	0.002	0.005	0.005	0.003	0.004
Ba	0.003	0.000	0.000	0.001	0.001	0.000	0.000	0.001	0.000	0.001	0.001	0.002	0.000	0.002
Ca	0.515	0.468	0.598	0.617	0.559	0.563	0.555	0.587	0.626	0.623	0.594	0.566	0.529	0.525
Na	0.455	0.500	0.380	0.360	0.412	0.408	0.412	0.386	0.362	0.366	0.386	0.415	0.444	0.448
K	0.028	0.031	0.019	0.017	0.022	0.020	0.018	0.019	0.020	0.016	0.019	0.020	0.023	0.025
Sum	5.014	5.007	5.011	5.007	5.004	5.004	5.002	5.005	5.011	5.013	5.009	5.009	5.007	5.009
Ab (mol%)	45.6	50.1	38.1	36.2	41.5	41.1	41.8	38.9	35.9	36.4	38.6	41.5	44.6	44.9
An (mol%)	51.6	46.8	59.9	62.0	56.3	56.8	56.4	59.2	62.2	62.0	59.5	56.5	53.2	52.6
Or (mol%)	2.8	3.1	1.9	1.7	2.2	2.0	1.8	1.9	1.9	1.6	1.9	2.0	2.3	2.5

Table D1 Feldspar analyses of the 2006 Merapi eruption (continued)

Sample	ME08-09-02	ME08-09-02	ME08-09-02	ME08-09-02	ME08-09-02	ME08-09-02	ME08-09-02	ME08-09-02	ME08-09-02	ME08-09-02	ME08-09-02	ME08-09-02	ME08-09-02	ME08-09-02
Sample Type	L1-S	L1-S	L1-S	L1-S	L1-S	L1-S	L1-S	L1-S	L1-S	L1-S	L1-S	L1-S	L1-S	L1-S
Point	1 / 32 .	1 / 33 .	1 / 34 .	1 / 35 .	1 / 36 .	1 / 37 .	1 / 38 .	1 / 39 .	1 / 40 .	1 / 41 .	1 / 42 .	1 / 43 .	1 / 44 .	1 / 45 .
Comment	ph	ph	ph	ph	ph	ph	ph	ph	ph	ph	ph	ph	ph	ph
SiO_2	56.53	56.68	57.28	57.70	55.96	57.23	57.69	56.44	54.31	56.07	56.90	56.83	56.98	55.71
TiO_2	0.02	0.03	0.02	0.02	0.02	0.02	0.01	0.02	0.02	0.03	0.04	0.02	0.04	0.03
Al_2O_3	27.05	26.47	26.42	26.02	27.10	26.55	26.38	26.80	28.37	27.10	26.68	26.80	26.50	27.46
FeO	0.49	0.50	0.43	0.48	0.47	0.46	0.48	0.45	0.55	0.47	0.48	0.46	0.51	0.45
MgO	0.04	0.05	0.03	0.05	0.04	0.04	0.03	0.02	0.05	0.04	0.04	0.04	0.06	0.04
CaO	9.52	8.89	8.71	8.31	9.62	8.78	8.46	9.13	10.99	9.62	8.94	9.05	8.78	9.88
SrO	0.18	0.16	0.10	0.08	0.13	0.08	0.05	0.16	0.16	0.10	0.12	0.11	0.17	0.18
BaO	0.01	0.06	0.03		0.09	0.09	0.18	0.10	0.04			0.06	0.16	0.11
Na_2O	5.91	6.11	6.20	6.29	5.73	6.19	6.33	5.99	4.98	5.81	6.08	6.01	6.19	5.75
K_2O	0.55	0.64	0.65	0.67	0.51	0.67	0.71	0.62	0.43	0.50	0.61	0.62	0.66	0.48
Sum	100.29	99.61	99.88	99.63	99.73	100.14	100.31	99.74	99.96	99.79	99.91	100.00	100.04	100.11
Si	2.544	2.567	2.581	2.603	2.535	2.575	2.589	2.554	2.464	2.536	2.566	2.561	2.570	2.517
Al	1.435	1.413	1.403	1.383	1.446	1.408	1.396	1.429	1.517	1.445	1.418	1.424	1.409	1.462
Ti	0.001	0.001	0.001	0.001	0.001	0.001	0.000	0.001	0.001	0.001	0.001	0.001	0.001	0.001
Fe	0.018	0.019	0.016	0.018	0.018	0.017	0.018	0.017	0.021	0.018	0.018	0.017	0.019	0.017
Mg	0.002	0.003	0.002	0.003	0.003	0.003	0.002	0.001	0.003	0.003	0.002	0.003	0.004	0.003
Sr	0.005	0.004	0.003	0.002	0.003	0.002	0.001	0.004	0.004	0.003	0.003	0.003	0.005	0.005
Ba	0.000	0.001	0.001	0.000	0.002	0.002	0.003	0.002	0.001	0.000	0.000	0.001	0.003	0.002
Ca	0.459	0.432	0.421	0.402	0.467	0.423	0.407	0.443	0.534	0.466	0.432	0.437	0.424	0.478
Na	0.515	0.536	0.542	0.550	0.504	0.540	0.550	0.526	0.438	0.510	0.532	0.526	0.541	0.504
K	0.032	0.037	0.038	0.038	0.030	0.038	0.041	0.036	0.025	0.029	0.035	0.036	0.038	0.028
Sum	5.011	5.013	5.006	4.999	5.008	5.009	5.008	5.012	5.008	5.009	5.007	5.007	5.014	5.017
Ab (mol%)	51.2	53.4	54.2	55.6	50.4	53.9	55.2	52.4	43.9	50.7	53.3	52.6	53.9	49.9
An (mol%)	45.6	42.9	42.1	40.6	46.7	42.3	40.8	44.1	53.5	46.4	43.3	43.8	42.3	47.4
Or (mol%)	3.1	3.7	3.8	3.9	3.0	3.8	4.1	3.5	2.5	2.9	3.5	3.6	3.8	2.8

Table D1 Feldspar analyses of the 2006 Merapi eruption (continued)

Sample	ME08-09-02	ME08-09-02	ME08-09-02	ME08-09-02	ME08-09-02	ME08-09-02	ME08-09-02	ME08-09-02	ME08-09-02	ME08-09-02	ME08-09-02	ME08-09-02	ME08-09-02	ME08-09-02
Sample Type	L1-S	L1-S	L1-S	L1-S	L1-S	L1-S	L1-S	L1-S	L1-S	L1-S	L1-S	L1-S	L1-S	L1-S
Point	1 / 46 .	1 / 47 .	1 / 48 .	1 / 49 .	1 / 50 .	1 / 51 .	1 / 53 .	1 / 54 .	1 / 55 .	8 / 1 .	10 / 1 .	11 / 1 .	12 / 1 .	2 / 1 .
Comment	ph	ph	ph	ph	ph	ph	ph	ph	ph-r	mph	mph	mph	mph	m
SiO_2	56.57	57.12	56.39	56.13	56.63	52.80	53.85	57.53	62.25	56.85	52.30	56.21	51.63	56.68
TiO_2	0.03	0.03	0.03	0.03	0.02	0.02	0.03	0.02	0.06	0.03	0.02	0.02	0.01	0.04
Al_2O_3	26.61	26.07	27.21	27.28	26.94	29.32	28.73	26.53	21.42	26.37	29.14	26.85	29.62	26.39
FeO	0.42	0.53	0.44	0.56	0.39	0.55	0.52	0.48	0.62	0.48	0.52	0.50	0.56	1.07
MgO	0.04	0.05	0.06	0.04	0.04	0.04	0.06	0.12	0.22	0.04	0.05	0.06	0.04	0.21
CaO	9.15	8.59	9.49	9.46	9.47	12.54	11.45	8.91	4.83	8.68	12.04	9.41	12.67	8.76
SrO	0.15	0.13	0.12	0.15	0.16	0.16	0.13	0.16	0.04	0.13	0.13	0.15	0.15	0.11
BaO		0.09	0.12	0.06	0.08	0.06	0.07		0.20					
Na_2O	5.91	6.17	5.76	5.73	5.92	4.14	4.72	6.22	7.03	5.95	4.18	5.53	3.87	5.84
K_2O	0.59	0.67	0.54	0.55	0.49	0.28	0.35	0.63	2.43	0.61	0.25	0.55	0.30	0.64
Sum	99.57	99.49	100.14	99.99	100.13	99.94	99.93	100.59	99.12	99.16	98.64	99.28	98.86	99.78
Si	2.562	2.587	2.540	2.534	2.551	2.404	2.445	2.576	2.814	2.579	2.407	2.551	2.377	2.565
Al	1.421	1.392	1.445	1.451	1.430	1.573	1.537	1.401	1.141	1.410	1.581	1.436	1.607	1.407
Ti	0.001	0.001	0.001	0.001	0.001	0.001	0.001	0.001	0.002	0.001	0.001	0.001	0.000	0.001
Fe	0.016	0.020	0.016	0.021	0.015	0.021	0.020	0.018	0.023	0.018	0.020	0.019	0.022	0.041
Mg	0.003	0.003	0.004	0.003	0.002	0.003	0.004	0.008	0.015	0.003	0.003	0.004	0.003	0.014
Sr	0.004	0.003	0.003	0.004	0.004	0.004	0.003	0.004	0.001	0.003	0.004	0.004	0.004	0.003
Ba	0.000	0.002	0.002	0.001	0.001	0.001	0.001	0.000	0.004	0.000	0.000	0.000	0.000	0.000
Ca	0.444	0.417	0.458	0.458	0.457	0.612	0.557	0.427	0.234	0.422	0.593	0.458	0.625	0.425
Na	0.519	0.542	0.503	0.502	0.517	0.365	0.416	0.540	0.617	0.524	0.373	0.486	0.345	0.513
K	0.034	0.039	0.031	0.031	0.028	0.016	0.020	0.036	0.140	0.035	0.015	0.032	0.018	0.037
Sum	5.003	5.006	5.003	5.006	5.006	5.000	5.004	5.011	4.991	4.995	4.996	4.990	5.001	5.005
Ab (mol%)	52.1	54.3	50.7	50.6	51.6	36.8	41.9	53.8	62.2	53.4	38.0	49.8	35.0	52.6
An (mol%)	44.5	41.8	46.2	46.2	45.6	61.6	56.1	42.6	23.6	43.0	60.5	46.9	63.2	43.6
Or (mol%)	3.4	3.9	3.1	3.2	2.8	1.6	2.0	3.6	14.2	3.6	1.5	3.3	1.8	3.8

Table D1 Feldspar analyses of the 2006 Merapi eruption (continued)

Sample	ME08-09-02	ME08-09-02	ME08-09-02	ME08-09-02	ME08-09-02	ME08-09-02	ME08-09-02	ME08-09-02	ME08-09-02	ME08-09-02	ME08-09-02	ME08-09-02	ME08-10	ME08-10
Sample Type	L1-S	L1-S	L1-S	L1-S	L1-S	L1-S	L1-S	L1-S	L1-S	L1-S	L1-S	L1-S	KB-S	KB-S
Point	3 / 1 .	4 / 1 .	1 / 1 .	2 / 1 .	3 / 1 .	4 / 1 .	1 / 1 .	3 / 1 .	4 / 1 .	6 / 1 .	16 / 1 .	17 / 1 .	1 / 1 .	2 / 1 .
Comment	m	m	m	m	m	m	m-c	m-c	m-c	m-c	m-c	m-c	ph-r	ph-c
SiO_2	61.51	58.90	63.12	58.90	61.65	59.38	57.62	62.54	57.78	61.29	55.88	58.12	54.20	50.88
TiO_2	0.15	0.03	0.12	0.02	0.07	0.04	0.09	0.10	0.05	0.04	0.06	0.06	0.02	0.02
Al_2O_3	23.90	25.07	21.69	25.37	23.34	25.18	26.65	23.37	26.53	24.43	27.48	26.35	28.15	30.54
FeO	1.02	0.54	0.89	0.61	0.81	0.76	0.49	0.59	0.48	0.49	0.49	0.44	0.49	0.53
MgO	0.06	0.03	0.05	0.03	0.04	0.08	0.06	0.04	0.05	0.05	0.08	0.04	0.05	0.04
CaO	5.69	7.44	4.96	7.78	6.02	7.09	9.17	5.94	8.99	7.23	10.18	8.79	10.72	13.77
SrO	0.04	0.09	0.02	0.15	0.06	0.05							0.10	0.12
BaO			0.13	0.12	0.10	0.08							0.05	0.03
Na_2O	6.88	6.50	6.69	6.43	6.57	6.56	5.90	6.81	6.12	6.66	5.35	5.99	5.00	3.50
K_2O	1.63	1.07	2.34	1.05	2.03	1.25	0.63	1.86	0.70	1.45	0.47	0.77	0.42	0.22
Sum	100.93	99.67	100.01	100.47	100.69	100.50	100.62	101.24	100.71	101.68	100.02	100.59	99.20	99.65
Si	2.730	2.652	2.822	2.638	2.746	2.655	2.576	2.761	2.582	2.702	2.520	2.597	2.473	2.331
Al	1.250	1.330	1.143	1.339	1.225	1.327	1.404	1.216	1.397	1.270	1.461	1.388	1.514	1.649
Ti	0.005	0.001	0.004	0.001	0.002	0.002	0.003	0.003	0.002	0.001	0.002	0.002	0.001	0.001
Fe	0.038	0.020	0.033	0.023	0.030	0.028	0.018	0.022	0.018	0.018	0.019	0.017	0.019	0.020
Mg	0.004	0.002	0.003	0.002	0.003	0.006	0.004	0.003	0.003	0.003	0.005	0.003	0.003	0.003
Sr	0.001	0.002	0.000	0.004	0.001	0.001	0.000	0.000	0.000	0.000	0.000	0.000	0.003	0.003
Ba	0.000	0.000	0.002	0.002	0.002	0.001	0.000	0.000	0.000	0.000	0.000	0.000	0.001	0.001
Ca	0.271	0.359	0.238	0.373	0.287	0.340	0.439	0.281	0.431	0.342	0.492	0.421	0.524	0.676
Na	0.592	0.568	0.580	0.558	0.567	0.568	0.511	0.583	0.530	0.569	0.468	0.519	0.442	0.311
K	0.092	0.062	0.133	0.060	0.116	0.071	0.036	0.105	0.040	0.082	0.027	0.044	0.024	0.013
Sum	4.982	4.996	4.959	5.001	4.980	5.000	4.992	4.972	5.003	4.987	4.994	4.989	5.003	5.006
Ab (mol%)	62.0	57.5	61.0	56.3	58.5	58.0	51.8	60.2	53.0	57.3	47.4	52.8	44.6	31.1
An (mol%)	28.3	36.3	25.0	37.7	29.6	34.7	44.5	29.0	43.0	34.4	49.9	42.8	52.9	67.6
Or (mol%)	9.7	6.2	14.0	6.1	11.9	7.3	3.6	10.8	4.0	8.2	2.8	4.5	2.5	1.3

Table D1 Feldspar analyses of the 2006 Merapi eruption (continued)

Sample	ME08-10	ME08-10	ME08-10	ME08-10	ME08-10	ME08-10	ME08-10	ME08-10	ME08-10	ME08-10	ME08-10	ME08-10	ME08-10	ME08-10
Sample Type	KB-S	KB-S	KB-S	KB-S	KB-S	KB-S	KB-S	KB-S	KB-S	KB-S	KB-S	KB-S	KB-S	KB-S
Point	2 / 1 .	2 / 2 .	2 / 3 .	2 / 4 .	2 / 5 .	2 / 6 .	2 / 7 .	2 / 8 .	2 / 9 .	2 / 10 .	2 / 11 .	2 / 12 .	2 / 13 .	2 / 14 .
Comment	ph-c	ph	ph	ph	ph	ph	ph	ph	ph	ph	ph	ph	ph	ph
SiO_2	51.39	52.56	51.60	50.65	50.52	49.77	49.80	50.80	52.14	53.87	54.53	56.11	56.77	59.88
TiO_2	0.02	0.03	0.03	0.02	0.03	0.02	0.01	0.03	0.02	0.03	0.03	0.03	0.03	0.06
Al_2O_3	30.38	29.31	30.39	31.21	31.12	31.85	31.36	30.88	29.65	28.89	28.55	27.56	26.52	24.09
FeO	0.48	0.58	0.62	0.57	0.69	0.54	0.51	0.57	0.58	0.67	0.53	0.51	0.48	0.65
MgO	0.05	0.05	0.03	0.06	0.05	0.05	0.04	0.06	0.04	0.05	0.06	0.05	0.07	0.04
CaO	13.43	12.37	13.30	14.05	14.08	14.63	14.55	13.78	12.42	11.51	10.99	9.67	8.85	6.42
SrO	0.14	0.12	0.12	0.17	0.08	0.09	0.08	0.13	0.17	0.16	0.15	0.17	0.14	0.11
BaO	0.00	0.05	0.00		0.09		0.03		0.09	0.01		0.10	0.12	0.06
Na_2O	3.62	3.86	3.65	3.32	3.29	2.95	3.03	3.59	4.12	4.75	4.89	5.62	5.96	6.28
K_2O	0.24	0.69	0.22	0.21	0.21	0.17	0.18	0.21	0.28	0.33	0.47	0.58	0.73	2.25
Sum	99.76	99.63	100.01	100.26	100.17	100.14	99.61	100.08	99.52	100.29	100.20	100.47	99.68	99.82
Si	2.347	2.402	2.352	2.308	2.306	2.274	2.286	2.319	2.385	2.438	2.465	2.525	2.568	2.699
Al	1.636	1.579	1.633	1.676	1.674	1.715	1.697	1.661	1.599	1.541	1.521	1.461	1.414	1.280
Ti	0.001	0.001	0.001	0.001	0.001	0.001	0.001	0.001	0.001	0.001	0.001	0.001	0.001	0.002
Fe	0.018	0.022	0.023	0.022	0.026	0.020	0.020	0.022	0.022	0.025	0.020	0.019	0.018	0.024
Mg	0.004	0.003	0.002	0.004	0.003	0.004	0.002	0.004	0.003	0.003	0.004	0.003	0.005	0.002
Sr	0.004	0.003	0.003	0.005	0.002	0.002	0.002	0.003	0.005	0.004	0.004	0.004	0.004	0.003
Ba	0.000	0.001	0.000	0.000	0.002	0.000	0.001	0.000	0.002	0.000	0.000	0.002	0.002	0.001
Ca	0.657	0.606	0.649	0.686	0.689	0.716	0.716	0.674	0.609	0.558	0.532	0.466	0.429	0.310
Na	0.321	0.342	0.322	0.294	0.291	0.261	0.270	0.318	0.366	0.417	0.429	0.491	0.523	0.549
K	0.014	0.040	0.013	0.012	0.012	0.010	0.011	0.012	0.016	0.019	0.027	0.033	0.042	0.129
Sum	5.001	4.999	4.998	5.006	5.007	5.003	5.005	5.014	5.006	5.008	5.002	5.006	5.006	4.999
Ab (mol%)	32.3	34.6	32.7	29.6	29.3	26.5	27.1	31.6	36.9	42.0	43.4	49.5	52.6	55.5
An (mol%)	66.3	61.3	66.0	69.2	69.4	72.5	71.9	67.2	61.4	56.1	53.9	47.1	43.2	31.4
Or (mol%)	1.4	4.1	1.3	1.2	1.2	1.0	1.1	1.2	1.6	1.9	2.8	3.4	4.2	13.1

Table D1 Feldspar analyses of the 2006 Merapi eruption (continued)

Sample	ME08-10	ME08-10	ME08-10	ME08-10	ME08-10	ME08-10	ME08-10	ME08-10	ME08-10	ME08-10	ME08-10	ME08-10	ME08-10	ME08-10
Sample Type	KB-S	KB-S	KB-S	KB-S	KB-S	KB-S	KB-S	KB-S	KB-S	KB-S	KB-S	KB-S	KB-S	KB-S
Point	2 / 15 .	2 / 16 .	2 / 17 .	2 / 18 .	2 / 19 .	3 / 1 .	4 / 1 .	2 / 1 .	3 / 1 .	4 / 1 .	5 / 1 .	6 / 1 .	1 / 1 .	2 / 1 .
Comment	ph	ph	ph	ph	ph	mph-r	mph-c	mph	mph	mph	mph	mph	m	m
SiO_2	61.83	60.50	60.35	60.52	65.32	58.47	53.76	52.45	55.25	56.04	55.69	56.46	56.12	54.07
TiO_2	0.04	0.02	0.01	0.01	0.01	0.02	0.02	0.02	0.03	0.02	0.02	0.02	0.03	0.02
Al_2O_3	23.05	24.44	24.33	23.71	20.30	25.35	28.15	28.42	26.91	26.65	27.11	26.56	26.94	28.29
FeO	0.60	0.56	0.50	0.52	0.55	0.56	0.54	0.51	0.58	0.52	0.55	0.50	0.65	0.63
MgO	0.04	0.02	0.02	0.03	0.03	0.03	0.05	0.03	0.06	0.05	0.04	0.05	0.04	0.03
CaO	5.36	6.43	6.29	5.60	2.03	7.61	10.97	11.57	9.89	8.93	9.71	8.91	9.14	10.92
SrO	0.05	0.01	0.09	0.08	0.03	0.12	0.13	0.13	0.14	0.13	0.10	0.13	0.13	0.11
BaO	0.21	0.11	0.15	0.10	0.38	0.08	0.05						0.03	0.02
Na_2O	6.58	6.95	7.21	7.32	6.72	6.44	4.77	4.34	5.29	5.68	5.44	5.63	5.63	4.91
K_2O	2.56	1.42	1.37	1.64	5.56	0.95	0.41	0.43	0.53	0.58	0.57	0.59	0.73	0.48
Sum	100.38	100.51	100.33	99.53	100.92	99.63	98.85	97.92	98.70	98.61	99.24	98.87	99.43	99.49
Si	2.765	2.699	2.699	2.725	2.912	2.637	2.464	2.431	2.528	2.558	2.532	2.568	2.547	2.464
Al	1.215	1.285	1.282	1.258	1.067	1.347	1.520	1.552	1.451	1.434	1.453	1.424	1.440	1.519
Ti	0.001	0.001	0.000	0.000	0.000	0.001	0.001	0.001	0.001	0.001	0.001	0.001	0.001	0.001
Fe	0.023	0.021	0.019	0.020	0.021	0.021	0.021	0.020	0.022	0.020	0.021	0.019	0.025	0.024
Mg	0.003	0.001	0.001	0.002	0.002	0.002	0.003	0.002	0.004	0.003	0.003	0.003	0.003	0.002
Sr	0.001	0.000	0.002	0.002	0.001	0.003	0.003	0.003	0.004	0.003	0.003	0.003	0.003	0.003
Ba	0.004	0.002	0.003	0.002	0.007	0.001	0.001	0.000	0.000	0.000	0.000	0.000	0.000	0.000
Ca	0.257	0.307	0.302	0.270	0.097	0.368	0.539	0.575	0.485	0.437	0.473	0.434	0.444	0.533
Na	0.570	0.601	0.625	0.639	0.581	0.563	0.424	0.390	0.470	0.503	0.479	0.497	0.495	0.434
K	0.146	0.081	0.078	0.094	0.316	0.055	0.024	0.026	0.031	0.034	0.033	0.034	0.042	0.028
Sum	4.985	4.999	5.012	5.012	5.003	4.998	4.999	5.000	4.996	4.993	4.997	4.984	5.001	5.007
Ab (mol%)	58.6	60.8	62.2	63.7	58.4	57.1	43.0	39.4	47.6	51.6	48.6	51.5	50.4	43.6
An (mol%)	26.4	31.1	30.0	26.9	9.7	37.3	54.6	58.0	49.2	44.9	48.0	45.0	45.2	53.6
Or (mol%)	15.0	8.2	7.8	9.4	31.8	5.5	2.4	2.6	3.2	3.5	3.4	3.5	4.3	2.8

Table D1 Feldspar analyses of the 2006 Merapi eruption (continued)

Sample	ME08-10	ME08-10	ME08-10	ME08-10	ME08-10	ME08-10	ME08-10	ME08-10	ME08-10	ME08-10	ME08-14	ME08-14	ME08-14	ME08-14
Sample Type	KB-S	KB-S	KB-S	KB-S	KB-S	KB-S	KB-S	KB-S	KB-S	KB-S	SD-S	SD-S	SD-S	SD-S
Point	7 / 1 .	8 / 1 .	11 / 1 .	12 / 1 .	7 / 1 .	8 / 1 .	9 / 1 .	10 / 1 .	11 / 1 .	24 / 1 .	2 / 2 .	2 / 3 .	2 / 4 .	2 / 5 .
Comment	m	m	m	m	m	m	m	m	m	m	ph-r	ph	ph	ph
SiO_2	52.42	56.35	55.67	60.72	58.06	60.79	59.19	53.69	58.41	58.31	52.22	55.01	54.90	53.88
TiO_2	0.02	0.04	0.03	-0.01	0.02	0.02	0.07	0.03	0.03	0.03	0.02	0.03	0.03	0.02
Al_2O_3	29.52	26.57	27.13	23.66	25.81	23.74	24.75	28.52	25.62	25.88	29.27	27.49	28.09	28.43
FeO	0.59	0.58	0.59	0.53	0.60	0.64	0.71	0.54	0.65	0.58	0.49	0.47	0.47	0.48
MgO	0.03	0.03	0.03	0.01	0.01	0.01	0.02	0.04	0.02	0.04	0.04	0.05	0.05	0.05
CaO	12.12	8.88	9.53	5.42	7.84	5.50	7.68	10.92	7.82	8.25	12.20	10.45	10.49	11.34
SrO	0.12	0.15	0.12	0.06	0.07	0.07	0.05	0.11	0.09		0.12	0.12	0.12	0.12
BaO	0.03	0.03	0.08	0.38	0.10	0.21	0.02		0.06					
Na_2O	4.19	5.69	5.51	6.89	6.47	7.04	6.31	4.80	6.57	6.03	4.09	5.06	5.00	4.63
K_2O	0.33	0.71	0.68	2.08	1.03	1.93	1.21	0.55	1.11	0.95	0.33	0.46	0.40	0.38
Sum	99.40	99.04	99.38	99.75	100.01	99.96	100.03	99.26	100.38	100.07	98.78	99.14	99.55	99.37
Si	2.397	2.564	2.531	2.734	2.614	2.729	2.660	2.453	2.621	2.617	2.401	2.506	2.490	2.456
Al	1.591	1.425	1.454	1.255	1.369	1.256	1.311	1.536	1.355	1.369	1.586	1.476	1.502	1.528
Ti	0.001	0.001	0.001	0.000	0.001	0.001	0.002	0.001	0.001	0.001	0.001	0.001	0.001	0.001
Fe	0.022	0.022	0.023	0.020	0.022	0.024	0.027	0.021	0.024	0.022	0.019	0.018	0.018	0.018
Mg	0.002	0.002	0.002	0.001	0.001	0.001	0.002	0.003	0.001	0.003	0.003	0.003	0.003	0.004
Sr	0.003	0.004	0.003	0.002	0.002	0.002	0.001	0.003	0.002	0.000	0.003	0.003	0.003	0.003
Ba	0.001	0.000	0.002	0.007	0.002	0.004	0.000	0.000	0.001	0.000	0.000	0.000	0.000	0.000
Ca	0.594	0.433	0.464	0.261	0.378	0.265	0.370	0.534	0.376	0.397	0.601	0.510	0.510	0.554
Na	0.372	0.502	0.485	0.601	0.565	0.613	0.549	0.425	0.571	0.524	0.365	0.447	0.440	0.410
K	0.019	0.041	0.039	0.119	0.059	0.110	0.069	0.032	0.064	0.054	0.019	0.027	0.023	0.022
Sum	5.002	4.994	5.004	5.000	5.013	5.004	4.992	5.007	5.018	4.987	4.997	4.991	4.990	4.995
Ab (mol%)	37.7	51.4	49.1	61.2	56.4	62.0	55.6	42.9	56.5	53.7	37.0	45.5	45.2	41.5
An (mol%)	60.3	44.4	46.9	26.6	37.7	26.8	37.4	53.9	37.2	40.7	61.0	51.8	52.4	56.2
Or (mol%)	1.9	4.2	4.0	12.1	5.9	11.2	7.0	3.2	6.3	5.6	2.0	2.7	2.4	2.3

Table D1 Feldspar analyses of the 2006 Merapi eruption (continued)

Sample	ME08-14	ME08-14	ME08-14	ME08-14	ME08-14	ME08-14	ME08-14	ME08-14	ME08-14	ME08-14	ME08-14	ME08-14	ME08-14	ME08-14
Sample Type	SD-S	SD-S	SD-S	SD-S	SD-S	SD-S	SD-S	SD-S	SD-S	SD-S	SD-S	SD-S	SD-S	SD-S
Point	2 / 6 .	2 / 7 .	2 / 8 .	2 / 9 .	2 / 10 .	2 / 11 .	2 / 12 .	2 / 13 .	2 / 15 .	3 / 2 .	3 / 3 .	3 / 4 .	3 / 5 .	3 / 6 .
Comment	ph	ph	ph	ph	ph	ph	ph	ph	ph-c	ph	ph	ph	ph	ph
SiO_2	54.37	54.93	53.01	53.45	54.04	54.00	54.28	53.39	54.37	56.85	51.01	50.88	51.47	55.41
TiO_2	0.02	0.03	0.02	0.02	0.02	0.03	0.03	0.03	0.02	0.02	0.02	0.02	0.02	0.02
Al_2O_3	28.12	27.36	28.46	28.55	28.43	28.25	27.69	27.79	28.03	26.22	30.68	30.30	29.30	27.06
FeO	0.50	0.47	0.50	0.48	0.48	0.48	0.50	0.49	0.45	0.48	0.54	0.51	0.54	0.48
MgO	0.04	0.05	0.05	0.05	0.05	0.05	0.05	0.04	0.05	0.04	0.04	0.04	0.03	0.04
CaO	10.92	10.46	11.36	11.51	11.17	11.06	10.71	11.37	10.92	9.18	13.62	13.67	12.92	9.98
SrO	0.13	0.13	0.12	0.13	0.13	0.12	0.12	0.12	0.13	0.12	0.12	0.10	0.12	0.11
BaO														
Na_2O	4.90	5.13	4.55	4.47	4.74	4.76	5.05	4.56	4.94	5.75	3.33	3.49	3.88	5.43
K_2O	0.37	0.43	0.35	0.36	0.40	0.39	0.40	0.37	0.39	0.56	0.18	0.23	0.33	0.48
Sum	99.37	98.99	98.42	99.03	99.50	99.14	98.84	98.16	99.31	99.22	99.55	99.26	98.62	99.01
Si	2.475	2.507	2.441	2.445	2.460	2.465	2.485	2.464	2.477	2.579	2.334	2.338	2.378	2.526
Al	1.509	1.472	1.545	1.540	1.525	1.520	1.494	1.512	1.505	1.401	1.655	1.641	1.596	1.454
Ti	0.001	0.001	0.001	0.001	0.001	0.001	0.001	0.001	0.001	0.001	0.001	0.001	0.001	0.001
Fe	0.019	0.018	0.019	0.018	0.018	0.018	0.019	0.019	0.017	0.018	0.021	0.020	0.021	0.018
Mg	0.003	0.003	0.003	0.003	0.004	0.003	0.003	0.003	0.003	0.003	0.003	0.003	0.002	0.003
Sr	0.003	0.003	0.003	0.003	0.004	0.003	0.003	0.003	0.003	0.003	0.003	0.003	0.003	0.003
Ba	0.000	0.000	0.000	0.000	0.000	0.000	0.000	0.000	0.000	0.000	0.000	0.000	0.000	0.000
Ca	0.533	0.511	0.560	0.564	0.545	0.541	0.525	0.562	0.533	0.446	0.668	0.673	0.639	0.488
Na	0.432	0.454	0.406	0.397	0.419	0.421	0.449	0.408	0.436	0.505	0.295	0.311	0.348	0.480
K	0.022	0.025	0.021	0.021	0.023	0.023	0.024	0.022	0.023	0.032	0.011	0.014	0.019	0.028
Sum	4.997	4.995	4.999	4.993	4.998	4.996	5.003	4.994	4.999	4.989	4.990	5.003	5.007	5.000
Ab (mol%)	43.8	45.8	41.1	40.4	42.4	42.8	45.0	41.1	44.0	51.4	30.3	31.2	34.5	48.2
An (mol%)	54.0	51.6	56.8	57.5	55.2	54.9	52.7	56.7	53.7	45.3	68.6	67.5	63.5	49.0
Or (mol%)	2.2	2.5	2.1	2.2	2.4	2.3	2.4	2.2	2.3	3.3	1.1	1.4	1.9	2.8

Table D1 Feldspar analyses of the 2006 Merapi eruption (continued)

Sample	ME08-14	ME08-14	ME08-14	ME08-14	ME08-14	ME08-14	ME08-14	ME08-14	ME08-14	ME08-14	ME08-14	ME08-14	ME08-14	ME08-14
Sample Type	SD-S	SD-S	SD-S	SD-S	SD-S	SD-S	SD-S	SD-S	SD-S	SD-S	SD-S	SD-S	SD-S	SD-S
Point	3 / 8 .	3 / 9 .	3 / 10 .	3 / 11 .	3 / 12 .	3 / 13 .	3 / 14 .	3 / 15 .	3 / 16 .	3 / 17 .	4 / 1 .	4 / 2 .	4 / 4 .	4 / 6 .
Comment	ph	ph	ph	ph	ph	ph	ph	ph	ph	ph-c	ph-r	ph	ph	ph
SiO_2	56.01	53.46	53.20	52.87	53.21	52.42	52.96	52.86	53.41	52.20	55.11	49.28	49.59	57.47
TiO_2	0.02	0.27	0.03	0.03	0.03	0.03	0.03	0.03	0.03	0.03	0.02	0.01	0.03	0.03
Al_2O_3	27.19	29.19	28.80	28.96	28.68	28.87	28.34	28.76	28.38	29.85	27.99	31.54	31.84	25.90
FeO	0.49	1.33	0.50	0.45	0.47	0.51	0.53	0.51	0.51	0.49	0.47	0.57	0.55	0.58
MgO	0.04	0.20	0.04	0.03	0.04	0.05	0.05	0.05	0.05	0.04	0.04	0.05	0.03	0.03
CaO	9.53	13.13	11.75	11.90	11.95	12.49	11.55	12.19	11.36	12.64	10.48	14.72	14.83	9.37
SrO	0.11	0.11	0.12	0.10	0.12	0.12	0.15	0.11	0.12	0.12	0.13	0.12	0.13	0.10
BaO														
Na_2O	5.65	3.37	4.39	4.41	4.40	4.13	4.53	4.31	4.59	3.97	5.03	2.82	2.72	4.78
K_2O	0.55	0.54	0.33	0.32	0.32	0.27	0.32	0.31	0.34	0.29	0.40	0.13	0.18	1.32
Sum	99.60	101.65	99.18	99.07	99.23	98.89	98.46	99.13	98.81	99.64	99.67	99.25	99.91	99.58
Si	2.536	2.401	2.432	2.421	2.433	2.410	2.440	2.422	2.449	2.382	2.496	2.272	2.271	2.599
Al	1.451	1.546	1.552	1.563	1.546	1.564	1.539	1.553	1.534	1.605	1.494	1.713	1.718	1.381
Ti	0.001	0.009	0.001	0.001	0.001	0.001	0.001	0.001	0.001	0.001	0.001	0.000	0.001	0.001
Fe	0.019	0.050	0.019	0.017	0.018	0.019	0.020	0.019	0.020	0.019	0.018	0.022	0.021	0.022
Mg	0.003	0.013	0.003	0.002	0.003	0.003	0.003	0.003	0.003	0.003	0.003	0.003	0.002	0.002
Sr	0.003	0.003	0.003	0.003	0.003	0.003	0.004	0.003	0.003	0.003	0.003	0.003	0.003	0.003
Ba	0.000	0.000	0.000	0.000	0.000	0.000	0.000	0.000	0.000	0.000	0.000	0.000	0.000	0.000
Ca	0.462	0.632	0.576	0.584	0.586	0.615	0.570	0.599	0.558	0.618	0.509	0.727	0.727	0.454
Na	0.496	0.294	0.389	0.391	0.390	0.368	0.405	0.383	0.408	0.352	0.442	0.252	0.242	0.419
K	0.032	0.031	0.019	0.019	0.019	0.016	0.019	0.018	0.020	0.017	0.023	0.008	0.010	0.076
Sum	5.002	4.979	4.995	5.001	4.998	4.999	5.001	5.001	4.997	4.999	4.988	5.001	4.995	4.956
Ab (mol%)	50.1	30.7	39.5	39.4	39.2	36.8	40.8	38.3	41.4	35.7	45.4	25.5	24.7	44.1
An (mol%)	46.7	66.0	58.5	58.8	58.9	61.6	57.4	59.9	56.6	62.6	52.3	73.7	74.3	47.8
Or (mol%)	3.2	3.3	2.0	1.9	1.9	1.6	1.9	1.8	2.0	1.7	2.4	0.8	1.1	8.0

Table D1 Feldspar analyses of the 2006 Merapi eruption (continued)

Sample	ME08-14	ME08-14	ME08-14	ME08-14	ME08-14	ME08-14	ME08-14	ME08-14	ME08-14	ME08-14	ME08-14	ME08-14	ME08-14	ME08-14
Sample Type	SD-S	SD-S	SD-S	SD-S	SD-S	SD-S	SD-S	SD-S	SD-S	SD-S	SD-S	SD-S	SD-S	SD-S
Point	4 / 7 .	4 / 8 .	4 / 9 .	4 / 11 .	4 / 12 .	5 / 1 .	5 / 2 .	5 / 3 .	5 / 4 .	5 / 5 .	5 / 6 .	5 / 7 .	19 / 1 .	20 / 1 .
Comment	ph	ph	ph	ph	ph-c	ph-r	ph	ph	ph	ph	ph	ph-c	mph-r	mph-c
SiO_2	49.98	49.72	46.22	46.65	50.91	57.00	54.89	50.98	49.73	48.18	45.36	45.24	58.02	47.99
TiO_2	0.01	0.02	0.01	0.02	0.02	0.01	0.02	0.02	0.03	0.02	0.01	0.01	0.02	0.01
Al_2O_3	31.11	31.33	33.28	33.65	31.18	24.86	26.10	30.20	30.28	32.13	34.41	34.17	25.49	32.19
FeO	0.50	0.53	0.59	0.54	0.51	0.45	0.50	0.55	0.57	0.58	0.57	0.51	0.48	0.46
MgO	0.04	0.04	0.02	0.02	0.01	0.02	0.05	0.04	0.05	0.03	0.03	0.02	0.03	0.03
CaO	14.26	14.57	17.06	17.03	14.33	8.56	8.85	13.37	13.88	15.74	17.89	17.74	7.85	15.69
SrO	0.15	0.12	0.11	0.13	0.10	0.05	0.12	0.12	0.10	0.12	0.10	0.10	0.09	0.14
BaO														
Na_2O	2.97	2.97	1.50	1.61	2.19	6.26	5.58	3.56	3.21	2.28	1.10	1.15	6.30	2.11
K_2O	0.21	0.17	0.08	0.07	0.84	0.85	0.55	0.21	0.19	0.11	0.03	0.03	0.77	0.10
Sum	99.25	99.49	98.90	99.72	100.10	98.06	96.66	99.05	98.03	99.20	99.50	98.97	99.06	98.75
Si	2.300	2.286	2.154	2.155	2.321	2.618	2.557	2.346	2.317	2.229	2.105	2.110	2.628	2.228
Al	1.687	1.698	1.828	1.832	1.675	1.346	1.433	1.637	1.662	1.752	1.882	1.878	1.361	1.761
Ti	0.000	0.001	0.000	0.001	0.001	0.000	0.001	0.001	0.001	0.001	0.000	0.000	0.001	0.000
Fe	0.019	0.020	0.023	0.021	0.019	0.017	0.019	0.021	0.022	0.022	0.022	0.020	0.018	0.018
Mg	0.003	0.003	0.002	0.001	0.001	0.001	0.004	0.003	0.003	0.002	0.002	0.001	0.002	0.002
Sr	0.004	0.003	0.003	0.003	0.003	0.001	0.003	0.003	0.003	0.003	0.003	0.003	0.002	0.004
Ba	0.000	0.000	0.000	0.000	0.000	0.000	0.000	0.000	0.000	0.000	0.000	0.000	0.000	0.000
Ca	0.703	0.718	0.852	0.843	0.700	0.421	0.442	0.659	0.693	0.780	0.889	0.886	0.381	0.780
Na	0.265	0.265	0.136	0.144	0.193	0.558	0.504	0.318	0.290	0.205	0.099	0.104	0.553	0.190
K	0.013	0.010	0.005	0.004	0.049	0.050	0.033	0.012	0.011	0.007	0.002	0.002	0.045	0.006
Sum	4.994	5.002	5.002	5.003	4.962	5.012	4.994	5.000	5.002	5.000	5.004	5.004	4.990	4.990
Ab (mol%)	27.0	26.7	13.7	14.5	20.5	54.2	51.5	32.1	29.2	20.7	10.0	10.4	56.5	19.5
An (mol%)	71.7	72.3	85.9	85.1	74.3	40.9	45.2	66.6	69.7	78.7	89.8	89.4	38.9	79.9
Or (mol%)	1.3	1.0	0.5	0.4	5.2	4.8	3.3	1.2	1.1	0.7	0.2	0.2	4.6	0.6

Table D1 Feldspar analyses of the 2006 Merapi eruption (continued)

Sample	ME08-14	ME08-14	ME08-14	ME08-14	ME08-14	ME08-14	ME08-14	ME08-14	ME08-14	ME08-14				
Sample Type	SD-S	SD-S	SD-S	SD-S	SD-S	SD-S	SD-S	SD-S	SD-S	SD-S				
Point	21 / 1 .	22 / 1 .	23 / 1 .	24 / 1 .	17 / 1 .	19 / 1 .	14 / 1 .	19 / 1 .	1 / 1 .	2 / 1 .				
Comment	mph-r	mph-c	mph-r	mph-c	m	m	m-r	m-c	m	m				
SiO_2	58.24	53.21	51.25	51.33	56.83	57.79	59.57	65.81	54.51	59.44				
TiO_2	0.02	0.02	0.02	0.02	0.03	0.03	0.05	0.09	0.05	0.01				
Al_2O_3	25.37	28.70	30.34	30.12	26.15	26.25	24.63	20.55	27.88	24.63				
FeO	0.51	0.53	0.53	0.51	0.52	0.51	0.52	0.60	0.58	0.44				
MgO	0.04	0.04	0.04	0.04	0.05	0.04	0.04	0.01	0.04	0.02				
CaO	7.67	11.53	13.46	13.24	8.51	8.26	6.86	3.52	11.02	6.90				
SrO	0.13	0.10	0.10	0.14	0.06	0.11			0.09	0.07				
BaO					0.16									
Na_2O	6.38	4.50	3.42	3.62	6.25	6.40	6.33	6.19	4.87	6.81				
K_2O	0.81	0.32	0.25	0.23	0.84	0.81	1.87	3.80	0.39	1.05				
Sum	99.19	98.95	99.42	99.26	99.41	100.20	99.86	100.58	99.46	99.38				
Si	2.635	2.437	2.348	2.355	2.579	2.595	2.678	2.912	2.481	2.678				
Al	1.353	1.549	1.638	1.629	1.399	1.389	1.305	1.072	1.496	1.308				
Ti	0.001	0.001	0.001	0.001	0.001	0.001	0.002	0.003	0.002	0.001				
Fe	0.019	0.020	0.020	0.020	0.020	0.019	0.020	0.022	0.022	0.016				
Mg	0.002	0.003	0.003	0.003	0.003	0.003	0.002	0.001	0.003	0.001				
Sr	0.003	0.003	0.003	0.004	0.002	0.003	0.000	0.000	0.002	0.002				
Ba	0.000	0.000	0.000	0.000	0.003	0.000	0.000	0.000	0.000	0.000				
Ca	0.372	0.566	0.661	0.651	0.414	0.398	0.330	0.167	0.537	0.333				
Na	0.560	0.400	0.304	0.322	0.550	0.557	0.552	0.531	0.430	0.595				
K	0.047	0.019	0.015	0.014	0.049	0.046	0.107	0.214	0.023	0.060				
Sum	4.992	4.997	4.992	4.998	5.020	5.011	4.997	4.922	4.996	4.995				
Ab (mol%)	57.2	40.6	31.0	32.6	54.3	55.6	55.8	58.2	43.4	60.2				
An (mol%)	38.0	57.5	67.4	66.0	40.9	39.7	33.4	18.3	54.3	33.7				
Or (mol%)	4.8	1.9	1.5	1.4	4.8	4.6	10.8	23.5	2.3	6.1				

Table D2 Pyroxene analyses of the 2006 Merapi eruption[1]

Sample	ME08-01	ME08-04-01	ME08-04-01	ME08-04-01	ME08-04-01	ME08-04-01	ME08-04-01	ME08-04-01	ME08-04-01	ME08-09-01	ME08-09-01	ME08-09-01	ME08-09-01	ME08-09-01	ME08-09-01	ME08-09-01	ME08-09-01	ME08-09-01	ME08-09-01
Sample Type[2]	L4-S	L8-S	L8-S	L8-S	L8-S	L8-S	L8-S	L8-S	L8-S	L1-S	L1-S	L1-S	L1-S	L1-S	L1-S	L1-S	L1-S	L1-S	L1-S
Point	56 / 1 .	47 / 1 .	48 / 1 .	51 / 1 .	52 / 1 .	45 / 1 .	46 / 1 .	49 / 1 .	50 / 1 .	6 / 1 .	7 / 1 .	12 / 1 .	13 / 1 .	19 / 1 .	20 / 1 .	21 / 1 .	22 / 1 .	33 / 1 .	34 / 1 .
Comment[3]	mph	m-r	m-c	m-c	m-c	mph-r	mph-c	m-r	m-c	ph	ph	ph	ph	ph	ph	ph	ph	ph	ph
Pyroxene Type	opx	cpx	cpx	cpx	cpx	opx	opx	opx	opx	cpx	cpx	cpx	cpx	cpx	cpx	cpx	cpx	cpx	cpx
SiO_2	52.64	52.30	50.59	51.35	52.23	53.59	52.98	53.67	53.72	52.57	52.86	52.56	52.15	52.78	52.48	52.92	52.95	52.87	52.96
TiO_2	0.28	0.38	0.60	0.45	0.41	0.16	0.22	0.23	0.22	0.36	0.42	0.33	0.38	0.41	0.39	0.26	0.38	0.31	0.39
Al_2O_3	1.52	1.58	3.43	2.34	2.14	0.61	1.06	0.97	0.87	1.94	1.91	1.96	1.89	2.10	2.07	1.95	1.74	1.92	1.72
Cr_2O_3	0.01	-0.01	0.01	0.00	-0.01	-0.01	0.01	-0.01	0.01	0.01	0.00	0.00	0.00	0.05	0.02	0.00	0.00	0.06	0.03
FeO	16.71	8.44	8.83	8.83	9.00	17.72	18.20	18.32	18.07	8.70	9.14	8.94	9.23	8.45	8.69	9.17	8.91	8.81	8.72
MnO	1.23	0.76	0.45	0.68	0.52	1.37	1.36	1.35	1.36	0.59	0.67	0.68	0.72	0.43	0.54	0.60	0.71	0.63	0.66
MgO	21.66	15.24	13.81	14.75	14.78	24.10	24.40	24.70	24.70	14.57	14.92	15.00	15.09	15.20	15.09	14.67	15.07	15.11	15.35
CaO	3.84	20.18	21.57	20.38	20.34	1.51	1.43	1.41	1.35	21.29	20.71	20.89	20.18	20.94	20.73	20.97	20.76	20.81	20.68
Na_2O	0.28	0.35	0.36	0.44	0.34	0.02	0.02	0.03	0.02	0.35	0.37	0.40	0.34	0.35	0.31	0.34	0.36	0.33	0.32
K_2O	0.25	0.03	0.01	0.01	0.00	0.03	0.01	0.02	0.00	0.00	0.00	0.00	0.00	0.00	0.00	0.00	0.00	0.01	0.00
Sum	98.41	99.26	99.66	99.21	99.77	99.10	99.68	100.69	100.32	100.38	101.00	100.76	99.99	100.69	100.33	100.87	100.89	100.84	100.83
Si	1.971	1.957	1.897	1.929	1.946	1.984	1.956	1.961	1.967	1.950	1.949	1.943	1.943	1.945	1.944	1.954	1.953	1.950	1.952
Al	0.067	0.070	0.152	0.104	0.094	0.027	0.046	0.042	0.038	0.085	0.083	0.086	0.083	0.091	0.090	0.085	0.076	0.083	0.075
Ti	0.008	0.011	0.017	0.013	0.011	0.004	0.006	0.006	0.006	0.010	0.012	0.009	0.011	0.011	0.011	0.007	0.011	0.009	0.011
Cr	0.000	0.000	0.000	0.000	0.000	0.000	0.000	0.000	0.000	0.000	0.000	0.000	0.000	0.002	0.001	0.000	0.000	0.002	0.001
Mg	1.209	0.850	0.772	0.826	0.821	1.330	1.343	1.346	1.348	0.805	0.820	0.827	0.838	0.835	0.834	0.807	0.829	0.831	0.844
Fe	0.523	0.264	0.277	0.277	0.281	0.549	0.562	0.560	0.553	0.270	0.282	0.276	0.288	0.260	0.269	0.283	0.275	0.272	0.269
Mn	0.039	0.024	0.014	0.021	0.016	0.043	0.042	0.042	0.042	0.018	0.021	0.021	0.023	0.013	0.017	0.019	0.022	0.020	0.021
Ca	0.154	0.809	0.867	0.820	0.812	0.060	0.056	0.055	0.053	0.846	0.818	0.828	0.806	0.827	0.823	0.830	0.821	0.822	0.817
Na	0.021	0.025	0.026	0.032	0.025	0.001	0.001	0.002	0.001	0.025	0.026	0.028	0.025	0.025	0.022	0.024	0.026	0.023	0.023
K	0.012	0.002	0.000	0.000	0.000	0.001	0.001	0.001	0.000	0.000	0.000	0.000	0.000	0.000	0.000	0.000	0.000	0.000	0.000
Sum	4.004	4.011	4.023	4.023	4.008	4.000	4.015	4.014	4.009	4.010	4.011	4.019	4.016	4.009	4.011	4.009	4.012	4.011	4.011
Si	1.969	1.951	1.887	1.918	1.943	1.984	1.949	1.954	1.962	1.945	1.944	1.934	1.935	1.941	1.939	1.949	1.947	1.944	1.947
Al	0.067	0.069	0.151	0.103	0.094	0.027	0.046	0.042	0.038	0.085	0.083	0.085	0.083	0.091	0.090	0.085	0.075	0.083	0.075
Ti	0.008	0.011	0.017	0.013	0.011	0.004	0.006	0.006	0.006	0.010	0.012	0.009	0.011	0.011	0.011	0.007	0.011	0.008	0.011
Cr	0.000	0.000	0.000	0.000	0.000	0.000	0.000	0.000	0.000	0.000	0.000	0.000	0.000	0.002	0.001	0.000	0.000	0.002	0.001
Fe^{3+}	0.011	0.033	0.069	0.068	0.023	0.000	0.045	0.041	0.026	0.030	0.033	0.056	0.049	0.028	0.032	0.026	0.034	0.034	0.033
Mg	1.208	0.848	0.768	0.821	0.820	1.331	1.338	1.341	1.345	0.803	0.818	0.823	0.835	0.833	0.831	0.806	0.826	0.829	0.841
Fe^{2+}	0.512	0.230	0.207	0.208	0.258	0.549	0.515	0.517	0.526	0.239	0.248	0.219	0.237	0.231	0.236	0.256	0.240	0.237	0.236
Mn	0.039	0.024	0.014	0.021	0.016	0.043	0.042	0.042	0.042	0.018	0.021	0.021	0.023	0.013	0.017	0.019	0.022	0.020	0.020
Ca	0.154	0.807	0.862	0.816	0.811	0.060	0.056	0.055	0.053	0.844	0.816	0.824	0.803	0.825	0.821	0.828	0.818	0.820	0.814
Na	0.021	0.025	0.026	0.032	0.025	0.001	0.001	0.002	0.001	0.025	0.026	0.028	0.024	0.025	0.022	0.024	0.026	0.023	0.023
K	0.012	0.002	0.000	0.000	0.000	0.001	0.001	0.001	0.000	0.000	0.000	0.000	0.000	0.000	0.000	0.000	0.000	0.000	0.000
Sum	4.000	4.000	4.000	4.000	4.000	4.000	4.000	4.000	4.000	4.000	4.000	4.000	4.000	4.000	4.000	4.000	4.000	4.000	4.000
Wo (mol%)	0.082	0.421	0.452	0.426	0.424	0.031	0.029	0.028	0.027	0.440	0.426	0.429	0.417	0.430	0.427	0.432	0.426	0.427	0.423
En (mol%)	0.641	0.442	0.403	0.429	0.429	0.686	0.685	0.686	0.690	0.419	0.427	0.428	0.434	0.434	0.433	0.421	0.431	0.432	0.437
Fs (mol%)	0.277	0.137	0.145	0.144	0.147	0.283	0.287	0.286	0.283	0.140	0.147	0.143	0.149	0.135	0.140	0.147	0.143	0.141	0.139

[1] Major element oxides in wt.%; number of cations based on 6 oxygens; endmembers calculated using the ferric form and total iron; [2] see Appendix A; [3] see Table D1

Table D2 Pyroxene analyses of the 2006 Merapi eruption (continued)

Sample	ME08-09-01	ME08-09-01	ME08-09-01	ME08-09-01	ME08-09-01	ME08-09-01	ME08-09-01	ME08-09-01	ME08-09-01	ME08-09-01	ME08-09-01	ME08-09-01	ME08-09-01	ME08-09-01	ME08-09-01	ME08-09-01	ME08-09-01	ME08-09-01	ME08-09-01
Sample Type[2]	L1-S	L1-S	L1-S	L1-S	L1-S	L1-S	L1-S	L1-S	L1-S	L1-S	L1-S	L1-S	L1-S	L1-S	L1-S	L1-S	L1-S	L1-S	L1-S
Point	2 / 1 .	13 / 1 .	18 / 1 .	23 / 1 .	26 / 1 .	6 / 1 .	7 / 1 .	12 / 1 .	13 / 1 .	19 / 1 .	20 / 1 .	21 / 1 .	22 / 1 .	33 / 1 .	34 / 1 .	2 / 1 .	13 / 1 .	18 / 1 .	23 / 1 .
Comment[3]	ph	ph	ph	ph	ph	ph	ph	ph	ph	ph	ph	ph	ph	ph	ph	ph	ph	ph	ph
Pyroxene Type	cpx	cpx	cpx	cpx	cpx	cpx	cpx	cpx	cpx	cpx	cpx	cpx	cpx	cpx	cpx	cpx	cpx	cpx	cpx
SiO_2	52.65	51.32	52.65	52.16	52.10	52.57	52.86	52.56	52.15	52.78	52.48	52.92	52.95	52.87	52.96	52.65	51.32	52.65	52.16
TiO_2	0.38	0.55	0.37	0.29	0.50	0.36	0.42	0.33	0.38	0.41	0.39	0.26	0.38	0.31	0.39	0.38	0.55	0.37	0.29
Al_2O_3	1.96	3.11	1.61	1.58	2.38	1.94	1.91	1.96	1.89	2.10	2.07	1.95	1.74	1.92	1.72	1.96	3.11	1.61	1.58
Cr_2O_3	0.00	0.02	0.00	0.04	0.02	0.01	0.00	0.00	0.00	0.05	0.02	0.00	0.00	0.06	0.03	0.00	0.02	0.00	0.04
FeO	8.56	8.84	8.78	8.73	8.67	8.70	9.14	8.94	9.23	8.45	8.69	9.17	8.91	8.81	8.72	8.56	8.84	8.78	8.73
MnO	0.59	0.58	0.72	0.71	0.54	0.59	0.67	0.68	0.72	0.43	0.54	0.60	0.71	0.63	0.66	0.59	0.58	0.72	0.71
MgO	15.20	14.16	14.87	14.94	14.49	14.57	14.92	15.00	15.09	15.20	15.09	14.67	15.07	15.11	15.35	15.20	14.16	14.87	14.94
CaO	20.59	20.97	20.49	20.45	20.80	21.29	20.71	20.89	20.18	20.94	20.73	20.97	20.76	20.81	20.68	20.59	20.97	20.49	20.45
Na_2O	0.33	0.35	0.34	0.37	0.35	0.35	0.37	0.40	0.34	0.35	0.31	0.34	0.36	0.33	0.32	0.33	0.35	0.34	0.37
K_2O	0.00	0.00	0.00	0.03	0.00	0.00	0.00	0.00	0.00	0.00	0.00	0.00	0.00	0.01	0.00	0.00	0.00	0.00	0.03
Sum	100.25	99.89	99.83	99.29	99.85	100.38	101.00	100.76	99.99	100.69	100.33	100.87	100.89	100.84	100.83	100.25	99.89	99.83	99.29
Si	1.950	1.915	1.961	1.955	1.940	1.950	1.949	1.943	1.943	1.945	1.944	1.954	1.953	1.950	1.952	1.950	1.915	1.961	1.955
Al	0.085	0.137	0.071	0.070	0.104	0.085	0.083	0.086	0.083	0.091	0.090	0.085	0.076	0.083	0.075	0.085	0.137	0.071	0.070
Ti	0.011	0.015	0.010	0.008	0.014	0.010	0.012	0.009	0.011	0.011	0.011	0.007	0.011	0.009	0.011	0.011	0.015	0.010	0.008
Cr	0.000	0.000	0.000	0.001	0.001	0.000	0.000	0.000	0.000	0.002	0.001	0.000	0.000	0.002	0.001	0.000	0.000	0.000	0.001
Mg	0.839	0.788	0.825	0.835	0.805	0.805	0.820	0.827	0.838	0.835	0.834	0.807	0.829	0.831	0.844	0.839	0.788	0.825	0.835
Fe	0.265	0.276	0.274	0.274	0.270	0.270	0.282	0.276	0.288	0.260	0.269	0.283	0.275	0.272	0.269	0.265	0.276	0.274	0.274
Mn	0.018	0.018	0.023	0.023	0.017	0.018	0.021	0.021	0.023	0.013	0.017	0.019	0.022	0.020	0.021	0.018	0.018	0.023	0.023
Ca	0.817	0.839	0.817	0.821	0.830	0.846	0.818	0.828	0.806	0.827	0.823	0.830	0.821	0.822	0.817	0.817	0.839	0.817	0.821
Na	0.023	0.025	0.025	0.027	0.025	0.025	0.026	0.028	0.025	0.025	0.022	0.024	0.026	0.023	0.023	0.023	0.025	0.025	0.027
K	0.000	0.000	0.000	0.001	0.000	0.000	0.000	0.000	0.000	0.000	0.000	0.000	0.000	0.000	0.000	0.000	0.000	0.000	0.001
Sum	4.009	4.013	4.006	4.015	4.006	4.010	4.011	4.019	4.016	4.009	4.011	4.009	4.012	4.011	4.011	4.009	4.013	4.006	4.015
Si	1.945	1.909	1.958	1.948	1.937	1.945	1.944	1.934	1.935	1.941	1.939	1.949	1.947	1.944	1.947	1.945	1.909	1.958	1.948
Al	0.085	0.136	0.071	0.070	0.104	0.085	0.083	0.085	0.083	0.091	0.090	0.085	0.075	0.083	0.075	0.085	0.136	0.071	0.070
Ti	0.011	0.015	0.010	0.008	0.014	0.010	0.012	0.009	0.011	0.011	0.011	0.007	0.011	0.008	0.011	0.011	0.015	0.010	0.008
Cr	0.000	0.000	0.000	0.001	0.001	0.000	0.000	0.000	0.000	0.002	0.001	0.000	0.000	0.002	0.001	0.000	0.000	0.000	0.001
Fe^{3+}	0.026	0.040	0.017	0.045	0.018	0.030	0.033	0.056	0.049	0.028	0.032	0.026	0.034	0.034	0.033	0.026	0.040	0.017	0.045
Mg	0.837	0.785	0.824	0.832	0.803	0.803	0.818	0.823	0.835	0.833	0.831	0.806	0.826	0.829	0.841	0.837	0.785	0.824	0.832
Fe^{2+}	0.238	0.235	0.256	0.228	0.252	0.239	0.248	0.219	0.237	0.231	0.236	0.256	0.240	0.237	0.236	0.238	0.235	0.256	0.228
Mn	0.018	0.018	0.023	0.023	0.017	0.018	0.021	0.021	0.023	0.013	0.017	0.019	0.022	0.020	0.020	0.018	0.018	0.023	0.023
Ca	0.815	0.836	0.816	0.818	0.829	0.844	0.816	0.824	0.803	0.825	0.821	0.828	0.818	0.820	0.814	0.815	0.836	0.816	0.818
Na	0.023	0.025	0.025	0.027	0.025	0.025	0.026	0.028	0.024	0.025	0.022	0.024	0.026	0.023	0.023	0.023	0.025	0.025	0.027
K	0.000	0.000	0.000	0.001	0.000	0.000	0.000	0.000	0.000	0.000	0.000	0.000	0.000	0.000	0.000	0.000	0.000	0.000	0.001
Sum	4.000	4.000	4.000	4.000	4.000	4.000	4.000	4.000	4.000	4.000	4.000	4.000	4.000	4.000	4.000	4.000	4.000	4.000	4.000
Wo (mol%)	0.425	0.441	0.427	0.426	0.436	0.440	0.426	0.429	0.417	0.430	0.427	0.432	0.426	0.427	0.423	0.425	0.441	0.427	0.426
En (mol%)	0.437	0.414	0.431	0.433	0.422	0.419	0.427	0.428	0.434	0.434	0.433	0.421	0.431	0.432	0.437	0.437	0.414	0.431	0.433
Fs (mol%)	0.138	0.145	0.143	0.142	0.142	0.140	0.147	0.143	0.149	0.135	0.140	0.147	0.143	0.141	0.139	0.138	0.145	0.143	0.142

Table D2 Pyroxene analyses of the 2006 Merapi eruption (continued)

Sample	ME08-09-01	ME08-09-02	ME08-09-02	ME08-09-02	ME08-09-02	ME08-09-02	ME08-09-02	ME08-09-02	ME08-09-02	ME08-09-02	ME08-09-02	ME08-09-02	ME08-09-02	ME08-09-02	ME08-09-02	ME08-09-02	ME08-09-02	ME08-09-02	ME08-09-02
Sample Type[2]	L1-S	L1-S	L1-S	L1-S	L1-S	L1-S	L1-S	L1-S	L1-S	L1-S	L1-S	L1-S	L1-S	L1-S	L1-S	L1-S	L1-S	L1-S	L1-S
Point	26 / 1 .	92 / 1 .	92 / 2 .	92 / 3 .	92 / 4 .	92 / 5 .	92 / 6 .	92 / 7 .	92 / 8 .	92 / 9 .	92 / 10 .	92 / 11 .	92 / 12 .	92 / 13 .	92 / 14 .	92 / 15 .	92 / 16 .	92 / 17 .	92 / 18 .
Comment[3]	ph	ph-r	ph	ph	ph	ph	ph	ph	ph	ph	ph	ph	ph	ph	ph	ph	ph	ph	ph
Pyroxene Type	cpx	cpx	cpx	cpx	cpx	cpx	cpx	cpx	cpx	cpx	cpx	cpx	cpx	cpx	cpx	cpx	cpx	cpx	cpx
SiO_2	52.10	52.84	52.00	52.31	52.22	50.82	52.41	50.93	51.38	50.53	50.65	51.66	51.11	51.45	51.56	51.21	52.04	51.40	50.65
TiO_2	0.50	0.33	0.38	0.35	0.33	0.39	0.33	0.36	0.39	0.52	0.52	0.39	0.46	0.38	0.40	0.37	0.38	0.39	0.49
Al_2O_3	2.38	1.39	1.65	1.51	1.53	2.14	1.38	1.47	2.28	3.07	3.01	1.84	2.51	1.78	2.32	2.64	1.69	1.59	2.63
Cr_2O_3	0.02	0.01	0.00	0.00	0.00	0.00	-0.02	0.01	0.01	0.00	-0.01	0.00	-0.01	0.01	-0.01	0.01	0.01	0.00	0.01
FeO	8.67	8.57	8.50	8.79	8.59	8.51	8.54	8.59	7.82	8.49	8.41	9.34	8.38	8.05	8.13	8.15	8.06	8.53	8.19
MnO	0.54	0.73	0.68	0.80	0.73	0.56	0.74	0.72	0.41	0.42	0.47	0.73	0.39	0.55	0.51	0.55	0.60	0.53	0.48
MgO	14.49	15.41	14.99	15.28	15.22	14.42	15.74	14.59	14.09	13.59	14.00	14.65	14.42	14.78	14.98	14.68	15.38	15.24	14.65
CaO	20.80	20.32	20.48	20.03	20.18	21.82	20.04	21.04	22.59	22.06	21.68	20.06	21.75	20.90	20.98	20.90	20.49	20.59	21.05
Na_2O	0.35	0.36	0.34	0.34	0.33	0.34	0.29	0.37	0.33	0.36	0.35	0.40	0.33	0.41	0.35	0.31	0.31	0.28	0.37
K_2O	0.00	0.02	0.00	0.00	0.00	0.00	0.00	0.00	0.00	0.00	0.00	0.00	0.00	0.00	0.00	0.00	0.00	0.00	0.00
Sum	99.85	99.97	99.00	99.43	99.12	98.98	99.45	98.08	99.30	99.04	99.10	99.08	99.34	98.30	99.21	98.81	98.96	98.56	98.52
Si	1.940	1.963	1.953	1.956	1.957	1.920	1.957	1.941	1.929	1.907	1.908	1.946	1.919	1.946	1.931	1.926	1.951	1.942	1.915
Al	0.104	0.061	0.073	0.067	0.068	0.095	0.061	0.066	0.101	0.136	0.134	0.082	0.111	0.079	0.102	0.117	0.075	0.071	0.117
Ti	0.014	0.009	0.011	0.010	0.009	0.011	0.009	0.010	0.011	0.015	0.015	0.011	0.013	0.011	0.011	0.010	0.011	0.011	0.014
Cr	0.001	0.000	0.000	0.000	0.000	0.000	-0.001	0.000	0.000	0.000	0.000	0.000	0.000	0.000	0.000	0.000	0.000	0.000	0.000
Mg	0.805	0.853	0.839	0.852	0.851	0.812	0.876	0.829	0.789	0.764	0.786	0.822	0.807	0.833	0.837	0.823	0.859	0.858	0.826
Fe	0.270	0.266	0.267	0.275	0.269	0.269	0.266	0.274	0.246	0.268	0.265	0.294	0.263	0.255	0.255	0.256	0.253	0.269	0.259
Mn	0.017	0.023	0.022	0.025	0.023	0.018	0.023	0.023	0.013	0.014	0.015	0.023	0.012	0.018	0.016	0.018	0.019	0.017	0.015
Ca	0.830	0.809	0.824	0.803	0.811	0.883	0.802	0.859	0.909	0.892	0.875	0.809	0.875	0.847	0.842	0.842	0.823	0.833	0.853
Na	0.025	0.026	0.025	0.025	0.024	0.025	0.021	0.027	0.024	0.027	0.026	0.029	0.024	0.030	0.025	0.023	0.022	0.020	0.027
K	0.000	0.001	0.000	0.000	0.000	0.000	0.000	0.000	0.000	0.000	0.000	0.000	0.000	0.000	0.000	0.000	0.000	0.000	0.000
Sum	4.006	4.011	4.013	4.013	4.011	4.033	4.014	4.030	4.021	4.023	4.023	4.017	4.025	4.018	4.019	4.016	4.012	4.022	4.026
Si	1.937	1.958	1.947	1.950	1.952	1.904	1.950	1.926	1.919	1.896	1.897	1.937	1.907	1.937	1.922	1.919	1.944	1.931	1.902
Al	0.104	0.061	0.073	0.067	0.067	0.094	0.061	0.065	0.100	0.136	0.133	0.081	0.110	0.079	0.102	0.117	0.074	0.071	0.116
Ti	0.014	0.009	0.011	0.010	0.009	0.011	0.009	0.010	0.011	0.015	0.015	0.011	0.013	0.011	0.011	0.010	0.011	0.011	0.014
Cr	0.001	0.000	0.000	0.000	0.000	0.000	-0.001	0.000	0.000	0.000	0.000	0.000	0.000	0.000	0.000	0.000	0.000	0.000	0.000
Fe^{3+}	0.018	0.032	0.038	0.038	0.034	0.099	0.043	0.088	0.064	0.069	0.070	0.051	0.073	0.055	0.057	0.048	0.037	0.066	0.078
Mg	0.803	0.851	0.837	0.849	0.848	0.805	0.873	0.823	0.784	0.760	0.782	0.819	0.803	0.830	0.833	0.820	0.857	0.854	0.820
Fe^{2+}	0.252	0.233	0.228	0.236	0.234	0.168	0.223	0.183	0.181	0.197	0.193	0.242	0.188	0.198	0.196	0.207	0.215	0.202	0.180
Mn	0.017	0.023	0.021	0.025	0.023	0.018	0.023	0.023	0.013	0.013	0.015	0.023	0.012	0.017	0.016	0.018	0.019	0.017	0.015
Ca	0.829	0.807	0.822	0.800	0.808	0.876	0.799	0.853	0.904	0.887	0.870	0.806	0.870	0.843	0.838	0.839	0.820	0.829	0.847
Na	0.025	0.026	0.025	0.025	0.024	0.024	0.021	0.027	0.024	0.027	0.026	0.029	0.024	0.030	0.025	0.023	0.022	0.020	0.027
K	0.000	0.001	0.000	0.000	0.000	0.000	0.000	0.000	0.000	0.000	0.000	0.000	0.000	0.000	0.000	0.000	0.000	0.000	0.000
Sum	4.000	4.000	4.000	4.000	4.000	4.000	4.000	4.000	4.000	4.000	4.000	4.000	4.000	4.000	4.000	4.000	4.000	4.000	4.000
Wo (mol%)	0.436	0.420	0.427	0.416	0.420	0.450	0.412	0.438	0.468	0.464	0.454	0.420	0.450	0.438	0.435	0.438	0.425	0.425	0.440
En (mol%)	0.422	0.442	0.435	0.442	0.441	0.413	0.450	0.423	0.406	0.397	0.408	0.427	0.415	0.431	0.433	0.428	0.444	0.438	0.426
Fs (mol%)	0.142	0.138	0.138	0.143	0.140	0.137	0.137	0.140	0.126	0.139	0.138	0.153	0.135	0.132	0.132	0.133	0.131	0.137	0.134

Table D2 Pyroxene analyses of the 2006 Merapi eruption (continued)

Sample	ME08-09-02	ME08-09-02	ME08-09-02	ME08-09-02	ME08-09-02	ME08-09-02	ME08-09-02	ME08-09-02	ME08-09-02	ME08-09-02	ME08-09-02	ME08-09-02	ME08-09-02	ME08-09-02	ME08-09-02	ME08-09-02	ME08-09-02	ME08-09-02	ME08-09-02
Sample Type[2]	L1-S	L1-S	L1-S	L1-S	L1-S	L1-S	L1-S	L1-S	L1-S	L1-S	L1-S	L1-S	L1-S	L1-S	L1-S	L1-S	L1-S	L1-S	L1-S
Point	92 / 19 .	92 / 20 .	92 / 21 .	92 / 22 .	92 / 23 .	92 / 24 .	92 / 25 .	92 / 26 .	92 / 29 .	92 / 31 .	92 / 32 .	92 / 33 .	92 / 36 .	92 / 37 .	92 / 38 .	92 / 39 .	92 / 40 .	37 / 1 .	38 / 1 .
Comment[3]	ph	ph	ph	ph	ph	ph	ph	ph	ph	ph	ph	ph	ph	ph	ph	ph	ph-c	ph-r	ph-c
Pyroxene Type	cpx	cpx	cpx	cpx	cpx	cpx	cpx	cpx	cpx	cpx	cpx	cpx	cpx	cpx	cpx	cpx	cpx	cpx	cpx
SiO_2	51.63	50.25	51.90	51.07	50.81	51.60	51.24	51.02	49.95	51.61	51.27	51.54	51.56	51.14	51.58	51.94	50.86	52.08	51.33
TiO_2	0.40	0.54	0.41	0.41	0.49	0.41	0.43	0.45	0.38	0.37	0.40	0.31	0.36	0.38	0.34	0.32	0.52	0.38	0.43
Al_2O_3	1.83	3.00	2.03	2.31	2.92	2.15	2.20	2.67	2.60	2.02	2.28	1.81	1.76	2.31	1.88	1.68	2.24	1.84	2.23
Cr_2O_3	0.01	-0.01	0.02	0.00	0.00	0.02	0.01	0.00	0.01	0.00	-0.01	0.01	0.00	0.02	-0.01	-0.01	-0.01	-0.01	-0.01
FeO	8.56	8.72	7.97	7.93	8.19	8.14	8.18	8.12	8.93	8.20	7.77	7.87	8.66	7.89	8.18	8.61	8.35	8.68	9.12
MnO	0.59	0.53	0.50	0.51	0.45	0.52	0.52	0.51	0.47	0.53	0.56	0.60	0.62	0.50	0.60	0.64	0.58	0.69	0.59
MgO	15.34	14.30	15.16	14.60	14.44	14.69	14.77	14.58	14.05	14.90	14.70	15.03	15.03	14.65	14.81	15.15	14.50	15.21	15.36
CaO	20.37	20.79	20.80	21.23	21.66	21.33	20.87	21.16	21.53	20.85	21.07	20.94	20.54	21.06	21.16	20.56	20.82	20.30	19.86
Na_2O	0.36	0.35	0.34	0.35	0.33	0.37	0.35	0.36	0.37	0.33	0.33	0.33	0.31	0.30	0.31	0.29	0.35	0.32	0.37
K_2O	0.00	0.01	0.03	0.00	0.00	0.00	0.00	0.00	0.00	0.00	0.00	0.00	0.02	0.00	0.00	0.00	0.02	0.02	0.00
Sum	99.10	98.49	99.17	98.41	99.29	99.23	98.58	98.89	98.30	98.81	98.38	98.43	98.86	98.24	98.85	99.19	98.23	99.51	99.29
Si	1.938	1.905	1.942	1.930	1.908	1.935	1.933	1.920	1.905	1.941	1.935	1.945	1.942	1.934	1.942	1.948	1.929	1.946	1.926
Al	0.081	0.134	0.090	0.103	0.129	0.095	0.098	0.119	0.117	0.089	0.102	0.080	0.078	0.103	0.084	0.074	0.100	0.081	0.099
Ti	0.011	0.015	0.011	0.012	0.014	0.012	0.012	0.013	0.011	0.010	0.011	0.009	0.010	0.011	0.010	0.009	0.015	0.011	0.012
Cr	0.000	0.000	0.001	0.000	0.000	0.001	0.000	0.000	0.000	0.000	0.000	0.000	0.000	0.000	0.000	0.000	0.000	0.000	0.000
Mg	0.859	0.808	0.846	0.822	0.808	0.821	0.831	0.818	0.799	0.836	0.827	0.845	0.844	0.826	0.831	0.847	0.820	0.848	0.859
Fe	0.269	0.277	0.249	0.251	0.257	0.255	0.258	0.256	0.285	0.258	0.245	0.248	0.273	0.249	0.258	0.270	0.265	0.271	0.286
Mn	0.019	0.017	0.016	0.016	0.014	0.017	0.017	0.016	0.015	0.017	0.018	0.019	0.020	0.016	0.019	0.020	0.019	0.022	0.019
Ca	0.820	0.844	0.834	0.860	0.871	0.857	0.843	0.853	0.880	0.840	0.852	0.847	0.829	0.853	0.853	0.826	0.846	0.813	0.798
Na	0.026	0.026	0.025	0.026	0.024	0.027	0.026	0.026	0.027	0.024	0.024	0.024	0.022	0.022	0.023	0.021	0.026	0.023	0.027
K	0.000	0.000	0.001	0.000	0.000	0.000	0.000	0.000	0.000	0.000	0.000	0.000	0.001	0.000	0.000	0.000	0.001	0.001	0.000
Sum	4.023	4.026	4.015	4.020	4.026	4.019	4.019	4.021	4.039	4.016	4.015	4.018	4.020	4.014	4.018	4.017	4.020	4.015	4.026
Si	1.927	1.892	1.935	1.921	1.895	1.926	1.924	1.910	1.886	1.934	1.928	1.936	1.933	1.927	1.933	1.940	1.920	1.939	1.914
Al	0.080	0.133	0.089	0.102	0.128	0.094	0.098	0.118	0.116	0.089	0.101	0.080	0.078	0.103	0.083	0.074	0.099	0.081	0.098
Ti	0.011	0.015	0.011	0.012	0.014	0.012	0.012	0.013	0.011	0.010	0.011	0.009	0.010	0.011	0.010	0.009	0.015	0.011	0.012
Cr	0.000	0.000	0.001	0.000	0.000	0.001	0.000	0.000	0.000	0.000	0.000	0.000	0.000	0.000	0.000	0.000	0.000	0.000	0.000
Fe^{3+}	0.069	0.078	0.044	0.058	0.078	0.057	0.055	0.063	0.117	0.047	0.044	0.053	0.060	0.043	0.055	0.050	0.059	0.045	0.078
Mg	0.854	0.803	0.843	0.818	0.803	0.818	0.827	0.814	0.791	0.832	0.824	0.842	0.840	0.823	0.827	0.844	0.816	0.844	0.854
Fe^{2+}	0.198	0.197	0.205	0.191	0.177	0.197	0.202	0.192	0.165	0.210	0.200	0.194	0.211	0.205	0.201	0.219	0.204	0.225	0.207
Mn	0.019	0.017	0.016	0.016	0.014	0.016	0.017	0.016	0.015	0.017	0.018	0.019	0.020	0.016	0.019	0.020	0.019	0.022	0.019
Ca	0.815	0.839	0.831	0.856	0.866	0.853	0.840	0.849	0.871	0.837	0.849	0.843	0.825	0.850	0.849	0.823	0.842	0.810	0.793
Na	0.026	0.026	0.025	0.025	0.024	0.027	0.026	0.026	0.027	0.024	0.024	0.024	0.022	0.022	0.023	0.021	0.026	0.023	0.027
K	0.000	0.000	0.001	0.000	0.000	0.000	0.000	0.000	0.000	0.000	0.000	0.000	0.001	0.000	0.000	0.000	0.001	0.001	0.000
Sum	4.000	4.000	4.000	4.000	4.000	4.000	4.000	4.000	4.000	4.000	4.000	4.000	4.000	4.000	4.000	4.000	4.000	4.000	4.000
Wo (mol%)	0.421	0.438	0.432	0.445	0.450	0.443	0.436	0.443	0.448	0.434	0.443	0.436	0.426	0.442	0.439	0.425	0.438	0.421	0.411
En (mol%)	0.441	0.419	0.438	0.425	0.417	0.425	0.430	0.425	0.407	0.432	0.430	0.436	0.434	0.428	0.428	0.436	0.425	0.439	0.442
Fs (mol%)	0.138	0.143	0.129	0.130	0.133	0.132	0.134	0.133	0.145	0.133	0.127	0.128	0.140	0.129	0.133	0.139	0.137	0.140	0.147

Table D2 Pyroxene analyses of the 2006 Merapi eruption (continued)

Sample	ME08-09-02	ME08-09-02	ME08-09-02	ME08-09-02	ME08-09-02	ME08-09-02	ME08-09-02	ME08-09-02	ME08-10	ME08-10	ME08-10	ME08-10	ME08-10	ME08-10	ME08-10	ME08-10	ME08-10	ME08-10	ME08-10
Sample Type[2]	L1-S	L1-S	L1-S	L1-S	L1-S	L1-S	L1-S	L1-S	KB-S	KB-S	KB-S	KB-S	KB-S	KB-S	KB-S	KB-S	KB-S	KB-S	KB-S
Point	42 / 1 .	43 / 1 .	44 / 1 .	39 / 1 .	40 / 1 .	41 / 1 .	27 / 1 .	28/ 1 .	5/ 1 .	6 / 1 .	90 / 1 .	90 / 4 .	90 / 5 .	90 / 6 .	90 / 7 .	90 / 8 .	90 / 9 .	90 / 10 .	90 / 11 .
Comment[3]	mph-c	mph-c	mph-r	mph-r	mph-c	mph-r	m-c	m-r	ph-r	ph-c	ph-r	ph	ph	ph	ph	ph	ph	ph	ph
Pyroxene Type	cpx	cpx	cpx	opx	opx	opx	opx	opx	cpx	cpx	cpx	cpx	cpx	cpx	cpx	cpx	cpx	cpx	cpx
SiO_2	51.84	48.00	51.46	53.44	54.06	53.37	53.69	53.52	52.36	51.06	50.83	50.03	51.54	50.06	50.56	46.47	51.07	51.07	51.04
TiO_2	0.34	1.19	0.39	0.23	0.15	0.22	0.28	0.25	0.34	0.50	0.54	0.54	0.41	0.57	0.54	1.16	0.46	0.41	0.42
Al_2O_3	1.39	5.98	1.90	0.99	0.49	1.08	1.42	1.34	1.43	2.98	2.43	3.10	1.95	3.05	2.85	6.74	2.26	1.99	2.19
Cr_2O_3	0.01	0.00	0.01	0.00	0.00	-0.01	0.00	0.00	0.00	0.01	0.00	-0.01	0.01	0.01	0.02	0.00	0.01	0.00	-0.01
FeO	9.04	9.34	8.95	18.44	18.37	18.12	17.52	17.47	8.82	8.11	8.95	8.83	9.10	9.16	8.97	9.92	8.96	8.77	8.25
MnO	0.74	0.33	0.58	1.40	1.45	1.37	1.32	1.39	0.68	0.45	0.69	0.48	0.70	0.60	0.56	0.30	0.60	0.63	0.50
MgO	15.24	12.36	14.80	24.38	24.84	24.43	23.28	23.52	15.19	13.92	14.66	13.51	14.93	14.23	14.33	11.84	14.73	14.88	14.61
CaO	19.91	22.23	20.90	1.47	1.40	1.39	1.99	1.97	20.30	22.16	20.09	21.35	19.95	20.49	20.64	22.01	20.29	20.30	21.31
Na_2O	0.30	0.34	0.37	0.02	0.04	0.05	0.07	0.04	0.35	0.29	0.36	0.42	0.37	0.40	0.35	0.35	0.37	0.36	0.32
K_2O	0.01	0.02	0.01	0.01	0.01	0.02	0.04	0.02	0.03	0.00	0.03	0.00	0.01	0.00	0.00	0.00	0.00	0.00	0.00
Sum	98.81	99.78	99.37	100.39	100.80	100.03	99.62	99.51	99.50	99.48	98.59	98.27	98.97	98.56	98.81	98.79	98.75	98.40	98.64
Si	1.954	1.811	1.934	1.961	1.973	1.962	1.976	1.973	1.958	1.914	1.923	1.905	1.941	1.900	1.911	1.779	1.928	1.934	1.928
Al	0.062	0.266	0.084	0.043	0.021	0.047	0.062	0.058	0.063	0.132	0.109	0.139	0.087	0.136	0.127	0.304	0.101	0.089	0.098
Ti	0.010	0.034	0.011	0.006	0.004	0.006	0.008	0.007	0.010	0.014	0.015	0.016	0.011	0.016	0.015	0.033	0.013	0.012	0.012
Cr	0.000	0.000	0.000	0.000	0.000	0.000	0.000	0.000	0.000	0.000	0.000	0.000	0.000	0.000	0.001	0.000	0.000	0.000	0.000
Mg	0.856	0.695	0.829	1.334	1.352	1.338	1.277	1.292	0.846	0.778	0.827	0.767	0.838	0.805	0.807	0.676	0.829	0.840	0.823
Fe	0.285	0.295	0.281	0.566	0.561	0.557	0.539	0.538	0.276	0.254	0.283	0.281	0.287	0.291	0.283	0.318	0.283	0.278	0.261
Mn	0.024	0.011	0.019	0.044	0.045	0.043	0.041	0.043	0.022	0.014	0.022	0.016	0.022	0.019	0.018	0.010	0.019	0.020	0.016
Ca	0.804	0.899	0.841	0.058	0.055	0.055	0.078	0.078	0.813	0.890	0.814	0.871	0.805	0.833	0.836	0.903	0.821	0.824	0.863
Na	0.022	0.025	0.027	0.001	0.003	0.003	0.005	0.003	0.025	0.021	0.027	0.031	0.027	0.029	0.025	0.026	0.027	0.026	0.024
K	0.000	0.001	0.000	0.000	0.000	0.001	0.002	0.001	0.001	0.000	0.002	0.000	0.000	0.000	0.000	0.000	0.000	0.000	0.000
Sum	4.016	4.035	4.027	4.012	4.014	4.011	3.989	3.994	4.014	4.017	4.022	4.025	4.018	4.030	4.023	4.049	4.022	4.023	4.023
Si	1.946	1.795	1.921	1.955	1.967	1.956	1.982	1.976	1.951	1.906	1.913	1.893	1.932	1.886	1.900	1.758	1.918	1.923	1.917
Al	0.061	0.264	0.083	0.043	0.021	0.047	0.062	0.058	0.063	0.131	0.108	0.138	0.086	0.135	0.126	0.300	0.100	0.088	0.097
Ti	0.010	0.033	0.011	0.006	0.004	0.006	0.008	0.007	0.009	0.014	0.015	0.015	0.011	0.016	0.015	0.033	0.013	0.011	0.012
Cr	0.000	0.000	0.000	0.000	0.000	0.000	0.000	0.000	0.000	0.000	0.000	0.000	0.000	0.000	0.000	0.000	0.000	0.000	0.000
Fe^{3+}	0.049	0.105	0.079	0.037	0.041	0.033	0.000	0.000	0.043	0.051	0.064	0.076	0.054	0.090	0.069	0.144	0.065	0.068	0.070
Mg	0.853	0.689	0.824	1.329	1.347	1.335	1.281	1.295	0.843	0.774	0.822	0.762	0.834	0.799	0.803	0.668	0.825	0.835	0.818
Fe^{2+}	0.235	0.187	0.200	0.528	0.518	0.522	0.541	0.539	0.232	0.202	0.218	0.203	0.231	0.199	0.213	0.170	0.216	0.208	0.190
Mn	0.024	0.011	0.018	0.043	0.045	0.043	0.041	0.044	0.022	0.014	0.022	0.015	0.022	0.019	0.018	0.010	0.019	0.020	0.016
Ca	0.801	0.891	0.836	0.058	0.055	0.055	0.079	0.078	0.810	0.886	0.810	0.865	0.801	0.827	0.831	0.892	0.817	0.819	0.858
Na	0.022	0.025	0.027	0.001	0.003	0.003	0.005	0.003	0.025	0.021	0.027	0.031	0.027	0.029	0.025	0.026	0.027	0.026	0.024
K	0.000	0.001	0.000	0.000	0.000	0.001	0.002	0.001	0.001	0.000	0.002	0.000	0.000	0.000	0.000	0.000	0.000	0.000	0.000
Sum	4.000	4.000	4.000	4.000	4.000	4.000	4.000	4.000	4.000	4.000	4.000	4.000	4.000	4.000	4.000	4.000	4.000	4.000	4.000
Wo (mol%)	0.413	0.476	0.431	0.029	0.028	0.028	0.041	0.041	0.420	0.463	0.423	0.454	0.417	0.432	0.434	0.476	0.425	0.424	0.443
En (mol%)	0.440	0.368	0.425	0.681	0.687	0.686	0.674	0.677	0.437	0.405	0.430	0.400	0.434	0.417	0.419	0.356	0.429	0.433	0.423
Fs (mol%)	0.147	0.156	0.144	0.289	0.285	0.286	0.285	0.282	0.143	0.132	0.147	0.147	0.149	0.151	0.147	0.167	0.146	0.143	0.134

Table D2 Pyroxene analyses of the 2006 Merapi eruption (continued)

Sample	ME08-10	ME08-10	ME08-10	ME08-10	ME08-10	ME08-10	ME08-10	ME08-10	ME08-10	ME08-10	ME08-10	ME08-10	ME08-10	ME08-10	ME08-10	ME08-10	ME08-10	ME08-10	ME08-10
Sample Type[2]	KB-S	KB-S	KB-S	KB-S	KB-S	KB-S	KB-S	KB-S	KB-S	KB-S	KB-S	KB-S	KB-S	KB-S	KB-S	KB-S	KB-S	KB-S	KB-S
Point	90 / 12 .	90 / 13 .	90 / 14 .	90 / 15 .	90 / 16 .	90 / 17 .	90 / 18 .	90 / 19 .	90 / 20 .	1 / 1 .	2 / 1 .	5 / 1 .	11/ 1 .	12 / 1 .	6 / 1 .	9 / 1 .	10 / 1 .	18 / 1 .	19 / 1 .
Comment[3]	ph	ph	ph	ph	ph	ph	ph	ph	ph-c	mph-r	mph-c	mph-c	mph-r	mph-c	m	mph-r	mph-c	mph-c	mph-c
Pyroxene Type	cpx	cpx	cpx	cpx	cpx	cpx	cpx	cpx	cpx	cpx	cpx	cpx	cpx	cpx	cpx	opx	opx	opx	opx
SiO_2	49.99	51.81	51.60	51.99	51.39	51.59	50.76	51.74	52.33	51.12	51.26	51.64	51.47	51.56	52.47	53.02	52.49	53.09	52.77
TiO_2	0.56	0.38	0.39	0.41	0.43	0.41	0.72	0.38	0.36	0.65	0.40	0.36	0.44	0.38	0.32	0.17	0.23	0.19	0.28
Al_2O_3	3.20	1.94	1.95	1.98	1.76	1.85	3.81	1.77	1.72	2.66	2.17	1.52	1.82	1.64	1.58	0.71	1.16	0.69	1.50
Cr_2O_3	0.00	-0.02	0.00	0.00	-0.02	-0.01	0.01	0.00	0.00	0.00	-0.01	-0.02	0.00	0.01	0.01	0.00	0.00	0.00	0.00
FeO	8.91	9.09	8.77	8.35	8.90	8.22	8.75	9.04	8.79	9.09	9.25	9.19	8.63	8.54	9.27	18.04	18.83	18.53	17.06
MnO	0.47	0.59	0.63	0.62	0.67	0.59	0.52	0.62	0.63	0.70	0.64	0.77	0.75	0.60	0.80	1.35	1.31	1.42	1.30
MgO	13.81	15.21	15.25	15.23	15.29	15.02	14.47	15.24	15.46	14.86	15.06	15.06	15.30	15.27	15.81	24.51	24.20	24.50	24.24
CaO	21.36	20.03	19.95	20.28	19.90	20.42	20.72	19.88	20.27	20.25	20.36	20.28	20.16	20.72	18.88	1.55	1.50	1.39	2.11
Na_2O	0.33	0.41	0.37	0.34	0.34	0.33	0.40	0.34	0.31	0.37	0.38	0.38	0.32	0.28	0.28	0.01	0.03	0.04	0.06
K_2O	0.00	0.00	0.00	0.00	0.00	0.00	0.00	0.00	0.00	0.01	0.01	0.00	0.02	0.01	0.06	0.03	0.01	0.01	0.01
Sum	98.64	99.43	98.91	99.20	98.67	98.43	100.17	99.00	99.88	99.71	99.51	99.19	98.91	98.99	99.47	99.39	99.77	99.86	99.32
Si	1.897	1.940	1.940	1.945	1.939	1.946	1.888	1.945	1.948	1.913	1.924	1.944	1.937	1.940	1.959	1.963	1.944	1.961	1.949
Al	0.143	0.086	0.086	0.087	0.078	0.082	0.167	0.078	0.076	0.117	0.096	0.067	0.081	0.073	0.069	0.031	0.051	0.030	0.065
Ti	0.016	0.011	0.011	0.012	0.012	0.011	0.020	0.011	0.010	0.018	0.011	0.010	0.012	0.011	0.009	0.005	0.007	0.005	0.008
Cr	0.000	-0.001	0.000	0.000	-0.001	0.000	0.000	0.000	0.000	0.000	0.000	0.000	0.000	0.000	0.000	0.000	0.000	0.000	0.000
Mg	0.781	0.849	0.855	0.850	0.860	0.845	0.803	0.854	0.858	0.829	0.842	0.845	0.858	0.856	0.880	1.353	1.337	1.349	1.335
Fe	0.283	0.285	0.276	0.261	0.281	0.259	0.272	0.284	0.274	0.284	0.290	0.289	0.272	0.269	0.289	0.559	0.583	0.572	0.527
Mn	0.015	0.019	0.020	0.020	0.021	0.019	0.016	0.020	0.020	0.022	0.020	0.025	0.024	0.019	0.025	0.042	0.041	0.045	0.041
Ca	0.868	0.804	0.804	0.813	0.805	0.825	0.826	0.801	0.809	0.812	0.819	0.818	0.813	0.835	0.755	0.062	0.060	0.055	0.083
Na	0.024	0.030	0.027	0.025	0.025	0.024	0.029	0.024	0.022	0.027	0.027	0.028	0.023	0.020	0.020	0.000	0.002	0.003	0.004
K	0.000	0.000	0.000	0.000	0.000	0.000	0.000	0.000	0.000	0.000	0.000	0.000	0.001	0.000	0.003	0.001	0.000	0.000	0.001
Sum	4.028	4.022	4.019	4.012	4.022	4.013	4.022	4.017	4.015	4.024	4.031	4.026	4.022	4.023	4.009	4.017	4.025	4.021	4.013
Si	1.884	1.930	1.931	1.939	1.929	1.940	1.878	1.937	1.940	1.902	1.909	1.931	1.927	1.929	1.954	1.955	1.932	1.951	1.943
Al	0.142	0.085	0.086	0.087	0.078	0.082	0.166	0.078	0.075	0.117	0.095	0.067	0.080	0.072	0.069	0.031	0.050	0.030	0.065
Ti	0.016	0.011	0.011	0.012	0.012	0.011	0.020	0.011	0.010	0.018	0.011	0.010	0.012	0.011	0.009	0.005	0.006	0.005	0.008
Cr	0.000	-0.001	0.000	0.000	0.000	0.000	0.000	0.000	0.000	0.000	0.000	0.000	0.000	0.000	0.000	0.000	0.000	0.000	0.000
Fe^{3+}	0.082	0.064	0.057	0.036	0.065	0.039	0.066	0.052	0.046	0.070	0.092	0.079	0.066	0.069	0.027	0.051	0.074	0.061	0.038
Mg	0.776	0.845	0.851	0.847	0.855	0.842	0.798	0.850	0.855	0.824	0.836	0.839	0.854	0.851	0.877	1.348	1.328	1.342	1.331
Fe^{2+}	0.199	0.219	0.218	0.224	0.215	0.220	0.205	0.231	0.226	0.212	0.196	0.209	0.204	0.198	0.261	0.505	0.506	0.508	0.488
Mn	0.015	0.019	0.020	0.020	0.021	0.019	0.016	0.020	0.020	0.022	0.020	0.024	0.024	0.019	0.025	0.042	0.041	0.044	0.040
Ca	0.862	0.799	0.800	0.810	0.800	0.823	0.821	0.797	0.805	0.807	0.813	0.813	0.809	0.830	0.753	0.061	0.059	0.055	0.083
Na	0.024	0.029	0.027	0.025	0.025	0.024	0.028	0.024	0.022	0.027	0.027	0.028	0.023	0.020	0.020	0.000	0.002	0.003	0.004
K	0.000	0.000	0.000	0.000	0.000	0.000	0.000	0.000	0.000	0.000	0.000	0.000	0.001	0.000	0.003	0.001	0.000	0.000	0.001
Sum	4.000	4.000	4.000	4.000	4.000	4.000	4.000	4.000	4.000	4.000	4.000	4.000	4.000	4.000	4.000	4.000	4.000	4.000	4.000
Wo (mol%)	0.449	0.415	0.416	0.423	0.414	0.428	0.434	0.413	0.417	0.422	0.420	0.419	0.419	0.426	0.392	0.031	0.030	0.028	0.043
En (mol%)	0.404	0.438	0.442	0.442	0.442	0.438	0.422	0.440	0.442	0.431	0.432	0.433	0.442	0.437	0.457	0.686	0.675	0.683	0.686
Fs (mol%)	0.146	0.147	0.143	0.136	0.144	0.134	0.143	0.147	0.141	0.148	0.149	0.148	0.140	0.137	0.150	0.283	0.295	0.290	0.271

Table D2 Pyroxene analyses of the 2006 Merapi eruption (continued)

Sample	ME08-10	ME08-10	ME08-10	ME08-10	ME08-14	ME08-14	ME08-14	ME08-14	ME08-14	ME08-14	ME08-14	ME08-14	ME08-14
Sample Type[2]	KB-S	KB-S	KB-S	KB-S	SD-S	SD-S	SD-S	SD-S	SD-S	SD-S	SD-S	SD-S	SD-S
Point	20 / 1 .	3 / 1 .	13/ 1 .	15 / 1 .	70 / 1 .	71 / 1 .	72 / 1 .	73 / 1 .	62 / 1 .	63 / 1 .	32 / 1 .	33 / 1 .	65 / 1 .
Comment[3]	mph-c	m	m-r	m-c	mph-c	mph-c	mph-c	m-c	mph-r	mph-c	m-r	m-c	m-c
Pyroxene Type	opx	opx	opx	opx	cpx	cpx	cpx	cpx	opx	opx	opx	opx	opx
SiO_2	51.95	53.71	52.70	53.48	52.25	52.71	52.06	52.36	53.65	54.10	53.85	53.45	53.96
TiO_2	0.25	0.19	0.23	0.21	0.36	0.33	0.38	0.35	0.17	0.17	0.24	0.27	0.16
Al_2O_3	1.27	0.88	1.06	1.01	1.63	1.34	1.67	1.49	0.66	0.84	1.09	1.21	0.44
Cr_2O_3	0.01	0.00	-0.01	0.00	0.00	-0.02	-0.01	-0.01	0.01	0.00	0.00	0.01	0.00
FeO	18.00	17.48	18.33	18.09	8.97	8.62	8.89	8.72	18.20	17.80	18.29	17.62	18.21
MnO	1.32	1.32	1.29	1.31	0.76	0.78	0.71	0.71	1.35	1.33	1.41	1.35	1.54
MgO	24.18	24.45	24.24	24.28	15.11	15.28	14.95	15.25	24.14	25.08	23.44	23.99	23.73
CaO	1.57	1.77	1.60	1.34	20.06	20.36	20.26	20.12	1.29	1.40	1.59	1.52	1.40
Na_2O	0.04	0.09	0.03	0.04	0.41	0.35	0.37	0.33	0.02	0.04	0.08	0.04	0.03
K_2O	0.01	0.04	0.01	0.02	0.01	0.01	0.01	0.02	0.02	0.01	0.12	0.01	0.03
Sum	98.61	99.94	99.49	99.78	99.56	99.76	99.28	99.34	99.52	100.77	100.10	99.45	99.51
Si	1.942	1.971	1.953	1.969	1.953	1.964	1.952	1.959	1.981	1.969	1.979	1.970	1.993
Al	0.056	0.038	0.046	0.044	0.072	0.059	0.074	0.066	0.029	0.036	0.047	0.053	0.019
Ti	0.007	0.005	0.007	0.006	0.010	0.009	0.011	0.010	0.005	0.005	0.007	0.007	0.004
Cr	0.000	0.000	0.000	0.000	0.000	-0.001	0.000	0.000	0.000	0.000	0.000	0.000	0.000
Mg	1.348	1.338	1.339	1.333	0.842	0.849	0.836	0.850	1.329	1.361	1.284	1.318	1.307
Fe	0.563	0.537	0.568	0.557	0.280	0.269	0.279	0.273	0.562	0.542	0.562	0.543	0.563
Mn	0.042	0.041	0.040	0.041	0.024	0.024	0.023	0.022	0.042	0.041	0.044	0.042	0.048
Ca	0.063	0.070	0.064	0.053	0.803	0.812	0.814	0.806	0.051	0.055	0.062	0.060	0.055
Na	0.003	0.007	0.002	0.003	0.029	0.025	0.027	0.024	0.001	0.003	0.006	0.003	0.002
K	0.000	0.002	0.001	0.001	0.001	0.000	0.000	0.001	0.001	0.000	0.006	0.000	0.001
Sum	4.024	4.008	4.019	4.005	4.016	4.011	4.014	4.011	4.001	4.010	3.997	3.997	3.994
Si	1.930	1.967	1.943	1.966	1.946	1.958	1.945	1.953	1.980	1.964	1.981	1.972	1.996
Al	0.056	0.038	0.046	0.044	0.071	0.059	0.073	0.065	0.029	0.036	0.047	0.053	0.019
Ti	0.007	0.005	0.007	0.006	0.010	0.009	0.011	0.010	0.005	0.005	0.007	0.007	0.004
Cr	0.000	0.000	0.000	0.000	0.000	-0.001	0.000	0.000	0.000	0.000	0.000	0.000	0.000
Fe^{3+}	0.073	0.025	0.057	0.016	0.047	0.032	0.042	0.034	0.003	0.031	0.000	0.000	0.000
Mg	1.340	1.335	1.332	1.331	0.839	0.846	0.833	0.848	1.329	1.357	1.285	1.319	1.309
Fe^{2+}	0.487	0.510	0.508	0.540	0.232	0.235	0.236	0.238	0.559	0.510	0.563	0.544	0.563
Mn	0.042	0.041	0.040	0.041	0.024	0.024	0.022	0.022	0.042	0.041	0.044	0.042	0.048
Ca	0.063	0.069	0.063	0.053	0.800	0.810	0.811	0.804	0.051	0.054	0.063	0.060	0.056
Na	0.003	0.007	0.002	0.003	0.029	0.025	0.027	0.024	0.001	0.003	0.006	0.003	0.002
K	0.000	0.002	0.001	0.001	0.001	0.000	0.000	0.001	0.001	0.000	0.006	0.000	0.001
Sum	4.000	4.000	4.000	4.000	4.000	4.000	4.000	4.000	4.000	4.000	4.000	4.000	4.000
Wo (mol%)	0.032	0.036	0.032	0.027	0.417	0.421	0.422	0.418	0.026	0.028	0.033	0.031	0.029
En (mol%)	0.683	0.688	0.679	0.686	0.437	0.440	0.433	0.441	0.684	0.695	0.673	0.686	0.679
Fs (mol%)	0.285	0.276	0.288	0.287	0.146	0.139	0.145	0.141	0.289	0.277	0.295	0.283	0.292

Table D3 Amphibole analyses of the 2006 Merapi eruption[1]

Sample	ME08-01	ME08-01	ME08-01	ME08-01	ME08-01	ME08-01	ME08-01	ME08-01	ME08-01	ME08-01	ME08-01	ME08-01	ME08-04-01	ME08-04-01
Sample Type[2]	L4-S	L4-S	L4-S	L4-S	L4-S	L4-S	L4-S	L4-S	L4-S	L4-S	L4-S	L4-S	L8-S	L8-S
DataSet/Point	1 / 1.	2 / 1.	38 / 1.	39 / 1.	40 / 1.	41 / 1.	43 / 1.	44 / 1.	46 / 1.	47 / 1.	50 / 1.	51 / 1.	56 / 1 .	57 / 1 .
Comment[3]	ph-c	ph-r	mph-c	mph-r	mph-c	mph-r	mph-c	mph-r	mph-c	mph-r	mph-c	mph-r	ph-c	ph-c
SiO_2	40.99	41.81	41.82	42.39	40.07	40.54	42.92	41.43	42.49	42.27	40.84	41.81	41.35	41.62
TiO_2	1.79	2.75	2.45	2.57	2.11	2.21	2.74	2.15	2.33	2.25	2.39	2.40	2.76	3.07
Al_2O_3	13.92	11.77	11.60	11.02	14.30	14.02	11.04	12.46	11.70	12.07	13.56	13.10	11.75	11.88
Cr_2O_3	0.01	0.02	0.01	0.00	0.00	0.03	0.00	0.02	0.00	0.00	0.01	0.02	0.02	0.00
FeO	12.69	14.62	12.81	12.94	14.37	13.63	12.52	12.86	12.72	13.07	13.01	12.96	13.43	13.08
MnO	0.19	0.50	0.37	0.43	0.20	0.20	0.41	0.24	0.32	0.32	0.20	0.25	0.40	0.34
MgO	12.84	12.03	13.40	13.34	11.80	12.40	13.78	13.10	13.40	13.33	12.80	12.76	12.80	13.28
CaO	11.88	11.47	11.30	11.15	11.96	11.83	11.27	11.82	11.55	11.68	11.88	11.48	11.40	11.07
Na_2O	2.21	2.25	2.28	2.32	2.24	2.23	2.36	2.26	2.27	2.27	2.32	2.42	2.40	2.32
K_2O	1.20	1.09	0.93	0.95	0.91	0.90	0.95	0.86	0.98	1.01	0.91	0.98	0.87	1.01
Cl	0.05	0.08	0.06	0.08	0.02	0.02	0.07	0.03	0.05	0.06	0.03	0.05	0.05	0.07
F	0.24	0.11	0.16	0.06	0.07	0.13	0.42	0.12	0.00	0.30	0.04	0.20	0.36	0.33
Sum	98.02	98.49	97.18	97.23	98.04	98.12	98.46	97.34	97.81	98.62	97.99	98.41	97.60	98.06
Si	6.009	6.152	6.155	6.236	5.900	5.935	6.246	6.105	6.212	6.156	5.982	6.097	6.113	6.082
Al	2.405	2.042	2.012	1.910	2.482	2.418	1.893	2.164	2.015	2.072	2.341	2.252	2.047	2.046
Ti	0.198	0.304	0.272	0.284	0.233	0.244	0.299	0.238	0.257	0.247	0.263	0.263	0.307	0.337
Cr	0.001	0.003	0.001	0.000	0.000	0.003	0.000	0.002	0.000	0.000	0.001	0.002	0.002	0.000
Fe^{3+}	0.596	0.583	0.748	0.696	0.669	0.710	0.663	0.607	0.601	0.649	0.610	0.574	0.648	0.801
Mg	2.806	2.638	2.939	2.925	2.590	2.707	2.988	2.877	2.921	2.894	2.795	2.775	2.821	2.893
Fe^{2+}	0.961	1.216	0.828	0.896	1.101	0.958	0.861	0.977	0.954	0.942	0.984	1.006	1.013	0.798
Mn	0.024	0.062	0.046	0.053	0.024	0.025	0.050	0.030	0.040	0.039	0.025	0.031	0.050	0.042
Ca	1.866	1.808	1.781	1.757	1.887	1.856	1.757	1.866	1.810	1.823	1.864	1.794	1.806	1.733
Na	0.627	0.641	0.650	0.663	0.638	0.632	0.665	0.647	0.643	0.640	0.660	0.683	0.687	0.659
K	0.224	0.204	0.174	0.178	0.171	0.168	0.177	0.161	0.183	0.187	0.171	0.183	0.165	0.188
Cl	0.012	0.021	0.015	0.019	0.006	0.004	0.018	0.007	0.013	0.015	0.006	0.011	0.013	0.016
F	0.113	0.053	0.075	0.028	0.032	0.059	0.194	0.055	0.000	0.136	0.020	0.091	0.167	0.152
Sum	15.718	15.652	15.606	15.597	15.696	15.656	15.598	15.674	15.636	15.650	15.694	15.659	15.658	15.581

[1] Major element oxides in wt.%; number of cations based on 23 oxygens; Fe^{3+} estimation assuming 13eCNK; cation sum excluding Cl and F; [2] see Appendix A; [3] see Table D1

Table D3 Amphibole analyses of the 2006 Merapi eruption (continued)

Sample	ME08-04-01	ME08-04-01	ME08-04-01	ME08-04-01	ME08-09-02	ME08-09-02	ME08-09-02	ME08-09-02	ME08-09-02	ME08-09-02	ME08-09-02	ME08-09-02	ME08-09-02	ME08-09-02
Sample Type	L8-S	L8-S	L8-S	L8-S	L1-S	L1-S	L1-S	L1-S	L1-S	L1-S	L1-S	L1-S	L1-S	L1-S
DataSet/Point	58 / 1 .	59 / 1 .	60 / 1 .	61 / 1 .	26 / 1 .	27 / 1 .	28 / 1 .	29 / 1 .	33 / 1 .	34 / 1 .	35 / 1 .	36 / 1 .	91 / 1 .	91 / 2 .
Comment	ph-c	mph-c	mph-r	mph-c	ph-r	ph-c	ph-c	ph-r	ph-r	ph-c	ph-r	ph-c	ph-r	ph
SiO_2	40.75	42.97	42.13	42.12	41.41	41.71	39.69	40.04	41.50	42.48	41.40	42.92	42.84	42.01
TiO_2	2.82	3.02	2.65	2.59	2.69	2.82	2.26	2.26	2.87	2.24	2.97	3.11	2.77	2.91
Al_2O_3	12.60	10.38	11.61	11.38	11.12	10.84	13.54	13.77	11.13	10.34	11.54	10.43	11.82	11.59
Cr_2O_3	0.00	0.01	-0.01	0.00	0.00	0.01	-0.01	0.01	-0.01	-0.01	0.01	-0.01	0.02	0.01
FeO	13.19	12.74	13.07	13.25	12.17	12.62	12.37	12.79	12.57	15.71	12.81	13.06	12.24	12.41
MnO	0.32	0.45	0.42	0.39	0.30	0.39	0.18	0.19	0.37	0.54	0.35	0.44	0.35	0.35
MgO	12.81	14.05	13.10	13.31	13.45	13.32	13.09	12.95	13.51	11.77	13.53	13.48	14.03	13.81
CaO	11.60	10.95	11.09	11.27	11.28	11.07	11.94	12.00	11.27	10.87	11.14	10.85	11.31	11.32
Na_2O	2.29	2.31	2.26	2.25	2.32	2.34	2.31	2.39	2.28	2.07	2.33	2.40	2.33	2.29
K_2O	1.00	0.92	1.02	1.00	0.94	1.03	0.97	0.98	0.93	1.07	0.99	1.06	0.90	0.98
Cl	0.03	0.08	0.07	0.06	0.05	0.08	0.02	0.02	0.05	0.10	0.06	0.10	0.05	0.06
F	0.20	0.24	0.20	0.22	0.17	0.17	0.39	0.39	0.19	0.13	0.20	0.17	0.23	0.20
Sum	97.61	98.13	97.61	97.86	95.91	96.39	96.75	97.79	96.66	97.31	97.33	98.02	98.88	97.95
Si	6.011	6.244	6.181	6.170	6.186	6.207	5.907	5.906	6.150	6.313	6.087	6.273	6.167	6.128
Al	2.192	1.778	2.008	1.965	1.957	1.901	2.374	2.393	1.943	1.811	1.999	1.797	2.005	1.992
Ti	0.312	0.330	0.292	0.286	0.303	0.315	0.252	0.251	0.320	0.250	0.329	0.341	0.300	0.320
Cr	0.000	0.001	-0.001	0.000	0.000	0.001	-0.001	0.001	-0.001	-0.001	0.001	-0.001	0.003	0.001
Fe^{3+}	0.652	0.840	0.728	0.760	0.603	0.650	0.649	0.631	0.709	0.804	0.809	0.698	0.756	0.745
Mg	2.817	3.043	2.864	2.907	2.996	2.955	2.905	2.847	2.985	2.607	2.965	2.938	3.010	3.002
Fe^{2+}	0.975	0.708	0.875	0.864	0.917	0.920	0.891	0.946	0.849	1.148	0.766	0.898	0.717	0.769
Mn	0.040	0.056	0.053	0.048	0.038	0.049	0.023	0.024	0.046	0.068	0.044	0.055	0.042	0.044
Ca	1.833	1.705	1.743	1.768	1.805	1.765	1.904	1.897	1.789	1.730	1.754	1.699	1.744	1.769
Na	0.655	0.651	0.643	0.640	0.673	0.676	0.667	0.683	0.656	0.597	0.664	0.679	0.650	0.648
K	0.187	0.171	0.191	0.188	0.179	0.196	0.184	0.183	0.176	0.202	0.186	0.198	0.166	0.182
Cl	0.008	0.021	0.016	0.016	0.013	0.021	0.004	0.005	0.013	0.026	0.015	0.025	0.013	0.014
F	0.094	0.111	0.093	0.102	0.080	0.079	0.184	0.184	0.088	0.060	0.091	0.080	0.103	0.093
Sum	15.675	15.528	15.577	15.596	15.657	15.637	15.756	15.764	15.621	15.530	15.605	15.576	15.559	15.599

Table D3 Amphibole analyses of the 2006 Merapi eruption (continued)

Sample	ME08-09-02	ME08-09-02	ME08-09-02	ME08-09-02	ME08-09-02	ME08-09-02	ME08-09-02	ME08-09-02	ME08-09-02	ME08-09-02	ME08-09-02	ME08-09-02	ME08-09-02	ME08-09-02
Sample Type	L1-S	L1-S	L1-S	L1-S	L1-S	L1-S	L1-S	L1-S	L1-S	L1-S	L1-S	L1-S	L1-S	L1-S
DataSet/Point	91 / 3 .	91 / 4 .	91 / 5 .	91 / 6 .	91 / 7 .	25 / 1 .	30 / 1 .	1 / 1 .	2 / 1 .	3 / 1 .	4 / 1 .	5 / 1 .	6 / 1 .	7 / 1 .
Comment	ph	ph	ph	ph	ph-c	mph-c	mph-c	mph-c	mph-c	mph-c	mph-c	mph-c	mph-c	mph-c
SiO_2	41.64	41.29	42.36	42.39	41.97	40.38	42.90	41.89	40.84	40.56	42.88	40.55	41.85	42.12
TiO_2	2.86	2.86	2.26	2.24	2.21	2.59	2.82	2.40	2.65	2.54	2.89	2.50	3.13	3.06
Al_2O_3	11.45	11.62	10.33	10.57	10.49	12.03	10.76	11.53	12.68	12.31	10.66	13.01	11.43	11.30
Cr_2O_3	0.01	0.00	0.01	0.01	0.01	0.02	0.00	0.00	0.00	-0.01	0.00	0.00	0.00	-0.01
FeO	12.36	12.81	14.72	14.61	15.46	12.70	12.53	13.72	12.89	13.19	12.87	13.39	12.62	12.35
MnO	0.35	0.36	0.43	0.50	0.53	0.27	0.38	0.36	0.23	0.23	0.43	0.24	0.41	0.42
MgO	13.47	13.55	12.58	12.36	11.82	13.07	14.18	12.72	13.41	13.00	13.79	13.17	13.68	13.46
CaO	11.31	11.36	11.00	10.83	10.95	11.63	11.14	11.76	11.87	11.44	11.18	11.65	10.99	11.16
Na_2O	2.28	2.23	2.10	2.02	2.11	2.34	2.31	2.33	2.43	2.29	2.39	2.39	2.38	2.41
K_2O	0.96	0.94	0.97	1.06	1.06	0.93	0.93	0.88	0.94	1.00	0.96	0.93	1.01	0.97
Cl	0.05	0.05	0.09	0.12	0.10	0.03	0.06	0.05	0.03	0.03	0.08	0.02	0.07	0.07
F	0.21	0.20	0.19	0.16	0.12	0.11	0.20	0.14	0.30	0.24	0.18	0.22	0.19	0.16
Sum	96.96	97.27	97.04	96.89	96.82	96.11	98.21	97.79	98.28	96.83	98.32	98.06	97.77	97.48
Si	6.151	6.076	6.281	6.289	6.271	6.044	6.222	6.186	5.982	6.021	6.243	5.936	6.115	6.187
Al	1.993	2.015	1.805	1.849	1.847	2.122	1.839	2.006	2.190	2.154	1.828	2.245	1.969	1.957
Ti	0.317	0.316	0.252	0.250	0.249	0.292	0.307	0.267	0.292	0.283	0.316	0.275	0.344	0.339
Cr	0.001	0.000	0.001	0.001	0.001	0.002	-0.001	0.000	0.000	-0.001	0.000	0.000	0.000	-0.001
Fe^{3+}	0.655	0.806	0.846	0.844	0.794	0.617	0.819	0.532	0.669	0.750	0.712	0.825	0.811	0.610
Mg	2.966	2.972	2.781	2.735	2.632	2.917	3.066	2.801	2.928	2.876	2.993	2.875	2.980	2.948
Fe^{2+}	0.873	0.771	0.979	0.969	1.137	0.973	0.701	1.163	0.910	0.888	0.854	0.814	0.731	0.908
Mn	0.044	0.044	0.055	0.063	0.067	0.034	0.047	0.045	0.029	0.029	0.054	0.030	0.051	0.052
Ca	1.790	1.791	1.748	1.722	1.752	1.866	1.732	1.862	1.862	1.820	1.745	1.827	1.720	1.757
Na	0.653	0.636	0.603	0.582	0.611	0.679	0.650	0.666	0.691	0.658	0.676	0.679	0.675	0.687
K	0.182	0.177	0.183	0.201	0.201	0.178	0.171	0.167	0.176	0.190	0.178	0.174	0.189	0.182
Cl	0.013	0.013	0.022	0.029	0.025	0.007	0.015	0.013	0.008	0.008	0.019	0.005	0.017	0.017
F	0.098	0.091	0.091	0.076	0.056	0.054	0.092	0.067	0.138	0.113	0.085	0.101	0.088	0.075
Sum	15.624	15.604	15.534	15.505	15.564	15.723	15.553	15.695	15.730	15.669	15.598	15.679	15.584	15.626

Table D3 Amphibole analyses of the 2006 Merapi eruption (continued)

Sample	ME08-09-02	ME08-09-02	ME08-09-02	ME08-09-02	ME08-09-02	ME08-09-02	ME08-09-02	ME08-09-02	ME08-09-02	ME08-09-02	ME08-09-02	ME08-10	ME08-10	ME08-10
Sample Type	L1-S	L1-S	L1-S	L1-S	L1-S	L1-S	L1-S	L1-S	L1-S	L1-S	L1-S	KB-S	KB-S	KB-S
DataSet/Point	8 / 1 .	9 / 1 .	1 / 1 .	2 / 1 .	3 / 1 .	4 / 1 .	5 / 1 .	6 / 1 .	7 / 1 .	8 / 1 .	9 / 1 .	7 / 1 .	8 / 1 .	6 / 1 .
Comment	mph-c	mph-c	mph	mph	mph	mph	mph	mph	mph	mph	mph	ph-r	ph-c	ph-r
SiO_2	42.70	42.29	41.89	40.84	40.56	42.88	40.55	41.85	42.12	42.70	42.29	40.40	40.31	40.23
TiO_2	2.93	2.95	2.40	2.65	2.54	2.89	2.50	3.13	3.06	2.93	2.95	2.41	2.55	2.34
Al_2O_3	11.12	11.30	11.53	12.68	12.31	10.66	13.01	11.43	11.30	11.12	11.30	13.09	13.15	12.61
Cr_2O_3	0.00	0.00	0.00	0.00	-0.01	0.00	0.00	0.00	-0.01	0.00	0.00	0.01	0.00	-0.01
FeO	13.06	12.58	13.72	12.89	13.19	12.87	13.39	12.62	12.35	13.06	12.58	12.81	12.74	12.51
MnO	0.43	0.43	0.36	0.23	0.23	0.43	0.24	0.41	0.42	0.43	0.43	0.21	0.20	0.18
MgO	13.92	13.79	12.72	13.41	13.00	13.79	13.17	13.68	13.46	13.92	13.79	12.74	12.69	13.00
CaO	11.08	11.06	11.76	11.87	11.44	11.18	11.65	10.99	11.16	11.08	11.06	11.90	11.87	11.84
Na_2O	2.50	2.42	2.33	2.43	2.29	2.39	2.39	2.38	2.41	2.50	2.42	2.20	2.33	2.25
K_2O	0.93	0.95	0.88	0.94	1.00	0.96	0.93	1.01	0.97	0.93	0.95	1.00	1.00	1.00
Cl	0.07	0.07	0.05	0.03	0.03	0.08	0.02	0.07	0.07	0.07	0.07	0.02	0.02	0.02
F	0.23	0.24	0.14	0.30	0.24	0.18	0.22	0.19	0.16	0.23	0.24	0.41	0.38	0.38
Sum	98.97	98.07	97.79	98.28	96.83	98.32	98.06	97.77	97.48	98.97	98.07	97.19	97.22	96.34
Si	6.165	6.159	6.186	5.982	6.021	6.243	5.936	6.115	6.187	6.165	6.159	6.001	5.993	6.022
Al	1.892	1.939	2.006	2.190	2.154	1.828	2.245	1.969	1.957	1.892	1.939	2.292	2.303	2.226
Ti	0.318	0.323	0.267	0.292	0.283	0.316	0.275	0.344	0.339	0.318	0.323	0.269	0.285	0.263
Cr	0.000	0.000	0.000	0.000	-0.001	0.000	0.000	0.000	-0.001	0.000	0.000	0.001	0.000	-0.002
Fe^{3+}	0.844	0.787	0.532	0.669	0.750	0.712	0.825	0.811	0.610	0.844	0.787	0.555	0.500	0.563
Mg	2.995	2.995	2.801	2.928	2.876	2.993	2.875	2.980	2.948	2.995	2.995	2.820	2.811	2.901
Fe^{2+}	0.733	0.745	1.163	0.910	0.888	0.854	0.814	0.731	0.908	0.733	0.745	1.035	1.083	1.003
Mn	0.052	0.052	0.045	0.029	0.029	0.054	0.030	0.051	0.052	0.052	0.052	0.026	0.025	0.023
Ca	1.713	1.726	1.862	1.862	1.820	1.745	1.827	1.720	1.757	1.713	1.726	1.894	1.891	1.900
Na	0.699	0.682	0.666	0.691	0.658	0.676	0.679	0.675	0.687	0.699	0.682	0.633	0.670	0.652
K	0.172	0.177	0.167	0.176	0.190	0.178	0.174	0.189	0.182	0.172	0.177	0.190	0.191	0.190
Cl	0.016	0.017	0.013	0.008	0.008	0.019	0.005	0.017	0.017	0.016	0.017	0.006	0.005	0.006
F	0.106	0.108	0.067	0.138	0.113	0.085	0.101	0.088	0.075	0.106	0.108	0.192	0.176	0.180
Sum	15.584	15.585	15.695	15.730	15.669	15.598	15.679	15.584	15.626	15.584	15.585	15.717	15.752	15.742

Table D3 Amphibole analyses of the 2006 Merapi eruption (continued)

Sample	ME08-10	ME08-10	ME08-14	ME08-14	ME08-14
Sample Type	KB-S	KB-S	SD-S	SD-S	SD-S
DataSet/Point	7 / 1 .	8 / 1 .	67 / 1 .	68 / 1 .	69 / 1 .
Comment	ph	ph-c	ph-c	ph-c	ph-c
SiO_2	40.41	41.85	42.01	42.07	40.11
TiO_2	2.78	3.34	3.43	2.61	2.63
Al_2O_3	11.65	10.26	11.04	11.29	12.67
Cr_2O_3	0.01	0.01	0.02	-0.01	0.00
FeO	13.43	11.83	11.94	11.88	12.97
MnO	0.30	0.25	0.39	0.38	0.24
MgO	12.82	13.67	13.72	14.06	13.03
CaO	11.11	11.25	11.08	11.09	11.56
Na_2O	2.47	2.30	2.50	2.56	2.29
K_2O	0.95	1.04	1.01	0.96	0.92
Cl	0.08	0.12	0.07	0.05	0.04
F	0.29	0.32	0.41	0.51	0.18
Sum	96.29	96.24	97.61	97.46	96.64
Si	6.050	6.257	6.179	6.176	5.959
Al	2.055	1.808	1.913	1.954	2.220
Ti	0.313	0.375	0.379	0.288	0.293
Cr	0.001	0.001	0.002	-0.001	0.000
Fe^{3+}	0.757	0.458	0.574	0.721	0.760
Mg	2.861	3.047	3.009	3.078	2.885
Fe^{2+}	0.925	1.021	0.895	0.737	0.852
Mn	0.038	0.032	0.048	0.048	0.031
Ca	1.782	1.801	1.746	1.745	1.841
Na	0.717	0.667	0.712	0.730	0.659
K	0.181	0.198	0.190	0.180	0.175
Cl	0.020	0.030	0.017	0.014	0.010
F	0.135	0.152	0.191	0.235	0.086
Sum	15.680	15.666	15.648	15.655	15.674

Table D4 Oxide analyses of the 2006 Merapi eruption[1]

Sample	ME08-04-01	ME08-04-01	ME08-04-01	ME08-04-01	ME08-09-02	ME08-09-02	ME08-09-02	ME08-09-02	ME08-09-02	ME08-09-02
Sample Type[2]	L8-S	L8-S	L8-S	L8-S	L1-S	L1-S	L1-S	L1-S	L1-S	L1-S
Point	78 / 1 .	79 / 1 .	80 / 1 .	81 / 1 .	82 / 1 .	83 / 1 .	84 / 1 .	85 / 1 .	36 / 1 .	40 / 1 .
Comment[3]	mph	mph	mph	mph	mph	mph	mph	mph	m	m
TiO_2	9.94	10.02	10.24	9.67	7.16	9.34	9.41	9.56	9.56	9.98
Al_2O_3	2.59	2.39	2.32	2.76	3.71	3.08	2.91	2.79	2.33	2.32
Cr_2O_3	0.00	0.00	0.00	0.00	0.02	0.04	0.01	0.01		
FeO	79.33	79.89	78.34	78.69	79.64	79.32	78.61	79.30	77.98	76.26
MnO	0.96	1.06	1.04	1.04	0.78	0.90	0.90	0.99	0.99	1.01
MgO	1.66	1.60	1.59	1.83	2.31	2.30	2.25	1.89	1.42	1.26
CaO	0.05	0.04	0.03	0.05	0.02	0.01	0.08	0.03	0.10	0.91
Total	94.52	94.99	93.56	94.03	93.63	95.00	94.18	94.58	92.37	91.74
Al	0.114	0.105	0.104	0.122	0.163	0.134	0.128	0.123	0.106	0.107
Ti	0.280	0.281	0.292	0.273	0.201	0.259	0.264	0.268	0.276	0.293
Cr	0.000	0.000	0.000	0.000	0.001	0.001	0.000	0.000	0.000	0.000
Fe^{3+}	1.327	1.333	1.313	1.332	1.435	1.346	1.343	1.341	1.342	1.306
Mg	0.093	0.089	0.090	0.102	0.128	0.126	0.125	0.105	0.081	0.074
Fe^{2+}	1.156	1.159	1.168	1.137	1.048	1.105	1.111	1.132	1.163	1.186
Mn	0.031	0.033	0.033	0.033	0.025	0.028	0.029	0.031	0.032	0.033
Sum	3.000	3.000	3.000	3.000	3.000	3.000	3.000	3.000	3.000	3.000
XUsp	0.297	0.297	0.308	0.291	0.219	0.278	0.282	0.286	0.291	0.310
XMt	0.703	0.703	0.692	0.709	0.781	0.722	0.718	0.714	0.709	0.690

[1] Major element oxides in wt.%; number of cations based on 4 oxygens; [2] see Appendix A; [3] see Table D1

Table D4 Oxide analyses of the 2006 Merapi eruption (continued)

Sample	ME08-10	ME08-10	ME08-10	ME08-10	ME08-14	ME08-14	ME08-14	ME08-14		
Sample Type	KB-S	KB-S	KB-S	KB-S	SD-S	SD-S	SD-S	SD-S		
Point	86 / 1 .	87 / 1 .	88 / 1 .	89 / 1 .	74 / 1 .	75 / 1 .	76 / 1 .	77 / 1 .		
Comment	mph	mph	mph	mph	mph	mph	mph	mph		
TiO_2	20.57	15.96	10.04	12.83	16.45	13.27	13.29	11.86		
Al_2O_3	1.33	1.31	2.04	1.10	0.85	1.11	2.87	4.39		
Cr_2O_3	0.01	0.01	0.02	0.03	0.03	0.02	0.01	0.01		
FeO	69.20	74.33	78.58	75.72	72.36	75.75	74.79	75.66		
MnO	0.57	0.41	0.52	0.38	0.37	0.41	1.08	2.32		
MgO	1.06	0.83	0.95	0.77	0.85	0.75	1.45	2.10		
CaO	0.01	0.02	0.01	0.03	0.03	0.03	0.07	0.02		
Total	92.75	92.87	92.17	90.86	90.94	91.34	93.55	96.36		
Al	0.061	0.060	0.093	0.051	0.040	0.051	0.128	0.188		
Ti	0.603	0.466	0.292	0.382	0.492	0.393	0.379	0.324		
Cr	0.000	0.000	0.001	0.001	0.001	0.000	0.000	0.000		
Fe^{3+}	0.733	1.008	1.322	1.184	0.976	1.161	1.113	1.162		
Mg	0.062	0.048	0.055	0.045	0.050	0.044	0.082	0.114		
Fe^{2+}	1.523	1.405	1.220	1.324	1.429	1.335	1.262	1.139		
Mn	0.019	0.014	0.017	0.013	0.013	0.014	0.035	0.071		
Sum	3.000	3.000	3.000	3.000	3.000	3.000	3.000	3.000		
XUsp	0.622	0.480	0.306	0.392	0.502	0.404	0.405	0.358		
XMt	0.378	0.520	0.694	0.608	0.498	0.596	0.595	0.642		

Table D5 Apatite analyses of the 2006 Merapi eruption[1]

Sample	ME08-01	ME08-01	ME08-09-01	ME08-09-01	ME08-09-01	ME08-09-01	ME08-09-01	ME08-09-01	ME08-09-01	ME08-09-01	ME08-09-01	ME08-09-01	ME08-09-01	ME08-09-01	ME08-09-01	ME08-09-01	ME08-09-01
Sample Type[2]	L4-S	L4-S	L1-S	L1-S	L1-S	L1-S	L1-S	L1-S	L1-S	L1-S	L1-S	L1-S	L1-S	L1-S	L1-S	L1-S	L1-S
Point	1 / 1 .	2 / 1 .	3 / 1 .	4 / 1 .	5 / 1 .	6 / 1 .	7 / 1 .	8 / 1 .	9 / 1 .	10 / 1 .	11 / 1 .	12 / 1 .	13 / 1 .	14 / 1 .	15 / 1 .	16 / 1 .	17 / 1 .
Comment[3]	pyx inc	pyx inc	MI PEC	MI PEC	pyx inc	MI PEC	pyx inc	pyx inc	pyx inc	pyx inc	pyx inc	pyx inc	pyx inc	pyx inc	pyx inc	pyx inc	pyx inc
P_2O_5	43.16	42.87	41.45	41.52	41.62	41.90	41.54	41.33	41.73	42.00	41.56	41.26	40.77	40.82	39.97	40.45	42.00
SiO_2	0.20	0.66	0.31	0.20	0.30	0.16	0.23	0.19	0.17	0.19	0.21	0.19	0.28	0.69	0.19	0.33	0.18
TiO_2	0.03	0.00	0.02	0.00	0.02	0.00	0.06	0.02	0.00	0.00	0.00	0.03	0.00	0.01	0.02	0.03	0.00
Al_2O_3	0.00	0.10	0.03	0.00	0.04	0.01	0.01	0.00	0.00	0.00	0.00	0.02	0.00	0.01	0.00	0.01	0.00
FeO	0.58	0.61	0.54	0.46	0.50	0.45	0.96	0.53	0.41	0.48	0.46	0.47	0.50	0.67	0.42	0.56	0.47
MnO	0.19	0.17	0.24	0.18	0.13	0.20	0.20	0.19	0.17	0.12	0.18	0.18	0.21	0.17	0.18	0.19	0.16
MgO	0.35	0.37	0.36	0.35	0.39	0.36	0.35	0.33	0.35	0.38	0.37	0.41	0.36	0.48	0.39	0.39	0.39
CaO	52.95	52.46	53.31	53.35	53.62	53.33	53.12	53.01	52.81	52.80	52.65	52.72	52.48	52.30	51.80	52.55	53.12
Na_2O	0.10	0.09	0.14	0.10	0.07	0.08	0.10	0.07	0.07	0.05	0.08	0.08	0.12	0.10	0.03	0.12	0.07
K_2O	0.01	0.04	0.02	0.01	0.00	0.01	0.00	0.02	0.00	0.00	0.00	0.00	0.02	0.00	0.03	0.00	0.00
Cl	1.14	1.03	1.05	1.06	0.87	1.06	1.20	1.12	1.05	0.86	1.02	1.01	1.05	0.97	1.04	1.08	0.80
F	4.36	4.03	4.29	4.02	3.56	3.92	3.95	4.58	4.50	4.55	4.40	4.30	3.73	4.15	4.53	4.02	3.87
F corr.	2.10	1.94	2.07	1.94	1.72	1.89	1.90	2.21	2.17	2.20	2.12	2.08	1.80	2.00	2.19	1.94	1.87
H_2O*	0.51	0.61	0.51	0.57	0.73	0.60	0.56	0.42	0.46	0.50	0.49	0.50	0.61	0.55	0.40	0.53	0.68
Subtotal	101.33	100.96	100.06	99.75	100.02	100.04	100.23	99.44	99.38	99.59	99.13	98.95	98.20	98.75	96.64	98.18	99.73
O=F,Cl	1.14	1.05	1.11	1.06	0.92	1.04	1.07	1.18	1.15	1.12	1.12	1.10	0.99	1.06	1.15	1.06	0.97
Sum	100.19	99.91	98.95	98.69	99.10	99.00	99.16	98.25	98.23	98.47	98.01	97.85	97.20	97.69	95.49	97.12	98.76
P	6.097	6.058	5.973	5.994	5.976	6.020	5.982	5.998	6.036	6.049	6.027	6.001	5.978	5.944	5.973	5.947	6.033
Si	0.034	0.110	0.052	0.034	0.051	0.027	0.038	0.033	0.029	0.033	0.036	0.033	0.049	0.118	0.034	0.058	0.030
Al	0.000	0.010	0.003	0.000	0.004	0.001	0.001	0.000	0.000	0.000	0.000	0.002	0.000	0.001	0.000	0.001	0.000
Ti	0.004	0.000	0.003	0.000	0.002	0.000	0.007	0.002	0.000	0.000	0.000	0.004	0.000	0.001	0.003	0.004	0.000
Fe	0.082	0.086	0.077	0.066	0.071	0.064	0.136	0.076	0.058	0.068	0.066	0.068	0.072	0.097	0.062	0.081	0.067
Mn	0.027	0.024	0.035	0.027	0.019	0.028	0.029	0.028	0.024	0.018	0.027	0.026	0.031	0.024	0.027	0.028	0.023
Mg	0.088	0.092	0.092	0.089	0.099	0.092	0.089	0.084	0.090	0.096	0.094	0.105	0.092	0.122	0.101	0.101	0.098
Ca	9.468	9.383	9.721	9.747	9.742	9.698	9.680	9.734	9.668	9.623	9.661	9.704	9.739	9.638	9.797	9.776	9.658
Na	0.032	0.029	0.047	0.033	0.023	0.026	0.033	0.023	0.023	0.017	0.025	0.025	0.042	0.032	0.011	0.040	0.023
K	0.002	0.009	0.005	0.002	0.001	0.001	0.001	0.005	0.001	0.000	0.000	0.000	0.004	0.000	0.006	0.001	0.000
Cl	0.323	0.291	0.303	0.307	0.250	0.306	0.346	0.324	0.303	0.246	0.295	0.295	0.308	0.283	0.310	0.316	0.230
F	1.109	1.026	1.114	1.047	0.921	1.016	1.024	1.197	1.175	1.181	1.150	1.128	0.985	1.090	1.220	1.065	1.002
OH*	0.568	0.684	0.583	0.646	0.829	0.678	0.630	0.478	0.522	0.573	0.555	0.577	0.708	0.627	0.470	0.618	0.768
Sum	17.833	17.802	18.007	17.991	17.988	17.956	17.997	17.982	17.929	17.903	17.936	17.968	18.006	17.978	18.013	18.037	17.932

[1] Major element oxides in wt.%; number of cations based on 25 oxygens; H_2O calculated on the basis of filling the C site (2); [2] see Appendix A; [3] pyx-pl-am inc = inclusion in pyroxene, plagioclase and amphibole, respectively, am rr = amphibole reaction rim, MI-PEC = post-entrapment crystal in melt inclusion; other abbreviations, see Table D1

Table D5 Apatite analyses of the 2006 Merapi eruption (continued)

Sample	ME08-09-01	ME08-09-01	ME08-14	ME08-14
Sample Type	L1-S	L1-S	SD-S	SD-S
Point	18 / 1 .	19 / 1 .	20 / 1 .	21 / 1 .
Comment	pyx inc	pyx inc	pyx inc	pyx inc
P_2O_5	41.42	41.01	42.03	42.43
SiO_2	0.22	0.16	0.30	0.64
TiO_2	0.01	0.03	0.02	0.00
Al_2O_3	0.00	0.00	0.01	0.03
FeO	0.57	0.51	0.62	0.76
MnO	0.18	0.16	0.19	0.19
MgO	0.37	0.35	0.38	0.49
CaO	52.73	52.98	52.85	52.13
Na_2O	0.11	0.07	0.06	0.11
K_2O	0.02	0.00	0.01	0.01
Cl	1.02	1.06	0.91	1.12
F	4.16	3.88	5.86	4.09
F corr.	2.01	1.87	2.83	1.97
H_2O*	0.54	0.58	0.20	0.56
Subtotal	99.17	98.77	100.42	100.45
O=F,Cl	1.07	1.03	1.40	1.08
Sum	98.10	97.75	99.02	99.36
P	6.009	5.983	6.029	6.041
Si	0.037	0.028	0.052	0.108
Al	0.000	0.000	0.001	0.003
Ti	0.001	0.004	0.003	0.000
Fe	0.081	0.073	0.087	0.107
Mn	0.026	0.024	0.028	0.027
Mg	0.093	0.089	0.095	0.124
Ca	9.681	9.782	9.595	9.395
Na	0.037	0.022	0.020	0.035
K	0.004	0.000	0.003	0.002
Cl	0.295	0.308	0.262	0.319
F	1.087	1.019	1.516	1.049
OH*	0.618	0.672	0.222	0.632
Sum	17.969	18.005	17.911	17.841

Table D6 Feldspar analyses of the 2010 Merapi eruption[1]

Sample	M11-06	M11-07	M11-07	M11-07	M11-07	M11-07	M11-07	M11-07	M11-15	M11-15	M11-15	M11-15	M11-24	M11-24
Sample Type[2]	DS	DD	DD	DD	DD	DD	DD	DD	DD	DD	DD	DD	DD	DD
Point	25 / 1 .	16 / 1 .	18 / 1 .	19 / 1 .	20 / 1 .	21 / 1 .	23 / 1 .	24 / 1 .	1 / 1 .	2 / 1 .	4 / 1 .	5 / 1 .	6 / 1 .	7 / 1 .
Comment[3]	ph-c	ph-r	ph-r	ph-r	ph-c	m	m	m	ph-c	ph-c	ph-r	ph-c	ph-c	ph-r
SiO_2	54.50	56.82	56.50	56.33	56.18	53.19	51.73	51.52	44.77	44.83	49.08	52.88	45.09	49.61
TiO_2	0.02	0.02	0.03	0.02	0.02	0.05	0.04	0.08	0.01	0.00	0.03	0.03	0.01	0.02
Al_2O_3	28.50	26.42	26.70	27.09	27.22	28.90	30.45	30.21	33.51	33.46	30.72	28.49	34.03	30.20
FeO	0.51	0.47	0.57	0.50	0.50	0.74	0.79	0.92	0.60	0.57	0.64	0.53	0.61	0.52
MgO	0.04	0.04	0.07	0.04	0.05	0.09	0.09	0.13	0.01	0.02	0.08	0.04	0.01	0.02
CaO	11.17	9.04	9.42	9.92	9.94	12.15	13.72	13.69	17.79	17.81	14.50	11.36	17.80	14.25
SrO	0.12	0.11	0.12	0.12	0.15	0.12	0.11	0.11	0.10	0.10	0.09	0.12	0.11	0.11
BaO	0.02	0.06	0.07	0.07	0.09	0.00	0.03	0.00						
Na_2O	5.16	6.08	5.98	5.71	5.87	4.61	3.66	3.74	1.25	1.27	3.10	4.79	1.21	3.36
K_2O	0.39	0.64	0.54	0.53	0.50	0.31	0.23	0.23	0.03	0.03	0.14	0.35	0.05	0.21
Sum	100.44	99.69	100.00	100.33	100.52	100.17	100.86	100.62	98.07	98.11	98.38	98.60	98.91	98.30
Si	2.460	2.570	2.551	2.537	2.528	2.417	2.343	2.341	2.111	2.113	2.285	2.434	2.107	2.310
Al	1.516	1.408	1.421	1.437	1.443	1.548	1.625	1.618	1.862	1.859	1.685	1.546	1.874	1.657
Ti	0.001	0.001	0.001	0.001	0.001	0.002	0.001	0.003	0.000	0.000	0.001	0.001	0.000	0.001
Fe	0.019	0.018	0.022	0.019	0.019	0.028	0.030	0.035	0.024	0.022	0.025	0.020	0.024	0.020
Mg	0.003	0.003	0.005	0.003	0.003	0.006	0.006	0.009	0.001	0.002	0.006	0.003	0.001	0.002
Sr	0.003	0.003	0.003	0.003	0.004	0.003	0.003	0.003	0.003	0.003	0.002	0.003	0.003	0.003
Ba	0.000	0.001	0.001	0.001	0.002	0.000	0.001	0.000	0.000	0.000	0.000	0.000	0.000	0.000
Ca	0.540	0.438	0.456	0.478	0.479	0.592	0.666	0.667	0.899	0.900	0.723	0.560	0.891	0.711
Na	0.452	0.533	0.523	0.499	0.512	0.407	0.321	0.329	0.115	0.116	0.280	0.428	0.110	0.303
K	0.023	0.037	0.031	0.030	0.029	0.018	0.013	0.013	0.002	0.002	0.008	0.021	0.003	0.013
Sum	5.018	5.011	5.014	5.008	5.020	5.019	5.010	5.018	5.016	5.016	5.016	5.016	5.012	5.019
Ab (mol%)	44.5	52.9	51.8	49.5	50.2	40.0	32.1	32.6	11.3	11.4	27.7	42.4	10.9	29.5
An (mol%)	53.3	43.5	45.1	47.5	47.0	58.2	66.6	66.1	88.6	88.4	71.5	55.6	88.8	69.2
Or (mol%)	2.2	3.7	3.1	3.0	2.8	1.7	1.3	1.3	0.2	0.2	0.8	2.0	0.3	1.2

[1] Major element oxides in wt.%; number of cations based on 8 oxygens; [2] see Appendix A; [3] see Table D1

Table D6 Feldspar analyses of the 2010 Merapi eruption (continued)

Sample	M11-24	M11-24	M11-24	M11-24	M11-24	M11-24	M11-24	M11-24	M11-24	M11-24	M11-24	M11-24	M11-24	M11-24
Sample Type	DD	DD	DD	DD	DD	DD	DD	DD	DD	DD	DD	DD	DD	DD
Point	8 / 1 .	18 / 1 .	1 / 1 .	1 / 2 .	1 / 3 .	1 / 4 .	1 / 5 .	1 / 6 .	1 / 7 .	1 / 8 .	1 / 9 .	1 / 10 .	1 / 11 .	1 / 12 .
Comment	ph-c	ph-c	ph-c	ph	ph	ph	ph	ph	ph	ph	ph	ph	ph	ph-r
SiO_2	44.76	45.24	45.45	45.58	45.41	45.80	45.97	45.75	45.31	45.73	47.58	48.62	48.85	50.60
TiO_2	0.01	0.03	0.02	0.03	0.00	0.01	0.01	0.02	0.00	0.00	0.03	0.04	0.02	0.01
Al_2O_3	33.85	33.85	34.02	33.95	34.20	33.89	33.83	33.72	34.00	34.00	32.78	32.01	31.51	30.75
FeO	0.50	0.38	0.58	0.62	0.57	0.58	0.62	0.57	0.52	0.65	0.54	0.62	0.63	0.58
MgO	0.01	0.00	0.01	0.01	0.02	0.01	0.02	0.01	0.01	0.02	0.02	0.03	0.03	0.03
CaO	17.73	17.34	17.70	17.75	17.68	17.54	17.62	17.46	17.81	17.57	16.10	15.44	14.92	13.95
SrO	0.09	0.11	0.11	0.11	0.11	0.09	0.09	0.11	0.10	0.08	0.09	0.11	0.10	0.12
BaO														
Na_2O	1.15	1.31	1.30	1.35	1.20	1.29	1.39	1.41	1.20	1.30	2.20	2.56	2.85	3.46
K_2O	0.04	0.05	0.05	0.05	0.04	0.08	0.05	0.06	0.05	0.05	0.09	0.13	0.17	0.23
Sum	98.14	98.31	99.25	99.46	99.22	99.27	99.59	99.11	99.01	99.40	99.43	99.56	99.10	99.73
Si	2.106	2.121	2.115	2.117	2.112	2.128	2.131	2.130	2.113	2.123	2.199	2.240	2.260	2.318
Al	1.878	1.870	1.866	1.859	1.875	1.856	1.848	1.850	1.869	1.860	1.785	1.738	1.718	1.660
Ti	0.000	0.001	0.001	0.001	0.000	0.000	0.000	0.001	0.000	0.000	0.001	0.001	0.001	0.000
Fe	0.020	0.015	0.023	0.024	0.022	0.022	0.024	0.022	0.020	0.025	0.021	0.024	0.025	0.022
Mg	0.001	0.000	0.001	0.001	0.001	0.000	0.001	0.001	0.001	0.001	0.001	0.002	0.002	0.002
Sr	0.002	0.003	0.003	0.003	0.003	0.002	0.002	0.003	0.003	0.002	0.002	0.003	0.003	0.003
Ba	0.000	0.000	0.000	0.000	0.000	0.000	0.000	0.000	0.000	0.000	0.000	0.000	0.000	0.000
Ca	0.894	0.871	0.883	0.884	0.881	0.873	0.875	0.871	0.890	0.874	0.797	0.762	0.740	0.685
Na	0.105	0.119	0.118	0.121	0.108	0.116	0.125	0.128	0.108	0.117	0.197	0.229	0.256	0.307
K	0.003	0.003	0.003	0.003	0.002	0.004	0.003	0.003	0.003	0.003	0.005	0.008	0.010	0.013
Sum	5.009	5.004	5.012	5.014	5.005	5.004	5.009	5.009	5.008	5.007	5.009	5.008	5.014	5.012
Ab (mol%)	10.5	12.0	11.7	12.0	10.9	11.7	12.4	12.7	10.8	11.8	19.7	22.9	25.4	30.5
An (mol%)	89.3	87.7	88.0	87.7	88.8	87.9	87.3	86.9	88.9	87.9	79.7	76.3	73.5	68.1
Or (mol%)	0.3	0.3	0.3	0.3	0.2	0.5	0.3	0.3	0.3	0.3	0.5	0.8	1.0	1.3

Table D6 Feldspar analyses of the 2010 Merapi eruption (continued)

Sample	M11-24	M11-26a	M11-26a	M11-26a	M11-26a	M11-26a	M11-26a	M11-26a	M11-26a	M11-26a	M11-26a	M11-27-2	M11-27-2	M11-27-2
Sample Type	DD	DD	DD	DD	DD	DD	DD	DD	DD	DD	DD	DD	DD	DD
Point	26 / 1 .	11 / 1 .	12 / 1 .	18 / 1 .	19 / 1 .	21 / 1 .	23 / 1 .	24 / 1 .	25 / 1 .	26 / 1 .	27 / 1 .	12 / 1 .	13 / 1 .	14 / 1 .
Comment	m	ph-c	ph-r	m	m	m	m	m	m	m	m	ph-r	ph-r	ph-r
SiO_2	53.56	44.85	52.87	51.68	51.50	51.37	51.13	54.77	51.05	49.22	53.81	49.89	55.78	55.80
TiO_2	0.05	0.00	0.01	0.04	0.03	0.04	0.03	0.05	0.04	0.03	0.02	0.02	0.03	0.03
Al_2O_3	28.53	33.99	28.89	29.43	29.43	29.59	29.67	26.56	31.42	30.69	28.70	31.61	26.83	27.63
FeO	0.58	0.58	0.58	0.93	0.87	0.82	0.73	0.84	0.67	0.95	0.60	0.53	0.50	0.53
MgO	0.03	0.02	0.05	0.09	0.10	0.10	0.08	0.08	0.03	0.26	0.05	0.04	0.05	0.04
CaO	11.62	18.13	11.71	12.88	12.85	12.85	13.10	10.97	14.72	15.53	11.36	14.77	9.87	10.11
SrO	0.14	0.10	0.11	0.16	0.13	0.12	0.12	0.07	0.11	0.06	0.14	0.13	0.10	0.13
BaO												0.03	0.05	0.06
Na_2O	4.31	1.09	4.62	3.93	4.00	3.81	3.82	4.38	2.87	2.37	4.81	3.14	5.78	5.70
K_2O	0.77	0.03	0.30	0.28	0.31	0.29	0.26	0.92	0.22	0.58	0.40	0.17	0.50	0.49
Sum	99.59	98.79	99.13	99.42	99.22	98.98	98.95	98.64	101.11	99.70	99.88	100.33	99.48	100.52
Si	2.444	2.100	2.422	2.373	2.370	2.367	2.358	2.518	2.307	2.273	2.444	2.278	2.534	2.511
Al	1.534	1.876	1.559	1.593	1.596	1.606	1.612	1.439	1.673	1.670	1.536	1.700	1.437	1.465
Ti	0.002	0.000	0.000	0.001	0.001	0.001	0.001	0.002	0.001	0.001	0.001	0.001	0.001	0.001
Fe	0.022	0.023	0.022	0.036	0.033	0.032	0.028	0.032	0.025	0.037	0.023	0.020	0.019	0.020
Mg	0.002	0.002	0.003	0.006	0.007	0.007	0.006	0.005	0.002	0.018	0.003	0.003	0.003	0.003
Sr	0.004	0.003	0.003	0.004	0.003	0.003	0.003	0.002	0.003	0.002	0.004	0.003	0.003	0.003
Ba	0.000	0.000	0.000	0.000	0.000	0.000	0.000	0.000	0.000	0.000	0.000	0.001	0.001	0.001
Ca	0.568	0.910	0.575	0.634	0.633	0.634	0.647	0.540	0.713	0.768	0.553	0.722	0.480	0.487
Na	0.381	0.099	0.410	0.350	0.357	0.341	0.342	0.391	0.251	0.212	0.424	0.278	0.509	0.498
K	0.045	0.002	0.017	0.016	0.018	0.017	0.016	0.054	0.013	0.034	0.023	0.010	0.029	0.028
Sum	5.001	5.013	5.012	5.013	5.019	5.008	5.013	4.983	4.987	5.015	5.010	5.015	5.016	5.018
Ab (mol%)	38.3	9.8	40.9	35.0	35.4	34.3	34.0	39.7	25.7	20.9	42.4	27.5	50.0	49.1
An (mol%)	57.2	90.1	57.3	63.4	62.8	64.0	64.4	54.8	73.0	75.7	55.3	71.5	47.2	48.1
Or (mol%)	4.5	0.2	1.7	1.6	1.8	1.7	1.5	5.5	1.3	3.4	2.3	1.0	2.8	2.8

Table D6 Feldspar analyses of the 2010 Merapi eruption (continued)

Sample	M11-27-2	M11-27-2	M11-27-2	M11-27-2	M11-27-2	M11-27-3	M11-27-3	M11-27-3	M11-27-3	M11-27-3	M11-27-3	M11-27-3	M11-27-3	M11-27-3
Sample Type	DD	DD	LG-Inc	LG-Inc	LG-Inc	DD	DD	DD	DD	DD	DD	DD	DD	DD
Point	17 / 1 .	18 / 1 .	44 / 1 .	45 / 1 .	46 / 1 .	19 / 1 .	20 / 1 .	21 / 1 .	22 / 1 .	23 / 1 .	24 / 1 .	25 / 1 .	26 / 1 .	27 / 1 .
Comment	m	m	m-c	m-r	m-c	ph-c	ph-c	ph-r	ph-r	ph-r	ph-c	ph-c	ph-r	ph-r
SiO_2	49.99	51.76	57.39	58.56	46.83	45.33	46.40	55.95	53.11	50.61	45.94	45.31	46.23	47.61
TiO_2	0.03	0.06	0.02	0.03	0.02	0.00	0.00	0.03	0.04	0.03	0.01	0.00	0.00	0.00
Al_2O_3	30.67	29.16	25.61	25.35	33.59	33.61	34.82	27.53	29.12	29.97	34.62	33.66	34.76	32.99
FeO	0.79	0.91	0.43	0.43	0.51	0.45	0.43	0.52	0.50	0.53	0.57	0.55	0.62	0.65
MgO	0.12	0.18	0.02	0.03	0.01	0.01	0.02	0.04	0.03	0.04	0.02	0.03	0.03	0.06
CaO	14.38	13.11	8.37	7.99	17.45	17.43	18.06	9.91	12.08	13.01	18.37	17.79	18.34	16.51
SrO	0.13	0.12	0.03	0.05	0.12	0.12	0.09	0.14	0.15	0.20	0.13	0.17	0.09	0.14
BaO	0.01	0.02	0.03	0.03	0.00									
Na_2O	3.26	4.03	6.42	6.55	1.80	1.40	1.31	5.72	4.63	3.85	1.18	1.39	1.27	2.16
K_2O	0.21	0.26	0.62	0.95	0.09	0.05	0.07	0.50	0.31	0.25	0.03	0.04	0.05	0.07
Sum	99.59	99.62	98.93	99.97	100.40	98.40	101.18	100.33	99.98	98.50	100.87	98.93	101.39	100.20
Si	2.300	2.374	2.607	2.633	2.152	2.126	2.116	2.519	2.415	2.344	2.106	2.118	2.108	2.188
Al	1.663	1.577	1.371	1.343	1.819	1.858	1.871	1.461	1.560	1.636	1.870	1.854	1.868	1.787
Ti	0.001	0.002	0.001	0.001	0.001	0.000	0.000	0.001	0.001	0.001	0.000	0.000	0.000	0.000
Fe	0.030	0.035	0.016	0.016	0.020	0.018	0.016	0.019	0.019	0.020	0.022	0.021	0.024	0.025
Mg	0.008	0.013	0.001	0.002	0.001	0.000	0.001	0.003	0.002	0.003	0.002	0.002	0.002	0.004
Sr	0.004	0.003	0.001	0.001	0.003	0.003	0.002	0.004	0.004	0.005	0.004	0.005	0.002	0.004
Ba	0.000	0.000	0.000	0.001	0.000	0.000	0.000	0.000	0.000	0.000	0.000	0.000	0.000	0.000
Ca	0.709	0.645	0.407	0.385	0.859	0.876	0.882	0.478	0.589	0.645	0.902	0.891	0.896	0.813
Na	0.290	0.359	0.566	0.571	0.160	0.128	0.116	0.499	0.408	0.346	0.105	0.126	0.112	0.193
K	0.012	0.015	0.036	0.054	0.005	0.003	0.004	0.028	0.018	0.015	0.002	0.002	0.003	0.004
Sum	5.019	5.022	5.007	5.007	5.020	5.011	5.009	5.013	5.017	5.017	5.012	5.019	5.015	5.017
Ab (mol%)	28.7	35.2	56.1	56.5	15.6	12.7	11.5	49.6	40.2	34.4	10.4	12.3	11.1	19.1
An (mol%)	70.1	63.3	40.4	38.1	83.9	87.0	88.1	47.5	58.0	64.1	89.4	87.5	88.6	80.5
Or (mol%)	1.2	1.5	3.6	5.4	0.5	0.3	0.4	2.8	1.8	1.5	0.2	0.2	0.3	0.4

Table D6 Feldspar analyses of the 2010 Merapi eruption (continued)

Sample	M11-27-3	M11-27-3	M11-27-3	M11-27-3	M11-27-3	M11-27-3	M11-27-3	M11-27-3	M11-27-3	M11-27-3	M11-27-3	M11-27-3	M11-27-3	M11-27-3
Sample Type	DD	DD	LG-Inc	LG-Inc	LG-Inc	LG-Inc	LG-Inc	LG-Inc	LG-Inc	LG-Inc	LG-Inc	LG-Inc	LG-Inc	LG-Inc
Point	38 / 1 .	44 / 1 .	12 / 1 .	13 / 1 .	14 / 1 .	15 / 1 .	16 / 1 .	28 / 1 .	30 / 1 .	31 / 1 .	32 / 1 .	33 / 1 .	34 / 1 .	35 / 1 .
Comment	m	m	ph-c	ph-c	ph	ph	ph-r	m	m	m	m	m	m	m
SiO_2	57.00	57.71	56.79	47.66	45.98	51.42	62.52	67.27	66.40	66.93	55.88	66.84	66.96	66.50
TiO_2	0.14	0.05	0.00	0.02	0.00	0.05	0.00	0.03	0.02	0.07	0.02	0.02	0.06	0.02
Al_2O_3	25.79	27.17	27.56	32.48	34.50	31.21	23.93	18.81	18.48	19.27	28.14	19.61	18.81	19.36
FeO	1.45	0.55	0.50	0.51	0.43	0.57	0.37	0.33	0.16	0.37	0.52	0.22	0.21	0.21
MgO	0.38	0.04	0.04	0.02	0.00	0.04	0.00	0.00	0.00	0.00	0.01	0.00	0.00	0.00
CaO	9.93	9.35	9.64	16.15	18.29	14.05	5.28	0.22	0.24	0.62	10.60	0.87	0.33	0.72
SrO	0.07	0.14	0.11	0.11	0.11	0.13	0.05	0.00	0.00	0.00	0.13	0.00	0.00	0.00
BaO														
Na_2O	4.76	6.24	5.99	2.28	1.33	3.60	8.14	4.84	4.94	5.62	5.64	6.12	5.23	6.03
K_2O	1.42	0.62	0.56	0.11	0.06	0.20	0.96	10.40	9.77	8.84	0.39	7.94	9.69	8.08
Sum	100.95	101.87	101.19	99.33	100.70	101.28	101.25	101.89	100.00	101.73	101.33	101.63	101.29	100.92
Si	2.565	2.557	2.533	2.206	2.110	2.319	2.750	2.995	3.003	2.973	2.496	2.963	2.992	2.969
Al	1.368	1.418	1.449	1.771	1.866	1.659	1.241	0.987	0.985	1.009	1.481	1.024	0.991	1.019
Ti	0.005	0.002	0.000	0.001	0.000	0.002	0.000	0.001	0.001	0.002	0.001	0.001	0.002	0.001
Fe	0.054	0.020	0.019	0.020	0.017	0.022	0.014	0.012	0.006	0.014	0.019	0.008	0.008	0.008
Mg	0.026	0.002	0.003	0.001	0.000	0.003	0.000	0.000	0.000	0.000	0.001	0.000	0.000	0.000
Sr	0.002	0.004	0.003	0.003	0.003	0.003	0.001	0.000	0.000	0.000	0.003	0.000	0.000	0.000
Ba	0.000	0.000	0.000	0.000	0.000	0.000	0.000	0.000	0.000	0.000	0.000	0.000	0.000	0.000
Ca	0.479	0.444	0.461	0.801	0.899	0.679	0.249	0.011	0.012	0.030	0.507	0.041	0.016	0.034
Na	0.416	0.536	0.518	0.205	0.118	0.315	0.694	0.418	0.433	0.484	0.488	0.526	0.453	0.522
K	0.082	0.035	0.032	0.006	0.004	0.012	0.054	0.591	0.564	0.501	0.022	0.449	0.552	0.460
Sum	4.995	5.018	5.017	5.014	5.018	5.013	5.003	5.014	5.003	5.012	5.019	5.012	5.014	5.012
Ab (mol%)	42.6	52.8	51.2	20.3	11.6	31.3	69.6	41.0	43.0	47.7	48.0	51.8	44.3	51.3
An (mol%)	49.1	43.7	45.6	79.1	88.1	67.5	25.0	1.0	1.2	2.9	49.8	4.1	1.6	3.4
Or (mol%)	8.4	3.5	3.1	0.6	0.4	1.2	5.4	58.0	55.9	49.4	2.2	44.2	54.1	45.3

Table D6 Feldspar analyses of the 2010 Merapi eruption (continued)

Sample	M11-27-3	M11-27-4	M11-27-4	M11-27-4	M11-27-4	M11-27-4	M11-27-4	M11-27-4	M11-27-4	M11-28a	M11-28a	M11-28a	M11-28a	M11-28a
Sample Type	LG-Inc	LG-Inc	LG-Inc	LG-Inc	LG-Inc	LG-Inc	LG-Inc	LG-Inc	LG-Inc	P5N-Sc	P5N-Sc	P5N-Sc	P5N-Sc	P5N-Sc
Point	36 / 1 .	76 / 1 .	78 / 1 .	80 / 1 .	81 / 1 .	87 / 1 .	88 / 1 .	90 / 1 .	92 / 1 .	15 / 1 .	16 / 1 .	17 / 1 .	18 / 1 .	19 / 1 .
Comment	m	ph-c	m	m	m	m	m	m	m	ph-r	ph-r	ph-r	ph-r	m
SiO_2	57.59	46.52	60.92	65.49	59.58	65.37	66.44	65.85	65.79	55.09	58.60	57.14	56.18	56.57
TiO_2	0.04	0.02	0.01	0.00	0.06	0.04	0.04	0.02	0.02	0.02	0.03	0.02	0.02	0.02
Al_2O_3	26.89	33.75	25.11	19.22	25.03	19.10	18.78	18.55	18.24	27.75	25.12	26.66	27.19	27.76
FeO	0.62	0.61	0.41	0.37	0.59	0.26	0.41	0.25	0.14	0.47	0.47	0.45	0.45	0.48
MgO	0.02	0.01	0.01	0.00	0.02	0.00	0.00	0.00	0.00	0.04	0.04	0.04	0.04	0.04
CaO	9.11	17.36	6.68	0.89	7.80	0.63	0.46	0.41	0.30	10.54	7.66	8.94	9.63	9.77
SrO	0.13	0.16	0.04	0.00	0.02	0.00	0.00	0.00	0.00	0.10	0.07	0.09	0.11	0.12
BaO										0.02	0.12	0.07	0.08	0.07
Na_2O	6.25	1.63	7.46	6.25	6.40	5.58	5.65	5.50	5.21	5.25	6.82	6.00	5.59	5.70
K_2O	0.51	0.06	0.90	7.50	0.89	8.58	8.87	8.87	9.48	0.46	0.80	0.57	0.53	0.54
Sum	101.15	100.13	101.52	99.72	100.39	99.55	100.65	99.45	99.18	99.74	99.73	99.98	99.81	101.07
Si	2.566	2.144	2.684	2.959	2.660	2.966	2.984	2.991	3.001	2.498	2.641	2.572	2.538	2.526
Al	1.412	1.833	1.304	1.023	1.317	1.021	0.994	0.993	0.980	1.483	1.334	1.414	1.448	1.461
Ti	0.001	0.001	0.000	0.000	0.002	0.001	0.001	0.001	0.001	0.001	0.001	0.001	0.001	0.001
Fe	0.023	0.024	0.015	0.014	0.022	0.010	0.016	0.009	0.005	0.018	0.018	0.017	0.017	0.018
Mg	0.001	0.001	0.000	0.000	0.001	0.000	0.000	0.000	0.000	0.003	0.002	0.003	0.003	0.003
Sr	0.003	0.004	0.001	0.000	0.000	0.000	0.000	0.000	0.000	0.003	0.002	0.002	0.003	0.003
Ba	0.000	0.000	0.000	0.000	0.000	0.000	0.000	0.000	0.000	0.000	0.002	0.001	0.001	0.001
Ca	0.435	0.857	0.315	0.043	0.373	0.031	0.022	0.020	0.015	0.512	0.370	0.431	0.466	0.467
Na	0.540	0.146	0.637	0.548	0.554	0.490	0.492	0.484	0.461	0.461	0.596	0.523	0.490	0.494
K	0.029	0.004	0.051	0.432	0.051	0.497	0.508	0.514	0.552	0.027	0.046	0.033	0.031	0.031
Sum	5.011	5.013	5.008	5.019	4.981	5.016	5.017	5.011	5.015	5.004	5.012	4.998	4.998	5.005
Ab (mol%)	53.8	14.5	63.5	53.5	56.6	48.2	48.1	47.6	44.9	46.1	58.9	53.0	49.7	49.8
An (mol%)	43.3	85.2	31.4	4.2	38.2	3.0	2.2	2.0	1.4	51.2	36.5	43.7	47.2	47.1
Or (mol%)	2.9	0.4	5.0	42.2	5.2	48.8	49.7	50.5	53.7	2.7	4.6	3.3	3.1	3.1

Table D6 Feldspar analyses of the 2010 Merapi eruption (continued)

Sample	M11-28a	M11-28a	M11-28a	M11-28a	M11-28a	M11-28a	M11-28a	M11-28a	M11-28a	M11-28a	M11-28a	M11-28b	M11-28b	M11-28b
Sample Type	P5N-Sc	P5N-Sc	P5N-Sc	P5N-Sc	P5N-Sc	P5N-Sc	P5N-Sc	P5N-Sc	P5N-Sc	P5N-Sc	P5N-Sc	P5N-LGD	P5N-LGD	P5N-LGD
Point	20 / 1 .	21 / 1 .	22 / 1 .	30 / 1 .	6 / 1 .	7 / 1 .	8 / 1 .	9 / 1 .	11 / 1 .	12 / 1 .	15 / 1 .	6 / 1 .	7 / 1 .	8 / 1 .
Comment	m	m	m	m	m	m	m	m	m	m	m	ph-r	ph-r	ph-r
SiO_2	51.20	60.88	51.97	52.94	48.19	51.46	54.42	47.69	48.88	48.01	62.18	57.08	52.47	57.09
TiO_2	0.02	0.05	0.02	0.02	0.00	0.04	0.01	0.01	0.03	0.02	0.05	0.03	0.02	0.03
Al_2O_3	30.85	24.22	30.15	29.06	32.80	30.72	28.52	32.34	31.77	32.18	23.11	26.94	30.04	25.43
FeO	0.48	0.56	0.55	0.51	0.59	0.51	0.45	0.57	0.63	0.58	0.51	0.53	0.54	0.54
MgO	0.05	0.05	0.05	0.04	0.07	0.07	0.05	0.06	0.08	0.07	0.04	0.03	0.03	0.06
CaO	14.10	6.36	13.26	12.24	16.20	13.95	11.19	16.04	15.49	16.07	5.39	9.37	13.01	8.99
SrO	0.12	0.07	0.11	0.11								0.10	0.12	0.10
BaO	0.00	0.07	0.00	0.00								0.08	0.03	0.05
Na_2O	3.48	7.11	3.87	4.44	2.20	3.48	4.91	2.20	2.38	2.26	7.31	5.96	4.11	5.98
K_2O	0.20	1.41	0.23	0.35	0.10	0.19	0.38	0.12	0.18	0.10	1.66	0.62	0.31	0.73
Sum	100.50	100.79	100.20	99.73	100.15	100.42	99.92	99.03	99.43	99.29	100.25	100.74	100.68	99.00
Si	2.326	2.708	2.363	2.413	2.209	2.336	2.464	2.211	2.252	2.220	2.768	2.556	2.375	2.600
Al	1.651	1.269	1.615	1.561	1.772	1.643	1.522	1.767	1.725	1.754	1.212	1.422	1.602	1.364
Ti	0.001	0.002	0.001	0.001	0.000	0.001	0.000	0.000	0.001	0.001	0.002	0.001	0.001	0.001
Fe	0.018	0.021	0.021	0.020	0.022	0.020	0.017	0.022	0.024	0.022	0.019	0.020	0.020	0.020
Mg	0.004	0.003	0.004	0.003	0.005	0.005	0.004	0.004	0.005	0.005	0.002	0.002	0.002	0.004
Sr	0.003	0.002	0.003	0.003	0.000	0.000	0.000	0.000	0.000	0.000	0.000	0.002	0.003	0.003
Ba	0.000	0.001	0.000	0.000	0.000	0.000	0.000	0.000	0.000	0.000	0.000	0.001	0.001	0.001
Ca	0.686	0.303	0.646	0.598	0.796	0.678	0.543	0.797	0.765	0.796	0.257	0.449	0.631	0.439
Na	0.306	0.613	0.341	0.393	0.196	0.307	0.431	0.198	0.213	0.202	0.631	0.518	0.360	0.528
K	0.012	0.080	0.014	0.021	0.006	0.011	0.022	0.007	0.011	0.006	0.094	0.035	0.018	0.043
Sum	5.007	5.002	5.006	5.012	5.006	5.000	5.002	5.007	4.996	5.007	4.987	5.008	5.012	5.002
Ab (mol%)	30.5	61.6	34.1	38.8	19.6	30.8	43.3	19.8	21.5	20.1	64.2	51.7	35.7	52.3
An (mol%)	68.3	30.4	64.6	59.1	79.8	68.1	54.5	79.5	77.4	79.3	26.2	44.8	62.5	43.5
Or (mol%)	1.2	8.0	1.3	2.0	0.6	1.1	2.2	0.7	1.1	0.6	9.6	3.5	1.8	4.2

Table D6 Feldspar analyses of the 2010 Merapi eruption (continued)

Sample	M11-28b	M11-28b	M11-33	M11-33	M11-33	M11-33	M11-33	M11-33	M11-38	M11-38	M11-38	M11-38	M11-38	M11-38
Sample Type	P5N-LGD	P5N-LGD	WP	WP	WP	WP	WP	WP	DD	DD	DD	DD	DD	LG-Inc
Point	10 / 1 .	19 / 1 .	20 / 1 .	21 / 1 .	22 / 1 .	41 / 1 .	44 / 1 .	47 / 1 .	27 / 1 .	28 / 1 .	29 / 1 .	30 / 1 .	32 / 1 .	47 / 1 .
Comment	ph-r	m	ph	ph-c	ph-r	m	m	m	m	m	m	m	m	m
SiO_2	58.26	57.14	45.33	45.15	56.98	57.50	58.82	57.56	51.73	60.57	52.65	56.63	53.89	66.02
TiO_2	0.02	0.03	0.02	0.04	0.01	0.02	0.03	0.02	0.05	0.11	0.05	0.03	0.04	0.00
Al_2O_3	26.26	26.95	33.78	33.73	26.42	26.17	23.58	25.69	29.88	24.38	29.13	27.87	27.51	20.30
FeO	0.51	0.59	0.49	0.56	0.45	0.48	0.90	0.50	0.80	1.09	0.77	0.68	0.70	0.27
MgO	0.03	0.01	0.01	0.03	0.03	0.03	0.69	0.03	0.08	0.17	0.08	0.05	0.10	0.00
CaO	8.49	9.50	17.76	17.66	8.53	8.17	6.94	7.68	13.16	7.33	12.43	10.14	10.55	1.05
SrO	0.07	0.06	0.08	0.10	0.09	0.10	0.07	0.11	0.13	0.06	0.10	0.10	0.12	0.03
BaO	0.07	0.02												
Na_2O	6.42	5.91	1.35	1.27	6.33	6.44	6.55	6.57	3.91	5.95	4.18	5.18	4.91	5.56
K_2O	0.74	0.61	0.06	0.04	0.62	0.80	1.21	0.95	0.26	1.84	0.43	0.71	0.66	8.13
Sum	100.89	100.82	98.87	98.57	99.46	99.72	98.79	99.12	99.99	101.51	99.82	101.39	98.47	101.38
Si	2.599	2.556	2.118	2.116	2.578	2.594	2.677	2.612	2.361	2.686	2.402	2.522	2.481	2.936
Al	1.381	1.421	1.860	1.863	1.409	1.392	1.265	1.374	1.607	1.274	1.566	1.463	1.493	1.064
Ti	0.001	0.001	0.001	0.001	0.000	0.001	0.001	0.001	0.002	0.004	0.002	0.001	0.001	0.000
Fe	0.019	0.022	0.019	0.022	0.017	0.018	0.034	0.019	0.031	0.041	0.029	0.025	0.027	0.010
Mg	0.002	0.001	0.000	0.002	0.002	0.002	0.047	0.002	0.006	0.011	0.006	0.003	0.007	0.000
Sr	0.002	0.002	0.002	0.003	0.002	0.003	0.002	0.003	0.003	0.002	0.003	0.002	0.003	0.001
Ba	0.001	0.000	0.000	0.000	0.000	0.000	0.000	0.000	0.000	0.000	0.000	0.000	0.000	0.000
Ca	0.406	0.455	0.889	0.887	0.413	0.395	0.339	0.373	0.643	0.348	0.608	0.484	0.520	0.050
Na	0.556	0.513	0.122	0.115	0.555	0.563	0.578	0.578	0.346	0.512	0.370	0.447	0.438	0.480
K	0.042	0.035	0.003	0.003	0.036	0.046	0.070	0.055	0.015	0.104	0.025	0.041	0.039	0.461
Sum	5.009	5.006	5.014	5.011	5.013	5.014	5.013	5.017	5.014	4.981	5.010	4.989	5.010	5.002
Ab (mol%)	55.4	51.1	12.0	11.5	55.3	56.1	58.5	57.4	34.5	53.1	36.9	46.0	43.9	48.4
An (mol%)	40.4	45.4	87.6	88.3	41.2	39.3	34.3	37.1	64.0	36.1	60.6	49.8	52.2	5.1
Or (mol%)	4.2	3.5	0.3	0.3	3.6	4.6	7.1	5.5	1.5	10.8	2.5	4.2	3.9	46.5

Table D6 Feldspar analyses of the 2010 Merapi eruption (continued)

Sample	M11-38	M11-38	M11-38	M11-38	M11-38	M11-38	M11-38	M11-48	M11-48	M11-48	M11-48	M11-48	M11-48	M11-48
Sample Type	LG-Inc	LG-Inc	LG-Inc	LG-Inc	LG-Inc	LG-Inc	LG-Inc	DD	DD	LG-Inc	LG-Inc	LG-Inc	LG-Inc	LG-Inc
Point	48 / 1 .	50 / 1 .	51 / 1 .	52 / 1 .	53 / 1 .	55 / 1 .	56 / 1 .	37 / 1 .	40 / 1 .	16 / 1 .	17 / 1 .	18 / 1 .	21 / 1 .	22 / 1 .
Comment	m	m	m	m	m	m	m	m	m	m	m	m	m	m
SiO_2	62.79	65.37	60.83	66.14	65.73	65.59	66.23	54.89	53.71	60.12	65.59	66.62	65.41	66.66
TiO_2	0.04	0.02	0.04	0.00	0.00	0.00	0.03	0.00	0.06	0.00	0.00	0.00	0.03	0.06
Al_2O_3	23.23	20.89	25.44	20.13	20.09	19.51	19.04	27.46	29.13	23.93	19.60	19.49	18.92	19.59
FeO	0.42	0.35	0.48	0.29	0.27	0.27	0.35	0.65	0.78	0.49	0.40	0.28	0.24	0.42
MgO	0.01	0.00	0.01	0.00	0.00	0.00	0.00	0.04	0.08	0.02	0.00	0.00	0.00	0.00
CaO	4.47	1.78	6.19	0.87	0.94	0.74	0.39	10.13	12.26	5.93	1.17	0.75	0.60	0.78
SrO	0.01	0.01	0.00	0.00	0.01	0.00	0.01	0.10	0.09	0.04	0.03	0.01	0.00	0.00
BaO														
Na_2O	7.59	6.49	7.33	5.30	5.47	5.23	4.73	5.30	4.21	7.52	5.87	5.83	5.55	5.76
K_2O	2.19	6.50	1.07	8.78	8.30	9.11	9.82	0.55	0.72	1.00	7.91	8.27	8.40	8.45
Sum	100.76	101.42	101.39	101.51	100.80	100.46	100.60	99.13	101.03	99.07	100.57	101.25	99.15	101.72
Si	2.781	2.900	2.681	2.943	2.941	2.955	2.981	2.504	2.421	2.713	2.945	2.966	2.975	2.960
Al	1.213	1.092	1.321	1.056	1.059	1.036	1.010	1.477	1.547	1.273	1.037	1.023	1.014	1.025
Ti	0.001	0.001	0.001	0.000	0.000	0.000	0.001	0.000	0.002	0.000	0.000	0.000	0.001	0.002
Fe	0.016	0.013	0.018	0.011	0.010	0.010	0.013	0.025	0.029	0.019	0.015	0.010	0.009	0.016
Mg	0.001	0.000	0.001	0.000	0.000	0.000	0.000	0.003	0.005	0.001	0.000	0.000	0.000	0.000
Sr	0.000	0.000	0.000	0.000	0.000	0.000	0.000	0.003	0.002	0.001	0.001	0.000	0.000	0.000
Ba	0.000	0.000	0.000	0.000	0.000	0.000	0.000	0.000	0.000	0.000	0.000	0.000	0.000	0.000
Ca	0.212	0.084	0.293	0.041	0.045	0.036	0.019	0.495	0.592	0.287	0.056	0.036	0.029	0.037
Na	0.652	0.558	0.626	0.458	0.474	0.457	0.413	0.469	0.368	0.658	0.511	0.503	0.490	0.495
K	0.124	0.368	0.060	0.498	0.474	0.524	0.564	0.032	0.041	0.058	0.453	0.470	0.487	0.479
Sum	5.000	5.016	5.001	5.007	5.003	5.018	5.001	5.007	5.008	5.009	5.018	5.008	5.006	5.013
Ab (mol%)	66.0	55.2	64.0	45.9	47.8	45.0	41.5	47.0	36.7	65.6	50.1	49.9	48.7	49.0
An (mol%)	21.5	8.4	29.9	4.1	4.5	3.5	1.9	49.7	59.1	28.6	5.5	3.6	2.9	3.7
Or (mol%)	12.5	36.4	6.1	50.0	47.7	51.5	56.6	3.2	4.1	5.8	44.4	46.6	48.4	47.3

Table D6 Feldspar analyses of the 2010 Merapi eruption (continued)

Sample	M11-50	M11-50	M11-50	M11-50	M11-51	M11-51	M11-51	M11-51	M11-51	M11-51	M11-51	M11-53-B3	M11-53-B3	M11-53-B3
Sample Type	WP	WP	WP	WP	GS	GS	GS	GS	GS	GS	GS	DS	DS	DS
Point	78 / 1 .	79 / 1 .	84 / 1 .	85 / 1 .	62 / 1 .	63 / 1 .	64 / 1 .	68 / 1 .	69 / 1 .	70 / 1 .	71 / 1 .	8 / 1 .	9 / 1 .	10 / 1 .
Comment	m	m	m	m	m	m	m	m	m	m	m	ph	m	m
SiO_2	58.45	65.04	61.11	59.40	53.94	53.78	53.09	51.02	52.90	53.42	58.72	47.67	51.61	52.19
TiO_2	0.05	0.04	0.06	0.04	0.02	0.04	0.04	0.03	0.02	0.05	0.03	0.00	0.04	0.02
Al_2O_3	25.93	20.91	24.80	25.34	28.19	28.16	28.91	29.62	28.60	28.61	25.66	32.60	29.72	29.48
FeO	0.48	0.35	0.49	0.45	0.73	0.75	0.74	0.77	0.48	0.73	0.67	0.56	0.80	0.80
MgO	0.04	0.00	0.01	0.03	0.07	0.06	0.07	0.10	0.03	0.09	0.25	0.02	0.08	0.10
CaO	8.20	2.58	6.59	7.61	10.89	11.25	11.85	13.17	11.67	11.57	7.68	16.15	12.77	12.72
SrO					0.16	0.15	0.12	0.15	0.11	0.18	0.08	0.12	0.12	0.14
BaO														
Na_2O	6.24	6.89	6.98	6.60	4.97	4.80	4.44	3.74	4.52	4.60	6.51	2.28	3.95	4.03
K_2O	0.83	4.62	1.19	1.03	0.40	0.45	0.34	0.30	0.42	0.35	0.98	0.11	0.26	0.33
Sum	100.22	100.43	101.21	100.50	99.38	99.43	99.61	98.90	98.74	99.60	100.58	99.52	99.36	99.78
Si	2.618	2.894	2.699	2.650	2.462	2.456	2.422	2.356	2.432	2.436	2.625	2.203	2.368	2.384
Al	1.369	1.097	1.291	1.333	1.516	1.516	1.554	1.612	1.549	1.538	1.352	1.776	1.607	1.587
Ti	0.002	0.001	0.002	0.001	0.001	0.002	0.001	0.001	0.001	0.002	0.001	0.000	0.001	0.001
Fe	0.018	0.013	0.018	0.017	0.028	0.028	0.028	0.030	0.018	0.028	0.025	0.022	0.031	0.030
Mg	0.003	0.000	0.001	0.002	0.005	0.004	0.005	0.007	0.002	0.006	0.017	0.001	0.006	0.007
Sr	0.000	0.000	0.000	0.000	0.004	0.004	0.003	0.004	0.003	0.005	0.002	0.003	0.003	0.004
Ba	0.000	0.000	0.000	0.000	0.000	0.000	0.000	0.000	0.000	0.000	0.000	0.000	0.000	0.000
Ca	0.393	0.123	0.312	0.364	0.533	0.550	0.579	0.652	0.574	0.565	0.368	0.800	0.628	0.622
Na	0.542	0.595	0.598	0.571	0.440	0.425	0.393	0.335	0.402	0.407	0.564	0.204	0.351	0.356
K	0.048	0.262	0.067	0.059	0.023	0.026	0.020	0.018	0.025	0.020	0.056	0.007	0.015	0.019
Sum	4.991	4.985	4.986	4.996	5.011	5.010	5.006	5.014	5.007	5.007	5.008	5.015	5.011	5.010
Ab (mol%)	55.1	60.7	61.2	57.5	44.2	42.4	39.6	33.3	40.2	41.0	57.1	20.2	35.3	35.7
An (mol%)	40.0	12.6	31.9	36.6	53.5	55.0	58.4	64.9	57.4	57.0	37.2	79.1	63.1	62.4
Or (mol%)	4.8	26.7	6.8	5.9	2.4	2.6	2.0	1.8	2.4	2.1	5.7	0.7	1.5	1.9

Table D6 Feldspar analyses of the 2010 Merapi eruption (continued)

Sample	M11-53-B3	M11-53-B3	M11-53-B3	M11-53-B3	M11-53-B3	M11-53-B3	M11-53-B3	M11-53-B3	M11-53-B4	M11-53-B4	M11-53-B4	M11-53-B4	M11-53-B4	M11-53-B4
Sample Type	DS	DS	DS	DS	DS	DS	DS	DS	WP	WP	WP	WP	WP	WP
Point	11 / 1 .	12 / 1 .	13 / 1 .	14 / 1 .	15 / 1 .	16 / 1 .	17 / 1 .	18 / 1 .	65 / 1 .	66 / 1 .	67 / 1 .	68 / 1 .	69 / 1 .	70 / 1 .
Comment	m	m	m	m	m	m	m	m	m	m	m	m	m	m
SiO_2	53.81	55.82	55.84	50.14	54.46	56.28	55.23	51.14	64.51	62.50	56.33	63.49	65.78	61.86
TiO_2	0.03	0.02	0.04	0.04	0.03	0.02	0.04	0.02	0.00	0.02	0.03	0.00	0.01	0.02
Al_2O_3	28.42	27.48	26.82	30.30	27.66	27.28	27.96	29.86	21.27	22.93	26.52	21.75	20.78	23.33
FeO	0.51	0.53	0.60	0.56	0.66	0.50	0.74	0.76	0.37	0.48	0.55	0.47	0.45	0.61
MgO	0.04	0.04	0.06	0.04	0.08	0.04	0.07	0.08	0.00	0.01	0.03	0.01	0.01	0.01
CaO	11.21	9.86	9.30	13.54	10.93	9.38	10.35	13.10	2.37	4.12	9.18	3.01	1.65	4.74
SrO	0.14	0.12	0.12	0.14	0.11	0.12	0.11	0.14	0.05	0.06	0.07	0.08	0.00	0.06
BaO														
Na_2O	4.83	5.57	5.73	3.48	4.93	5.91	5.45	3.81	6.57	7.20	5.85	6.95	6.16	7.24
K_2O	0.41	0.51	0.57	0.24	0.52	0.59	0.49	0.23	5.39	3.19	0.62	4.24	6.43	2.36
Sum	99.41	99.95	99.08	98.47	99.37	100.13	100.43	99.13	100.52	100.51	99.19	100.00	101.27	100.25
Si	2.454	2.521	2.543	2.325	2.484	2.536	2.490	2.354	2.878	2.786	2.560	2.845	2.915	2.762
Al	1.528	1.463	1.439	1.656	1.487	1.449	1.486	1.620	1.118	1.205	1.421	1.148	1.085	1.228
Ti	0.001	0.001	0.001	0.001	0.001	0.001	0.001	0.001	0.000	0.001	0.001	0.000	0.000	0.001
Fe	0.019	0.020	0.023	0.022	0.025	0.019	0.028	0.029	0.014	0.018	0.021	0.018	0.017	0.023
Mg	0.003	0.003	0.004	0.003	0.006	0.003	0.005	0.005	0.000	0.001	0.002	0.001	0.001	0.001
Sr	0.004	0.003	0.003	0.004	0.003	0.003	0.003	0.004	0.001	0.002	0.002	0.002	0.000	0.002
Ba	0.000	0.000	0.000	0.000	0.000	0.000	0.000	0.000	0.000	0.000	0.000	0.000	0.000	0.000
Ca	0.548	0.477	0.454	0.672	0.534	0.453	0.500	0.646	0.113	0.197	0.447	0.144	0.078	0.227
Na	0.427	0.488	0.506	0.312	0.436	0.516	0.476	0.340	0.568	0.622	0.515	0.604	0.530	0.627
K	0.024	0.029	0.033	0.014	0.030	0.034	0.028	0.013	0.307	0.181	0.036	0.242	0.364	0.135
Sum	5.007	5.005	5.006	5.009	5.005	5.014	5.018	5.012	5.000	5.012	5.005	5.004	4.989	5.004
Ab (mol%)	42.8	49.1	50.9	31.3	43.6	51.4	47.4	34.0	57.5	62.2	51.6	61.0	54.5	63.4
An (mol%)	54.8	48.0	45.7	67.3	53.4	45.2	49.8	64.6	11.5	19.7	44.8	14.6	8.1	23.0
Or (mol%)	2.4	2.9	3.3	1.4	3.0	3.4	2.8	1.3	31.0	18.1	3.6	24.5	37.4	13.6

Table D6 Feldspar analyses of the 2010 Merapi eruption (continued)

Sample	M11-53-B4	M11-53-B4	M11-54-3	M11-54-3	M11-54-3	M11-54-3	M11-54-3	M11-54-3	M11-54-3	M11-54-3	M11-54-3	M11-54-3	M11-54-3	M11-54-3
Sample Type	WP	WP	DD	DD	DD	DD	DD	DD	DD	DD	DD	DD	DD	DD
Point	71 / 1 .	74 / 1 .	1 / 1 .	1 / 2 .	1 / 3 .	1 / 4 .	1 / 5 .	1 / 6 .	1 / 7 .	1 / 8 .	1 / 9 .	1 / 11 .	1 / 12 .	1 / 13 .
Comment	m	m	ph-c	ph	ph	ph	ph	ph	ph	ph	ph	ph	ph	ph
SiO_2	63.14	64.08	48.22	47.68	48.23	48.47	48.10	47.91	47.56	47.52	48.73	48.29	50.16	47.70
TiO_2	0.01	0.01	0.02	0.01	0.03	0.00	0.00	0.04	0.01	0.03	0.00	0.01	0.04	0.06
Al_2O_3	22.72	21.62	33.28	33.45	32.90	32.63	33.27	32.86	33.38	33.46	32.80	33.19	31.66	33.28
FeO	0.42	0.37	0.51	0.56	0.58	0.52	0.51	0.52	0.55	0.55	0.55	0.57	0.55	0.52
MgO	0.01	0.00	0.05	0.05	0.04	0.04	0.04	0.03	0.05	0.05	0.05	0.05	0.06	0.05
CaO	3.66	2.55	16.27	16.80	16.25	16.09	16.40	16.36	16.54	16.68	16.17	16.15	14.84	16.51
SrO	0.03	0.01												
BaO														
Na_2O	7.16	6.96	2.05	1.80	2.01	2.17	1.95	1.86	1.90	1.71	2.13	2.11	2.81	1.94
K_2O	3.44	4.93	0.13	0.10	0.13	0.14	0.12	0.12	0.12	0.11	0.15	0.14	0.26	0.13
Sum	100.57	100.53	100.52	100.44	100.17	100.06	100.39	99.70	100.11	100.10	100.57	100.50	100.38	100.19
Si	2.808	2.858	2.201	2.182	2.209	2.221	2.198	2.205	2.183	2.180	2.222	2.204	2.284	2.187
Al	1.191	1.137	1.790	1.804	1.776	1.762	1.792	1.782	1.805	1.810	1.763	1.786	1.699	1.798
Ti	0.000	0.000	0.001	0.000	0.001	0.000	0.000	0.001	0.000	0.001	0.000	0.000	0.001	0.002
Fe	0.016	0.014	0.020	0.022	0.022	0.020	0.019	0.020	0.021	0.021	0.021	0.022	0.021	0.020
Mg	0.000	0.000	0.003	0.003	0.003	0.003	0.003	0.002	0.004	0.003	0.003	0.003	0.004	0.004
Sr	0.001	0.000	0.000	0.000	0.000	0.000	0.000	0.000	0.000	0.000	0.000	0.000	0.000	0.000
Ba	0.000	0.000	0.000	0.000	0.000	0.000	0.000	0.000	0.000	0.000	0.000	0.000	0.000	0.000
Ca	0.174	0.122	0.795	0.823	0.798	0.790	0.803	0.806	0.813	0.820	0.790	0.790	0.724	0.811
Na	0.617	0.602	0.181	0.159	0.178	0.192	0.173	0.166	0.169	0.152	0.188	0.186	0.248	0.173
K	0.195	0.281	0.008	0.006	0.008	0.008	0.007	0.007	0.007	0.006	0.009	0.008	0.015	0.008
Sum	5.002	5.014	4.998	4.999	4.994	4.998	4.995	4.989	5.003	4.993	4.995	5.000	4.997	5.002
Ab (mol%)	62.6	59.9	18.4	16.1	18.1	19.4	17.6	16.9	17.1	15.5	19.1	18.9	25.1	17.4
An (mol%)	17.7	12.2	80.8	83.3	81.1	79.8	81.7	82.4	82.2	83.8	80.1	80.2	73.3	81.8
Or (mol%)	19.8	27.9	0.8	0.6	0.8	0.8	0.7	0.7	0.7	0.6	0.9	0.8	1.5	0.8

Table D6 Feldspar analyses of the 2010 Merapi eruption (continued)

Sample	M11-54-3	M11-54-3	M11-54-3	M11-54-3	M11-54-3	M11-54-3	M11-54-3	M11-54-3	M11-54-3	M11-54-3	M11-54-3	M11-54-3	M11-54-3	M11-54-3
Sample Type	DD	DD	DD	DD	DD	DD	DD	DD	DD	DD	DD	DD	DD	DD
Point	1 / 14 .	1 / 15 .	1 / 16 .	1 / 17 .	1 / 18 .	1 / 19 .	1 / 20 .	1 / 21 .	1 / 22 .	1 / 23 .	1 / 24 .	1 / 25 .	1 / 26 .	1 / 27 .
Comment	ph	ph	ph	ph	ph	ph	ph	ph	ph	ph	ph	ph	ph	ph
SiO_2	48.68	51.17	49.02	48.31	48.24	48.22	48.58	48.76	48.65	50.03	48.45	49.21	49.63	49.79
TiO_2	0.04	0.06	0.02	0.03	0.03	0.03	0.02	0.00	0.02	0.04	0.00	0.00	0.01	0.04
Al_2O_3	32.65	30.85	32.36	32.63	32.48	32.97	33.15	32.26	32.45	31.80	32.52	32.83	31.24	32.02
FeO	0.52	0.52	0.53	0.53	0.53	0.54	0.53	0.53	0.53	0.53	0.54	0.53	0.55	0.53
MgO	0.04	0.04	0.05	0.05	0.05	0.04	0.05	0.06	0.06	0.05	0.03	0.03	0.04	0.04
CaO	16.14	13.98	15.69	15.92	16.00	16.21	16.20	15.85	15.86	14.98	16.19	16.24	15.19	15.50
SrO														
BaO														
Na_2O	2.24	3.20	2.51	2.11	2.10	1.97	2.12	2.34	2.29	2.80	2.33	2.21	2.85	2.95
K_2O	0.15	0.34	0.18	0.14	0.13	0.12	0.14	0.14	0.14	0.17	0.15	0.12	0.22	0.22
Sum	100.44	100.16	100.35	99.72	99.54	100.10	100.79	99.93	100.00	100.40	100.22	101.16	99.72	101.08
Si	2.223	2.329	2.239	2.220	2.222	2.209	2.211	2.236	2.230	2.278	2.220	2.230	2.279	2.259
Al	1.757	1.655	1.742	1.767	1.763	1.780	1.778	1.744	1.753	1.706	1.756	1.753	1.691	1.712
Ti	0.001	0.002	0.001	0.001	0.001	0.001	0.001	0.000	0.001	0.001	0.000	0.000	0.000	0.001
Fe	0.020	0.020	0.020	0.020	0.020	0.021	0.020	0.020	0.020	0.020	0.021	0.020	0.021	0.020
Mg	0.003	0.003	0.003	0.003	0.003	0.003	0.003	0.004	0.004	0.003	0.002	0.002	0.002	0.003
Sr	0.000	0.000	0.000	0.000	0.000	0.000	0.000	0.000	0.000	0.000	0.000	0.000	0.000	0.000
Ba	0.000	0.000	0.000	0.000	0.000	0.000	0.000	0.000	0.000	0.000	0.000	0.000	0.000	0.000
Ca	0.789	0.682	0.768	0.784	0.789	0.795	0.790	0.779	0.779	0.731	0.795	0.788	0.747	0.753
Na	0.198	0.282	0.222	0.188	0.187	0.175	0.187	0.208	0.204	0.247	0.207	0.194	0.254	0.259
K	0.009	0.020	0.010	0.008	0.008	0.007	0.008	0.008	0.008	0.010	0.009	0.007	0.013	0.013
Sum	5.000	4.993	5.006	4.993	4.993	4.991	4.997	5.000	4.999	4.996	5.010	4.994	5.008	5.020
Ab (mol%)	19.9	28.7	22.2	19.2	19.0	17.9	19.0	20.9	20.6	25.0	20.5	19.6	25.1	25.3
An (mol%)	79.2	69.3	76.8	80.0	80.2	81.4	80.2	78.3	78.6	74.0	78.7	79.7	73.7	73.5
Or (mol%)	0.9	2.0	1.0	0.8	0.8	0.7	0.8	0.8	0.8	1.0	0.8	0.7	1.3	1.3

Table D6 Feldspar analyses of the 2010 Merapi eruption (continued)

Sample	M11-54-3	M11-54-3	M11-54-3	M11-54-3	M11-54-3	M11-54-3	M11-54-3	M11-54-3	M11-54-3	M11-54-3	M11-54-3	M11-54-3	M11-54-3	M11-54-3
Sample Type	DD	DD	DD	DD	DD	DD	DD	DD	DD	DD	DD	DD	DD	DD
Point	1 / 28 .	1 / 29 .	1 / 30 .	1 / 31 .	1 / 32 .	1 / 34 .	1 / 35 .	1 / 36 .	1 / 37 .	1 / 38 .	1 / 40 .	1 / 41 .	1 / 42 .	1 / 44 .
Comment	ph	ph	ph	ph	ph	ph	ph	ph	ph	ph	ph	ph	ph	ph
SiO_2	50.16	50.56	50.39	47.73	47.74	47.49	48.75	47.80	47.02	49.68	51.14	51.12	49.59	46.84
TiO_2	0.03	0.05	0.03	0.00	0.03	0.02	0.03	0.11	0.07	0.00	0.03	0.03	0.03	0.04
Al_2O_3	32.02	31.39	31.66	33.50	33.42	33.59	32.96	31.67	33.83	31.98	31.16	30.81	32.17	33.97
FeO	0.52	0.48	0.50	0.55	0.50	0.51	0.56	0.82	0.53	0.53	0.50	0.49	0.53	0.52
MgO	0.04	0.03	0.05	0.04	0.04	0.03	0.03	0.08	0.04	0.04	0.05	0.04	0.05	0.05
CaO	15.31	14.86	14.69	16.69	16.45	16.90	16.14	15.50	17.07	15.37	14.00	13.94	15.69	17.27
SrO														
BaO														
Na_2O	2.96	2.98	2.88	1.75	1.88	1.78	2.12	2.19	1.54	2.60	3.08	3.24	2.77	1.51
K_2O	0.17	0.18	0.19	0.09	0.10	0.09	0.17	0.19	0.08	0.18	0.28	0.24	0.20	0.10
Sum	101.20	100.52	100.39	100.34	100.15	100.40	100.77	98.37	100.17	100.38	100.23	99.90	101.02	100.29
Si	2.269	2.297	2.291	2.184	2.188	2.174	2.218	2.231	2.158	2.265	2.324	2.331	2.251	2.150
Al	1.707	1.681	1.697	1.807	1.805	1.812	1.768	1.742	1.830	1.718	1.669	1.656	1.721	1.837
Ti	0.001	0.002	0.001	0.000	0.001	0.001	0.001	0.004	0.002	0.000	0.001	0.001	0.001	0.001
Fe	0.020	0.018	0.019	0.021	0.019	0.019	0.021	0.032	0.020	0.020	0.019	0.019	0.020	0.020
Mg	0.002	0.002	0.003	0.003	0.003	0.002	0.002	0.006	0.003	0.003	0.003	0.003	0.003	0.003
Sr	0.000	0.000	0.000	0.000	0.000	0.000	0.000	0.000	0.000	0.000	0.000	0.000	0.000	0.000
Ba	0.000	0.000	0.000	0.000	0.000	0.000	0.000	0.000	0.000	0.000	0.000	0.000	0.000	0.000
Ca	0.742	0.723	0.716	0.818	0.808	0.829	0.787	0.775	0.840	0.750	0.681	0.681	0.763	0.849
Na	0.259	0.262	0.254	0.155	0.167	0.158	0.187	0.198	0.137	0.230	0.271	0.286	0.243	0.134
K	0.010	0.010	0.011	0.005	0.006	0.005	0.010	0.012	0.005	0.010	0.016	0.014	0.011	0.006
Sum	5.011	4.997	4.992	4.993	4.995	5.001	4.995	4.999	4.995	4.997	4.984	4.990	5.015	5.001
Ab (mol%)	25.6	26.3	25.9	15.8	17.0	15.9	19.0	20.1	14.0	23.2	28.0	29.2	23.9	13.6
An (mol%)	73.4	72.6	73.0	83.6	82.4	83.5	80.0	78.7	85.5	75.7	70.4	69.4	75.0	85.8
Or (mol%)	1.0	1.0	1.1	0.5	0.6	0.6	1.0	1.2	0.5	1.0	1.6	1.4	1.1	0.6

Table D6 Feldspar analyses of the 2010 Merapi eruption (continued)

Sample	M11-54-3	M11-54-3	M11-54-3	M11-54-3	M11-54-3	M11-54-3	M11-54-3	M11-54-3	M11-54-3	M11-54-3	M11-54-3	M11-54-3	M11-54-3	M11-54-3
Sample Type	DD	DD	DD	DD	DD	DD	DD	DD	DD	DD	DD	DD	DD	DD
Point	1 / 45 .	1 / 46 .	1 / 47 .	1 / 48 .	1 / 49 .	1 / 50 .	1 / 51 .	1 / 52 .	1 / 53 .	1 / 54 .	1 / 55 .	1 / 56 .	1 / 57 .	1 / 60 .
Comment	ph	ph	ph	ph	ph	ph	ph	ph	ph	ph	ph	ph	ph	ph
SiO_2	46.89	48.88	51.78	52.00	54.16	55.46	54.68	53.15	53.59	53.69	52.86	52.83	56.73	50.52
TiO_2	0.00	0.03	0.06	0.00	0.05	0.03	0.02	0.06	0.04	0.03	0.01	0.02	0.04	0.04
Al_2O_3	33.82	32.63	30.59	30.41	29.24	28.11	28.45	29.69	29.55	29.09	30.31	30.29	27.67	31.17
FeO	0.51	0.51	0.51	0.50	0.50	0.50	0.51	0.50	0.51	0.51	0.54	0.53	0.50	0.56
MgO	0.04	0.03	0.05	0.05	0.05	0.04	0.06	0.05	0.04	0.05	0.05	0.05	0.03	0.06
CaO	17.25	15.91	13.54	13.56	11.90	10.79	11.32	12.47	12.36	12.07	12.69	12.88	10.57	14.37
SrO														
BaO														
Na_2O	1.47	2.26	3.69	3.43	4.45	4.95	4.75	4.03	4.12	4.18	3.87	3.90	5.58	2.99
K_2O	0.08	0.13	0.28	0.28	0.40	0.48	0.45	0.34	0.36	0.38	0.35	0.29	0.72	0.21
Sum	100.06	100.39	100.50	100.22	100.74	100.35	100.24	100.29	100.55	99.99	100.66	100.79	101.84	99.92
Si	2.156	2.231	2.347	2.360	2.436	2.495	2.468	2.404	2.416	2.433	2.384	2.381	2.520	2.307
Al	1.832	1.755	1.634	1.626	1.550	1.491	1.513	1.583	1.570	1.553	1.611	1.609	1.449	1.678
Ti	0.000	0.001	0.002	0.000	0.002	0.001	0.001	0.002	0.001	0.001	0.000	0.001	0.001	0.002
Fe	0.020	0.020	0.019	0.019	0.019	0.019	0.019	0.019	0.019	0.019	0.020	0.020	0.019	0.021
Mg	0.003	0.002	0.003	0.003	0.003	0.003	0.004	0.003	0.002	0.003	0.003	0.004	0.002	0.004
Sr	0.000	0.000	0.000	0.000	0.000	0.000	0.000	0.000	0.000	0.000	0.000	0.000	0.000	0.000
Ba	0.000	0.000	0.000	0.000	0.000	0.000	0.000	0.000	0.000	0.000	0.000	0.000	0.000	0.000
Ca	0.850	0.778	0.657	0.659	0.573	0.520	0.548	0.604	0.597	0.586	0.613	0.622	0.503	0.703
Na	0.131	0.200	0.324	0.302	0.388	0.432	0.416	0.353	0.360	0.367	0.338	0.341	0.480	0.264
K	0.005	0.008	0.016	0.016	0.023	0.027	0.026	0.020	0.021	0.022	0.020	0.017	0.041	0.012
Sum	4.996	4.994	5.004	4.986	4.993	4.988	4.995	4.989	4.987	4.984	4.989	4.993	5.015	4.991
Ab (mol%)	13.3	20.3	32.5	30.9	39.4	44.1	42.0	36.1	36.8	37.7	34.8	34.8	46.9	27.0
An (mol%)	86.2	79.0	65.9	67.4	58.3	53.1	55.4	61.8	61.1	60.1	63.1	63.5	49.1	71.8
Or (mol%)	0.5	0.8	1.6	1.7	2.3	2.8	2.6	2.0	2.1	2.2	2.1	1.7	4.0	1.3

Table D6 Feldspar analyses of the 2010 Merapi eruption (continued)

Sample	M11-54-3	M11-54-3	M11-54-3	M11-54-3	M11-54-3	M11-54-3	M11-54-3	M11-54-3	M11-54-3	M11-54-3	M11-54-3	M11-54-3	M11-54-3	M11-54-3
Sample Type	DD	DD	DD	DD	DD	DD	DD	DD	DD	DD	DD	DD	DD	DD
Point	1 / 61 .	1 / 62 .	1 / 63 .	1 / 64 .	1 / 65 .	1 / 66 .	1 / 67 .	1 / 68 .	1 / 69 .	1 / 70 .	1 / 71 .	1 / 72 .	1 / 73 .	1 / 74 .
Comment	ph	ph	ph	ph	ph	ph	ph	ph	ph	ph	ph	ph	ph	ph-r
SiO_2	50.70	51.18	49.20	50.22	52.11	51.23	50.95	50.97	50.66	52.18	54.45	54.12	57.44	60.56
TiO_2	0.05	0.05	0.01	0.06	0.04	0.03	0.02	0.05	0.02	0.03	0.03	0.03	0.08	0.08
Al_2O_3	31.38	30.63	32.12	31.28	30.01	31.02	30.95	30.87	31.10	30.62	28.71	27.91	26.97	24.41
FeO	0.53	0.50	0.54	0.52	0.49	0.47	0.53	0.54	0.50	0.53	0.47	0.49	0.47	0.45
MgO	0.06	0.04	0.04	0.05	0.04	0.03	0.04	0.04	0.03	0.05	0.03	0.04	0.04	0.03
CaO	14.35	13.64	15.41	14.70	13.33	13.69	14.11	13.98	14.28	13.44	11.31	10.88	9.47	6.77
SrO														
BaO														
Na_2O	3.05	3.20	2.48	2.91	3.69	3.18	3.34	3.22	3.01	3.83	4.74	4.81	5.93	6.40
K_2O	0.21	0.31	0.18	0.20	0.29	0.28	0.23	0.26	0.20	0.26	0.37	0.36	0.47	2.28
Sum	100.33	99.54	99.97	99.93	99.99	99.92	100.16	99.93	99.79	100.92	100.11	98.64	100.87	100.97
Si	2.305	2.340	2.253	2.295	2.371	2.332	2.321	2.325	2.314	2.354	2.460	2.479	2.563	2.696
Al	1.682	1.650	1.733	1.685	1.609	1.664	1.661	1.660	1.674	1.628	1.529	1.507	1.418	1.281
Ti	0.002	0.002	0.000	0.002	0.001	0.001	0.001	0.002	0.001	0.001	0.001	0.001	0.003	0.003
Fe	0.020	0.019	0.021	0.020	0.019	0.018	0.020	0.021	0.019	0.020	0.018	0.019	0.017	0.017
Mg	0.004	0.003	0.003	0.003	0.003	0.002	0.003	0.003	0.002	0.003	0.002	0.003	0.003	0.002
Sr	0.000	0.000	0.000	0.000	0.000	0.000	0.000	0.000	0.000	0.000	0.000	0.000	0.000	0.000
Ba	0.000	0.000	0.000	0.000	0.000	0.000	0.000	0.000	0.000	0.000	0.000	0.000	0.000	0.000
Ca	0.699	0.668	0.756	0.720	0.650	0.668	0.689	0.683	0.699	0.649	0.547	0.534	0.452	0.323
Na	0.269	0.284	0.221	0.258	0.326	0.280	0.295	0.285	0.266	0.335	0.415	0.427	0.513	0.552
K	0.012	0.018	0.010	0.011	0.017	0.016	0.014	0.015	0.012	0.015	0.021	0.021	0.027	0.129
Sum	4.993	4.984	4.996	4.995	4.995	4.983	5.002	4.993	4.987	5.006	4.993	4.990	4.996	5.002
Ab (mol%)	27.4	29.3	22.4	26.0	32.8	29.1	29.6	28.9	27.2	33.5	42.2	43.5	51.7	55.0
An (mol%)	71.3	68.9	76.6	72.8	65.5	69.2	69.1	69.5	71.6	65.0	55.7	54.4	45.6	32.1
Or (mol%)	1.3	1.8	1.0	1.2	1.7	1.7	1.4	1.5	1.2	1.5	2.2	2.1	2.7	12.9

Table D6 Feldspar analyses of the 2010 Merapi eruption (continued)

Sample	M11-54-3	M11-54-3	M11-54-3	M11-54-3	M11-54-3	M11-54-3	M11-54-3	M11-54-3	M11-54-3	M11-54-3	M11-54-3	M11-54-3	M11-54-3	M11-54-3
Sample Type	DD	DD	DD	DD	DD	DD	DD	DD	DD	DD	DD	DD	DD	DD
Point	2 / 1 .	2 / 3 .	2 / 5 .	2 / 7 .	2 / 11 .	2 / 14 .	2 / 15 .	2 / 16 .	2 / 17 .	2 / 18 .	2 / 19 .	2 / 20 .	2 / 21 .	2 / 22 .
Comment	ph-c	ph	ph	ph	ph	ph	ph	ph	ph	ph	ph	ph	ph	ph
SiO_2	55.19	57.54	57.84	54.93	51.25	53.96	53.34	52.89	52.08	51.89	50.60	49.70	47.62	47.25
TiO_2	0.01	0.05	0.04	0.03	0.01	0.00	0.02	0.04	0.04	0.03	0.02	0.04	0.06	0.01
Al_2O_3	27.75	26.80	25.90	28.13	30.82	29.05	29.04	28.50	29.39	30.35	31.13	31.65	32.21	32.96
FeO	0.48	0.50	0.48	0.45	0.51	0.49	0.49	0.46	0.49	0.48	0.50	0.51	0.49	0.49
MgO	0.05	0.05	0.04	0.03	0.05	0.05	0.05	0.05	0.05	0.05	0.04	0.05	0.05	0.04
CaO	10.95	9.42	8.79	11.06	14.21	11.89	12.01	11.89	12.38	13.39	14.30	14.91	16.02	16.26
SrO														
BaO														
Na_2O	5.22	5.92	6.14	5.04	3.46	4.51	4.34	4.31	4.23	3.85	3.14	2.79	2.14	1.93
K_2O	0.54	0.79	0.89	0.70	0.28	0.37	0.37	0.30	0.32	0.31	0.21	0.17	0.13	0.11
Sum	100.21	101.07	100.11	100.36	100.60	100.31	99.66	98.43	98.98	100.35	99.92	99.81	98.72	99.04
Si	2.493	2.567	2.601	2.480	2.326	2.437	2.427	2.435	2.391	2.355	2.310	2.276	2.214	2.190
Al	1.477	1.409	1.372	1.496	1.648	1.547	1.557	1.546	1.590	1.624	1.675	1.708	1.765	1.800
Ti	0.000	0.002	0.001	0.001	0.000	0.000	0.001	0.001	0.001	0.001	0.001	0.001	0.002	0.000
Fe	0.018	0.019	0.018	0.017	0.019	0.019	0.018	0.018	0.019	0.018	0.019	0.019	0.019	0.019
Mg	0.004	0.003	0.003	0.002	0.004	0.003	0.003	0.003	0.004	0.004	0.003	0.003	0.003	0.003
Sr	0.000	0.000	0.000	0.000	0.000	0.000	0.000	0.000	0.000	0.000	0.000	0.000	0.000	0.000
Ba	0.000	0.000	0.000	0.000	0.000	0.000	0.000	0.000	0.000	0.000	0.000	0.000	0.000	0.000
Ca	0.530	0.450	0.424	0.535	0.691	0.575	0.585	0.587	0.609	0.651	0.699	0.731	0.798	0.807
Na	0.457	0.512	0.535	0.441	0.305	0.395	0.383	0.385	0.377	0.339	0.278	0.248	0.193	0.173
K	0.031	0.045	0.051	0.040	0.016	0.022	0.021	0.018	0.019	0.018	0.012	0.010	0.008	0.007
Sum	5.012	5.006	5.005	5.012	5.010	4.997	4.996	4.992	5.010	5.010	4.997	4.997	5.002	5.000
Ab (mol%)	44.9	50.8	53.0	43.4	30.1	39.8	38.7	38.9	37.5	33.6	28.1	25.1	19.3	17.6
An (mol%)	52.0	44.7	42.0	52.6	68.3	58.0	59.1	59.3	60.6	64.6	70.7	73.9	79.9	81.8
Or (mol%)	3.1	4.5	5.1	3.9	1.6	2.2	2.2	1.8	1.9	1.8	1.2	1.0	0.8	0.7

Table D6 Feldspar analyses of the 2010 Merapi eruption (continued)

Sample	M11-54-3	M11-54-3	M11-54-3	M11-54-3	M11-54-3	M11-54-3	M11-54-3	M11-54-3	M11-54-3	M11-54-3	M11-54-3	M11-54-3	M11-54-3	M11-54-3
Sample Type	DD	DD	DD	DD	DD	DD	DD	DD	DD	DD	DD	DD	DD	DD
Point	2 / 23 .	2 / 24 .	2 / 25 .	2 / 26 .	2 / 27 .	2 / 28 .	2 / 29 .	2 / 30 .	2 / 31 .	2 / 32 .	2 / 33 .	2 / 37 .	2 / 38 .	2 / 41 .
Comment	ph	ph	ph	ph	ph	ph	ph	ph	ph	ph	ph	ph	ph	ph
SiO_2	47.61	48.04	47.75	47.64	47.78	47.47	47.68	48.00	47.86	48.04	47.42	48.24	48.18	48.51
TiO_2	0.02	0.01	0.06	0.03	0.04	0.00	0.00	0.00	0.00	0.00	0.05	0.04	0.01	0.04
Al_2O_3	32.50	32.45	33.08	32.90	32.85	33.06	32.98	32.49	32.70	32.51	33.39	32.28	32.08	32.27
FeO	0.48	0.49	0.52	0.49	0.51	0.53	0.49	0.52	0.51	0.54	0.56	0.55	1.47	0.54
MgO	0.06	0.04	0.05	0.05	0.05	0.06	0.05	0.05	0.05	0.05	0.05	0.06	0.07	0.06
CaO	15.92	15.77	16.21	16.32	16.14	16.50	16.36	16.00	16.10	15.89	16.32	15.76	15.04	15.56
SrO														
BaO														
Na_2O	2.09	2.14	1.98	2.04	2.11	1.86	1.98	2.26	2.22	2.22	1.99	2.39	2.52	2.34
K_2O	0.14	0.16	0.13	0.12	0.13	0.13	0.12	0.14	0.14	0.14	0.11	0.14	0.17	0.15
Sum	98.82	99.10	99.78	99.60	99.61	99.61	99.66	99.45	99.58	99.39	99.90	99.45	99.53	99.46
Si	2.210	2.221	2.196	2.197	2.202	2.189	2.196	2.215	2.207	2.217	2.180	2.225	2.227	2.234
Al	1.778	1.769	1.793	1.788	1.784	1.797	1.790	1.767	1.777	1.768	1.810	1.755	1.748	1.752
Ti	0.001	0.000	0.002	0.001	0.002	0.000	0.000	0.000	0.000	0.000	0.002	0.001	0.000	0.001
Fe	0.019	0.019	0.020	0.019	0.020	0.021	0.019	0.020	0.020	0.021	0.021	0.021	0.057	0.021
Mg	0.004	0.003	0.003	0.004	0.004	0.004	0.004	0.003	0.003	0.004	0.004	0.004	0.005	0.004
Sr	0.000	0.000	0.000	0.000	0.000	0.000	0.000	0.000	0.000	0.000	0.000	0.000	0.000	0.000
Ba	0.000	0.000	0.000	0.000	0.000	0.000	0.000	0.000	0.000	0.000	0.000	0.000	0.000	0.000
Ca	0.792	0.781	0.799	0.806	0.797	0.815	0.807	0.791	0.795	0.785	0.804	0.779	0.745	0.768
Na	0.188	0.192	0.176	0.182	0.188	0.167	0.177	0.202	0.198	0.198	0.177	0.214	0.226	0.209
K	0.008	0.009	0.008	0.007	0.008	0.007	0.007	0.008	0.008	0.008	0.007	0.008	0.010	0.009
Sum	4.999	4.995	4.997	5.003	5.003	5.000	5.001	5.007	5.008	5.002	5.005	5.007	5.017	4.997
Ab (mol%)	19.0	19.6	18.0	18.3	18.9	16.8	17.9	20.2	19.8	20.0	17.9	21.4	23.0	21.2
An (mol%)	80.2	79.5	81.3	81.0	80.3	82.4	81.4	79.0	79.4	79.1	81.4	77.8	76.0	77.9
Or (mol%)	0.8	0.9	0.8	0.7	0.8	0.8	0.7	0.8	0.8	0.9	0.7	0.8	1.0	0.9

Table D6 Feldspar analyses of the 2010 Merapi eruption (continued)

Sample	M11-54-3	M11-54-3	M11-54-3	M11-54-3	M11-54-3	M11-54-3	M11-54-3	M11-54-3	M11-54-3	M11-54-3	M11-54-3	M11-54-3	M11-54-3	M11-54-3
Sample Type	DD	DD	DD	DD	DD	DD	DD	DD	DD	DD	DD	DD	DD	DD
Point	2 / 42 .	2 / 43 .	2 / 44 .	2 / 45 .	2 / 46 .	2 / 47 .	2 / 48 .	2 / 49 .	2 / 50 .	2 / 51 .	2 / 52 .	2 / 53 .	2 / 54 .	2 / 55 .
Comment	ph	ph	ph	ph	ph	ph	ph	ph	ph	ph	ph	ph	ph	ph
SiO_2	48.80	48.90	48.58	48.56	51.40	53.62	52.95	51.16	52.58	52.79	52.27	52.19	50.73	49.48
TiO_2	0.04	0.05	0.00	0.02	0.04	0.05	0.03	0.04	0.02	0.08	0.02	0.04	0.07	0.04
Al_2O_3	32.19	31.90	32.24	32.17	30.80	28.66	29.21	29.47	29.76	29.56	29.74	29.92	30.54	31.50
FeO	0.52	0.49	0.54	0.56	0.51	0.47	0.50	0.49	0.50	0.48	0.50	0.52	0.54	0.59
MgO	0.07	0.06	0.06	0.05	0.05	0.06	0.04	0.05	0.06	0.06	0.08	0.07	0.05	0.06
CaO	15.46	15.09	15.49	15.55	13.34	11.42	12.27	12.81	12.74	12.23	12.62	12.55	13.55	14.77
SrO														
BaO														
Na_2O	2.47	2.42	2.40	2.39	3.71	4.56	4.18	3.80	4.05	4.20	3.99	4.00	3.39	2.71
K_2O	0.16	0.17	0.15	0.16	0.31	0.41	0.36	0.32	0.35	0.36	0.32	0.33	0.27	0.19
Sum	99.71	99.07	99.46	99.44	100.16	99.25	99.55	98.15	100.05	99.77	99.54	99.61	99.14	99.35
Si	2.241	2.256	2.237	2.237	2.338	2.446	2.414	2.371	2.389	2.402	2.386	2.380	2.332	2.277
Al	1.743	1.735	1.750	1.747	1.651	1.541	1.569	1.610	1.593	1.585	1.600	1.608	1.654	1.708
Ti	0.001	0.002	0.000	0.001	0.001	0.002	0.001	0.001	0.001	0.003	0.001	0.001	0.002	0.002
Fe	0.020	0.019	0.021	0.021	0.019	0.018	0.019	0.019	0.019	0.018	0.019	0.020	0.021	0.023
Mg	0.005	0.004	0.004	0.003	0.003	0.004	0.003	0.004	0.004	0.004	0.005	0.004	0.003	0.004
Sr	0.000	0.000	0.000	0.000	0.000	0.000	0.000	0.000	0.000	0.000	0.000	0.000	0.000	0.000
Ba	0.000	0.000	0.000	0.000	0.000	0.000	0.000	0.000	0.000	0.000	0.000	0.000	0.000	0.000
Ca	0.761	0.746	0.765	0.768	0.650	0.558	0.599	0.636	0.620	0.596	0.617	0.613	0.667	0.728
Na	0.220	0.217	0.214	0.213	0.327	0.403	0.370	0.341	0.356	0.371	0.353	0.354	0.302	0.242
K	0.010	0.010	0.009	0.009	0.018	0.024	0.021	0.019	0.020	0.021	0.019	0.019	0.016	0.011
Sum	5.000	4.988	5.000	5.000	5.008	4.995	4.996	5.002	5.002	4.999	4.999	5.000	4.998	4.994
Ab (mol%)	22.2	22.3	21.7	21.5	32.8	40.9	37.3	34.3	35.8	37.5	35.7	35.9	30.6	24.6
An (mol%)	76.9	76.7	77.4	77.5	65.3	56.7	60.5	63.8	62.2	60.4	62.4	62.2	67.7	74.2
Or (mol%)	1.0	1.0	0.9	0.9	1.8	2.4	2.1	1.9	2.0	2.1	1.9	1.9	1.6	1.1

Table D6 Feldspar analyses of the 2010 Merapi eruption (continued)

Sample	M11-54-3	M11-54-3	M11-54-3	M11-54-3	M11-54-3	M11-54-3	M11-54-3	M11-54-3	M11-54-3	M11-54-3	M11-54-3	M11-54-3	M11-54-3	M11-54-3
Sample Type	DD	DD	DD	DD	DD	DD	DD	DD	DD	DD	DD	DD	DD	DD
Point	2 / 56 .	2 / 57 .	2 / 58 .	2 / 59 .	2 / 60 .	2 / 61 .	2 / 62 .	2 / 63 .	2 / 64 .	2 / 65 .	2 / 66 .	2 / 67 .	2 / 68 .	2 / 69 .
Comment	ph	ph	ph	ph	ph	ph	ph	ph	ph	ph	ph	ph	ph	ph
SiO_2	49.54	48.94	48.92	48.93	51.08	52.55	48.97	48.60	52.87	55.44	54.56	54.05	53.88	54.08
TiO_2	0.05	0.02	0.00	0.02	0.04	0.04	0.02	0.03	0.01	0.01	0.07	0.03	0.00	0.05
Al_2O_3	31.38	31.64	31.84	32.10	30.73	30.26	32.17	32.24	29.35	27.85	28.46	28.97	28.49	28.48
FeO	0.60	0.64	0.61	0.58	0.53	0.54	0.63	0.55	0.49	0.49	0.48	0.50	0.52	0.53
MgO	0.06	0.07	0.04	0.05	0.05	0.05	0.05	0.06	0.06	0.05	0.04	0.05	0.06	0.05
CaO	14.60	14.97	15.07	15.35	13.81	12.91	15.37	15.41	12.16	10.29	11.00	11.53	11.39	11.28
SrO														
BaO														
Na_2O	2.78	2.57	2.56	2.52	3.58	3.80	2.45	2.33	4.09	5.18	4.75	4.54	4.62	4.63
K_2O	0.21	0.18	0.20	0.18	0.31	0.36	0.17	0.15	0.37	0.54	0.48	0.43	0.43	0.45
Sum	99.22	99.04	99.24	99.72	100.12	100.50	99.81	99.37	99.39	99.83	99.83	100.08	99.40	99.53
Si	2.282	2.261	2.256	2.247	2.328	2.376	2.247	2.239	2.412	2.506	2.470	2.445	2.455	2.459
Al	1.703	1.723	1.731	1.738	1.651	1.613	1.739	1.750	1.578	1.484	1.519	1.544	1.529	1.526
Ti	0.002	0.001	0.000	0.001	0.001	0.001	0.001	0.001	0.000	0.000	0.002	0.001	0.000	0.002
Fe	0.023	0.025	0.024	0.022	0.020	0.020	0.024	0.021	0.019	0.018	0.018	0.019	0.020	0.020
Mg	0.004	0.004	0.003	0.003	0.003	0.003	0.004	0.004	0.004	0.003	0.002	0.004	0.004	0.003
Sr	0.000	0.000	0.000	0.000	0.000	0.000	0.000	0.000	0.000	0.000	0.000	0.000	0.000	0.000
Ba	0.000	0.000	0.000	0.000	0.000	0.000	0.000	0.000	0.000	0.000	0.000	0.000	0.000	0.000
Ca	0.721	0.741	0.745	0.755	0.674	0.626	0.755	0.761	0.594	0.498	0.533	0.559	0.556	0.549
Na	0.249	0.230	0.229	0.224	0.316	0.333	0.218	0.208	0.362	0.454	0.417	0.398	0.408	0.408
K	0.013	0.011	0.011	0.010	0.018	0.021	0.010	0.009	0.022	0.031	0.028	0.025	0.025	0.026
Sum	4.995	4.997	4.999	5.001	5.012	4.993	4.997	4.993	4.990	4.994	4.990	4.993	4.997	4.993
Ab (mol%)	25.3	23.4	23.3	22.7	31.3	34.0	22.2	21.3	37.0	46.2	42.7	40.5	41.3	41.5
An (mol%)	73.4	75.5	75.6	76.3	66.9	63.9	76.9	77.8	60.8	50.7	54.5	57.0	56.2	55.9
Or (mol%)	1.3	1.1	1.2	1.0	1.8	2.1	1.0	0.9	2.2	3.2	2.8	2.5	2.5	2.6

Table D6 Feldspar analyses of the 2010 Merapi eruption (continued)

Sample	M11-54-3	M11-54-3	M11-54-3	M11-54-3	M11-54-3	M11-54-3	M11-54-3	M11-54-3	M11-54-3	M11-54-3	M11-54-3	M11-54-3	M11-54-3	M11-61
Sample Type	DD	DD	DD	DD	DD	DD	DD	DD	DD	DD	DD	DD	DD	WP
Point	2 / 70 .	2 / 71 .	2 / 72 .	2 / 73 .	2 / 74 .	2 / 75 .	2 / 76 .	2 / 77 .	2 / 78 .	2 / 81 .	2 / 82 .	2 / 83 .	2 / 84 .	2 / 1 .
Comment	ph	ph	ph	ph	ph	ph	ph	ph	ph	ph	ph	ph	ph	m
SiO_2	53.25	53.74	54.22	54.28	54.63	53.84	54.22	55.32	54.13	54.32	50.78	53.03	55.42	57.58
TiO_2	0.01	0.07	0.03	0.00	0.03	0.00	0.00	0.00	0.04	0.02	0.04	0.08	0.03	0.02
Al_2O_3	29.38	28.82	28.16	28.18	28.12	28.84	28.70	27.68	28.72	28.31	31.12	29.58	28.56	26.04
FeO	0.53	0.52	0.52	0.54	0.50	0.54	0.53	0.53	0.52	0.43	0.47	0.46	0.46	0.46
MgO	0.05	0.06	0.04	0.04	0.05	0.04	0.05	0.05	0.04	0.03	0.03	0.04	0.04	0.04
CaO	12.08	11.66	11.07	11.04	11.02	11.54	11.42	10.37	11.38	11.17	13.88	12.34	11.07	8.22
SrO														0.12
BaO														
Na_2O	4.33	4.41	4.80	4.89	4.87	4.42	4.75	5.14	4.67	4.86	3.38	4.14	5.13	6.40
K_2O	0.40	0.38	0.46	0.45	0.50	0.40	0.41	0.55	0.41	0.43	0.21	0.44	0.49	0.71
Sum	100.03	99.66	99.29	99.42	99.71	99.61	100.07	99.63	99.90	99.58	99.91	100.11	101.20	99.59
Si	2.415	2.442	2.471	2.471	2.478	2.446	2.454	2.507	2.453	2.468	2.317	2.405	2.478	2.600
Al	1.571	1.543	1.512	1.512	1.503	1.544	1.530	1.478	1.534	1.516	1.673	1.581	1.505	1.386
Ti	0.000	0.002	0.001	0.000	0.001	0.000	0.000	0.000	0.001	0.001	0.001	0.003	0.001	0.001
Fe	0.020	0.020	0.020	0.020	0.019	0.020	0.020	0.020	0.020	0.016	0.018	0.017	0.017	0.017
Mg	0.004	0.004	0.003	0.003	0.003	0.003	0.003	0.003	0.003	0.002	0.002	0.003	0.003	0.002
Sr	0.000	0.000	0.000	0.000	0.000	0.000	0.000	0.000	0.000	0.000	0.000	0.000	0.000	0.003
Ba	0.000	0.000	0.000	0.000	0.000	0.000	0.000	0.000	0.000	0.000	0.000	0.000	0.000	0.000
Ca	0.587	0.568	0.541	0.538	0.536	0.562	0.554	0.503	0.552	0.544	0.679	0.599	0.530	0.398
Na	0.381	0.389	0.424	0.432	0.428	0.389	0.417	0.451	0.410	0.428	0.299	0.364	0.444	0.560
K	0.023	0.022	0.027	0.026	0.029	0.023	0.024	0.032	0.024	0.025	0.012	0.026	0.028	0.041
Sum	5.001	4.990	4.998	5.002	4.997	4.988	5.001	4.996	4.996	5.000	5.001	4.997	5.005	5.007
Ab (mol%)	38.4	39.7	42.8	43.3	43.1	40.0	41.9	45.7	41.6	42.9	30.2	36.8	44.3	56.1
An (mol%)	59.3	58.0	54.5	54.0	54.0	57.7	55.7	51.0	56.0	54.6	68.5	60.6	52.9	39.8
Or (mol%)	2.3	2.3	2.7	2.6	2.9	2.4	2.4	3.2	2.4	2.5	1.3	2.6	2.8	4.1

Table D6 Feldspar analyses of the 2010 Merapi eruption (continued)

Sample	M11-61	M11-61	M11-61	M11-61	M11-75	M11-75	M11-75	M11-75	M11-75	M11-75	M11-93	M11-93	M11-93	M11-93
Sample Type	WP	WP	WP	WP	GS	GS	GS	GS	GS	GS	GS	GS	GS	GS
Point	3 / 1 .	5 / 1 .	7 / 1 .	10 / 1 .	51 / 1 .	52 / 1 .	54 / 1 .	57 / 1 .	58 / 1 .	59 / 1 .	15 / 1 .	16 / 1 .	11 / 1 .	12 / 1 .
Comment	m	m	m	m	m	m	m	m	m	m	ph-c	ph-c	mph-c	mph-r
SiO_2	59.04	61.31	57.61	52.67	60.69	56.59	51.82	59.36	60.83	62.10	46.34	53.70	49.47	55.49
TiO_2	0.02	0.00	0.03	0.02	0.08	0.01	0.01	0.04	0.08	0.11	0.00	0.02	0.01	0.01
Al_2O_3	25.41	24.16	25.47	29.08	24.19	27.47	30.43	25.34	24.20	23.46	33.48	28.68	31.26	27.51
FeO	0.45	0.53	0.55	0.53	0.62	0.51	0.54	0.52	0.55	0.72	0.47	0.45	0.50	0.50
MgO	0.03	0.05	0.37	0.05	0.04	0.06	0.07	0.04	0.06	0.05	0.02	0.03	0.02	0.04
CaO	7.13	5.55	8.21	12.02	6.84	10.06	13.51	7.55	6.67	6.35	17.03	11.14	14.59	9.78
SrO	0.16	0.08	0.10	0.14							0.11	0.12	0.11	0.12
BaO														
Na_2O	6.78	7.25	6.29	4.38	6.88	5.34	3.60	6.78	6.80	6.77	1.61	5.01	3.08	5.70
K_2O	1.11	1.50	0.73	0.33	1.29	0.53	0.34	0.87	1.22	1.75	0.07	0.39	0.17	0.50
Sum	100.14	100.44	99.36	99.21	100.63	100.59	100.32	100.50	100.41	101.32	99.13	99.53	99.20	99.66
Si	2.646	2.728	2.608	2.412	2.702	2.535	2.353	2.649	2.709	2.745	2.153	2.446	2.282	2.515
Al	1.342	1.267	1.359	1.569	1.269	1.451	1.629	1.333	1.270	1.222	1.833	1.540	1.699	1.469
Ti	0.001	0.000	0.001	0.001	0.003	0.000	0.000	0.001	0.003	0.004	0.000	0.001	0.000	0.000
Fe	0.017	0.020	0.021	0.020	0.023	0.019	0.021	0.020	0.021	0.027	0.018	0.017	0.019	0.019
Mg	0.002	0.003	0.025	0.003	0.002	0.004	0.004	0.003	0.004	0.003	0.001	0.002	0.001	0.003
Sr	0.004	0.002	0.003	0.004	0.000	0.000	0.000	0.000	0.000	0.000	0.003	0.003	0.003	0.003
Ba	0.000	0.000	0.000	0.000	0.000	0.000	0.000	0.000	0.000	0.000	0.000	0.000	0.000	0.000
Ca	0.342	0.264	0.398	0.590	0.327	0.483	0.657	0.361	0.318	0.301	0.848	0.543	0.721	0.475
Na	0.589	0.626	0.552	0.389	0.594	0.464	0.317	0.586	0.587	0.580	0.145	0.442	0.276	0.501
K	0.064	0.085	0.042	0.019	0.074	0.030	0.019	0.050	0.070	0.099	0.004	0.023	0.010	0.029
Sum	5.008	4.995	5.009	5.007	4.994	4.987	5.001	5.002	4.981	4.980	5.005	5.016	5.011	5.015
Ab (mol%)	59.2	64.2	55.6	39.0	59.7	47.5	31.9	58.8	60.2	59.2	14.5	43.8	27.4	49.9
An (mol%)	34.4	27.1	40.1	59.1	32.9	49.4	66.1	36.2	32.6	30.7	85.1	53.9	71.6	47.3
Or (mol%)	6.4	8.7	4.2	1.9	7.4	3.1	2.0	5.0	7.1	10.1	0.4	2.3	1.0	2.9

Table D6 Feldspar analyses of the 2010 Merapi eruption (continued)

Sample	M11-93	M11-93	M11-93	M11-93	M11-131	M11-131	M11-131	M11-131	M11-135	M11-135	M11-138a	M11-138a	M11-138a	M11-138a
Sample Type	GS	GS	GS	GS	LG-Inc	LG-Inc	LG-Inc	LG-Inc	LG-Inc	LG-Inc	GS	GS	GS	GS
Point	27 / 1 .	28 / 1 .	29 / 1 .	36 / 1 .	41 / 1 .	43 / 1 .	58 / 1 .	60 / 1 .	15 / 1 .	16 / 1 .	1 / 1 .	2 / 1 .	5 / 1 .	7 / 1 .
Comment	m	m	m	m	m	m	m	m	m	m	m	m	m	m
SiO_2	58.52	55.82	57.63	54.35	65.91	66.31	58.81	66.79	65.68	64.23	61.00	62.47	63.67	64.99
TiO_2	0.03	0.04	0.03	0.02	0.02	0.02	0.06	0.04	0.16	0.08	0.04	0.02	0.00	0.00
Al_2O_3	25.65	27.14	26.19	27.69	19.14	18.88	25.49	18.87	19.41	20.73	24.19	23.16	22.33	20.59
FeO	0.58	0.48	0.55	0.60	0.29	0.34	0.43	0.21	0.50	0.57	0.45	0.45	0.43	0.35
MgO	0.02	0.04	0.03	0.03	0.00	0.00	0.04	0.00	0.01	0.03	0.00	0.00	0.01	0.00
CaO	7.37	9.36	8.17	10.25	0.59	0.31	7.70	0.44	1.18	3.09	5.63	4.45	3.42	1.41
SrO	0.12	0.13	0.08	0.11							0.02	0.06	0.04	0.03
BaO														
Na_2O	6.77	5.93	6.48	5.34	6.19	5.44	6.70	5.35	5.27	6.89	7.71	8.17	7.91	6.84
K_2O	0.96	0.53	0.87	0.47	7.26	8.60	0.90	8.54	7.93	4.02	1.16	1.40	2.59	5.77
Sum	100.02	99.46	100.03	98.88	99.40	99.90	100.11	100.24	100.14	99.64	100.20	100.18	100.39	99.98
Si	2.629	2.533	2.594	2.488	2.976	2.990	2.636	2.997	2.956	2.882	2.719	2.778	2.827	2.912
Al	1.358	1.451	1.389	1.494	1.019	1.003	1.346	0.998	1.030	1.096	1.271	1.214	1.168	1.088
Ti	0.001	0.001	0.001	0.001	0.001	0.001	0.002	0.001	0.005	0.003	0.001	0.001	0.000	0.000
Fe	0.022	0.018	0.021	0.023	0.011	0.013	0.016	0.008	0.019	0.021	0.017	0.017	0.016	0.013
Mg	0.002	0.003	0.002	0.002	0.000	0.000	0.002	0.000	0.001	0.002	0.000	0.000	0.001	0.000
Sr	0.003	0.004	0.002	0.003	0.000	0.000	0.000	0.000	0.000	0.000	0.001	0.002	0.001	0.001
Ba	0.000	0.000	0.000	0.000	0.000	0.000	0.000	0.000	0.000	0.000	0.000	0.000	0.000	0.000
Ca	0.355	0.455	0.394	0.503	0.029	0.015	0.370	0.021	0.057	0.149	0.269	0.212	0.163	0.067
Na	0.590	0.522	0.566	0.474	0.542	0.476	0.582	0.466	0.460	0.599	0.666	0.704	0.681	0.594
K	0.055	0.030	0.050	0.027	0.418	0.495	0.051	0.489	0.455	0.230	0.066	0.079	0.147	0.330
Sum	5.014	5.017	5.018	5.015	4.994	4.993	5.006	4.980	4.982	4.982	5.010	5.006	5.003	5.006
Ab (mol%)	59.0	51.8	56.0	47.2	54.8	48.3	58.0	47.7	47.3	61.3	66.6	70.7	68.8	59.9
An (mol%)	35.5	45.2	39.0	50.1	2.9	1.5	36.8	2.1	5.9	15.2	26.9	21.3	16.4	6.8
Or (mol%)	5.5	3.0	5.0	2.7	42.3	50.2	5.1	50.1	46.8	23.5	6.6	8.0	14.8	33.3

Table D6 Feldspar analyses of the 2010 Merapi eruption (continued)

Sample	M11-138a	M11-138a	M11-138a	DD10	DD10	DD10	DD10	DD10	DD10	DD10	DD10	DD10	DD10	DD10
Sample Type	GS	GS	GS	DD	DD	DD	DD	DD	DD	DD	DD	DD	DD	DD
Point	8 / 1 .	9 / 1 .	10 / 1 .	15 / 1 .	16 / 1 .	17 / 1 .	18 / 1 .	19 / 1 .	20 / 1 .	38 / 1 .	39 / 1 .	41 / 1 .	42 / 1 .	43 / 1 .
Comment	m	m	m	ph-r	ph-r	ph-r	ph-r	ph-c	ph-c	m	m	m	m	m
SiO_2	64.88	46.05	50.34	53.34	57.23	56.38	56.91	45.49	45.65	51.56	51.73	57.59	51.46	51.67
TiO_2	0.00	0.01	0.01	0.03	0.03	0.02	0.02	0.01	0.01	0.03	0.04	0.02	0.03	0.03
Al_2O_3	19.68	33.13	30.96	28.06	26.96	27.69	27.07	34.75	34.85	30.68	30.40	27.04	30.36	30.30
FeO	0.34	0.66	0.58	0.51	0.49	0.49	0.48	0.53	0.55	0.69	0.82	0.50	0.83	0.87
MgO	0.00	0.00	0.00	0.04	0.05	0.05	0.05	0.03	0.03	0.08	0.11	0.03	0.10	0.10
CaO	1.08	16.27	14.44	11.11	9.34	10.08	9.32	18.39	18.35	13.69	13.62	9.01	13.52	13.55
SrO	0.00	0.07	0.10	0.14	0.12	0.13	0.11	0.08	0.12	0.12	0.15	0.11	0.16	0.18
BaO				0.06	0.02	0.05	0.06	0.00	0.00	0.04	0.04	0.04	0.01	0.03
Na_2O	5.90	1.73	3.04	4.91	5.87	5.62	5.98	1.02	0.99	3.66	3.68	6.22	3.63	3.61
K_2O	7.47	0.26	0.34	0.38	0.58	0.52	0.56	0.03	0.04	0.18	0.23	0.53	0.24	0.22
Sum	99.35	98.18	99.80	98.60	100.69	101.03	100.56	100.33	100.60	100.73	100.81	101.08	100.34	100.55
Si	2.941	2.160	2.307	2.455	2.561	2.521	2.552	2.096	2.097	2.337	2.345	2.566	2.342	2.348
Al	1.051	1.832	1.672	1.522	1.422	1.459	1.430	1.886	1.886	1.639	1.624	1.420	1.629	1.622
Ti	0.000	0.000	0.000	0.001	0.001	0.001	0.001	0.000	0.000	0.001	0.001	0.001	0.001	0.001
Fe	0.013	0.026	0.022	0.020	0.018	0.018	0.018	0.020	0.021	0.026	0.031	0.019	0.032	0.033
Mg	0.000	0.000	0.000	0.003	0.003	0.003	0.003	0.002	0.002	0.005	0.007	0.002	0.007	0.007
Sr	0.000	0.002	0.003	0.004	0.003	0.003	0.003	0.002	0.003	0.003	0.004	0.003	0.004	0.005
Ba	0.000	0.000	0.000	0.001	0.000	0.001	0.001	0.000	0.000	0.001	0.001	0.001	0.000	0.001
Ca	0.052	0.818	0.709	0.548	0.448	0.483	0.448	0.907	0.903	0.665	0.661	0.430	0.660	0.659
Na	0.519	0.157	0.270	0.438	0.509	0.487	0.520	0.091	0.088	0.322	0.324	0.537	0.320	0.318
K	0.432	0.015	0.020	0.022	0.033	0.030	0.032	0.002	0.003	0.010	0.013	0.030	0.014	0.013
Sum	5.009	5.010	5.002	5.014	4.999	5.007	5.008	5.008	5.005	5.009	5.011	5.007	5.009	5.005
Ab (mol%)	51.7	15.9	27.0	43.5	51.4	48.7	52.0	9.1	8.9	32.3	32.4	53.9	32.2	32.1
An (mol%)	5.2	82.6	71.0	54.3	45.2	48.3	44.8	90.7	90.8	66.7	66.2	43.1	66.4	66.6
Or (mol%)	43.1	1.6	2.0	2.2	3.3	3.0	3.2	0.2	0.3	1.0	1.3	3.0	1.4	1.3

Table D6 Feldspar analyses of the 2010 Merapi eruption (continued)

Sample	DD10													
Sample Type	DD													
Point	44 / 1 .													
Comment	m													
SiO_2	51.72													
TiO_2	0.03													
Al_2O_3	29.36													
FeO	0.78													
MgO	0.12													
CaO	12.62													
SrO	0.13													
BaO	0.07													
Na_2O	3.92													
K_2O	0.28													
Sum	99.02													
Si	2.380													
Al	1.592													
Ti	0.001													
Fe	0.030													
Mg	0.008													
Sr	0.003													
Ba	0.001													
Ca	0.622													
Na	0.350													
K	0.017													
Sum	5.005													
Ab (mol%)	35.4													
An (mol%)	63.0													
Or (mol%)	1.7													

Table D7 Pyroxene analyses of the 2010 Merapi eruption[1]

Sample	M11-02	M11-02	M11-02	M11-02	M11-02	M11-02	M11-02	M11-02	M11-02	M11-06	M11-06	M11-06	M11-06	M11-06	M11-06	M11-06	M11-07	M11-07	M11-07
Sample Type[2]	DS	DS	DS	DS	DS	DS	DS	DS	DS	DS	DS	DS	DS	DS	DS	DS	DD	DD	DD
Point	2 / 1 .	6 / 1 .	8 / 1 .	10 / 1 .	13 / 1 .	15 / 1 .	17 / 1 .	19 / 1 .	21 / 1 .	2 / 1 .	6 / 1 .	8 / 1 .	10 / 1 .	12 / 1 .	14 / 1 .	19 / 1 .	1 / 1 .	5 / 1 .	25 / 1 .
Comment[3]	ph	ph	ph	ph	ph	ph	ph	ph	ph	ph	ph	ph	ph	ph	ph	ph	ph	ph	ph
Pyroxene Type	cpx	cpx	cpx	cpx	cpx	cpx	cpx	cpx	cpx	cpx	cpx	cpx	cpx	cpx	cpx	cpx	cpx	cpx	cpx
SiO_2	50.87	52.20	53.10	52.20	52.16	52.99	52.06	52.06	52.10	52.62	52.25	52.58	52.16	51.85	52.60	52.53	51.73	51.25	51.60
TiO_2	0.51	0.41	0.38	0.39	0.50	0.37	0.38	0.40	0.38	0.38	0.40	0.41	0.44	0.40	0.33	0.39	0.45	0.44	0.54
Al_2O_3	3.03	1.94	1.76	1.86	2.57	1.69	1.86	1.95	2.09	1.80	1.99	1.79	2.24	2.35	1.44	1.86	2.94	2.26	2.74
Cr_2O_3	0.01	-0.01	0.00	0.00	0.00	0.00	0.00	0.02	0.01	0.01	-0.01	0.00	-0.01	0.01	-0.01	0.02	0.00	0.01	-0.02
FeO	7.98	8.85	7.50	8.64	8.39	8.51	9.61	8.59	8.16	8.59	8.92	9.04	8.38	8.96	8.90	9.04	9.10	8.57	9.34
MnO	0.36	0.65	0.54	0.63	0.60	0.64	0.64	0.60	0.61	0.66	0.60	0.69	0.61	0.56	0.73	0.67	0.61	0.57	0.69
MgO	13.82	14.63	15.73	15.33	15.13	15.83	15.20	15.60	15.37	14.82	14.93	15.26	15.37	14.78	15.73	15.40	14.37	14.69	15.13
CaO	22.74	21.03	21.82	21.09	21.55	20.61	20.48	20.94	21.26	21.48	21.08	20.62	21.05	21.25	20.46	20.73	21.16	21.59	20.31
Na_2O	0.33	0.44	0.26	0.38	0.35	0.33	0.39	0.35	0.36	0.38	0.41	0.43	0.39	0.37	0.34	0.37	0.46	0.39	0.39
K_2O	0.01	0.00	0.01	0.01	0.01	0.01	0.02	0.00	0.01	0.03	0.01	0.01	0.01	0.00	0.00	0.02	0.02	0.01	0.12
Sum	99.65	100.16	101.10	100.53	101.26	101.00	100.64	100.51	100.34	100.77	100.56	100.84	100.66	100.53	100.51	101.03	100.83	99.78	100.85
Si	1.906	1.943	1.946	1.935	1.918	1.948	1.933	1.929	1.931	1.946	1.937	1.943	1.928	1.925	1.948	1.938	1.916	1.919	1.911
Al	0.134	0.085	0.076	0.081	0.112	0.073	0.082	0.085	0.091	0.078	0.087	0.078	0.098	0.103	0.063	0.081	0.129	0.100	0.120
Ti	0.014	0.011	0.010	0.011	0.014	0.010	0.011	0.011	0.011	0.011	0.011	0.011	0.012	0.011	0.009	0.011	0.012	0.012	0.015
Cr	0.000	0.000	0.000	0.000	0.000	0.000	0.000	0.000	0.000	0.000	0.000	0.000	0.000	0.000	0.000	0.000	0.000	0.000	0.000
Mg	0.772	0.812	0.859	0.847	0.830	0.868	0.842	0.862	0.850	0.817	0.825	0.841	0.847	0.818	0.868	0.847	0.793	0.820	0.835
Fe	0.250	0.276	0.230	0.268	0.258	0.262	0.298	0.266	0.253	0.266	0.277	0.279	0.259	0.278	0.276	0.279	0.282	0.268	0.289
Mn	0.011	0.021	0.017	0.020	0.019	0.020	0.020	0.019	0.019	0.021	0.019	0.022	0.019	0.018	0.023	0.021	0.019	0.018	0.022
Ca	0.913	0.839	0.857	0.838	0.849	0.812	0.815	0.832	0.844	0.851	0.838	0.817	0.834	0.845	0.812	0.820	0.840	0.866	0.806
Na	0.024	0.032	0.019	0.027	0.025	0.023	0.028	0.025	0.026	0.027	0.029	0.031	0.028	0.027	0.024	0.026	0.033	0.029	0.028
K	0.000	0.000	0.000	0.000	0.000	0.001	0.001	0.000	0.000	0.001	0.000	0.001	0.001	0.000	0.000	0.001	0.001	0.001	0.006
Sum	4.025	4.019	4.015	4.027	4.025	4.017	4.030	4.030	4.026	4.019	4.023	4.022	4.026	4.026	4.023	4.024	4.025	4.033	4.031
Si	1.894	1.934	1.939	1.922	1.907	1.940	1.919	1.915	1.919	1.937	1.926	1.932	1.916	1.913	1.937	1.926	1.904	1.903	1.896
Al	0.133	0.085	0.076	0.081	0.111	0.073	0.081	0.085	0.091	0.078	0.087	0.078	0.097	0.102	0.062	0.081	0.128	0.099	0.119
Ti	0.014	0.011	0.010	0.011	0.014	0.010	0.011	0.011	0.011	0.010	0.011	0.011	0.012	0.011	0.009	0.011	0.012	0.012	0.015
Cr	0.000	0.000	0.000	0.000	0.000	0.000	0.000	0.000	0.000	0.000	0.000	0.000	0.000	0.000	0.000	0.000	0.000	0.000	0.000
Fe^{3+}	0.075	0.056	0.044	0.081	0.074	0.050	0.088	0.088	0.076	0.055	0.069	0.067	0.076	0.076	0.070	0.072	0.073	0.099	0.093
Mg	0.767	0.808	0.856	0.841	0.825	0.864	0.836	0.855	0.844	0.813	0.821	0.836	0.842	0.813	0.863	0.842	0.789	0.813	0.829
Fe^{2+}	0.174	0.218	0.185	0.185	0.183	0.210	0.208	0.176	0.175	0.209	0.206	0.211	0.181	0.200	0.204	0.205	0.207	0.167	0.194
Mn	0.011	0.021	0.017	0.020	0.019	0.020	0.020	0.019	0.019	0.021	0.019	0.021	0.019	0.018	0.023	0.021	0.019	0.018	0.021
Ca	0.907	0.835	0.854	0.832	0.844	0.808	0.809	0.825	0.839	0.847	0.833	0.812	0.829	0.840	0.807	0.815	0.835	0.859	0.800
Na	0.024	0.032	0.019	0.027	0.025	0.023	0.028	0.025	0.026	0.027	0.029	0.031	0.028	0.026	0.024	0.026	0.033	0.028	0.028
K	0.000	0.000	0.000	0.000	0.000	0.001	0.001	0.000	0.000	0.001	0.000	0.001	0.001	0.000	0.000	0.001	0.001	0.001	0.006
Sum	4.000	4.000	4.000	4.000	4.000	4.000	4.000	4.000	4.000	4.000	4.000	4.000	4.000	4.000	4.000	4.000	4.000	4.000	4.000
Wo (mol%)	0.472	0.435	0.440	0.429	0.438	0.418	0.417	0.424	0.434	0.440	0.432	0.422	0.430	0.435	0.415	0.421	0.439	0.443	0.417
En (mol%)	0.399	0.422	0.442	0.434	0.428	0.447	0.431	0.440	0.436	0.423	0.426	0.434	0.437	0.421	0.444	0.435	0.414	0.420	0.433
Fs (mol%)	0.129	0.143	0.118	0.137	0.133	0.135	0.153	0.136	0.130	0.137	0.143	0.144	0.134	0.143	0.141	0.143	0.147	0.137	0.150

[1] Major element oxides in wt.%; number of cations based on 6 oxygens; endmembers calculated using the ferric form and total iron; [2] see Appendix A; [3] see Table D1

Table D7 Pyroxene analyses of the 2010 Merapi eruption (continued)

Sample	M11-07	M11-07	M11-07	M11-07	M11-07	M11-07	M11-07	M11-07	M11-07	M11-07	M11-18	M11-18	M11-18	M11-18	M11-18	M11-18	M11-24	M11-24	M11-25
Sample Type	DD	DD	DD	DD	DD	DD	LG-Inc	LG-Inc	LG-Inc	LG-Inc	WP	WP	WP	WP	WP	WP	DD	DD	DD
Point	26 / 1 .	28 / 1 .	29 / 1 .	30 / 1 .	31 / 1 .	32 / 1 .	58 / 1 .	54 / 1 .	52 / 1 .	56 / 1 .	4 / 1 .	5 / 1 .	9 / 1 .	12 / 1 .	8 / 1 .	11 / 1 .	10 / 1 .	11 / 1 .	32 / 1 .
Comment	ph	ph	m-c	m-r	m-c	m-c	ph	m	m	m	ph	ph	mph-c	mph-c	mph-r	mph-r	mph-r	mph-r	ph
Pyroxene Type	cpx	cpx	cpx	cpx	cpx	cpx	cpx	cpx	opx	opx	cpx	cpx	cpx	cpx	cpx	cpx	cpx (green)	cpx (green)	cpx
SiO_2	52.47	52.43	51.53	50.89	49.63	49.29	51.46	53.00	54.43	52.74	52.44	52.06	52.86	51.84	52.44	50.01	48.48	48.19	52.14
TiO_2	0.27	0.43	0.53	0.65	0.80	0.90	0.37	0.36	0.19	0.20	0.44	0.64	0.30	0.52	0.27	0.79	0.39	0.37	0.52
Al_2O_3	1.35	1.98	2.33	3.79	4.13	4.60	2.74	1.11	0.85	0.57	2.18	2.35	1.56	2.76	1.64	5.05	1.97	1.83	2.68
Cr_2O_3	0.01	-0.01	0.00	-0.01	0.00	0.00	0.02	0.00	0.01	0.00	0.01	0.01	0.01	0.00	0.00	0.00	0.00	0.04	0.01
FeO	9.25	9.41	9.19	9.65	9.78	10.16	8.64	10.66	17.77	21.07	9.07	8.43	8.94	8.64	8.87	8.81	17.16	17.30	9.13
MnO	0.75	0.71	0.54	0.54	0.38	0.38	0.62	0.99	1.31	1.94	0.66	0.59	0.85	0.54	0.78	0.37	0.91	0.87	0.68
MgO	15.06	15.24	14.91	14.79	13.43	13.45	14.00	14.69	24.95	21.77	15.06	14.52	15.09	14.63	14.95	12.98	7.07	7.00	14.49
CaO	20.94	20.49	20.89	20.76	22.00	21.57	21.88	20.22	1.55	1.59	19.99	21.01	20.20	21.17	20.22	22.35	22.78	22.97	20.52
Na_2O	0.41	0.39	0.26	0.24	0.23	0.24	0.40	0.41	0.03	0.03	0.38	0.39	0.39	0.33	0.38	0.38	0.32	0.29	0.41
K_2O	0.00	0.01	0.04	0.14	0.01	0.02	0.01	0.02	0.00	0.06	0.00	0.00	0.00	0.00	0.02	0.00	0.02	0.00	0.00
Sum	100.52	101.08	100.23	101.45	100.40	100.61	100.14	101.45	101.08	99.96	100.23	100.00	100.19	100.42	99.55	100.74	99.10	98.88	100.58
Si	1.951	1.936	1.920	1.878	1.860	1.845	1.920	1.960	1.973	1.975	1.945	1.936	1.962	1.922	1.959	1.858	1.921	1.918	1.931
Al	0.059	0.086	0.102	0.165	0.183	0.203	0.121	0.048	0.036	0.025	0.095	0.103	0.068	0.120	0.072	0.221	0.092	0.086	0.117
Ti	0.008	0.012	0.015	0.018	0.023	0.025	0.010	0.010	0.005	0.005	0.012	0.018	0.008	0.014	0.007	0.022	0.012	0.011	0.014
Cr	0.000	0.000	0.000	0.000	0.000	0.000	0.001	0.000	0.000	0.000	0.000	0.000	0.000	0.000	0.000	0.000	0.000	0.001	0.000
Mg	0.835	0.839	0.828	0.814	0.750	0.750	0.778	0.810	1.349	1.215	0.832	0.805	0.835	0.809	0.833	0.719	0.418	0.416	0.800
Fe	0.287	0.291	0.286	0.298	0.306	0.318	0.270	0.330	0.539	0.660	0.281	0.262	0.278	0.268	0.277	0.274	0.569	0.576	0.283
Mn	0.024	0.022	0.017	0.017	0.012	0.012	0.019	0.031	0.040	0.062	0.021	0.019	0.027	0.017	0.025	0.012	0.031	0.029	0.021
Ca	0.834	0.810	0.834	0.821	0.883	0.865	0.875	0.801	0.060	0.064	0.794	0.837	0.803	0.841	0.810	0.890	0.967	0.980	0.814
Na	0.030	0.028	0.019	0.017	0.017	0.017	0.029	0.029	0.002	0.002	0.027	0.028	0.028	0.024	0.027	0.027	0.024	0.023	0.030
K	0.000	0.000	0.002	0.007	0.000	0.001	0.000	0.001	0.000	0.003	0.000	0.000	0.000	0.000	0.001	0.000	0.001	0.000	0.000
Sum	4.027	4.023	4.024	4.034	4.035	4.037	4.024	4.021	4.004	4.010	4.009	4.008	4.010	4.015	4.011	4.023	4.034	4.039	4.011
Si	1.937	1.924	1.909	1.862	1.844	1.828	1.909	1.950	1.971	1.970	1.941	1.932	1.957	1.915	1.954	1.848	1.905	1.899	1.926
Al	0.059	0.086	0.102	0.163	0.181	0.201	0.120	0.048	0.036	0.025	0.095	0.103	0.068	0.120	0.072	0.220	0.091	0.085	0.117
Ti	0.008	0.012	0.015	0.018	0.022	0.025	0.010	0.010	0.005	0.005	0.012	0.018	0.008	0.014	0.007	0.022	0.011	0.011	0.014
Cr	0.000	0.000	0.000	0.000	0.000	0.000	0.001	0.000	0.000	0.000	0.000	0.000	0.000	0.000	0.000	0.000	0.000	0.001	0.000
Fe^{3+}	0.081	0.070	0.071	0.100	0.103	0.111	0.071	0.062	0.013	0.029	0.026	0.025	0.029	0.045	0.033	0.068	0.101	0.116	0.033
Mg	0.829	0.834	0.823	0.807	0.744	0.744	0.774	0.806	1.347	1.212	0.831	0.803	0.833	0.806	0.830	0.715	0.414	0.412	0.798
Fe^{2+}	0.205	0.219	0.213	0.195	0.201	0.204	0.197	0.266	0.525	0.629	0.255	0.236	0.248	0.222	0.243	0.204	0.462	0.454	0.250
Mn	0.024	0.022	0.017	0.017	0.012	0.012	0.019	0.031	0.040	0.061	0.021	0.019	0.027	0.017	0.025	0.011	0.030	0.029	0.021
Ca	0.829	0.806	0.829	0.814	0.876	0.857	0.870	0.797	0.060	0.063	0.793	0.835	0.801	0.838	0.807	0.885	0.959	0.970	0.812
Na	0.029	0.028	0.018	0.017	0.017	0.017	0.029	0.029	0.002	0.002	0.027	0.028	0.028	0.024	0.027	0.027	0.024	0.022	0.030
K	0.000	0.000	0.002	0.007	0.000	0.001	0.000	0.001	0.000	0.003	0.000	0.000	0.000	0.000	0.001	0.000	0.001	0.000	0.000
Sum	4.000	4.000	4.000	4.000	4.000	4.000	4.000	4.000	4.000	4.000	4.000	4.000	4.000	4.000	4.000	4.000	4.000	4.000	4.000
Wo (mol%)	0.426	0.418	0.428	0.425	0.455	0.447	0.455	0.413	0.031	0.033	0.416	0.440	0.419	0.439	0.422	0.473	0.495	0.497	0.429
En (mol%)	0.427	0.432	0.425	0.421	0.387	0.388	0.405	0.417	0.692	0.627	0.436	0.423	0.436	0.422	0.434	0.382	0.214	0.211	0.422
Fs (mol%)	0.147	0.150	0.147	0.154	0.158	0.164	0.140	0.170	0.277	0.340	0.147	0.138	0.145	0.140	0.144	0.145	0.291	0.292	0.149

Table D7 Pyroxene analyses of the 2010 Merapi eruption (continued)

Sample	M11-25	M11-25	M11-25	M11-25	M11-25	M11-25	M11-25	M11-25	M11-26a	M11-26a	M11-26a	M11-26a	M11-26a	M11-26a	M11-26a	M11-26a	M11-26a	M11-26a
Sample Type	DD	DD	DD	DD	DD	DD	DD	DD	DD	DD	DD	DD	DD	DD	DD	DD	DD	DD
Point	34 / 1 .	37 / 1 .	40 / 1 .	44 / 1 .	50 / 1 .	56 / 1 .	58 / 1 .	60 / 1 .	6 / 1 .	7 / 1 .	8 / 1 .	13 / 1 .	14 / 1 .	15 / 1 .	16 / 1 .	13 / 1 .	14 / 1 .	15 / 1 .	16 / 1 .
Comment	ph	ph	ph	ph	ph	ph	ph	ph	ph	ph	ph	ph	ph	ph	ph	ph-c	ph-c	ph-r	ph-r
Pyroxene Type	cpx	cpx	cpx	cpx	cpx	cpx	cpx	cpx	cpx	cpx	cpx	cpx	cpx	cpx	cpx	cpx	cpx	cpx	cpx
SiO_2	52.02	52.44	51.85	52.44	52.63	52.02	52.24	50.79	51.52	51.94	47.57	51.61	51.73	51.44	51.26	51.61	51.73	51.44	51.26
TiO_2	0.43	0.33	0.39	0.42	0.42	0.29	0.36	0.45	0.43	0.38	1.17	0.23	0.30	0.06	0.27	0.23	0.30	0.06	0.27
Al_2O_3	2.57	1.80	2.25	1.75	1.91	1.62	1.83	2.35	1.91	1.68	5.82	1.55	2.19	0.38	0.70	1.55	2.19	0.38	0.70
Cr_2O_3	0.00	0.00	0.00	0.00	0.02	0.01	0.00	0.01	0.01	0.00	0.02	0.00	0.07	0.00	0.00	0.00	0.07	0.00	0.00
FeO	8.02	7.66	8.45	8.18	8.60	8.97	9.01	8.50	9.13	9.22	9.68	9.28	8.70	13.64	14.65	9.28	8.70	13.64	14.65
MnO	0.35	0.46	0.51	0.62	0.60	0.71	0.63	0.46	0.74	0.73	0.30	0.61	0.73	0.58	0.51	0.61	0.73	0.58	0.51
MgO	14.26	15.33	14.97	14.88	15.24	15.13	15.01	14.33	15.15	14.97	12.36	14.00	14.37	11.44	12.16	14.00	14.37	11.44	12.16
CaO	22.38	21.20	20.78	19.37	20.49	20.32	20.24	21.83	20.15	20.44	22.18	21.45	21.35	21.23	19.04	21.45	21.35	21.23	19.04
Na_2O	0.25	0.37	0.39	0.38	0.33	0.38	0.42	0.38	0.40	0.43	0.37	0.26	0.37	0.17	0.27	0.26	0.37	0.17	0.27
K_2O	0.03	0.00	0.01	0.01	0.01	0.00	0.01	0.01	0.00	0.00	0.02	0.00	0.00	0.00	0.03	0.00	0.00	0.00	0.03
Sum	100.31	99.59	99.59	98.05	100.25	99.48	99.77	99.11	99.44	99.79	99.48	98.99	99.80	98.95	98.88	98.99	99.80	98.95	98.88
Si	1.930	1.951	1.936	1.975	1.949	1.949	1.949	1.916	1.933	1.943	1.805	1.951	1.935	1.985	1.976	1.951	1.935	1.985	1.976
Al	0.112	0.079	0.099	0.078	0.084	0.072	0.081	0.104	0.084	0.074	0.260	0.069	0.096	0.017	0.032	0.069	0.096	0.017	0.032
Ti	0.012	0.009	0.011	0.012	0.012	0.008	0.010	0.013	0.012	0.011	0.033	0.006	0.008	0.002	0.008	0.006	0.008	0.002	0.008
Cr	0.000	0.000	0.000	0.000	0.000	0.000	0.000	0.000	0.000	0.000	0.000	0.000	0.002	0.000	0.000	0.000	0.002	0.000	0.000
Mg	0.789	0.850	0.833	0.835	0.841	0.845	0.835	0.806	0.847	0.835	0.699	0.789	0.801	0.658	0.699	0.789	0.801	0.658	0.699
Fe	0.249	0.238	0.264	0.258	0.266	0.281	0.281	0.268	0.286	0.288	0.307	0.294	0.272	0.440	0.472	0.294	0.272	0.440	0.472
Mn	0.011	0.014	0.016	0.020	0.019	0.023	0.020	0.015	0.023	0.023	0.010	0.019	0.023	0.019	0.017	0.019	0.023	0.019	0.017
Ca	0.890	0.845	0.831	0.782	0.813	0.816	0.809	0.882	0.810	0.819	0.902	0.869	0.856	0.878	0.786	0.869	0.856	0.878	0.786
Na	0.018	0.027	0.028	0.028	0.023	0.028	0.031	0.028	0.029	0.031	0.027	0.019	0.027	0.013	0.020	0.019	0.027	0.013	0.020
K	0.002	0.000	0.000	0.001	0.000	0.000	0.001	0.000	0.000	0.000	0.001	0.000	0.000	0.000	0.001	0.000	0.000	0.000	0.001
Sum	4.011	4.014	4.018	3.988	4.009	4.021	4.016	4.033	4.027	4.025	4.045	4.017	4.021	4.011	4.011	4.017	4.021	4.011	4.011
Si	1.924	1.944	1.927	1.981	1.945	1.938	1.941	1.900	1.920	1.931	1.785	1.943	1.925	1.979	1.970	1.943	1.925	1.979	1.970
Al	0.112	0.079	0.098	0.078	0.083	0.071	0.080	0.104	0.084	0.074	0.257	0.069	0.096	0.017	0.032	0.069	0.096	0.017	0.032
Ti	0.012	0.009	0.011	0.012	0.012	0.008	0.010	0.013	0.012	0.011	0.033	0.006	0.008	0.002	0.008	0.006	0.008	0.002	0.008
Cr	0.000	0.000	0.000	0.000	0.000	0.000	0.000	0.000	0.000	0.000	0.000	0.000	0.002	0.000	0.000	0.000	0.002	0.000	0.000
Fe^{3+}	0.034	0.041	0.054	0.000	0.026	0.063	0.048	0.098	0.080	0.074	0.134	0.051	0.062	0.034	0.033	0.051	0.062	0.034	0.033
Mg	0.786	0.847	0.829	0.838	0.840	0.841	0.832	0.800	0.842	0.829	0.692	0.786	0.797	0.656	0.697	0.786	0.797	0.656	0.697
Fe^{2+}	0.214	0.196	0.209	0.258	0.239	0.216	0.232	0.168	0.204	0.213	0.170	0.241	0.209	0.405	0.438	0.241	0.209	0.405	0.438
Mn	0.011	0.014	0.016	0.020	0.019	0.023	0.020	0.014	0.023	0.023	0.010	0.019	0.023	0.019	0.016	0.019	0.023	0.019	0.016
Ca	0.887	0.842	0.827	0.784	0.811	0.811	0.806	0.875	0.805	0.814	0.892	0.865	0.851	0.875	0.784	0.865	0.851	0.875	0.784
Na	0.018	0.027	0.028	0.028	0.023	0.028	0.030	0.028	0.029	0.031	0.027	0.019	0.027	0.013	0.020	0.019	0.027	0.013	0.020
K	0.002	0.000	0.000	0.001	0.000	0.000	0.001	0.000	0.000	0.000	0.001	0.000	0.000	0.000	0.001	0.000	0.000	0.000	0.001
Sum	4.000	4.000	4.000	4.000	4.000	4.000	4.000	4.000	4.000	4.000	4.000	4.000	4.000	4.000	4.000	4.000	4.000	4.000	4.000
Wo (mol%)	0.462	0.437	0.431	0.417	0.423	0.420	0.420	0.451	0.417	0.422	0.472	0.445	0.444	0.444	0.402	0.445	0.444	0.444	0.402
En (mol%)	0.409	0.440	0.432	0.446	0.438	0.435	0.434	0.412	0.436	0.430	0.367	0.404	0.415	0.333	0.357	0.404	0.415	0.333	0.357
Fs (mol%)	0.129	0.123	0.137	0.137	0.139	0.145	0.146	0.137	0.147	0.149	0.161	0.150	0.141	0.223	0.241	0.150	0.141	0.223	0.241

Table D7 Pyroxene analyses of the 2010 Merapi eruption (continued)

Sample	M11-26a	M11-26a	M11-26a	M11-26a	M11-26a	M11-26a	M11-27-1	M11-27-1	M11-27-1	M11-27-1	M11-27-1	M11-27-1	M11-27-2	M11-27-2	M11-27-2	M11-27-2	M11-27-2	M11-27-2	M11-27-2
Sample Type	DD	DD	DD	DD	DD	DD	DD	DD	DD	DD	DD	DD	DD	DD	DD	DD	DD	LG-Inc	LG-Inc
Point	6 / 1 .	7 / 1 .	8 / 1 .	30 / 1 .	31 / 1 .	5 / 1 .	2 / 1 .	5 / 1 .	8 / 1 .	11 / 1 .	15 / 1 .	20 / 1 .	23 / 1 .	24 / 1 .	25 / 1 .	20 / 1 .	21 / 1 .	42 / 1 .	43 / 1 .
Comment	ph	ph-r	ph-r	mph-c	mph-r	ph-c	ph	ph	ph	ph	ph	ph	ph	ph	ph	m-c	m-c	ph	ph
Pyroxene Type	cpx	cpx	cpx	cpx	cpx	opx	cpx	cpx	cpx	cpx	cpx	cpx	cpx	cpx	cpx	cpx	cpx	cpx	cpx
SiO_2	51.52	51.94	47.57	51.86	46.20	53.37	52.45	50.24	52.22	52.51	51.12	52.19	50.05	50.90	52.63	51.60	50.27	51.55	52.57
TiO_2	0.43	0.38	1.17	0.37	1.61	0.16	0.36	0.57	0.34	0.35	0.53	0.39	0.68	0.55	0.43	0.41	0.71	0.39	0.36
Al_2O_3	1.91	1.68	5.82	1.67	5.50	0.75	1.70	2.77	1.49	1.53	2.89	1.83	4.57	3.15	2.12	2.92	3.50	1.59	1.68
Cr_2O_3	0.01	0.00	0.02	0.00	0.02	0.00	-0.01	0.00	-0.01	-0.01	0.00	-0.01	0.02	0.01	0.00	0.01	0.01	0.02	0.00
FeO	9.13	9.22	9.68	8.75	10.12	17.47	9.71	9.56	8.99	8.82	8.67	9.50	8.46	9.29	8.61	10.14	9.70	9.51	7.19
MnO	0.74	0.73	0.30	0.79	0.45	1.16	0.79	0.63	0.74	0.74	0.45	0.71	0.43	0.54	0.71	0.83	0.42	0.89	0.62
MgO	15.15	14.97	12.36	15.15	12.84	25.11	14.72	14.03	15.18	15.20	14.21	15.45	13.76	14.39	15.52	15.04	14.02	14.51	14.90
CaO	20.15	20.44	22.18	20.22	21.22	1.48	20.17	21.25	20.69	20.61	22.22	20.59	22.25	20.83	20.69	19.42	21.35	19.83	22.11
Na_2O	0.40	0.43	0.37	0.36	0.40	0.04	0.47	0.47	0.35	0.36	0.33	0.38	0.41	0.39	0.36	0.33	0.25	0.40	0.46
K_2O	0.00	0.00	0.02	0.00	0.00	0.00	0.01	0.01	0.01	0.01	0.01	0.01	0.36	0.00	0.08	0.35	0.03	0.01	0.00
Sum	99.44	99.79	99.48	99.16	98.36	99.54	100.38	99.52	100.01	100.10	100.44	101.05	101.00	100.04	101.15	101.04	100.26	98.69	99.88
Si	1.933	1.943	1.805	1.947	1.781	1.965	1.952	1.897	1.948	1.953	1.904	1.931	1.858	1.902	1.935	1.912	1.882	1.952	1.953
Al	0.084	0.074	0.260	0.074	0.250	0.033	0.075	0.123	0.065	0.067	0.127	0.080	0.200	0.139	0.092	0.128	0.154	0.071	0.074
Ti	0.012	0.011	0.033	0.010	0.047	0.004	0.010	0.016	0.010	0.010	0.015	0.011	0.019	0.015	0.012	0.011	0.020	0.011	0.010
Cr	0.000	0.000	0.000	0.000	0.001	0.000	0.000	0.000	0.000	0.000	0.000	0.000	0.000	0.000	0.000	0.000	0.000	0.001	0.000
Mg	0.847	0.835	0.699	0.848	0.738	1.378	0.817	0.790	0.844	0.843	0.789	0.852	0.762	0.801	0.851	0.831	0.782	0.819	0.825
Fe	0.286	0.288	0.307	0.275	0.326	0.538	0.302	0.302	0.280	0.274	0.270	0.294	0.263	0.290	0.265	0.314	0.303	0.301	0.223
Mn	0.023	0.023	0.010	0.025	0.015	0.036	0.025	0.020	0.023	0.023	0.014	0.022	0.013	0.017	0.022	0.026	0.013	0.028	0.020
Ca	0.810	0.819	0.902	0.813	0.876	0.058	0.804	0.860	0.827	0.821	0.887	0.816	0.885	0.834	0.815	0.771	0.856	0.804	0.880
Na	0.029	0.031	0.027	0.026	0.030	0.003	0.034	0.035	0.026	0.026	0.024	0.028	0.029	0.029	0.026	0.024	0.018	0.029	0.033
K	0.000	0.000	0.001	0.000	0.000	0.000	0.001	0.000	0.001	0.000	0.001	0.000	0.017	0.000	0.004	0.016	0.001	0.001	0.000
Sum	4.027	4.025	4.045	4.019	4.062	4.016	4.018	4.043	4.023	4.017	4.030	4.033	4.046	4.028	4.022	4.033	4.031	4.017	4.017
Si	1.920	1.931	1.785	1.938	1.753	1.957	1.943	1.877	1.936	1.945	1.890	1.915	1.836	1.889	1.925	1.896	1.867	1.944	1.944
Al	0.084	0.074	0.257	0.073	0.246	0.033	0.074	0.122	0.065	0.067	0.126	0.079	0.198	0.138	0.091	0.127	0.153	0.070	0.073
Ti	0.012	0.011	0.033	0.010	0.046	0.004	0.010	0.016	0.010	0.010	0.015	0.011	0.019	0.015	0.012	0.011	0.020	0.011	0.010
Cr	0.000	0.000	0.000	0.000	0.001	0.000	0.000	0.000	0.000	0.000	0.000	0.000	0.000	0.000	0.000	0.000	0.000	0.001	0.000
Fe^{3+}	0.080	0.074	0.134	0.055	0.184	0.047	0.055	0.127	0.069	0.051	0.090	0.098	0.138	0.082	0.064	0.098	0.092	0.050	0.051
Mg	0.842	0.829	0.692	0.844	0.726	1.373	0.813	0.782	0.839	0.839	0.783	0.845	0.753	0.796	0.846	0.824	0.776	0.815	0.821
Fe^{2+}	0.204	0.213	0.170	0.218	0.137	0.489	0.246	0.172	0.209	0.222	0.178	0.194	0.122	0.206	0.199	0.213	0.209	0.250	0.172
Mn	0.023	0.023	0.010	0.025	0.014	0.036	0.025	0.020	0.023	0.023	0.014	0.022	0.013	0.017	0.022	0.026	0.013	0.028	0.019
Ca	0.805	0.814	0.892	0.810	0.863	0.058	0.801	0.850	0.822	0.818	0.880	0.810	0.875	0.828	0.811	0.764	0.850	0.801	0.876
Na	0.029	0.031	0.027	0.026	0.029	0.003	0.034	0.034	0.025	0.026	0.024	0.027	0.029	0.028	0.026	0.024	0.018	0.029	0.033
K	0.000	0.000	0.001	0.000	0.000	0.000	0.001	0.000	0.001	0.000	0.001	0.000	0.017	0.000	0.004	0.016	0.001	0.001	0.000
Sum	4.000	4.000	4.000	4.000	4.000	4.000	4.000	4.000	4.000	4.000	4.000	4.000	4.000	4.000	4.000	4.000	4.000	4.000	4.000
Wo (mol%)	0.417	0.422	0.472	0.420	0.452	0.029	0.418	0.441	0.424	0.424	0.456	0.416	0.463	0.433	0.422	0.402	0.441	0.418	0.456
En (mol%)	0.436	0.430	0.367	0.438	0.380	0.698	0.425	0.405	0.433	0.435	0.405	0.434	0.399	0.416	0.441	0.434	0.403	0.426	0.428
Fs (mol%)	0.147	0.149	0.161	0.142	0.168	0.272	0.157	0.155	0.144	0.142	0.139	0.150	0.138	0.151	0.137	0.164	0.156	0.157	0.116

Table D7 Pyroxene analyses of the 2010 Merapi eruption (continued)

Sample	M11-27-2	M11-27-2	M11-27-2	M11-27-2	M11-27-3	M11-27-3	M11-27-3	M11-27-3	M11-27-3	M11-27-3	M11-27-3	M11-27-3	M11-27-3	M11-27-3	M11-27-3	M11-27-3	M11-27-3	M11-27-3	M11-27-3
Sample Type	LG-Inc	LG-Inc	LG-Inc	LG-Inc	DD	DD	DD	DD	DD	DD	DD	DD	DD	DD	DD	DD	DD	DD	DD
Point	35 / 1 .	36 / 1 .	37 / 1 .	41 / 1 .	28 / 1 .	29 / 1 .	30 / 1 .	31 / 1 .	33 / 1 .	34 / 1 .	35 / 1 .	36 / 1 .	28 / 1 .	33 / 1 .	29 / 1 .	34 / 1 .	30 / 1 .	35 / 1 .	31 / 1 .
Comment	m	m	m	m	ph	ph	ph	ph	ph	ph	ph	ph	ph-c	ph-c	ph-c	ph-c	ph-r	ph-r	ph-r
Pyroxene Type	cpx	opx	opx	opx	cpx	cpx	cpx	cpx	cpx	cpx	cpx	cpx	cpx	cpx	cpx	cpx	cpx	cpx	cpx
SiO_2	52.40	53.14	54.16	52.77	51.57	51.75	51.59	52.09	47.00	46.45	44.62	44.65	51.57	47.00	51.75	46.45	51.59	44.62	52.09
TiO_2	0.30	0.20	0.18	0.25	0.42	0.39	0.40	0.50	1.06	1.16	1.66	1.67	0.42	1.06	0.39	1.16	0.40	1.66	0.50
Al_2O_3	1.19	0.74	0.92	1.01	2.24	1.76	1.81	1.83	7.06	7.60	8.94	8.90	2.24	7.06	1.76	7.60	1.81	8.94	1.83
Cr_2O_3	0.00	-0.01	0.01	0.01	0.00	0.02	0.00	0.00	0.00	0.00	0.00	0.00	0.00	0.00	0.02	0.00	0.00	0.00	0.00
FeO	9.14	20.34	17.06	21.67	8.79	9.01	9.07	9.58	8.48	8.99	10.61	10.57	8.79	8.48	9.01	8.99	9.07	10.61	9.58
MnO	0.88	1.45	1.24	1.67	0.60	0.68	0.75	0.71	0.23	0.19	0.19	0.24	0.60	0.23	0.68	0.19	0.75	0.19	0.71
MgO	15.15	23.03	25.42	21.54	15.21	15.43	14.88	15.04	12.22	11.90	10.89	10.88	15.21	12.22	15.43	11.90	14.88	10.89	15.04
CaO	20.23	1.42	1.62	1.39	20.68	20.28	20.76	20.71	23.36	23.20	22.68	22.51	20.68	23.36	20.28	23.20	20.76	22.68	20.71
Na_2O	0.33	0.03	0.02	0.02	0.39	0.34	0.38	0.46	0.30	0.30	0.34	0.35	0.39	0.30	0.34	0.30	0.38	0.34	0.46
K_2O	0.03	0.02	0.00	0.04	0.01	0.02	0.02	0.05	0.00	0.00	0.00	0.01	0.01	0.00	0.02	0.00	0.02	0.00	0.05
Sum	99.65	100.37	100.63	100.35	99.92	99.69	99.66	100.97	99.71	99.80	99.94	99.77	99.92	99.71	99.69	99.80	99.66	99.94	100.97
Si	1.961	1.968	1.967	1.968	1.924	1.936	1.934	1.931	1.775	1.757	1.700	1.703	1.924	1.775	1.936	1.757	1.934	1.700	1.931
Al	0.052	0.032	0.039	0.044	0.098	0.078	0.080	0.080	0.314	0.339	0.402	0.400	0.098	0.314	0.078	0.339	0.080	0.402	0.080
Ti	0.008	0.006	0.005	0.007	0.012	0.011	0.011	0.014	0.030	0.033	0.048	0.048	0.012	0.030	0.011	0.033	0.011	0.048	0.014
Cr	0.000	0.000	0.000	0.000	0.000	0.001	0.000	0.000	0.000	0.000	0.000	0.000	0.000	0.000	0.001	0.000	0.000	0.000	0.000
Mg	0.845	1.271	1.376	1.198	0.846	0.860	0.832	0.831	0.688	0.671	0.619	0.619	0.846	0.688	0.860	0.671	0.832	0.619	0.831
Fe	0.286	0.630	0.518	0.676	0.274	0.282	0.284	0.297	0.268	0.284	0.338	0.337	0.274	0.268	0.282	0.284	0.284	0.338	0.297
Mn	0.028	0.045	0.038	0.053	0.019	0.022	0.024	0.022	0.007	0.006	0.006	0.008	0.019	0.007	0.022	0.006	0.024	0.006	0.022
Ca	0.811	0.056	0.063	0.055	0.827	0.813	0.834	0.822	0.945	0.940	0.926	0.920	0.827	0.945	0.813	0.940	0.834	0.926	0.822
Na	0.024	0.002	0.002	0.002	0.028	0.025	0.027	0.033	0.022	0.022	0.025	0.026	0.028	0.022	0.025	0.022	0.027	0.025	0.033
K	0.002	0.001	0.000	0.002	0.001	0.001	0.001	0.002	0.000	0.000	0.000	0.000	0.001	0.000	0.001	0.000	0.001	0.000	0.002
Sum	4.017	4.012	4.009	4.005	4.029	4.027	4.028	4.033	4.049	4.052	4.064	4.062	4.029	4.049	4.027	4.052	4.028	4.064	4.033
Si	1.952	1.962	1.963	1.966	1.910	1.923	1.921	1.915	1.753	1.734	1.674	1.677	1.910	1.753	1.923	1.734	1.921	1.674	1.915
Al	0.052	0.032	0.039	0.044	0.098	0.077	0.080	0.079	0.310	0.335	0.395	0.394	0.098	0.310	0.077	0.335	0.080	0.395	0.079
Ti	0.008	0.006	0.005	0.007	0.012	0.011	0.011	0.014	0.030	0.033	0.047	0.047	0.012	0.030	0.011	0.033	0.011	0.047	0.014
Cr	0.000	0.000	0.000	0.000	0.000	0.001	0.000	0.000	0.000	0.000	0.000	0.000	0.000	0.000	0.001	0.000	0.000	0.000	0.000
Fe^{3+}	0.052	0.035	0.027	0.014	0.087	0.081	0.084	0.097	0.146	0.154	0.189	0.183	0.087	0.146	0.081	0.154	0.084	0.189	0.097
Mg	0.841	1.268	1.373	1.196	0.840	0.855	0.826	0.824	0.680	0.662	0.609	0.610	0.840	0.680	0.855	0.662	0.826	0.609	0.824
Fe^{2+}	0.233	0.593	0.489	0.662	0.185	0.199	0.198	0.197	0.119	0.127	0.144	0.149	0.185	0.119	0.199	0.127	0.198	0.144	0.197
Mn	0.028	0.045	0.038	0.053	0.019	0.021	0.024	0.022	0.007	0.006	0.006	0.007	0.019	0.007	0.021	0.006	0.024	0.006	0.022
Ca	0.808	0.056	0.063	0.055	0.821	0.807	0.828	0.816	0.934	0.928	0.911	0.906	0.821	0.934	0.807	0.928	0.828	0.911	0.816
Na	0.024	0.002	0.002	0.002	0.028	0.025	0.027	0.033	0.022	0.022	0.025	0.026	0.028	0.022	0.025	0.022	0.027	0.025	0.033
K	0.002	0.001	0.000	0.002	0.001	0.001	0.001	0.002	0.000	0.000	0.000	0.000	0.001	0.000	0.001	0.000	0.001	0.000	0.002
Sum	4.000	4.000	4.000	4.000	4.000	4.000	4.000	4.000	4.000	4.000	4.000	4.000	4.000	4.000	4.000	4.000	4.000	4.000	4.000
Wo (mol%)	0.418	0.029	0.032	0.029	0.425	0.416	0.428	0.422	0.497	0.496	0.492	0.490	0.425	0.497	0.416	0.496	0.428	0.492	0.422
En (mol%)	0.435	0.649	0.703	0.621	0.435	0.440	0.427	0.426	0.362	0.354	0.329	0.330	0.435	0.362	0.440	0.354	0.427	0.329	0.426
Fs (mol%)	0.147	0.322	0.265	0.350	0.141	0.144	0.146	0.152	0.141	0.150	0.180	0.180	0.141	0.141	0.144	0.150	0.146	0.180	0.152

Table D7 Pyroxene analyses of the 2010 Merapi eruption (continued)

Sample	M11-27-3	M11-27-3	M11-27-3	M11-27-3	M11-27-3	M11-27-3	M11-27-3	M11-27-3	M11-27-3	M11-27-4	M11-27-4	M11-27-4	M11-27-4	M11-27-4	M11-27-4	M11-27-4	M11-27-4	M11-27-4
Sample Type	DD	LG-Inc	LG-Inc	LG-Inc	LG-Inc	LG-Inc	LG-Inc	LG-Inc	LG-Inc	LG-Inc	LG-Inc	LG-Inc	LG-Inc	LG-Inc	LG-Inc	LG-Inc	LG-Inc	LG-Inc
Point	36 / 1 .	24 / 1 .	25 / 1 .	26 / 1 .	27 / 1 .	24 / 1 .	25 / 1 .	26 / 1 .	27 / 1 .	1 / 1 .	2 / 1 .	3 / 1 .	4 / 1 .	5 / 1 .	6 / 1 .	51 / 1 .	52 / 1 .	53 / 1 .	54 / 1 .
Comment	ph-r	ph	ph	ph	ph	ph-r	ph-r	ph-c	ph-c	ph	ph	ph	ph	ph	ph	ph	ph	ph	ph
Pyroxene Type	cpx	cpx	cpx	cpx	cpx	cpx	cpx	cpx	cpx	cpx	cpx	cpx	cpx	cpx	cpx	cpx	cpx	cpx	cpx
SiO_2	44.65	47.02	47.62	51.20	51.10	47.02	47.62	51.20	51.10	47.65	47.49	48.11	51.67	50.95	50.89	51.61	51.44	49.16	48.31
TiO_2	1.67	1.25	1.02	0.46	0.59	1.25	1.02	0.46	0.59	1.00	1.14	0.96	0.36	0.57	0.55	0.34	0.34	0.62	0.87
Al_2O_3	8.90	6.10	5.73	2.24	2.30	6.10	5.73	2.24	2.30	5.63	6.12	5.65	1.90	2.78	2.72	1.67	1.42	4.02	4.70
Cr_2O_3	0.00	0.02	0.04	0.05	0.00	0.02	0.04	0.05	0.00	0.03	0.01	0.00	0.03	0.02	0.00	0.00	0.02	0.00	0.00
FeO	10.57	9.42	9.21	9.51	9.09	9.42	9.21	9.51	9.09	8.86	9.62	8.91	8.88	8.72	8.79	8.91	8.70	8.68	8.81
MnO	0.24	0.34	0.33	0.71	0.53	0.34	0.33	0.71	0.53	0.26	0.34	0.29	0.68	0.49	0.56	0.88	0.67	0.35	0.36
MgO	10.88	12.26	12.53	14.69	14.89	12.26	12.53	14.69	14.89	12.64	12.29	12.72	15.24	14.71	14.79	14.92	15.19	13.44	12.94
CaO	22.51	22.60	23.04	20.41	20.71	22.60	23.04	20.41	20.71	22.60	22.48	22.70	20.65	20.79	21.08	19.74	20.61	22.40	22.58
Na_2O	0.35	0.36	0.36	0.43	0.35	0.36	0.36	0.43	0.35	0.35	0.37	0.34	0.36	0.37	0.41	0.36	0.28	0.27	0.32
K_2O	0.01	0.00	0.00	0.01	0.00	0.00	0.00	0.01	0.00	0.00	0.02	0.00	0.00	0.00	0.00	0.05	0.01	0.00	0.00
Sum	99.77	99.38	99.88	99.71	99.57	99.38	99.88	99.71	99.57	99.03	99.87	99.69	99.77	99.38	99.80	98.48	98.68	98.94	98.89
Si	1.703	1.788	1.801	1.922	1.917	1.788	1.801	1.922	1.917	1.811	1.796	1.816	1.932	1.911	1.905	1.952	1.944	1.864	1.838
Al	0.400	0.274	0.255	0.099	0.102	0.274	0.255	0.099	0.102	0.252	0.273	0.252	0.084	0.123	0.120	0.074	0.063	0.180	0.211
Ti	0.048	0.036	0.029	0.013	0.017	0.036	0.029	0.013	0.017	0.029	0.032	0.027	0.010	0.016	0.015	0.010	0.010	0.018	0.025
Cr	0.000	0.001	0.001	0.002	0.000	0.001	0.001	0.002	0.000	0.001	0.000	0.000	0.001	0.001	0.000	0.000	0.001	0.000	0.000
Mg	0.619	0.695	0.706	0.822	0.833	0.695	0.706	0.822	0.833	0.717	0.693	0.716	0.850	0.823	0.825	0.841	0.856	0.760	0.734
Fe	0.337	0.300	0.291	0.298	0.285	0.300	0.291	0.298	0.285	0.282	0.304	0.281	0.278	0.274	0.275	0.282	0.275	0.275	0.280
Mn	0.008	0.011	0.011	0.023	0.017	0.011	0.011	0.023	0.017	0.009	0.011	0.009	0.021	0.016	0.018	0.028	0.022	0.011	0.011
Ca	0.920	0.921	0.934	0.821	0.832	0.921	0.934	0.821	0.832	0.921	0.911	0.918	0.827	0.836	0.845	0.800	0.834	0.910	0.920
Na	0.026	0.026	0.026	0.031	0.026	0.026	0.026	0.031	0.026	0.026	0.027	0.025	0.026	0.027	0.030	0.026	0.020	0.020	0.024
K	0.000	0.000	0.000	0.000	0.000	0.000	0.000	0.000	0.000	0.000	0.001	0.000	0.000	0.000	0.000	0.003	0.000	0.000	0.000
Sum	4.062	4.052	4.055	4.031	4.028	4.052	4.055	4.031	4.028	4.046	4.049	4.044	4.029	4.024	4.034	4.016	4.025	4.038	4.044
Si	1.677	1.766	1.777	1.907	1.903	1.766	1.777	1.907	1.903	1.791	1.775	1.796	1.918	1.900	1.889	1.944	1.932	1.847	1.818
Al	0.394	0.270	0.252	0.098	0.101	0.270	0.252	0.098	0.101	0.249	0.269	0.249	0.083	0.122	0.119	0.074	0.063	0.178	0.209
Ti	0.047	0.035	0.029	0.013	0.017	0.035	0.029	0.013	0.017	0.028	0.032	0.027	0.010	0.016	0.015	0.010	0.010	0.017	0.025
Cr	0.000	0.001	0.001	0.002	0.000	0.001	0.001	0.002	0.000	0.001	0.000	0.000	0.001	0.000	0.000	0.000	0.001	0.000	0.000
Fe^{3+}	0.183	0.153	0.162	0.092	0.085	0.153	0.162	0.092	0.085	0.137	0.144	0.130	0.086	0.073	0.102	0.046	0.074	0.114	0.129
Mg	0.610	0.686	0.697	0.816	0.827	0.686	0.697	0.816	0.827	0.708	0.685	0.708	0.844	0.818	0.818	0.838	0.850	0.753	0.726
Fe^{2+}	0.149	0.143	0.125	0.204	0.199	0.143	0.125	0.204	0.199	0.141	0.156	0.149	0.189	0.199	0.171	0.234	0.199	0.159	0.148
Mn	0.007	0.011	0.010	0.022	0.017	0.011	0.010	0.022	0.017	0.008	0.011	0.009	0.021	0.015	0.017	0.028	0.021	0.011	0.011
Ca	0.906	0.909	0.921	0.815	0.826	0.909	0.921	0.815	0.826	0.910	0.900	0.908	0.821	0.831	0.838	0.797	0.829	0.901	0.910
Na	0.026	0.026	0.026	0.031	0.026	0.026	0.026	0.031	0.026	0.025	0.026	0.025	0.026	0.026	0.030	0.026	0.020	0.020	0.023
K	0.000	0.000	0.000	0.000	0.000	0.000	0.000	0.000	0.000	0.000	0.001	0.000	0.000	0.000	0.000	0.003	0.000	0.000	0.000
Sum	4.000	4.000	4.000	4.000	4.000	4.000	4.000	4.000	4.000	4.000	4.000	4.000	4.000	4.000	4.000	4.000	4.000	4.000	4.000
Wo (mol%)	0.490	0.481	0.483	0.423	0.427	0.481	0.483	0.423	0.427	0.480	0.477	0.479	0.423	0.433	0.434	0.416	0.425	0.468	0.476
En (mol%)	0.330	0.363	0.366	0.423	0.427	0.363	0.366	0.423	0.427	0.373	0.363	0.374	0.435	0.426	0.424	0.437	0.435	0.391	0.379
Fs (mol%)	0.180	0.156	0.151	0.154	0.146	0.156	0.151	0.154	0.146	0.147	0.159	0.147	0.142	0.142	0.141	0.146	0.140	0.142	0.145

Table D7 Pyroxene analyses of the 2010 Merapi eruption (continued)

Sample	M11-27-4	M11-27-4	M11-27-4	M11-27-4	M11-27-4	M11-27-4	M11-27-4	M11-27-4	M11-27-4	M11-27-4	M11-27-4	M11-27-4	M11-27-4	M11-27-4	M11-27-4	M11-27-4	M11-27-4	M11-27-4	M11-27-4
Sample Type	LG-Inc	LG-Inc	LG-Inc	LG-Inc	LG-Inc	LG-Inc	LG-Inc	LG-Inc	LG-Inc	LG-Inc	LG-Inc	LG-Inc	LG-Inc	LG-Inc	LG-Inc	LG-Inc	LG-Inc	LG-Inc	LG-Inc
Point	55 / 1 .	34 / 1 .	35 / 1 .	4 / 1 .	5 / 1 .	6 / 1 .	47 / 1 .	48 / 1 .	55 / 1 .	52 / 1 .	53 / 1 .	54 / 1 .	51 / 1 .	1 / 1 .	2 / 1 .	3 / 1 .	77 / 1 .	32 / 1 .	33 / 1 .
Comment	ph	ph	ph	ph	ph	ph	ph	ph	ph	ph	ph	ph	ph	ph-r	ph-r	ph-r	ph-c	ph	ph
Pyroxene Type	cpx	cpx	cpx	cpx	cpx	cpx	cpx	cpx	cpx	cpx	cpx	cpx	cpx	cpx	cpx	cpx	cpx	opx	opx
SiO_2	49.32	51.81	51.53	51.67	50.95	50.89	51.44	52.28	49.32	51.44	49.16	48.31	51.61	47.65	47.49	48.11	51.37	53.45	53.42
TiO_2	0.75	0.39	0.39	0.36	0.57	0.55	0.44	0.38	0.75	0.34	0.62	0.87	0.34	1.00	1.14	0.96	0.51	0.23	0.18
Al_2O_3	3.92	1.92	2.12	1.90	2.78	2.72	2.32	1.54	3.92	1.42	4.02	4.70	1.67	5.63	6.12	5.65	2.40	0.91	0.72
Cr_2O_3	0.00	0.00	0.01	0.03	0.02	0.00	0.00	0.00	0.00	0.02	0.00	0.00	0.00	0.03	0.01	0.00	0.01	0.02	0.01
FeO	8.18	9.58	8.89	8.88	8.72	8.79	8.31	8.59	8.18	8.70	8.68	8.81	8.91	8.86	9.62	8.91	8.93	18.73	18.67
MnO	0.34	0.68	0.71	0.68	0.49	0.56	0.51	0.69	0.34	0.67	0.35	0.36	0.88	0.26	0.34	0.29	0.56	1.28	1.33
MgO	13.53	15.29	15.15	15.24	14.71	14.79	14.73	15.77	13.53	15.19	13.44	12.94	14.92	12.64	12.29	12.72	15.05	24.34	24.46
CaO	22.43	20.14	20.40	20.65	20.79	21.08	21.63	20.55	22.43	20.61	22.40	22.58	19.74	22.60	22.48	22.70	20.25	1.37	1.42
Na_2O	0.36	0.36	0.41	0.36	0.37	0.41	0.30	0.28	0.36	0.28	0.27	0.32	0.36	0.35	0.37	0.34	0.40	0.03	0.03
K_2O	0.00	0.01	0.00	0.00	0.00	0.00	0.02	0.01	0.00	0.01	0.00	0.00	0.05	0.00	0.02	0.00	0.00	0.00	0.00
Sum	98.84	100.17	99.62	99.77	99.38	99.80	99.70	100.09	98.84	98.68	98.94	98.89	98.48	99.03	99.87	99.69	99.48	100.35	100.24
Si	1.868	1.932	1.929	1.932	1.911	1.905	1.923	1.943	1.868	1.944	1.864	1.838	1.952	1.811	1.796	1.816	1.924	1.963	1.965
Al	0.175	0.084	0.094	0.084	0.123	0.120	0.102	0.067	0.175	0.063	0.180	0.211	0.074	0.252	0.273	0.252	0.106	0.039	0.031
Ti	0.021	0.011	0.011	0.010	0.016	0.015	0.013	0.011	0.021	0.010	0.018	0.025	0.010	0.029	0.032	0.027	0.014	0.006	0.005
Cr	0.000	0.000	0.000	0.001	0.001	0.000	0.000	0.000	0.000	0.001	0.000	0.000	0.000	0.001	0.000	0.000	0.000	0.001	0.000
Mg	0.764	0.850	0.846	0.850	0.823	0.825	0.821	0.874	0.764	0.856	0.760	0.734	0.841	0.717	0.693	0.716	0.840	1.333	1.341
Fe	0.259	0.299	0.278	0.278	0.274	0.275	0.260	0.267	0.259	0.275	0.275	0.280	0.282	0.282	0.304	0.281	0.280	0.575	0.574
Mn	0.011	0.021	0.022	0.021	0.016	0.018	0.016	0.022	0.011	0.022	0.011	0.011	0.028	0.009	0.011	0.009	0.018	0.040	0.041
Ca	0.911	0.805	0.818	0.827	0.836	0.845	0.866	0.818	0.911	0.834	0.910	0.920	0.800	0.921	0.911	0.918	0.812	0.054	0.056
Na	0.027	0.026	0.030	0.026	0.027	0.030	0.022	0.020	0.027	0.020	0.020	0.024	0.026	0.026	0.027	0.025	0.029	0.002	0.002
K	0.000	0.000	0.000	0.000	0.000	0.000	0.001	0.000	0.000	0.000	0.000	0.000	0.003	0.000	0.001	0.000	0.000	0.000	0.000
Sum	4.036	4.028	4.028	4.029	4.024	4.034	4.024	4.022	4.036	4.025	4.038	4.044	4.016	4.046	4.049	4.044	4.023	4.012	4.016
Si	1.851	1.919	1.915	1.918	1.900	1.889	1.912	1.932	1.851	1.932	1.847	1.818	1.944	1.791	1.775	1.796	1.913	1.957	1.957
Al	0.174	0.084	0.093	0.083	0.122	0.119	0.102	0.067	0.174	0.063	0.178	0.209	0.074	0.249	0.269	0.249	0.105	0.039	0.031
Ti	0.021	0.011	0.011	0.010	0.016	0.015	0.012	0.011	0.021	0.010	0.017	0.025	0.010	0.028	0.032	0.027	0.014	0.006	0.005
Cr	0.000	0.000	0.000	0.001	0.000	0.000	0.000	0.000	0.000	0.001	0.000	0.000	0.000	0.001	0.000	0.000	0.000	0.001	0.000
Fe^{3+}	0.107	0.083	0.084	0.086	0.073	0.102	0.072	0.067	0.107	0.074	0.114	0.129	0.046	0.137	0.144	0.130	0.070	0.037	0.048
Mg	0.757	0.844	0.840	0.844	0.818	0.818	0.816	0.869	0.757	0.850	0.753	0.726	0.838	0.708	0.685	0.708	0.835	1.328	1.336
Fe^{2+}	0.149	0.213	0.192	0.189	0.199	0.171	0.186	0.199	0.149	0.199	0.159	0.148	0.234	0.141	0.156	0.149	0.209	0.537	0.524
Mn	0.011	0.021	0.022	0.021	0.015	0.017	0.016	0.022	0.011	0.021	0.011	0.011	0.028	0.008	0.011	0.009	0.018	0.040	0.041
Ca	0.902	0.799	0.812	0.821	0.831	0.838	0.861	0.814	0.902	0.829	0.901	0.910	0.797	0.910	0.900	0.908	0.808	0.054	0.056
Na	0.026	0.026	0.030	0.026	0.026	0.030	0.022	0.020	0.026	0.020	0.020	0.023	0.026	0.025	0.026	0.025	0.029	0.002	0.002
K	0.000	0.000	0.000	0.000	0.000	0.000	0.001	0.000	0.000	0.000	0.000	0.000	0.003	0.000	0.001	0.000	0.000	0.000	0.000
Sum	4.000	4.000	4.000	4.000	4.000	4.000	4.000	4.000	4.000	4.000	4.000	4.000	4.000	4.000	4.000	4.000	4.000	4.000	4.000
Wo (mol%)	0.471	0.412	0.421	0.423	0.433	0.434	0.445	0.418	0.471	0.425	0.468	0.476	0.416	0.480	0.477	0.479	0.420	0.027	0.028
En (mol%)	0.395	0.435	0.435	0.435	0.426	0.424	0.422	0.446	0.395	0.435	0.391	0.379	0.437	0.373	0.363	0.374	0.435	0.679	0.680
Fs (mol%)	0.134	0.153	0.143	0.142	0.142	0.141	0.133	0.136	0.134	0.140	0.142	0.145	0.146	0.147	0.159	0.147	0.145	0.293	0.291

Table D7 Pyroxene analyses of the 2010 Merapi eruption (continued)

Sample	M11-27-4	M11-27-4	M11-27-4	M11-27-4	M11-27-4	M11-27-4	M11-27-4	M11-27-4	M11-27-5	M11-27-5	M11-27-5	M11-27-5	M11-27-5	M11-27-5	M11-27-5	M11-27-5	M11-27-5	M11-27-5	M11-27-5
Sample Type	LG-Inc	LG-Inc	LG-Inc	LG-Inc	LG-Inc	LG-Inc	LG-Inc	LG-Inc	DD	DD	DD	DD	DD	DD	DD	DD	DD	DD	DD
Point	45 / 1 .	46 / 1 .	56 / 1 .	27 / 1 .	28 / 1 .	29 / 1 .	30 / 1 .	31 / 1 .	124 / 1 .	126 / 1 .	127 / 1 .	128 / 1 .	129 / 1 .	130 / 1 .	88 / 1 .	90 / 1 .	94 / 1 .	99 / 1 .	102 / 1 .
Comment	ph	ph	mph	mph-c	mph-c	mph-r	mph-r	mph-r	ph	ph	ph	ph	ph	ph	ph	ph	ph	ph	ph
Pyroxene Type	opx	opx	opx	opx	opx	opx	opx	opx	cpx	cpx	cpx	cpx	cpx	cpx	cpx	cpx	cpx	cpx	cpx
SiO_2	53.99	53.52	52.01	53.63	53.16	51.97	52.17	51.62	51.61	52.33	52.41	50.59	52.85	52.41	51.69	52.09	52.05	52.95	52.61
TiO_2	0.18	0.15	0.11	0.18	0.21	0.18	0.12	0.23	0.36	0.36	0.32	0.67	0.30	0.17	0.32	0.29	0.53	0.31	0.32
Al_2O_3	0.55	0.68	0.21	0.71	0.88	0.53	0.24	0.43	1.78	1.74	1.88	3.68	1.86	1.67	1.84	1.51	2.55	1.39	1.50
Cr_2O_3	0.03	0.00	0.01	0.03	0.00	0.00	0.01	0.00	0.00	0.05	0.00	0.00	0.01	0.03	0.00	0.00	0.00	0.01	0.00
FeO	17.70	18.28	24.07	18.15	18.58	22.88	23.62	24.03	9.78	9.18	8.78	8.56	8.93	10.93	8.79	8.90	8.98	8.79	8.75
MnO	1.25	1.32	2.38	1.37	1.44	2.10	2.63	2.34	0.73	0.73	0.58	0.40	0.68	0.58	0.63	0.77	0.72	0.66	0.74
MgO	25.11	24.76	19.71	24.74	24.47	20.50	19.88	19.43	15.25	15.19	14.55	14.07	15.10	13.61	14.96	15.08	14.52	15.13	15.19
CaO	1.47	1.40	1.08	1.49	1.44	1.32	1.14	1.29	19.41	20.16	21.52	21.78	20.67	20.92	20.37	20.43	20.56	20.48	20.71
Na_2O	0.01	0.02	0.02	0.03	0.04	0.03	0.01	0.02	0.47	0.41	0.36	0.38	0.36	0.33	0.38	0.37	0.36	0.32	0.34
K_2O	0.00	0.01	0.02	0.01	0.01	0.01	0.01	0.03	0.00	0.00	0.00	0.00	0.00	0.00	0.00	0.01	0.04	0.00	0.02
Sum	100.29	100.15	99.63	100.34	100.22	99.54	99.82	99.43	99.38	100.15	100.39	100.12	100.76	100.65	98.99	99.45	100.30	100.02	100.18
Si	1.973	1.966	1.984	1.966	1.957	1.972	1.984	1.975	1.939	1.947	1.947	1.887	1.951	1.957	1.944	1.952	1.933	1.967	1.955
Al	0.024	0.029	0.010	0.031	0.038	0.024	0.011	0.020	0.079	0.076	0.082	0.162	0.081	0.073	0.082	0.067	0.112	0.061	0.066
Ti	0.005	0.004	0.003	0.005	0.006	0.005	0.003	0.007	0.010	0.010	0.009	0.019	0.008	0.005	0.009	0.008	0.015	0.009	0.009
Cr	0.001	0.000	0.000	0.001	0.000	0.000	0.000	0.000	0.000	0.001	0.000	0.000	0.000	0.001	0.000	0.000	0.000	0.000	0.000
Mg	1.369	1.356	1.121	1.352	1.343	1.160	1.127	1.108	0.854	0.843	0.806	0.782	0.831	0.758	0.839	0.842	0.804	0.838	0.842
Fe	0.541	0.562	0.768	0.556	0.572	0.726	0.751	0.769	0.307	0.285	0.273	0.267	0.276	0.341	0.277	0.279	0.279	0.273	0.272
Mn	0.039	0.041	0.077	0.043	0.045	0.067	0.085	0.076	0.023	0.023	0.018	0.012	0.021	0.018	0.020	0.024	0.023	0.021	0.023
Ca	0.058	0.055	0.044	0.059	0.057	0.054	0.047	0.053	0.781	0.804	0.856	0.870	0.818	0.837	0.821	0.820	0.818	0.815	0.824
Na	0.001	0.001	0.001	0.002	0.003	0.002	0.001	0.001	0.034	0.029	0.026	0.027	0.026	0.024	0.028	0.027	0.026	0.023	0.024
K	0.000	0.000	0.001	0.001	0.000	0.000	0.001	0.001	0.000	0.000	0.000	0.000	0.000	0.000	0.000	0.001	0.002	0.000	0.001
Sum	4.010	4.016	4.009	4.014	4.020	4.012	4.008	4.010	4.028	4.019	4.016	4.027	4.013	4.013	4.020	4.020	4.010	4.005	4.016
Si	1.969	1.959	1.979	1.959	1.947	1.967	1.980	1.970	1.926	1.938	1.939	1.874	1.945	1.950	1.935	1.942	1.928	1.964	1.947
Al	0.023	0.029	0.010	0.030	0.038	0.024	0.011	0.019	0.078	0.076	0.082	0.161	0.081	0.073	0.081	0.066	0.111	0.061	0.066
Ti	0.005	0.004	0.003	0.005	0.006	0.005	0.003	0.007	0.010	0.010	0.009	0.019	0.008	0.005	0.009	0.008	0.015	0.009	0.009
Cr	0.001	0.000	0.000	0.001	0.000	0.000	0.000	0.000	0.000	0.001	0.000	0.000	0.000	0.001	0.000	0.000	0.000	0.000	0.000
Fe^{3+}	0.030	0.048	0.028	0.043	0.060	0.035	0.025	0.030	0.084	0.056	0.048	0.080	0.038	0.040	0.058	0.060	0.031	0.016	0.048
Mg	1.365	1.351	1.118	1.347	1.336	1.157	1.124	1.105	0.848	0.839	0.802	0.777	0.828	0.755	0.835	0.838	0.802	0.836	0.838
Fe^{2+}	0.510	0.512	0.738	0.511	0.509	0.689	0.724	0.737	0.221	0.228	0.223	0.185	0.237	0.300	0.217	0.217	0.247	0.256	0.223
Mn	0.038	0.041	0.077	0.042	0.045	0.067	0.085	0.076	0.023	0.023	0.018	0.012	0.021	0.018	0.020	0.024	0.023	0.021	0.023
Ca	0.057	0.055	0.044	0.058	0.056	0.054	0.046	0.053	0.776	0.800	0.853	0.864	0.815	0.834	0.817	0.816	0.816	0.814	0.821
Na	0.001	0.001	0.001	0.002	0.003	0.002	0.001	0.001	0.034	0.029	0.026	0.027	0.026	0.024	0.028	0.027	0.026	0.023	0.024
K	0.000	0.000	0.001	0.001	0.000	0.000	0.001	0.001	0.000	0.000	0.000	0.000	0.000	0.000	0.000	0.001	0.002	0.000	0.001
Sum	4.000	4.000	4.000	4.000	4.000	4.000	4.000	4.000	4.000	4.000	4.000	4.000	4.000	4.000	4.000	4.000	4.000	4.000	4.000
Wo (mol%)	0.029	0.028	0.023	0.030	0.029	0.028	0.024	0.027	0.402	0.416	0.443	0.453	0.425	0.432	0.424	0.422	0.430	0.423	0.425
En (mol%)	0.696	0.687	0.580	0.687	0.681	0.598	0.586	0.574	0.440	0.436	0.416	0.408	0.432	0.391	0.433	0.434	0.423	0.435	0.434
Fs (mol%)	0.275	0.285	0.397	0.283	0.290	0.374	0.390	0.398	0.158	0.148	0.141	0.139	0.143	0.176	0.143	0.144	0.147	0.142	0.140

Table D7 Pyroxene analyses of the 2010 Merapi eruption (continued)

Sample	M11-27-5	M11-27-5	M11-27-6	M11-27-6	M11-27-6	M11-27-6	M11-27-6	M11-27-6	M11-27-6	M11-27-6	M11-27-6	M11-27-6	M11-27-6	M11-27-6	M11-27-6	M11-27-6	M11-27-6	M11-28a	M11-28a
Sample Type	DD	DD	LG-Inc	LG-Inc	LG-Inc	LG-Inc	LG-Inc	LG-Inc	LG-Inc	LG-Inc	LG-Inc	LG-Inc	LG-Inc	LG-Inc	LG-Inc	LG-Inc	LG-Inc	P5N-Sc	P5N-Sc
Point	105 / 1 .	111 / 1 .	28 / 1 .	29 / 1 .	30 / 1 .	33 / 1 .	34 / 1 .	33 / 1 .	28 / 1 .	29 / 1 .	30 / 1 .	34 / 1 .	36 / 1 .	32 / 1 .	37 / 1 .	35 / 1 .	38 / 1 .	7 / 1 .	8 / 1 .
Comment	ph	ph	ph	ph	ph	ph	ph	ph-c	ph	ph	ph	ph-r	ph-c	ph-c	ph-r	ph-r	ph-r	ph	ph
Pyroxene Type	cpx	cpx	cpx	cpx	cpx	cpx	cpx	cpx	cpx	cpx	cpx	cpx	cpx	cpx	cpx	cpx	cpx	cpx	cpx
SiO_2	52.84	52.94	50.01	49.92	52.01	52.46	48.76	52.46	50.01	49.92	52.01	48.76	53.68	52.76	52.57	51.41	52.62	53.06	52.02
TiO_2	0.29	0.30	0.64	0.66	0.37	0.30	0.78	0.30	0.64	0.66	0.37	0.78	0.20	0.18	0.21	0.22	0.20	0.35	0.47
Al_2O_3	1.42	1.58	4.49	4.40	1.83	1.54	4.59	1.54	4.49	4.40	1.83	4.59	0.90	0.90	0.88	1.01	0.72	1.43	2.31
Cr_2O_3	0.01	0.01	0.10	0.06	0.00	0.00	0.00	0.00	0.10	0.06	0.00	0.00	0.00	0.00	0.00	0.00	0.00	-0.01	0.00
FeO	8.62	8.64	6.49	6.47	8.78	9.39	10.58	9.39	6.49	6.47	8.78	10.58	17.70	21.46	21.22	24.16	21.56	9.23	8.50
MnO	0.73	0.77	0.14	0.13	0.71	0.63	0.56	0.63	0.14	0.13	0.71	0.56	1.05	1.00	1.56	1.71	1.59	0.75	0.56
MgO	14.98	15.19	14.76	14.74	15.54	16.39	12.71	16.39	14.76	14.74	15.54	12.71	25.42	22.66	22.33	19.76	22.01	15.05	15.10
CaO	20.70	20.51	22.98	23.47	20.49	18.98	21.36	18.98	22.98	23.47	20.49	21.36	1.41	1.24	1.42	1.60	1.48	20.50	20.40
Na_2O	0.34	0.35	0.27	0.25	0.36	0.26	0.39	0.26	0.27	0.25	0.36	0.39	0.02	0.02	0.02	0.02	0.02	0.37	0.39
K_2O	0.02	0.01	0.01	0.01	0.00	0.00	0.02	0.00	0.01	0.01	0.00	0.02	0.00	0.00	0.00	0.00	0.03	0.02	0.00
Sum	99.95	100.29	99.88	100.11	100.07	99.95	99.76	99.95	99.88	100.11	100.07	99.76	100.37	100.22	100.20	99.89	100.22	100.74	99.75
Si	1.965	1.961	1.858	1.854	1.936	1.949	1.847	1.949	1.858	1.854	1.936	1.847	1.960	1.963	1.960	1.955	1.966	1.962	1.937
Al	0.062	0.069	0.197	0.193	0.080	0.068	0.205	0.068	0.197	0.193	0.080	0.205	0.039	0.039	0.039	0.045	0.032	0.062	0.101
Ti	0.008	0.008	0.018	0.018	0.010	0.008	0.022	0.008	0.018	0.018	0.010	0.022	0.005	0.005	0.006	0.006	0.006	0.010	0.013
Cr	0.000	0.000	0.003	0.002	0.000	0.000	0.000	0.000	0.003	0.002	0.000	0.000	0.000	0.000	0.000	0.000	0.000	0.000	0.000
Mg	0.831	0.839	0.818	0.816	0.862	0.908	0.718	0.908	0.818	0.816	0.862	0.718	1.384	1.256	1.241	1.120	1.226	0.829	0.838
Fe	0.268	0.268	0.202	0.201	0.273	0.292	0.335	0.292	0.202	0.201	0.273	0.335	0.540	0.668	0.662	0.768	0.674	0.285	0.265
Mn	0.023	0.024	0.004	0.004	0.022	0.020	0.018	0.020	0.004	0.004	0.022	0.018	0.032	0.031	0.049	0.055	0.050	0.023	0.018
Ca	0.825	0.814	0.915	0.934	0.817	0.756	0.867	0.756	0.915	0.934	0.817	0.867	0.055	0.050	0.057	0.065	0.059	0.812	0.814
Na	0.025	0.025	0.020	0.018	0.026	0.019	0.029	0.019	0.020	0.018	0.026	0.029	0.002	0.001	0.001	0.002	0.002	0.027	0.028
K	0.001	0.001	0.000	0.001	0.000	0.000	0.001	0.000	0.000	0.001	0.000	0.001	0.000	0.000	0.000	0.000	0.001	0.001	0.000
Sum	4.008	4.009	4.034	4.040	4.027	4.019	4.043	4.019	4.034	4.040	4.027	4.043	4.016	4.013	4.015	4.017	4.014	4.011	4.013
Si	1.961	1.957	1.842	1.836	1.923	1.940	1.828	1.940	1.842	1.836	1.923	1.828	1.952	1.956	1.953	1.947	1.959	1.956	1.930
Al	0.062	0.069	0.195	0.191	0.080	0.067	0.203	0.067	0.195	0.191	0.080	0.203	0.038	0.039	0.038	0.045	0.031	0.062	0.101
Ti	0.008	0.008	0.018	0.018	0.010	0.008	0.022	0.008	0.018	0.018	0.010	0.022	0.005	0.005	0.006	0.006	0.006	0.010	0.013
Cr	0.000	0.000	0.003	0.002	0.000	0.000	0.000	0.000	0.003	0.002	0.000	0.000	0.000	0.000	0.000	0.000	0.000	0.000	0.000
Fe^{3+}	0.024	0.026	0.102	0.118	0.080	0.056	0.126	0.056	0.102	0.118	0.080	0.126	0.049	0.040	0.045	0.050	0.043	0.033	0.040
Mg	0.829	0.837	0.811	0.808	0.856	0.904	0.710	0.904	0.811	0.808	0.856	0.710	1.378	1.252	1.237	1.115	1.221	0.827	0.835
Fe^{2+}	0.243	0.241	0.098	0.081	0.191	0.235	0.205	0.235	0.098	0.081	0.191	0.205	0.489	0.625	0.614	0.715	0.628	0.251	0.224
Mn	0.023	0.024	0.004	0.004	0.022	0.020	0.018	0.020	0.004	0.004	0.022	0.018	0.032	0.031	0.049	0.055	0.050	0.023	0.018
Ca	0.823	0.812	0.907	0.924	0.812	0.752	0.858	0.752	0.907	0.924	0.812	0.858	0.055	0.049	0.056	0.065	0.059	0.810	0.811
Na	0.025	0.025	0.020	0.017	0.026	0.019	0.028	0.019	0.020	0.017	0.026	0.028	0.002	0.001	0.001	0.002	0.002	0.027	0.028
K	0.001	0.001	0.000	0.001	0.000	0.000	0.001	0.000	0.000	0.001	0.000	0.001	0.000	0.000	0.000	0.000	0.001	0.001	0.000
Sum	4.000	4.000	4.000	4.000	4.000	4.000	4.000	4.000	4.000	4.000	4.000	4.000	4.000	4.000	4.000	4.000	4.000	4.000	4.000
Wo (mol%)	0.429	0.424	0.473	0.479	0.419	0.386	0.452	0.386	0.473	0.479	0.419	0.452	0.028	0.025	0.029	0.033	0.030	0.421	0.425
En (mol%)	0.432	0.437	0.423	0.418	0.442	0.464	0.374	0.464	0.423	0.418	0.442	0.374	0.699	0.637	0.633	0.573	0.626	0.430	0.437
Fs (mol%)	0.139	0.139	0.104	0.103	0.140	0.149	0.175	0.149	0.104	0.103	0.140	0.175	0.273	0.338	0.338	0.393	0.344	0.148	0.138

Table D7 Pyroxene analyses of the 2010 Merapi eruption (continued)

Sample	M11-28a	M11-28a	M11-28a	M11-28a	M11-28a	M11-28a	M11-28a	M11-28a	M11-28a	M11-28a	M11-28a	M11-28b	M11-28b	M11-28b	M11-28b	M11-28b	M11-28b	M11-28b	M11-28b
Sample Type	P5N-Sc	P5N-Sc	P5N-Sc	P5N-Sc	P5N-Sc	P5N-Sc	P5N-Sc	P5N-Sc	P5N-Sc	P5N-Sc	P5N-Sc	P5N-LGD	P5N-LGD	P5N-LGD	P5N-LGD	P5N-LGD	P5N-LGD	P5N-LGD	P5N-LGD
Point	10 / 1 .	11 / 1 .	12 / 1 .	13 / 1 .	14 / 1 .	26 / 1 .	29 / 1 .	23 / 1 .	25 / 1 .	27 / 1 .	29 / 1 .	1 / 1 .	2 / 1 .	4 / 1 .	5 / 1 .	6 / 1 .	7 / 1 .	8 / 1 .	9 / 1 .
Comment	ph	ph	ph	ph	ph	ph	ph	m-c	m-c	m-c	m-c	ph	ph	ph	ph	ph	ph	ph	ph
Pyroxene Type	cpx	cpx	cpx	cpx	cpx	cpx	cpx	cpx	cpx	cpx	opx	cpx	cpx	cpx	cpx	cpx	cpx	cpx	cpx
SiO_2	52.27	53.02	52.33	52.41	51.94	52.58	52.40	48.89	50.94	52.27	54.25	52.13	49.22	52.97	52.36	53.06	51.46	51.35	52.73
TiO_2	0.41	0.40	0.27	0.36	0.32	0.29	0.37	1.09	0.75	0.12	0.18	0.41	0.71	0.46	0.46	0.37	0.27	0.53	0.35
Al_2O_3	1.99	1.79	1.94	1.69	1.74	1.73	2.42	5.79	4.27	0.84	0.87	2.08	3.46	2.31	2.47	1.62	1.17	2.55	2.02
Cr_2O_3	0.02	0.01	0.01	0.00	-0.01	0.04	0.00	-0.01	-0.01	-0.01	0.01	0.01	0.01	0.01	0.01	0.01	0.00	0.00	0.01
FeO	8.73	8.90	10.01	9.33	11.46	9.11	8.84	9.77	8.84	13.04	18.53	8.40	8.81	8.51	8.57	8.93	8.73	9.12	8.79
MnO	0.65	0.72	0.73	0.79	0.67	0.71	0.57	0.39	0.30	0.41	1.47	0.62	0.47	0.65	0.54	0.74	0.59	0.79	0.62
MgO	15.32	15.29	14.05	15.16	13.33	14.97	14.32	12.19	13.65	12.56	24.59	14.95	13.97	15.26	15.05	15.52	14.64	14.45	15.29
CaO	20.63	20.66	20.88	20.24	20.69	20.64	21.48	22.28	22.23	20.96	1.38	21.37	21.97	20.51	21.10	20.43	21.06	21.14	20.88
Na_2O	0.37	0.33	0.38	0.41	0.37	0.40	0.36	0.39	0.29	0.21	0.03	0.35	0.43	0.41	0.37	0.37	0.39	0.40	0.31
K_2O	0.00	0.02	0.00	0.00	0.00	0.00	0.01	0.01	0.02	0.03	0.02	0.01	0.01	0.03	0.00	0.03	0.02	0.08	0.00
Sum	100.39	101.14	100.61	100.40	100.51	100.48	100.76	100.78	101.28	100.44	101.32	100.33	99.05	101.11	100.94	101.06	98.32	100.42	101.00
Si	1.938	1.950	1.948	1.947	1.948	1.950	1.938	1.827	1.879	1.974	1.970	1.935	1.867	1.943	1.929	1.953	1.955	1.914	1.942
Al	0.087	0.078	0.085	0.074	0.077	0.076	0.106	0.255	0.186	0.037	0.037	0.091	0.155	0.100	0.107	0.070	0.052	0.112	0.088
Ti	0.011	0.011	0.008	0.010	0.009	0.008	0.010	0.031	0.021	0.003	0.005	0.011	0.020	0.013	0.013	0.010	0.008	0.015	0.010
Cr	0.001	0.000	0.000	0.000	0.000	0.001	0.000	0.000	0.000	0.000	0.000	0.000	0.000	0.000	0.000	0.000	0.000	0.000	0.000
Mg	0.847	0.838	0.779	0.840	0.745	0.828	0.789	0.679	0.751	0.707	1.331	0.827	0.790	0.835	0.827	0.851	0.829	0.803	0.839
Fe	0.271	0.274	0.312	0.290	0.359	0.283	0.273	0.305	0.273	0.412	0.563	0.261	0.280	0.261	0.264	0.275	0.277	0.284	0.271
Mn	0.020	0.022	0.023	0.025	0.021	0.022	0.018	0.012	0.009	0.013	0.045	0.020	0.015	0.020	0.017	0.023	0.019	0.025	0.019
Ca	0.819	0.814	0.833	0.806	0.832	0.820	0.851	0.892	0.879	0.848	0.054	0.850	0.893	0.806	0.833	0.805	0.857	0.844	0.824
Na	0.026	0.023	0.028	0.030	0.027	0.029	0.026	0.028	0.021	0.016	0.002	0.025	0.031	0.029	0.026	0.026	0.029	0.029	0.022
K	0.000	0.001	0.000	0.000	0.000	0.000	0.000	0.000	0.001	0.002	0.001	0.001	0.000	0.001	0.000	0.001	0.001	0.004	0.000
Sum	4.020	4.012	4.015	4.021	4.018	4.017	4.012	4.029	4.019	4.013	4.008	4.021	4.051	4.009	4.017	4.015	4.026	4.031	4.015
Si	1.928	1.944	1.940	1.937	1.939	1.942	1.932	1.814	1.870	1.968	1.966	1.925	1.843	1.939	1.921	1.945	1.942	1.900	1.935
Al	0.086	0.077	0.085	0.074	0.077	0.075	0.105	0.253	0.185	0.037	0.037	0.091	0.153	0.100	0.107	0.070	0.052	0.111	0.087
Ti	0.011	0.011	0.008	0.010	0.009	0.008	0.010	0.030	0.021	0.003	0.005	0.011	0.020	0.013	0.013	0.010	0.008	0.015	0.010
Cr	0.001	0.000	0.000	0.000	0.000	0.001	0.000	0.000	0.000	0.000	0.000	0.000	0.000	0.000	0.000	0.000	0.000	0.000	0.000
Fe^{3+}	0.061	0.036	0.046	0.063	0.054	0.052	0.036	0.087	0.055	0.038	0.024	0.062	0.152	0.027	0.051	0.046	0.079	0.093	0.046
Mg	0.843	0.836	0.776	0.835	0.742	0.824	0.787	0.674	0.747	0.705	1.329	0.823	0.780	0.833	0.823	0.848	0.824	0.797	0.836
Fe^{2+}	0.209	0.237	0.264	0.226	0.304	0.230	0.236	0.216	0.216	0.373	0.537	0.198	0.124	0.234	0.212	0.228	0.197	0.190	0.224
Mn	0.020	0.022	0.023	0.025	0.021	0.022	0.018	0.012	0.009	0.013	0.045	0.019	0.015	0.020	0.017	0.023	0.019	0.025	0.019
Ca	0.815	0.812	0.830	0.802	0.828	0.817	0.849	0.885	0.875	0.846	0.054	0.846	0.882	0.804	0.830	0.802	0.851	0.838	0.821
Na	0.026	0.023	0.027	0.030	0.027	0.028	0.026	0.028	0.021	0.016	0.002	0.025	0.031	0.029	0.026	0.026	0.029	0.029	0.022
K	0.000	0.001	0.000	0.000	0.000	0.000	0.000	0.000	0.001	0.002	0.001	0.001	0.000	0.001	0.000	0.001	0.001	0.004	0.000
Sum	4.000	4.000	4.000	4.000	4.000	4.000	4.000	4.000	4.000	4.000	4.000	4.000	4.000	4.000	4.000	4.000	4.000	4.000	4.000
Wo (mol%)	0.423	0.423	0.433	0.416	0.429	0.425	0.445	0.475	0.462	0.431	0.028	0.439	0.455	0.424	0.433	0.417	0.436	0.437	0.426
En (mol%)	0.437	0.435	0.405	0.434	0.385	0.429	0.412	0.362	0.395	0.360	0.684	0.427	0.403	0.439	0.430	0.441	0.422	0.416	0.434
Fs (mol%)	0.140	0.142	0.162	0.150	0.186	0.146	0.143	0.163	0.143	0.209	0.289	0.135	0.142	0.137	0.137	0.142	0.141	0.147	0.140

Table D7 Pyroxene analyses of the 2010 Merapi eruption (continued)

Sample	M11-28b	M11-28b	M11-28b	M11-28b	M11-28b	M11-33	M11-33	M11-33	M11-33	M11-33	M11-33	M11-33	M11-33	M11-33	M11-33	M11-33	M11-33	M11-33	M11-33
Sample Type	P5N-LGD	P5N-LGD	P5N-LGD	P5N-LGD	P5N-LGD	WP	WP	WP	WP	WP	WP	WP	WP	WP	WP	WP	WP	WP	WP
Point	20 / 1 .	21 / 1 .	15 / 1 .	16 / 1 .	17 / 1 .	1 / 1 .	10 / 1 .	23 / 1 .	25 / 1 .	1 / 1 .	23 / 1 .	10 / 1 .	25 / 1 .	27 / 1 .	9 / 1 .	11 / 1 .	12 / 1 .	28 / 1 .	29 / 1 .
Comment	m-r	m-c	m-c	m-r	m-c	ph	ph	ph	ph	ph-c	ph-c	ph-r	ph-r	m	ph-r	ph	ph	m	m
Pyroxene Type	cpx	cpx	opx	opx	opx	cpx	cpx	cpx	cpx	cpx	cpx	cpx	cpx	cpx	opx	opx	opx	opx	opx
SiO_2	52.31	52.55	54.44	53.80	53.06	47.70	51.87	46.34	51.22	47.70	46.34	51.87	51.22	51.83	52.61	53.53	53.72	52.78	52.79
TiO_2	0.40	0.41	0.17	0.21	0.19	0.96	0.35	1.19	0.63	0.96	1.19	0.35	0.63	0.35	0.25	0.20	0.15	0.32	0.23
Al_2O_3	2.42	1.69	0.65	0.90	0.90	5.80	1.41	7.00	2.42	5.80	7.00	1.41	2.42	1.45	1.62	0.84	0.54	0.97	1.19
Cr_2O_3	0.00	-0.01	0.01	0.00	-0.01	0.01	0.00	0.03	0.06	0.01	0.03	0.00	0.06	0.00	0.00	0.00	0.00	0.00	0.00
FeO	9.03	9.04	18.17	18.23	20.73	8.76	8.39	9.22	8.71	8.76	9.22	8.39	8.71	8.30	18.09	18.09	17.80	17.68	17.62
MnO	0.78	0.79	1.40	1.47	1.58	0.30	0.79	0.23	0.72	0.30	0.23	0.79	0.72	0.71	1.16	1.17	1.32	1.39	1.34
MgO	14.85	15.09	24.85	24.39	22.08	12.79	15.67	11.87	14.78	12.79	11.87	15.67	14.78	15.15	24.66	24.94	24.90	24.39	24.34
CaO	20.55	20.20	1.42	1.70	1.77	22.20	20.41	22.17	20.45	22.20	22.17	20.41	20.45	20.35	1.29	1.31	1.34	1.53	1.45
Na_2O	0.37	0.38	0.02	0.03	0.06	0.33	0.31	0.35	0.40	0.33	0.35	0.31	0.40	0.34	0.03	0.02	0.02	0.01	0.02
K_2O	0.21	0.01	0.02	0.04	0.15	0.00	0.01	0.00	0.01	0.00	0.00	0.01	0.01	0.09	0.00	0.01	0.02	0.03	0.04
Sum	100.93	100.16	101.14	100.77	100.51	98.85	99.21	98.39	99.40	98.85	98.39	99.21	99.40	98.57	99.72	100.10	99.81	99.10	99.01
Si	1.933	1.953	1.976	1.965	1.970	1.813	1.945	1.776	1.921	1.813	1.776	1.945	1.921	1.955	1.940	1.964	1.975	1.958	1.958
Al	0.105	0.074	0.028	0.039	0.039	0.260	0.062	0.316	0.107	0.260	0.316	0.062	0.107	0.065	0.070	0.036	0.024	0.043	0.052
Ti	0.011	0.012	0.005	0.006	0.005	0.027	0.010	0.034	0.018	0.027	0.034	0.010	0.018	0.010	0.007	0.005	0.004	0.009	0.006
Cr	0.000	0.000	0.000	0.000	0.000	0.000	0.000	0.001	0.002	0.000	0.001	0.000	0.002	0.000	0.000	0.000	0.000	0.000	0.000
Mg	0.818	0.836	1.345	1.329	1.222	0.725	0.876	0.678	0.827	0.725	0.678	0.876	0.827	0.852	1.355	1.364	1.365	1.349	1.346
Fe	0.279	0.281	0.552	0.557	0.643	0.278	0.263	0.295	0.273	0.278	0.295	0.263	0.273	0.262	0.558	0.555	0.547	0.548	0.547
Mn	0.024	0.025	0.043	0.046	0.050	0.010	0.025	0.008	0.023	0.010	0.008	0.025	0.023	0.023	0.036	0.036	0.041	0.044	0.042
Ca	0.814	0.804	0.055	0.067	0.071	0.904	0.820	0.910	0.822	0.904	0.910	0.820	0.822	0.823	0.051	0.051	0.053	0.061	0.058
Na	0.027	0.027	0.001	0.002	0.004	0.025	0.022	0.026	0.029	0.025	0.026	0.022	0.029	0.025	0.002	0.001	0.001	0.001	0.001
K	0.010	0.000	0.001	0.002	0.007	0.000	0.000	0.000	0.000	0.000	0.000	0.000	0.000	0.004	0.000	0.000	0.001	0.001	0.002
Sum	4.021	4.012	4.006	4.011	4.011	4.042	4.025	4.044	4.022	4.042	4.044	4.025	4.022	4.017	4.019	4.014	4.010	4.013	4.011
Si	1.923	1.947	1.974	1.960	1.964	1.794	1.934	1.756	1.911	1.794	1.756	1.934	1.911	1.946	1.930	1.957	1.970	1.952	1.952
Al	0.105	0.074	0.028	0.039	0.039	0.257	0.062	0.313	0.106	0.257	0.313	0.062	0.106	0.064	0.070	0.036	0.024	0.042	0.052
Ti	0.011	0.011	0.005	0.006	0.005	0.027	0.010	0.034	0.018	0.027	0.034	0.010	0.018	0.010	0.007	0.005	0.004	0.009	0.006
Cr	0.000	0.000	0.000	0.000	0.000	0.000	0.000	0.001	0.002	0.000	0.001	0.000	0.002	0.000	0.000	0.000	0.000	0.000	0.000
Fe^{3+}	0.064	0.037	0.018	0.034	0.033	0.125	0.073	0.131	0.064	0.125	0.131	0.073	0.064	0.052	0.058	0.041	0.031	0.039	0.034
Mg	0.814	0.834	1.343	1.325	1.219	0.717	0.871	0.671	0.822	0.717	0.671	0.871	0.822	0.848	1.348	1.359	1.361	1.344	1.342
Fe^{2+}	0.214	0.243	0.533	0.522	0.608	0.151	0.188	0.161	0.208	0.151	0.161	0.188	0.208	0.209	0.497	0.513	0.514	0.507	0.511
Mn	0.024	0.025	0.043	0.045	0.050	0.010	0.025	0.007	0.023	0.010	0.007	0.025	0.023	0.023	0.036	0.036	0.041	0.043	0.042
Ca	0.809	0.802	0.055	0.066	0.070	0.895	0.815	0.900	0.817	0.895	0.900	0.815	0.817	0.819	0.051	0.051	0.052	0.061	0.057
Na	0.027	0.027	0.001	0.002	0.004	0.024	0.022	0.025	0.029	0.024	0.025	0.022	0.029	0.024	0.002	0.001	0.001	0.001	0.001
K	0.010	0.000	0.001	0.002	0.007	0.000	0.000	0.000	0.000	0.000	0.000	0.000	0.000	0.004	0.000	0.000	0.001	0.001	0.002
Sum	4.000	4.000	4.000	4.000	4.000	4.000	4.000	4.000	4.000	4.000	4.000	4.000	4.000	4.000	4.000	4.000	4.000	4.000	4.000
Wo (mol%)	0.426	0.419	0.028	0.034	0.036	0.474	0.419	0.483	0.428	0.474	0.483	0.419	0.428	0.425	0.026	0.026	0.027	0.031	0.030
En (mol%)	0.428	0.435	0.689	0.681	0.631	0.380	0.447	0.360	0.430	0.380	0.360	0.447	0.430	0.440	0.690	0.692	0.695	0.689	0.690
Fs (mol%)	0.146	0.146	0.283	0.285	0.332	0.146	0.134	0.157	0.142	0.146	0.157	0.134	0.142	0.135	0.284	0.282	0.279	0.280	0.280

Table D7 Pyroxene analyses of the 2010 Merapi eruption (continued)

Sample	M11-33	M11-34	M11-34	M11-34	M11-34	M11-34	M11-34	M11-34	M11-34	M11-34	M11-34	M11-38	M11-38	M11-38	M11-48	M11-48	M11-48	M11-48	M11-48
Sample Type	WP	DD	DD	DD	DD	DD	DD	DD	DD	DD	DD	DD	DD	DD	LGD	LGD	LGD	LGD	LGD
Point	30 / 1 .	11 / 1 .	14 / 1 .	18 / 1 .	19 / 1 .	20 / 1 .	21 / 1 .	22 / 1 .	23 / 1 .	24 / 1 .	8 / 1 .	35 / 1 .	37 / 1 .	38 / 1 .	4 / 1 .	5 / 1 .	6 / 1 .	7 / 1 .	2 / 1 .
Comment	m	ph	ph	ph	ph	ph	ph	ph	ph	ph	ph	m	m	m	ph	ph	ph	ph	ph
Pyroxene Type	opx	cpx	cpx	cpx	cpx	cpx	cpx	cpx	cpx	cpx	cpx	cpx	cpx	cpx	cpx	cpx	cpx	cpx	cpx
SiO_2	53.03	52.44	50.78	52.49	48.27	48.13	46.34	47.48	48.17	48.65	51.82	48.11	48.76	47.02	51.18	47.15	45.83	51.73	50.70
TiO_2	0.21	0.39	0.52	0.39	0.33	0.39	0.65	0.52	0.35	0.27	0.46	0.99	1.05	1.45	0.56	1.04	1.41	0.38	0.48
Al_2O_3	0.83	2.02	2.79	1.87	1.27	1.66	2.62	2.11	1.48	1.23	2.69	7.55	4.16	5.91	2.42	6.72	7.70	1.66	2.83
Cr_2O_3	0.01	0.08	0.00	0.00	0.00	0.00	0.00	0.00	0.00	0.00	0.01	0.00	0.01	0.02	0.00	0.01	0.03	0.00	0.00
FeO	17.61	8.29	8.70	8.58	23.01	22.58	24.22	22.87	23.09	23.19	8.28	10.09	10.27	10.16	8.38	9.24	9.72	9.13	9.00
MnO	1.41	0.58	0.49	0.60	0.71	0.73	0.70	0.70	0.74	0.84	0.50	0.34	0.54	0.38	0.38	0.28	0.34	0.75	0.65
MgO	24.67	15.07	14.59	15.25	3.57	3.84	2.70	3.47	3.58	3.51	14.68	11.30	13.85	12.19	14.65	12.30	11.74	15.14	14.50
CaO	1.46	21.06	20.82	20.58	22.53	22.75	22.48	22.65	22.61	22.59	21.49	21.20	19.54	21.39	22.14	22.37	22.11	20.62	20.92
Na_2O	0.02	0.34	0.36	0.37	0.26	0.28	0.28	0.25	0.26	0.27	0.34	0.25	0.27	0.32	0.38	0.39	0.36	0.38	0.35
K_2O	0.02	0.00	0.00	0.00	0.00	0.00	0.00	0.00	0.00	0.00	0.00	0.03	0.08	0.08	0.00	0.00	0.00	0.02	0.00
Sum	99.26	100.26	99.06	100.12	99.95	100.36	100.00	100.05	100.29	100.56	100.26	99.85	98.52	98.94	100.09	99.51	99.24	99.81	99.44
Si	1.962	1.943	1.912	1.948	1.946	1.930	1.885	1.914	1.937	1.950	1.923	1.809	1.859	1.797	1.910	1.786	1.747	1.936	1.906
Al	0.036	0.088	0.124	0.082	0.060	0.078	0.126	0.100	0.070	0.058	0.118	0.335	0.187	0.266	0.106	0.300	0.346	0.073	0.125
Ti	0.006	0.011	0.015	0.011	0.010	0.012	0.020	0.016	0.011	0.008	0.013	0.028	0.030	0.042	0.016	0.029	0.040	0.011	0.014
Cr	0.000	0.002	0.000	0.000	0.000	0.000	0.000	0.000	0.000	0.000	0.000	0.000	0.000	0.001	0.000	0.000	0.001	0.000	0.000
Mg	1.361	0.833	0.819	0.843	0.215	0.229	0.164	0.208	0.215	0.210	0.812	0.633	0.787	0.694	0.815	0.694	0.667	0.845	0.813
Fe	0.545	0.257	0.274	0.266	0.776	0.757	0.824	0.771	0.776	0.777	0.257	0.317	0.327	0.325	0.262	0.293	0.310	0.286	0.283
Mn	0.044	0.018	0.016	0.019	0.024	0.025	0.024	0.024	0.025	0.028	0.016	0.011	0.017	0.012	0.012	0.009	0.011	0.024	0.021
Ca	0.058	0.836	0.840	0.818	0.973	0.978	0.979	0.978	0.974	0.970	0.854	0.854	0.798	0.876	0.886	0.908	0.903	0.827	0.843
Na	0.002	0.025	0.027	0.026	0.020	0.022	0.022	0.020	0.021	0.021	0.024	0.018	0.020	0.024	0.027	0.029	0.027	0.028	0.026
K	0.001	0.000	0.000	0.000	0.000	0.000	0.000	0.000	0.000	0.000	0.000	0.001	0.004	0.004	0.000	0.000	0.000	0.001	0.000
Sum	4.015	4.013	4.025	4.014	4.024	4.031	4.044	4.030	4.028	4.023	4.017	4.006	4.029	4.041	4.034	4.049	4.052	4.030	4.030
Si	1.955	1.937	1.900	1.941	1.934	1.915	1.864	1.899	1.923	1.939	1.915	1.806	1.845	1.779	1.894	1.764	1.724	1.922	1.892
Al	0.036	0.088	0.123	0.082	0.060	0.078	0.124	0.100	0.070	0.058	0.117	0.334	0.186	0.264	0.106	0.297	0.341	0.073	0.124
Ti	0.006	0.011	0.015	0.011	0.010	0.012	0.020	0.016	0.011	0.008	0.013	0.028	0.030	0.041	0.016	0.029	0.040	0.011	0.014
Cr	0.000	0.002	0.000	0.000	0.000	0.000	0.000	0.000	0.000	0.000	0.000	0.000	0.000	0.001	0.000	0.000	0.001	0.000	0.000
Fe^{3+}	0.044	0.039	0.075	0.041	0.072	0.091	0.129	0.090	0.083	0.069	0.052	0.017	0.087	0.123	0.102	0.145	0.155	0.091	0.090
Mg	1.356	0.830	0.814	0.841	0.213	0.228	0.162	0.207	0.213	0.209	0.809	0.632	0.781	0.687	0.808	0.686	0.659	0.838	0.807
Fe^{2+}	0.499	0.217	0.198	0.224	0.699	0.660	0.686	0.675	0.688	0.703	0.204	0.300	0.238	0.199	0.157	0.145	0.150	0.193	0.191
Mn	0.044	0.018	0.015	0.019	0.024	0.025	0.024	0.024	0.025	0.028	0.016	0.011	0.017	0.012	0.012	0.009	0.011	0.024	0.021
Ca	0.058	0.834	0.835	0.816	0.967	0.970	0.969	0.970	0.967	0.965	0.851	0.853	0.792	0.867	0.878	0.897	0.892	0.821	0.837
Na	0.002	0.024	0.026	0.026	0.020	0.022	0.022	0.019	0.020	0.021	0.024	0.018	0.019	0.024	0.027	0.029	0.026	0.027	0.026
K	0.001	0.000	0.000	0.000	0.000	0.000	0.000	0.000	0.000	0.000	0.000	0.001	0.004	0.004	0.000	0.000	0.000	0.001	0.000
Sum	4.000	4.000	4.000	4.000	4.000	4.000	4.000	4.000	4.000	4.000	4.000	4.000	4.000	4.000	4.000	4.000	4.000	4.000	4.000
Wo (mol%)	0.029	0.434	0.435	0.424	0.496	0.498	0.498	0.500	0.496	0.496	0.444	0.473	0.417	0.462	0.451	0.479	0.480	0.422	0.435
En (mol%)	0.693	0.432	0.424	0.437	0.109	0.117	0.083	0.106	0.109	0.107	0.422	0.351	0.411	0.366	0.415	0.366	0.355	0.432	0.419
Fs (mol%)	0.278	0.133	0.142	0.138	0.395	0.386	0.419	0.394	0.395	0.397	0.134	0.176	0.171	0.171	0.133	0.154	0.165	0.146	0.146

Table D7 Pyroxene analyses of the 2010 Merapi eruption (continued)

Sample	M11-48	M11-48	M11-48	M11-48	M11-48	M11-48	M11-50	M11-50	M11-50	M11-50	M11-50	M11-50	M11-50	M11-50	M11-50	M11-50	M11-50	M11-50	M11-50
Sample Type	LGD	LGD	LGD	LGD	LGD	LGD	WP	WP	WP	WP	WP	WP	WP	WP	WP	WP	WP	WP	WP
Point	4 / 1 .	5 / 1 .	6 / 1 .	7 / 1 .	28 / 1 .	1 / 1 .	2 / 1 .	3 / 1 .	10 / 1 .	11 / 1 .	13 / 1 .	21 / 1 .	22 / 1 .	26 / 1 .	105 / 1 .	106 / 1 .	107 / 1 .	108 / 1 .	3 / 1 .
Comment	ph-c	ph-c	ph-r	ph-r	m	ph	ph	ph	ph	ph	ph	ph	ph	ph	ph	ph	ph	ph	ph
Pyroxene Type	cpx	cpx	cpx	cpx	pig	opx	cpx	cpx	cpx	cpx	cpx	cpx	cpx	cpx	cpx	cpx	cpx	cpx	cpx
SiO_2	51.18	47.15	45.83	51.73	52.60	52.90	53.20	52.29	52.93	50.93	51.86	51.58	51.71	51.76	51.83	50.11	48.04	51.27	53.02
TiO_2	0.56	1.04	1.41	0.38	0.39	0.19	0.35	0.38	0.34	0.52	0.47	0.53	0.37	0.46	0.27	0.52	0.88	0.39	0.38
Al_2O_3	2.42	6.72	7.70	1.66	0.82	1.34	1.43	2.24	1.61	3.35	2.39	2.81	2.34	2.72	1.66	3.29	5.56	1.82	2.24
Cr_2O_3	0.00	0.01	0.03	0.00	0.00	0.03	0.01	0.00	0.04	0.00	0.02	0.00	0.01	0.01	0.00	0.01	0.00	0.00	0.03
FeO	8.38	9.24	9.72	9.13	20.85	18.48	9.00	8.72	8.78	9.49	8.39	8.94	9.12	7.79	8.88	8.50	8.71	9.01	8.47
MnO	0.38	0.28	0.34	0.75	1.57	1.08	0.79	0.63	0.71	0.57	0.53	0.61	0.73	0.29	0.64	0.39	0.26	0.63	0.63
MgO	14.65	12.30	11.74	15.14	19.49	24.62	15.32	14.44	15.22	14.22	14.46	14.48	14.45	14.31	15.12	14.26	13.01	14.66	15.19
CaO	22.14	22.37	22.11	20.62	4.06	1.40	20.39	21.05	20.30	20.42	21.31	20.64	20.52	22.46	20.19	21.99	22.16	20.63	20.38
Na_2O	0.38	0.39	0.36	0.38	0.20	0.03	0.37	0.39	0.33	0.40	0.30	0.36	0.35	0.25	0.38	0.31	0.33	0.37	0.37
K_2O	0.00	0.00	0.00	0.02	0.06	0.01	0.00	0.00	0.00	0.00	0.00	0.00	0.01	0.00	0.00	0.00	0.00	0.01	0.00
Sum	100.09	99.51	99.24	99.81	100.04	100.09	100.86	100.15	100.26	99.90	99.73	99.95	99.62	100.05	98.97	99.39	98.95	98.77	100.71
Si	1.910	1.786	1.747	1.936	1.977	1.946	1.962	1.944	1.961	1.905	1.935	1.923	1.936	1.924	1.950	1.886	1.822	1.938	1.951
Al	0.106	0.300	0.346	0.073	0.037	0.058	0.062	0.098	0.070	0.148	0.105	0.123	0.103	0.119	0.073	0.146	0.248	0.081	0.097
Ti	0.016	0.029	0.040	0.011	0.011	0.005	0.010	0.011	0.010	0.015	0.013	0.015	0.010	0.013	0.008	0.015	0.025	0.011	0.011
Cr	0.000	0.000	0.001	0.000	0.000	0.001	0.000	0.000	0.001	0.000	0.001	0.000	0.000	0.000	0.000	0.000	0.000	0.000	0.001
Mg	0.815	0.694	0.667	0.845	1.092	1.350	0.842	0.800	0.840	0.793	0.804	0.805	0.806	0.793	0.848	0.800	0.736	0.826	0.833
Fe	0.262	0.293	0.310	0.286	0.655	0.569	0.278	0.271	0.272	0.297	0.262	0.279	0.286	0.242	0.279	0.268	0.276	0.285	0.261
Mn	0.012	0.009	0.011	0.024	0.050	0.034	0.025	0.020	0.022	0.018	0.017	0.019	0.023	0.009	0.020	0.013	0.008	0.020	0.020
Ca	0.886	0.908	0.903	0.827	0.164	0.055	0.806	0.838	0.806	0.818	0.852	0.824	0.823	0.895	0.814	0.887	0.900	0.836	0.803
Na	0.027	0.029	0.027	0.028	0.014	0.002	0.026	0.028	0.024	0.029	0.021	0.026	0.026	0.018	0.028	0.022	0.024	0.027	0.027
K	0.000	0.000	0.000	0.001	0.003	0.000	0.000	0.000	0.000	0.000	0.000	0.000	0.000	0.000	0.000	0.000	0.000	0.000	0.000
Sum	4.034	4.049	4.052	4.030	4.003	4.020	4.010	4.010	4.006	4.022	4.010	4.014	4.015	4.013	4.020	4.037	4.041	4.024	4.003
Si	1.894	1.764	1.724	1.922	1.976	1.936	1.957	1.939	1.958	1.894	1.930	1.916	1.929	1.918	1.940	1.869	1.804	1.927	1.949
Al	0.106	0.297	0.341	0.073	0.036	0.058	0.062	0.098	0.070	0.147	0.105	0.123	0.103	0.119	0.073	0.145	0.246	0.081	0.097
Ti	0.016	0.029	0.040	0.011	0.011	0.005	0.010	0.011	0.010	0.014	0.013	0.015	0.010	0.013	0.007	0.015	0.025	0.011	0.011
Cr	0.000	0.000	0.001	0.000	0.000	0.001	0.000	0.000	0.001	0.000	0.001	0.000	0.000	0.000	0.000	0.000	0.000	0.000	0.001
Fe^{3+}	0.102	0.145	0.155	0.091	0.008	0.060	0.031	0.031	0.017	0.065	0.029	0.042	0.044	0.038	0.060	0.110	0.121	0.071	0.009
Mg	0.808	0.686	0.659	0.838	1.091	1.343	0.840	0.798	0.839	0.789	0.802	0.802	0.803	0.790	0.844	0.793	0.728	0.821	0.833
Fe^{2+}	0.157	0.145	0.150	0.193	0.647	0.505	0.246	0.239	0.254	0.230	0.232	0.236	0.241	0.204	0.218	0.155	0.153	0.212	0.252
Mn	0.012	0.009	0.011	0.024	0.050	0.034	0.025	0.020	0.022	0.018	0.017	0.019	0.023	0.009	0.020	0.012	0.008	0.020	0.019
Ca	0.878	0.897	0.892	0.821	0.163	0.055	0.803	0.836	0.805	0.814	0.850	0.821	0.820	0.892	0.810	0.879	0.891	0.831	0.803
Na	0.027	0.029	0.026	0.027	0.014	0.002	0.026	0.028	0.024	0.029	0.021	0.026	0.025	0.018	0.028	0.022	0.024	0.027	0.027
K	0.000	0.000	0.000	0.001	0.003	0.000	0.000	0.000	0.000	0.000	0.000	0.000	0.000	0.000	0.000	0.000	0.000	0.000	0.000
Sum	4.000	4.000	4.000	4.000	4.000	4.000	4.000	4.000	4.000	4.000	4.000	4.000	4.000	4.000	4.000	4.000	4.000	4.000	4.000
Wo (mol%)	0.451	0.479	0.480	0.422	0.086	0.028	0.418	0.439	0.420	0.429	0.444	0.432	0.430	0.464	0.419	0.454	0.471	0.429	0.424
En (mol%)	0.415	0.366	0.355	0.432	0.571	0.684	0.437	0.419	0.438	0.416	0.419	0.422	0.421	0.411	0.437	0.409	0.385	0.424	0.439
Fs (mol%)	0.133	0.154	0.165	0.146	0.343	0.288	0.144	0.142	0.142	0.156	0.137	0.146	0.149	0.126	0.144	0.137	0.144	0.146	0.137

Table D7 Pyroxene analyses of the 2010 Merapi eruption (continued)

Sample	M11-50	M11-50	M11-50	M11-50	M11-50	M11-50	M11-50	M11-50	M11-50	M11-50	M11-50	M11-50	M11-50	M11-50	M11-51	M11-51	M11-51	M11-51	M11-51
Sample Type	WP	WP	WP	WP	WP	WP	WP	WP	WP	WP	WP	WP	WP	WP	GS	GS	GS	GS	GS
Point	6 / 1 .	10 / 1 .	12 / 1 .	16 / 1 .	18 / 1 .	22 / 1 .	24 / 1 .	26 / 1 .	27 / 1 .	32 / 1 .	87 / 1 .	88 / 1 .	91 / 1 .	92 / 1 .	8 / 1 .	9 / 1 .	10 / 1 .	11 / 1 .	48 / 1 .
Comment	ph	ph	ph	ph	ph	ph	ph	ph	ph	ph	m	m	m	m	ph	ph	ph	ph	ph
Pyroxene Type	cpx	cpx	cpx	cpx	cpx	cpx	cpx	cpx	cpx	cpx	opx	opx	opx	opx	cpx	cpx	cpx	cpx	cpx
SiO_2	52.83	52.53	52.87	53.55	51.66	53.46	50.74	52.70	51.71	53.41	53.59	53.86	54.17	53.88	51.38	48.55	51.53	51.78	51.18
TiO_2	0.47	0.44	0.36	0.33	0.58	0.33	0.39	0.44	0.57	0.32	0.23	0.23	0.12	0.22	0.47	0.93	0.43	0.39	0.47
Al_2O_3	2.21	1.84	1.71	1.53	3.29	1.92	1.89	2.17	3.23	1.62	0.99	0.81	0.52	0.89	2.17	4.75	2.08	1.77	2.28
Cr_2O_3	0.00	0.04	0.00	0.02	0.01	0.03	0.00	0.01	0.01	0.01	0.00	0.02	0.00	0.03	0.02	0.02	0.05	0.00	0.00
FeO	8.05	8.97	9.47	8.66	9.22	9.13	8.74	8.73	8.83	9.03	20.09	20.20	17.85	18.19	9.03	8.88	8.79	8.69	8.17
MnO	0.50	0.66	0.75	0.79	0.64	0.71	0.63	0.61	0.54	0.77	1.65	1.55	1.38	1.50	0.64	0.40	0.55	0.69	0.45
MgO	15.18	14.99	14.69	15.22	14.22	15.02	15.10	14.90	14.05	14.86	21.94	22.07	24.11	23.48	14.90	12.94	15.19	15.06	14.76
CaO	21.00	20.19	20.31	20.40	20.65	20.20	20.33	20.46	21.14	20.26	1.96	1.67	1.82	1.63	20.19	21.76	20.07	20.43	21.17
Na_2O	0.36	0.41	0.41	0.39	0.44	0.39	0.39	0.38	0.37	0.43	0.08	0.05	0.03	0.02	0.38	0.39	0.37	0.38	0.32
K_2O	0.00	0.00	0.00	0.01	0.00	0.00	0.01	0.00	0.00	0.00	0.04	0.02	0.01	0.02	0.00	0.01	0.00	0.01	0.00
Sum	100.59	100.06	100.57	100.91	100.70	101.18	98.22	100.39	100.44	100.70	100.56	100.47	100.01	99.86	99.18	98.62	99.05	99.20	98.81
Si	1.946	1.952	1.959	1.969	1.913	1.962	1.928	1.949	1.918	1.970	1.980	1.989	1.988	1.984	1.931	1.848	1.936	1.944	1.928
Al	0.096	0.081	0.075	0.066	0.144	0.083	0.084	0.095	0.141	0.070	0.043	0.035	0.022	0.039	0.096	0.213	0.092	0.078	0.101
Ti	0.013	0.012	0.010	0.009	0.016	0.009	0.011	0.012	0.016	0.009	0.006	0.006	0.003	0.006	0.013	0.027	0.012	0.011	0.013
Cr	0.000	0.001	0.000	0.001	0.000	0.001	0.000	0.000	0.000	0.000	0.000	0.000	0.000	0.001	0.001	0.001	0.001	0.000	0.000
Mg	0.834	0.831	0.812	0.834	0.785	0.822	0.855	0.822	0.777	0.817	1.209	1.215	1.319	1.289	0.835	0.734	0.850	0.842	0.829
Fe	0.248	0.279	0.293	0.266	0.285	0.280	0.278	0.270	0.274	0.279	0.621	0.624	0.548	0.560	0.284	0.283	0.276	0.273	0.257
Mn	0.016	0.021	0.024	0.025	0.020	0.022	0.020	0.019	0.017	0.024	0.052	0.048	0.043	0.047	0.020	0.013	0.018	0.022	0.014
Ca	0.829	0.804	0.806	0.804	0.819	0.794	0.828	0.811	0.840	0.801	0.078	0.066	0.071	0.064	0.813	0.887	0.807	0.822	0.854
Na	0.025	0.030	0.030	0.028	0.031	0.028	0.029	0.028	0.027	0.031	0.006	0.003	0.002	0.001	0.028	0.028	0.027	0.028	0.024
K	0.000	0.000	0.000	0.001	0.000	0.000	0.000	0.000	0.000	0.000	0.002	0.001	0.001	0.001	0.000	0.000	0.000	0.000	0.000
Sum	4.006	4.010	4.008	4.003	4.014	4.001	4.033	4.005	4.009	4.001	3.996	3.989	3.998	3.992	4.021	4.033	4.019	4.020	4.020
Si	1.943	1.947	1.955	1.968	1.906	1.961	1.912	1.947	1.913	1.970	1.982	1.994	1.989	1.988	1.921	1.832	1.926	1.934	1.918
Al	0.096	0.080	0.074	0.066	0.143	0.083	0.084	0.094	0.141	0.070	0.043	0.035	0.023	0.039	0.096	0.211	0.091	0.078	0.101
Ti	0.013	0.012	0.010	0.009	0.016	0.009	0.011	0.012	0.016	0.009	0.006	0.006	0.003	0.006	0.013	0.026	0.012	0.011	0.013
Cr	0.000	0.001	0.000	0.001	0.000	0.001	0.000	0.000	0.000	0.000	0.000	0.000	0.000	0.001	0.001	0.001	0.001	0.000	0.000
Fe^{3+}	0.018	0.029	0.025	0.008	0.043	0.004	0.100	0.015	0.027	0.003	0.000	0.000	0.000	0.000	0.063	0.099	0.057	0.060	0.061
Mg	0.832	0.829	0.810	0.834	0.782	0.822	0.848	0.821	0.775	0.817	1.210	1.218	1.320	1.291	0.831	0.728	0.846	0.838	0.825
Fe^{2+}	0.230	0.249	0.268	0.258	0.241	0.276	0.176	0.255	0.246	0.276	0.621	0.626	0.548	0.561	0.220	0.181	0.218	0.211	0.196
Mn	0.016	0.021	0.024	0.025	0.020	0.022	0.020	0.019	0.017	0.024	0.052	0.049	0.043	0.047	0.020	0.013	0.017	0.022	0.014
Ca	0.827	0.802	0.805	0.803	0.816	0.794	0.821	0.810	0.838	0.800	0.078	0.066	0.072	0.064	0.809	0.880	0.804	0.818	0.850
Na	0.025	0.029	0.029	0.028	0.031	0.028	0.029	0.028	0.027	0.031	0.006	0.003	0.002	0.001	0.027	0.028	0.027	0.028	0.023
K	0.000	0.000	0.000	0.001	0.000	0.000	0.000	0.000	0.000	0.000	0.002	0.001	0.001	0.001	0.000	0.000	0.000	0.000	0.000
Sum	4.000	4.000	4.000	4.000	4.000	4.000	4.000	4.000	4.000	4.000	4.000	4.000	4.000	4.000	4.000	4.000	4.000	4.000	4.000
Wo (mol%)	0.434	0.420	0.422	0.422	0.434	0.419	0.422	0.426	0.444	0.422	0.041	0.035	0.037	0.034	0.421	0.466	0.418	0.424	0.440
En (mol%)	0.436	0.434	0.425	0.438	0.415	0.433	0.436	0.432	0.411	0.431	0.634	0.638	0.680	0.674	0.432	0.385	0.440	0.435	0.427
Fs (mol%)	0.130	0.146	0.153	0.140	0.151	0.148	0.142	0.142	0.145	0.147	0.325	0.327	0.283	0.293	0.147	0.148	0.143	0.141	0.133

Table D7 Pyroxene analyses of the 2010 Merapi eruption (continued)

Sample	M11-51	M11-51	M11-51	M11-51	M11-51	M11-51	M11-51	M11-51	M11-51	M11-51	M11-53-B4	M11-53-B4	M11-53-B4	M11-53-B4	M11-53-B4	M11-53-B4	M11-53-B4	M11-53-B4	M11-53-B4
Sample Type	GS	GS	GS	GS	GS	GS	GS	GS	GS	GS	WP	WP	WP	WP	WP	WP	WP	WP	WP
Point	49 / 1 .	8 / 1 .	10 / 1 .	48 / 1 .	49 / 1 .	9 / 1 .	11 / 1 .	59 / 1 .	56 / 1 .	58 / 1 .	21 / 1 .	22 / 1 .	23 / 1 .	24 / 1 .	53 / 1 .	54 / 1 .	46 / 1 .	47 / 1 .	51 / 1 .
Comment	ph	ph-c	ph-c	ph-c	ph-c	ph-r	ph-r	m	m	m	ph-c	ph-c	ph-r	ph-r	mph	mph	mph-c	mph-r	mph
Pyroxene Type	cpx	cpx	cpx	cpx	cpx	cpx	cpx	cpx	opx	opx	cpx	cpx	cpx	cpx	cpx	cpx	cpx	cpx	opx
SiO_2	51.81	51.38	51.53	51.18	51.81	48.55	51.78	49.55	53.13	53.02	50.90	51.38	52.19	51.16	52.44	51.82	51.67	51.99	53.67
TiO_2	0.38	0.47	0.43	0.47	0.38	0.93	0.39	0.95	0.22	0.23	0.64	0.48	0.39	0.48	0.39	0.41	0.37	0.35	0.17
Al_2O_3	1.63	2.17	2.08	2.28	1.63	4.75	1.77	4.47	0.94	1.07	3.03	2.57	1.58	2.48	1.67	1.95	1.64	1.52	0.87
Cr_2O_3	0.01	0.02	0.05	0.00	0.01	0.02	0.00	0.00	0.00	0.00	0.00	0.00	0.00	0.03	0.00	0.03	0.02	0.00	0.00
FeO	8.66	9.03	8.79	8.17	8.66	8.88	8.69	9.57	17.48	17.93	8.62	8.80	8.68	8.14	8.95	8.76	9.06	8.99	17.40
MnO	0.73	0.64	0.55	0.45	0.73	0.40	0.69	0.53	1.32	1.35	0.51	0.52	0.70	0.45	0.66	0.65	0.73	0.77	1.08
MgO	15.06	14.90	15.19	14.76	15.06	12.94	15.06	13.22	24.54	24.19	14.34	15.05	15.33	14.61	15.35	14.98	15.04	14.99	25.20
CaO	20.18	20.19	20.07	21.17	20.18	21.76	20.43	20.40	1.36	1.78	21.19	20.27	20.55	21.65	20.09	20.79	19.93	20.10	1.35
Na_2O	0.36	0.38	0.37	0.32	0.36	0.39	0.38	0.42	0.42	0.01	0.38	0.37	0.34	0.32	0.36	0.35	0.39	0.39	0.04
K_2O	0.03	0.00	0.00	0.00	0.03	0.01	0.01	0.18	0.44	0.03	0.01	0.01	0.00	0.00	0.00	0.00	0.00	0.02	0.01
Sum	98.85	99.18	99.05	98.81	98.85	98.62	99.20	99.30	99.84	99.61	99.62	99.46	99.76	99.31	99.92	99.74	98.85	99.12	99.79
Si	1.950	1.931	1.936	1.928	1.950	1.848	1.944	1.870	1.959	1.959	1.906	1.923	1.947	1.919	1.952	1.936	1.948	1.954	1.968
Al	0.072	0.096	0.092	0.101	0.072	0.213	0.078	0.199	0.041	0.047	0.134	0.113	0.069	0.110	0.073	0.086	0.073	0.068	0.038
Ti	0.011	0.013	0.012	0.013	0.011	0.027	0.011	0.027	0.006	0.006	0.018	0.014	0.011	0.013	0.011	0.011	0.010	0.010	0.005
Cr	0.000	0.001	0.001	0.000	0.000	0.001	0.000	0.000	0.000	0.000	0.000	0.000	0.000	0.001	0.000	0.001	0.001	0.000	0.000
Mg	0.845	0.835	0.850	0.829	0.845	0.734	0.842	0.744	1.349	1.332	0.801	0.839	0.853	0.817	0.851	0.834	0.845	0.840	1.377
Fe	0.273	0.284	0.276	0.257	0.273	0.283	0.273	0.302	0.539	0.554	0.270	0.275	0.271	0.255	0.279	0.274	0.286	0.282	0.533
Mn	0.023	0.020	0.018	0.014	0.023	0.013	0.022	0.017	0.041	0.042	0.016	0.017	0.022	0.014	0.021	0.021	0.023	0.024	0.034
Ca	0.814	0.813	0.807	0.854	0.814	0.887	0.822	0.825	0.054	0.070	0.850	0.813	0.821	0.870	0.801	0.832	0.805	0.809	0.053
Na	0.026	0.028	0.027	0.024	0.026	0.028	0.028	0.030	0.030	0.001	0.028	0.027	0.025	0.023	0.026	0.026	0.028	0.028	0.003
K	0.001	0.000	0.000	0.000	0.001	0.000	0.000	0.009	0.021	0.001	0.001	0.000	0.000	0.000	0.000	0.000	0.000	0.001	0.001
Sum	4.016	4.021	4.019	4.020	4.016	4.033	4.020	4.023	4.040	4.013	4.023	4.021	4.020	4.024	4.014	4.022	4.019	4.017	4.010
Si	1.943	1.921	1.926	1.918	1.943	1.832	1.934	1.859	1.940	1.952	1.895	1.913	1.938	1.908	1.945	1.926	1.938	1.946	1.962
Al	0.072	0.096	0.091	0.101	0.072	0.211	0.078	0.198	0.040	0.046	0.133	0.113	0.069	0.109	0.073	0.086	0.073	0.067	0.037
Ti	0.011	0.013	0.012	0.013	0.011	0.026	0.011	0.027	0.006	0.006	0.018	0.013	0.011	0.013	0.011	0.011	0.010	0.010	0.005
Cr	0.000	0.001	0.001	0.000	0.000	0.001	0.000	0.000	0.000	0.000	0.000	0.000	0.000	0.001	0.000	0.001	0.001	0.000	0.000
Fe^{3+}	0.048	0.063	0.057	0.061	0.048	0.099	0.060	0.069	0.119	0.039	0.069	0.062	0.059	0.070	0.041	0.064	0.057	0.051	0.031
Mg	0.842	0.831	0.846	0.825	0.842	0.728	0.838	0.740	1.336	1.328	0.796	0.835	0.848	0.812	0.848	0.830	0.841	0.836	1.374
Fe^{2+}	0.223	0.220	0.218	0.196	0.223	0.181	0.211	0.232	0.415	0.514	0.199	0.212	0.211	0.184	0.237	0.208	0.227	0.230	0.501
Mn	0.023	0.020	0.017	0.014	0.023	0.013	0.022	0.017	0.041	0.042	0.016	0.016	0.022	0.014	0.021	0.021	0.023	0.024	0.034
Ca	0.811	0.809	0.804	0.850	0.811	0.880	0.818	0.820	0.053	0.070	0.845	0.808	0.817	0.865	0.798	0.828	0.801	0.806	0.053
Na	0.026	0.027	0.027	0.023	0.026	0.028	0.028	0.030	0.030	0.001	0.028	0.027	0.025	0.023	0.026	0.025	0.028	0.028	0.003
K	0.001	0.000	0.000	0.000	0.001	0.000	0.000	0.009	0.020	0.001	0.001	0.000	0.000	0.000	0.000	0.000	0.000	0.001	0.001
Sum	4.000	4.000	4.000	4.000	4.000	4.000	4.000	4.000	4.000	4.000	4.000	4.000	4.000	4.000	4.000	4.000	4.000	4.000	4.000
Wo (mol%)	0.421	0.421	0.418	0.440	0.421	0.466	0.424	0.441	0.028	0.036	0.443	0.422	0.422	0.448	0.415	0.429	0.416	0.419	0.027
En (mol%)	0.438	0.432	0.440	0.427	0.438	0.385	0.435	0.398	0.695	0.681	0.417	0.436	0.438	0.421	0.441	0.430	0.437	0.435	0.701
Fs (mol%)	0.141	0.147	0.143	0.133	0.141	0.148	0.141	0.161	0.278	0.283	0.140	0.143	0.139	0.131	0.144	0.141	0.148	0.146	0.272

Table D7 Pyroxene analyses of the 2010 Merapi eruption (continued)

Sample	M11-53-B4	M11-53-B4	M11-53-B4	M11-54-3	M11-54-3	M11-55	M11-55	M11-55	M11-55	M11-55	M11-55	M11-55	M11-55	M11-55	M11-55	M11-55	M11-55	M11-55
Sample Type	WP	WP	WP	DD	LG-Inc	WP	WP	WP	WP	WP	WP	WP	WP	WP	WP	WP	WP	WP
Point	52 / 1 .	56 / 1 .	57 / 1 .	56 / 1 .	64 / 1 .	3 / 1 .	5 / 1 .	7 / 1 .	39 / 1 .	43 / 1 .	139 / 1 .	140 / 1 .	141 / 1 .	142 / 1 .	143 / 1 .	144 / 1 .	145 / 1 .	146 / 1 .	147 / 1 .
Comment	mph	m	m	ph	ph	ph	ph	ph	ph	ph	ph	ph	ph	ph	ph	ph	ph	ph	ph
Pyroxene Type	opx	opx	opx	cpx	opx	cpx	cpx	cpx	cpx	cpx	cpx	cpx	cpx	cpx	cpx	cpx	cpx	cpx	cpx
SiO_2	53.62	51.78	52.51	53.05	54.13	51.79	51.77	52.48	52.15	53.08	50.68	52.65	51.96	52.01	52.53	51.74	52.98	52.95	52.02
TiO_2	0.17	0.22	0.20	0.31	0.11	0.37	0.33	0.33	0.36	0.30	0.71	0.41	0.38	0.41	0.28	0.33	0.47	0.43	0.43
Al_2O_3	0.81	0.66	0.64	1.67	0.39	2.43	2.30	2.01	2.29	1.61	4.17	2.09	2.23	2.67	1.67	1.81	1.82	2.37	2.05
Cr_2O_3	0.03	0.00	0.00	0.03	0.02	0.00	0.02	0.01	0.00	0.00	0.01	0.00	0.02	0.00	0.00	0.03	0.00	0.00	0.04
FeO	17.38	22.94	21.17	8.76	20.71	7.95	8.44	8.45	8.47	8.44	8.50	8.56	8.56	8.67	9.17	9.14	9.11	8.86	8.94
MnO	1.13	1.86	1.68	0.69	1.26	0.44	0.45	0.52	0.58	0.70	0.30	0.46	0.57	0.51	0.63	0.66	0.74	0.65	0.67
MgO	25.25	20.01	21.84	15.11	22.94	14.74	14.57	14.89	14.80	15.08	13.93	15.22	15.29	15.03	15.09	15.11	15.42	15.05	14.91
CaO	1.42	1.71	1.53	20.71	1.15	21.38	21.11	20.98	20.71	20.66	21.88	20.57	20.41	20.60	20.59	20.32	20.03	20.43	20.57
Na_2O	0.02	0.05	0.04	0.36	0.02	0.34	0.38	0.36	0.37	0.43	0.35	0.33	0.37	0.38	0.38	0.42	0.38	0.35	0.35
K_2O	0.01	0.05	0.03	0.02	0.00	0.00	0.00	0.00	0.01	0.00	0.00	0.00	0.00	0.00	0.00	0.00	0.00	0.00	0.00
Sum	99.84	99.27	99.63	100.70	100.73	99.44	99.36	100.02	99.74	100.30	100.52	100.30	99.80	100.29	100.34	99.56	100.93	101.09	99.97
Si	1.966	1.972	1.971	1.958	1.993	1.934	1.938	1.949	1.942	1.964	1.880	1.947	1.935	1.928	1.951	1.939	1.951	1.945	1.939
Al	0.035	0.029	0.028	0.073	0.017	0.107	0.102	0.088	0.100	0.070	0.182	0.091	0.098	0.117	0.073	0.080	0.079	0.102	0.090
Ti	0.005	0.006	0.006	0.009	0.003	0.010	0.009	0.009	0.010	0.008	0.020	0.012	0.011	0.011	0.008	0.009	0.013	0.012	0.012
Cr	0.001	0.000	0.000	0.001	0.000	0.000	0.001	0.000	0.000	0.000	0.000	0.000	0.001	0.000	0.000	0.001	0.000	0.000	0.001
Mg	1.380	1.136	1.222	0.831	1.259	0.821	0.813	0.824	0.822	0.832	0.771	0.839	0.849	0.830	0.835	0.844	0.846	0.824	0.828
Fe	0.533	0.731	0.665	0.270	0.638	0.248	0.264	0.262	0.264	0.261	0.264	0.265	0.267	0.269	0.285	0.286	0.281	0.272	0.279
Mn	0.035	0.060	0.053	0.022	0.039	0.014	0.014	0.016	0.018	0.022	0.009	0.014	0.018	0.016	0.020	0.021	0.023	0.020	0.021
Ca	0.056	0.070	0.062	0.819	0.045	0.856	0.847	0.835	0.827	0.819	0.870	0.815	0.814	0.818	0.819	0.816	0.790	0.804	0.821
Na	0.002	0.003	0.003	0.026	0.001	0.024	0.027	0.026	0.026	0.031	0.025	0.024	0.027	0.028	0.027	0.030	0.027	0.025	0.025
K	0.001	0.002	0.001	0.001	0.000	0.000	0.000	0.000	0.001	0.000	0.000	0.000	0.000	0.000	0.000	0.000	0.000	0.000	0.000
Sum	4.013	4.010	4.011	4.009	3.996	4.014	4.015	4.010	4.011	4.008	4.021	4.008	4.019	4.016	4.018	4.027	4.010	4.005	4.016
Si	1.960	1.967	1.966	1.954	1.995	1.927	1.931	1.944	1.937	1.960	1.870	1.944	1.926	1.920	1.942	1.926	1.946	1.942	1.931
Al	0.035	0.029	0.028	0.073	0.017	0.107	0.101	0.088	0.100	0.070	0.181	0.091	0.097	0.116	0.073	0.079	0.079	0.102	0.090
Ti	0.005	0.006	0.006	0.009	0.003	0.010	0.009	0.009	0.010	0.008	0.020	0.011	0.010	0.011	0.008	0.009	0.013	0.012	0.012
Cr	0.001	0.000	0.000	0.001	0.000	0.000	0.001	0.000	0.000	0.000	0.000	0.000	0.001	0.000	0.000	0.001	0.000	0.000	0.001
Fe^{3+}	0.038	0.030	0.032	0.028	0.000	0.042	0.045	0.031	0.032	0.023	0.064	0.023	0.055	0.049	0.055	0.079	0.030	0.014	0.048
Mg	1.376	1.133	1.219	0.829	1.260	0.818	0.810	0.822	0.820	0.830	0.767	0.838	0.845	0.827	0.831	0.838	0.844	0.823	0.825
Fe^{2+}	0.494	0.699	0.631	0.242	0.638	0.205	0.218	0.230	0.231	0.238	0.199	0.242	0.210	0.219	0.228	0.205	0.250	0.258	0.229
Mn	0.035	0.060	0.053	0.022	0.039	0.014	0.014	0.016	0.018	0.022	0.009	0.014	0.018	0.016	0.020	0.021	0.023	0.020	0.021
Ca	0.056	0.070	0.061	0.817	0.045	0.853	0.843	0.833	0.824	0.817	0.865	0.813	0.811	0.815	0.816	0.811	0.788	0.803	0.818
Na	0.002	0.003	0.003	0.026	0.001	0.024	0.027	0.026	0.026	0.031	0.025	0.024	0.026	0.027	0.027	0.030	0.027	0.025	0.025
K	0.001	0.002	0.001	0.001	0.000	0.000	0.000	0.000	0.001	0.000	0.000	0.000	0.000	0.000	0.000	0.000	0.000	0.000	0.000
Sum	4.000	4.000	4.000	4.000	4.000	4.000	4.000	4.000	4.000	4.000	4.000	4.000	4.000	4.000	4.000	4.000	4.000	4.000	4.000
Wo (mol%)	0.028	0.036	0.032	0.426	0.023	0.445	0.440	0.434	0.432	0.428	0.457	0.425	0.422	0.427	0.422	0.419	0.412	0.423	0.426
En (mol%)	0.701	0.587	0.627	0.433	0.648	0.426	0.423	0.429	0.430	0.435	0.405	0.437	0.440	0.433	0.431	0.434	0.441	0.434	0.430
Fs (mol%)	0.271	0.377	0.341	0.141	0.328	0.129	0.137	0.137	0.138	0.137	0.138	0.138	0.138	0.140	0.147	0.147	0.146	0.143	0.144

Table D7 Pyroxene analyses of the 2010 Merapi eruption (continued)

Sample	M11-55	M11-61	M11-61	M11-75	M11-75	M11-75	M11-75	M11-75	M11-75	M11-75	M11-75	M11-75	M11-75	M11-75	M11-75	M11-75	M11-75	M11-75	M11-75
Sample Type	WP	WP	WP	GS	GS	GS	GS	GS	GS	GS	GS	GS	GS	GS	GS	GS	GS	GS	GS
Point	148 / 1 .	13 / 1 .	14 / 1 .	25 / 1 .	26 / 1 .	27 / 1 .	28 / 1 .	29 / 1 .	30 / 1 .	31 / 1 .	32 / 1 .	33 / 1 .	34 / 1 .	35 / 1 .	36 / 1 .	111 / 1 .	112 / 1 .	113 / 1 .	114 / 1 .
Comment	ph	m	m	ph	ph	ph	ph	ph	ph	ph	ph	ph	ph	ph	ph	ph	ph	ph	ph
Pyroxene Type	cpx	opx	opx	cpx	cpx	cpx	cpx	cpx	cpx	cpx	cpx	cpx	cpx	cpx	cpx	cpx	cpx	cpx	cpx
SiO_2	51.78	54.01	53.86	52.47	52.98	52.82	49.86	52.44	53.09	52.34	52.40	52.59	52.04	52.29	52.82	51.00	52.35	52.29	52.80
TiO_2	0.39	0.17	0.15	0.32	0.25	0.31	0.64	0.45	0.31	0.37	0.33	0.34	0.40	0.26	0.30	0.44	0.31	0.41	0.32
Al_2O_3	1.76	0.62	0.45	1.93	1.65	1.84	4.64	2.08	1.82	2.05	1.73	1.90	2.09	2.18	1.58	1.88	1.74	2.15	1.81
Cr_2O_3	0.05	0.03	0.04	0.00	0.00	0.01	0.04	0.04	0.03	0.03	0.00	0.01	0.00	0.04	0.04	0.00	0.01	0.00	0.01
FeO	9.14	17.69	18.06	8.79	8.97	8.95	9.05	8.79	8.81	8.92	8.93	8.32	8.72	8.80	8.86	8.46	8.38	8.64	8.58
MnO	0.68	1.41	1.38	0.54	0.73	0.64	0.46	0.64	0.66	0.64	0.70	0.66	0.59	0.70	0.72	0.58	0.69	0.62	0.65
MgO	15.14	24.76	24.03	15.23	15.09	15.19	13.09	14.67	15.13	15.21	14.82	15.30	14.76	14.81	15.25	15.05	15.22	15.10	15.23
CaO	20.08	1.33	1.58	20.77	20.64	20.54	22.19	21.21	20.65	20.43	20.73	21.05	21.01	20.62	20.72	20.75	20.66	20.62	20.57
Na_2O	0.39	0.02	0.03	0.38	0.36	0.33	0.37	0.40	0.42	0.34	0.36	0.30	0.37	0.33	0.34	0.36	0.33	0.30	0.34
K_2O	0.00	0.02	0.03	0.00	0.00	0.00	0.00	0.00	0.00	0.00	0.00	0.00	0.00	0.01	0.00	0.00	0.01	0.01	0.00
Sum	99.40	100.05	99.61	100.43	100.67	100.64	100.34	100.72	100.92	100.32	100.00	100.47	99.99	100.05	100.62	98.52	99.67	100.14	100.32
Si	1.942	1.979	1.987	1.944	1.958	1.952	1.863	1.940	1.955	1.941	1.952	1.945	1.939	1.945	1.954	1.930	1.951	1.941	1.954
Al	0.078	0.027	0.020	0.084	0.072	0.080	0.204	0.091	0.079	0.090	0.076	0.083	0.092	0.096	0.069	0.084	0.076	0.094	0.079
Ti	0.011	0.005	0.004	0.009	0.007	0.009	0.018	0.013	0.008	0.010	0.009	0.009	0.011	0.007	0.008	0.012	0.009	0.011	0.009
Cr	0.001	0.001	0.001	0.000	0.000	0.000	0.001	0.001	0.001	0.001	0.000	0.000	0.000	0.001	0.001	0.000	0.000	0.000	0.000
Mg	0.846	1.353	1.322	0.841	0.831	0.837	0.729	0.809	0.831	0.841	0.823	0.844	0.820	0.821	0.841	0.849	0.846	0.835	0.840
Fe	0.287	0.542	0.557	0.272	0.277	0.276	0.283	0.272	0.271	0.277	0.278	0.257	0.272	0.274	0.274	0.268	0.261	0.268	0.266
Mn	0.022	0.044	0.043	0.017	0.023	0.020	0.015	0.020	0.020	0.020	0.022	0.021	0.019	0.022	0.023	0.019	0.022	0.019	0.020
Ca	0.807	0.052	0.062	0.824	0.818	0.813	0.888	0.841	0.815	0.812	0.827	0.834	0.839	0.822	0.821	0.841	0.825	0.820	0.816
Na	0.028	0.001	0.002	0.027	0.026	0.024	0.027	0.028	0.030	0.024	0.026	0.022	0.026	0.024	0.024	0.026	0.023	0.022	0.024
K	0.000	0.001	0.001	0.000	0.000	0.000	0.000	0.000	0.000	0.000	0.000	0.000	0.000	0.000	0.000	0.000	0.000	0.001	0.000
Sum	4.022	4.004	4.000	4.019	4.012	4.011	4.029	4.015	4.011	4.016	4.014	4.015	4.017	4.012	4.015	4.029	4.014	4.012	4.009
Si	1.931	1.977	1.987	1.935	1.953	1.946	1.850	1.933	1.950	1.934	1.945	1.938	1.931	1.939	1.946	1.916	1.945	1.935	1.950
Al	0.077	0.027	0.020	0.084	0.072	0.080	0.203	0.091	0.079	0.089	0.076	0.083	0.092	0.095	0.069	0.083	0.076	0.094	0.079
Ti	0.011	0.005	0.004	0.009	0.007	0.009	0.018	0.012	0.008	0.010	0.009	0.009	0.011	0.007	0.008	0.012	0.009	0.011	0.009
Cr	0.001	0.001	0.001	0.000	0.000	0.000	0.001	0.001	0.001	0.001	0.000	0.000	0.000	0.001	0.001	0.000	0.000	0.000	0.000
Fe^{3+}	0.064	0.012	0.000	0.056	0.035	0.034	0.087	0.046	0.034	0.046	0.041	0.045	0.052	0.035	0.045	0.086	0.041	0.035	0.027
Mg	0.842	1.351	1.322	0.837	0.829	0.835	0.724	0.806	0.829	0.837	0.820	0.840	0.816	0.819	0.838	0.843	0.843	0.833	0.839
Fe^{2+}	0.221	0.530	0.557	0.215	0.242	0.242	0.194	0.225	0.236	0.229	0.236	0.212	0.219	0.238	0.228	0.180	0.219	0.232	0.238
Mn	0.022	0.044	0.043	0.017	0.023	0.020	0.014	0.020	0.020	0.020	0.022	0.021	0.019	0.022	0.023	0.019	0.022	0.019	0.020
Ca	0.802	0.052	0.062	0.820	0.815	0.811	0.882	0.838	0.813	0.809	0.825	0.831	0.835	0.819	0.818	0.835	0.822	0.818	0.814
Na	0.028	0.001	0.002	0.027	0.026	0.024	0.027	0.028	0.030	0.024	0.026	0.022	0.026	0.024	0.024	0.026	0.023	0.022	0.024
K	0.000	0.001	0.001	0.000	0.000	0.000	0.000	0.000	0.000	0.000	0.000	0.000	0.000	0.000	0.000	0.000	0.000	0.001	0.000
Sum	4.000	4.000	4.000	4.000	4.000	4.000	4.000	4.000	4.000	4.000	4.000	4.000	4.000	4.000	4.000	4.000	4.000	4.000	4.000
Wo (mol%)	0.416	0.027	0.032	0.425	0.424	0.422	0.467	0.438	0.425	0.421	0.429	0.431	0.435	0.429	0.424	0.430	0.427	0.426	0.424
En (mol%)	0.436	0.695	0.681	0.434	0.432	0.434	0.384	0.421	0.433	0.436	0.427	0.436	0.425	0.429	0.434	0.434	0.438	0.434	0.437
Fs (mol%)	0.148	0.278	0.287	0.141	0.144	0.144	0.149	0.141	0.141	0.143	0.144	0.133	0.141	0.143	0.142	0.137	0.135	0.139	0.138

Table D7 Pyroxene analyses of the 2010 Merapi eruption (continued)

Sample	M11-75	M11-75	M11-75	M11-75	M11-75	M11-75	M11-75	M11-75	M11-75	M11-75	M11-75	M11-75	M11-80	M11-80	M11-93	M11-93	M11-93	M11-93	M11-93
Sample Type	GS	GS	GS	GS	GS	GS	GS	GS	GS	GS	GS	GS	DD	DD	GS	GS	GS	GS	GS
Point	115 / 1 .	116 / 1 .	117 / 1 .	118 / 1 .	119 / 1 .	120 / 1 .	122 / 1 .	123 / 1 .	3 / 1 .	4 / 1 .	9 / 1 .	8 / 1 .	47 / 1 .	49 / 1 .	1 / 1 .	2 / 1 .	13 / 1 .	14 / 1 .	26 / 1 .
Comment	ph	ph	ph	ph	ph	ph	ph	ph	mph-c	mph-r	mph-r	mph-c	ph	mph	ph	ph	ph	ph	ph
Pyroxene Type	cpx	cpx	cpx	cpx	cpx	cpx	cpx	cpx	cpx	cpx	cpx	opx	op	opx	cpx	cpx	cpx	cpx	cpx
SiO_2	52.66	52.02	51.80	52.23	51.80	52.67	52.44	52.07	53.03	52.51	47.10	54.76	53.86	54.08	51.42	51.38	51.79	50.89	51.96
TiO_2	0.35	0.48	0.38	0.49	0.52	0.39	0.35	0.49	0.30	0.38	1.08	0.14	0.20	0.11	0.44	0.51	0.40	0.54	0.36
Al_2O_3	1.79	2.44	2.18	2.39	2.60	1.98	1.86	2.08	1.44	2.18	6.60	0.53	0.90	0.47	2.30	2.43	1.87	2.88	1.58
Cr_2O_3	0.05	0.00	0.01	0.01	0.02	0.00	0.00	0.00	0.00	0.04	0.02	0.00	0.00	0.00	0.00	0.02	0.00	0.03	0.01
FeO	8.77	8.66	8.43	8.93	8.52	8.45	8.60	8.32	9.06	8.78	9.66	17.90	17.97	17.17	8.69	7.89	8.70	8.51	8.92
MnO	0.61	0.53	0.48	0.60	0.47	0.58	0.56	0.51	0.75	0.73	0.29	1.44	1.36	1.31	0.52	0.47	0.63	0.55	0.70
MgO	14.93	14.96	14.89	15.12	15.00	15.32	15.09	14.79	14.97	14.98	11.47	24.71	24.22	24.51	15.10	14.71	15.38	14.34	15.41
CaO	20.55	20.84	21.38	20.22	20.83	20.64	20.62	21.00	20.73	20.60	22.79	1.45	1.60	2.03	20.48	21.80	20.28	21.05	20.22
Na_2O	0.37	0.38	0.40	0.39	0.37	0.37	0.32	0.41	0.40	0.35	0.33	0.04	0.06	0.03	0.32	0.31	0.38	0.39	0.36
K_2O	0.00	0.00	0.00	0.00	0.00	0.00	0.00	0.00	0.00	0.00	0.00	0.00	0.00	0.00	0.00	0.00	0.00	0.01	0.00
Sum	100.07	100.30	99.95	100.38	100.13	100.39	99.83	99.67	100.67	100.56	99.33	100.98	100.18	99.70	99.28	99.51	99.42	99.18	99.53
Si	1.956	1.930	1.931	1.935	1.924	1.947	1.951	1.942	1.962	1.942	1.793	1.988	1.974	1.986	1.928	1.922	1.938	1.913	1.945
Al	0.078	0.107	0.096	0.105	0.114	0.086	0.082	0.092	0.063	0.095	0.296	0.023	0.039	0.020	0.101	0.107	0.082	0.127	0.070
Ti	0.010	0.013	0.011	0.014	0.014	0.011	0.010	0.014	0.008	0.011	0.031	0.004	0.006	0.003	0.012	0.014	0.011	0.015	0.010
Cr	0.001	0.000	0.000	0.000	0.001	0.000	0.000	0.000	0.000	0.001	0.001	0.000	0.000	0.000	0.000	0.001	0.000	0.001	0.000
Mg	0.827	0.827	0.828	0.835	0.831	0.844	0.837	0.823	0.826	0.826	0.651	1.337	1.324	1.342	0.844	0.820	0.858	0.804	0.860
Fe	0.273	0.269	0.263	0.277	0.265	0.261	0.268	0.260	0.280	0.272	0.307	0.543	0.551	0.527	0.272	0.247	0.272	0.268	0.279
Mn	0.019	0.017	0.015	0.019	0.015	0.018	0.018	0.016	0.024	0.023	0.009	0.044	0.042	0.041	0.017	0.015	0.020	0.018	0.022
Ca	0.818	0.828	0.854	0.802	0.829	0.817	0.822	0.839	0.822	0.817	0.929	0.056	0.063	0.080	0.823	0.874	0.813	0.848	0.811
Na	0.026	0.027	0.029	0.028	0.026	0.026	0.023	0.030	0.029	0.025	0.024	0.003	0.004	0.002	0.024	0.022	0.028	0.028	0.026
K	0.000	0.000	0.000	0.000	0.000	0.000	0.000	0.000	0.000	0.000	0.000	0.000	0.000	0.000	0.000	0.000	0.000	0.000	0.000
Sum	4.008	4.017	4.025	4.013	4.018	4.012	4.010	4.014	4.013	4.011	4.041	3.999	4.003	4.002	4.021	4.021	4.023	4.022	4.023
Si	1.952	1.921	1.918	1.928	1.915	1.942	1.946	1.935	1.956	1.937	1.775	1.989	1.973	1.985	1.918	1.912	1.927	1.903	1.933
Al	0.078	0.106	0.095	0.104	0.113	0.086	0.081	0.091	0.062	0.095	0.293	0.023	0.039	0.020	0.101	0.106	0.082	0.127	0.069
Ti	0.010	0.013	0.011	0.014	0.014	0.011	0.010	0.014	0.008	0.011	0.030	0.004	0.006	0.003	0.012	0.014	0.011	0.015	0.010
Cr	0.001	0.000	0.000	0.000	0.001	0.000	0.000	0.000	0.000	0.001	0.001	0.000	0.000	0.000	0.000	0.001	0.000	0.001	0.000
Fe^{3+}	0.023	0.052	0.075	0.040	0.053	0.035	0.030	0.041	0.039	0.034	0.120	0.000	0.008	0.005	0.063	0.063	0.070	0.065	0.070
Mg	0.825	0.823	0.822	0.832	0.827	0.842	0.835	0.820	0.823	0.824	0.644	1.338	1.323	1.341	0.840	0.816	0.853	0.799	0.855
Fe^{2+}	0.249	0.215	0.186	0.236	0.210	0.226	0.237	0.218	0.241	0.237	0.184	0.543	0.542	0.522	0.208	0.182	0.201	0.201	0.208
Mn	0.019	0.017	0.015	0.019	0.015	0.018	0.018	0.016	0.023	0.023	0.009	0.044	0.042	0.041	0.017	0.015	0.020	0.017	0.022
Ca	0.816	0.825	0.848	0.800	0.825	0.815	0.820	0.836	0.819	0.814	0.920	0.056	0.063	0.080	0.818	0.869	0.809	0.843	0.806
Na	0.026	0.027	0.029	0.028	0.026	0.026	0.023	0.029	0.029	0.025	0.024	0.003	0.004	0.002	0.023	0.022	0.028	0.028	0.026
K	0.000	0.000	0.000	0.000	0.000	0.000	0.000	0.000	0.000	0.000	0.000	0.000	0.000	0.000	0.000	0.000	0.000	0.000	0.000
Sum	4.000	4.000	4.000	4.000	4.000	4.000	4.000	4.000	4.000	4.000	4.000	4.000	4.000	4.000	4.000	4.000	4.000	4.000	4.000
Wo (mol%)	0.427	0.431	0.439	0.419	0.431	0.425	0.427	0.437	0.426	0.427	0.492	0.029	0.032	0.041	0.424	0.450	0.418	0.442	0.416
En (mol%)	0.431	0.430	0.426	0.436	0.432	0.439	0.434	0.428	0.428	0.432	0.345	0.690	0.683	0.688	0.435	0.423	0.441	0.419	0.441
Fs (mol%)	0.142	0.140	0.135	0.145	0.138	0.136	0.139	0.135	0.145	0.142	0.163	0.281	0.284	0.271	0.141	0.127	0.140	0.139	0.143

Table D7 Pyroxene analyses of the 2010 Merapi eruption (continued)

Sample	M11-93	M11-93	M11-93	M11-93	M11-93	M11-93	M11-93	M11-130	M11-130	M11-130	M11-130	M11-130	M11-130	M11-131	M11-131	M11-131	M11-131	M11-131	M11-135
Sample Type	GS	GS	GS	GS	GS	GS	GS	LG-Inc	LG-Inc	LG-Inc	LG-Inc	LG-Inc	LG-Inc	DD	DD	DD	DD	LG-Inc	LG-Inc
Point	22 / 1 .	23 / 1 .	1 / 1 .	13 / 1 .	26 / 1 .	2 / 1 .	14 / 1 .	4 / 1 .	5 / 1 .	8 / 1 .	9 / 1 .	10 / 1 .	11 / 1 .	17 / 1 .	18 / 1 .	21 / 1 .	6 / 1 .	36 / 1 .	11 / 1 .
Comment	ph	ph	ph-c	ph-c	ph-c	ph-r	ph-r	ph	ph	ph	ph	ph	ph	ph	ph	ph	m	mph	mph
Pyroxene Type	cpx	cpx	cpx	cpx	cpx	cpx	cpx	cpx	cpx	cpx	cpx	cpx	cpx	cpx	cpx	cpx	cpx	opx	pig
SiO_2	50.51	51.20	51.42	51.79	51.96	51.38	50.89	52.08	52.38	50.85	51.56	52.10	51.21	52.50	51.64	52.32	52.26	53.59	52.42
TiO_2	0.55	0.49	0.44	0.40	0.36	0.51	0.54	0.41	0.39	0.57	0.34	0.34	0.46	0.36	0.54	0.31	0.31	0.18	0.18
Al_2O_3	3.04	2.09	2.30	1.87	1.58	2.43	2.88	2.15	2.15	3.25	2.74	1.68	2.42	1.65	2.90	1.87	1.45	0.87	0.21
Cr_2O_3	0.00	0.00	0.00	0.00	0.01	0.02	0.03	0.00	0.03	0.00	0.01	0.00	0.02	0.03	0.00	0.00	0.04	0.00	0.00
FeO	9.46	9.07	8.69	8.70	8.92	7.89	8.51	8.71	8.73	8.25	8.33	8.41	8.68	8.94	8.37	8.54	8.65	17.20	25.13
MnO	0.60	0.75	0.52	0.63	0.70	0.47	0.55	0.53	0.65	0.40	0.47	0.70	0.58	0.69	0.41	0.69	0.68	1.21	1.53
MgO	14.53	14.87	15.10	15.38	15.41	14.71	14.34	14.79	15.01	14.11	14.45	15.44	14.89	14.76	14.16	14.80	15.17	24.72	16.56
CaO	19.86	20.05	20.48	20.28	20.22	21.80	21.05	20.94	20.65	21.81	21.72	20.35	20.88	20.89	22.14	20.54	20.72	1.76	4.00
Na_2O	0.41	0.38	0.32	0.38	0.36	0.31	0.39	0.33	0.39	0.36	0.39	0.33	0.37	0.44	0.35	0.37	0.36	0.04	0.12
K_2O	0.00	0.00	0.00	0.00	0.00	0.00	0.01	0.00	0.00	0.00	0.00	0.00	0.00	0.00	0.00	0.06	0.00	0.00	0.00
Sum	98.97	98.91	99.28	99.42	99.53	99.51	99.18	99.94	100.38	99.60	100.01	99.34	99.52	100.26	100.50	99.50	99.64	99.56	100.16
Si	1.906	1.931	1.928	1.938	1.945	1.922	1.913	1.939	1.941	1.903	1.921	1.948	1.919	1.952	1.916	1.955	1.953	1.971	2.005
Al	0.135	0.093	0.101	0.082	0.070	0.107	0.127	0.094	0.094	0.143	0.120	0.074	0.107	0.072	0.127	0.082	0.064	0.038	0.010
Ti	0.016	0.014	0.012	0.011	0.010	0.014	0.015	0.012	0.011	0.016	0.009	0.010	0.013	0.010	0.015	0.009	0.009	0.005	0.005
Cr	0.000	0.000	0.000	0.000	0.000	0.001	0.001	0.000	0.001	0.000	0.000	0.000	0.001	0.001	0.000	0.000	0.001	0.000	0.000
Mg	0.817	0.836	0.844	0.858	0.860	0.820	0.804	0.821	0.829	0.787	0.803	0.861	0.832	0.818	0.783	0.824	0.845	1.355	0.944
Fe	0.299	0.286	0.272	0.272	0.279	0.247	0.268	0.271	0.270	0.258	0.259	0.263	0.272	0.278	0.260	0.267	0.270	0.529	0.804
Mn	0.019	0.024	0.017	0.020	0.022	0.015	0.018	0.017	0.020	0.013	0.015	0.022	0.018	0.022	0.013	0.022	0.022	0.038	0.049
Ca	0.803	0.810	0.823	0.813	0.811	0.874	0.848	0.835	0.820	0.875	0.867	0.815	0.838	0.832	0.880	0.822	0.829	0.069	0.164
Na	0.030	0.028	0.024	0.028	0.026	0.022	0.028	0.024	0.028	0.026	0.028	0.024	0.027	0.032	0.025	0.027	0.026	0.003	0.009
K	0.000	0.000	0.000	0.000	0.000	0.000	0.000	0.000	0.000	0.000	0.000	0.000	0.000	0.000	0.000	0.003	0.000	0.000	0.000
Sum	4.026	4.023	4.021	4.023	4.023	4.021	4.022	4.014	4.015	4.022	4.023	4.017	4.028	4.017	4.018	4.010	4.019	4.007	3.990
Si	1.894	1.920	1.918	1.927	1.933	1.912	1.903	1.933	1.934	1.893	1.910	1.940	1.906	1.944	1.907	1.950	1.944	1.967	2.010
Al	0.135	0.092	0.101	0.082	0.069	0.106	0.127	0.094	0.094	0.142	0.119	0.074	0.106	0.072	0.126	0.082	0.064	0.038	0.010
Ti	0.015	0.014	0.012	0.011	0.010	0.014	0.015	0.012	0.011	0.016	0.009	0.010	0.013	0.010	0.015	0.009	0.009	0.005	0.005
Cr	0.000	0.000	0.000	0.000	0.000	0.001	0.001	0.000	0.001	0.000	0.000	0.000	0.001	0.001	0.000	0.000	0.001	0.000	0.000
Fe^{3+}	0.076	0.068	0.063	0.070	0.070	0.063	0.065	0.041	0.043	0.065	0.070	0.051	0.082	0.051	0.055	0.031	0.057	0.021	0.000
Mg	0.812	0.831	0.840	0.853	0.855	0.816	0.799	0.818	0.826	0.783	0.798	0.857	0.826	0.815	0.780	0.822	0.841	1.353	0.947
Fe^{2+}	0.220	0.217	0.208	0.201	0.208	0.182	0.201	0.230	0.226	0.192	0.188	0.211	0.188	0.226	0.204	0.235	0.212	0.507	0.806
Mn	0.019	0.024	0.017	0.020	0.022	0.015	0.017	0.017	0.020	0.013	0.015	0.022	0.018	0.022	0.013	0.022	0.021	0.038	0.050
Ca	0.798	0.805	0.818	0.809	0.806	0.869	0.843	0.833	0.817	0.870	0.862	0.812	0.833	0.829	0.876	0.820	0.825	0.069	0.164
Na	0.030	0.028	0.023	0.028	0.026	0.022	0.028	0.024	0.028	0.026	0.028	0.024	0.027	0.031	0.025	0.027	0.026	0.003	0.009
K	0.000	0.000	0.000	0.000	0.000	0.000	0.000	0.000	0.000	0.000	0.000	0.000	0.000	0.000	0.000	0.003	0.000	0.000	0.000
Sum	4.000	4.000	4.000	4.000	4.000	4.000	4.000	4.000	4.000	4.000	4.000	4.000	4.000	4.000	4.000	4.000	4.000	4.000	4.000
Wo (mol%)	0.418	0.419	0.424	0.418	0.416	0.450	0.442	0.433	0.427	0.456	0.449	0.420	0.432	0.432	0.458	0.430	0.426	0.035	0.086
En (mol%)	0.426	0.433	0.435	0.441	0.441	0.423	0.419	0.426	0.432	0.410	0.416	0.444	0.428	0.424	0.407	0.431	0.435	0.694	0.494
Fs (mol%)	0.156	0.148	0.141	0.140	0.143	0.127	0.139	0.141	0.141	0.134	0.134	0.136	0.140	0.144	0.135	0.139	0.139	0.271	0.420

Table D7 Pyroxene analyses of the 2010 Merapi eruption (continued)

Sample	M11-138a	DD10	DD10	DD10	DD10	DD10	DD10	DD10	DD10	DD10	DD10	DD10	DD10	DD10	DD10	DD10	DD10		
Sample Type	GS	DD	DD	DD	DD	DD	DD	DD	DD	DD	DD	LG-Inc	LG-Inc	LG-Inc	LG-Inc	LG-Inc	LG-Inc		
Point	19 / 1 .	6 / 1 .	7 / 1 .	24 / 1 .	29 / 1 .	32 / 1 .	36 / 1 .	45 / 1 .	47 / 1 .	49 / 1 .	46 / 1 .	62 / 1 .	64 / 1 .	58 / 1 .	59 / 1 .	60 / 1 .	56 / 1 .		
Comment	m	ph	ph	ph	ph	ph	m-c	m-r	m-c	m-c	m-c	ph	ph	m	m	m	m		
Pyroxene Type	opx	cpx	cpx	cpx	cpx	cpx	cpx	cpx	cpx	cpx	opx	cpx	cpx	cpx	cpx	cpx	opx		
SiO_2	55.32	52.39	51.78	52.47	52.65	52.34	45.75	48.91	49.24	53.49	54.43	51.76	52.72	52.88	52.65	52.83	54.11		
TiO_2	0.31	0.26	0.53	0.36	0.34	0.39	1.79	0.85	1.13	0.33	0.20	0.26	0.38	0.34	0.34	0.33	0.16		
Al_2O_3	1.63	1.85	2.75	1.69	1.53	1.85	7.25	5.64	5.63	1.34	1.08	1.70	2.06	1.61	1.67	1.52	0.61		
Cr_2O_3	0.00	-0.01	0.01	0.02	0.00	-0.01	0.00	0.00	0.01	-0.03	0.00	-0.01	0.01	-0.01	-0.01	0.01	0.00		
FeO	9.81	10.41	9.14	8.66	8.76	8.73	10.55	9.77	9.39	8.45	18.51	9.26	8.15	8.78	8.13	8.70	17.23		
MnO	1.42	0.81	0.51	0.71	0.76	0.69	0.34	0.62	0.42	0.70	1.37	0.79	0.57	0.71	0.61	0.73	1.37		
MgO	28.23	13.62	15.33	15.09	15.03	14.56	11.12	12.89	12.90	16.15	24.58	14.40	15.23	15.28	14.80	15.12	25.03		
CaO	1.52	21.31	20.66	20.59	20.69	21.03	21.47	20.10	21.79	20.42	1.39	20.10	21.60	20.68	22.09	20.89	1.33		
Na_2O	0.05	0.44	0.43	0.38	0.35	0.39	0.42	0.46	0.39	0.26	0.03	0.37	0.29	0.36	0.31	0.36	0.02		
K_2O	0.14	0.00	0.00	0.02	0.05	0.04	0.04	0.68	0.17	0.02	0.01	0.00	0.00	0.00	0.04	0.00	0.00		
Sum	98.44	101.09	101.13	100.00	100.15	100.01	98.74	99.90	101.07	101.14	101.60	98.63	101.00	100.64	100.64	100.50	99.87		
Si	1.985	1.948	1.909	1.952	1.957	1.950	1.758	1.841	1.830	1.961	1.969	1.957	1.940	1.954	1.948	1.956	1.981		
Al	0.069	0.081	0.119	0.074	0.067	0.081	0.328	0.250	0.247	0.058	0.046	0.076	0.089	0.070	0.073	0.066	0.026		
Ti	0.008	0.007	0.015	0.010	0.010	0.011	0.052	0.024	0.032	0.009	0.006	0.007	0.011	0.010	0.010	0.009	0.004		
Cr	0.000	0.000	0.000	0.001	0.000	0.000	0.000	0.000	0.000	-0.001	0.000	0.000	0.000	0.000	0.000	0.000	0.000		
Mg	1.510	0.755	0.843	0.837	0.833	0.809	0.637	0.723	0.715	0.883	1.326	0.812	0.835	0.842	0.816	0.835	1.366		
Fe	0.294	0.324	0.282	0.269	0.272	0.272	0.339	0.308	0.292	0.259	0.560	0.293	0.251	0.271	0.252	0.269	0.527		
Mn	0.043	0.025	0.016	0.022	0.024	0.022	0.011	0.020	0.013	0.022	0.042	0.025	0.018	0.022	0.019	0.023	0.043		
Ca	0.059	0.849	0.816	0.821	0.824	0.840	0.884	0.811	0.868	0.802	0.054	0.814	0.851	0.819	0.876	0.829	0.052		
Na	0.004	0.032	0.031	0.027	0.025	0.028	0.032	0.034	0.028	0.018	0.002	0.027	0.021	0.026	0.022	0.026	0.002		
K	0.006	0.000	0.000	0.001	0.002	0.002	0.002	0.032	0.008	0.001	0.000	0.000	0.000	0.000	0.002	0.000	0.000		
Sum	3.978	4.021	4.031	4.015	4.014	4.014	4.043	4.043	4.033	4.011	4.004	4.011	4.015	4.014	4.018	4.014	4.002		
Si	1.996	1.938	1.895	1.944	1.950	1.943	1.739	1.822	1.815	1.955	1.967	1.952	1.932	1.947	1.940	1.950	1.980		
Al	0.069	0.081	0.118	0.074	0.067	0.081	0.325	0.247	0.245	0.058	0.046	0.076	0.089	0.070	0.073	0.066	0.026		
Ti	0.008	0.007	0.015	0.010	0.010	0.011	0.051	0.024	0.031	0.009	0.006	0.007	0.011	0.010	0.010	0.009	0.004		
Cr	0.000	0.000	0.000	0.001	0.000	0.000	0.000	0.000	0.000	-0.001	0.000	0.000	0.000	0.000	0.000	0.000	0.000		
Fe^{3+}	0.000	0.062	0.094	0.045	0.041	0.041	0.127	0.127	0.097	0.034	0.012	0.034	0.045	0.043	0.053	0.042	0.006		
Mg	1.518	0.751	0.836	0.834	0.830	0.806	0.630	0.716	0.709	0.880	1.324	0.809	0.832	0.839	0.813	0.832	1.366		
Fe^{2+}	0.296	0.260	0.186	0.223	0.230	0.230	0.208	0.177	0.193	0.225	0.547	0.258	0.204	0.228	0.198	0.227	0.521		
Mn	0.043	0.025	0.016	0.022	0.024	0.022	0.011	0.019	0.013	0.022	0.042	0.025	0.018	0.022	0.019	0.023	0.042		
Ca	0.059	0.844	0.810	0.818	0.821	0.837	0.875	0.802	0.861	0.800	0.054	0.812	0.848	0.816	0.872	0.826	0.052		
Na	0.004	0.032	0.030	0.027	0.025	0.028	0.031	0.033	0.028	0.018	0.002	0.027	0.020	0.026	0.022	0.025	0.002		
K	0.007	0.000	0.000	0.001	0.002	0.002	0.002	0.032	0.008	0.001	0.000	0.000	0.000	0.000	0.002	0.000	0.000		
Sum	4.000	4.000	4.000	4.000	4.000	4.000	4.000	4.000	4.000	4.000	4.000	4.000	4.000	4.000	4.000	4.000	4.000		
Wo (mol%)	0.031	0.440	0.421	0.426	0.427	0.437	0.475	0.440	0.463	0.413	0.028	0.424	0.439	0.424	0.451	0.429	0.027		
En (mol%)	0.811	0.392	0.434	0.434	0.432	0.421	0.343	0.393	0.381	0.454	0.684	0.423	0.431	0.436	0.420	0.432	0.702		
Fs (mol%)	0.158	0.168	0.145	0.140	0.141	0.142	0.182	0.167	0.156	0.133	0.289	0.153	0.129	0.140	0.129	0.139	0.271		

Table D8 Amphibole analyses of the 2010 Merapi eruption[1]

Sample	M11-01	M11-01	M11-07	M11-07	M11-07	M11-07	M11-07	M11-07	M11-07	M11-07	M11-07	M11-07	M11-07	M11-07
Sample Type[2]	DD	DD	DD	DD	DD	DD	DD	DD	DD	DD	DD	DD	LG-Inc	LG-Inc
DataSet/Point	4 / 1 .	5 / 1 .	3 / 1 .	4 / 1 .	7 / 1 .	8 / 1 .	9 / 1 .	10 / 1 .	11 / 1 .	12 / 1 .	13 / 1 .	14 / 1 .	42 / 1 .	43 / 1 .
Comment[3]	ph-r	ph-c	mph-c	mph-c	mph-r	mph-c	mph-c	mph-c	mph-c	mph-c	mh-r	mph-c	ph-c	ph-r
SiO_2	40.87	40.25	40.95	39.76	40.05	41.07	42.50	42.64	39.79	40.05	40.46	40.50	42.75	42.01
TiO_2	2.93	2.08	2.31	2.35	2.52	2.45	2.72	3.03	2.40	2.16	2.20	2.46	2.53	2.48
Al_2O_3	12.29	14.11	12.50	13.10	13.56	12.49	11.27	11.02	14.41	14.31	13.87	13.08	11.40	12.11
Cr_2O_3	0.01	0.01	-0.01	0.01	0.00	0.00	0.00	-0.01	0.01	0.03	0.00	-0.03	0.01	0.01
FeO	12.57	11.74	14.52	12.79	12.76	14.38	12.80	12.26	12.44	12.26	11.82	13.41	13.23	13.36
MnO	0.30	0.13	0.38	0.20	0.20	0.30	0.37	0.39	0.12	0.16	0.14	0.29	0.30	0.30
MgO	13.47	13.83	12.22	12.84	12.87	12.65	13.85	14.27	13.20	13.16	13.37	12.63	13.76	13.22
CaO	11.56	12.15	11.64	11.85	12.06	11.76	11.36	11.31	12.15	12.21	12.09	11.80	11.62	11.53
Na_2O	2.52	2.35	2.37	2.28	2.30	2.34	2.37	2.51	2.37	2.25	2.36	2.35	2.66	2.66
K_2O	1.15	1.28	0.97	0.85	0.96	1.03	0.97	0.92	0.99	1.14	0.97	0.98	0.65	0.72
Cl	0.08	0.03	0.04	0.02	0.02	0.05	0.06	0.06	0.02	0.01	0.02	0.03	0.04	0.05
F	0.49	0.18	0.12	0.10	0.14	0.14	0.26	0.27	0.07	0.08	0.11	0.16	0.44	0.64
Sum	98.25	98.13	98.01	96.15	97.43	98.65	98.53	98.66	97.97	97.83	97.41	97.65	99.37	99.09
Si	6.010	5.879	6.043	5.942	5.920	6.015	6.173	6.176	5.828	5.878	5.950	5.981	6.180	6.117
Al	2.130	2.430	2.175	2.307	2.362	2.156	1.929	1.880	2.487	2.476	2.405	2.276	1.942	2.078
Ti	0.324	0.229	0.256	0.264	0.280	0.269	0.298	0.330	0.265	0.239	0.243	0.273	0.275	0.272
Cr	0.001	0.001	-0.001	0.002	0.000	-0.001	0.000	-0.001	0.001	0.003	0.000	-0.003	0.001	0.001
Fe^{3+}	0.624	0.648	0.686	0.659	0.580	0.731	0.749	0.724	0.658	0.590	0.544	0.627	0.682	0.661
Mg	2.952	3.011	2.688	2.861	2.836	2.762	3.000	3.082	2.882	2.880	2.931	2.781	2.966	2.868
Fe^{2+}	0.922	0.787	1.107	0.939	0.998	1.030	0.806	0.761	0.865	0.914	0.909	1.029	0.917	0.966
Mn	0.037	0.015	0.047	0.025	0.025	0.037	0.046	0.048	0.015	0.019	0.018	0.036	0.037	0.038
Ca	1.822	1.901	1.841	1.898	1.909	1.845	1.768	1.755	1.906	1.921	1.905	1.867	1.800	1.799
Na	0.719	0.665	0.678	0.662	0.658	0.663	0.666	0.704	0.672	0.641	0.672	0.674	0.745	0.751
K	0.215	0.238	0.183	0.161	0.182	0.193	0.179	0.170	0.185	0.213	0.182	0.184	0.120	0.134
Cl	0.020	0.008	0.010	0.005	0.005	0.012	0.014	0.015	0.004	0.004	0.004	0.009	0.010	0.013
F	0.230	0.083	0.057	0.047	0.065	0.064	0.119	0.122	0.034	0.039	0.049	0.074	0.199	0.293
Sum	15.756	15.803	15.702	15.721	15.749	15.701	15.613	15.629	15.764	15.775	15.759	15.725	15.665	15.684

[1] Major element oxides in wt.%; number of cations based on 23 oxygens; Fe^{3+} estimation assuming 13eCNK; cation sum excluding Cl and F; [2] see Appendix A; [3] see Table D1

Table D8 Amphibole analyses of the 2010 Merapi eruption (continued)

Sample	M11-07	M11-07	M11-07	M11-15	M11-15	M11-15	M11-15	M11-18	M11-18	M11-18	M11-18	M11-18	M11-18	M11-18
Sample Type	LG-Inc	LG-Inc	LG-Inc	DD	DD	DD	DD	WP	WP	WP	WP	WP	WP	WP
DataSet/Point	44 / 1 .	45 / 1 .	46 / 1 .	11 / 1 .	12 / 1 .	13 / 1 .	14 / 1 .	13 / 1 .	14 / 1 .	15 / 1 .	41 / 1 .	42 / 1 .	43 / 1 .	44 / 1 .
Comment	ph-c	ph-c	ph-r	mph-c	mph-c	mph-c	mph-c	ph-c	ph	ph-r	ph-c	ph	ph-r	ph-c
SiO_2	42.24	42.61	42.28	40.97	41.52	42.19	39.78	41.82	40.73	40.54	43.02	41.14	40.86	40.31
TiO_2	2.87	2.94	5.48	3.03	3.11	2.98	2.79	1.73	1.94	1.96	2.71	2.31	2.80	2.08
Al_2O_3	11.57	11.13	10.52	11.52	11.53	10.69	12.48	12.56	13.65	14.43	10.96	13.14	12.75	13.19
Cr_2O_3	0.01	0.00	-0.01	0.00	0.00	0.00	0.00	0.00	0.02	0.01	0.01	0.01	0.00	0.01
FeO	12.20	13.15	14.88	12.54	12.45	12.00	12.97	12.53	12.56	12.64	12.40	12.67	12.94	15.99
MnO	0.34	0.40	0.53	0.38	0.33	0.39	0.22	0.17	0.22	0.27	0.30	0.19	0.32	0.40
MgO	13.84	13.31	12.39	13.58	13.61	14.05	12.81	13.16	12.71	12.65	13.78	13.13	12.79	10.68
CaO	11.52	11.19	11.26	11.18	11.12	11.04	11.57	11.91	11.93	11.93	11.20	12.04	11.70	11.64
Na_2O	2.46	2.47	2.21	2.45	2.40	2.38	2.35	2.33	2.22	2.28	2.37	2.37	2.38	2.24
K_2O	0.97	1.05	1.09	0.91	0.94	0.91	1.00	0.82	1.05	1.09	0.98	0.94	0.95	1.12
Cl	0.06	0.10	0.14	0.05	0.06	0.08	0.04	0.02	0.03	0.04	0.09	0.03	0.04	0.04
F	0.61	0.20	0.58	0.26	0.21	0.28	0.11	0.33	0.20	0.25	0.31	0.36	0.29	0.40
Sum	98.70	98.54	101.36	96.87	97.29	96.98	96.14	97.39	97.26	98.07	98.13	98.33	97.82	98.10
Si	6.158	6.216	6.096	6.061	6.104	6.210	5.964	6.165	6.022	5.942	6.272	6.029	6.025	6.020
Al	1.989	1.914	1.788	2.008	1.997	1.854	2.206	2.183	2.378	2.492	1.884	2.269	2.217	2.322
Ti	0.315	0.322	0.594	0.337	0.344	0.329	0.315	0.192	0.216	0.216	0.297	0.255	0.311	0.234
Cr	0.001	0.000	-0.001	0.000	0.000	0.000	0.000	0.000	0.002	0.001	0.001	0.001	0.000	0.001
Fe^{3+}	0.586	0.617	0.534	0.779	0.744	0.736	0.643	0.521	0.529	0.591	0.624	0.532	0.555	0.583
Mg	3.007	2.895	2.664	2.995	2.983	3.082	2.862	2.893	2.801	2.765	2.996	2.869	2.811	2.377
Fe^{2+}	0.901	0.988	1.260	0.772	0.786	0.740	0.983	1.024	1.025	0.959	0.888	1.021	1.041	1.413
Mn	0.042	0.049	0.065	0.048	0.041	0.049	0.028	0.022	0.027	0.033	0.037	0.024	0.040	0.051
Ca	1.800	1.750	1.739	1.772	1.751	1.741	1.859	1.881	1.890	1.873	1.750	1.890	1.849	1.863
Na	0.696	0.698	0.619	0.702	0.683	0.679	0.684	0.665	0.637	0.648	0.669	0.675	0.680	0.648
K	0.181	0.196	0.201	0.172	0.177	0.170	0.192	0.153	0.198	0.203	0.182	0.175	0.179	0.213
Cl	0.014	0.024	0.035	0.013	0.015	0.019	0.010	0.006	0.007	0.009	0.021	0.007	0.009	0.011
F	0.283	0.093	0.265	0.120	0.098	0.129	0.052	0.156	0.091	0.114	0.144	0.167	0.134	0.190
Sum	15.677	15.643	15.559	15.645	15.611	15.591	15.735	15.700	15.725	15.725	15.601	15.740	15.708	15.724

Table D8 Amphibole analyses of the 2010 Merapi eruption (continued)

Sample	M11-18	M11-18	M11-18	M11-18	M11-24	M11-24	M11-24	M11-24	M11-24	M11-24	M11-24	M11-24	M11-24	M11-26a
Sample Type	WP	WP	WP	WP	DD	DD	DD	DD	DD	DD	DD	DD	DD	DD
DataSet/Point	45 / 1 .	47 / 1 .	48 / 1 .	49 / 1 .	1 / 1 .	2 / 1 .	3 / 1 .	12 / 1 .	13 / 1 .	14 / 1 .	15 / 1 .	16 / 1 .	17 / 1 .	1 / 1 .
Comment	ph	ph-c	ph-c	ph-r	mph-c	mph-c	mph-c	mph-c	mph-r	mph-c	mph-c	mph-c	mph-c	ph-c
SiO_2	42.53	42.52	42.80	42.66	41.29	41.99	41.25	40.12	40.45	42.95	42.98	43.21	41.72	41.94
TiO_2	1.91	2.62	2.48	2.58	2.99	3.00	2.77	2.36	2.51	3.11	3.04	2.91	3.16	2.60
Al_2O_3	10.91	11.16	11.15	11.18	11.35	11.29	12.02	13.60	12.61	10.14	10.13	9.98	11.23	11.66
Cr_2O_3	0.02	0.00	0.02	0.00	0.00	0.02	0.02	0.05	0.02	0.01	0.00	0.00	0.02	0.00
FeO	15.27	12.85	12.84	12.72	12.02	12.31	12.46	12.74	12.97	12.27	12.09	12.02	12.92	12.18
MnO	0.47	0.37	0.39	0.35	0.35	0.40	0.31	0.12	0.25	0.44	0.43	0.44	0.40	0.32
MgO	11.37	13.33	13.13	13.24	13.75	13.69	13.42	13.02	13.16	14.28	14.27	14.44	13.47	14.10
CaO	12.69	11.15	11.23	11.45	11.23	11.21	11.53	12.00	11.38	10.88	10.71	11.01	10.96	11.14
Na_2O	1.82	2.28	2.26	2.24	2.42	2.34	2.45	2.35	2.43	2.34	2.42	2.47	2.48	2.37
K_2O	0.96	0.96	1.00	0.98	0.88	0.93	0.86	0.96	0.81	0.98	0.95	0.94	0.97	1.00
Cl	0.05	0.08	0.09	0.07	0.06	0.07	0.03	0.02	0.02	0.09	0.09	0.10	0.08	0.06
F	0.41	0.04	0.30	0.22	0.24	0.27	0.16	0.08	0.07	0.41	0.40	0.40	0.22	0.18
Sum	98.41	97.34	97.68	97.68	96.57	97.51	97.27	97.42	96.67	97.91	97.51	97.93	97.63	97.53
Si	6.358	6.241	6.290	6.271	6.116	6.161	6.080	5.918	5.982	6.262	6.281	6.303	6.124	6.118
Al	1.923	1.930	1.931	1.937	1.981	1.953	2.087	2.364	2.199	1.743	1.744	1.716	1.942	2.005
Ti	0.215	0.289	0.274	0.285	0.333	0.331	0.307	0.262	0.279	0.341	0.334	0.320	0.349	0.285
Cr	0.002	0.000	0.002	0.000	0.000	0.002	0.002	0.006	0.002	0.001	0.000	0.000	0.002	0.001
Fe^{3+}	0.152	0.675	0.569	0.522	0.696	0.697	0.634	0.626	0.822	0.805	0.809	0.724	0.775	0.850
Mg	2.533	2.918	2.876	2.900	3.037	2.995	2.948	2.863	2.903	3.103	3.110	3.140	2.947	3.066
Fe^{2+}	1.757	0.902	1.009	1.041	0.793	0.813	0.902	0.946	0.783	0.691	0.669	0.743	0.811	0.637
Mn	0.060	0.046	0.048	0.044	0.044	0.049	0.039	0.015	0.031	0.054	0.053	0.054	0.049	0.039
Ca	2.033	1.754	1.768	1.803	1.782	1.763	1.821	1.896	1.803	1.700	1.677	1.721	1.724	1.741
Na	0.527	0.647	0.645	0.640	0.694	0.666	0.699	0.671	0.697	0.663	0.685	0.697	0.705	0.670
K	0.183	0.180	0.188	0.183	0.166	0.173	0.161	0.181	0.152	0.182	0.177	0.175	0.182	0.187
Cl	0.013	0.019	0.022	0.017	0.014	0.017	0.008	0.005	0.006	0.023	0.023	0.025	0.020	0.014
F	0.195	0.017	0.141	0.102	0.113	0.127	0.075	0.035	0.031	0.189	0.184	0.183	0.104	0.083
Sum	15.743	15.582	15.601	15.626	15.642	15.602	15.681	15.749	15.653	15.545	15.539	15.593	15.610	15.598

Table D8 Amphibole analyses of the 2010 Merapi eruption (continued)

Sample	M11-26a	M11-26a	M11-26a	M11-27-1	M11-27-2	M11-27-2	M11-27-2	M11-27-2	M11-27-2	M11-27-2	M11-27-2	M11-27-2	M11-27-2	M11-27-3
Sample Type	DD	DD	DD	DD	DD	DD	DD	DD	DD	DD	DD	DD	LG-Inc	DD
DataSet/Point	2 / 1 .	3 / 1 .	4 / 1 .	13 / 1 .	2 / 1 .	3 / 1 .	4 / 1 .	5 / 1 .	6 / 1 .	7 / 1 .	8 / 1 .	9 / 1 .	1 / 1 .	1 / 1 .
Comment	ph-c	ph-r	ph-r	ph	mph-c	mph-r	mph-c	mph-c	mph-c	mph-c	mph-c	mph-r	mph-c	ph
SiO_2	42.14	40.65	41.24	40.16	39.83	39.82	40.16	39.83	41.61	41.66	41.43	40.68	42.71	42.08
TiO_2	2.51	2.75	3.02	2.39	2.19	2.51	2.60	2.25	2.95	2.94	2.03	2.35	2.98	2.80
Al_2O_3	11.53	12.62	12.18	12.82	14.48	13.93	13.70	14.49	12.01	11.69	12.68	13.72	11.15	11.29
Cr_2O_3	0.03	0.00	0.02	0.00	0.00	0.00	0.00	0.00	0.00	0.00	0.07	0.00	0.00	0.00
FeO	12.42	12.82	12.49	14.81	12.35	12.89	13.18	11.97	13.02	12.62	13.11	12.81	12.79	13.53
MnO	0.36	0.25	0.30	0.39	0.15	0.21	0.20	0.16	0.33	0.37	0.20	0.18	0.41	0.37
MgO	14.10	13.05	13.19	11.63	13.32	12.93	12.82	13.46	13.40	13.58	13.14	12.75	13.81	13.50
CaO	10.97	11.45	11.47	11.88	12.12	11.80	11.99	12.22	11.61	11.46	11.77	11.74	11.13	11.15
Na_2O	2.34	2.38	2.40	2.29	2.27	2.27	2.32	2.33	2.42	2.40	2.26	2.34	2.50	2.42
K_2O	0.93	0.98	0.99	1.15	1.01	0.94	0.93	0.98	1.02	0.96	0.87	0.95	0.95	1.01
Cl	0.05	0.04	0.05	0.07	0.01	0.02	0.02	0.01	0.05	0.05	0.02	0.02	0.07	0.09
F	0.20	0.10	0.12	0.44	0.10	0.10	0.11	0.09	0.25	0.25	0.07	0.12	0.98	0.24
Sum	97.57	97.10	97.46	98.04	97.83	97.41	98.01	97.80	98.65	97.97	97.66	97.68	99.48	98.49
Si	6.131	6.006	6.076	5.993	5.827	5.859	5.896	5.829	6.069	6.101	6.073	5.975	6.189	6.130
Al	1.977	2.198	2.114	2.254	2.496	2.415	2.370	2.500	2.064	2.018	2.191	2.375	1.904	1.938
Ti	0.275	0.306	0.335	0.268	0.241	0.277	0.287	0.247	0.324	0.324	0.223	0.260	0.325	0.307
Cr	0.004	0.000	0.002	0.000	0.001	0.000	0.000	0.000	0.000	0.000	0.009	0.001	0.000	0.000
Fe^{3+}	0.954	0.688	0.571	0.544	0.736	0.769	0.659	0.670	0.648	0.676	0.705	0.614	0.734	0.837
Mg	3.058	2.874	2.897	2.588	2.905	2.837	2.805	2.938	2.915	2.966	2.871	2.793	2.983	2.931
Fe^{2+}	0.557	0.897	0.968	1.304	0.775	0.818	0.959	0.795	0.940	0.869	0.902	0.959	0.816	0.811
Mn	0.044	0.032	0.037	0.049	0.019	0.026	0.025	0.020	0.040	0.046	0.025	0.023	0.050	0.046
Ca	1.711	1.812	1.810	1.900	1.899	1.860	1.885	1.917	1.815	1.798	1.849	1.847	1.728	1.741
Na	0.659	0.682	0.685	0.661	0.643	0.649	0.660	0.660	0.684	0.681	0.642	0.668	0.703	0.684
K	0.172	0.185	0.186	0.219	0.188	0.176	0.175	0.183	0.189	0.179	0.162	0.179	0.176	0.187
Cl	0.013	0.010	0.013	0.018	0.003	0.005	0.004	0.003	0.013	0.014	0.005	0.006	0.018	0.023
F	0.094	0.047	0.055	0.208	0.046	0.044	0.050	0.041	0.114	0.115	0.034	0.056	0.448	0.113
Sum	15.542	15.679	15.681	15.781	15.731	15.685	15.721	15.759	15.688	15.658	15.654	15.693	15.607	15.612

Table D8 Amphibole analyses of the 2010 Merapi eruption (continued)

Sample	M11-27-3	M11-27-3	M11-27-3	M11-27-3	M11-27-3	M11-27-3	M11-27-3	M11-27-3	M11-27-3	M11-27-3	M11-27-3	M11-27-3	M11-27-4	M11-27-4
Sample Type	DD	DD	DD	DD	DD	DD	DD	DD	LG-Inc	LG-Inc	LG-Inc	LG-Inc	LG-Inc	LG-Inc
DataSet/Point	2 / 1 .	3 / 1 .	4 / 1 .	14 / 1 .	15 / 1 .	16 / 1 .	17 / 1 .	18 / 1 .	8 / 1 .	9 / 1 .	10 / 1 .	11 / 1 .	7 / 1 .	8 / 1 .
Comment	ph	ph	ph	mph	mph	mph	mph	mph	ph	ph	ph	ph	ph-c	ph-c
SiO_2	41.99	42.08	42.19	40.80	41.13	39.97	41.16	43.08	41.84	41.54	41.63	41.59	39.85	40.99
TiO_2	2.97	2.73	2.70	2.37	2.49	2.39	2.79	2.88	3.02	3.10	3.04	3.24	2.51	2.40
Al_2O_3	11.22	11.17	11.10	12.82	12.78	13.68	12.02	10.12	11.23	11.25	11.19	11.26	12.12	12.58
Cr_2O_3	0.00	0.00	0.00	0.01	0.00	0.05	0.00	0.04	0.00	0.00	0.03	0.00	0.00	0.04
FeO	13.02	13.08	12.74	13.01	12.42	12.85	12.89	12.57	12.59	12.76	12.91	12.55	12.39	13.07
MnO	0.39	0.37	0.39	0.20	0.20	0.17	0.28	0.48	0.33	0.35	0.35	0.32	0.41	0.38
MgO	13.44	13.71	13.73	13.27	13.68	13.06	13.19	14.11	13.45	13.28	13.20	13.32	13.45	13.01
CaO	11.02	11.28	11.17	11.97	12.01	12.02	11.71	11.08	11.42	11.27	11.22	11.25	11.23	11.90
Na_2O	2.49	2.45	2.41	2.29	2.29	2.26	2.33	2.39	2.28	2.34	2.27	2.39	2.45	2.55
K_2O	0.98	0.98	0.99	0.80	0.82	0.89	0.93	0.97	1.25	1.22	1.21	1.11	0.94	0.98
Cl	0.08	0.09	0.08	0.04	0.03	0.02	0.08	0.10	0.14	0.12	0.13	0.08	0.06	0.05
F	0.25	0.40	0.37	0.14	0.12	0.09	0.31	0.37	0.43	0.30	0.25	0.40	0.62	0.54
Sum	97.85	98.35	97.87	97.72	97.96	97.44	97.72	98.19	97.98	97.54	97.43	97.51	96.03	98.49
Si	6.155	6.147	6.180	5.991	6.007	5.885	6.073	6.282	6.167	6.143	6.157	6.149	5.969	6.034
Al	1.938	1.924	1.916	2.219	2.200	2.374	2.091	1.740	1.950	1.961	1.951	1.963	2.140	2.183
Ti	0.328	0.299	0.298	0.261	0.273	0.264	0.310	0.315	0.334	0.344	0.338	0.360	0.283	0.266
Cr	0.000	0.000	0.000	0.001	0.000	0.005	0.000	0.004	0.000	0.000	0.004	0.000	0.000	0.005
Fe^{3+}	0.745	0.773	0.756	0.708	0.681	0.719	0.598	0.744	0.553	0.590	0.622	0.562	0.860	0.548
Mg	2.936	2.985	2.999	2.905	2.978	2.868	2.901	3.066	2.955	2.928	2.910	2.935	3.004	2.856
Fe^{2+}	0.851	0.825	0.804	0.890	0.836	0.864	0.992	0.788	0.999	0.988	0.974	0.990	0.692	1.061
Mn	0.048	0.046	0.048	0.025	0.025	0.021	0.036	0.060	0.041	0.044	0.043	0.040	0.052	0.048
Ca	1.730	1.766	1.752	1.883	1.879	1.896	1.851	1.731	1.804	1.786	1.777	1.782	1.802	1.877
Na	0.708	0.695	0.684	0.652	0.649	0.645	0.668	0.675	0.652	0.671	0.651	0.684	0.712	0.728
K	0.184	0.183	0.185	0.150	0.153	0.166	0.176	0.180	0.235	0.231	0.228	0.209	0.179	0.184
Cl	0.021	0.023	0.021	0.010	0.007	0.005	0.019	0.024	0.034	0.031	0.034	0.021	0.016	0.013
F	0.117	0.185	0.171	0.067	0.054	0.041	0.146	0.171	0.201	0.140	0.116	0.189	0.296	0.251
Sum	15.622	15.644	15.622	15.685	15.680	15.707	15.695	15.586	15.691	15.687	15.656	15.675	15.693	15.788

Table D8 Amphibole analyses of the 2010 Merapi eruption (continued)

Sample	M11-27-4	M11-27-6	M11-27-6	M11-27-6	M11-27-6	M11-27-6	M11-27-6	M11-27-6	M11-27-6	M11-27-6	M11-27-6	M11-28b	M11-33	M11-33
Sample Type	LG-Inc	LG-Inc	LG-Inc	LG-Inc	LG-Inc	LG-Inc	LG-Inc	LG-Inc	LG-Inc	LG-Inc	LG-Inc	LG-Inc	WP	WP
DataSet/Point	9 / 1 .	1 / 1 .	2 / 1 .	3 / 1 .	4 / 1 .	49 / 1 .	50 / 1 .	51 / 1 .	52 / 1 .	53 / 1 .	54 / 1 .	9 / 1 .	5 / 1 .	6 / 1 .
Comment	ph-c	ph	ph	ph	ph	mph	mph	mph	mph	mph	mph	ph-c	mph-c	mph-c
SiO_2	41.20	40.64	40.69	40.91	40.78	39.30	40.61	39.67	41.66	39.45	42.15	42.75	41.30	39.30
TiO_2	3.54	1.77	1.75	1.69	1.80	2.28	2.38	2.19	2.46	2.22	2.77	2.93	2.62	2.43
Al_2O_3	11.71	13.92	13.75	13.73	13.78	14.79	12.96	14.94	12.43	14.86	11.35	11.21	11.65	13.87
Cr_2O_3	0.00	0.08	0.12	0.09	0.14	0.01	0.00	0.00	0.01	0.00	0.00	-0.01	0.01	0.00
FeO	13.25	10.23	10.09	10.38	10.02	12.44	13.20	12.80	12.37	12.39	12.59	12.44	13.31	12.88
MnO	0.40	0.07	0.07	0.16	0.11	0.15	0.21	0.14	0.19	0.17	0.34	0.40	0.34	0.15
MgO	13.02	14.83	15.01	15.83	15.07	12.97	12.95	12.84	13.70	13.09	13.61	13.94	12.70	12.62
CaO	11.19	12.22	12.30	11.86	12.37	12.19	11.98	12.30	12.02	12.24	11.63	11.25	11.67	11.74
Na_2O	2.59	2.18	2.12	2.27	2.16	2.29	2.41	2.27	2.32	2.29	2.38	2.45	2.36	2.27
K_2O	1.06	1.53	1.59	1.57	1.62	1.01	0.96	1.10	0.77	1.05	0.96	0.97	0.97	0.94
Cl	0.10	0.01	0.01	0.06	0.00	0.02	0.03	0.02	0.04	0.02	0.07	0.07	0.06	0.03
F	0.77	0.41	0.44	0.56	0.73	0.10	0.10	0.09	0.16	0.05	0.18	0.29	0.11	0.13
Sum	98.82	97.89	97.95	99.13	98.60	97.57	97.77	98.36	98.13	97.82	98.03	98.69	97.09	96.35
Si	6.053	5.925	5.932	5.854	5.929	5.784	5.986	5.801	6.078	5.785	6.177	6.197	6.146	5.860
Al	2.027	2.392	2.363	2.315	2.361	2.566	2.251	2.576	2.137	2.568	1.959	1.915	2.043	2.437
Ti	0.391	0.194	0.192	0.182	0.196	0.253	0.264	0.241	0.270	0.244	0.306	0.319	0.294	0.272
Cr	0.000	0.009	0.014	0.010	0.017	0.001	0.000	0.000	0.001	0.000	0.000	-0.001	0.001	0.001
Fe^{3+}	0.629	0.643	0.637	1.048	0.609	0.672	0.598	0.637	0.605	0.679	0.568	0.691	0.489	0.712
Mg	2.851	3.224	3.261	3.377	3.266	2.846	2.845	2.799	2.980	2.863	2.973	3.012	2.817	2.806
Fe^{2+}	0.999	0.604	0.593	0.194	0.609	0.859	1.029	0.928	0.904	0.840	0.975	0.817	1.168	0.894
Mn	0.050	0.008	0.009	0.019	0.013	0.019	0.027	0.017	0.024	0.021	0.043	0.049	0.043	0.019
Ca	1.761	1.909	1.922	1.819	1.927	1.922	1.892	1.927	1.879	1.924	1.826	1.747	1.861	1.876
Na	0.738	0.615	0.600	0.630	0.608	0.653	0.688	0.645	0.657	0.650	0.676	0.688	0.682	0.657
K	0.198	0.285	0.295	0.287	0.301	0.190	0.180	0.204	0.144	0.196	0.179	0.180	0.185	0.179
Cl	0.024	0.002	0.002	0.014	0.001	0.005	0.006	0.005	0.010	0.004	0.017	0.016	0.014	0.007
F	0.359	0.189	0.204	0.255	0.336	0.048	0.044	0.040	0.072	0.023	0.083	0.134	0.051	0.059
Sum	15.696	15.808	15.817	15.735	15.836	15.765	15.760	15.776	15.680	15.770	15.682	15.614	15.727	15.711

Table D8 Amphibole analyses of the 2010 Merapi eruption (continued)

Sample	M11-33	M11-33	M11-33	M11-33	M11-33	M11-34	M11-34	M11-34	M11-34	M11-38	M11-38	M11-38	M11-38	M11-38
Sample Type	WP	WP	WP	WP	WP	DD	DD	DD	DD	DD	DD	DD	DD	DD
DataSet/Point	13 / 1 .	14 / 1 .	15 / 1 .	18 / 1 .	19 / 1 .	1 / 1 .	2 / 1 .	3 / 1 .	4 / 1 .	1 / 1 .	2 / 1 .	3 / 1 .	4 / 1 .	15 / 1 .
Comment	mph-c	mph-c	mph-r	mph-c	mph-r	mph-c	mph-c	mph-r	mph-c	ph-c	ph-c	ph-r	ph-r	ph
SiO_2	40.72	41.87	42.61	39.85	39.04	40.35	40.55	39.96	40.48	40.15	39.99	40.66	40.21	39.64
TiO_2	2.83	2.85	3.21	2.31	2.48	2.14	2.34	2.22	1.81	2.49	2.42	2.29	2.35	2.25
Al_2O_3	12.29	11.43	10.59	13.74	13.70	13.78	13.40	13.84	13.27	13.69	14.17	13.16	13.42	14.29
Cr_2O_3	0.00	0.03	0.00	0.00	0.01	0.01	0.02	0.00	0.00	0.00	0.03	0.01	0.02	0.00
FeO	12.94	12.43	12.43	13.21	12.83	12.80	12.88	12.72	14.92	12.08	12.46	12.24	12.39	12.96
MnO	0.29	0.35	0.40	0.20	0.18	0.17	0.25	0.18	0.35	0.13	0.14	0.20	0.21	0.17
MgO	13.23	13.59	13.89	12.76	12.63	12.65	12.70	12.64	11.60	13.13	13.22	13.31	13.09	12.97
CaO	11.58	11.28	11.04	11.84	11.61	12.14	11.99	12.29	11.97	11.61	12.02	11.83	11.96	11.98
Na_2O	2.45	2.38	2.38	2.31	2.26	2.23	2.27	2.22	2.26	2.25	2.32	2.24	2.26	2.33
K_2O	0.90	0.99	1.07	0.96	0.89	1.02	1.00	1.04	0.96	1.07	1.09	0.91	0.93	0.95
Cl	0.05	0.05	0.09	0.02	0.02	0.02	0.03	0.01	0.06	0.03	0.02	0.02	0.03	0.02
F	0.25	0.25	0.35	0.13	0.25	0.10	0.13	0.19	0.06	0.06	0.01	0.06	0.06	0.06
Sum	97.52	97.51	98.05	97.33	95.90	97.42	97.57	97.31	97.75	96.69	97.90	96.94	96.92	97.60
Si	6.006	6.154	6.227	5.886	5.849	5.966	5.987	5.932	6.198	5.936	5.855	5.996	5.949	5.823
Al	2.137	1.980	1.825	2.391	2.418	2.402	2.332	2.422	2.071	2.385	2.445	2.288	2.340	2.474
Ti	0.314	0.315	0.353	0.257	0.280	0.238	0.260	0.248	0.228	0.277	0.267	0.254	0.261	0.248
Cr	0.000	0.003	0.000	0.000	0.002	0.001	0.002	0.000	0.001	0.000	0.004	0.001	0.002	0.000
Fe^{3+}	0.694	0.663	0.685	0.735	0.769	0.511	0.542	0.473	0.546	0.663	0.674	0.658	0.621	0.772
Mg	2.910	2.976	3.026	2.810	2.821	2.789	2.796	2.796	2.664	2.894	2.886	2.925	2.888	2.841
Fe^{2+}	0.902	0.865	0.834	0.897	0.838	1.072	1.049	1.106	1.243	0.830	0.852	0.852	0.912	0.820
Mn	0.036	0.044	0.050	0.024	0.023	0.021	0.031	0.022	0.049	0.016	0.018	0.025	0.026	0.021
Ca	1.830	1.776	1.728	1.873	1.864	1.923	1.896	1.954	1.882	1.839	1.885	1.870	1.896	1.885
Na	0.699	0.678	0.673	0.661	0.655	0.640	0.649	0.640	0.611	0.646	0.659	0.641	0.647	0.663
K	0.170	0.186	0.200	0.181	0.170	0.192	0.188	0.197	0.156	0.203	0.204	0.172	0.176	0.177
Cl	0.012	0.013	0.022	0.005	0.005	0.005	0.008	0.003	0.015	0.006	0.006	0.005	0.007	0.004
F	0.116	0.116	0.163	0.061	0.120	0.046	0.061	0.089	0.030	0.028	0.004	0.028	0.029	0.027
Sum	15.699	15.640	15.602	15.716	15.689	15.755	15.733	15.790	15.649	15.688	15.748	15.682	15.719	15.726

Table D8 Amphibole analyses of the 2010 Merapi eruption (continued)

Sample	M11-38	M11-38	M11-38	M11-38	M11-38	M11-38	M11-38	M11-38	M11-38	M11-38	M11-38	M11-38	M11-38	M11-38
Sample Type	DD	DD	DD	DD	DD	DD	DD	DD	DD	DD	DD	DD	DD	DD
DataSet/Point	16 / 1 .	17 / 1 .	18 / 1 .	19 / 1 .	20 / 1 .	21 / 1 .	22 / 1 .	23 / 1 .	24 / 1 .	5 / 1 .	6 / 1 .	7 / 1 .	8 / 1 .	9 / 1 .
Comment	ph	ph	ph	ph	ph	ph	ph	ph	ph	mph-c	mph-c	mph-c	mph-r	mph-r
SiO_2	39.68	39.76	39.67	39.74	39.57	39.68	39.40	39.54	39.61	39.52	42.38	42.22	40.22	39.62
TiO_2	2.27	2.28	2.26	2.25	2.19	2.17	2.14	2.23	2.34	1.96	3.20	3.14	2.70	2.31
Al_2O_3	14.44	14.42	14.71	14.63	14.82	14.55	14.43	14.62	14.24	14.53	10.62	10.81	13.31	14.33
Cr_2O_3	0.02	0.00	0.01	0.00	0.02	0.02	0.00	0.01	0.00	0.00	0.02	0.00	0.04	0.00
FeO	12.75	12.74	12.30	12.26	12.57	12.46	12.42	12.33	12.53	13.82	13.47	13.64	12.57	12.76
MnO	0.14	0.20	0.15	0.14	0.08	0.11	0.16	0.11	0.17	0.20	0.45	0.47	0.23	0.20
MgO	12.89	12.84	12.98	12.94	12.90	12.94	13.14	12.89	12.79	12.33	13.15	12.91	13.13	12.96
CaO	12.06	11.89	12.18	12.10	12.04	12.12	12.02	12.10	12.04	11.62	10.80	10.88	11.89	11.86
Na_2O	2.26	2.36	2.27	2.25	2.27	2.23	2.22	2.23	2.26	2.20	2.32	2.34	2.28	2.35
K_2O	1.00	0.98	1.04	1.08	1.09	1.10	1.08	1.09	1.03	0.94	1.22	1.16	0.89	0.96
Cl	0.02	0.02	0.02	0.01	0.01	0.02	0.02	0.01	0.02	0.03	0.12	0.12	0.03	0.02
F	0.10	0.10	0.05	0.03	0.06	0.06	0.01	0.05	0.09	0.07	0.23	0.22	0.08	0.10
Sum	97.63	97.60	97.65	97.43	97.60	97.49	97.04	97.20	97.12	97.22	97.97	97.91	97.37	97.46
Si	5.835	5.845	5.829	5.848	5.812	5.842	5.812	5.836	5.862	5.823	6.222	6.211	5.924	5.826
Al	2.502	2.498	2.547	2.537	2.566	2.526	2.509	2.543	2.484	2.523	1.837	1.875	2.311	2.484
Ti	0.251	0.252	0.249	0.249	0.242	0.241	0.237	0.248	0.261	0.217	0.353	0.347	0.299	0.256
Cr	0.002	0.000	0.001	0.000	0.002	0.002	0.000	0.001	0.000	0.000	0.002	0.000	0.005	0.000
Fe^{3+}	0.691	0.704	0.617	0.608	0.685	0.637	0.752	0.618	0.608	0.924	0.726	0.693	0.668	0.767
Mg	2.824	2.814	2.843	2.838	2.824	2.841	2.890	2.837	2.822	2.709	2.877	2.831	2.884	2.840
Fe^{2+}	0.877	0.861	0.894	0.901	0.859	0.898	0.780	0.903	0.943	0.778	0.928	0.985	0.881	0.802
Mn	0.018	0.025	0.019	0.017	0.009	0.014	0.020	0.013	0.021	0.025	0.055	0.058	0.029	0.025
Ca	1.900	1.873	1.918	1.908	1.894	1.913	1.900	1.913	1.909	1.833	1.699	1.715	1.876	1.868
Na	0.646	0.674	0.647	0.641	0.647	0.638	0.636	0.638	0.649	0.629	0.661	0.668	0.652	0.669
K	0.187	0.184	0.196	0.203	0.204	0.207	0.204	0.205	0.195	0.177	0.228	0.218	0.166	0.180
Cl	0.006	0.006	0.006	0.003	0.002	0.004	0.005	0.003	0.005	0.007	0.030	0.030	0.007	0.005
F	0.045	0.047	0.023	0.016	0.026	0.027	0.003	0.025	0.040	0.032	0.108	0.102	0.038	0.045
Sum	15.733	15.731	15.761	15.752	15.745	15.758	15.740	15.756	15.753	15.640	15.587	15.601	15.695	15.718

Table D8 Amphibole analyses of the 2010 Merapi eruption (continued)

Sample	M11-38	M11-38	M11-38	M11-38	M11-38	M11-38	M11-48	M11-48	M11-48	M11-48	M11-48	M11-48	M11-48	M11-50
Sample Type	DD	DD	DD	DD	DD	DD	DD	DD	DD	LG-Inc	LG-Inc	LG-Inc	LG-Inc	WP
DataSet/Point	10 / 1 .	11 / 1 .	12 / 1 .	13 / 1 .	45 / 1 .	46 / 1 .	33 / 1 .	34 / 1 .	35 / 1 .	3 / 1 .	10 / 1 .	11 / 1 .	12 / 1 .	27 / 1 .
Comment	mph-c	mph-c	mph-r	mph-r	mph-c	mph-c	mph-c	mph-r	mph	mph-c	mph	mph	mph	ph
SiO_2	41.13	40.82	40.68	42.11	42.20	41.61	41.52	39.92	40.09	40.27	39.53	41.04	39.40	42.15
TiO_2	2.53	2.46	2.50	2.51	2.79	2.62	1.98	2.28	2.28	2.41	2.26	2.58	2.18	2.72
Al_2O_3	12.62	12.92	12.84	13.46	11.71	12.11	11.07	13.56	13.79	13.30	14.36	12.61	14.62	11.46
Cr_2O_3	0.00	0.00	0.00	0.01	0.02	0.00	0.05	0.00	0.00	0.03	0.00	0.03	0.00	0.00
FeO	13.77	14.14	13.57	12.58	13.40	12.64	18.03	13.29	13.16	12.80	12.80	13.38	12.44	12.44
MnO	0.30	0.32	0.25	0.17	0.47	0.40	0.50	0.26	0.14	0.16	0.14	0.35	0.17	0.32
MgO	12.58	12.33	12.45	13.12	13.28	13.58	10.37	12.84	12.84	13.10	13.21	13.17	13.08	13.67
CaO	11.59	11.76	11.41	11.30	11.35	11.23	11.49	12.09	12.02	11.99	11.97	11.10	12.16	11.43
Na_2O	2.30	2.29	2.31	2.32	2.37	2.41	1.78	2.28	2.27	2.28	2.32	2.52	2.31	2.28
K_2O	0.99	0.92	0.93	0.98	0.83	1.06	1.13	0.91	0.96	1.00	1.06	1.01	1.07	0.89
Cl	0.04	0.04	0.04	0.03	0.04	0.06	0.10	0.03	0.03	0.03	0.02	0.06	0.01	0.06
F	0.05	0.06	0.10	0.15	0.38	0.52	0.09	0.06	0.07	0.17	0.50	0.16	0.14	0.37
Sum	97.90	98.04	97.08	98.74	98.85	98.23	98.10	97.51	97.64	97.54	98.18	98.01	97.56	97.78
Si	6.047	6.005	6.021	6.077	6.128	6.077	6.200	5.891	5.900	5.940	5.795	5.995	5.800	6.175
Al	2.186	2.240	2.241	2.289	2.005	2.085	1.948	2.359	2.392	2.312	2.482	2.172	2.536	1.978
Ti	0.280	0.272	0.278	0.272	0.305	0.288	0.222	0.253	0.252	0.267	0.249	0.283	0.241	0.299
Cr	0.000	0.000	0.000	0.001	0.002	0.000	0.006	0.000	0.000	0.004	0.000	0.003	0.000	0.000
Fe^{3+}	0.666	0.672	0.701	0.689	0.773	0.791	0.796	0.708	0.685	0.640	0.814	0.892	0.683	0.672
Mg	2.757	2.704	2.748	2.822	2.875	2.957	2.309	2.826	2.818	2.880	2.888	2.869	2.870	2.984
Fe^{2+}	1.027	1.067	0.979	0.829	0.855	0.753	1.455	0.932	0.935	0.938	0.755	0.743	0.848	0.853
Mn	0.038	0.039	0.031	0.021	0.058	0.050	0.063	0.032	0.018	0.020	0.018	0.043	0.021	0.039
Ca	1.826	1.854	1.810	1.747	1.766	1.757	1.838	1.912	1.895	1.895	1.880	1.737	1.919	1.794
Na	0.657	0.652	0.664	0.649	0.668	0.683	0.515	0.652	0.648	0.653	0.658	0.715	0.658	0.648
K	0.186	0.173	0.175	0.180	0.154	0.197	0.215	0.171	0.180	0.189	0.199	0.188	0.202	0.166
Cl	0.010	0.010	0.010	0.008	0.011	0.014	0.024	0.008	0.007	0.006	0.005	0.015	0.003	0.014
F	0.024	0.026	0.047	0.069	0.173	0.238	0.040	0.028	0.031	0.078	0.232	0.072	0.064	0.171
Sum	15.669	15.679	15.649	15.575	15.589	15.638	15.567	15.734	15.723	15.737	15.737	15.639	15.779	15.608

Table D8 Amphibole analyses of the 2010 Merapi eruption (continued)

Sample	M11-50	M11-50	M11-50	M11-50	M11-50	M11-51	M11-51	M11-51	M11-51	M11-51	M11-51	M11-51	M11-51	M11-51
Sample Type	WP	WP	WP	WP	WP	GS	GS	GS	GS	GS	GS	GS	GS	GS
DataSet/Point	28 / 1 .	43 / 1 .	56 / 1 .	57 / 1 .	58 / 1 .	1 / 1 .	2 / 1 .	3 / 1 .	4 / 1 .	6 / 1 .	7 / 1 .	15 / 1 .	16 / 1 .	17 / 1 .
Comment	ph	ph	ph	ph	ph	ph-c	ph-c	ph-c	ph-c	ph-c	ph-c	ph-c	ph-c	ph-r
SiO_2	42.57	42.09	42.46	42.78	42.59	40.71	41.83	42.17	40.75	39.68	39.61	40.54	41.73	42.18
TiO_2	2.71	2.75	3.11	2.35	2.90	2.91	3.26	2.70	2.77	2.30	2.26	3.20	3.29	3.24
Al_2O_3	11.27	11.30	11.33	11.48	11.32	12.07	11.18	11.21	12.17	13.99	14.23	12.32	11.09	11.04
Cr_2O_3	0.00	0.00	0.00	0.00	0.01	0.00	0.03	0.00	0.03	0.00	0.01	0.01	0.00	0.02
FeO	12.39	12.25	12.69	11.99	12.41	12.60	12.37	12.62	13.04	12.41	12.89	13.24	13.15	13.12
MnO	0.37	0.33	0.32	0.33	0.38	0.38	0.33	0.34	0.30	0.15	0.18	0.36	0.36	0.34
MgO	13.88	13.49	13.58	14.09	13.61	13.23	13.64	13.43	13.06	12.80	12.80	12.72	13.29	13.50
CaO	11.35	11.27	10.95	11.17	11.09	10.95	10.88	11.11	11.49	11.91	12.12	11.17	10.80	10.82
Na_2O	2.32	2.40	2.37	2.46	2.49	2.41	2.38	2.33	2.39	2.24	2.24	2.43	2.40	2.33
K_2O	0.88	0.90	0.96	0.89	0.98	1.01	1.02	0.93	0.93	1.09	1.16	1.07	1.10	1.16
Cl	0.06	0.05	0.07	0.06	0.08	0.07	0.08	0.07	0.04	0.02	0.02	0.05	0.10	0.10
F	0.37	0.48	0.29	0.47	0.55	0.35	0.27	0.18	0.24	0.23	0.37	0.29	0.33	0.29
Sum	98.16	97.31	98.14	98.07	98.39	96.69	97.25	97.09	97.20	96.82	97.90	97.41	97.64	98.13
Si	6.200	6.211	6.183	6.222	6.214	6.035	6.149	6.210	6.032	5.897	5.845	6.001	6.137	6.159
Al	1.935	1.964	1.944	1.968	1.946	2.109	1.938	1.946	2.123	2.450	2.475	2.149	1.922	1.901
Ti	0.297	0.305	0.341	0.257	0.318	0.325	0.360	0.299	0.308	0.257	0.250	0.357	0.363	0.355
Cr	0.000	0.000	0.000	0.000	0.001	0.000	0.003	0.000	0.003	0.000	0.001	0.001	0.000	0.002
Fe^{3+}	0.712	0.584	0.746	0.736	0.637	0.811	0.744	0.689	0.690	0.600	0.642	0.693	0.782	0.805
Mg	3.013	2.966	2.948	3.054	2.960	2.923	2.989	2.949	2.882	2.836	2.816	2.808	2.915	2.938
Fe^{2+}	0.797	0.927	0.800	0.722	0.878	0.751	0.776	0.865	0.924	0.942	0.949	0.947	0.835	0.796
Mn	0.046	0.042	0.039	0.041	0.047	0.047	0.041	0.042	0.038	0.019	0.022	0.045	0.045	0.043
Ca	1.771	1.781	1.708	1.740	1.733	1.739	1.713	1.754	1.822	1.896	1.916	1.771	1.701	1.694
Na	0.654	0.687	0.670	0.694	0.704	0.692	0.679	0.666	0.685	0.646	0.642	0.697	0.684	0.659
K	0.163	0.169	0.178	0.165	0.183	0.192	0.191	0.174	0.176	0.206	0.218	0.202	0.207	0.215
Cl	0.014	0.013	0.018	0.014	0.019	0.019	0.019	0.017	0.010	0.005	0.006	0.014	0.024	0.025
F	0.170	0.225	0.135	0.215	0.254	0.162	0.125	0.083	0.111	0.108	0.171	0.137	0.155	0.133
Sum	15.588	15.638	15.556	15.599	15.620	15.623	15.583	15.594	15.683	15.747	15.776	15.670	15.593	15.568

Table D8 Amphibole analyses of the 2010 Merapi eruption (continued)

Sample	M11-51	M11-51	M11-51	M11-51	M11-51	M11-51	M11-53-B3	M11-53-B3	M11-53-B3	M11-53-B3	M11-53-B3	M11-53-B3	M11-53-B4	M11-53-B4
Sample Type	GS	GS	GS	GS	GS	GS	DS	DS	DS	DS	DS	DS	P5N-WP	P5N-WP
DataSet/Point	18 / 1 .	38 / 1 .	39 / 1 .	41 / 1 .	42 / 1 .	47 / 1 .	1 / 1 .	2 / 1 .	3 / 1 .	4 / 1 .	5 / 1 .	6 / 1 .	1 / 1 .	2 / 1 .
Comment	ph-r	mph-c	mph-r	mph-c	mph-r	mph-c	mph-c	mph-r	mph-c	mph-c	mph-c	mph-c	ph-c	ph-c
SiO_2	42.02	41.93	40.38	42.64	42.16	41.04	42.25	40.62	39.85	41.72	41.34	41.80	41.12	39.73
TiO_2	3.19	3.08	2.50	2.86	3.01	2.95	3.05	2.52	2.14	3.09	2.80	2.82	2.48	2.38
Al_2O_3	11.05	11.21	13.08	10.56	11.07	12.09	10.90	13.15	14.50	11.39	11.81	11.90	12.59	14.18
Cr_2O_3	0.00	0.00	0.00	0.01	0.00	0.00	0.02	0.03	0.02	0.02	0.00	0.00	0.00	0.02
FeO	13.02	12.76	12.85	12.26	12.69	12.48	12.46	12.20	12.00	12.24	12.39	12.38	12.08	12.88
MnO	0.39	0.38	0.23	0.38	0.38	0.28	0.39	0.16	0.16	0.38	0.37	0.29	0.17	0.13
MgO	13.40	13.39	12.90	13.81	13.59	13.14	13.61	13.06	13.32	13.76	13.43	13.54	13.63	13.01
CaO	10.69	11.00	11.58	10.94	10.97	11.43	10.94	11.74	11.85	11.43	11.49	11.12	11.58	11.90
Na_2O	2.36	2.37	2.25	2.35	2.31	2.37	2.38	2.29	2.33	2.34	2.36	2.34	2.37	2.33
K_2O	1.10	1.00	0.89	0.92	1.00	0.94	0.95	0.91	1.05	0.93	0.92	0.91	1.29	1.23
Cl	0.11	0.07	0.03	0.09	0.09	0.04	0.08	0.02	0.01	0.06	0.05	0.06	0.06	0.02
F	0.34	0.25	0.12	0.20	0.18	0.16	0.23	0.11	0.32	0.23	0.11	0.15	0.30	0.17
Sum	97.68	97.43	96.80	96.99	97.44	96.92	97.26	96.81	97.55	97.61	97.08	97.31	97.66	97.98
Si	6.163	6.165	5.976	6.271	6.182	6.079	6.211	6.011	5.848	6.124	6.103	6.124	6.047	5.834
Al	1.910	1.943	2.281	1.830	1.912	2.110	1.889	2.293	2.508	1.971	2.055	2.055	2.182	2.454
Ti	0.352	0.341	0.278	0.316	0.332	0.328	0.337	0.281	0.236	0.341	0.311	0.310	0.275	0.263
Cr	0.000	0.000	0.000	0.001	0.000	0.000	0.002	0.004	0.002	0.002	0.000	0.000	0.000	0.002
Fe^{3+}	0.825	0.717	0.726	0.705	0.772	0.588	0.711	0.569	0.737	0.657	0.632	0.749	0.606	0.711
Mg	2.930	2.935	2.846	3.027	2.971	2.902	2.981	2.881	2.913	3.011	2.956	2.958	2.988	2.849
Fe^{2+}	0.772	0.852	0.864	0.802	0.784	0.958	0.821	0.941	0.736	0.846	0.898	0.767	0.881	0.871
Mn	0.049	0.047	0.029	0.047	0.047	0.035	0.049	0.020	0.020	0.047	0.046	0.037	0.022	0.016
Ca	1.679	1.733	1.836	1.724	1.723	1.814	1.723	1.861	1.863	1.798	1.818	1.746	1.825	1.872
Na	0.672	0.675	0.646	0.669	0.655	0.681	0.679	0.657	0.662	0.667	0.676	0.664	0.675	0.665
K	0.205	0.187	0.167	0.172	0.186	0.178	0.178	0.171	0.196	0.175	0.174	0.170	0.243	0.230
Cl	0.027	0.017	0.007	0.021	0.023	0.010	0.019	0.005	0.002	0.015	0.012	0.014	0.014	0.005
F	0.158	0.115	0.055	0.092	0.083	0.073	0.107	0.052	0.149	0.108	0.053	0.072	0.138	0.079
Sum	15.556	15.595	15.649	15.566	15.565	15.674	15.580	15.689	15.721	15.640	15.668	15.581	15.742	15.767

Table D8 Amphibole analyses of the 2010 Merapi eruption (continued)

Sample	M11-53-B4	M11-53-B4	M11-53-B4	M11-53-B4	M11-53-B4	M11-53-B4	M11-54-3	M11-54-3	M11-54-3	M11-54-3	M11-54-3	M11-54-3	M11-54-3	M11-54-3
Sample Type	P5N-WP	P5N-WP	P5N-WP	P5N-WP	P5N-WP	P5N-WP	DD	DD	DD	DD	DD	DD	DD	LG-Inc
DataSet/Point	3 / 1 .	4 / 1 .	27 / 1 .	28 / 1 .	29 / 1 .	30 / 1 .	53 / 1 .	57 / 1 .	58 / 1 .	59 / 1 .	60 / 1 .	61 / 1 .	62 / 1 .	1 / 1 .
Comment	ph-r	ph-r	ph-c	ph-c	ph-r	ph-r	mph-r	mph-c	mph-r	mph-c	mph-r	mph-c	mph-r	ph
SiO_2	39.22	39.19	40.28	40.69	40.49	40.33	40.44	42.80	43.93	40.26	41.14	43.24	42.78	40.24
TiO_2	2.39	2.38	2.03	1.95	2.57	2.17	2.29	2.72	2.61	1.80	2.02	2.56	2.65	2.42
Al_2O_3	14.33	14.34	14.27	14.05	12.80	13.50	13.72	10.78	11.37	14.32	13.33	10.89	11.22	14.35
Cr_2O_3	0.02	0.05	0.01	0.01	0.00	0.01	0.00	0.01	0.01	0.03	0.01	0.00	0.00	0.03
FeO	12.47	12.80	10.72	11.00	12.40	12.36	12.98	12.76	12.23	11.83	12.44	12.64	12.66	13.26
MnO	0.14	0.18	0.12	0.13	0.35	0.32	0.19	0.45	0.38	0.13	0.17	0.39	0.40	0.12
MgO	13.08	13.02	14.10	14.05	13.34	13.24	12.97	13.53	12.92	13.31	13.17	13.89	13.42	12.84
CaO	12.11	12.11	11.97	11.75	11.26	11.54	12.15	11.28	10.99	12.32	12.25	11.12	11.21	12.71
Na_2O	2.34	2.35	2.19	2.23	2.38	2.36	2.22	2.33	2.46	2.11	2.22	2.34	2.33	1.49
K_2O	1.14	1.13	1.43	1.43	1.18	1.27	0.81	0.97	1.11	1.13	0.91	0.91	0.89	1.31
Cl	0.02	0.03	0.02	0.03	0.09	0.04	0.02	0.09	0.07	0.01	0.02	0.08	0.07	0.02
F	0.55	0.61	0.30	0.26	0.53	0.62	0.00	0.21	0.29	0.00	0.02	0.11	0.33	0.26
Sum	97.82	98.17	97.45	97.58	97.38	97.76	97.80	97.91	98.38	97.24	97.71	98.16	97.98	99.04
Si	5.796	5.778	5.902	5.944	5.977	5.942	5.927	6.267	6.409	5.924	6.039	6.274	6.253	5.857
Al	2.496	2.492	2.465	2.419	2.228	2.345	2.371	1.861	1.955	2.483	2.306	1.862	1.933	2.461
Ti	0.266	0.264	0.224	0.215	0.285	0.240	0.253	0.299	0.287	0.199	0.223	0.279	0.292	0.265
Cr	0.003	0.005	0.001	0.001	0.000	0.002	0.000	0.001	0.001	0.003	0.002	0.000	0.000	0.003
Fe^{3+}	0.658	0.708	0.634	0.686	0.785	0.731	0.670	0.626	0.315	0.571	0.513	0.751	0.641	0.662
Mg	2.881	2.861	3.079	3.061	2.936	2.908	2.834	2.954	2.809	2.919	2.881	3.003	2.924	2.785
Fe^{2+}	0.884	0.870	0.680	0.658	0.746	0.792	0.921	0.937	1.178	0.885	1.015	0.783	0.907	0.951
Mn	0.017	0.022	0.015	0.016	0.044	0.040	0.023	0.055	0.047	0.016	0.022	0.048	0.050	0.015
Ca	1.917	1.913	1.879	1.840	1.781	1.821	1.908	1.769	1.718	1.942	1.926	1.728	1.755	1.982
Na	0.672	0.673	0.622	0.631	0.680	0.675	0.632	0.661	0.696	0.601	0.632	0.658	0.660	0.421
K	0.215	0.213	0.268	0.266	0.222	0.240	0.152	0.180	0.206	0.212	0.171	0.168	0.166	0.243
Cl	0.004	0.006	0.004	0.007	0.022	0.010	0.005	0.022	0.018	0.003	0.005	0.020	0.018	0.004
F	0.259	0.283	0.141	0.122	0.248	0.290	0.000	0.099	0.136	0.000	0.010	0.051	0.154	0.122
Sum	15.804	15.798	15.769	15.737	15.683	15.736	15.691	15.610	15.620	15.754	15.729	15.554	15.582	15.646

Table D8 Amphibole analyses of the 2010 Merapi eruption (continued)

Sample	M11-54-3	M11-54-3	M11-54-3	M11-54-3	M11-54-3	M11-54-3	M11-55	M11-55	M11-55	M11-55	M11-55	M11-55	M11-55	M11-55
Sample Type	LG-Inc	LG-Inc	LG-Inc	LG-Inc	LG-Inc	LG-Inc	WP	WP	WP	WP	WP	WP	WP	WP
DataSet/Point	1 / 2 .	1 / 3 .	1 / 4 .	1 / 5 .	1 / 6 .	1 / 7 .	37 / 1 .	37 / 2 .	37 / 3 .	37 / 4 .	37 / 5 .	37 / 6 .	37 / 7 .	37 / 8 .
Comment	ph	ph	ph	ph	ph	ph	ph	ph	ph	ph	ph	ph	ph	ph
SiO_2	40.03	39.98	39.76	39.82	39.87	40.05	41.22	41.29	41.34	41.42	41.08	41.20	41.34	41.29
TiO_2	1.79	1.92	1.87	1.76	1.72	1.78	1.74	1.71	1.69	1.79	1.65	1.64	1.77	1.75
Al_2O_3	14.58	14.66	14.53	14.73	14.51	14.30	13.25	13.60	13.76	13.84	13.84	13.35	13.71	13.49
Cr_2O_3	0.01	0.00	0.01	0.01	0.00	0.03	0.06	0.03	0.07	0.08	0.06	0.05	0.06	0.06
FeO	12.36	12.21	12.31	12.12	12.25	12.11	11.16	11.68	10.31	10.10	10.19	10.19	10.24	10.36
MnO	0.10	0.14	0.15	0.11	0.14	0.11	0.22	0.14	0.09	0.08	0.10	0.09	0.08	0.11
MgO	13.11	12.96	13.11	13.12	13.07	13.07	13.94	13.53	14.62	14.71	14.53	14.67	14.62	14.69
CaO	12.36	12.42	12.28	12.33	12.32	12.46	11.81	11.88	12.08	12.00	11.95	12.08	11.99	12.08
Na_2O	2.18	2.14	2.19	2.16	2.17	2.15	2.25	2.18	2.22	2.19	2.12	2.13	2.14	2.16
K_2O	1.07	1.07	1.03	1.04	1.03	1.03	1.21	1.18	1.14	1.13	1.12	1.17	1.17	1.18
Cl	0.02	0.01	0.01	0.01	0.01	0.02	0.01	0.01	0.00	0.01	0.01	0.00	0.01	0.01
F	0.03	0.02	0.04	0.00	0.00	0.44	0.27	0.23	0.12	0.00	0.12	0.00	0.00	0.26
Sum	97.63	97.53	97.28	97.20	97.08	97.56	97.13	97.46	97.44	97.35	96.77	96.58	97.12	97.44
Si	5.877	5.882	5.857	5.863	5.882	5.918	6.056	6.053	6.013	6.011	6.004	6.040	6.018	6.017
Al	2.524	2.543	2.522	2.556	2.524	2.490	2.295	2.349	2.358	2.368	2.385	2.306	2.352	2.317
Ti	0.198	0.212	0.207	0.195	0.191	0.198	0.192	0.189	0.185	0.195	0.181	0.181	0.194	0.192
Cr	0.001	0.000	0.001	0.001	0.000	0.004	0.007	0.004	0.008	0.009	0.007	0.006	0.007	0.007
Fe^{3+}	0.616	0.540	0.657	0.625	0.622	0.518	0.619	0.594	0.635	0.654	0.686	0.627	0.656	0.658
Mg	2.869	2.842	2.879	2.879	2.874	2.879	3.052	2.957	3.171	3.182	3.166	3.206	3.173	3.192
Fe^{2+}	0.902	0.963	0.860	0.867	0.890	0.979	0.752	0.838	0.619	0.572	0.560	0.622	0.590	0.604
Mn	0.012	0.017	0.018	0.014	0.018	0.014	0.027	0.017	0.011	0.009	0.012	0.011	0.009	0.014
Ca	1.944	1.957	1.937	1.945	1.948	1.973	1.858	1.865	1.883	1.866	1.871	1.897	1.870	1.886
Na	0.620	0.611	0.624	0.618	0.620	0.615	0.640	0.619	0.625	0.617	0.601	0.607	0.603	0.611
K	0.200	0.202	0.194	0.195	0.193	0.195	0.226	0.220	0.212	0.209	0.209	0.219	0.217	0.219
Cl	0.004	0.003	0.003	0.003	0.002	0.005	0.002	0.002	0.001	0.002	0.003	0.001	0.002	0.003
F	0.016	0.007	0.017	0.002	0.000	0.207	0.126	0.107	0.057	0.000	0.055	0.000	0.000	0.119
Sum	15.764	15.770	15.755	15.757	15.761	15.783	15.725	15.705	15.720	15.692	15.681	15.722	15.690	15.715

Table D8 Amphibole analyses of the 2010 Merapi eruption (continued)

Sample	M11-55	M11-55	M11-55	M11-75	M11-75	M11-75	M11-75	M11-75	M11-75	M11-75	M11-75	M11-80	M11-80	M11-80
Sample Type	WP	WP	WP	GS	GS	GS	GS	GS	GS	GS	GS	DD	DD	DD
DataSet/Point	44 / 1 .	45 / 1 .	46 / 1 .	1 / 1 .	2 / 1 .	6 / 1 .	7 / 1 .	10 / 1 .	11 / 1 .	12 / 1 .	13 / 1 .	1 / 1 .	2 / 1 .	3 / 1 .
Comment	ph-c	ph-c	ph-c	ph	mph	mph-c	mph-r	mph-c	mph-r	mph-c	mph-r	ph-c	ph-c	ph-r
SiO_2	41.71	41.38	41.10	42.06	42.56	40.71	42.38	42.76	42.70	43.10	41.97	40.51	40.97	40.58
TiO_2	2.48	2.42	2.41	2.47	2.18	2.28	2.54	2.66	2.73	2.55	2.38	2.15	2.39	2.27
Al_2O_3	12.50	12.85	12.97	11.82	11.16	13.24	11.26	10.92	11.34	10.70	11.49	14.02	12.96	13.76
Cr_2O_3	0.00	0.00	0.02	0.01	0.00	0.00	0.02	0.00	0.01	0.01	0.02	0.00	0.01	0.00
FeO	13.81	12.88	13.26	12.60	13.90	13.03	12.65	12.89	12.64	13.12	13.62	13.38	13.06	12.99
MnO	0.33	0.30	0.29	0.30	0.41	0.23	0.35	0.38	0.36	0.46	0.36	0.21	0.23	0.21
MgO	12.46	12.85	12.76	13.27	12.87	12.85	13.47	13.63	13.48	13.33	12.65	12.54	12.69	12.57
CaO	11.23	11.57	11.62	11.85	11.41	12.00	11.55	11.19	11.48	11.24	11.77	11.84	11.45	11.78
Na_2O	2.38	2.34	2.34	2.28	2.17	2.24	2.32	2.29	2.28	2.28	2.21	2.27	2.37	2.29
K_2O	1.03	0.98	1.03	0.88	0.88	0.86	0.91	0.93	0.91	0.98	0.99	1.06	1.07	1.02
Cl	0.07	0.05	0.05	0.05	0.07	0.04	0.05	0.08	0.07	0.09	0.07	0.03	0.07	0.03
F	0.26	0.30	0.32	0.23	0.07	0.11	0.30	0.19	0.20	0.25	0.11	0.41	0.44	0.30
Sum	98.26	97.90	98.16	97.81	97.69	97.57	97.78	97.91	98.19	98.11	97.64	98.43	97.70	97.79
Si	6.112	6.077	6.032	6.183	6.250	5.996	6.224	6.242	6.231	6.304	6.210	5.937	6.046	5.976
Al	2.159	2.224	2.244	2.048	1.932	2.298	1.948	1.878	1.950	1.845	2.003	2.421	2.255	2.388
Ti	0.273	0.267	0.266	0.273	0.241	0.252	0.280	0.292	0.300	0.280	0.265	0.237	0.265	0.251
Cr	0.000	0.000	0.002	0.001	0.000	0.000	0.002	0.000	0.001	0.001	0.002	0.000	0.002	0.000
Fe^{3+}	0.676	0.597	0.643	0.488	0.715	0.621	0.576	0.731	0.583	0.632	0.494	0.670	0.622	0.595
Mg	2.722	2.813	2.791	2.909	2.818	2.821	2.948	2.966	2.931	2.908	2.791	2.739	2.791	2.759
Fe^{2+}	1.017	0.985	0.985	1.060	0.992	0.983	0.978	0.843	0.959	0.974	1.191	0.970	0.990	1.005
Mn	0.041	0.037	0.036	0.037	0.051	0.029	0.043	0.047	0.045	0.056	0.045	0.026	0.029	0.027
Ca	1.763	1.821	1.827	1.867	1.795	1.893	1.817	1.751	1.795	1.762	1.865	1.859	1.810	1.858
Na	0.677	0.665	0.665	0.651	0.618	0.638	0.662	0.649	0.644	0.647	0.635	0.645	0.677	0.654
K	0.192	0.184	0.193	0.165	0.164	0.162	0.170	0.173	0.170	0.183	0.187	0.199	0.201	0.192
Cl	0.018	0.011	0.011	0.012	0.018	0.009	0.013	0.019	0.016	0.022	0.018	0.007	0.017	0.007
F	0.118	0.139	0.149	0.105	0.034	0.049	0.139	0.085	0.091	0.116	0.050	0.191	0.205	0.140
Sum	15.632	15.670	15.686	15.683	15.577	15.693	15.648	15.572	15.609	15.592	15.687	15.703	15.688	15.705

Table D8 Amphibole analyses of the 2010 Merapi eruption (continued)

Sample	M11-80	M11-80	M11-80	M11-80	M11-80	M11-80	M11-80	M11-80	M11-80	M11-80	M11-80	M11-93	M11-93	M11-93
Sample Type	DD	DD	DD	DD	DD	DD	DD	DD	DD	DD	DD	DS	DS	DS
DataSet/Point	25 / 1 .	26 / 1 .	24 / 1 .	36 / 1 .	37 / 1 .	40 / 1.	41 / 1.	43 / 1.	44 / 1 .	45 / 1.	48 / 1 .	5 / 1 .	6 / 1 .	7 / 1 .
Comment	mph-c	mph-r	mph	mph-c	mph-r	mph	mph	mph	mph-c	mph-r	ph	mph-c	mph-c	mph-r
SiO_2	42.85	41.35	41.45	42.37	42.46	43.78	41.62	41.72	40.88	41.33	43.08	39.65	42.39	41.91
TiO_2	2.23	1.99	2.57	2.95	2.95	2.40	2.32	2.38	2.51	2.37	2.79	2.30	2.47	2.35
Al_2O_3	11.33	13.28	12.47	10.50	10.36	10.41	12.35	12.37	12.75	12.55	11.06	14.08	10.61	12.27
Cr_2O_3	0.02	0.01	0.01	0.00	0.00	0.03	0.02	0.01	0.03	0.04	0.01	0.02	0.00	0.00
FeO	12.29	11.91	12.80	12.00	12.11	12.53	12.63	12.64	12.86	12.43	12.50	13.03	14.56	13.25
MnO	0.30	0.16	0.30	0.38	0.40	0.40	0.22	0.24	0.19	0.24	0.36	0.19	0.56	0.31
MgO	14.06	13.70	13.01	13.92	13.82	13.96	13.18	13.11	12.90	13.09	13.82	12.88	12.39	13.26
CaO	11.13	11.93	11.57	11.07	11.01	10.92	11.83	11.71	11.80	11.98	11.09	11.76	10.92	11.67
Na_2O	2.30	2.26	2.30	2.29	2.29	2.33	2.30	2.30	2.32	2.26	2.38	2.37	2.21	2.34
K_2O	1.08	1.04	0.89	1.04	1.05	0.85	0.85	0.90	0.86	0.86	0.97	0.95	1.07	0.85
Cl	0.11	0.03	0.04	0.09	0.10	0.08	0.02	0.04	0.03	0.02	0.08	0.02	0.11	0.04
F	0.39	0.36	0.26	0.29	0.20	0.17	0.06	0.01	0.08	0.05	0.13	0.11	0.15	0.20
Sum	98.07	98.00	97.65	96.88	96.74	97.84	97.40	97.41	97.21	97.21	98.27	97.36	97.42	98.44
Si	6.232	6.039	6.094	6.254	6.276	6.359	6.125	6.135	6.042	6.103	6.251	5.841	6.271	6.105
Al	1.942	2.285	2.160	1.827	1.805	1.783	2.143	2.143	2.221	2.184	1.891	2.444	1.850	2.107
Ti	0.244	0.218	0.284	0.327	0.328	0.262	0.256	0.263	0.279	0.264	0.305	0.255	0.275	0.257
Cr	0.002	0.001	0.001	0.000	0.000	0.003	0.002	0.001	0.004	0.004	0.001	0.002	0.000	0.000
Fe^{3+}	0.786	0.633	0.615	0.659	0.647	0.761	0.549	0.547	0.569	0.479	0.700	0.794	0.763	0.708
Mg	3.048	2.982	2.851	3.064	3.044	3.023	2.892	2.874	2.841	2.881	2.991	2.828	2.732	2.879
Fe^{2+}	0.709	0.823	0.958	0.822	0.850	0.761	1.005	1.008	1.020	1.056	0.817	0.811	1.039	0.906
Mn	0.037	0.020	0.037	0.047	0.050	0.049	0.028	0.030	0.024	0.030	0.044	0.024	0.070	0.038
Ca	1.734	1.867	1.823	1.750	1.743	1.699	1.864	1.844	1.869	1.895	1.724	1.856	1.730	1.821
Na	0.648	0.640	0.656	0.655	0.655	0.656	0.657	0.656	0.664	0.646	0.671	0.676	0.633	0.661
K	0.200	0.193	0.166	0.195	0.199	0.158	0.159	0.169	0.162	0.163	0.179	0.178	0.201	0.157
Cl	0.027	0.007	0.010	0.022	0.025	0.019	0.005	0.009	0.008	0.006	0.021	0.006	0.029	0.009
F	0.178	0.167	0.121	0.137	0.091	0.078	0.028	0.003	0.036	0.023	0.059	0.050	0.070	0.091
Sum	15.583	15.701	15.646	15.601	15.597	15.512	15.680	15.669	15.696	15.704	15.573	15.710	15.564	15.640

Table D8 Amphibole analyses of the 2010 Merapi eruption (continued)

Sample	M11-93	M11-93	M11-93	M11-93	M11-93	M11-93	M11-93	M11-93	M11-93	M11-131	M11-131	M11-131	M11-131	M11-131
Sample Type	DS	DS	DS	DS	DS	DS	DS	DS	DS	DD	DD	DD	DD	DD
DataSet/Point	8 / 1 .	9 / 1 .	10 / 1 .	18 / 1 .	19 / 1 .	20 / 1 .	21 / 1 .	24 / 1 .	25 / 1 .	1 / 1 .	2 / 1 .	3 / 1 .	4 / 1 .	5 / 1 .
Comment	mph-c	mph-r	mph-c	mph-r	mph-c	mph-c	mph-r	mph-c	mph-r	mph-c	mph-r	mph-r	mph-c	mph-r
SiO_2	41.33	40.88	41.69	41.56	41.96	41.68	41.42	41.57	41.93	40.89	40.53	40.29	39.50	40.37
TiO_2	2.71	2.43	2.66	2.87	3.02	2.75	2.28	2.70	2.62	2.19	2.07	2.28	1.97	2.34
Al_2O_3	11.91	12.48	11.86	11.47	11.06	10.72	11.17	11.54	11.26	12.01	13.26	13.63	14.15	13.78
Cr_2O_3	0.02	0.01	0.00	0.00	0.00	0.01	0.01	0.00	0.03	0.01	0.01	0.01	0.01	0.01
FeO	14.14	12.95	12.85	12.68	13.11	18.31	18.41	13.33	13.48	15.91	12.60	12.51	15.62	12.55
MnO	0.45	0.25	0.36	0.37	0.39	0.47	0.54	0.42	0.41	0.44	0.20	0.19	0.21	0.16
MgO	12.32	13.17	13.43	13.43	13.37	9.82	9.92	13.04	13.14	10.68	12.76	12.51	11.40	12.71
CaO	11.37	11.82	11.45	11.16	10.97	10.64	10.74	11.30	11.21	11.88	12.15	11.93	11.54	12.18
Na_2O	2.31	2.33	2.34	2.31	2.37	2.04	2.05	2.31	2.27	2.05	2.19	2.18	2.00	2.21
K_2O	1.04	0.89	0.99	0.98	1.02	1.22	1.15	1.06	1.03	1.12	0.78	0.97	0.87	0.81
Cl	0.07	0.03	0.07	0.07	0.09	0.17	0.14	0.06	0.09	0.10	0.02	0.02	0.02	0.03
F	0.20	0.21	0.22	0.25	0.17	0.14	0.13	0.23	0.25	0.00	0.00	0.04	0.07	0.15
Sum	97.88	97.46	97.92	97.14	97.54	97.99	97.94	97.56	97.71	97.28	96.57	96.55	97.36	97.29
Si	6.106	6.032	6.108	6.127	6.164	6.246	6.193	6.131	6.166	6.159	6.025	5.997	5.842	5.967
Al	2.074	2.170	2.047	1.994	1.915	1.893	1.969	2.006	1.951	2.132	2.323	2.391	2.467	2.400
Ti	0.301	0.270	0.293	0.318	0.334	0.310	0.256	0.299	0.290	0.248	0.232	0.255	0.220	0.260
Cr	0.002	0.001	0.000	0.000	0.000	0.001	0.001	0.000	0.003	0.001	0.001	0.002	0.001	0.001
Fe^{3+}	0.655	0.655	0.707	0.747	0.767	0.749	0.877	0.702	0.758	0.402	0.513	0.486	1.015	0.502
Mg	2.713	2.897	2.933	2.952	2.928	2.194	2.211	2.867	2.881	2.399	2.828	2.775	2.513	2.800
Fe^{2+}	1.092	0.944	0.867	0.816	0.844	1.546	1.425	0.943	0.900	1.602	1.054	1.071	0.917	1.049
Mn	0.057	0.032	0.044	0.046	0.048	0.060	0.068	0.052	0.051	0.056	0.025	0.024	0.026	0.021
Ca	1.799	1.868	1.798	1.763	1.727	1.709	1.721	1.786	1.766	1.918	1.936	1.902	1.829	1.929
Na	0.660	0.666	0.663	0.659	0.676	0.594	0.594	0.660	0.649	0.598	0.631	0.629	0.573	0.634
K	0.196	0.168	0.185	0.184	0.192	0.232	0.219	0.200	0.193	0.216	0.147	0.185	0.164	0.152
Cl	0.019	0.008	0.017	0.016	0.023	0.044	0.036	0.015	0.022	0.025	0.006	0.006	0.006	0.006
F	0.091	0.096	0.103	0.116	0.080	0.068	0.059	0.106	0.115	0.000	0.000	0.018	0.035	0.070
Sum	15.655	15.702	15.646	15.606	15.595	15.535	15.534	15.645	15.608	15.733	15.714	15.716	15.566	15.715

Table D8 Amphibole analyses of the 2010 Merapi eruption (continued)

Sample	M11-131	M11-131	M11-131	M11-131	M11-131	M11-131	M11-131	M11-131	M11-131	M11-131	M11-131	M11-131	M11-131	M11-131
Sample Type	DD	DD	DD	DD	DD	DD	DD	DD	DD	DD	DD	DD	DD	DD
DataSet/Point	7 / 1 .	8 / 1 .	9 / 1 .	10 / 1 .	11 / 1 .	12 / 1 .	13 / 1 .	14 / 1 .	15 / 1 .	22 / 1 .	29 / 1 .	30 / 1 .	31 / 1 .	32 / 1 .
Comment	mph-r	mph-c	mph-c	mph-c	mph-r	mph-c	mph-r	mph-c	mph-c	mph-c	mph-c	mph-c	mph-r	mph-r
SiO_2	40.54	40.96	40.23	39.79	39.96	42.29	42.63	41.02	42.24	42.53	41.58	41.60	39.84	40.11
TiO_2	1.97	1.89	2.02	2.01	2.04	2.55	2.63	2.22	2.62	2.51	2.11	2.16	2.46	2.29
Al_2O_3	13.35	13.25	13.50	14.33	14.54	11.75	11.33	13.06	11.41	11.31	11.49	11.35	13.62	13.53
Cr_2O_3	0.01	0.02	0.00	0.03	0.01	0.00	0.01	0.03	0.01	0.01	0.01	0.01	0.01	0.00
FeO	12.95	12.31	12.61	12.56	12.20	12.24	12.68	12.69	12.62	13.32	16.65	16.63	12.46	13.32
MnO	0.19	0.13	0.15	0.12	0.13	0.33	0.43	0.22	0.38	0.38	0.49	0.46	0.18	0.24
MgO	12.71	13.04	12.69	12.61	12.88	13.41	13.27	12.95	13.60	13.13	10.55	10.59	12.78	12.26
CaO	12.25	12.25	12.28	12.15	12.47	11.63	11.54	12.13	11.49	11.37	11.77	11.71	12.25	12.23
Na_2O	2.18	2.18	2.21	2.11	2.12	2.31	2.28	2.16	2.25	2.31	1.90	1.90	2.18	2.17
K_2O	0.87	0.98	0.89	1.03	1.05	0.92	0.94	0.78	0.91	1.03	1.23	1.22	0.85	0.87
Cl	0.03	0.03	0.02	0.01	0.02	0.06	0.09	0.02	0.06	0.09	0.11	0.10	0.02	0.02
F	0.05	0.02	0.00	0.00	0.00	0.17	0.01	0.05	0.18	0.12	0.02	0.11	0.01	0.00
Sum	97.10	97.03	96.60	96.75	97.42	97.65	97.82	97.31	97.78	98.09	97.91	97.83	96.66	97.03
Si	6.010	6.061	5.994	5.904	5.893	6.208	6.247	6.045	6.183	6.228	6.228	6.238	5.927	5.967
Al	2.332	2.310	2.371	2.506	2.528	2.032	1.958	2.269	1.968	1.951	2.029	2.006	2.387	2.371
Ti	0.220	0.210	0.226	0.224	0.226	0.281	0.290	0.246	0.288	0.276	0.238	0.243	0.275	0.256
Cr	0.001	0.003	0.000	0.003	0.001	0.000	0.001	0.003	0.002	0.001	0.001	0.002	0.002	0.000
Fe^{3+}	0.526	0.452	0.463	0.570	0.489	0.501	0.520	0.550	0.676	0.624	0.473	0.481	0.513	0.495
Mg	2.808	2.876	2.818	2.788	2.831	2.935	2.898	2.846	2.967	2.865	2.357	2.367	2.835	2.719
Fe^{2+}	1.080	1.072	1.109	0.989	1.016	1.002	1.034	1.014	0.868	1.007	1.613	1.605	1.038	1.162
Mn	0.024	0.016	0.019	0.015	0.017	0.041	0.053	0.027	0.047	0.047	0.062	0.058	0.023	0.030
Ca	1.945	1.942	1.960	1.932	1.971	1.830	1.812	1.916	1.801	1.784	1.889	1.881	1.953	1.949
Na	0.627	0.625	0.637	0.606	0.606	0.657	0.649	0.618	0.638	0.655	0.552	0.553	0.627	0.627
K	0.165	0.184	0.169	0.196	0.198	0.172	0.176	0.146	0.171	0.193	0.235	0.234	0.160	0.165
Cl	0.007	0.007	0.006	0.003	0.005	0.014	0.021	0.004	0.016	0.021	0.028	0.025	0.006	0.005
F	0.022	0.010	0.000	0.000	0.000	0.081	0.006	0.022	0.083	0.053	0.011	0.052	0.006	0.000
Sum	15.737	15.751	15.766	15.733	15.774	15.658	15.637	15.680	15.610	15.632	15.676	15.668	15.741	15.740

Table D8 Amphibole analyses of the 2010 Merapi eruption (continued)

Sample	M11-131	M11-131	M11-131	M11-138a	M11-138a	DD10	DD10	DD10	DD10	DD10	DD10	DD10	DD10	DD10
Sample Type	DD	LG-Inc	LG-Inc	GS	GS	DD	DD	DD	DD	DD	DD	DD	DD	DD
DataSet/Point	33 / 1 .	27 / 1 .	28 / 1 .	27 / 1 .	28 / 1 .	1 / 1 .	2 / 1 .	3 / 1 .	4 / 1 .	12 / 1 .	13 / 1 .	10 / 1 .	11 / 1 .	14 / 1 .
Comment	mph-r	mph-c	mph-r	ph-c	ph-c	ph-r	ph-c	ph-c	ph-r	ph-c	ph-r	mph-c	mph-c	mph-c
SiO_2	40.75	40.65	42.08	42.67	42.46	42.32	41.49	42.75	40.67	41.10	42.65	40.86	42.39	43.55
TiO_2	2.51	2.12	2.54	3.09	3.18	2.61	2.80	2.97	2.27	2.51	3.09	2.31	2.68	2.79
Al_2O_3	13.63	13.17	12.35	10.33	11.10	11.29	12.70	11.81	13.48	13.47	11.06	13.67	11.85	10.89
Cr_2O_3	0.03	0.00	0.01	0.00	0.00	0.00	0.00	0.00	0.01	0.01	0.01	0.00	0.00	-0.02
FeO	12.53	12.79	12.24	12.87	12.70	14.12	12.93	13.03	13.71	12.64	13.22	12.90	12.63	12.30
MnO	0.20	0.17	0.26	0.42	0.41	0.45	0.29	0.36	0.23	0.21	0.46	0.23	0.33	0.38
MgO	12.73	12.87	13.07	13.76	13.80	12.83	13.15	13.64	12.94	12.97	13.63	12.80	13.31	14.26
CaO	12.15	12.22	11.65	10.92	11.05	11.43	11.64	11.21	12.12	11.91	10.86	12.10	11.65	11.27
Na_2O	2.24	2.21	2.29	2.37	2.41	2.32	2.47	2.53	2.38	2.46	2.44	2.39	2.34	2.37
K_2O	0.84	0.86	0.98	1.14	1.00	1.04	1.00	0.99	0.94	0.96	1.03	0.92	1.00	0.95
Cl	0.02	0.01	0.03	0.11	0.09	0.08	0.04	0.06	0.02	0.03	0.08	0.02	0.05	0.07
F	0.17	0.00	0.15	0.30	0.24	0.23	0.22	0.21	0.11	0.32	0.27	0.12	0.27	0.29
Sum	97.79	97.06	97.65	97.98	98.44	98.73	98.73	99.56	98.88	98.58	98.79	98.33	98.50	99.09
Si	5.996	6.019	6.182	6.247	6.169	6.188	6.045	6.145	5.926	6.006	6.177	5.984	6.188	6.268
Al	2.363	2.298	2.137	1.782	1.901	1.946	2.182	2.001	2.315	2.321	1.887	2.359	2.039	1.847
Ti	0.277	0.236	0.281	0.340	0.348	0.286	0.307	0.321	0.248	0.276	0.336	0.254	0.294	0.302
Cr	0.004	0.000	0.001	0.000	0.000	0.000	0.000	0.000	0.001	0.001	0.001	0.000	0.000	-0.002
Fe^{3+}	0.459	0.519	0.433	0.730	0.761	0.674	0.598	0.727	0.704	0.509	0.842	0.517	0.502	0.705
Mg	2.793	2.841	2.863	3.004	2.988	2.797	2.856	2.923	2.811	2.825	2.943	2.795	2.896	3.059
Fe^{2+}	1.082	1.066	1.071	0.846	0.783	1.053	0.977	0.840	0.967	1.036	0.759	1.063	1.039	0.775
Mn	0.025	0.021	0.032	0.052	0.051	0.056	0.036	0.043	0.028	0.026	0.056	0.029	0.041	0.046
Ca	1.915	1.938	1.833	1.714	1.720	1.790	1.817	1.727	1.892	1.865	1.686	1.899	1.823	1.738
Na	0.638	0.634	0.653	0.674	0.678	0.657	0.697	0.704	0.673	0.697	0.684	0.679	0.663	0.660
K	0.158	0.163	0.184	0.212	0.186	0.195	0.186	0.182	0.174	0.179	0.190	0.172	0.186	0.174
Cl	0.005	0.003	0.008	0.026	0.022	0.020	0.011	0.015	0.005	0.007	0.021	0.005	0.013	0.018
F	0.078	0.000	0.071	0.139	0.108	0.107	0.101	0.097	0.049	0.146	0.123	0.055	0.127	0.134
Sum	15.711	15.735	15.670	15.600	15.585	15.642	15.700	15.613	15.739	15.741	15.560	15.750	15.672	15.572

Table D9 Oxide analyses of the 2010 Merapi eruption[1]

Sample	M11-07	M11-07	M11-07	M11-07	M11-07	M11-15	M11-15	M11-27-2	M11-27-2	M11-27-2
Sample Type[2]	DD	DD	DD	DD	DD	DD	DD	DD	DD	DD
Point	35 / 1 .	36 / 1 .	37 / 1 .	39 / 1 .	40 / 1 .	19 / 1 .	20 / 1 .	27 / 1 .	28 / 1 .	29 / 1 .
Comment[3]	mph-c	mph-c	mph-c	mph-c	mph-c	mph	mph	mph-c	mph-c	mph-c
TiO_2	9.28	9.31	9.55	9.59	9.34	9.59	9.60	9.61	7.71	9.41
Al_2O_3	3.05	3.36	2.93	2.90	3.25	3.00	2.96	2.79	3.51	2.94
Cr_2O_3	0.00	0.01	0.02	0.01	0.02	0.02	0.02	0.01	0.02	0.02
FeO	79.38	79.22	78.87	79.37	78.01	78.56	77.64	79.21	80.66	79.37
MnO	0.84	0.81	0.85	0.84	0.79	0.92	0.81	0.87	0.85	0.83
MgO	2.57	2.61	2.45	2.48	2.57	2.41	2.35	2.45	2.45	2.59
CaO	0.06	0.05	0.55	0.01	0.67	0.06	0.08	0.07	0.01	0.02
Total	95.19	95.37	95.23	95.21	94.64	94.56	93.45	95.01	95.21	95.18
Al	0.132	0.145	0.128	0.126	0.142	0.131	0.131	0.122	0.152	0.127
Ti	0.257	0.257	0.266	0.266	0.261	0.268	0.271	0.267	0.213	0.261
Cr	0.000	0.000	0.000	0.000	0.000	0.001	0.001	0.000	0.000	0.001
Fe^{3+}	1.354	1.341	1.339	1.342	1.334	1.333	1.326	1.344	1.422	1.351
Mg	0.141	0.143	0.135	0.136	0.142	0.133	0.132	0.135	0.134	0.142
Fe^{2+}	1.089	1.089	1.104	1.103	1.094	1.105	1.114	1.105	1.052	1.093
Mn	0.026	0.025	0.027	0.026	0.025	0.029	0.026	0.027	0.026	0.026
Sum	3.000	3.000	3.000	3.000	3.000	3.000	3.000	3.000	3.000	3.000
XUsp	0.275	0.277	0.284	0.284	0.282	0.287	0.290	0.284	0.230	0.278
XMt	0.725	0.723	0.716	0.716	0.718	0.713	0.710	0.716	0.770	0.722

[1] Major element oxides in wt.%; number of cations based on 4 oxygens; [2] see Appendix A; [3] pyx inc = inclusion in pyroxene; other abbreviations, see Table D1

Table D9 Oxide analyses of the 2010 Merapi eruption (continued)

Sample	M11-27-2	M11-27-2	M11-27-2	M11-27-2	M11-27-2	M11-28a	M11-28a	M11-28a	M11-28a	M11-28a
Sample Type	DD	DD	LG-Inc	LG-Inc	LG-Inc	P5N-Sc	P5N-Sc	P5N-Sc	P5N-Sc	P5N-Sc
Point	30 / 1 .	31 / 1 .	32 / 1 .	33 / 1 .	34 / 1 .	3 / 1 .	4 / 1 .	5 / 1 .	6 / 1 .	21 / 1 .
Comment	mph-c	mph-c	mph-c	mph-c	mph-c	mph-c	mph-c	mph-c	mph-c	mph
TiO_2	9.61	9.39	11.13	9.24	10.91	9.88	9.20	6.04	9.39	8.77
Al_2O_3	2.67	3.25	1.09	2.09	1.06	2.48	3.14	3.86	3.09	2.54
Cr_2O_3	0.02	0.02	0.00	0.02	0.02	0.01	0.01	0.22	0.01	
FeO	79.79	79.28	81.52	80.63	80.48	79.48	80.01	81.74	79.16	78.37
MnO	0.91	0.82	0.94	0.89	0.88	1.10	0.97	0.64	0.96	0.98
MgO	2.38	2.54	0.87	1.57	0.80	1.99	2.14	2.35	2.39	1.83
CaO	0.03	0.02	0.03	0.02	0.10	0.04	0.02	0.00	0.02	0.06
Total	95.40	95.33	95.58	94.46	94.26	94.96	95.49	94.84	95.01	92.55
Al	0.116	0.141	0.048	0.093	0.048	0.108	0.136	0.167	0.135	0.114
Ti	0.266	0.259	0.314	0.261	0.313	0.276	0.254	0.167	0.261	0.251
Cr	0.000	0.001	0.000	0.001	0.000	0.000	0.000	0.006	0.000	0.000
Fe^{3+}	1.351	1.340	1.323	1.386	1.326	1.339	1.355	1.493	1.344	1.383
Mg	0.131	0.139	0.049	0.088	0.046	0.110	0.117	0.129	0.131	0.104
Fe^{2+}	1.107	1.094	1.236	1.145	1.239	1.131	1.107	1.018	1.099	1.116
Mn	0.028	0.026	0.030	0.028	0.028	0.034	0.030	0.020	0.030	0.032
Sum	3.000	3.000	3.000	3.000	3.000	3.000	3.000	3.000	3.000	3.000
XUsp	0.283	0.279	0.322	0.273	0.320	0.292	0.273	0.183	0.279	0.267
XMt	0.717	0.721	0.678	0.727	0.680	0.708	0.727	0.817	0.721	0.733

Table D9 Oxide analyses of the 2010 Merapi eruption (continued)

Sample	M11-28a	M11-28a	M11-28b	M11-28b	M11-28b	M11-28b	M11-28b	M11-38	M11-38	M11-38
Sample Type	P5N-Sc	P5N-Sc	P5N-LGD	P5N-LGD	P5N-LGD	P5N-LGD	P5N-LGD	DD	DD	DD
Point	22 / 1 .	23 / 1 .	1 / 1 .	2 / 1 .	3 / 1 .	4 / 1 .	5 / 1 .	40 / 1 .	41 / 1 .	42 / 1 .
Comment	mph	mph	mph-c	mph-c	mph-c	mph-c	mph-c	m	m	m
TiO_2	8.63	9.10	12.05	11.77	10.08	10.32	10.03	7.99	9.89	8.72
Al_2O_3	2.81	2.04	1.47	1.48	2.21	1.91	2.39	3.33	2.76	3.05
Cr_2O_3			0.01	0.00	0.03	0.01	0.00	0.02	0.00	0.00
FeO	78.60	78.51	79.27	80.28	80.25	80.06	80.21	77.81	77.26	77.74
MnO	0.92	1.04	0.74	0.78	0.86	0.88	0.82	0.75	0.75	0.75
MgO	1.96	1.68	0.68	0.70	1.12	1.05	1.24	2.14	0.96	1.11
CaO	0.02	0.02	0.02	0.02	0.02	0.01	0.02	0.27	0.17	0.19
Total	92.94	92.38	94.23	95.03	94.57	94.24	94.70	92.30	91.80	91.55
Al	0.125	0.092	0.066	0.066	0.098	0.085	0.105	0.149	0.126	0.139
Ti	0.246	0.262	0.345	0.334	0.285	0.294	0.283	0.229	0.288	0.254
Cr	0.000	0.000	0.000	0.000	0.001	0.000	0.000	0.001	0.000	0.000
Fe^{3+}	1.383	1.384	1.243	1.265	1.330	1.327	1.329	1.393	1.297	1.353
Mg	0.111	0.096	0.039	0.039	0.063	0.059	0.070	0.121	0.056	0.064
Fe^{2+}	1.105	1.132	1.283	1.270	1.195	1.206	1.187	1.083	1.208	1.165
Mn	0.030	0.034	0.024	0.025	0.028	0.028	0.026	0.024	0.025	0.025
Sum	3.000	3.000	3.000	3.000	3.000	3.000	3.000	3.000	3.000	3.000
XUsp	0.262	0.275	0.357	0.346	0.300	0.307	0.299	0.247	0.308	0.273
XMt	0.738	0.725	0.643	0.654	0.700	0.693	0.701	0.753	0.692	0.727

Table D9 Oxide analyses of the 2010 Merapi eruption (continued)

Sample	M11-38	M11-48	M11-48	M11-48	M11-48	M11-50	M11-50	M11-50	M11-51	M11-51
Sample Type	DD	LG-Inc	LG-Inc	LG-Inc	LG-Inc	WP	WP	WP	GS	GS
Point	44 / 1 .	23 / 1 .	24 / 1 .	25 / 1 .	27 / 1 .	6 / 1.	7 / 1.	14 / 1 .	50 / 1 .	53 / 1 .
Comment	m	m	m	m	m	pyx inc	pyx inc	mph	m	m
TiO_2	7.60	9.92	11.50	10.72	24.35	8.85	9.32	10.17	9.95	10.74
Al_2O_3	5.23	1.98	0.86	1.58	1.64	2.02	1.44	1.29	2.18	2.08
Cr_2O_3	0.00	0.00	0.00	0.00	0.00				0.00	0.00
FeO	71.02	77.21	78.47	77.89	66.22	79.48	79.91	79.27	76.67	77.11
MnO	0.63	0.79	1.06	1.06	1.08	0.92	0.89	0.96	0.98	1.04
MgO	1.50	1.46	1.17	1.22	1.65	1.85	1.46	1.57	1.62	1.75
CaO	1.65	0.60	0.12	0.24	0.11	0.13	0.16	0.02	0.13	0.18
Total	87.63	91.97	93.19	92.71	95.05	93.24	93.17	93.27	91.52	92.90
Al	0.250	0.091	0.039	0.072	0.073	0.090	0.065	0.058	0.100	0.094
Ti	0.232	0.290	0.333	0.311	0.695	0.252	0.268	0.292	0.290	0.309
Cr	0.000	0.000	0.000	0.000	0.000	0.000	0.000	0.000	0.000	0.000
Fe^{3+}	1.287	1.329	1.295	1.306	0.536	1.405	1.399	1.359	1.321	1.289
Mg	0.091	0.084	0.067	0.070	0.094	0.104	0.083	0.089	0.094	0.100
Fe^{2+}	1.120	1.179	1.231	1.206	1.567	1.118	1.156	1.172	1.164	1.175
Mn	0.022	0.026	0.035	0.035	0.035	0.030	0.029	0.031	0.032	0.034
Sum	3.000	3.000	3.000	3.000	3.000	3.000	3.000	3.000	3.000	3.000
XUsp	0.265	0.304	0.340	0.323	0.722	0.264	0.277	0.300	0.305	0.324
XMt	0.735	0.696	0.660	0.677	0.278	0.736	0.723	0.700	0.695	0.676

Table D9 Oxide analyses of the 2010 Merapi eruption (continued)

Sample	M11-53-B4	M11-53-B4	M11-53-B4	M11-61	M11-61	M11-75	M11-75	M11-75	M11-75	M11-75
Sample Type	P5N-WP	P5N-WP	P5N-WP	WP	WP	GS	GS	GS	GS	GS
Point	60 / 1 .	63 / 1 .	64 / 1 .	16 / 1 .	18 / 1 .	15 / 1 .	16 / 1 .	17 / 1 .	18 / 1 .	19 / 1 .
Comment	m	m	m	m	m	mph	mph	mph	mph	mph
TiO_2	10.85	10.59	10.90	10.13	9.56	8.13	8.32	8.13	8.24	8.48
Al_2O_3	1.38	1.37	1.48	2.25	2.58	2.90	2.78	2.95	2.88	2.95
Cr_2O_3	0.03	0.00	0.00	0.01	0.00					
FeO	77.75	77.83	78.51	78.18	78.03	78.59	78.37	78.44	78.65	77.27
MnO	0.99	0.88	0.95	0.95	0.87	0.77	0.83	0.82	0.84	0.85
MgO	1.31	1.27	1.28	1.78	1.74	2.17	2.57	2.26	2.36	2.05
CaO	0.11	0.10	0.20	0.10	0.12	0.05	0.04	0.19	0.02	1.21
Total	92.41	92.03	93.32	93.41	92.90	92.61	92.90	92.79	92.99	92.81
Al	0.063	0.063	0.067	0.100	0.116	0.130	0.123	0.132	0.128	0.133
Ti	0.315	0.309	0.314	0.289	0.274	0.232	0.236	0.231	0.233	0.245
Cr	0.001	0.000	0.000	0.000	0.000	0.000	0.000	0.000	0.000	0.000
Fe^{3+}	1.306	1.319	1.305	1.321	1.337	1.407	1.405	1.406	1.405	1.378
Mg	0.075	0.073	0.073	0.101	0.099	0.123	0.144	0.127	0.133	0.117
Fe^{2+}	1.208	1.207	1.210	1.158	1.147	1.084	1.065	1.078	1.074	1.100
Mn	0.032	0.029	0.031	0.031	0.028	0.025	0.027	0.026	0.027	0.028
Sum	3.000	3.000	3.000	3.000	3.000	3.000	3.000	3.000	3.000	3.000
XUsp	0.326	0.319	0.325	0.304	0.290	0.248	0.251	0.248	0.249	0.262
XMt	0.674	0.681	0.675	0.696	0.710	0.752	0.749	0.752	0.751	0.738

Table D9 Oxide analyses of the 2010 Merapi eruption (continued)

Sample	M11-75	M11-75	M11-75	M11-75	M11-75	M11-138	M11-138	M11-138	M11-138	DD10
Sample Type	GS	GS	GS	GS	GS	GS	GS	GS	GS	DD
Point	20 / 1 .	21 / 1 .	22 / 1 .	23 / 1 .	24 / 1 .	23 / 1 .	24 / 1 .	25 / 1 .	26 / 1 .	5 / 1 .
Comment	mph	mph	mph	mph	mph	mph-c	mph-c	mph-r	mph-r	pyx inc
TiO_2	8.47	8.30	8.64	8.58	8.88	16.74	12.09	18.63	14.43	7.38
Al_2O_3	3.14	3.07	2.73	2.72	2.83	1.78	1.40	2.21	2.16	3.88
Cr_2O_3						0.01	0.05	0.00	0.00	0.01
FeO	78.54	75.96	79.04	78.90	78.92	72.65	76.19	68.87	73.58	80.52
MnO	0.83	0.82	0.77	0.90	0.91	0.43	0.45	0.10	0.18	0.65
MgO	2.55	2.49	2.43	2.32	2.41	1.04	1.02	0.52	0.54	2.33
CaO	0.04	1.84	0.03	0.03	0.04	0.02	0.05	0.11	0.05	0.01
Total	93.57	92.49	93.63	93.44	93.99	92.68	91.25	90.45	90.93	94.79
Al	0.138	0.140	0.121	0.120	0.125	0.081	0.065	0.104	0.101	0.169
Ti	0.238	0.241	0.243	0.242	0.249	0.488	0.357	0.560	0.429	0.204
Cr	0.000	0.000	0.000	0.000	0.000	0.000	0.001	0.000	0.000	0.000
Fe^{3+}	1.386	1.379	1.393	1.395	1.377	0.942	1.220	0.776	1.041	1.423
Mg	0.142	0.143	0.135	0.130	0.134	0.060	0.060	0.031	0.032	0.128
Fe^{2+}	1.069	1.071	1.084	1.084	1.087	1.414	1.282	1.525	1.391	1.056
Mn	0.026	0.027	0.024	0.029	0.029	0.014	0.015	0.004	0.006	0.020
Sum	3.000	3.000	3.000	3.000	3.000	3.000	3.000	3.000	3.000	3.000
XUsp	0.256	0.259	0.259	0.258	0.266	0.509	0.369	0.591	0.452	0.223
XMt	0.744	0.741	0.741	0.742	0.734	0.491	0.631	0.409	0.548	0.777

Table D9 Oxide analyses of the 2010 Merapi eruption (continued)

Sample	DD10	DD10	DD10	DD10	DD10	DD10	DD10	DD10	DD10	
Sample Type	DD	DD	DD	DD	LG-Inc	LG-Inc	LG-Inc	LG-Inc	LG-Inc	
Point	21 / 1 .	22 / 1 .	23 / 1 .	33 / 1 .	50 / 1 .	51 / 1 .	52 / 1 .	53 / 1 .	54 / 1 .	
Comment	mph	mph-c	mph-c	mph-r	mph-c	mph-c	mph-c	mph-c	mph-c	
TiO_2	9.67	7.49	9.05	9.66	10.31	10.39	10.18	10.83	10.23	
Al_2O_3	2.87	3.49	3.45	3.39	1.06	1.07	1.24	1.05	1.04	
Cr_2O_3	0.01	0.10	0.02	0.01	0.02	0.02	0.02	-0.01	0.03	
FeO	79.04	81.30	79.60	77.93	80.25	81.71	80.43	80.17	81.22	
MnO	0.91	0.69	0.79	0.87	1.02	1.06	1.05	1.00	1.01	
MgO	2.47	2.38	2.60	2.48	1.04	0.98	0.96	1.29	1.07	
CaO	0.01	0.02	0.01	0.02	0.03	0.02	0.79	0.02	0.04	
Total	94.98	95.48	95.51	94.36	93.74	95.24	94.68	94.35	94.65	
Al	0.125	0.151	0.149	0.148	0.048	0.047	0.056	0.047	0.046	
Ti	0.269	0.206	0.249	0.270	0.296	0.294	0.292	0.309	0.291	
Cr	0.000	0.003	0.001	0.000	0.001	0.000	0.001	0.000	0.001	
Fe^{3+}	1.337	1.434	1.353	1.312	1.359	1.365	1.360	1.336	1.371	
Mg	0.136	0.130	0.142	0.137	0.059	0.055	0.054	0.073	0.060	
Fe^{2+}	1.104	1.055	1.083	1.105	1.204	1.205	1.203	1.204	1.198	
Mn	0.028	0.021	0.024	0.027	0.033	0.034	0.034	0.032	0.032	
Sum	3.000	3.000	3.000	3.000	3.000	3.000	3.000	3.000	3.000	
XUsp	0.287	0.223	0.269	0.291	0.303	0.301	0.300	0.316	0.298	
XMt	0.713	0.777	0.731	0.709	0.697	0.699	0.700	0.684	0.702	

Table D10 Apatite analyses of the 2010 Merapi eruption[1]

Sample	M11-26a	M11-26a	M11-26a	M11-27-3	M11-27-3	M11-27-3	M11-27-3	M11-27-5	M11-27-5	M11-27-5	M11-27-5	M11-27-5	M11-27-5	M11-27-5	M11-27-5	M11-27-5	M11-27-5
Sample Type[2]	DD	DD	DD	LG-Inc	LG-Inc	LG-Inc	LG-Inc	DD	DD	DD	DD	DD	DD	DD	DD	DD	DD
Point	1 / 1 .	2 / 1 .	3 / 1 .	4 / 1 .	5 / 1 .	6 / 1 .	7 / 1 .	8 / 1 .	9 / 1 .	10 / 1 .	11 / 1 .	13 / 1 .	14 / 1 .	15 / 1 .	16 / 1 .	17 / 1 .	18 / 1 .
Comment[3]	pyx inc	pyx inc	pyx inc	pyx inc	pyx inc	pyx inc	pyx inc	pyx inc	pyx inc	pyx inc	pyx inc	pyx inc	pyx inc	pyx inc	pyx inc	pyx inc	pyx inc
P_2O_5	40.29	40.43	40.38	42.94	42.19	42.41	41.89	42.13	42.51	41.81	41.98	42.10	42.60	42.02	41.84	42.66	42.53
SiO_2	0.32	0.29	0.54	0.23	0.51	0.46	0.43	0.16	0.15	0.38	0.14	0.19	0.63	0.22	0.18	0.17	0.26
TiO_2								0.00	0.04	0.00	0.00	0.05	0.02	0.00	0.00	0.00	0.04
Al_2O_3								0.00	0.00	0.00	0.00	0.00	0.03	0.02	0.00	0.00	0.01
FeO	0.66	0.62	1.37	0.60	0.66	0.50	0.48	0.44	0.41	0.60	0.44	0.57	0.69	0.66	0.47	0.44	0.53
MnO	0.18	0.14	0.29	0.19	0.24	0.20	0.17	0.14	0.19	0.18	0.17	0.19	0.23	0.23	0.21	0.18	0.21
MgO	0.24	0.24	0.26	0.22	0.06	0.11	0.12	0.40	0.37	0.36	0.37	0.37	0.57	0.40	0.38	0.36	0.37
CaO	51.46	52.40	51.84	54.85	54.29	54.37	53.71	53.08	52.91	52.52	52.74	52.76	52.47	52.39	52.84	52.79	52.58
Na_2O	0.09	0.05	0.12	0.14	0.14	0.11	0.06	0.07	0.08	0.17	0.05	0.05	0.11	0.09	0.07	0.11	0.07
K_2O	0.05	0.00	0.04	0.00	0.02	0.03	0.02	0.00	0.00	0.01	0.00	0.01	0.00	0.02	0.00	0.00	0.00
Cl	1.15	1.19	1.48	0.90	1.52	0.82	1.09	0.81	1.02	1.04	1.02	1.11	1.10	1.13	1.03	1.03	1.04
F	4.09	3.63	5.10	3.55	3.69	4.06	4.24	4.15	3.93	4.19	4.66	4.25	4.21	3.87	4.00	4.19	3.76
F corr.	1.97	1.75	2.46	1.71	1.78	1.96	2.05	2.00	1.89	2.02	2.25	2.05	2.03	1.87	1.93	2.02	1.81
H_2O*	0.48	0.59	0.19	0.77	0.56	0.66	0.52	0.61	0.62	0.54	0.43	0.51	0.55	0.59	0.58	0.56	0.65
Subtotal	96.89	97.70	98.97	102.55	101.97	101.64	100.53	99.84	100.20	99.62	99.61	99.97	101.02	99.62	99.53	100.31	100.11
O=F,Cl	1.09	1.00	1.37	0.92	1.09	1.01	1.11	1.03	1.03	1.08	1.18	1.11	1.10	1.04	1.04	1.08	1.00
Sum	95.80	96.69	97.60	101.63	100.87	100.63	99.42	98.81	99.17	98.53	98.43	98.85	99.92	98.58	98.49	99.23	99.11
P	5.995	5.969	5.935	6.009	5.974	5.991	5.997	6.045	6.073	6.025	6.054	6.047	6.033	6.051	6.035	6.086	6.074
Si	0.056	0.051	0.094	0.037	0.085	0.077	0.072	0.026	0.026	0.064	0.024	0.032	0.106	0.038	0.031	0.028	0.043
Al	0.000	0.000	0.000	0.000	0.000	0.000	0.000	0.000	0.000	0.000	0.000	0.000	0.003	0.002	0.000	0.000	0.001
Ti	0.000	0.000	0.000	0.000	0.000	0.000	0.000	0.000	0.005	0.000	0.000	0.007	0.003	0.000	0.000	0.000	0.005
Fe	0.097	0.091	0.198	0.082	0.092	0.070	0.067	0.062	0.058	0.085	0.063	0.081	0.097	0.093	0.067	0.062	0.075
Mn	0.027	0.021	0.043	0.027	0.034	0.028	0.024	0.020	0.027	0.027	0.024	0.028	0.033	0.033	0.030	0.026	0.030
Mg	0.064	0.063	0.067	0.055	0.015	0.028	0.029	0.101	0.092	0.092	0.095	0.092	0.142	0.102	0.096	0.090	0.094
Ca	9.691	9.792	9.642	9.715	9.729	9.721	9.731	9.640	9.566	9.579	9.626	9.592	9.404	9.549	9.645	9.531	9.505
Na	0.032	0.015	0.042	0.045	0.045	0.037	0.020	0.023	0.026	0.055	0.018	0.017	0.035	0.028	0.024	0.035	0.023
K	0.012	0.001	0.008	0.001	0.004	0.007	0.003	0.000	0.000	0.002	0.001	0.002	0.000	0.004	0.000	0.000	0.000
Cl	0.342	0.351	0.435	0.251	0.431	0.233	0.314	0.233	0.291	0.299	0.294	0.318	0.310	0.325	0.296	0.294	0.299
F	1.098	0.966	1.350	0.895	0.943	1.035	1.095	1.074	1.011	1.088	1.213	1.101	1.074	1.004	1.039	1.077	0.968
OH*	0.560	0.684	0.215	0.854	0.627	0.732	0.591	0.694	0.698	0.613	0.493	0.581	0.616	0.671	0.664	0.628	0.733
Sum	17.974	18.003	18.029	17.972	17.978	17.958	17.944	17.917	17.873	17.927	17.904	17.900	17.854	17.899	17.929	17.859	17.851

[1] Major element oxides in wt.%; number of cations based on 25 oxygens; H_2O calculated on the basis of filling the C site (2); [2] see Appendix A; [3] pyx-pl-am inc = inclusion in pyroxene, plagioclase and amphibole, respectively, am rr = amphibole reaction rim, MI-PEC = post-entrapment crystal in melt inclusion; other abbreviations, see Table D1

Table D10 Apatite analyses of the 2010 Merapi eruption (continued)

Sample	M11-27-5	M11-27-5	M11-27-5	M11-27-5	M11-27-5	M11-27-5	M11-27-5	M11-27-5	M11-27-5	M11-27-5	M11-27-5	M11-27-5	M11-27-5	M11-28a	M11-28a	M11-33	M11-33
Sample Type	DD	DD	DD	DD	DD	DD	DD	DD	DD	DD	DD	DD	DD	P5N-Sc	P5N-Sc	WP	WP
Point	19 / 1 .	20 / 1 .	21 / 1 .	22 / 1 .	23 / 1 .	24 / 1 .	25 / 1 .	26 / 1 .	27 / 1 .	28 / 1 .	29 / 1 .	30 / 1 .	31 / 1 .	32 / 1 .	33 / 1 .	34 / 1 .	35 / 1 .
Comment	pyx inc	pyx inc	MI PEC	pyx inc	pyx inc	pyx inc	pyx inc	pyx inc	pyx inc	pyx inc	pyx inc	pyx inc	pyx inc	pl inc	pyx inc	pyx inc	pyx inc
P_2O_5	42.60	42.81	42.41	42.93	42.17	42.86	42.70	40.44	40.95	41.78	41.79	41.80	41.93	42.73	42.59	41.09	41.41
SiO_2	0.18	0.16	0.22	0.26	0.20	0.28	0.16	0.15	0.22	0.30	0.19	0.20	0.18	0.30	0.24	0.39	0.36
TiO_2	0.00	0.00	0.01	0.01	0.04	0.05	0.00	0.61	0.00	0.01	0.00	0.00	0.02	0.01	0.01		
Al_2O_3	0.00	0.00	0.00	0.01	0.02	0.00	0.01	0.10	0.00	0.00	0.00	0.00	0.00	0.06	0.00		
FeO	0.46	0.50	0.51	0.53	0.97	0.85	0.62	5.24	0.47	0.45	0.39	0.49	0.48	0.39	0.55	1.05	0.56
MnO	0.16	0.18	0.22	0.19	0.20	0.18	0.18	0.26	0.19	0.21	0.17	0.14	0.21	0.17	0.21	0.23	0.22
MgO	0.36	0.37	0.38	0.36	0.36	0.38	0.34	0.42	0.38	0.36	0.37	0.40	0.37	0.36	0.35	0.33	0.28
CaO	52.76	52.62	52.78	52.81	52.56	52.49	52.80	49.80	52.91	52.96	53.12	53.16	53.17	53.30	53.42	51.77	52.18
Na_2O	0.06	0.09	0.04	0.06	0.10	0.06	0.05	0.05	0.07	0.15	0.09	0.02	0.11	0.06	0.11	0.12	0.08
K_2O	0.02	0.00	0.02	0.04	0.01	0.02	0.01	0.00	0.00	0.00	0.00	0.00	0.00	0.01	0.02	0.02	0.01
Cl	1.03	1.03	1.10	1.11	1.06	1.01	1.03	0.98	1.05	1.08	1.03	0.87	1.05	1.07	0.99	1.08	0.81
F	4.59	3.79	3.74	3.76	3.79	4.16	3.72	3.95	4.62	4.53	4.88	4.34	4.52	4.31	4.36	4.30	3.56
F corr.	2.21	1.83	1.80	1.81	1.83	2.01	1.79	1.91	2.23	2.19	2.36	2.09	2.18	2.08	2.11	2.07	1.72
H_2O*	0.47	0.65	0.64	0.65	0.64	0.58	0.67	0.59	0.42	0.45	0.38	0.55	0.47	0.53	0.54	0.48	0.72
Subtotal	100.30	100.24	100.14	100.78	100.13	100.76	100.35	100.53	98.89	99.93	99.88	99.71	100.16	101.07	101.12	98.63	98.35
O=F,Cl	1.16	1.00	1.01	1.01	1.01	1.07	0.99	1.02	1.18	1.16	1.22	1.08	1.15	1.12	1.11	1.12	0.91
Sum	99.14	99.24	99.13	99.76	99.13	99.69	99.36	99.51	97.71	98.76	98.66	98.64	99.00	99.95	100.01	97.51	97.44
P	6.085	6.100	6.066	6.089	6.044	6.085	6.086	5.879	5.978	6.015	6.023	6.020	6.023	6.056	6.044	6.002	6.027
Si	0.030	0.027	0.036	0.044	0.034	0.047	0.027	0.025	0.038	0.051	0.033	0.033	0.030	0.050	0.040	0.067	0.062
Al	0.000	0.000	0.000	0.001	0.002	0.000	0.001	0.010	0.000	0.000	0.000	0.000	0.000	0.006	0.000	0.000	0.000
Ti	0.000	0.000	0.001	0.002	0.005	0.006	0.000	0.079	0.000	0.001	0.000	0.000	0.003	0.001	0.002	0.000	0.000
Fe	0.064	0.071	0.072	0.074	0.137	0.119	0.088	0.753	0.068	0.064	0.055	0.069	0.068	0.054	0.077	0.152	0.080
Mn	0.023	0.026	0.031	0.027	0.028	0.026	0.026	0.038	0.027	0.030	0.024	0.019	0.030	0.023	0.029	0.034	0.031
Mg	0.090	0.093	0.095	0.091	0.090	0.094	0.085	0.106	0.098	0.091	0.093	0.101	0.094	0.090	0.087	0.084	0.073
Ca	9.538	9.491	9.553	9.479	9.534	9.431	9.523	9.161	9.774	9.649	9.689	9.689	9.667	9.561	9.593	9.571	9.611
Na	0.018	0.030	0.014	0.018	0.033	0.019	0.015	0.015	0.024	0.048	0.030	0.008	0.036	0.019	0.036	0.038	0.026
K	0.004	0.000	0.005	0.007	0.001	0.004	0.001	0.000	0.000	0.000	0.001	0.000	0.000	0.001	0.004	0.004	0.003
Cl	0.293	0.293	0.316	0.314	0.303	0.288	0.293	0.284	0.306	0.312	0.296	0.252	0.301	0.304	0.281	0.316	0.236
F	1.181	0.973	0.964	0.961	0.979	1.066	0.955	1.036	1.216	1.176	1.269	1.127	1.171	1.102	1.117	1.131	0.934
OH*	0.526	0.733	0.720	0.725	0.718	0.646	0.753	0.680	0.478	0.512	0.435	0.621	0.528	0.594	0.602	0.553	0.830
Sum	17.853	17.837	17.874	17.831	17.908	17.831	17.851	18.066	18.007	17.949	17.948	17.940	17.950	17.862	17.913	17.952	17.912

Table D10 Apatite analyses of the 2010 Merapi eruption (continued)

Sample	M11-33	M11-38	M11-48	M11-48	M11-50	M11-50	M11-50	M11-50	M11-50	M11-50	M11-50	M11-50	M11-50	M11-50	M11-50	M11-50	M11-50
Sample Type	WP	DD	LG-Inc	LG-Inc	WP	WP	WP	WP	WP	WP	WP	WP	WP	WP	WP	WP	WP
Point	36 / 1 .	37 / 1 .	38 / 1 .	39 / 1 .	40 / 1 .	41 / 1 .	42 / 1 .	43 / 1 .	44 / 1 .	45 / 1 .	46 / 1 .	47 / 1 .	48 / 1 .	49 / 1 .	50 / 1 .	51 / 1 .	52 / 1 .
Comment	pyx inc	am inc	pyx inc	pyx inc	pyx inc	mph	pyx inc	pyx inc	MI PEC	pyx inc	pyx inc	pyx inc	pyx inc	pyx inc	pyx inc	pyx inc	pl inc
P_2O_5	41.76	41.09	42.31	42.34	40.55	39.52	40.63	43.36	43.15	43.10	42.82	42.18	42.33	41.70	41.90	41.21	40.56
SiO_2	0.33	0.41	0.18	0.22	0.29	0.44	0.19	0.15	0.15	0.24	0.19	0.23	0.19	0.22	0.88	0.19	0.24
TiO_2					0.03	0.00	0.00	0.00	0.00	0.00	0.00	0.06	0.01	0.09	0.04	0.00	0.00
Al_2O_3					0.01	0.00	0.00	0.00	0.00	0.01	0.00	0.03	0.00	0.02	0.03	0.01	0.00
FeO	0.59	0.55	0.49	0.52	0.60	0.67	0.46	0.51	0.59	0.48	0.52	1.00	0.41	1.74	1.18	0.38	0.28
MnO	0.16	0.13	0.18	0.17	0.21	0.20	0.22	0.19	0.14	0.23	0.15	0.22	0.16	0.22	0.17	0.17	0.16
MgO	0.24	0.71	0.23	0.20	0.39	0.37	0.38	0.38	0.34	0.34	0.42	0.29	0.35	0.33	0.56	0.36	0.23
CaO	52.12	53.34	53.78	53.65	52.98	52.64	53.18	53.40	52.70	52.60	52.67	52.42	52.80	52.10	52.28	52.73	52.89
Na_2O	0.11	0.12	0.06	0.05	0.08	0.24	0.09	0.09	0.10	0.08	0.05	0.08	0.05	0.06	0.12	0.08	0.11
K_2O	0.00	0.07	0.01	0.01	0.01	0.03	0.01	0.00	0.01	0.02	0.00	0.01	0.01	0.00	0.01	0.00	0.00
Cl	1.23	0.57	0.78	0.89	1.08	1.12	1.12	1.04	1.37	1.14	0.86	1.19	1.24	1.11	0.95	1.01	1.69
F	4.34	2.77	3.83	3.79	4.10	3.69	4.01	4.24	4.52	4.10	4.15	4.04	3.99	4.98	3.82	4.28	4.69
F corr.	2.09	1.34	1.85	1.83	1.98	1.78	1.94	2.05	2.18	1.98	2.00	1.95	1.93	2.40	1.84	2.07	2.26
H_2O*	0.45	0.98	0.70	0.69	0.52	0.58	0.53	0.57	0.41	0.56	0.61	0.54	0.54	0.34	0.67	0.51	0.22
Subtotal	99.08	99.30	100.58	100.57	98.74	97.60	98.73	101.72	101.13	100.78	100.28	100.20	100.01	100.34	100.62	98.70	98.64
O=F,Cl	1.16	0.69	0.96	0.97	1.08	1.00	1.07	1.10	1.23	1.09	1.04	1.09	1.09	1.26	0.99	1.10	1.34
Sum	97.92	98.61	99.62	99.59	97.66	96.59	97.66	100.63	99.90	99.69	99.25	99.11	98.92	99.08	99.63	97.60	97.30
P	6.055	5.927	6.030	6.036	5.936	5.871	5.948	6.097	6.117	6.111	6.096	6.049	6.069	6.008	5.966	6.007	5.970
Si	0.056	0.070	0.031	0.037	0.051	0.077	0.032	0.024	0.025	0.040	0.032	0.039	0.033	0.037	0.148	0.032	0.041
Al	0.000	0.000	0.000	0.000	0.001	0.000	0.000	0.000	0.000	0.001	0.000	0.003	0.000	0.002	0.003	0.001	0.000
Ti	0.000	0.000	0.000	0.000	0.004	0.000	0.000	0.000	0.000	0.000	0.000	0.008	0.002	0.012	0.004	0.000	0.000
Fe	0.084	0.078	0.069	0.073	0.086	0.098	0.066	0.070	0.082	0.067	0.073	0.141	0.057	0.248	0.166	0.054	0.040
Mn	0.023	0.018	0.026	0.024	0.031	0.030	0.032	0.026	0.020	0.033	0.021	0.032	0.023	0.032	0.025	0.025	0.023
Mg	0.061	0.180	0.057	0.051	0.100	0.097	0.098	0.094	0.084	0.085	0.104	0.072	0.087	0.084	0.141	0.093	0.061
Ca	9.564	9.738	9.700	9.679	9.814	9.898	9.852	9.504	9.454	9.439	9.491	9.514	9.582	9.500	9.420	9.728	9.851
Na	0.038	0.039	0.021	0.017	0.028	0.082	0.030	0.028	0.032	0.027	0.017	0.025	0.017	0.020	0.038	0.028	0.036
K	0.000	0.015	0.001	0.002	0.003	0.007	0.001	0.000	0.001	0.005	0.000	0.003	0.001	0.000	0.002	0.000	0.000
Cl	0.357	0.164	0.224	0.255	0.316	0.334	0.327	0.292	0.387	0.322	0.246	0.342	0.355	0.320	0.270	0.293	0.499
F	1.134	0.721	0.985	0.974	1.082	0.988	1.058	1.075	1.154	1.047	1.065	1.045	1.032	1.293	0.980	1.125	1.245
OH*	0.509	1.114	0.791	0.771	0.602	0.679	0.615	0.633	0.458	0.631	0.689	0.613	0.613	0.387	0.750	0.581	0.256
Sum	17.880	18.066	17.935	17.919	18.054	18.161	18.060	17.844	17.816	17.808	17.833	17.887	17.871	17.944	17.912	17.968	18.022

Table D10 Apatite analyses of the 2010 Merapi eruption (continued)

Sample	M11-50	M11-51	M11-51	M11-51	M11-51	M11-51	M11-51	M11-53-B4	M11-53-B4	M11-55	M11-55	M11-55	M11-75	M11-75	M11-75	M11-75	M11-75
Sample Type	WP	GS	GS	GS	GS	GS	GS	P5N-WP	P5N-WP	WP	WP	WP	GS	GS	GS	GS	GS
Point	53 / 1 .	54 / 1 .	55 / 1 .	56 / 1 .	57 / 1 .	58 / 1 .	59 / 1 .	60 / 1 .	61 / 1 .	62 / 1 .	63 / 1 .	64 / 1 .	65 / 1 .	66 / 1 .	67 / 1 .	68 / 1 .	69 / 1 .
Comment	pyx inc	pyx inc	pyx inc	pyx inc	am inc	am rr	am inc	pyx inc	pyx inc	pyx inc	mph	am inc	pyx inc	pyx inc	pyx inc	pyx inc	pyx inc
P_2O_5	41.01	40.48	41.58	41.71	41.43	40.82	41.00	40.39	41.05	40.55	41.95	40.41	40.25	41.13	40.64	42.22	42.72
SiO_2	0.28	0.17	0.16	0.18	0.18	0.17	0.17	0.35	0.28	0.44	0.62	0.88	0.52	0.17	0.18	0.16	0.27
TiO_2	0.00									0.06	0.04	0.00	0.00	0.05	0.00	0.02	0.00
Al_2O_3	0.01									1.09	0.05	0.10	0.04	0.00	0.00	0.00	0.00
FeO	0.45	0.54	0.52	1.38	0.54	0.51	0.60	0.56	0.67	0.80	0.57	0.88	0.65	0.66	0.46	0.48	0.59
MnO	0.23	0.22	0.22	0.18	0.13	0.17	0.24	0.16	0.13	0.18	0.21	0.17	0.18	0.19	0.19	0.15	0.20
MgO	0.27	0.22	0.24	0.24	0.26	0.23	0.25	0.23	0.21	0.35	0.28	0.41	0.40	0.37	0.36	0.37	0.36
CaO	52.80	52.13	53.45	52.39	52.45	51.78	52.06	52.39	53.09	51.64	52.11	51.99	52.87	53.09	53.24	53.34	53.18
Na_2O	0.06	0.08	0.06	0.06	0.05	0.08	0.10	0.16	0.08	0.15	0.12	0.17	0.14	0.07	0.05	0.05	0.12
K_2O	0.02	0.01	0.00	0.02	0.01	0.00	0.03	0.01	0.05	0.02	0.08	0.02	0.03	0.01	0.00	0.00	0.01
Cl	1.13	1.20	0.78	1.00	0.78	0.81	0.87	0.83	1.08	1.06	1.08	1.12	1.18	1.11	1.05	0.97	1.12
F	4.77	3.82	3.10	3.45	3.43	3.23	3.01	3.28	3.34	4.98	4.55	4.26	4.24	4.37	4.21	3.67	4.07
F corr.	2.30	1.84	1.50	1.66	1.65	1.56	1.45	1.58	1.61	2.40	2.19	2.06	2.04	2.11	2.03	1.77	1.97
H_2O*	0.36	0.53	0.85	0.72	0.76	0.77	0.82	0.76	0.70	0.34	0.45	0.48	0.46	0.47	0.50	0.69	0.57
Subtotal	98.93	97.43	99.34	99.55	98.24	96.90	97.60	97.42	98.94	99.07	99.75	98.68	98.77	99.42	98.71	100.22	101.11
O=F,Cl	1.22	1.05	0.81	0.92	0.87	0.84	0.81	0.85	0.92	1.25	1.17	1.12	1.13	1.14	1.09	0.96	1.08
Sum	97.70	96.38	98.54	98.63	97.37	96.07	96.79	96.57	98.02	97.82	98.58	97.56	97.64	98.28	97.62	99.26	100.03
P	5.986	5.995	6.003	6.025	6.037	6.033	6.022	5.960	5.975	5.897	6.030	5.905	5.900	5.976	5.951	6.038	6.058
Si	0.049	0.029	0.027	0.031	0.031	0.029	0.030	0.061	0.048	0.075	0.106	0.152	0.091	0.029	0.031	0.027	0.045
Al	0.001	0.000	0.000	0.000	0.000	0.000	0.000	0.000	0.000	0.110	0.005	0.010	0.004	0.000	0.000	0.000	0.000
Ti	0.000	0.000	0.000	0.000	0.000	0.000	0.000	0.000	0.000	0.008	0.005	0.000	0.000	0.007	0.000	0.003	0.000
Fe	0.065	0.079	0.074	0.198	0.078	0.075	0.087	0.082	0.096	0.114	0.081	0.126	0.094	0.095	0.066	0.067	0.082
Mn	0.034	0.032	0.031	0.026	0.019	0.026	0.035	0.024	0.019	0.027	0.031	0.025	0.027	0.028	0.027	0.022	0.028
Mg	0.069	0.057	0.061	0.061	0.067	0.059	0.066	0.061	0.053	0.089	0.070	0.105	0.102	0.095	0.093	0.094	0.090
Ca	9.755	9.770	9.765	9.577	9.672	9.686	9.677	9.784	9.780	9.504	9.479	9.615	9.808	9.760	9.865	9.654	9.544
Na	0.019	0.027	0.019	0.020	0.017	0.027	0.035	0.053	0.028	0.051	0.039	0.058	0.048	0.023	0.018	0.016	0.040
K	0.004	0.003	0.000	0.004	0.003	0.000	0.006	0.002	0.010	0.004	0.017	0.005	0.007	0.001	0.000	0.000	0.002
Cl	0.331	0.356	0.225	0.288	0.229	0.240	0.256	0.245	0.315	0.308	0.311	0.327	0.347	0.321	0.307	0.277	0.319
F	1.254	1.020	0.807	0.897	0.900	0.860	0.798	0.873	0.877	1.306	1.179	1.123	1.119	1.145	1.112	0.945	1.042
OH*	0.415	0.623	0.969	0.815	0.871	0.900	0.946	0.883	0.808	0.386	0.510	0.549	0.533	0.534	0.581	0.778	0.639
Sum	17.982	17.993	17.979	17.943	17.923	17.934	17.957	18.027	18.008	17.879	17.863	18.001	18.080	18.013	18.052	17.921	17.889

Table D10 Apatite analyses of the 2010 Merapi eruption (continued)

Sample	M11-130	M11-130	M11-130	M11-130	M11-130	M11-130	M11-131										
Sample Type	LG-Inc	LG-Inc	LG-Inc	LG-Inc	LG-Inc	LG-Inc	LG-Inc										
Point	70 / 1 .	71 / 1 .	72 / 1 .	73 / 1 .	74 / 1 .	75 / 1 .	76 / 1 .										
Comment	pyx inc	pyx inc	pyx inc	pyx inc	pyx inc	pyx inc	mph										
P_2O_5	41.01	41.61	41.29	40.50	40.98	40.35	42.56										
SiO_2	0.19	0.21	0.16	0.21	0.18	0.23	0.22										
TiO_2	0.06	0.00	0.02	0.00	0.03	0.03	0.07										
Al_2O_3	0.00	0.00	0.01	0.00	0.01	0.00	0.00										
FeO	0.71	1.16	0.80	0.57	0.83	0.52	0.74										
MnO	0.15	0.14	0.17	0.14	0.16	0.16	0.16										
MgO	0.32	0.29	0.31	0.35	0.35	0.33	0.34										
CaO	53.56	53.41	53.55	53.17	53.40	53.02	53.51										
Na_2O	0.09	0.17	0.11	0.08	0.08	0.07	0.10										
K_2O	0.00	0.01	0.02	0.05	0.00	0.00	0.02										
Cl	1.19	1.51	1.54	1.54	1.62	1.10	0.99										
F	5.42	5.12	4.99	5.39	5.00	5.11	4.48										
F corr.	2.61	2.47	2.41	2.60	2.41	2.46	2.16										
H_2O*	0.21	0.21	0.22	0.11	0.19	0.28	0.51										
Subtotal	100.10	101.19	100.61	99.30	100.25	98.55	101.39										
O=F,Cl	1.37	1.38	1.36	1.44	1.38	1.28	1.13										
Sum	98.73	99.81	99.25	97.86	98.87	97.27	100.26										
P	5.947	5.975	5.964	5.939	5.949	5.937	6.032										
Si	0.032	0.035	0.027	0.036	0.031	0.040	0.037										
Al	0.000	0.000	0.001	0.000	0.001	0.000	0.000										
Ti	0.008	0.000	0.002	0.000	0.004	0.004	0.008										
Fe	0.101	0.165	0.115	0.082	0.119	0.075	0.104										
Mn	0.022	0.021	0.024	0.021	0.023	0.024	0.023										
Mg	0.081	0.073	0.080	0.090	0.090	0.084	0.084										
Ca	9.832	9.706	9.789	9.869	9.809	9.872	9.599										
Na	0.031	0.055	0.037	0.025	0.026	0.024	0.033										
K	0.001	0.002	0.005	0.011	0.000	0.001	0.004										
Cl	0.345	0.434	0.444	0.451	0.472	0.323	0.282										
F	1.416	1.325	1.300	1.425	1.309	1.354	1.143										
OH*	0.239	0.242	0.256	0.124	0.219	0.323	0.575										
Sum	18.055	18.030	18.044	18.073	18.052	18.062	17.925										

Table D11 Olivine analyses of the 2010 Merapi eruption[1]

Sample	M11-33	M11-33	M11-54-3	M11-135									
Sample Type[2]	WP	WP	LG-Inc	LG-Inc									
Point	7 / 1 .	8 / 1 .	63 / 1 .	22 / 1 .									
Comment[3]	ph-c	ph-c	ph-c	mph									
SiO_2	36.70	36.69	36.40	34.09									
TiO_2	0.01	0.01	0.00	0.09									
Al_2O_3	0.01	0.01	0.00	0.34									
Cr_2O_3	0.00	0.00	0.01	0.00									
FeO	28.98	29.20	35.25	41.10									
MnO	1.33	1.33	1.39	1.49									
MgO	33.10	33.12	27.78	20.75									
CaO	0.12	0.13	0.13	0.33									
Na_2O	0.00	0.00	0.00	0.06									
K_2O	0.00	0.00	0.00	0.01									
Sum	100.26	100.51	100.95	98.27									
Si	0.990	0.988	1.004	1.003									
Al	0.000	0.000	0.000	0.012									
Ti	0.000	0.000	0.000	0.002									
Cr	0.000	0.000	0.000	0.000									
Mg	1.331	1.330	1.142	0.911									
Fe	0.654	0.658	0.813	1.012									
Mn	0.030	0.030	0.032	0.037									
Ca	0.004	0.004	0.004	0.010									
Na	0.000	0.000	0.000	0.004									
K	0.000	0.000	0.000	0.000									
Sum	3.010	3.011	2.996	2.991									
Fo (mol%)	67.060	66.908	58.417	47.370									
Fa (mol%)	32.940	33.092	41.583	52.630									

[1] Major element oxides in wt.%; number of cations based on 4 oxygens; [2] see Appendix A; [3] see Table D1

Table D12 Biotite analyses of the 2010 Merapi eruption[1]

Sample	M11-27-3	M11-27-3	M11-27-3	M11-27-3	M11-27-3	M11-27-3	M11-27-3	M11-27-3	M11-27-3	M11-27-3	M11-27-3	M11-27-3	M11-27-3	M11-27-4	M11-27-4	M11-27-4	M11-27-4	M11-27-4	M11-27-4
Sample Type[2]	LG-Inc	LG-Inc	LG-Inc	LG-Inc	LG-Inc	LG-Inc	LG-Inc	LG-Inc	LG-Inc	LG-Inc	LG-Inc	LG-Inc	LG-Inc	LG-Inc	LG-Inc	LG-Inc	LG-Inc	LG-Inc	LG-Inc
Point	1 / 1 .	2 / 1 .	3 / 1 .	4 / 1 .	5 / 1 .	6 / 1 .	7 / 1 .	8 / 1 .	9 / 1 .	10 / 1 .	11 / 1 .	12 / 1 .	13 / 1 .	14 / 1 .	15 / 1 .	16 / 1 .	17 / 1 .	18 / 1 .	19 / 1 .
Comment[3]	m	m	m	m	m	m	m	m	m	m	m	m	m	m	m	m	m	m	m
SiO_2	36.77	37.01	36.76	37.98	37.53	38.29	37.63	37.34	37.61	37.79	37.75	37.18	37.40	37.77	37.59	37.98	37.89	36.80	37.52
TiO_2	4.45	4.74	4.64	4.96	3.88	4.44	3.99	4.17	4.52	4.21	4.64	5.21	5.09	4.44	4.56	3.95	3.59	4.45	4.03
Al_2O_3	12.74	12.99	12.98	12.93	12.93	12.71	12.85	13.01	13.08	13.11	12.79	13.24	13.35	13.00	13.01	13.14	13.29	12.93	13.08
Cr_2O_3	0.02	0.00	0.00	0.00	0.00	0.03	0.01	0.00	0.00	0.02	0.00	0.00	0.00	0.01	0.00	0.00	0.00	0.00	0.00
FeO	15.48	13.87	15.50	14.85	14.92	11.96	14.90	15.16	13.73	15.00	14.32	13.67	13.74	14.94	15.05	12.96	14.01	14.50	15.63
MnO	0.26	0.20	0.23	0.26	0.26	0.22	0.30	0.21	0.20	0.28	0.29	0.19	0.27	0.33	0.26	0.20	0.25	0.24	0.21
MgO	14.91	15.27	15.32	14.47	15.48	15.08	15.66	15.47	16.31	15.76	15.74	15.80	16.09	15.54	15.66	17.18	16.72	15.88	15.33
CaO	0.03	0.10	0.06	0.04	0.04	0.02	0.01	0.03	0.02	0.03	0.03	0.01	0.01	0.01	0.00	0.05	0.08	0.19	0.06
Na_2O	0.74	0.76	0.80	0.77	0.79	0.77	0.75	0.78	0.77	0.70	0.74	0.77	0.78	0.71	0.72	0.76	0.79	0.74	0.82
K_2O	9.33	9.06	8.96	8.90	9.48	9.36	9.48	9.47	9.47	9.60	9.28	9.21	9.16	9.68	9.54	9.49	9.40	8.67	9.21
Cl	0.23	0.18	0.17	0.19	0.18	0.21	0.21	0.15	0.16	0.20	0.16	0.15	0.14	0.19	0.19	0.22	0.18	0.20	0.17
F	1.46	1.28	1.18	2.57	2.97	1.38	2.23	1.87	0.94	0.86	1.45	0.88	1.12	0.99	1.16	3.76	3.64	1.56	3.16
H_2O*	3.20	3.31	3.38	2.74	2.54	3.25	2.89	3.07	3.54	3.58	3.29	3.56	3.48	3.52	3.43	2.21	2.27	3.18	2.47
Subtotal	99.61	98.75	99.97	100.66	101.02	97.72	100.91	100.73	100.37	101.15	100.46	99.87	100.63	101.13	101.18	101.92	102.13	99.33	101.68
O=F,Cl	0.67	0.58	0.54	1.12	1.29	0.63	0.99	0.82	0.43	0.41	0.65	0.40	0.50	0.46	0.53	1.64	1.57	0.70	1.37
Sum	98.94	98.17	99.44	99.53	99.72	97.09	99.92	99.90	99.93	100.74	99.81	99.47	100.13	100.67	100.64	100.28	100.55	98.63	100.32
Si	5.584	5.605	5.539	5.686	5.640	5.803	5.638	5.600	5.594	5.609	5.633	5.550	5.546	5.614	5.589	5.623	5.617	5.561	5.614
Al total	2.281	2.319	2.305	2.282	2.290	2.270	2.269	2.299	2.293	2.294	2.249	2.330	2.334	2.277	2.280	2.293	2.323	2.302	2.306
Ti	0.509	0.540	0.526	0.559	0.438	0.506	0.449	0.470	0.506	0.470	0.521	0.585	0.567	0.497	0.510	0.440	0.401	0.505	0.453
Cr	0.002	0.000	0.000	0.000	0.000	0.003	0.002	0.000	0.000	0.002	0.000	0.000	0.000	0.001	0.000	0.000	0.000	0.000	0.000
Fe	1.966	1.757	1.954	1.859	1.876	1.516	1.867	1.902	1.707	1.862	1.787	1.706	1.704	1.857	1.871	1.605	1.738	1.832	1.956
Mn	0.033	0.025	0.030	0.033	0.034	0.028	0.038	0.027	0.026	0.036	0.036	0.023	0.033	0.041	0.033	0.025	0.032	0.031	0.027
Mg	3.375	3.448	3.442	3.228	3.468	3.407	3.497	3.459	3.616	3.486	3.501	3.515	3.556	3.443	3.470	3.791	3.696	3.577	3.418
Ca	0.004	0.016	0.010	0.006	0.006	0.004	0.001	0.004	0.004	0.004	0.005	0.002	0.001	0.002	0.000	0.008	0.012	0.031	0.009
Na	0.217	0.223	0.233	0.224	0.231	0.226	0.217	0.228	0.223	0.201	0.213	0.224	0.223	0.204	0.207	0.219	0.227	0.216	0.238
K	1.807	1.750	1.722	1.699	1.817	1.809	1.812	1.812	1.796	1.818	1.767	1.754	1.733	1.835	1.808	1.793	1.778	1.671	1.758
Cl	0.058	0.046	0.044	0.048	0.045	0.054	0.054	0.039	0.040	0.051	0.040	0.038	0.036	0.049	0.048	0.056	0.045	0.051	0.043
F	0.703	0.612	0.562	1.216	1.413	0.662	1.058	0.888	0.444	0.403	0.686	0.413	0.526	0.466	0.548	1.762	1.708	0.747	1.493
OH*	3.239	3.342	3.394	2.736	2.542	3.283	2.888	3.073	3.516	3.546	3.274	3.549	3.438	3.485	3.404	2.182	2.247	3.202	2.464
Sum	19.778	19.682	19.760	19.576	19.800	19.572	19.791	19.800	19.764	19.783	19.712	19.689	19.698	19.770	19.769	19.797	19.823	19.726	19.778
Mg#	63.2	66.2	63.8	63.5	64.9	69.2	65.2	64.5	67.9	65.2	66.2	67.3	67.6	65.0	65.0	70.3	68.0	66.1	63.6

[1] Major element oxides in wt.%; number of cations based on 22 oxygens; H_2O calculations after Tindle and Webb (1990); [2] see Appendix A; [3] see Table D1

Table D12 Biotite analyses of the 2010 Merapi eruption (continued)

Sample	M11-27-4	M11-27-4	M11-27-4	M11-27-4	M11-33	M11-131	M11-131	M11-131
Sample Type	LG-Inc	LG-Inc	LG-Inc	LG-Inc	WP	LG-Inc	LG-Inc	LG-Inc
Point	20 / 1 .	21 / 1 .	22 / 1 .	23 / 1 .	24 / 1 .	25 / 1 .	26 / 1 .	27 / 1 .
Comment	m	m	m	m	m	m	m	m
SiO_2	37.94	37.66	37.65	37.53	36.55	40.03	40.94	40.88
TiO_2	3.63	4.24	4.14	4.64	5.05	3.89	3.94	4.22
Al_2O_3	13.01	13.15	12.97	13.19	14.06	13.44	14.63	12.71
Cr_2O_3	0.00	0.00	0.03	0.00	0.00	0.00	0.00	0.00
FeO	14.13	15.58	13.88	14.66	14.56	13.78	12.81	13.31
MnO	0.20	0.32	0.23	0.28	0.24	0.27	0.23	0.21
MgO	16.64	15.54	16.10	15.70	15.47	13.12	12.53	13.19
CaO	0.04	0.03	0.02	0.06	0.06	0.08	0.97	0.68
Na_2O	0.75	0.79	0.77	0.77	0.85	1.22	1.12	0.84
K_2O	9.41	9.48	9.24	9.40	9.05	8.60	7.96	8.41
Cl	0.27	0.18	0.17	0.16	0.12	0.14	0.18	0.20
F	3.52	2.05	1.23	1.55	0.56	1.29	1.87	2.25
H_2O*	2.29	3.02	3.38	3.26	3.73	3.38	3.17	2.93
Subtotal	101.83	102.05	99.80	101.18	100.30	99.24	100.34	99.81
O=F,Cl	1.54	0.91	0.55	0.69	0.26	0.57	0.83	0.99
Sum	100.28	101.14	99.24	100.49	100.04	98.66	99.51	98.82
Si	5.643	5.588	5.636	5.577	5.446	5.961	5.986	6.059
Al total	2.281	2.300	2.289	2.310	2.468	2.358	2.521	2.220
Ti	0.407	0.473	0.467	0.518	0.566	0.436	0.433	0.470
Cr	0.000	0.000	0.003	0.000	0.000	0.000	0.000	0.000
Fe	1.758	1.934	1.738	1.821	1.814	1.716	1.567	1.649
Mn	0.025	0.040	0.029	0.036	0.030	0.034	0.028	0.026
Mg	3.690	3.437	3.593	3.478	3.436	2.912	2.732	2.913
Ca	0.006	0.005	0.003	0.009	0.010	0.013	0.152	0.107
Na	0.216	0.228	0.222	0.221	0.245	0.353	0.317	0.240
K	1.785	1.794	1.764	1.781	1.720	1.633	1.485	1.591
Cl	0.069	0.045	0.043	0.039	0.030	0.035	0.045	0.050
F	1.654	0.964	0.581	0.726	0.262	0.608	0.866	1.053
OH*	2.277	2.991	3.376	3.234	3.709	3.357	3.089	2.898
Sum	19.810	19.799	19.744	19.751	19.736	19.417	19.222	19.276
Mg#	67.7	64.0	67.4	65.6	65.5	62.9	63.6	63.8

Table D13 Cristobalite analyses of the 2010 Merapi eruption[1]

Sample	Sample Type[2]	Point	Comment[3]		SiO_2	TiO_2	Al_2O_3	FeO	MnO	MgO	CaO	Na_2O	K_2O	Sum
M11-27-3	LG-Inc	38 / 1 .	gm / pm		100.71	0.10	0.28	0.05	0.00	0.01	0.00	0.05	0.06	101.25
M11-27-3	LG-Inc	39 / 1 .	gm / pm		100.74	0.09	0.18	0.06	0.09	0.00	0.01	0.00	0.06	101.24
M11-27-3	LG-Inc	40 / 1 .	gm / pm		101.00	0.08	0.09	0.06	0.00	0.00	0.03	0.00	0.02	101.28
M11-27-3	LG-Inc	41 / 1 .	gm / pm		100.59	0.10	0.11	0.03	0.00	0.00	0.03	0.02	0.02	100.89
M11-27-3	LG-Inc	42 / 1 .	gm / pm		98.45	0.08	0.16	0.06	0.00	0.00	0.01	0.00	0.02	98.78
M11-27-4	LG-Inc	41 / 1 .	gm / pm		98.24	0.05	0.08	0.01	0.00	0.00	0.01			98.40
M11-27-4	LG-Inc	42 / 1 .	gm / pm		98.62	0.05	0.08	0.04	0.01	0.00	0.02			98.80
M11-27-4	LG-Inc	57 / 1 .	gm / pm		98.54	0.05	0.08	0.00	0.00	0.00	0.02			98.69
M11-27-4	LG-Inc	58 / 1 .	gm / pm		98.08	0.06	0.08	0.06	0.00	0.00	0.01			98.30
M11-27-4	LG-Inc	59 / 1 .	gm / pm		98.81	0.08	0.10	0.05	0.02	0.00	0.01			99.07
M11-34	DD	59 / 1 .	gm / pm		100.71	0.03	0.36	0.11	0.02	0.01	0.21	0.18	0.11	101.72
M11-34	DD	60 / 1 .	gm / pm		100.91	0.00	0.11	0.02	0.00	0.00	0.05	0.07	0.03	101.19
M11-48	LG-Inc	14 / 1 .	gm / pm		98.12	0.08	0.08	0.08	0.01	0.01	0.00			98.38
M11-48	LG-Inc	15 / 1 .	gm / pm		96.65	0.09	0.86	0.05	0.00	0.00	0.03			97.69
M11-54-3	LG-Inc	65 / 1 .	gm / pm		98.84	0.09	0.48	0.05	0.00	0.00	0.03	0.22	0.05	99.76
M11-54-3	LG-Inc	66 / 1 .	gm / pm		99.88	0.07	0.49	0.06	0.00	0.00	0.04	0.26	0.05	100.85
M11-131	LG-Inc	44 / 1 .	gm / pm		99.32	0.03	0.08	0.04	0.00	0.00	0.01	0.00	0.00	99.49
M11-131	LG-Inc	45 / 1 .	gm / pm		99.77	0.02	0.07	0.01	0.01	0.00	0.01	0.00	0.01	99.90
M11-131	LG-Inc	46 / 1 .	gm / pm		101.03	0.02	0.07	0.04	0.00	0.01	0.00	0.00	0.01	101.17
M11-131	LG-Inc	47 / 1 .	gm / pm		100.63	0.02	0.09	0.03	0.00	0.00	0.00	0.01	0.00	100.78
M11-131	LG-Inc	55 / 1 .	gm / pm		100.14	0.04	0.08	0.12	0.01	0.01	0.00	0.00	0.01	100.42
M11-131	LG-Inc	56 / 1 .	gm / pm		101.44	0.05	0.11	0.06	0.00	0.01	0.01	0.00	0.00	101.68
M11-131	LG-Inc	57 / 1 .	gm / pm		101.70	0.00	0.07	0.03	0.00	0.00	0.01	0.00	0.01	101.82
M11-131	LG-Inc	59 / 1 .	gm / pm		99.92	0.07	0.73	0.14	0.02	0.00	0.03	0.19	0.30	101.41
M11-131	LG-Inc	63 / 1 .	gm / pm		100.80	0.04	0.10	0.14	0.01	0.00	0.02	0.00	0.02	101.14
M11-135	LG-Inc	2 / 1 .	gm / pm		99.96	0.15	1.12	0.13	0.00	0.00	0.07	0.71	0.01	102.15
M11-135	LG-Inc	3 / 1 .	gm / pm		97.41	0.15	1.23	0.09	0.00	0.00	0.06	0.63	0.02	99.60
M11-135	LG-Inc	6 / 1 .	gm / pm		99.14	0.15	1.50	0.10	0.01	0.00	0.06	0.89	0.01	101.84
M11-135	LG-Inc	7 / 1 .	gm / pm		98.29	0.14	1.73	0.14	0.00	0.00	0.07	0.99	0.01	101.37
M11-135	LG-Inc	8 / 1 .	gm / pm		99.04	0.16	1.14	0.10	0.02	0.00	0.04	0.66	0.01	101.17
M11-138	SD-S	29 / 1 .	gm / pm		97.44	0.03	0.79	0.26	0.02	0.02	0.05			98.61

[1] Major element oxides in wt.%; [2] see Appendix A; [3] gm / pm = groundmass / post-magmatic (vapour phase crystallisation) phase

Table D14 Amphibole analyses from plutonic inclusions (magmatic cumulates) in the 2006 and 2010 Merapi eruption products[1]

Sample	C02	C02	C02	C02	C02	C02	C02	C02	C02	C02	C02	C02	C02	C02
Sample Type[2]	Pl-Inc	Pl-Inc	Pl-Inc	Pl-Inc	Pl-Inc	Pl-Inc	Pl-Inc	Pl-Inc	Pl-Inc	Pl-Inc	Pl-Inc	Pl-Inc	Pl-Inc	Pl-Inc
DataSet/Point	2 / 1 .	3 / 1 .	4 / 1 .	11 / 1 .	12 / 1 .	19 / 1 .	25 / 1 .	26 / 1 .	2 / 1 .	3 / 1 .	4 / 1 .	11 / 1 .	12 / 1 .	19 / 1 .
Comment[3]	ph	ph	ph	ph-r	ph-r	ph	ph	ph	ph	ph	ph	ph-r	ph-r	ph
SiO_2	40.21	39.93	40.13	40.12	40.05	41.68	40.10	40.00	40.21	39.93	40.13	40.12	40.05	41.68
TiO_2	2.24	2.21	2.24	2.26	2.26	2.12	2.23	2.19	2.24	2.21	2.24	2.26	2.26	2.12
Al_2O_3	14.57	14.77	14.68	14.64	14.54	12.85	14.29	14.46	14.57	14.77	14.68	14.64	14.54	12.85
Cr_2O_3	0.00	-0.02	0.01	0.00	0.00	0.00	0.01	-0.01	0.00	-0.02	0.01	0.00	0.00	0.00
FeO	12.25	12.41	13.05	12.45	12.45	11.88	13.19	12.19	12.25	12.41	13.05	12.45	12.45	11.88
MnO	0.14	0.14	0.14	0.16	0.14	0.14	0.19	0.16	0.14	0.14	0.14	0.16	0.14	0.14
MgO	13.07	12.78	12.76	13.03	13.14	14.04	12.87	12.95	13.07	12.78	12.76	13.03	13.14	14.04
CaO	12.27	12.33	12.31	12.25	12.33	12.06	12.25	12.23	12.27	12.33	12.31	12.25	12.33	12.06
Na_2O	2.23	2.38	2.33	2.26	2.26	2.40	2.27	2.21	2.23	2.38	2.33	2.26	2.26	2.40
K_2O	1.22	1.20	1.20	1.25	1.20	1.30	1.26	1.19	1.22	1.20	1.20	1.25	1.20	1.30
Cl	0.02	0.02	0.02	0.02	0.02	0.04	0.02	0.02	0.02	0.02	0.02	0.02	0.02	0.04
F	0.09	0.20	0.10	0.17	0.11	0.12	0.22	0.13	0.09	0.20	0.10	0.17	0.11	0.12
Sum	98.29	98.35	98.97	98.61	98.50	98.63	98.89	97.73	98.29	98.35	98.97	98.61	98.50	98.63
Si	5.879	5.863	5.850	5.857	5.850	6.061	5.858	5.887	5.879	5.863	5.850	5.857	5.850	6.061
Al	2.511	2.556	2.522	2.519	2.503	2.202	2.460	2.509	2.511	2.556	2.522	2.519	2.503	2.202
Ti	0.246	0.244	0.246	0.249	0.248	0.232	0.245	0.243	0.246	0.244	0.246	0.249	0.248	0.232
Cr	0.000	-0.002	0.001	0.000	0.000	0.000	0.001	-0.001	0.000	-0.002	0.001	0.000	0.000	0.000
Fe^{3+}	0.533	0.450	0.560	0.565	0.578	0.537	0.621	0.521	0.533	0.450	0.560	0.565	0.578	0.537
Mg	2.849	2.798	2.774	2.835	2.862	3.043	2.802	2.842	2.849	2.798	2.774	2.835	2.862	3.043
Fe^{2+}	0.965	1.074	1.032	0.955	0.943	0.907	0.991	0.979	0.965	1.074	1.032	0.955	0.943	0.907
Mn	0.018	0.017	0.017	0.020	0.018	0.017	0.023	0.020	0.018	0.017	0.017	0.020	0.018	0.017
Ca	1.923	1.940	1.924	1.916	1.930	1.879	1.918	1.929	1.923	1.940	1.924	1.916	1.930	1.879
Na	0.632	0.678	0.658	0.640	0.641	0.678	0.643	0.631	0.632	0.678	0.658	0.640	0.641	0.678
K	0.228	0.225	0.222	0.233	0.224	0.240	0.235	0.223	0.228	0.225	0.222	0.233	0.224	0.240
Cl	0.00	0.01	0.01	0.00	0.00	0.01	0.00	0.01	0.00	0.01	0.01	0.00	0.00	0.01
F	0.04	0.09	0.05	0.08	0.05	0.06	0.10	0.06	0.04	0.09	0.05	0.08	0.05	0.06
Sum	15.783	15.842	15.803	15.789	15.795	15.796	15.796	15.783	15.783	15.842	15.803	15.789	15.795	15.796

[1] Major element oxides in wt.%; number of cations based on 23 oxygens; Fe^{3+} estimation assuming 13eCNK; cation sum excluding Cl and F; [2] see Appendix A; [3] see Table D1

Table D14 Amphibole analyses from plutonic inclusions (magmatic cumulates) in the 2006 and 2010 Merapi eruption products (continued)

Sample	C02	C02	M07C	M07C	M07C	M07C	M07C	M07C	M07C	M07C	M11-01C	M11-01C	M11-01C	
Sample Type	Pl-Inc	Pl-Inc	Pl-Inc	Pl-Inc	Pl-Inc	Pl-Inc	Pl-Inc	Pl-Inc	Pl-Inc	Pl-Inc	Pl-Inc	Pl-Inc	Pl-Inc	
DataSet/Point	25 / 1 .	26 / 1 .	1 / 1 .	2 / 1 .	7 / 1 .	10 / 1 .	11 / 1 .	12 / 1 .	13 / 1 .	22 / 1 .	3 / 1 .	10 / 1 .	11 / 1 .	
Comment	ph	ph	ph-c	ph-r	ph-r	ph-c	ph-c	ph-r	ph	ph	ph	ph-c	ph-c	
SiO_2	40.10	40.00	40.50	40.32	40.03	40.12	40.16	42.03	40.30	40.32	41.35	40.20	40.93	
TiO_2	2.23	2.19	2.01	2.02	2.27	2.06	2.08	2.88	2.00	2.05	3.24	2.43	2.34	
Al_2O_3	14.29	14.46	14.33	14.43	14.23	14.45	14.52	11.61	14.41	13.93	12.46	13.99	14.11	
Cr_2O_3	0.01	-0.01	0.01	0.01	0.03	0.00	0.03	0.03	0.01	0.02	0.02	0.01	0.01	
FeO	13.19	12.19	11.14	11.64	11.89	11.40	10.32	11.77	10.62	10.16	12.66	12.70	12.74	
MnO	0.19	0.16	0.11	0.12	0.12	0.13	0.11	0.17	0.09	0.09	0.26	0.21	0.20	
MgO	12.87	12.95	14.19	13.78	13.50	13.72	14.55	14.24	14.60	14.65	13.29	12.99	12.95	
CaO	12.25	12.23	12.31	12.28	12.12	12.20	12.47	11.64	12.42	12.39	11.51	12.11	11.92	
Na_2O	2.27	2.21	2.20	2.25	2.69	2.27	2.17	2.44	2.24	2.12	2.47	2.39	2.52	
K_2O	1.26	1.19	1.26	1.25	1.25	1.23	1.41	1.06	1.37	1.45	1.14	1.12	1.11	
Cl	0.02	0.02	0.01	0.01	0.02	0.02	0.01	0.06	0.01	0.01	0.08	0.03	0.04	
F	0.22	0.13	0.06	0.38	0.10	0.10	0.08	0.15	0.07	0.08	0.46	0.51	0.55	
Sum	98.89	97.73	98.13	98.49	98.24	97.69	97.89	98.09	98.15	97.25	98.94	98.67	99.42	
Si	5.858	5.887	5.885	5.874	5.867	5.874	5.849	6.131	5.852	5.909	6.033	5.894	5.948	
Al	2.460	2.509	2.454	2.478	2.458	2.493	2.491	1.995	2.466	2.406	2.143	2.417	2.417	
Ti	0.245	0.243	0.220	0.221	0.250	0.227	0.227	0.316	0.218	0.225	0.356	0.268	0.256	
Cr	0.001	-0.001	0.001	0.001	0.004	0.000	0.004	0.003	0.002	0.002	0.002	0.002	0.002	
Fe^{3+}	0.621	0.521	0.650	0.632	0.501	0.608	0.587	0.582	0.641	0.557	0.571	0.568	0.543	
Mg	2.802	2.842	3.073	2.993	2.950	2.995	3.160	3.097	3.161	3.201	2.891	2.838	2.805	
Fe^{2+}	0.991	0.979	0.704	0.787	0.956	0.787	0.669	0.854	0.649	0.688	0.973	0.990	1.005	
Mn	0.023	0.020	0.013	0.015	0.015	0.017	0.013	0.021	0.011	0.011	0.032	0.026	0.025	
Ca	1.918	1.929	1.917	1.916	1.903	1.913	1.946	1.819	1.932	1.946	1.799	1.902	1.857	
Na	0.643	0.631	0.619	0.634	0.763	0.643	0.612	0.690	0.632	0.602	0.697	0.679	0.711	
K	0.235	0.223	0.233	0.232	0.233	0.229	0.262	0.197	0.254	0.272	0.212	0.209	0.207	
Cl	0.00	0.01	0.00	0.00	0.00	0.00	0.00	0.02	0.00	0.00	0.02	0.01	0.01	
F	0.10	0.06	0.03	0.17	0.05	0.04	0.04	0.07	0.03	0.04	0.21	0.24	0.25	
Sum	15.796	15.783	15.769	15.783	15.900	15.785	15.820	15.706	15.818	15.820	15.708	15.790	15.774	

Table E1 Major element and volatile (F, Cl, S) concentrations in melt inclusions in the 2006 Merapi eruption products obtained by electron microprobe analysis[1]

Sample	Sample Type[2]	Point	Host Mineral[3]		SiO_2	TiO_2	Al_2O_3	FeO	MnO	MgO	CaO	Na_2O	K_2O	P_2O_5	Sum		F	Cl	S
ME08-04-01	L8-S	12 / 1 .	cpx		66.71	0.40	16.12	2.59	0.13	0.27	1.05	4.94	6.37	0.14	98.73		111	2692	91
ME08-04-01	L8-S	14 / 1 .	cpx		67.51	0.56	14.89	1.67	0.09	0.23	1.19	4.66	4.80	0.15	95.75		1212	2735	188
ME08-04-01	L8-S	15 / 1 .	cpx		65.51	0.39	15.51	1.79	0.07	0.15	1.58	4.95	4.98	0.17	95.09		827	3179	122
ME08-09-01	L1-S	12 / 1 .	cpx		67.01	0.38	14.79	3.08	0.16	1.31	2.71	4.55	6.00	0.08	100.07		740	2430	90
ME08-09-01	L1-S	4 / 1 .	cpx		66.80	0.47	17.62	1.95	0.11	0.85	3.12	4.61	4.21	0.17	99.90		130	2410	225
ME08-09-01	L1-S	3 / 1 .	cpx		67.09	0.48	15.92	2.06	0.10	0.79	2.11	4.59	4.88	0.14	98.16		1330	3100	190
ME08-09-01	L1-S	21 / 1 .	cpx		65.69	0.41	16.35	2.52	0.11	0.34	1.15	5.07	5.97	0.17	97.79		1520	2780	75
ME08-09-01	L1-S	22 / 1 .	cpx		66.39	0.38	16.54	2.52	0.09	0.34	1.13	5.23	6.11	0.14	98.88		1790	2780	35
ME08-09-01	L1-S	24 / 1 .	cpx		68.12	0.51	16.20	2.69	0.15	0.33	1.18	4.73	6.17	0.14	100.21		1140	3720	10
ME08-09-01	L1-S	25 / 1 .	cpx		67.02	0.48	16.09	2.81	0.12	0.34	1.26	4.67	6.24	0.20	99.22		n.d.	3710	50
ME08-09-01	L1-S	14 / 1 .	cpx		68.32	0.43	15.68	2.74	0.11	0.27	1.28	5.87	5.40	0.15	100.24		990	3380	160
ME08-09-01	L1-S	15 / 1 .	cpx		68.46	0.44	15.85	2.69	0.07	0.25	1.25	6.04	5.45	0.14	100.63		820	3350	175
ME08-09-01	L1-S	1 / 1 .	cpx		67.87	0.33	16.28	2.60	0.11	0.35	0.94	5.02	6.33	0.16	99.98		800	2640	85
ME08-09-01	L1-S	3 / 1 .	cpx		68.34	0.32	16.08	2.95	0.10	0.35	0.97	5.02	6.25	0.14	100.53		280	2570	5
ME08-09-01	L1-S	8 / 1 .	cpx		67.79	0.42	14.95	2.96	0.12	0.67	1.52	4.66	5.86	0.13	99.09		1400	2930	95
ME08-09-01	L1-S	29 / 1 .	cpx		66.19	0.54	15.88	1.55	0.11	0.35	1.65	4.59	4.38	0.17	95.39		210	2670	130
ME08-09-01	L1-S	30 / 1 .	cpx		68.19	0.39	16.24	1.90	0.08	0.30	1.55	4.98	4.64	0.14	98.42		2050	3050	245
ME08-09-01	L1-S	31 / 1 .	cpx		67.89	0.46	16.26	1.76	0.11	0.24	1.58	4.56	4.63	0.14	97.62		770	2980	160
ME08-09-01	L1-S	32 / 1 .	cpx		64.11	0.78	16.23	2.83	0.06	0.74	1.79	6.70	6.00	0.10	99.35		330	2910	285
ME08-09-01	L1-S	25 / 1 .	cpx		66.46	0.40	16.01	2.54	0.13	0.15	1.33	6.89	5.40	0.11	99.40		1180	2960	95
ME08-09-01	L1-S	26 / 1 .	cpx		67.84	0.40	16.05	2.42	0.08	0.21	1.10	6.65	5.44	0.12	100.30		170	2580	80
ME08-09-01	L1-S	27 / 1 .	cpx		67.86	0.36	16.09	2.36	0.08	0.19	1.11	6.84	5.45	0.13	100.48		40	2510	20
ME08-09-02	L1-S	1 / 1 .	cpx		65.87	0.51	16.01	2.41	0.13	0.38	1.30	6.00	5.40	0.11	98.12		998	2611	200
ME08-09-02	L1-S	2 / 1 .	cpx		66.57	0.42	15.74	2.64	0.17	0.27	1.11	5.15	6.40	0.16	98.62		850	2640	82
ME08-09-02	L1-S	3 / 1 .	cpx		65.71	0.49	15.79	2.22	0.14	0.65	1.44	4.32	5.34	0.16	96.26		991	2810	224
ME08-09-02	L1-S	4 / 1 .	cpx		64.98	0.89	15.21	2.07	0.11	0.34	1.26	4.82	5.53	0.13	95.32		1080	3194	107
ME08-09-02	L1-S	5 / 1 .	cpx		65.90	0.45	15.51	1.99	0.17	0.43	1.67	4.74	5.01	0.15	96.02		1387	2444	192
ME08-09-02	L1-S	6 / 1 .	cpx		67.47	0.52	15.14	1.97	0.12	0.55	1.61	4.41	4.75	0.14	96.68		1493	2744	112
ME08-09-02	L1-S	7 / 1 .	cpx		64.96	0.78	16.49	1.66	0.11	0.39	2.37	5.17	3.28	0.28	95.48		1275	2049	736
ME08-09-02	L1-S	8 / 1 .	cpx		63.86	0.51	16.92	1.61	0.11	0.53	2.06	4.92	4.51	0.22	95.25		1307	2205	694
ME08-09-02	L1-S	9 / 1 .	cpx		66.15	0.41	15.98	1.95	0.11	0.26	1.68	4.95	4.42	0.15	96.05		1149	2658	318
ME08-09-02	L1-S	10 / 1 .	cpx		66.18	0.37	15.80	2.07	0.04	0.43	1.33	4.86	5.12	0.16	96.35		1292	2850	179
ME08-09-02	L1-S	11 / 1 .	cpx		65.89	0.56	16.41	2.11	0.11	0.58	1.99	5.02	4.97	0.17	97.83		526	2389	120
ME08-10	KB-S	16 / 1 .	cpx		64.50	0.66	15.82	2.67	0.08	0.21	0.90	6.24	6.66	0.10	97.84		244	2757	176
ME08-10	KB-S	18 / 1 .	cpx		69.14	0.48	13.69	2.59	0.17	0.36	1.17	3.27	6.95	0.18	98.00		844	3104	85
ME08-10	KB-S	19 / 1 .	cpx		68.77	0.36	15.25	1.16	0.05	0.29	1.18	5.03	4.63	0.15	96.88		732	3032	99
ME08-10	KB-S	20 / 1 .	cpx		68.90	0.57	13.64	2.11	0.05	0.30	1.08	3.60	6.96	0.16	97.37		987	3088	60
ME08-10	KB-S	21 / 1 .	cpx		67.77	0.39	15.62	1.75	0.11	0.45	1.27	4.17	7.31	0.13	98.98		855	2483	68
ME08-10	KB-S	22 / 1 .	cpx		67.62	0.30	15.04	1.42	0.10	0.26	0.98	4.93	5.59	0.13	96.38		661	3184	394
ME08-14	SD-S	24 / 1 .	cpx		66.09	0.26	16.37	1.63	0.04	0.26	0.97	5.54	5.84	0.13	97.14		676	3120	312

[1] Major element oxides in wt.%; volatile elements (F, Cl, S) in ppm; [2] see Appendix A; [3] host mineral: cpx = clinopyroxene

Table E2 Major element and volatile (F, Cl, S) concentrations in groundmass glass in the 2006 Merapi eruption products obtained by electron microprobe analysis[1]

Sample	Sample Type[2]	Point			SiO_2	TiO_2	Al_2O_3	FeO	MnO	MgO	CaO	Na_2O	K_2O	P_2O_5	Sum		F	Cl	S
ME08-01	L4-S	20 / 1 .			70.54	0.45	14.48	2.53	0.03	0.23	0.81	4.50	6.21	0.12	100.33		1334	2295	50
ME08-01	L4-S	21 / 1 .			69.87	0.55	14.55	2.76	0.14	0.30	0.82	4.44	6.28	0.13	100.34		1462	2443	9
ME08-01	L4-S	22 / 1 .			70.72	0.44	14.84	2.59	0.19	0.33	0.77	4.49	6.17	0.12	101.07		1505	1875	n.d.
ME08-01	L4-S	23 / 1 .			70.12	0.50	14.82	2.96	0.10	0.26	0.81	4.32	6.48	0.11	100.88		957	2424	n.d.
ME08-01	L4-S	24 / 1 .			70.10	0.47	14.41	2.49	0.13	0.25	0.82	4.40	6.37	0.13	100.09		1450	2116	50
ME08-01	L4-S	25 / 1 .			70.16	0.51	14.36	2.40	0.09	0.22	0.76	4.40	6.32	0.11	99.75		1907	2079	23
ME08-01	L4-S	26 / 1 .			70.39	0.50	14.53	2.59	0.15	0.21	0.86	4.32	6.31	0.11	100.28		644	2295	n.d.
ME08-01	L4-S	27 / 1 .			70.73	0.54	14.06	2.44	0.12	0.22	0.70	4.42	6.06	0.10	99.94		2349	2102	90
ME08-01	L4-S	28 / 1 .			70.88	0.51	14.37	2.79	0.15	0.22	0.79	4.30	6.36	0.15	100.90		1416	2181	117
ME08-01	L4-S	29 / 1 .			70.31	0.49	14.95	2.41	0.08	0.22	0.81	4.23	6.62	0.09	100.62		1637	2305	54
ME08-01	L4-S	30 / 1 .			70.74	0.52	14.69	2.51	0.19	0.17	0.81	4.42	6.40	0.10	100.89		1528	1914	n.d.
ME08-03-02	L6-S	20 / 1 .			73.61	0.45	12.90	2.40	0.12	0.17	0.60	3.68	6.39	0.04	100.65		n.d.	2250	5
ME08-03-02	L6-S	21 / 1 .			74.40	0.51	12.37	2.38	0.14	0.13	0.37	3.67	6.34	0.08	100.83		1322	2487	n.d.
ME08-03-02	L6-S	22 / 1 .			74.78	0.45	12.62	2.49	0.09	0.28	0.40	3.59	6.43	0.05	101.65		1124	2406	18
ME08-03-02	L6-S	23 / 1 .			74.22	0.44	12.64	2.39	0.10	0.25	0.57	3.54	6.41	0.08	100.94		314	2446	23
ME08-03-02	L6-S	24 / 1 .			74.46	0.42	12.65	2.28	0.07	0.25	0.60	3.75	6.25	0.05	101.14		558	2601	18
ME08-03-02	L6-S	25 / 1 .			74.92	0.48	12.49	2.32	0.11	0.21	0.60	3.51	6.40	0.09	101.51		653	2577	122
ME08-03-02	L6-S	26 / 1 .			74.66	0.48	12.71	2.06	0.07	0.34	0.49	3.46	6.36	0.07	101.17		1488	2214	n.d.
ME08-03-02	L6-S	27 / 1 .			74.33	0.49	12.30	2.42	0.17	0.23	0.59	3.63	6.20	0.05	100.87		879	2387	n.d.
ME08-03-02	L6-S	28 / 1 .			74.25	0.46	12.50	2.47	0.04	0.28	0.52	3.64	6.42	0.02	100.97		428	2483	95
ME08-04-01	L8-S	1 / 1 .			72.57	0.58	13.60	2.57	0.04	0.20	0.58	4.25	6.34	0.09	101.11		749	1824	n.d.
ME08-04-01	L8-S	2 / 1 .			72.78	0.52	13.33	2.53	0.08	0.25	0.63	3.97	6.35	0.12	100.99		1080	2084	32
ME08-04-01	L8-S	3 / 1 .			71.70	0.60	13.58	2.60	0.15	0.25	0.53	4.14	6.38	0.10	100.37		1096	1779	n.d.
ME08-04-01	L8-S	4 / 1 .			72.76	0.54	13.84	2.80	0.10	0.28	0.90	3.57	6.12	0.13	101.39		1175	1889	27
ME08-04-01	L8-S	5 / 1 .			72.79	0.48	13.41	2.67	0.21	0.24	0.62	4.04	6.46	0.13	101.41		664	1980	n.d.
ME08-04-01	L8-S	6 / 1 .			72.72	0.50	13.74	2.70	0.02	0.24	0.57	3.90	6.48	0.12	101.36		1372	1981	n.d.
ME08-04-01	L8-S	7 / 1 .			71.79	0.45	14.71	2.35	0.13	0.22	0.86	4.39	5.85	0.07	101.13		735	1794	n.d.
ME08-04-01	L8-S	9 / 1 .			73.05	0.48	13.97	2.53	-0.01	0.20	0.59	4.42	6.63	0.11	102.28		1012	1643	23
ME08-04-01	L8-S	10 / 1 .			72.37	0.50	13.42	2.56	0.13	0.23	0.64	4.09	6.56	0.10	100.92		905	1852	108
ME08-07	L10-S	29 / 1 .			72.88	0.49	13.46	2.35	0.09	0.20	0.64	4.14	6.73	0.08	101.43		1644	1940	n.d.
ME08-07	L10-S	30 / 1 .			72.28	0.47	13.93	2.25	0.15	0.30	0.55	4.14	6.62	0.07	101.07		728	1780	n.d.
ME08-07	L10-S	31 / 1 .			72.17	0.54	13.53	2.51	0.09	0.24	0.58	3.87	6.53	0.10	100.47		576	1908	n.d.
ME08-07	L10-S	32 / 1 .			72.24	0.46	13.40	2.36	0.16	0.25	0.54	3.98	6.35	0.07	100.06		100	2226	n.d.
ME08-07	L10-S	33 / 1 .			73.23	0.51	13.78	2.23	0.09	0.23	0.54	3.99	6.51	0.08	101.50		806	1603	32
ME08-07	L10-S	34 / 1 .			73.28	0.49	13.59	2.20	0.13	0.28	0.52	4.13	6.42	0.09	101.46		987	1670	14
ME08-07	L10-S	35 / 1 .			72.87	0.45	13.60	2.41	0.11	0.24	0.56	4.07	6.50	0.12	101.19		789	1623	n.d.
ME08-07	L10-S	36 / 1 .			73.36	0.49	13.61	2.40	0.20	0.29	0.59	4.04	6.50	0.10	102.06		828	1640	58
ME08-07	L10-S	37 / 1 .			73.35	0.48	13.47	2.44	0.06	0.20	0.56	3.84	6.67	0.08	101.56		1048	1762	n.d.
ME08-07	L10-S	38 / 1 .			72.35	0.49	13.38	2.38	0.09	0.20	0.59	4.08	6.64	0.13	100.63		667	1811	32
ME08-08-03	L1-D	11 / 1 .			72.69	0.46	13.50	2.06	0.07	0.21	0.60	3.72	6.50	0.07	100.17		543	1754	32

[1] Major element oxides in wt.%; volatile elements (F, Cl, S) in ppm; [2] see Appendix A; n.d. = not detected

Table E2 Major element and volatile (F, Cl, S) concentrations in groundmass glass in the 2006 Merapi eruption products (continued)

Sample	Sample Type	Point			SiO_2	TiO_2	Al_2O_3	FeO	MnO	MgO	CaO	Na_2O	K_2O	P_2O_5	Sum		F	Cl	S
ME08-08-03	L1-D	12 / 1 .			73.70	0.46	13.64	2.09	0.14	0.25	0.62	3.98	6.54	0.04	101.72		603	1559	45
ME08-08-03	L1-D	13 / 1 .			74.11	0.49	12.97	2.36	0.15	0.25	0.59	3.65	6.25	0.11	101.18		207	1887	95
ME08-08-03	L1-D	16 / 1 .			74.29	0.44	13.24	2.12	0.08	0.17	0.60	3.77	6.49	0.11	101.67		1358	1615	n.d.
ME08-08-03	L1-D	18 / 1 .			74.05	0.52	12.80	2.51	0.09	0.30	0.59	3.54	6.48	0.08	101.32		832	1989	18
ME08-08-03	L1-D	19 / 1 .			73.74	0.46	13.32	2.22	0.08	0.20	0.63	3.70	6.35	0.05	101.08		1208	1894	27
ME08-09-02	L1-S	1 / 1 .			72.14	0.54	13.49	2.51	0.08	0.21	0.68	3.98	6.65	0.10	100.72		563	2545	41
ME08-09-02	L1-S	2 / 1 .			71.80	0.58	13.43	2.69	0.10	0.21	0.66	3.89	6.58	0.11	100.47		1306	2737	77
ME08-09-02	L1-S	3 / 1 .			72.22	0.53	13.65	2.50	0.15	0.20	0.65	4.03	6.49	0.11	100.79		263	2236	5
ME08-09-02	L1-S	4 / 1 .			72.26	0.57	13.55	2.68	0.12	0.20	0.71	4.00	6.38	0.11	100.98		954	2590	n.d.
ME08-09-02	L1-S	5 / 1 .			72.27	0.58	13.48	2.47	0.13	0.22	0.65	3.83	6.37	0.14	100.51		1054	2739	n.d.
ME08-09-02	L1-S	6 / 1 .			72.23	0.57	14.16	2.72	0.06	0.20	0.69	4.10	6.49	0.09	101.81		906	2915	14
ME08-09-02	L1-S	7 / 1 .			72.46	0.62	13.42	2.37	0.18	0.24	0.66	3.97	6.41	0.13	100.80		579	2544	5
ME08-09-02	L1-S	9 / 1 .			72.29	0.57	13.54	2.60	0.07	0.24	0.61	4.10	6.09	0.13	100.68		1047	2305	n.d.
ME08-09-02	L1-S	10 / 1 .			71.02	0.57	13.86	2.67	0.11	0.22	0.67	4.18	6.34	0.09	100.28		965	2915	n.d.
ME08-10	KB-S	11 / 1 .			74.70	0.43	12.74	2.13	0.08	0.18	0.44	3.59	6.77	0.05	101.28		768	806	n.d.
ME08-10	KB-S	12 / 1 .			73.82	0.48	12.72	2.21	0.12	0.22	0.44	3.95	6.55	0.06	100.71		774	622	n.d.
ME08-10	KB-S	13 / 1 .			74.05	0.46	12.30	2.29	0.02	0.23	0.49	4.01	6.40	0.05	100.61		810	367	n.d.
ME08-10	KB-S	14 / 1 .			73.91	0.49	12.40	2.48	0.08	0.23	0.27	3.78	6.40	0.08	100.31		248	669	18
ME08-10	KB-S	15 / 1 .			74.79	0.47	12.75	2.45	0.09	0.18	0.56	3.71	6.52	0.09	101.90		1196	1433	n.d.
ME08-10	KB-S	16 / 1 .			75.32	0.42	12.70	2.06	0.09	0.14	0.42	3.39	6.58	0.06	101.42		905	1206	118
ME08-10	KB-S	18 / 1 .			74.44	0.43	13.36	1.50	0.02	0.12	0.35	3.68	6.56	0.06	100.68		748	443	n.d.
ME08-14	SD-S	31 / 1 .			75.30	0.45	12.09	2.19	0.11	0.10	0.42	3.52	6.24	0.10	100.65		n.d.	1206	n.d.
ME08-14	SD-S	32 / 1 .			74.65	0.48	13.46	1.70	0.04	0.09	0.48	4.12	5.91	0.09	101.14		27	801	n.d.
ME08-14	SD-S	33 / 1 .			73.10	0.40	13.94	1.58	0.04	0.11	0.38	4.07	7.02	0.08	100.87		n.d.	1006	9

Table E3 Major element and volatile (F, Cl, S) concentrations in melt inclusions in the 2010 Merapi eruption products obtained by electron microprobe analysis[1]

Sample	Sample Type[2]	Point	Host Mineral[3]		SiO_2	TiO_2	Al_2O_3	FeO	MnO	MgO	CaO	Na_2O	K_2O	P_2O_5	Sum		F	Cl	S
M11-02	DS	4 / 1 .	cpx		66.08	0.40	16.28	2.72	0.17	0.26	1.34	7.10	5.77	0.10	100.20		959	2610	26
M11-02	DS	5 / 1 .	cpx		64.97	0.38	16.25	2.98	0.13	0.69	2.15	6.70	5.50	0.08	99.83		1067	2743	139
M11-02	DS	7 / 1 .	cpx		66.53	0.51	15.63	2.05	0.16	0.68	1.58	4.93	5.09	0.15	97.31		1211	2659	306
M11-02	DS	9 / 1 .	cpx		67.10	0.40	16.37	2.67	0.06	0.67	1.83	4.73	5.38	0.11	99.33		1500	2837	181
M11-02	DS	11 / 1 .	cpx		64.95	0.45	14.69	2.32	0.15	1.38	2.57	4.23	5.18	0.20	96.13		2483	2906	254
M11-02	DS	12 / 1 .	cpx		65.60	0.39	15.89	1.85	0.07	0.52	1.68	4.86	5.25	0.17	96.30		2097	3044	226
M11-02	DS	14 / 1 .	cpx		64.73	0.40	16.20	2.21	0.15	0.67	1.55	4.98	4.82	0.18	95.90		1263	2434	206
M11-02	DS	16 / 1 .	cpx		63.85	0.77	16.43	3.34	0.03	0.26	1.33	7.79	5.90	0.15	99.85		714	2617	125
M11-02	DS	18 / 1 .	cpx		65.17	0.36	15.74	2.34	0.06	1.15	2.09	4.94	4.20	0.19	96.24		1297	2620	134
M11-02	DS	20 / 1 .	cpx		64.51	0.61	15.94	3.55	0.09	0.33	1.27	7.94	5.46	0.11	99.80		1691	1491	76
M11-06	DS	1 / 1 .	cpx		66.80	0.38	15.57	2.70	0.13	0.24	1.62	5.39	6.92	0.14	99.90		2245	2918	207
M11-06	DS	3 / 1 .	cpx		64.25	0.13	16.56	0.96	0.00	0.02	0.64	7.10	4.87	0.12	94.64		1494	713	126
M11-06	DS	9 / 1 .	cpx		65.65	0.41	18.00	2.56	0.08	0.71	1.82	5.31	5.72	0.19	100.45		1057	2657	228
M11-06	DS	11 / 1 .	cpx		63.60	0.45	17.50	2.23	0.11	0.34	2.57	5.48	4.38	0.25	96.91		1458	2657	276
M11-06	DS	13 / 1 .	cpx		65.86	0.36	15.72	2.98	0.19	0.27	1.58	5.38	7.29	0.13	99.75		1436	2625	89
M11-06	DS	16 / 1 .	cpx		68.16	0.54	15.79	2.83	0.04	0.34	2.47	4.56	6.56	0.19	101.50		1332	2445	188
M11-06	DS	18 / 1 .	cpx		67.08	0.42	15.93	2.42	0.01	0.30	1.57	5.26	4.28	0.13	97.41		1388	2748	160
M11-07	DD	6 / 1 .	cpx		68.00	0.44	15.16	2.91	0.09	0.50	1.47	5.17	5.01	0.12	98.88		402	2640	104
M11-07	DD	57 / 1 .	cpx		68.87	0.31	15.39	2.11	0.12	0.53	1.47	5.01	4.88	0.03	98.73		977	3047	9
M11-18	WP	2 / 1 .	cpx		65.78	0.28	18.19	1.67	0.07	0.22	2.82	5.27	4.49	0.07	98.87		1750	1920	35
M11-26a	DD	9 / 1 .	cpx		66.24	0.50	17.68	3.59	0.15	0.51	2.02	4.25	5.91	0.17	101.03		770	3217	n.d.
M11-26a	DD	10 / 1 .	cpx		66.41	0.52	17.33	3.49	0.23	0.47	1.67	4.65	6.46	0.17	101.42		667	2982	15
M11-27-1	DD	1 / 1 .	cpx		66.05	0.46	15.05	3.08	0.14	0.34	1.54	5.69	5.03	0.16	97.55		2088	2642	210
M11-27-1	DD	3 / 1 .	cpx		67.87	0.40	16.12	2.93	0.15	0.36	1.13	4.91	6.69	0.10	100.66		1977	2869	118
M11-27-1	DD	4 / 1 .	cpx		68.90	0.77	15.59	0.68	0.05	0.00	1.95	4.46	5.20	0.15	97.75		833	1720	124
M11-27-1	DD	6 / 1 .	cpx		67.28	0.44	15.79	2.45	0.15	0.29	1.13	5.28	6.94	0.13	99.89		926	2925	268
M11-27-1	DD	7 / 1 .	cpx		67.08	0.39	16.41	2.48	0.07	0.27	1.24	5.29	6.84	0.11	100.19		1384	2745	96
M11-27-1	DD	10 / 1 .	cpx		66.56	0.37	15.68	2.82	0.14	0.28	1.20	5.00	6.52	0.11	98.68		1445	2850	139
M11-27-1	DD	12 / 1 .	cpx		68.45	0.36	16.03	2.71	0.16	0.28	1.11	4.95	6.98	0.11	101.13		1999	2700	152
M11-27-1	DD	14 / 1 .	cpx		68.02	0.48	15.85	2.88	0.20	0.39	1.13	4.73	6.94	0.10	100.71		345	2668	70
M11-27-1	DD	19 / 1 .	cpx		66.45	0.42	16.24	3.05	0.15	0.33	1.40	5.80	6.29	0.12	100.26		826	2649	220
M11-27-2	DD	10 / 1 .	cpx		67.49	0.49	15.50	3.05	0.13	0.49	1.59	4.99	5.03	0.10	98.85		1871	2645	141
M11-27-5	DD	n.a.	cpx		64.11	0.38	15.32	2.84	0.13	0.16	0.90	5.65	5.50	0.16	95.13		n.d.	2940	95
M11-27-5	DD	n.a.	cpx		63.98	0.35	14.91	2.87	0.14	0.77	1.81	5.42	6.27	0.12	96.64		670	2770	40
M11-27-5	DD	n.a.	cpx		66.71	0.41	15.61	2.95	0.20	0.81	1.85	4.60	6.27	0.12	99.52		330	2700	n.d.
M11-27-5	DD	n.a.	cpx		67.29	0.44	16.16	1.66	0.06	0.07	1.73	5.00	4.88	0.17	97.45		n.d.	2350	225
M11-27-5	DD	n.a.	cpx		65.65	0.40	16.70	1.87	0.04	0.38	2.50	4.69	4.07	0.20	96.50		740	2060	355
M11-27-5	DD	n.a.	cpx		68.78	0.34	16.81	0.83	0.07	0.20	1.92	4.87	5.12	0.16	99.09		760	3150	210
M11-27-5	DD	n.a.	cpx		67.52	0.44	15.97	2.67	0.13	0.29	1.22	5.13	6.31	0.13	99.81		450	2690	105
M11-27-5	DD	n.a.	cpx		67.29	0.40	15.92	2.78	0.12	0.28	1.23	4.98	6.22	0.12	99.32		270	2820	45

[1] Major element oxides in wt.%; volatile elements (F, Cl, S) in ppm; [2] see Appendix A; [3] host mineral: cpx = clinopyroxene, am = amphibole, pl = plagioclase; [4] connected to groundmass; n.d. = not detected

Table E3 Major element and volatile (F, Cl, S) concentrations in melt inclusions in the 2010 Merapi eruption products (continued)

Sample	Sample Type	Point	Host Mineral		SiO_2	TiO_2	Al_2O_3	FeO	MnO	MgO	CaO	Na_2O	K_2O	P_2O_5	Sum		F	Cl	S
M11-27-5	DD	n.a.	cpx		63.58	0.42	14.91	3.05	0.12	0.51	1.81	4.08	6.33	0.18	95.00		510	2610	10
M11-27-5	DD	n.a.	cpx		66.93	0.38	16.36	2.76	0.12	0.36	1.52	4.88	6.22	0.15	99.67		1130	2830	10
M11-27-5	DD	n.a.	cpx		67.03	0.50	16.73	2.40	0.06	0.09	0.57	6.52	5.82	0.13	99.83		1210	2880	110
M11-27-5	DD	n.a.	cpx		66.81	0.45	16.76	2.22	0.06	0.04	0.47	6.64	5.91	0.10	99.45		1400	2430	215
M11-28a	P5N-Sc	24 / 1 .	cpx		65.41	0.29	15.94	2.21	0.11	0.73	2.25	4.78	4.43	0.10	96.25		n.d.	2390	135
M11-28a	P5N-Sc	25 / 1 .	cpx		65.72	0.29	16.04	2.23	0.15	0.61	1.99	2.71	4.42	0.13	94.27		1570	2590	300
M11-28a	P5N-Sc	27 / 1 .	cpx[4]		68.47	0.36	15.95	2.10	0.13	0.32	1.07	4.78	5.91	0.14	99.24		480	2600	10
M11-28a	P5N-Sc	28 / 1 .	cpx[4]		68.06	0.35	16.20	2.09	0.10	0.31	1.05	4.78	5.84	0.15	98.93		660	2910	n.d.
M11-33	WP	16 / 1 .	am		66.23	0.42	16.62	2.93	0.14	0.42	1.81	5.13	5.32	0.17	99.19		444	2762	163
M11-50	WP	n.a.	cpx		65.50	0.38	16.83	2.80	0.11	0.53	1.59	5.26	5.57	0.15	98.70		2390	2670	90
M11-50	WP	n.a.	cpx		64.50	0.37	16.51	2.87	0.12	0.52	1.57	4.85	5.65	0.15	97.10		1090	2650	110
M11-50	WP	n.a.	cpx		65.03	0.39	16.31	2.84	0.11	0.53	1.76	5.24	4.90	0.19	97.29		460	2470	120
M11-50	WP	n.a.	cpx		62.20	0.32	17.74	2.72	0.12	0.54	3.20	4.30	4.77	0.17	96.09		930	3960	390
M11-50	WP	n.a.	cpx		67.01	0.42	16.02	2.60	0.12	0.82	1.76	4.92	5.42	0.16	99.24		1070	2900	80
M11-50	WP	n.a.	cpx		65.79	0.40	15.62	2.84	0.11	1.07	2.04	4.81	5.35	0.13	98.17		270	2830	105
M11-50	WP	n.a.	cpx		69.47	0.33	13.72	2.00	0.08	0.25	0.75	3.91	6.09	0.08	96.67		830	5130	110
M11-50	WP	n.a.	cpx		70.44	0.36	13.96	2.13	0.09	0.29	0.87	4.07	5.95	0.04	98.19		750	4570	55
M11-50	WP	n.a.	cpx		66.92	0.36	15.81	2.56	0.13	0.60	1.93	4.65	4.69	0.15	97.82		370	2770	135
M11-50	WP	n.a.	cpx		67.90	0.36	15.34	2.56	0.11	0.51	1.34	4.92	5.44	0.10	98.57		570	3020	95
M11-50	WP	n.a.	cpx		67.71	0.39	16.09	2.45	0.07	0.41	1.29	5.06	5.61	0.13	99.21		260	2900	85
M11-50	WP	n.a.	cpx		67.87	0.42	15.99	2.45	0.12	0.39	1.24	4.93	5.56	0.12	99.09		510	2970	125
M11-50	WP	n.a.	cpx		67.94	0.36	16.20	2.54	0.11	0.45	1.32	4.97	5.66	0.10	99.63		n.d.	2840	75
M11-50	WP	n.a.	cpx		67.83	0.41	15.98	2.57	0.12	0.46	1.31	4.85	5.61	0.12	99.28		850	2810	170
M11-50	WP	n.a.	cpx		67.62	0.37	16.00	2.60	0.12	0.43	1.35	4.80	5.63	0.12	99.04		710	2860	140
M11-50	WP	n.a.	cpx		67.48	0.37	15.99	2.60	0.14	0.43	1.36	4.97	5.57	0.11	99.03		760	2890	85
M11-50	WP	n.a.	cpx		64.27	0.28	15.24	2.67	0.11	0.97	2.16	5.00	5.26	0.14	96.09		1740	2470	20
M11-50	WP	n.a.	cpx		68.07	0.36	15.47	2.84	0.12	0.90	2.20	4.75	5.43	0.14	100.26		420	2660	90
M11-50	WP	n.a.	cpx		67.85	0.43	15.98	2.74	0.11	0.43	1.43	4.88	5.54	0.11	99.49		n.d.	2810	130
M11-50	WP	n.a.	cpx		67.32	0.37	16.22	2.59	0.09	0.44	1.44	5.00	5.56	0.11	99.12		870	2550	275
M11-50	WP	n.a.	cpx		65.73	0.45	15.86	2.57	0.12	0.57	1.41	4.36	5.32	0.12	96.51		810	3220	160
M11-51	GS	43 / 1 .	am		66.55	0.31	16.80	2.94	0.15	0.50	1.74	5.43	6.28	0.13	100.83		504	2958	70
M11-51	GS	44 / 1 .	pl		69.61	0.60	14.56	3.52	0.08	0.58	0.89	4.01	6.10	0.11	100.06		408	2820	70
M11-53-B4	P5N-WP	48 / 1 .	cpx		69.00	0.30	16.86	1.58	0.08	0.28	0.93	4.64	6.68	0.10	100.44		635	2298	n.d.
M11-53-B4	P5N-WP	49 / 1 .	cpx		69.84	0.32	14.84	1.82	0.09	0.18	0.54	4.29	6.30	0.08	98.31		948	3215	942
M11-54-3	DD	54 / 1 .	cpx		67.52	0.44	15.61	2.77	0.13	0.35	1.55	5.16	6.07	0.14	99.74		800	2730	110
M11-54-3	DD	55 / 1 .	cpx		67.34	0.37	15.79	2.72	0.11	0.29	1.49	4.99	6.12	0.12	99.34		n.d.	2780	95
M11-55	WP	1 / 1 .	cpx		64.85	0.42	16.49	2.47	0.06	1.12	2.94	4.54	4.97	0.21	98.07		n.d.	4130	460
M11-55	WP	2 / 1 .	cpx		65.19	0.42	16.85	2.35	0.08	0.65	2.08	4.29	5.19	0.22	97.32		580	3900	475
M11-55	WP	4 / 1 .	cpx		64.86	0.30	17.32	2.29	0.08	0.72	2.27	4.77	4.50	0.12	97.24		1240	3960	255
M11-55	WP	6 / 1 .	cpx		66.69	0.42	15.14	2.14	0.09	0.47	1.18	4.16	6.00	0.24	96.52		850	4300	175

Table E3 Major element and volatile (F, Cl, S) concentrations in melt inclusions in the 2010 Merapi eruption products (continued)

Sample	Sample Type	Point	Host Mineral		SiO_2	TiO_2	Al_2O_3	FeO	MnO	MgO	CaO	Na_2O	K_2O	P_2O_5	Sum		F	Cl	S
M11-55	WP	42 / 1 .	cpx		68.75	0.41	15.25	1.97	0.13	0.48	1.14	4.42	5.49	0.10	98.13		1320	2950	130
M11-55	WP	n.a.	cpx		70.55	0.29	14.14	2.12	0.07	0.28	0.76	4.26	5.84	0.03	98.35		420	2440	45
M11-55	WP	n.a.	cpx		68.80	0.29	14.41	2.43	0.12	0.58	1.31	4.42	6.00	0.07	98.43		1060	3810	n.d.
M11-55	WP	n.a.	cpx		70.55	0.36	14.21	2.22	0.10	0.30	0.88	4.54	5.65	0.05	98.85		930	2820	50
M11-55	WP	n.a.	cpx		66.81	0.44	15.34	2.29	0.12	0.37	1.03	4.85	5.82	0.08	97.13		1110	3850	80
M11-75	GS	5 / 1 .	cpx		66.51	0.42	15.52	3.09	0.14	1.16	2.44	4.53	4.71	0.14	98.66		760	2980	410
M11-75	GS	14 / 1 .	am		66.21	0.30	16.57	3.02	0.14	0.42	0.88	6.13	6.03	0.13	99.83		480	2540	75
M11-75	GS	n.a.	cpx		67.87	0.48	16.25	2.41	0.07	0.24	1.22	6.04	5.29	0.11	99.99		n.d.	2910	60
M11-75	GS	n.a.	cpx		67.42	0.43	16.34	2.62	0.12	0.18	1.05	6.22	5.18	0.16	99.72		970	2710	45
M11-75	GS	n.a.	cpx		66.06	0.50	16.48	2.25	0.09	0.36	1.55	4.62	5.46	0.14	97.50		1160	3470	205
M11-75	GS	n.a.	cpx		65.03	0.40	15.31	1.94	0.08	0.50	1.66	4.87	5.10	0.22	95.12		660	3200	80
M11-75	GS	n.a.	cpx		62.66	0.54	16.45	2.75	0.11	0.40	1.90	4.32	4.63	0.25	94.00		560	2760	180
M11-75	GS	n.a.	cpx		64.73	0.42	15.89	1.93	0.06	0.54	1.61	4.70	5.13	0.17	95.17		n.d.	3180	315
M11-75	GS	n.a.	cpx		65.58	0.41	16.07	1.79	0.06	0.33	1.60	4.64	5.10	0.15	95.74		310	3260	220
M11-75	GS	n.a.	cpx		64.50	0.41	15.89	1.89	0.11	0.46	1.58	4.46	5.12	0.15	94.57		n.d.	3300	245
M11-75	GS	n.a.	cpx		67.30	0.38	16.04	1.90	0.09	0.25	1.30	4.79	5.22	0.12	97.38		750	2860	180
M11-75	GS	n.a.	cpx		67.85	0.40	16.82	1.79	0.09	0.16	1.52	4.98	4.93	0.14	98.69		140	2770	445
M11-75	GS	n.a.	cpx		69.15	0.50	16.60	1.76	0.08	0.23	1.38	5.40	4.90	0.12	100.10		1480	2620	90
M11-80	DD	39 / 1 .	am		64.92	0.60	16.01	3.09	0.16	0.88	1.63	4.58	6.02	0.12	98.01		2440	2450	50
M11-93	DS	3 / 1 .	cpx		68.32	0.40	17.18	2.36	0.12	0.25	1.22	3.73	6.05	0.12	99.75		1196	3204	80
M11-130	LG-Inc	n.a.	cpx		78.48	0.45	10.98	1.27	0.03	0.08	0.29	2.86	5.69	0.04	100.17		840	1850	n.d.
M11-130	LG-Inc	n.a.	cpx		78.25	0.45	11.00	1.23	0.03	0.07	0.28	2.86	5.72	0.05	99.92		n.d.	1940	n.d.
M11-130	LG-Inc	n.a.	cpx		69.71	0.24	16.31	1.45	0.05	0.29	1.23	4.58	5.55	0.19	99.59		1040	3660	30
M11-130	LG-Inc	n.a.	cpx		69.49	0.24	16.32	1.25	0.05	0.27	1.24	4.71	5.56	0.24	99.38		1190	3590	75
M11-131	DD	19 / 1 .	cpx		67.51	0.43	15.39	2.69	0.13	0.55	1.62	4.04	6.16	0.10	98.61		920	2780	80
M11-131	DD	20 / 1 .	cpx		67.66	0.36	15.81	2.56	0.05	0.11	0.53	5.07	6.04	0.08	98.27		1110	3410	115
DD10	DD10	25 / 1 .	cpx		67.28	0.61	16.11	3.69	0.21	0.36	1.66	4.74	6.42	0.11	101.17		533	2368	186
DD10	DD10	28 / 1 .	cpx		66.90	0.40	15.69	3.24	0.12	0.21	1.58	5.21	6.26	0.10	99.72		1232	2488	235

Table E4 Major element and volatile (F, Cl, S) concentrations in groundmass glass in the 2010 Merapi eruption products obtained by electron microprobe analysis[1]

Sample	Sample Type[2]	Point			SiO_2	TiO_2	Al_2O_3	FeO	MnO	MgO	CaO	Na_2O	K_2O	P_2O_5	Sum		F	Cl	S
M11-02	DS	5 / 1 .			67.57	0.44	15.86	2.60	0.16	0.74	1.85	5.13	5.15	0.15	100.01		1384	1823	36
M11-06	DS	28 / 1 .			66.99	0.41	15.70	3.22	0.18	0.71	1.49	4.72	6.75	0.14	100.94		1785	2428	49
M11-28a	P5N-Sc	2 / 1 .			70.52	0.38	15.49	2.24	0.13	0.33	1.36	4.72	5.48	0.09	101.02		280	2380	5
M11-28a	P5N-Sc	3 / 1 .			68.33	0.36	14.58	2.34	0.11	0.33	1.19	4.29	5.58	0.06	97.44		340	2390	40
M11-33	WP	48 / 1 .			68.82	0.39	15.57	2.19	0.11	0.33	1.41	4.65	5.63	0.11	99.61		1121	2749	45
M11-33	WP	50 / 1 .			67.61	0.43	15.18	3.77	0.23	0.41	1.36	3.79	5.39	0.14	98.55		632	1834	n.d.
M11-33	WP	51 / 1 .			68.22	0.48	14.45	2.07	0.09	0.40	1.10	4.15	5.98	0.12	97.62		1825	3550	30
M11-50	WP	6 / 1 .			69.15	0.34	16.23	2.58	0.11	0.45	1.24	4.86	5.58	0.12	100.95		290	2570	30
M11-50	WP	7 / 1 .			68.48	0.34	15.17	2.40	0.11	0.43	1.34	4.47	5.19	0.14	98.48		1520	2410	150
M11-50	WP	8 / 1 .			68.22	0.42	14.99	2.37	0.10	0.36	1.14	4.25	5.28	0.13	97.57		460	2580	155
M11-50	WP	18 / 1 .			68.59	0.27	17.30	1.86	0.07	0.31	1.87	5.07	5.15	0.09	100.89		890	1980	115
M11-51	GS	72 / 1 .			70.22	0.51	14.97	2.55	0.12	0.28	1.07	4.25	6.47	0.15	100.85		2305	476	5
M11-51	GS	73 / 1 .			71.57	0.52	14.67	2.30	0.18	0.31	0.88	3.93	6.60	0.18	101.46		2191	923	35
M11-51	GS	74 / 1 .			72.24	0.52	14.48	2.40	0.12	0.29	0.78	3.88	6.35	0.10	101.44		2308	466	50
M11-51	GS	75 / 1 .			71.30	0.49	14.27	2.48	0.15	0.52	0.75	3.99	6.39	0.20	100.79		1854	702	5
M11-51	GS	76 / 1 .			70.70	0.47	15.01	2.17	0.13	0.23	1.04	4.23	6.35	0.12	100.66		1603	458	70
M11-53-B3	DS	19 / 1 .			68.50	0.42	15.95	2.71	0.10	0.54	1.41	4.42	5.91	0.14	100.40		2138	957	n.d.
M11-53-B3	DS	20 / 1 .			67.41	0.44	15.63	2.78	0.14	0.53	1.22	4.45	5.86	0.12	98.79		2098	n.d.	n.d.
M11-53-B3	DS	21 / 1 .			68.98	0.47	15.86	2.85	0.14	0.47	1.21	4.60	6.04	0.11	101.00		2256	517	n.d.
M11-53-B3	DS	22 / 1 .			69.09	0.44	16.11	2.70	0.04	0.54	1.37	4.58	5.91	0.13	101.19		2478	277	70
M11-53-B3	DS	23 / 1 .			69.42	0.55	15.55	2.92	0.12	0.38	1.21	4.28	5.95	0.17	100.92		2509	1314	10
M11-53-B3	DS	24 / 1 .			69.30	0.53	15.72	2.89	0.21	0.43	1.23	4.36	5.93	0.14	101.08		2637	879	n.d.
M11-53-B3	DS	25 / 1 .			69.40	0.53	15.78	2.89	0.15	0.48	1.31	4.52	6.03	0.18	101.54		2123	490	18
M11-53-B3	DS	26 / 1 .			69.01	0.51	15.82	2.75	0.16	0.44	1.19	4.53	5.85	0.16	100.69		2243	414	50
M11-53-B3	DS	27 / 1 .			68.99	0.48	15.65	2.73	0.07	0.42	1.24	4.46	6.04	0.19	100.65		2575	1255	n.d.
M11-53-B3	DS	28 / 1 .			69.40	0.50	15.64	2.85	0.16	0.44	1.27	4.60	5.80	0.15	101.11		2439	664	25
M11-53-B3	DS	29 / 1 .			69.17	0.48	15.81	2.71	0.10	0.43	1.34	4.40	5.82	0.18	100.77		2411	836	n.d.
M11-53-B3	DS	30 / 1 .			68.25	0.43	15.44	2.63	0.12	0.44	1.27	4.16	5.92	0.16	99.14		2394	799	80
M11-53-B4	P5N-WP	75 / 1 .			76.20	0.35	12.30	1.39	0.00	0.15	0.35	3.12	6.06	0.03	100.15		1187	746	n.d.
M11-53-B4	P5N-WP	77 / 1 .			76.31	0.32	12.40	1.33	0.05	0.10	0.31	3.22	6.17	0.04	100.33		790	n.d.	n.d.
M11-53-B4	P5N-WP	78 / 1 .			76.58	0.33	12.72	1.23	0.00	0.12	0.29	3.25	6.12	0.02	100.83		1012	633	n.d.
M11-53-B4	P5N-WP	79 / 1 .			75.88	0.33	12.92	1.02	0.02	0.10	0.44	3.18	6.09	0.03	100.07		686	n.d.	n.d.
M11-53-B4	P5N-WP	80 / 1 .			75.69	0.33	12.56	1.27	0.00	0.11	0.24	3.29	6.20	0.00	99.90		1213	663	65
M11-53-B4	P5N-WP	81 / 1 .			75.94	0.31	12.53	1.46	0.05	0.13	0.29	3.11	6.17	0.04	100.21		954	628	40
M11-53-B4	P5N-WP	82 / 1 .			76.31	0.34	12.32	1.27	0.00	0.12	0.31	3.03	6.26	0.01	100.08		851	n.d.	68
M11-53-B4	P5N-WP	83 / 1 .			74.30	0.31	12.32	1.25	0.07	0.12	0.25	3.11	6.00	0.03	97.96		1487	292	55
M11-53-B4	P5N-WP	84 / 1 .			77.00	0.34	12.53	1.30	0.05	0.13	0.18	3.26	6.06	0.01	101.16		1507	1511	n.d.
M11-55	WP	104 / 1 .			69.52	0.25	15.18	1.62	0.08	0.19	1.17	4.78	5.49	0.06	98.59		550	1860	50
M11-61	WP	23 / 1 .			68.33	0.41	14.90	1.92	0.13	0.32	1.08	4.01	5.78	0.10	97.47		2199	2758	9
M11-61	WP	25 / 1 .			70.27	0.45	14.52	2.33	0.07	0.35	0.86	3.59	6.09	0.08	98.94		1095	2209	5

[1] Major element oxides in wt.%; volatile elements (F, Cl, S) in ppm; [2] see Appendix A; n.d. = not detected

Table E4 Major element and volatile (F, Cl, S) concentrations in groundmass glass in the 2010 Merapi eruption products (continued)

Sample	Sample Type	Point			SiO_2	TiO_2	Al_2O_3	FeO	MnO	MgO	CaO	Na_2O	K_2O	P_2O_5	Sum		F	Cl	S
M11-75	GS	43 / 1 .			70.65	0.41	15.16	2.36	0.12	0.25	1.16	4.21	5.81	0.13	100.50		370	1910	95
M11-75	GS	44 / 1 .			70.21	0.40	15.55	2.40	0.10	0.33	1.38	4.65	5.59	0.16	100.96		630	1390	n.d.
M11-75	GS	45 / 1 .			69.78	0.41	14.96	2.32	0.12	0.26	1.14	4.44	5.46	0.13	99.27		390	1820	15
M11-75	GS	46 / 1 .			70.33	0.44	15.10	2.60	0.12	0.40	1.18	4.26	5.81	0.16	100.80		1020	3060	n.d.
M11-75	GS	47 / 1 .			70.67	0.46	14.78	2.49	0.13	0.28	1.03	4.17	5.73	0.15	100.11		490	1720	n.d.
M11-75	GS	48 / 1 .			70.76	0.52	14.66	2.50	0.09	0.34	0.93	4.15	5.84	0.18	100.14		180	1680	n.d.
M11-75	GS	49 / 1 .			71.17	0.49	14.48	2.45	0.14	0.29	0.90	4.17	5.83	0.18	100.43		1050	2060	70
M11-75	GS	50 / 1 .			70.92	0.41	15.04	2.43	0.11	0.31	1.02	4.39	5.96	0.14	101.04		1540	1540	n.d.
M11-93	DS	38 / 1 .			72.43	0.42	13.80	2.27	0.09	0.16	0.58	3.87	6.47	0.08	100.45		1332	1477	n.d.
M11-93	DS	39 / 1 .			72.53	0.43	13.62	2.05	0.12	0.22	0.58	3.95	6.39	0.04	100.16		221	2071	n.d.
M11-93	DS	41 / 1 .			72.66	0.44	13.62	2.11	0.08	0.19	0.59	3.86	6.34	0.05	100.13		n.d.	2027	n.d.
M11-131	LG-Inc	48 / 1 .			71.71	0.06	14.79	0.73	0.00	0.04	0.44	3.79	6.75	0.01	98.56		1360	1000	10
M11-131	LG-Inc	49 / 1 .			72.04	0.14	14.30	0.91	0.02	0.09	0.38	3.91	6.58	0.02	98.65		1670	860	n.d.

Table F1 Light lithophile, volatile and some major element concentrations in melt inclusions in the 2006 Merapi eruption products obtained by ion probe analysis[1]

Sample	Sample Type[2]	Point	Host Mineral[3]	H_2O (wt.%)	Li (ppm)	Be (ppm)	B (ppm)	F (ppm)	MgO (wt.%)	TiO_2 (wt.%)	*CO_2 (ppm)*	*MgO (wt. %)*
ME08-09-01	L1-S	20	cpx	3.73	31	1	51	1256	0.87	0.51		
ME08-09-01	L1-S	24	cpx	2.77	29	1	44	1172	0.34	0.60		
ME08-09-01	L1-S	25	cpx	3.33	28	1	44	1009	0.22	0.45	*158*	*0.28*
ME08-09-01	L1-S	26	cpx	1.13	47	2	46	796	0.22	0.47	*3*	*0.22*
ME08-09-01	L1-S	26-2	cpx								*4*	*0.21*
ME08-09-01	L1-S	27	cpx	1.93	63	1	47	1060	0.37	1.22	*510*	*0.22*
ME08-09-01	L1-S	28	cpx	0.65	33	2	51	708	0.34	0.41	*1*	*0.67*
ME08-09-01	L1-S	85	cpx	0.23	34	2	48	887	0.36	0.40	*7*	*0.36*
ME08-09-01	L1-S	86	cpx	0.83	34	1	42	808	0.33	0.47	*2421*	*0.32*
ME08-09-01	L1-S	87	cpx	0.42	20	2	48	882	0.40	0.47	*7*	
ME08-09-01	L1-S	88	cpx	0.82	35	2	47	682	0.36	0.32	*9*	*0.35*
ME08-09-01	L1-S	89	cpx	2.65	30	1	44	1256	0.47	0.41	*134*	

[1] Results shown *in italics* (last two columns) obtained at high mass resolution; [2] see Appendix A; [3] host mineral: cpx = clinopyroxene

Table F2 Light lithophile, volatile and some major element concentrations in melt inclusions in the 2010 Merapi eruption products obtained by ion probe analysis[1]

Sample	Sample Type[2]	Point	Host Mineral[3]	H_2O (wt.%)	Li (ppm)	Be (ppm)	B (ppm)	F (ppm)	MgO (wt.%)	TiO_2 (wt.%)	*CO_2 (ppm)*	*MgO (wt. %)*
M11-27-5	DD	11	cpx	0.84	46	2	43	611	0.18	0.41		
M11-27-5	DD	12	cpx	3.62	26	1	48	723	0.40	0.53		
M11-27-5	DD	103	cpx	0.77	54	1	44	749	0.18	0.42		
M11-27-5	DD	104	cpx	0.25	37	2	45	1104	0.57	0.43		
M11-27-5	DD	105	cpx	2.94	25	1	44	855	0.06	0.34		
M11-27-5	DD	18	cpx	0.78	28	1	45	542	0.10	0.34		
M11-27-5	DD	19	cpx	0.40	43	2	44	517	0.31	0.42		
M11-27-5	DD	106	cpx	2.80	28	1	46	751	0.07	0.86		
M11-27-5	DD	108	cpx	0.22	39	2	48	1078	0.47	0.43		
M11-27-5	DD	99	cpx	0.16	41	2	35	1614	0.79	0.58		
M11-27-5	DD	93	cpx	1.13	68	1	41	982	0.12	0.56	*5*	*0.48*
M11-27-5	DD	94	cpx	1.69	20	1	50	1091	0.55	0.85	*12*	
M11-50	WP	57	cpx	1.90	27	1	45	734	0.49	0.43	*543*	*0.48*
M11-50	WP	58	cpx	3.91	29	1	69	1142	0.70	0.35	*695*	*0.67*
M11-50	WP	59	cpx	2.11	34	1	42	793	0.52	0.36	*97*	*0.52*
M11-50	WP	60	cpx	3.48	24	1	49	921	0.59	0.44	*283*	*0.61*
M11-50	WP	62	cpx	1.19	32	3	84	837	0.34	0.40		*0.44*
M11-50	WP	64	cpx	3.79	29	1	40	1532	0.91	0.42	*534*	*0.55*
M11-50	WP	73	cpx	2.08	31	2	47	915	0.45	0.40	*3016*	*0.44*
M11-50	WP	74	cpx	1.92	30	2	47	821	0.44	0.42	*1167*	*0.43*
M11-50	WP	74-2	cpx								*146*	*0.42*
M11-50	WP	76	cpx	2.19	34	2	44	1019	0.56	0.44		
M11-50	WP	75	cpx	2.23	26	2	51	575	0.26	0.27		
M11-50	WP	77	cpx	3.28	23	2	47	868	0.61	0.39		
M11-50	WP	78	cpx	2.46	30	2	50	772	0.37	0.46	*2213*	*0.37*
M11-50	WP	79	cpx	2.31	33	2	48	874	0.40	0.43	*51*	*0.39*
M11-50	WP	80	cpx	1.91	26	2	45	644	0.40	0.33	*31*	*0.51*
M11-50	WP	81	cpx	1.97	31	2	47	994	0.54	0.40	*15*	*0.42*
M11-50	WP	82	cpx	2.02	30	2	47	937	0.42	0.44		
M11-50	WP	83	cpx	1.88	31	1	47	670	0.48	0.40	*193*	*0.48*

[1] Results shown *in italics* (last two columns) obtained at high mass resolution; [2] see Appendix A; [3] host mineral: cpx = clinopyroxene

Table F2 Light lithophile, volatile and some major element concentrations in melt inclusions in the 2010 Merapi eruption products obtained by ion probe analysis[1]

Sample	Sample Type	Point	Host Mineral	H_2O (wt.%)	Li (ppm)	Be (ppm)	B (ppm)	F (ppm)	MgO (wt.%)	TiO_2 (wt.%)	*CO_2 (ppm)*	*MgO (wt. %)*
M11-55	WP	5	cpx	1.83	29	2	71	565	0.30	0.33		
M11-55	WP	6	cpx	1.62	31	2	70	621	0.35	0.33		
M11-55	WP	7	cpx	2.04	34	2	58	775	0.40	0.42		
M11-55	WP	8	cpx	2.37	31	2	67	673	0.63	0.35		
M11-55	WP	9	cpx	1.38	27	2	55	573	0.58	0.32		
M11-75	GS	49	cpx	1.08	30	2	47	677	0.26	0.43	*109*	*0.26*
M11-75	GS	51	cpx	1.27	34	2	45	976	0.18	0.42	*18*	*0.21*
M11-75	GS	53	cpx	3.66	27	1	49	987	0.42	0.55	*65*	*0.48*
M11-75	GS	54	cpx	1.32	25	2	48	1426	0.25	0.46		
M11-75	GS	56	cpx	3.08	26	1	42	1241	0.31	0.49		
M11-75	GS	50	cpx	3.83	27	1	48	1336	0.54	0.42	*146*	*0.62*
M11-75	GS	44	cpx	3.39	25	2	47	949	0.26	0.43		
M11-75	GS	45	cpx	2.79	25	2	48	845	0.34	0.56	*86*	*0.29*
M11-75	GS	46	cpx	3.94	32	1	41	823	0.20	0.66		
M11-130	LG-Inc	72	cpx	0.14	26	3	109	195	0.09	0.42		
M11-130	LG-Inc	70	cpx	0.35	72	2	52	421	0.29	0.24		

Eruption: 2006
Sample No: ME08-01
Lithology: 2006 dome scoria
Stage: III (Kali Gendol, L4)

Mid Inter	ln(pop den)	ln(min PD)	ln(max PD)	Cry num	Vol %	Vol from inter area (%)	18.01	Size inter	No. of crys
0.2404	6.44	Infinity	7.14	6.95E+01	6.13E+00	**Total number from CSD**	1030000.00	0.1	1
0.1517	7.29	Infinity	8.02	1.02E+02	2.26E+00	**Total vol (%) from CSD**	38.90	0.0631	1
0.0957	10.76	10.42	11.02	2.08E+03	1.16E+01			0.0398	12
0.0604	12.47	12.24	12.65	7.21E+03	1.01E+01			0.0251	27
0.0381	14.05	13.89	14.18	2.21E+04	7.777			0.0158	53
0.024	15.55	15.43	15.65	6.24E+04	5.506			0.01	95
0.0152	16.63	16.52	16.72	1.16E+05	2.572			0.0063	115
0.0096	17.38	17.25	17.48	1.55E+05	0.862			0.004	102
0.006	18.51	18.4	18.61	3.04E+05	0.425			0.0025	124
0.0038	18.71	18.54	18.86	2.35E+05	0.082			0.0016	70
0.0024	18.52	18.14	18.8	1.23E+05	0.01			0.001	31
0.0015	16.73	Infinity	17.73	1.29E+04	0.00E+00			0.0006	4
								0.0004	0

Eruption: 2006
Sample No: ME08-02-02
Lithology: 2006 dome scoria
Stage: III (Kali Gendol, L5)

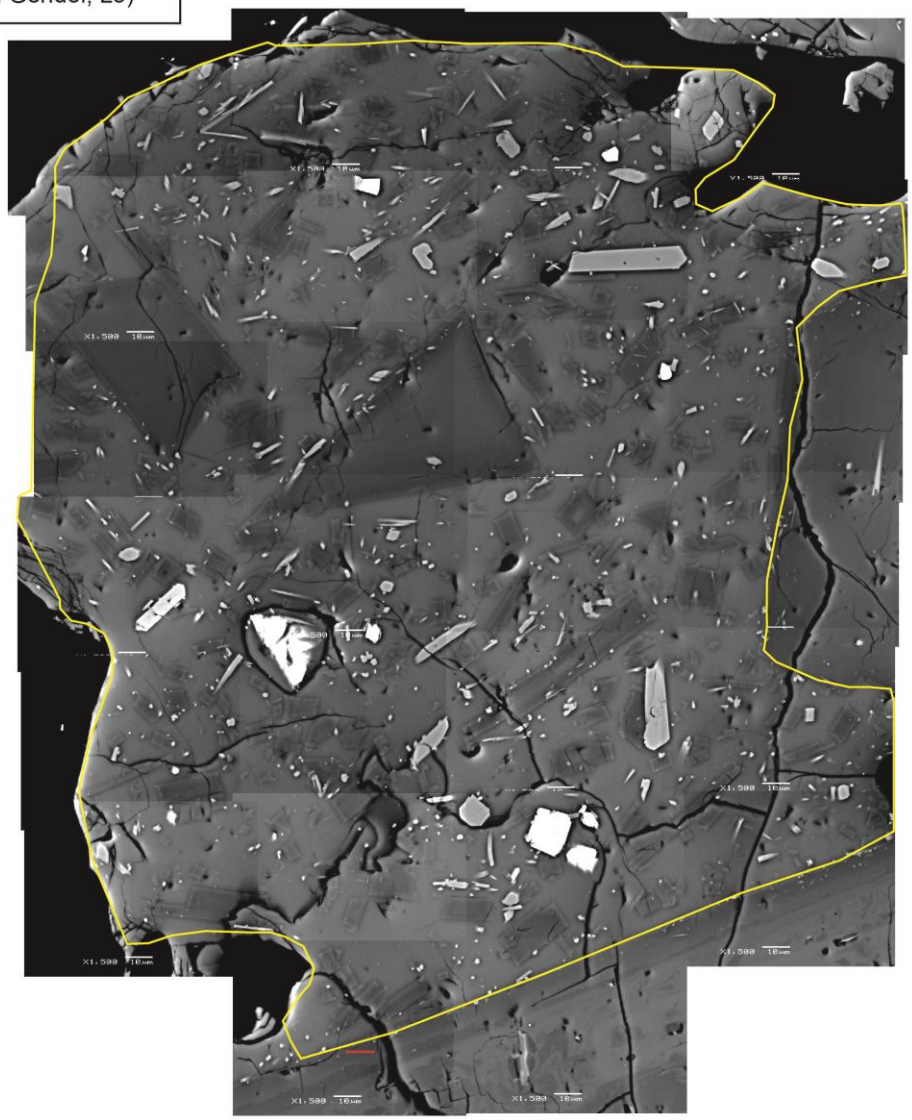

Mid Inter	ln(pop den)	ln(min PD)	ln(max PD)	Cry num	Vol %	Vol from inter area (%)	21.87	Size inter	No. of crys
0.229	7.65	6.79	8.1	2.21E+02	19.88	Total number from CSD	990000.00	0.1	3
0.1445	8.03	6.39	8.62	2.05E+02	4.628	Total vol (%) from CSD	42.50	0.0631	2
0.0912	10.56	10.14	10.85	1.61E+03	9.166			0.0398	9
0.0575	12.61	12.4	12.79	7.96E+03	11.35			0.0251	28
0.0363	14.43	14.29	14.55	3.08E+04	11.04			0.0158	69
0.0229	15.67	15.55	15.77	6.71E+04	6.042			0.01	98
0.0144	16.89	16.8	16.98	1.45E+05	3.27			0.0063	135
0.0091	17.72	17.61	17.81	2.07E+05	1.177			0.004	128
0.0058	18.31	18.17	18.42	2.36E+05	0.336			0.0025	98
0.0036	18.42	18.2	18.61	1.68E+05	0.06			0.0016	52
0.0023	18.35	17.88	18.67	9.80E+04	0.008			0.001	25
0.0014								0.0006	0
0.0009								0.0004	0
0.0006	18.52	Infinity	19.22	2.93E+04	0			0.0003	1
								0.0002	0

Eruption: 2006
Sample No: ME08-03-02
Lithology: 2006 dome scoria
Stage: III (Kali Gendol, L6)

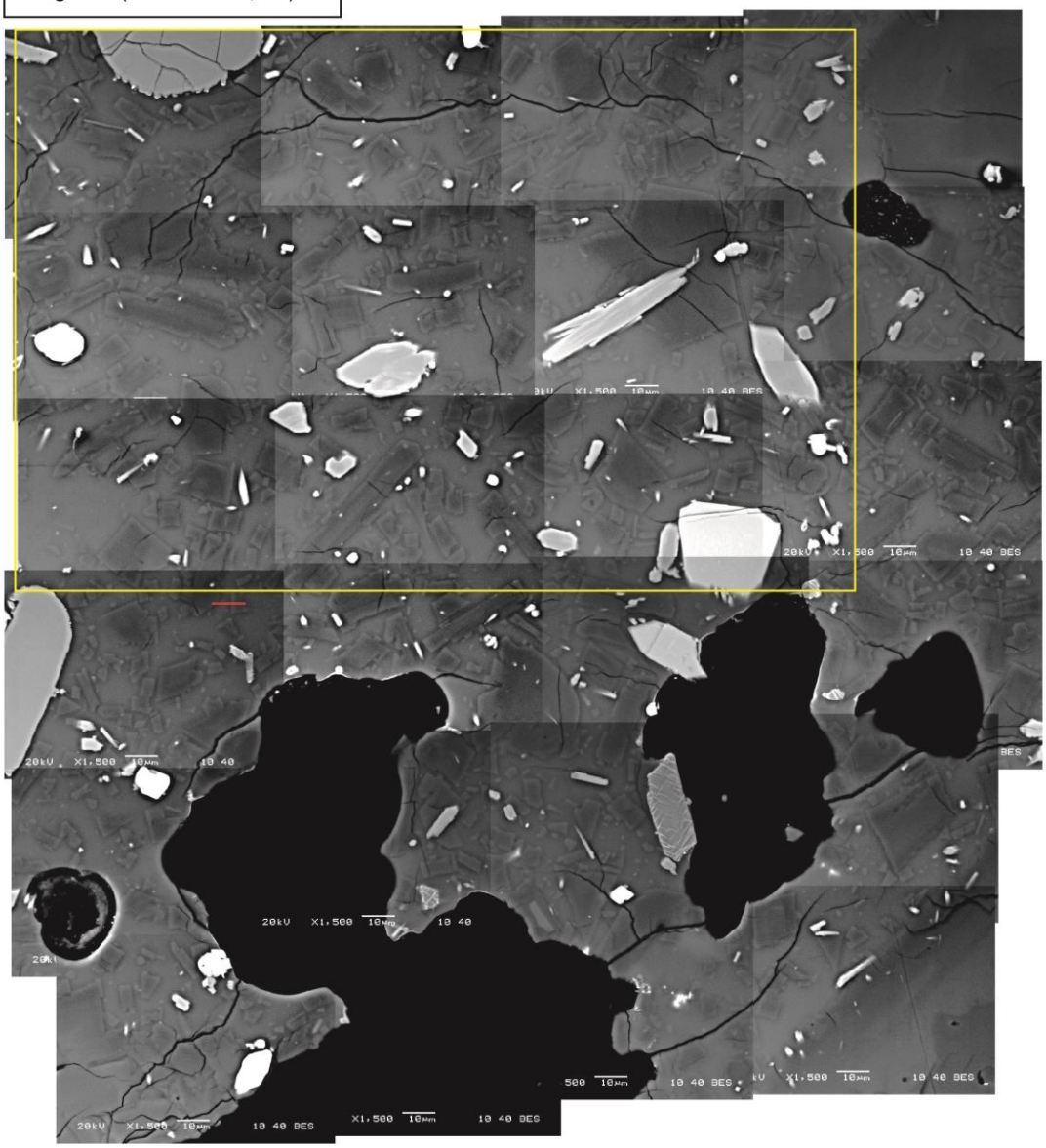

Mid Inter	ln(pop den)	ln(min PD)	ln(max PD)	Cry num	Vol %	Vol from inter area (%)	33.74	Size inter	No. of crys
0.1146	10.05	9.35	10.45	1.22E+03	2.04E+01	Total number from CSD	3080000.00	0.0631	4
0.0723	11.11	10.45	11.51	2.23E+03	9.39E+00	Total vol (%) from CSD	58.60	0.0398	5
0.0456	13.65	13.42	13.84	1.79E+04	18.87			0.0251	24
0.0288	15.07	14.89	15.23	4.67E+04	12.37			0.0158	41
0.0182	16.68	16.55	16.79	1.46E+05	9.736			0.01	81
0.0115	17.91	17.8	18.01	3.17E+05	5.313			0.0063	114
0.0072	18.67	18.55	18.78	4.29E+05	1.805			0.004	104
0.0046	19.78	19.67	19.88	8.21E+05	0.867			0.0025	124
0.0029	20	19.82	20.15	6.42E+05	0.17			0.0016	73
0.0018	20.47	20.24	20.66	6.52E+05	0.043			0.001	50
0.0011	Over							0.0006	5
								0.0004	0

Eruption: 2006
Sample No: ME08-04-01
Lithology: 2006 dome scoria
Stage: III (Kali Gendol, L8)

Mid Inter	ln(pop den)	ln(min PD)	ln(max PD)	Cry num	Vol %	Vol from inter area (%)	31.83	Size inter	No. of crys
0.3526	6.91	5.68	7.44	1.62E+02	2.52E+01	Total number from CSD	1030000.00	0.1	2
0.2225	7	Infinity	7.76	1.12E+02	4.38E+00	Total vol (%) from CSD	88.00	0.0631	1
0.1404	10.69	10.37	10.92	2.83E+03	2.77E+01			0.0398	14
0.0886	12.2	11.97	12.38	8.09E+03	1.99E+01			0.0251	26
0.0559	14.07	13.94	14.19	3.32E+04	20.53			0.0158	67
0.0353	15.31	15.19	15.41	7.20E+04	11.18			0.01	94
0.0222	16.51	16.41	16.6	1.51E+05	5.898			0.0063	126
0.014	17.16	17.04	17.27	1.84E+05	1.799			0.004	102
0.0089	18.22	18.1	18.31	3.32E+05	0.817			0.0025	115
0.0056	18.21	18.01	18.37	2.08E+05	0.128			0.0016	54
0.0035	16.95	15.29	17.55	3.74E+04	0.005			0.001	14
0.0022	16.68	Infinity	17.38	1.80E+04	0			0.0006	2
								0.0004	0

Eruption: 2006
Sample No: ME08-07
Lithology: 2006 dome scoria
Stage: III (Kali Gendol, L10)

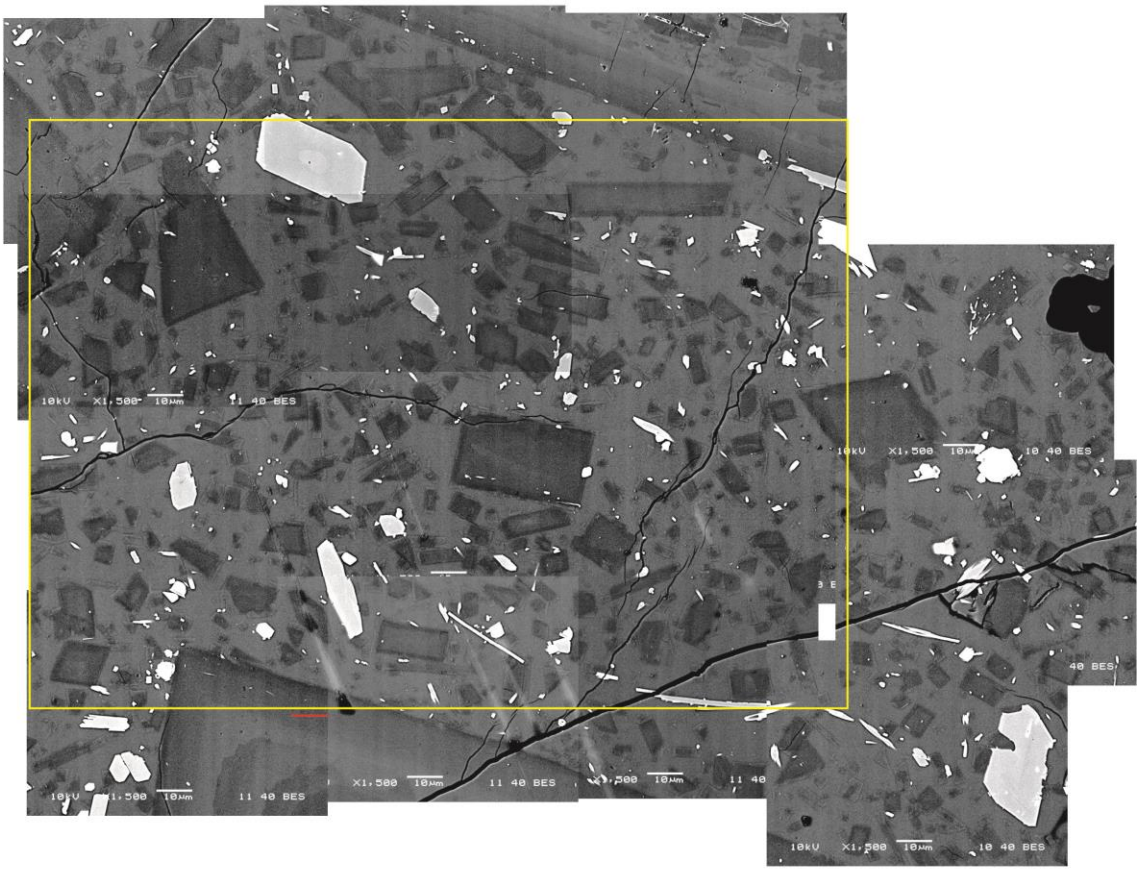

Mid Inter	ln(pop den)	ln(min PD)	ln(max PD)	Cry num	Vol %	Vol from inter area (%)	31.99	Size inter	No. of crys
0.0867	10.45	9.59	10.91	1.38E+03	1.88E+01	Total number from CSD	3650000.00	0.0631	3
0.0547	10.77	8.79	11.39	1.20E+03	4.09E+00	Total vol (%) from CSD	53.30	0.0398	2
0.0345	13.81	13.49	14.05	1.58E+04	13.5			0.0251	14
0.0218	15.76	15.58	15.91	7.01E+04	15.06			0.0158	40
0.0137	17.53	17.42	17.64	2.60E+05	14.05			0.01	95
0.0087	18.73	18.63	18.83	5.46E+05	7.406			0.0063	132
0.0055	19.44	19.32	19.55	6.99E+05	2.383			0.004	117
0.0035	20.13	19.99	20.25	8.80E+05	0.753			0.0025	99
0.0022	20.39	20.16	20.57	7.16E+05	0.154			0.0016	62
0.0014	20	19.35	20.39	3.06E+05	0.016			0.001	25
0.0009	19.78	18.49	20.33	1.56E+05	0.002			0.0006	6
								0.0004	0

Eruption: 2006
Sample No: ME08-08-03
Lithology: 2006 dome prism. joint
Stage: II (Kali Gendol, L1)

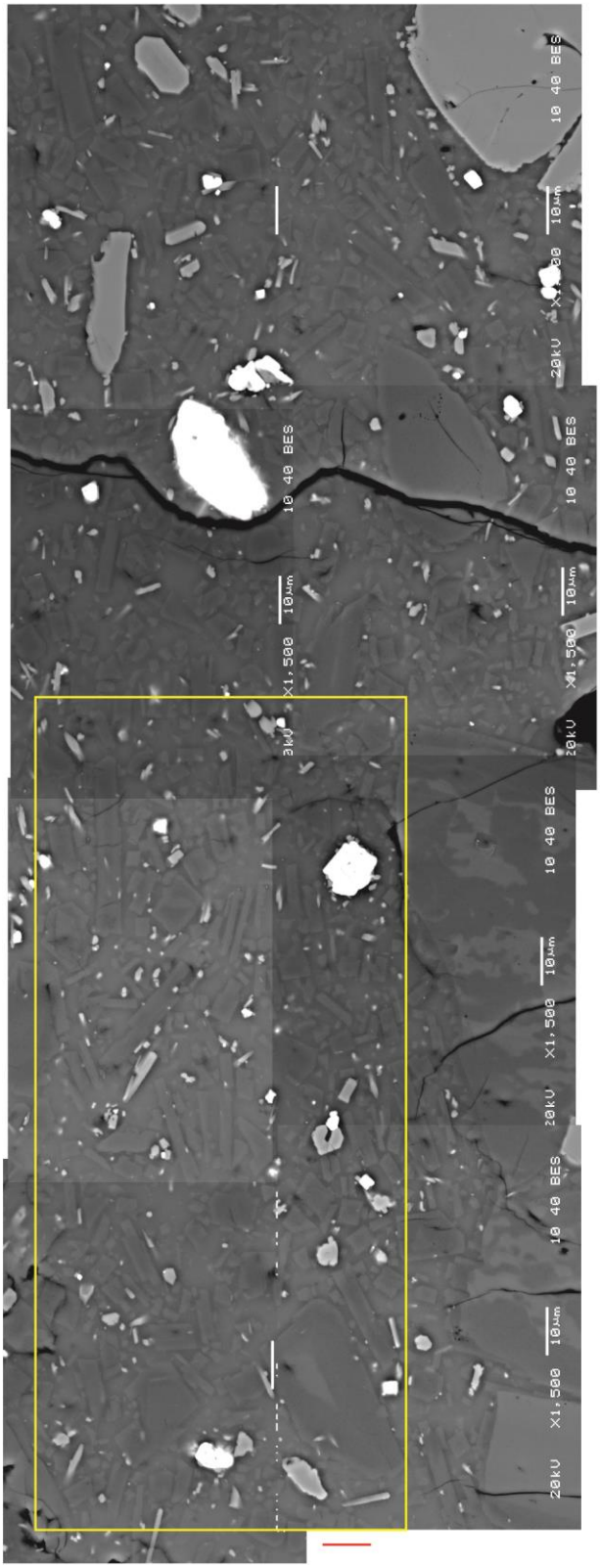

Mid Inter	ln(pop den)	ln(min PD)	ln(max PD)	Cry num	Vol %	Vol from inter area (%)		32.87	Size inter	No. of crys
0.0769	10.48	Infinity	11.17	1.25E+03	1.69E+01	Total number from CSD	17300000.00		0.0631	1
0.0485	12.02	10.61	12.59	3.72E+03	1.26E+01	Total vol (%) from CSD	78.30		0.0398	2
0.0306	14.06	13.49	14.41	1.79E+04	15.24				0.0251	6
0.0193	16.38	16.14	16.57	1.15E+05	24.63				0.0158	24
0.0122	18	17.84	18.14	3.68E+05	19.75				0.01	50
0.0077	19.02	18.85	19.16	6.42E+05	8.653				0.0063	59
0.0048	20.39	20.26	20.5	1.60E+06	5.406				0.004	91
0.0031	21.68	21.57	21.77	3.66E+06	3.107				0.0025	132
0.0019	22.57	22.46	22.67	5.63E+06	1.201				0.0016	136
0.0012	22.96	22.8	23.09	5.23E+06	0.28				0.001	93
0.0008	Over								0.0006	17
0.0005	Over								0.0004	2
0.0003									0.0003	0
0.0002	Over								0.0002	1
									0.0001	0

Eruption: 2006
Sample No: ME08-09-02
Lithology: 2006 dome scoria
Stage: II (K. Gendol, L1)

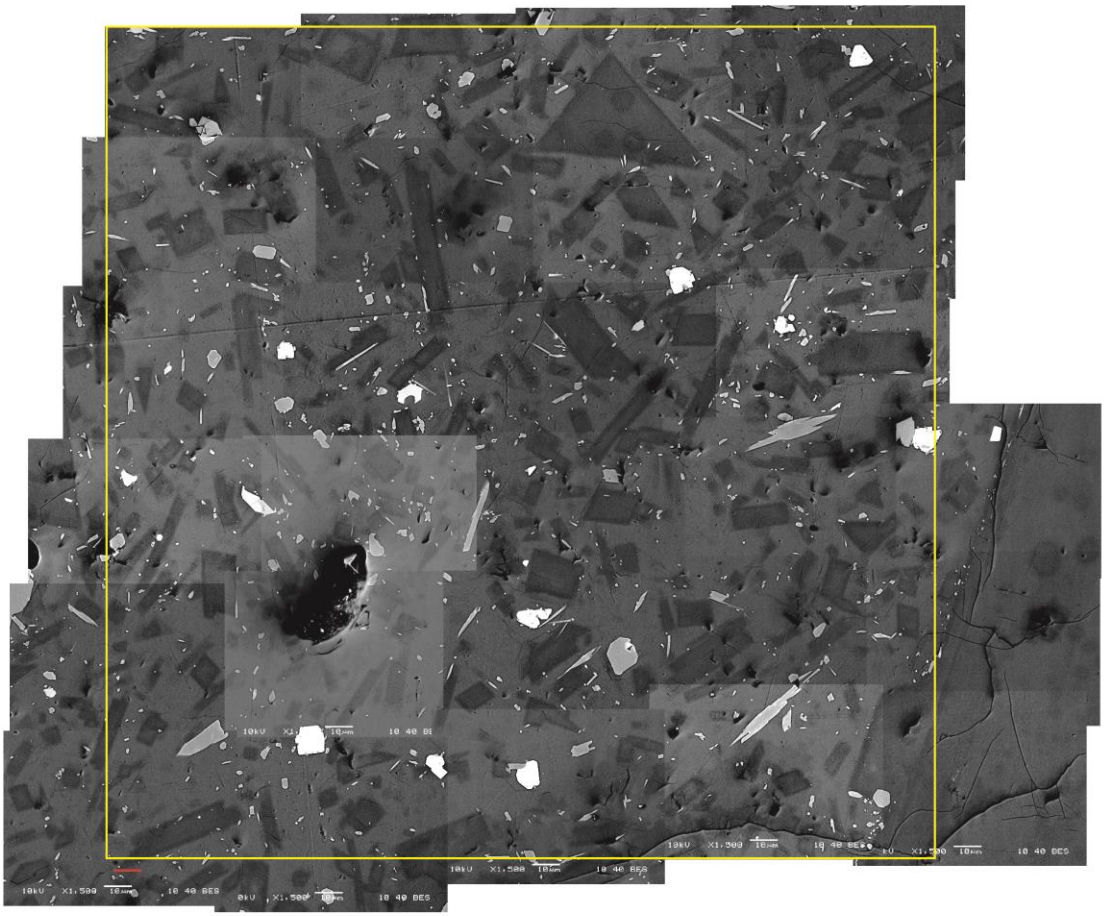

Mid Inter	ln(pop den)	ln(min PD)	ln(max PD)	Cry num	Vol %	Vol from inter area (%)	26.19	Size inter	No. of crys
0.2671	6.23	Infinity	6.92	6.22E+01	6.09E+00	Total number from CSD	515000.00	0.1	1
0.1685	9.54	9.18	9.8	1.08E+03	2.65E+01	Total vol (%) from CSD	91.50	0.0631	11
0.1063	11.07	10.81	11.28	3.15E+03	1.95E+01			0.0398	21
0.0671	13.03	12.89	13.16	1.41E+04	21.97			0.0251	59
0.0423	14.39	14.27	14.49	3.45E+04	13.46			0.0158	93
0.0267	15.5	15.39	15.59	6.60E+04	6.467			0.01	115
0.0169	16.4	16.29	16.5	1.03E+05	2.542			0.0063	117
0.0106	17.11	16.99	17.22	1.33E+05	0.819			0.004	99
0.0067	17.44	17.26	17.6	1.16E+05	0.18			0.0025	61
0.0042	16.94	16.42	17.28	4.42E+04	0.017			0.0016	21
0.0027	16.29	14.38	16.91	1.46E+04	0.001			0.001	4
								0.0006	0

Eruption: 2006
Sample No: ME08-10
Lithology: 2006 dome scoria
Stage: I (Kali Bebeng)

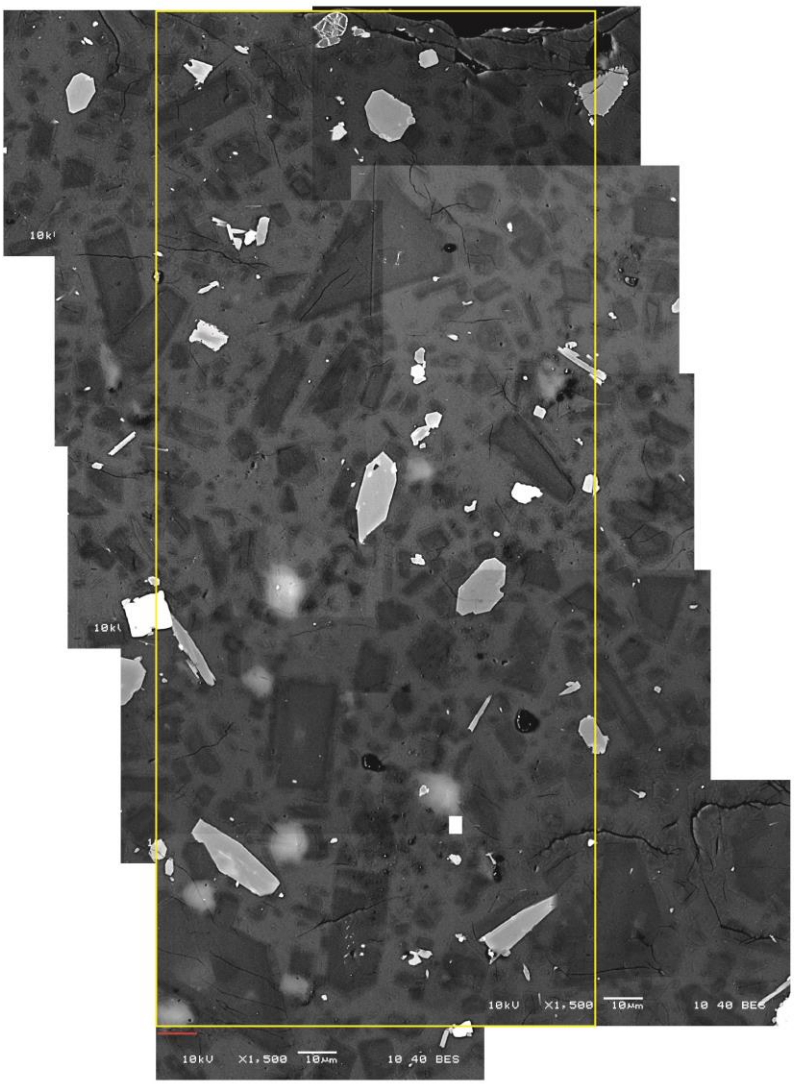

Mid Inter	ln(pop den)	ln(min PD)	ln(max PD)	Cry num	Vol %	Vol from inter area (%)	38.51	Size inter	No. of crys
0.089	9.5	Infinity	10.2	5.49E+02	8.57E+00	Total number from CSD	4870000.00	0.0631	1
0.0561	12.01	11.4	12.39	4.25E+03	1.66E+01	Total vol (%) from CSD	87.20	0.0398	5
0.0354	13.47	13.02	13.77	1.15E+04	11.33			0.0251	9
0.0224	15.95	15.77	16.1	8.67E+04	21.44			0.0158	41
0.0141	17.41	17.28	17.53	2.37E+05	14.73			0.01	74
0.0089	18.8	18.69	18.89	5.98E+05	9.327			0.0063	120
0.0056	19.63	19.52	19.74	8.71E+05	3.412			0.004	119
0.0035	20.66	20.55	20.76	1.53E+06	1.508			0.0025	133
0.0022	20.28	19.99	20.5	6.58E+05	0.162			0.0016	55
0.0014	21.02	20.72	21.25	8.75E+05	0.054			0.001	42
0.0009	Over							0.0006	11
0.0006	Over							0.0004	3
0.0004								0.0003	0
0.0002	Over							0.0002	1
								0.0001	0

Eruption: 2006
Sample No: ME08-11-01
Lithology: 2006 dome scoria
Stage: I (Kali Bebeng)

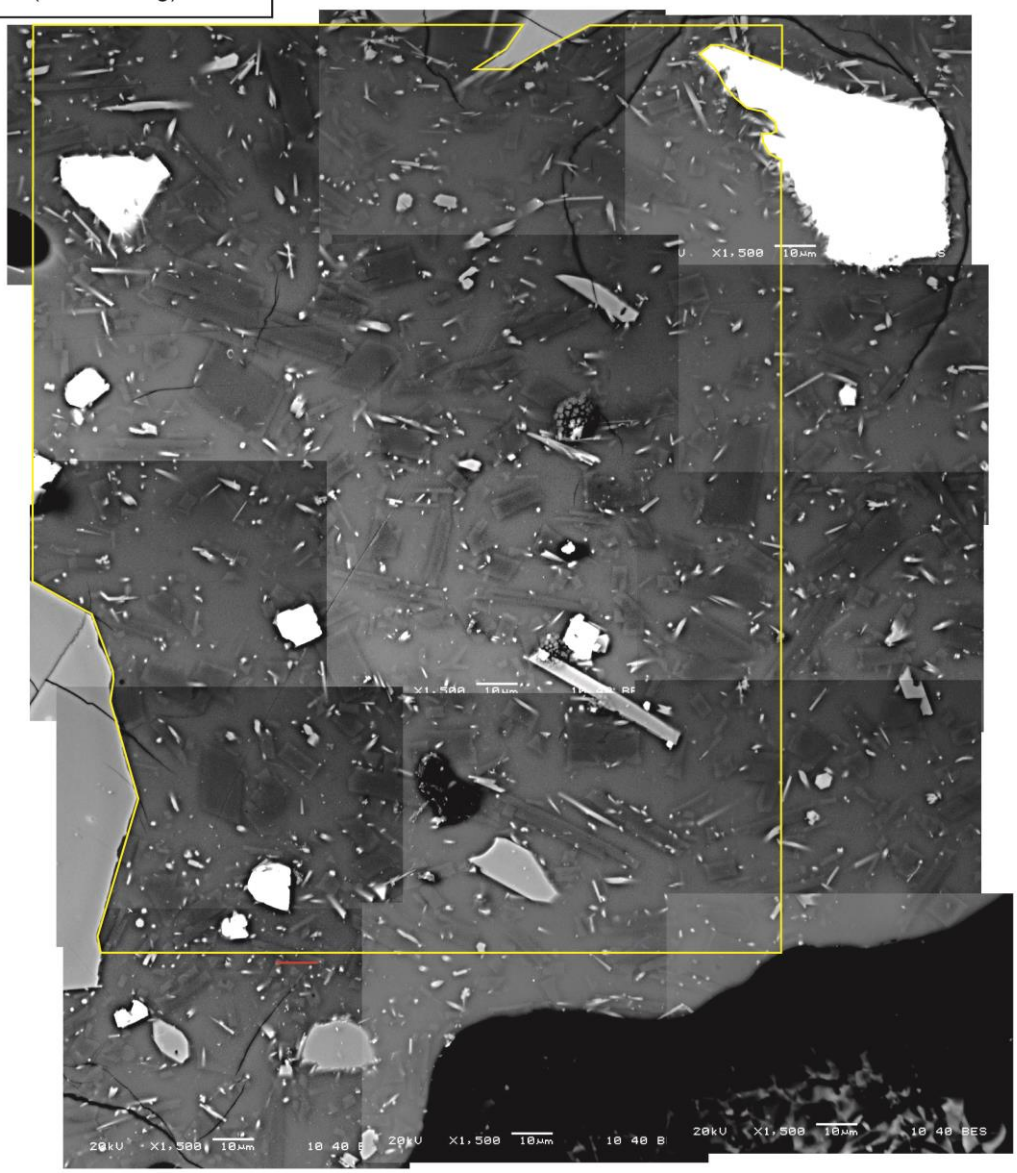

Mid Inter	ln(pop den)	ln(min PD)	ln(max PD)	Cry num	Vol %	Vol from inter area (%)	20.36	Size inter	No. of crys
0.1854	7.79	Infinity	8.48	2.05E+02	5.56E+00	Total number from CSD	2230000.00	0.0631	1
0.117	10.64	10.16	10.97	2.26E+03	1.54E+01	Total vol (%) from CSD	65.70	0.0398	7
0.0738	12.6	12.34	12.81	1.01E+04	17.21			0.0251	20
0.0466	14.15	13.96	14.3	2.99E+04	12.81			0.0158	38
0.0294	15.76	15.63	15.87	9.45E+04	10.18			0.01	76
0.0185	17.09	16.99	17.18	2.25E+05	6.104			0.0063	116
0.0117	18.08	17.98	18.17	3.83E+05	2.607			0.004	128
0.0074	19.08	18.99	19.17	6.60E+05	1.127			0.0025	141
0.0047	19.25	19.09	19.39	4.91E+05	0.21			0.0016	76
0.0029	18.98	18.62	19.25	2.38E+05	0.025			0.001	31
0.0019	18.52	17.66	18.97	9.41E+04	0.002			0.0006	7
								0.0004	0

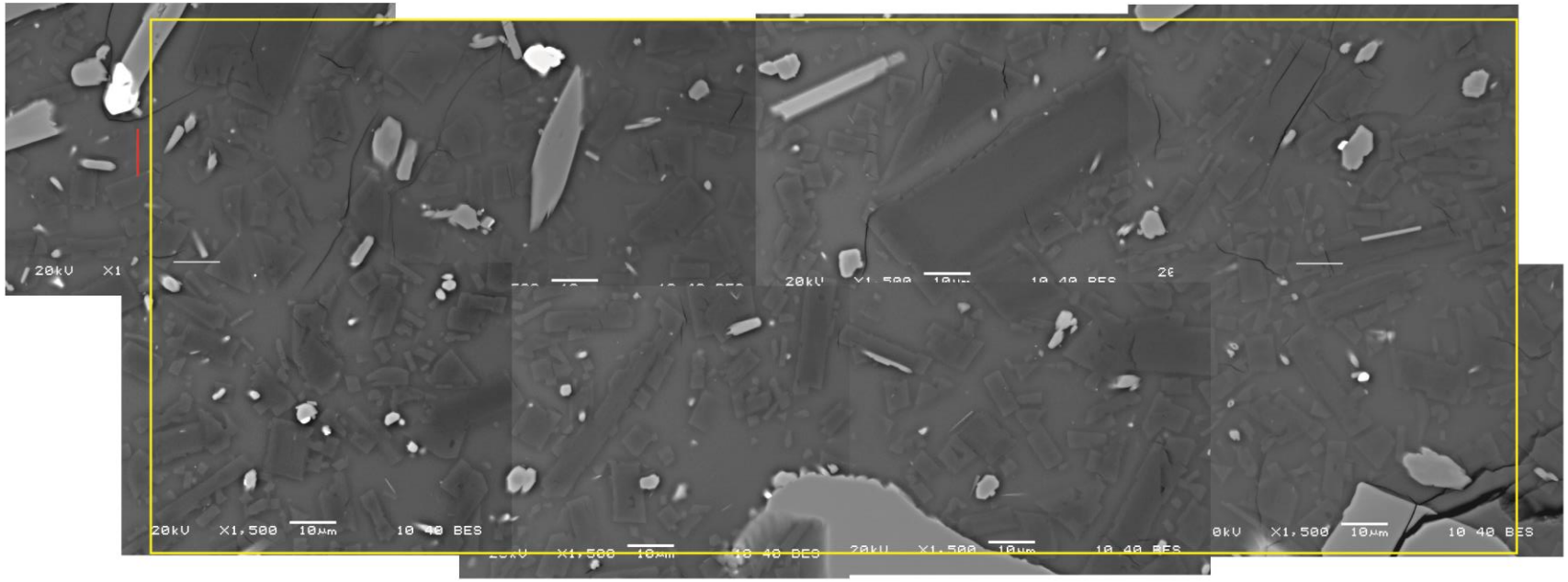

Eruption: 2006
Sample No: ME08-12
Lithology: 2006 dense prismatically jointed
Stage: I (Kali Bebeng)

Mid Inter	ln(pop den)	ln(min PD)	ln(max PD)	Cry num	Vol %	Vol from inter area (%)	34.37	Size inter	No. of crys
0.1946	7.86	Infinity	8.55	2.32E+02	1.78E+01	Total number from CSD	3420000.00	0.1	1
0.1228	8.68	Infinity	9.42	3.33E+02	6.40E+00	Total vol (%) from CSD	82.70	0.0631	1
0.0775	11.63	11.14	11.95	4.00E+03	1.93E+01			0.0398	7
0.0489	13.41	13.12	13.64	1.50E+04	1.82E+01			0.0251	17
0.0308	15.35	15.19	15.49	6.60E+04	20.1			0.0158	47
0.0195	16.84	16.72	16.95	1.85E+05	14.15			0.01	85
0.0123	17.99	17.88	18.09	3.66E+05	7.042			0.0063	110
0.0077	18.81	18.69	18.91	5.25E+05	2.534			0.004	105
0.0049	19.78	19.67	19.89	8.80E+05	1.067			0.0025	112
0.0031	20.2	20.03	20.34	8.41E+05	0.256			0.0016	76
0.0019	20.21	19.89	20.44	5.34E+05	0.04			0.001	38
0.0012	Over							0.0006	4
								0.0004	0

Eruption: 2006
Sample No: ME08-14
Lithology: 2006 dome scoria
Stage: IV (Remnant dome)

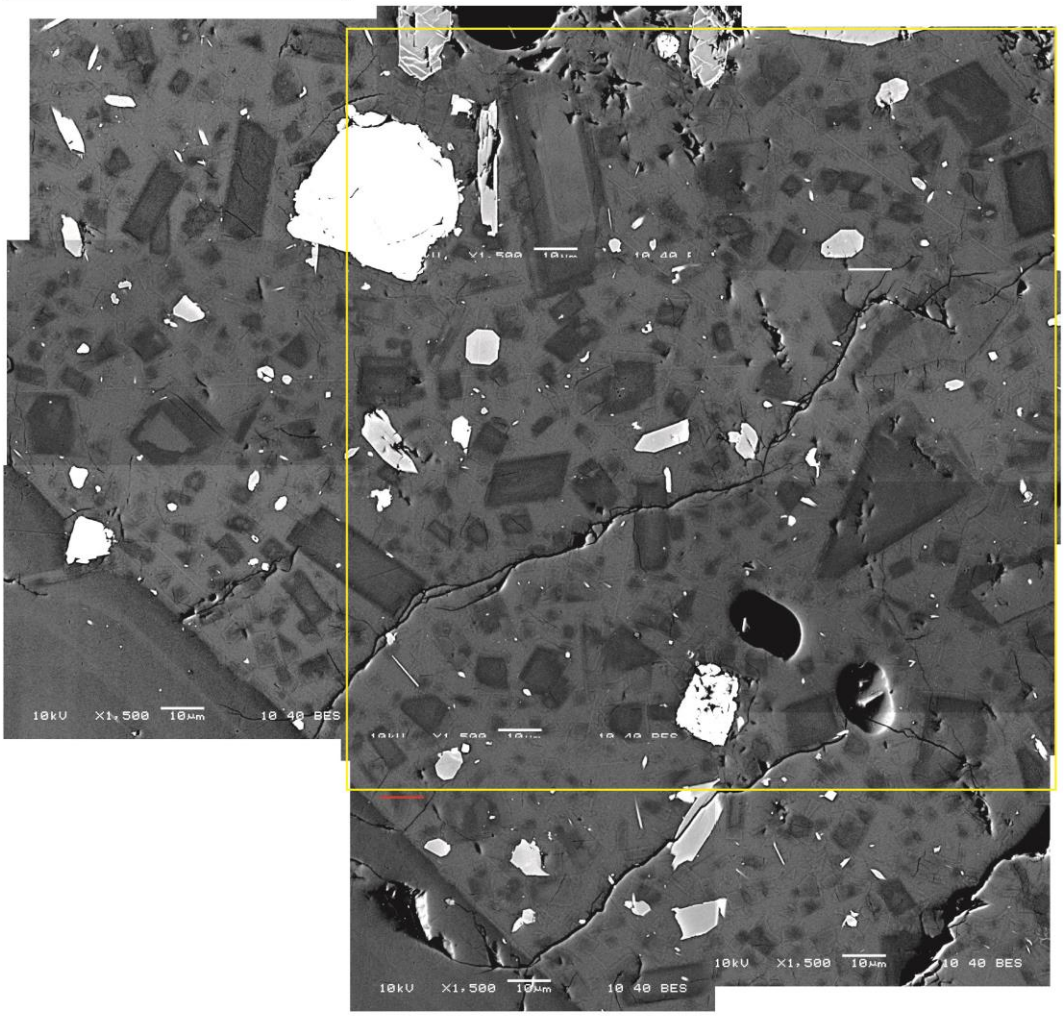

Mid Inter	ln(pop den)	ln(min PD)	ln(max PD)	Cry num	Vol %	Vol from inter area (%)	37.56	Size inter	No. of crys
0.0716	10.4	9.18	10.94	1.09E+03	1.42E+01	Total number from CSD	4700000.00	0.0631	2
0.0452	11.63	10.6	12.12	2.33E+03	7.66E+00	Total vol (%) from CSD	56.40	0.0398	3
0.0285	13.99	13.63	14.25	1.56E+04	12.9			0.0251	12
0.018	15.88	15.67	16.05	6.50E+04	13.47			0.0158	32
0.0114	17.84	17.73	17.95	2.94E+05	15.28			0.01	91
0.0072	19.24	19.15	19.33	7.48E+05	9.786			0.0063	153
0.0045	20.04	19.93	20.13	1.05E+06	3.449			0.004	150
0.0029	20.93	20.82	21.03	1.62E+06	1.333			0.0025	151
0.0018	20.82	20.58	21.01	9.09E+05	0.188			0.0016	79
0.0011	Over							0.001	18
0.0007	Over							0.0006	2
								0.0004	0

Eruption: 2010
Sample No: M11-01
Lithology: 2010 dome (dense)
Stage: 4

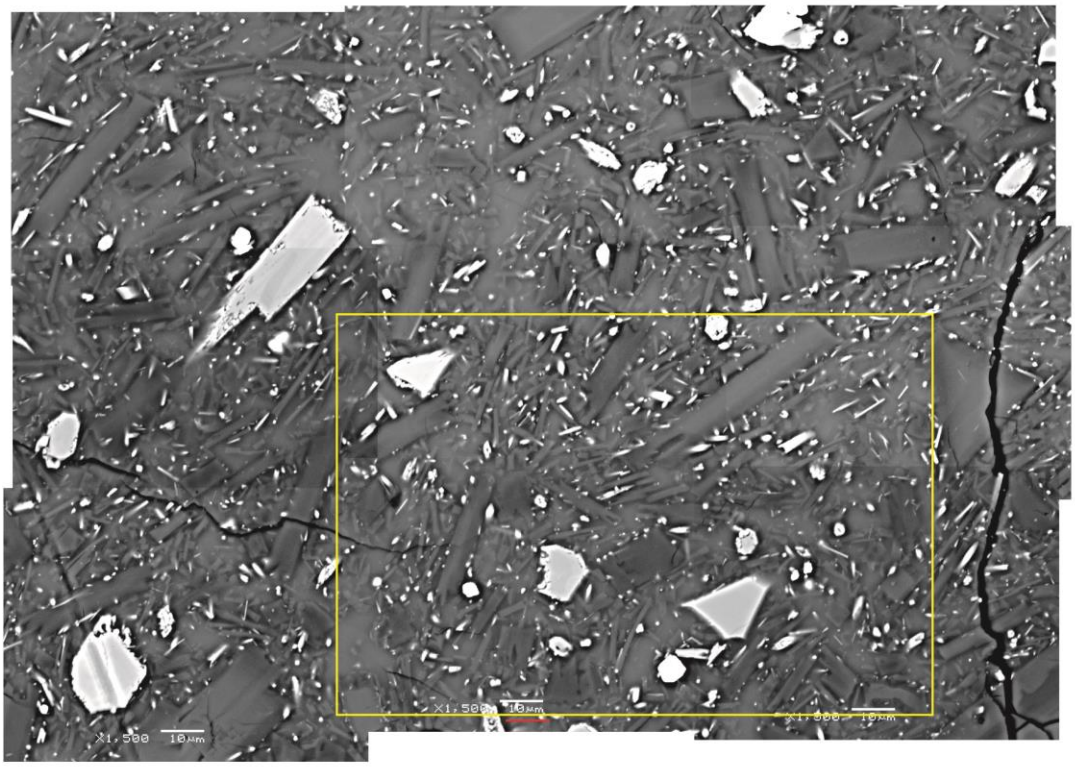

Mid Inter	ln(pop den)	ln(min PD)	ln(max PD)	Cry num	Vol %	Vol from inter area (%)	25.66	Size inter	No. of crys
0.3371	7.76	Infinity	8.45	362	19.82	**Total number from CSD**	8880000.00	0.0631	1
0.2127	9.35	8.07	9.89	1.13E+03	15.47	**Total vol (%) from CSD**	106.00	0.0398	2
0.1342	11.53	11.05	11.85	6.28E+03	21.69			0.0251	7
0.0847	13.76	13.54	13.95	3.70E+04	32.12			0.0158	26
0.0534	15.15	14.98	15.3	9.33E+04	20.33			0.01	42
0.0337	16.73	16.61	16.84	2.86E+05	15.62			0.0063	81
0.0213	18.05	17.95	18.14	6.76E+05	9.293			0.004	122
0.0134	19.28	19.2	19.36	1.47E+06	5.063			0.0025	168
0.0085	20.16	20.07	20.24	2.22E+06	1.926			0.0016	164
0.0053	20.6	20.49	20.71	2.18E+06	0.475			0.001	107
0.0034	20.64	20.45	20.81	1.43E+06	0.078			0.0006	50
0.0021	19.59	18.52	20.09	3.15E+05	0.004			0.0004	13
0.0013	19.89	18.49	20.46	2.70E+05	0			0.0003	5
0.0008	20.29	18.63	20.88	2.52E+05	0			0.0002	2
								0.0001	0

Eruption: 2010
Sample No: M11-02
Lithology: 2010 Dome (scoriaceous)
Stage: 4

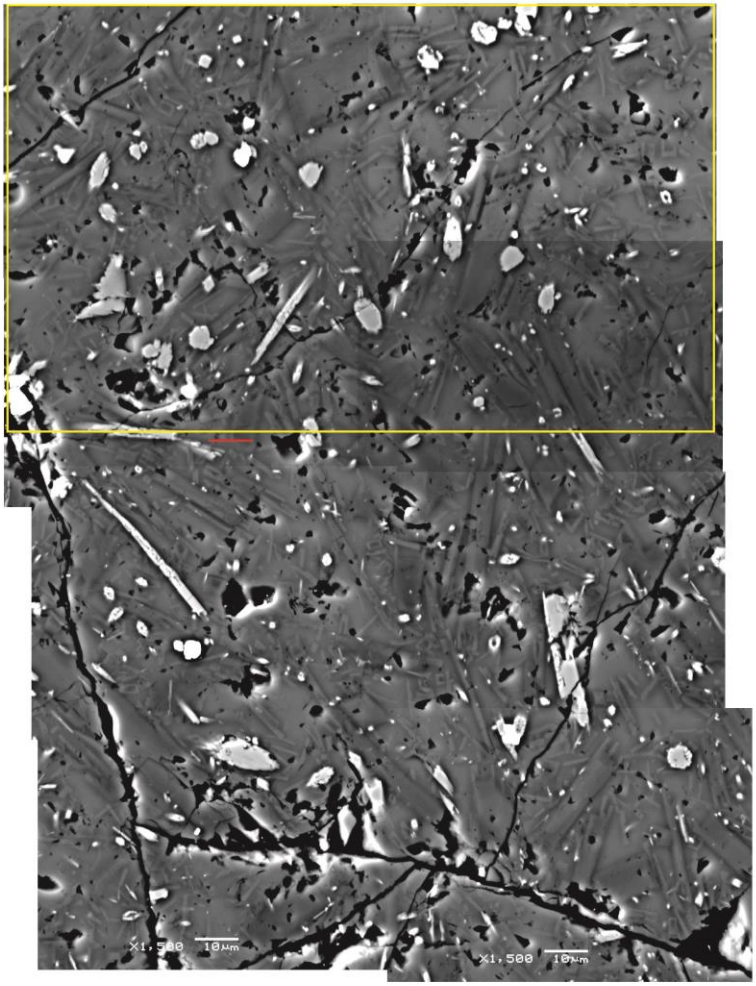

Mid Inter	ln(pop den)	ln(min PD)	ln(max PD)	Cry num	Vol %	Vol from inter area (%)	23.89	Size inter	No. of crys
0.158	9.04	Infinity	9.73	613	7.372	Total number from CSD	10900000.00	0.0631	1
0.0997	11.05	10.17	11.51	2.88E+03	8.692	Total vol (%) from CSD	59.50	0.0398	3
0.0629	13.06	12.65	13.35	1.36E+04	10.34			0.0251	9
0.0397	14.87	14.63	15.07	5.26E+04	10.01			0.0158	22
0.025	16.61	16.45	16.75	1.89E+05	9.037			0.01	50
0.0158	18.3	18.2	18.39	6.45E+05	7.755			0.0063	108
0.01	19.38	19.28	19.46	1.19E+06	3.604			0.004	129
0.0063	20.61	20.53	20.69	2.60E+06	1.968			0.0025	178
0.004	21.17	21.07	21.26	2.85E+06	0.543			0.0016	130
0.0025	21.4	21.24	21.54	2.27E+06	0.108			0.001	73
0.0016	21.13	20.76	21.4	1.09E+06	0.013			0.0006	30
0.001	Over								
0.0006	Over								

Eruption: 2010
Sample No: M11-15
Lithology: 2010 dome (dense)
Stage: 4

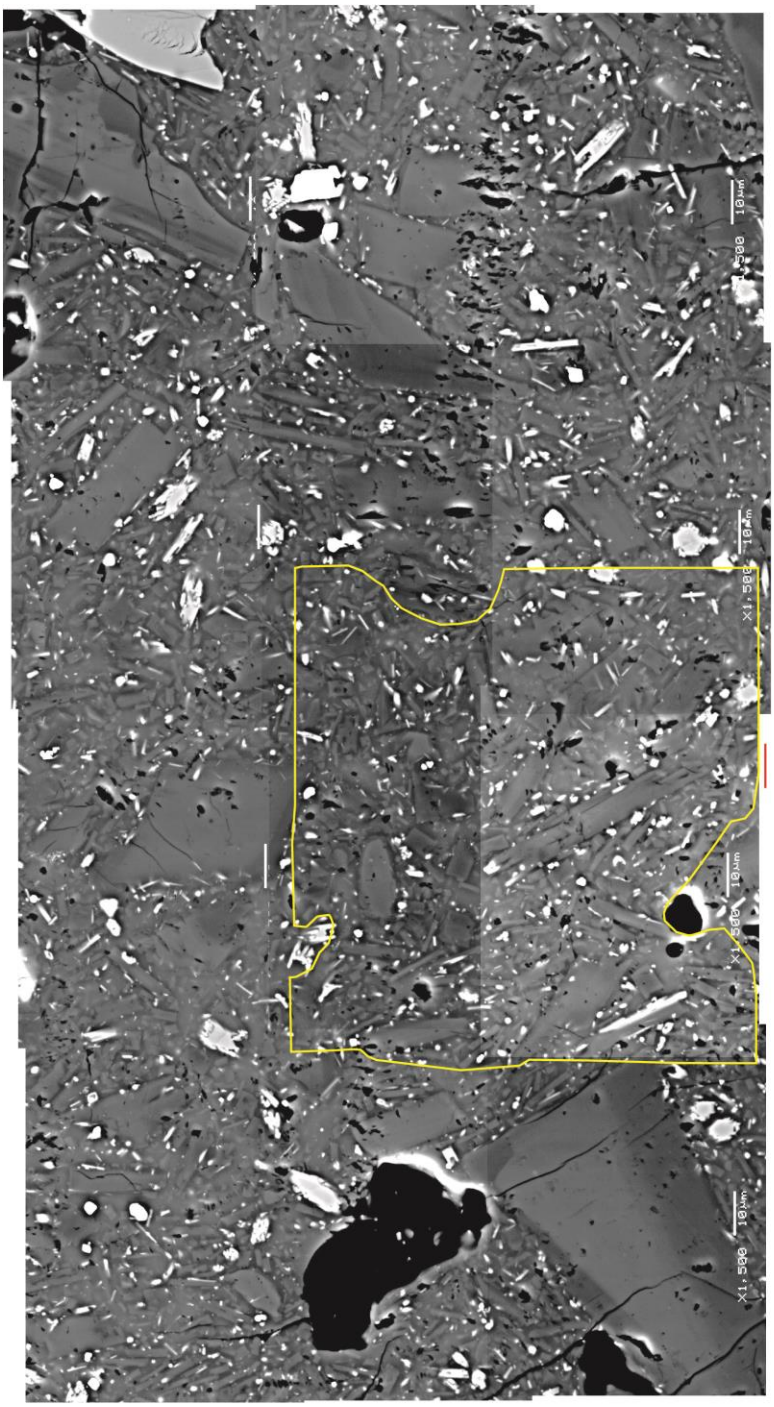

Mid Inter	ln(pop den)	ln(min PD)	ln(max PD)	Cry num	Vol %
0.0997	11.41	10.55	11.87	4.15E+03	22.57
0.0629	13.52	13.13	13.8	2.15E+04	29.33
0.0397	14.57	14.2	14.84	3.90E+04	13.35
0.025	16.33	16.1	16.51	1.42E+05	12.24
0.0158	17.96	17.81	18.09	4.59E+05	9.931
0.01	19.5	19.39	19.6	1.36E+06	7.375
0.0063	20.83	20.74	20.91	3.21E+06	4.387
0.004	21.71	21.62	21.8	4.92E+06	1.688
0.0025	21.99	21.86	22.12	4.11E+06	0.354
0.0016	22.12	21.89	22.31	2.95E+06	0.063
0.001	20.19	Infinity	21.15	2.68E+05	0.001
0.0006	20.99	19.25	21.59	3.77E+05	0

Vol from inter area (%)	27.86
Total number from CSD	17500000.00
Total vol (%) from CSD	78.70

Size inter	No. of crys
0.0398	3
0.0251	10
0.0158	12
0.01	27
0.0063	55
0.004	103
0.0025	156
0.0016	157
0.001	93
0.0006	50
0.0004	10
0.0003	2
0.0002	0

Eruption: 2010
Sample No: M11-50
Lithology: 2010 White Pumice
Stage: 6

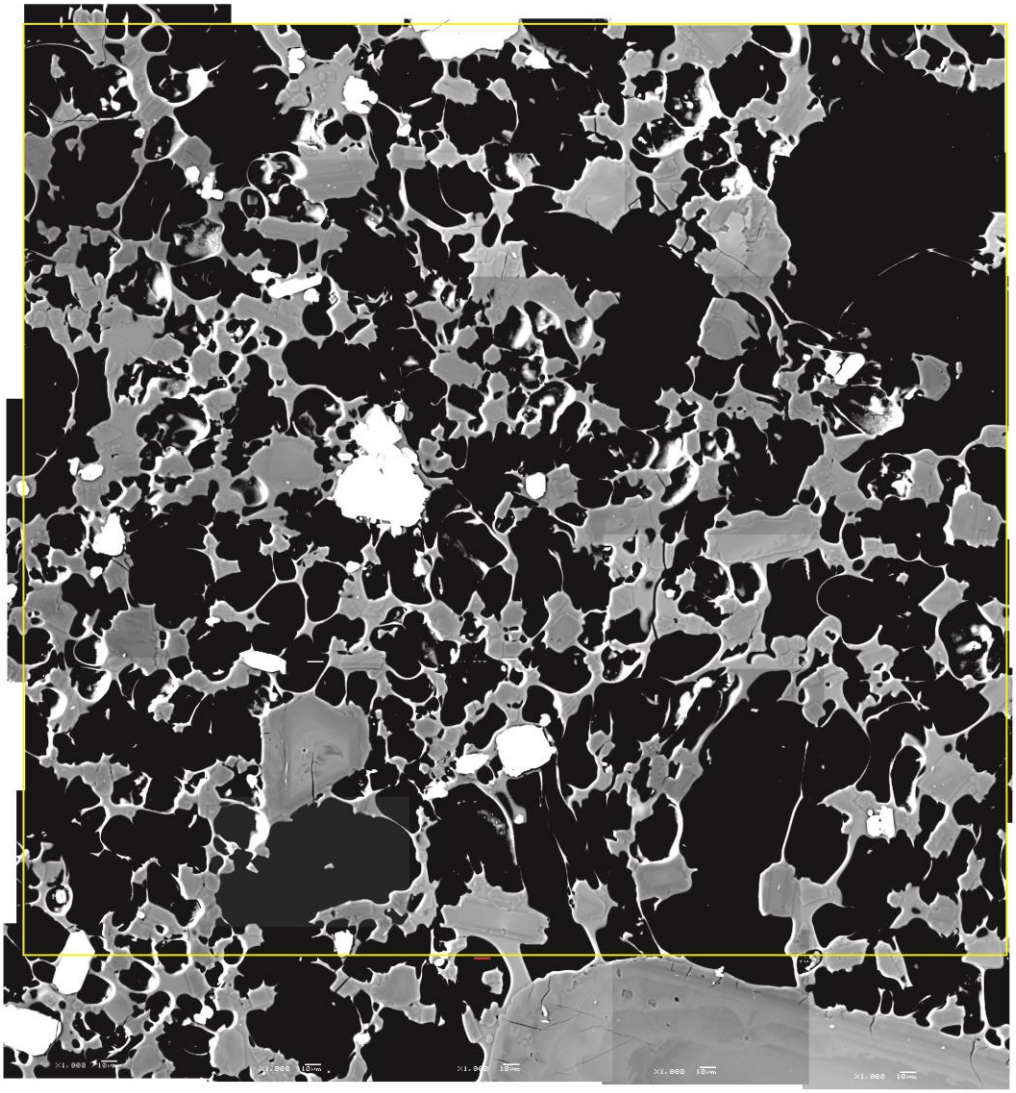

Mid Inter	ln(pop den)	ln(min PD)	ln(max PD)	Cry num	Vol %	Vol from inter area (%)	34.39	Size inter	No. of crys
0.1045	8.58	7.72	9.04	256	14.25	Total number from CSD	635000.00	0.1	3
0.066	9.69	8.89	10.13	492	6.874	Total vol (%) from CSD	48.60	0.0631	3
0.0416	12.18	11.9	12.4	3.73E+03	13.06			0.0398	18
0.0263	13.99	13.82	14.14	1.45E+04	12.74			0.0251	45
0.0166	15.83	15.73	15.93	5.74E+04	12.69			0.0158	107
0.0105	17.11	17.02	17.19	1.30E+05	7.231			0.01	168
0.0066	17.77	17.66	17.87	1.58E+05	2.207			0.0063	143
0.0042	18.24	18.09	18.36	1.59E+05	0.558			0.004	108
0.0026	18.35	18.08	18.56	1.12E+05	0.098			0.0025	61
0.0017	Over							0.0016	22
0.001	Over							0.001	7
0.0007	Over							0.0006	1
0.0004	Over							0.0004	1
								0.0003	0

Eruption: 2010
Sample No: M11-51
Lithology: 2010 Grey Scoria
Stage: 6

Mid Inter	ln(pop den)	ln(min PD)	ln(max PD)	Cry num	Vol %	Vol from inter area (%)	24.17	Size inter	No. of crys
0.1253	10.91	10.22	11.32	3.16E+03	27.41	Total number from CSD	13600000.00	0.0398	4
0.0791	12.35	11.85	12.68	8.43E+03	18.38	Total vol (%) from CSD	99.50	0.0251	7
0.0499	14.16	13.88	14.39	3.26E+04	17.84			0.0158	17
0.0315	16.02	15.84	16.16	1.31E+05	18			0.01	43
0.0199	17.38	17.24	17.5	3.22E+05	11.11			0.0063	68
0.0125	18.36	18.23	18.48	5.45E+05	4.727			0.004	75
0.0079	20	19.91	20.08	1.77E+06	3.856			0.0025	149
0.005	20.79	20.69	20.88	2.45E+06	1.343			0.0016	137
0.0031	21.78	21.68	21.87	4.17E+06	0.573			0.001	148
0.002	22.02	21.87	22.14	3.33E+06	0.115			0.0006	84
0.0013	21.77	21.44	22.02	1.65E+06	0.014			0.0004	35
0.0008	20.07	Infinity	21.13	1.90E+05	0			0.0003	8
0.0005	21.91	21.16	22.33	7.51E+05	0			0.0002	4
								0.0001	0

Eruption: 2010
Sample No: M11-55
Lithology: 2010 White pumice
Stage: 6

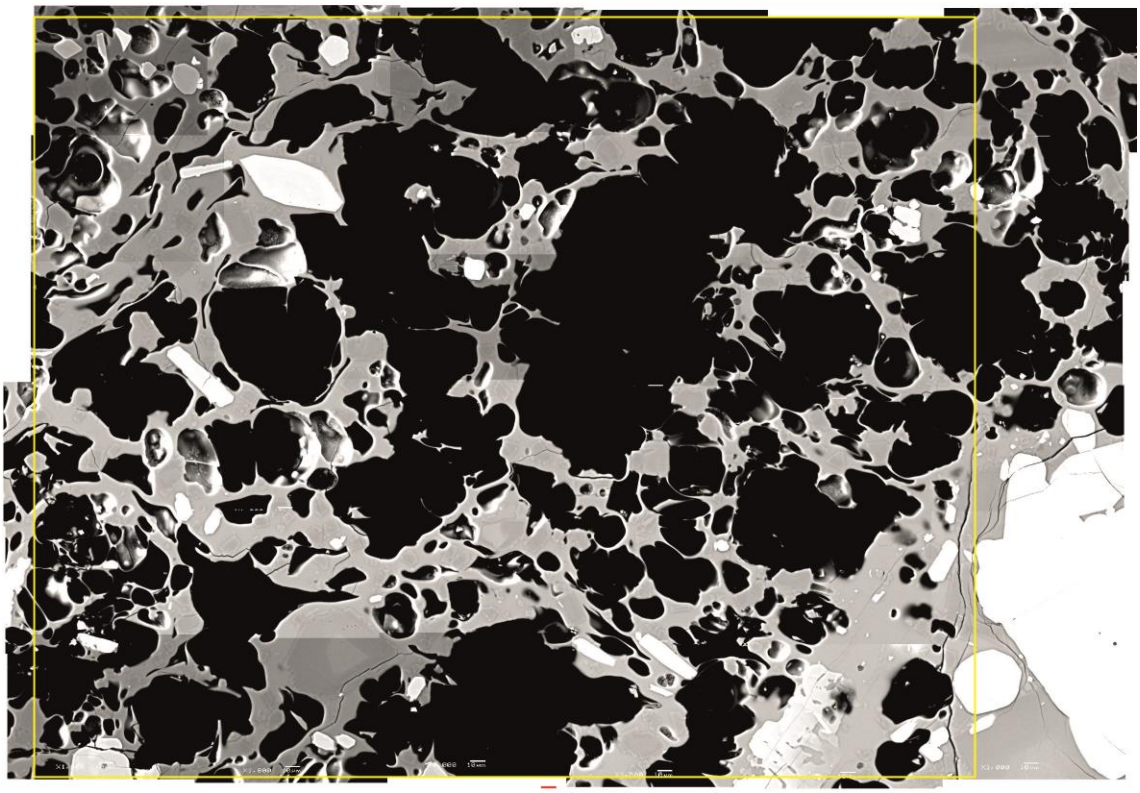

Mid Inter	ln(pop den)	ln(min PD)	ln(max PD)	Cry num	Vol %	Vol from inter area (%)	17.69	Size inter	No. of crys
0.0801	7.9	Infinity	8.6	99.7	3.592	Total number from CSD	998000.00	0.1	1
0.0506						Total vol (%) from CSD	21.00	0.0631	0
0.0319	11.68	11.2	12	1.74E+03	3.946			0.0398	7
0.0201	13.61	13.35	13.83	7.58E+03	4.329			0.0251	20
0.0127	15.91	15.78	16.02	4.73E+04	6.78			0.0158	78
0.008	16.93	16.8	17.04	8.29E+04	2.985			0.01	94
0.0051	18.53	18.45	18.61	2.60E+05	2.352			0.0063	181
0.0032	18.73	18.59	18.85	2.01E+05	0.455			0.004	110
0.002	19.23	19.04	19.38	2.07E+05	0.118			0.0025	80
0.0013	19.18	18.77	19.47	1.25E+05	0.017			0.0016	45
0.0008	18.85	17.18	19.44	5.64E+04	0.002			0.001	21
0.0005	17.57	Infinity	19.09	9.94E+03	0			0.0006	5
0.0003	19.99	19.03	20.47	7.03E+04	0			0.0004	3
								0.0003	0

Eruption: 2010
Sample No: M11-75
Lithology: 2010 Grey scoria
Stage: 6

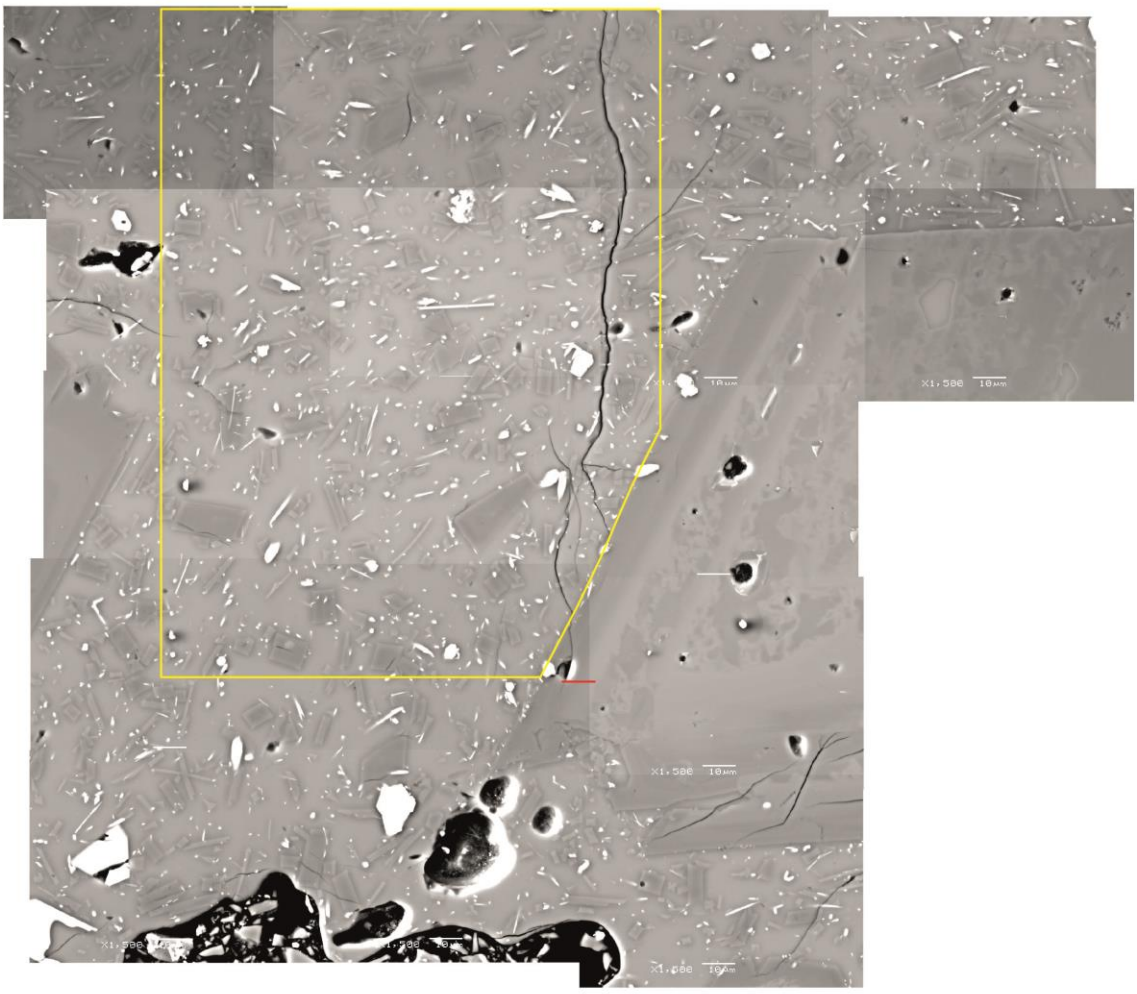

Mid Inter	ln(pop den)	ln(min PD)	ln(max PD)	Cry num	Vol %	Vol from inter area (%)	14.44	Size inter	No. of crys
0.2127	7.82	Infinity	8.51	244	3.357	Total number from CSD	2850000.00	0.0398	1
0.1342	10.68	10.2	11	2.69E+03	9.301	Total vol (%) from CSD	50.40	0.0251	7
0.0847	12.74	12.5	12.94	1.33E+04	11.54			0.0158	22
0.0534	14.52	14.36	14.65	4.96E+04	10.79			0.01	52
0.0337	16.05	15.94	16.15	1.46E+05	7.961			0.0063	97
0.0213	17.35	17.25	17.43	3.34E+05	4.594			0.004	142
0.0134	18.4	18.32	18.48	6.07E+05	2.095			0.0025	165
0.0085	18.93	18.82	19.02	6.46E+05	0.56			0.0016	116
0.0053	19.34	19.2	19.47	6.18E+05	0.134			0.001	74
0.0034	19.45	19.2	19.64	4.32E+05	0.023			0.0006	37
0.0021	Over							0.0004	3
0.0013	Over							0.0003	1
								0.0002	0